VI

# Focused Fundamental Research

Introduction

Cathode Development

Anode Development

Electrolyte Development

Cell Analysis, Modeling, and Fabrication

Diagnostics

Beyond Lithium-Ion Battery Technologies

# VI. Focused Fundamental Research

## VI.A Introduction

The focused fundamental research program, also called the Batteries for Advanced Transportation Technologies (BATT) Program, is supported by the VTO to research and analyze new materials for high-performance, next generation, rechargeable batteries for use in HEVs, PHEVs, and EVs. The effort in FY 2013 continued the increased emphasis on high-energy materials for PHEV and EV batteries and expanded efforts into technologies for enabling the use of Li metal anodes.

### Background and Program Context

The BATT Program addresses the fundamental problems of chemical and mechanical instabilities that have slowed the development of automotive batteries with acceptable cost, performance, life, and safety. The aim is to develop and test new materials and to use traditional and novel diagnostics and modeling methods to better understand cell and material performance and lifetime limitations before initiating battery scale-up and development. Emphasis is placed on the synthesis of components into cells with determination of failure modes, while continuing with materials synthesis and evaluation, advanced diagnostics, and improved model development. Battery chemistries are monitored continuously with timely substitution of more promising components. This is done with advice from within the BATT Program and from outside experts, including consultation with automotive companies and DOE. Also factored into the BATT Program direction is the monitoring of world-wide battery R&D activities. The Program not only supports research that leads to improvements to existing materials, but also into high-risk "leap-frog" technologies that might have a tremendous impact in the marketplace. An overview of the approach used in this program is shown in Figure VI - 1. BATT serves as a bridge between the basic science efforts in DOE and the applied offices, allowing translation of fundamental science into new battery chemistries.

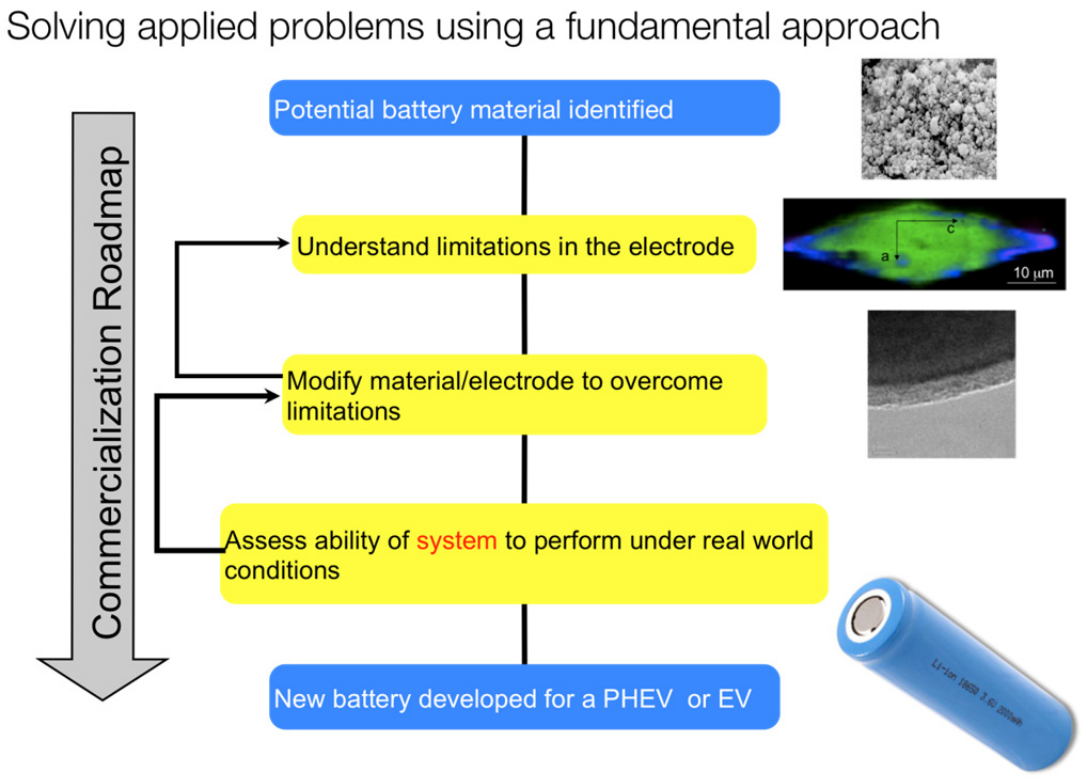


Figure VI - 1: BATT approach overview

The work is administered by the Lawrence Berkeley National Laboratory (LBNL), with principal researchers from LBNL, five additional national laboratories, fourteen universities, and two commercial companies. The program is organized into the following areas:

- Cathode Development..
- Anode Development.
- Electrolytes Development.
- Cell Analysis, Modeling, and Fabrication.
- Diagnostics.
- Beyond Lithium-ion Technologies.

The BATT Program has an enviable team of principal investigators, many of them world renowned, who push the battery field forward in each of these areas. The focus areas include advanced architectures that increase the energy and decrease the cost of batteries via "engineering" approaches and new materials that focus on advancing the state of the art in the short term (e.g., silcon anodes, high voltage electrolytes) and leapfrog chemistries for the long term (e..g, Lithium metal anode, sulfur and oxygen cathodes). This balanced materials effort is made more robust by coupling them with modeling at different length scale, microscopy and spectroscopy with *in situ* focus, and advanced electrochemical characterization. This is illustrated in Figure VI - 2.

The whole effort is undertaken in a coordinated fashion with focus groups formed to solve big challenges. Two such focus groups that bear mention is charged with solving the mechanical damage and surface instability of silicon anodes, and understanding the alleviating the problems at high voltages. Both teams bring together researchers with focus on material synthesis, advanced diagnostics and modeling to understand the issues and propose solutions.

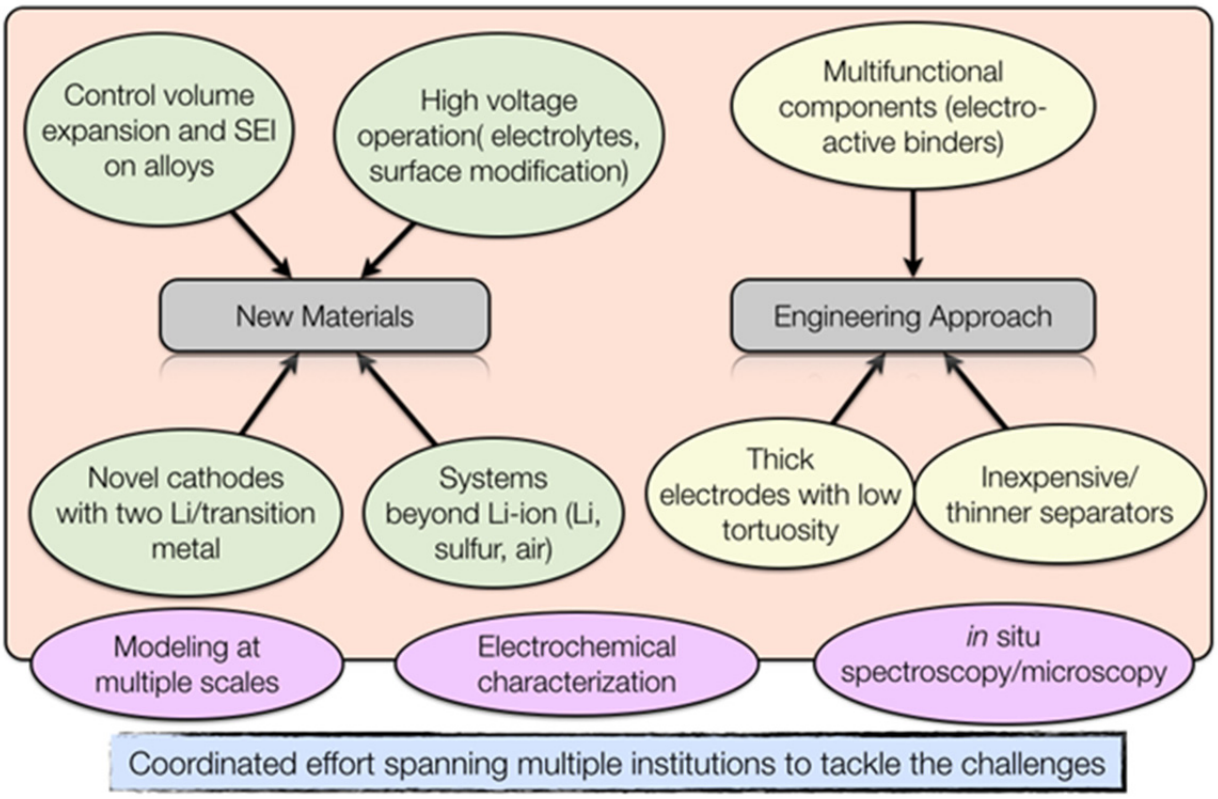


**Figure VI - 2: BATT focus areas**

This section summarizes the research activities of this program in FY 2013. The website for the BATT Program is found at http://batt.lbl.gov. Brief descriptions of each research area are as follows.

***Cathode Development*** aims to find novel cathode materials and processing methods that offer significant improvements in volumetric and specific energy and/or power over current state of the art materials, like LiCoO2. Current projects include work on the high voltage, high-energy layered/layered or Li rich cathode materials, investigating Li bearing mixed polyanion glasses, investigating polyanions that may cycle more than one Li ion per transition metal ion (e.g., silicates), optimization of ion transport in high-energy composite cathodes, and developing *in situ* reactors designed to investigate solvothermal synthesis reactions in real-time using synchrotron-based tools.

***Anode Development*** involves a significant focus on silicon, which offers ten times the capacity of currently used graphite anodes. Researchers are investigating several forms of Si, including nanowires, nanoparticles, clathrate structures, and others. They are also investigating methods for stabilizing Si and Sn composite negative electrodes, including the use of Cu foam current collectors, atomic layer deposition to stabilize alloy electrodes, and a number of Si/carbon nanocomposite materials. It also involves research on metal-based high capacity Li-ion anodes, layered nanolaminates for use in lithium battery anodes, nanoscale composite hetero-structures and thermoplastic resin binders.

***Electrolyte Development*** includes research efforts focused on expanding the temperature range of cells, additives to stabilize the negative and positive interfaces, development of new overcharge shuttles to further stabilize Li-ion cells, new ionic liquids to enable higher voltage windows, sulfone liquids and sulfate/triflate solids for high voltage electrolytes, bifunctional electrolytes for lithium-ion batteries, interfacial and bulk properties and stability studies and first principles modeling to understand and construct a more stable SEI.

***Cell Analysis, Modeling, and Fabrication*** involve several modeling approaches used to understand cell and fundamental material properties, including ab-initio calculations, macroscopic cell calculations, and finite element simulations. Standard cell making and testing techniques are developed and applied to provide a common evaluation process for new materials. Projects might involve predicting microstructure and performance for optimal cell fabrication, assembly of battery materials and electrodes, predicting and understanding novel electrode materials from first-principles, electrode fabrication and materials benchmarking, and the design and scalable assembly of high density low tortuosity electrodes.

***Diagnostics*** involve the use of advanced diagnostics techniques, such as FTIR, X-ray absorption fine structure (XAFS), X-ray diffraction (XRD, nuclear magnetic resonance (NMR) and other techniques to investigate interfacial and other properties in Li-ion batteries. Sample projects include those using DOE's user facilities, advanced *in situ* diagnostic techniques, study of interfacial processes, *in situ* electron microscopy of electrical energy storage materials, microscopy investigation on the fading mechanism of electrode materials, and NMR and pulse field gradient studies of SEI and electrode structure.

***Beyond Lithium-ion Technologies*** study issues critical to the realization of beyond Lithium-ion technologies. Two of the most promising (Lithium/Sulfur and Lithium/Air) require the use of a lithium metal anode. The main focus is to devise new methods to understand and stabilize lithium metal anodes (against mossy Li formation and dendrites) to bring about leaps in energy density without compromising durability and safety. LBNL, ANL and ORNL have partnered to design a series of projects that utilize recent advances in ceramic electrolyte materials, polymer science, and materials characterization to stabilize lithium metal anodes. Inorganic solid state lithium-ion conductors have been proposed as protective electrolyte layers in a lithium metal cell that contains a second, liquid electrolyte in contact with the cathode. The team is also studying various Li metal protective films and dopants that lead to a stable Li/electrolyte interface and permit long-term and stable cycling. Some projects focus on lithium selenium and selenium sulfur couple and composite electrolytes to stabilize metallic lithium anodes.

The BATT Program regularly solicits new proposals in each of the above-listed areas. BATT Program management regularly accepts unsolicited proposals on any advanced energy storage technology that can significantly advance the state-of-the-art and is appropriate for the R&D focus of the BATT Program. Unsolicited proposals are reviewed separately but by using a process similar to that for the solicited proposals.

# VI.B Cathode Development

## VI.B.1 Novel Cathode Materials and Processing Methods (ANL)

**Michael Thackeray**
Argonne National Laboratory

9700 South Cass Avenue
Argonne, IL 60439
Phone: (630) 252-9184; Fax: (630) 252-4176
E-mail: thackeray@anl.gov

Collaborators
ANL: J. R. Croy, D. Kim, R. Benedek, V. G. Pol, S. V. Pol, C. S. Johnson, J. T. Vaughey, K. G. Gallagher,
ANL's ABR 'Voltage Fade' team
APS: M. Balasubramanian, Y. Ren
Industry: Envia, BASF, Toda, LG Chem

Start Date: October 2011
Projected End Date: September 2015

### Objectives

- Design high capacity, high-power and low cost cathodes for PHEVs and EVs.
- Improve the design, composition and performance of Mn-based cathodes.
- Explore novel processing routes for advanced electrodes with effective architectural designs.
- Use atomic-scale modeling as a guide to identify, design and understand the structural features and electrochemical properties of advanced cathode materials.

### Technical Barriers

- Low energy density
- Poor low temperature operation
- Abuse tolerance limitations

### Technical Targets

- 142 Wh/kg, 317 W/kg (PHEV 40 mile requirement)
- Cycle life: 5000 cycles
- Calendar life: 15 years

### Accomplishments

- Identified promising electrode compositions and syntheses to achieve high capacity electrodes with stable surfaces and high rate capabilities.
- Identified changes to $Li_2MnO_3$-like environments as a possible trigger for continued voltage fade on high voltage cycling.
- Evaluated the effect of coatings on voltage fade.

✧ ✧ ✧ ✧ ✧

### Introduction

$Li_2MnO_3$-stabilized composite electrode structures, such as 'layered-layered' $xLi_2MnO_3•(1-x)LiMO_2$ (M=Mn, Ni, Co), 'layered-spinel' $xLi_2MnO_3•(1-x)LiM_2O_4$ and even more complex 'layered-layered-spinel' $y\{xLi_2MnO_3•(1-x)LiMO_2\}•(1-y)LiM_2O_4$ systems are receiving international attention because they can provide rechargeable capacities between 200 and 250 mAh/g between 4.6 and 2.0 V vs. lithium. They offer, today, perhaps the best opportunity to make a significant improvement to the energy output and to improve the abuse tolerance of state-of-the-art, commercial lithium-ion cells in order to meet or exceed the 40-mile electric range targets of PHEVs. These manganese-rich composite cathode structures have to be electrochemically activated above 4.4 V in order to access the high capacity. Unfortunately, this process compromises the rate capability of these electrodes, which also suffer from voltage decay on cycling, thereby compromising the energy and power output of the cells and preventing their implementation in practical systems. This project directly addresses these limitations and challenges. A novel processing route using $Li_2MnO_3$ as a precursor to synthesize composite electrode structures is being explored. The technique is simple, versatile and seemingly low cost; it offers the possibility of opening the door to wide exploitation and, in particular, of synthesizing and tailoring composite electrode structures, including new systems, thereby enhancing the electrochemical properties of lithium-ion cells to meet the performance targets of PHEVs.

## Approach

- Exploit the concept, and optimize the performance, of structurally-integrated, high-capacity electrodes, particularly 'layered-layered' $xLi_2MnO_3•(1-x)LiMO_2$ (M=Mn, Ni, Co) and 'layered-layered-spinel' $y\{xLi_2MnO_3•(1-x)LiMO_2\}•(1-y)LiM_2O_4$ electrodes.
- Explore new processing routes to prepare composite electrodes that provide acceptable capacity, power, and life.
- Design effective surface structures to protect the underlying metal oxide particles from the electrolyte and to improve their rate capability when charged at high potentials.
- Use first principles modeling to aid the design of bulk and surface cathode structures and to understand electrochemical phenomena.

## Results

**High Capacity $xLi_2MnO_3•(1-x)LiMO_2$ Cathodes.** $xLi_2MnO_3•(1-x)LiMO_2$ (M = Mn, Ni, Co) high capacity cathode materials are currently viewed as the most viable options for achieving near-term performance goals for PHEVs. The $Li_2MnO_3$ component in these composite structures can serve as both a stabilizing agent and a source of 'excess' capacity relative to layered $LiMO_2$ (M = Mn, Ni, Co), materials. A detailed electrochemical study to explore the compositional space and to understand the important and complex role played by the $Li_2MnO_3$ component for $xLi_2MnO_3•(1-x)LiMn_{0.5}Ni_{0.5}O_2$ electrode materials (x = 0, 0.1, 0.3, and 0.5), was completed.

Figure VI - 3(a-d) show differential capacity plots of $Li/xLi_2MnO_3•(1-x)LiMn_{0.5}Ni_{0.5}O_2$ cells cycled at room temperature over three consecutive voltage windows after an initial activation to 4.7 V. Cycles were conducted at 5 mA/g in order to approach near equilibrium states during charge and discharge.

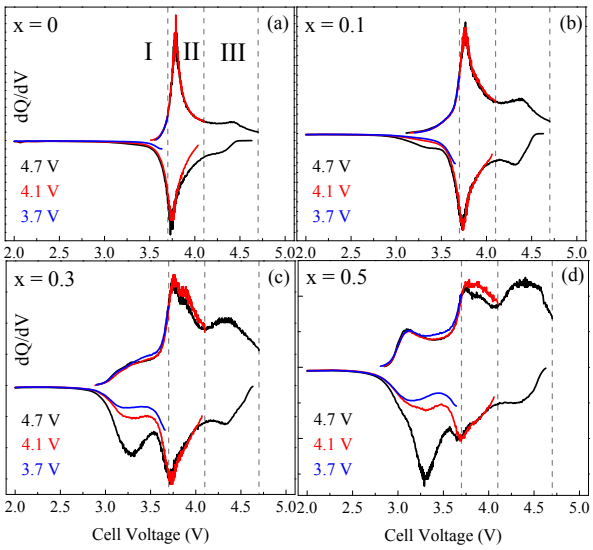


**Figure VI - 3: dQ/dV data taken over consecutive voltage windows of 2.0-3.7, 2.0-4.1, and 2.0-4.7 V at 5 mA/g for $Li/xLi_2MnO_3•(1-x)LiNi_{0.5}Mn_{0.5}O_2$ cells with various values of x after activation to 4.7 V. x values are provided at the upper left of each panel; data from each window are color-coded for clarity**

It was observed that with increasing $Li_2MnO_3$ content, x, significant capacity was generated in the low-voltage (2.0-3.7 V) and high-voltage (4.1-4.7 V) regions. Furthermore, a new process developed at ~3.8 V on charge as a consequence of the 'activation' process. From Figure VI - 3b-d, it is evident that some of the capacity extracted above ~4.0 V on charge was not delivered on discharge until ~3.2 V with substantial hysteresis occurring for x = 0.3, and 0.5.

Figure VI - 4a shows the difference in charge and discharge voltages at 50% state-of-charge for the 2.0-4.7 V windows shown in Figure VI - 3(black curves). The hysteresis clearly increases as a function of x. Extended cycling and monitoring of the capacity in each voltage window, as in Figure VI - 3, revealed that the high voltage charge capacity (>~4.0 V) decreased with cycling, concomitant with an increase in the low voltage (<~3.7 V) charge capacity. This low-voltage capacity is directly related to the continuously fading voltage profiles in composite materials and is a strong function of $Li_2MnO_3$ content (Figure VI - 4b). Furthermore, the data demonstrate that the hysteresis and voltage fade phenomena are correlated.

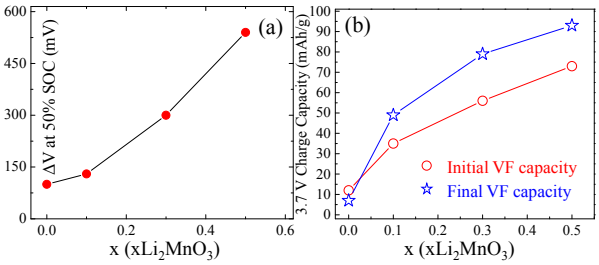


**Figure VI - 4: (a) Hysteresis as a function of x measured as the difference between charge and discharge voltages (ΔV) at 50% SOC. (b) Growing capacity associated with the initial (cycle 2, circles) and final (cycle 30, stars) voltage fade of the material (2.0-3.7 V charge capacity) as a function of x**

To better understand the structure of $xLi_2MnO_3$•(1-x)$LiMn_{0.5}Ni_{0.5}O_2$ materials as a function of $Li_2MnO_3$ content, x, X-ray absorption spectroscopy (XANES, EXAFS) studies were conducted on the as-prepared cathodes. Figure VI - 5a and b show the Mn and Ni K-edge XANES, respectively, of all samples (x = 0, 0.1, 0.2, 0.3) as well as $Li_2MnO_3$ and NiO references. It was observed that the average oxidation states of Mn and Ni were $Mn^{4+}$ and $Ni^{2+}$ for all values of x, in agreement with the respective references. This implies that substantial ordering occurs between Ni and Mn for all samples and reveals a strong tendency for charge ordering between Mn and Ni.

Figure VI - 6a and b show the corresponding Mn and Ni K-edge EXAFS data, respectively. Several interesting trends appeared in the Mn EXAFS data. Most apparent was the clear decrease in the first-shell Mn-metal correlations at ~2.5 Å (uncorrected for photoelectron wave shift). This trend reveals that the excess lithium in the transition metal layers preferentially orders with manganese on increasing x ($Li_2MnO_3$ content). The peaks between ~4-6 Å (arrowed) also show a strong shift towards the corresponding peaks of the $Li_2MnO_3$ reference at $x \geq 0.3$, indicating a tendency of the local Mn environment towards that of pure $Li_2MnO_3$ with increasing x. The Ni K EXAFS data in Figure VI - 6b reveal that the Ni environment of the composite material has stronger $LiMO_2$ character (e.g., Ni-M coordination of ~6) that was relatively unchanged on increasing x with the exception of decreasing intensity at ~4 Å. This peak arises from the exchange of Li and Ni between the layers in these materials, indicating that increasing the $Li_2MnO_3$ content enhances the layering of the structure. In combination with the Mn EXAFS data of Figure VI - 6a, for which no intensity at 4 Å was observed for any x, it was concluded that Li/Ni exchange occurs predominantly within the $LiMn_{0.5}Ni_{0.5}O_2$ component.

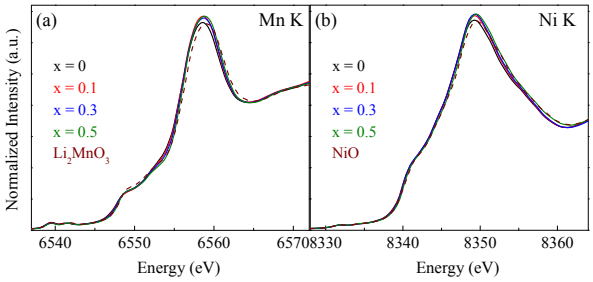


**Figure VI - 5: (a) Mn and (b) Ni K-edge XANES data of the as-prepared $xLi_2MnO_3$•(1-x)$LiMn_{0.5}Ni_{0.5}O_2$ cathodes along with $Li_2MnO_3$ and NiO reference spectra**

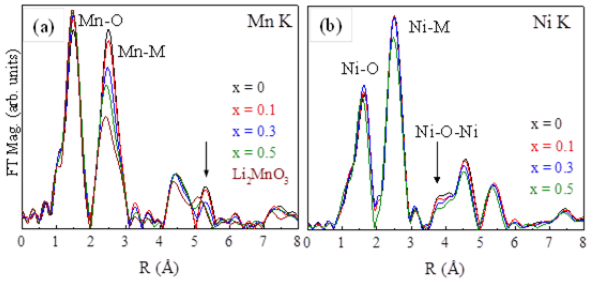


**Figure VI - 6: (a) Mn and (b) Ni K-edge EXAFS of the as-prepared $xLi_2MnO_3$•(1-x)$LiMn_{0.5}Ni_{0.5}O_2$ cathodes for various values of x**

Finally, in order to explore how synthesis conditions affect the formation of $Li_2MnO_3$ and $LiMO_2$ domains and the subsequent electrochemistry, a detailed synthesis study was combined with EXAFS to probe the structures of as-prepared cathodes. Figure VI - 7a and b show Mn and Co K-edge EXAFS, respectively, of $0.5Li_2MnO_3$•$0.5LiCoO_2$ cathode powders annealed via three different routes. All samples were annealed at 550°C in air followed by an annealing at 850°C, also in air. Subsequently, the samples were either 1) allowed to cool naturally in the furnace (uncontrolled), 2) slow-cooled by a programmed temperature profile (controlled), or 3) quenched (quenched). The EXAFS data in Figure VI - 7 reveal that that the local structure of all samples is essentially identical. It is known that voltage fade and hysteresis persist in similar samples prepared via different synthesis routes. Therefore, these data imply that the domain structure within these materials is largely insensitive to synthesis conditions, while charge ordering becomes a dominant driving factor in controlling their structural evolution.

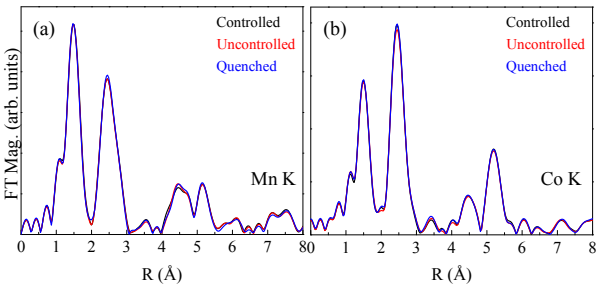


**Figure VI - 7: (a) Mn and (b) Co K-edge EXAFS data of $0.5Li_2MnO_3$•$0.5LiCoO_2$ powders prepared under different annealing conditions**

## Conclusions and Future Directions

*Conclusions*

- A detailed electrochemical study of $xLi_2MnO_3$•$(1-x)LiNi_{0.5}Mn_{0.5}O_2$ cathodes has revealed that the voltage fade and hysteresis phenomena are correlated and may be related to the same mechanisms. Furthermore, both voltage fade and hysteresis are a strong function of the $Li_2MnO_3$ content, each increasing with increasing $Li_2MnO_3$.
- X-ray absorption data reveal a strong preferential ordering of lithium and manganese with increasing x in $xLi_2MnO_3$•$(1-x)LiMn_{0.5}Ni_{0.5}O_2$. While the local environment of manganese tends towards that of pure $Li_2MnO_3$, the local nickel environment remains similar to that of $LiMO_2$. Manganese and nickel EXAFS data combine to reveal that Li/Ni exchange occurs predominantly within the $LiMn_{0.5}Ni_{0.5}O_2$ component.
- EXAFS studies of $0.5Li_2MnO_3$•$0.5LiCoO_2$ synthesized under various conditions reveals that the local, electrochemically-relevant structure of layered-layered materials is largely insensitive to synthesis conditions. Furthermore, all samples showed distinctly different manganese and cobalt environments revealing the composite nature of the materials under all synthesis conditions.

*Future Directions*

- Continue to explore the complex, critical role played by $Li_2MnO_3$ and the stabilizing interactions of manganese and nickel in composite cathode structures to optimize structural stability during cycling and capacity/energy generation.
- Explore composite cathode structures with low ($x \leq 0.4$) and high ($x \geq 0.6$) $Li_2MnO_3$ content with the goal of tailoring the size and stabilization of $Li_2MnO_3$-like domains.
- Evaluate sonochemical coatings against wet-chemical and atomic layer deposition methods to identify optimum materials for protecting composite particle surfaces.
- Use theory to understand surface degradation in manganese-based cathode materials.

## FY 2013 Publications/Patents/Presentations

1. D. Kim, G. Sandi, Jason R. Croy, K. Gallagher, S.-H. Kang, E. Lee, M. Slater, C. Johnson, and M. Thackeray, "Composite 'Layered-Layered-Spinel' Cathode Structures for Lithium-Ion Batteries," *JES* **160**, A31 (2013).
2. J. R. Croy, K. Gallagher, M. Balasubramanian, Z. Chen, Y. Ren, D. Kim, S.-H. Kang, D. Dees, and M. Thackeray, "Examining Hysteresis in Composite $xLi_2MnO_3$•$(1-x)LiMO_2$ Cathode Structures," *Phys. Chem. C* **117**, 6525 (2013).
3. K. Gallagher, J. R. Croy, M. Balasubramanian, M. Bettge, D. Abraham, A. Burrell, and M. Thackeray, "Correlating Hysteresis and Voltage Fade in Lithium- and Manganese-rich Layered Transition-Metal Oxide Electrodes," *Electrochem. Comm.* **33**, 96 (2013).
4. D. Kim, J. R. Croy, and M. Thackeray, *Comments on* "Stabilizing Layered Manganese Oxide Electrodes for Li Batteries," *Electrochem. Comm.* **36**, 103 (2013).
5. J. R. Croy, K. Gallagher, M. Balasubramanian, B. Long, and M. Thackeray, "Quantifying Hysteresis and Voltage Fade in $xLi_2MnO_3$•$(1-x)LiMn_{0.5}Ni_{0.5}O_2$ Electrodes as a Function of $Li_2MnO_3$ Content," (submitted).
6. M. M. Thackeray, D. Kim and J. Croy, "Electrode Structures and Surfaces for Li Batteries," USPTO, Filed November 19, 2012.
7. M. M. Thackeray, C. S. Johnson and S.-H. Kang, "Electrode Structures and Surfaces for Li Batteries," USPTO, Filed January 14, 2013.
8. M.M. Thackeray, "Development of High-Capacity Cathode Materials with Integrated Structures," *2013 DOE Annual Peer Review Meeting,* May 2013, Washington, DC.
9. J. R. Croy, K. Gallagher, M. Balasubramanian, B. Long, M. Thackeray, T. Burrell, D. Dees, Z. Chen, D. Abraham, M. Bettge, Y. Ren, "Structural and Electrochemical Insights on the Mechanisms of Voltage Fade and Hysteresis in Composite $xLi_2MnO_3$•$(1-x)LiMO_2$ Electrodes," *ABAA 6,* Argonne, IL, September 10, 2013 (Invited).
10. J. R. Croy, K. Gallagher, M. Balasubramanian, B. Long, M. Thackeray, "The Next Generation of Lithium-Ion Batteries: Challenges and

Opportunities," Ball State University, Muncie, Indiana, September 5, 2013 (Invited).

11. M. M. Thackeray, "Recent Developments in Lithium Battery Materials Research," Presentations to Samsung SDI, LG Chem (Korea); Nissan Research Center, Toda Kogyo (Japan), August 30 - September 2, 2013.
12. M. M. Thackeray, "Designing Energy Storage Materials: Intuition vs. Computation," *The Materials Genome Initiative Grand Challenges Summit,* Rockville, Maryland, June 25-26, 2013.
13. M. M. Thackeray, J. R. Croy, D. Kim, B. R. Long, V. G. Pol, S. V. Pol, M. Balasubramanian, Y. Ren and R. Benedek, "Design and Evaluation of High Capacity Cathodes," *DOE Annual Merit Review,* Vehicle Technologies Program, Arlington, Virginia, May 13-17, 2013.
14. J. R. Croy, K. Gallagher, M. Balasubramanian, B. Long, M. Thackeray, Challenges of Composite, High-Capacity, Li-Ion Cathodes," *Advanced Photon Source User's Meeting,* Argonne National Laboratory, IL, May 7, 2013 (Invited).
15. M. M. Thackeray, J. R. Croy, L. Trahey, V. G. Pol, M. Balasubramanian, K. G. Gallagher, J. Wen, M. Krumpelt, M. Chan, S. Kirklin, D. Miller, C. Wolverton, "Confronting the Challenges of High-Capacity Cathodes and Anodes for Lithium Batteries," *International Battery Association Meeting,* Barcelona, Spain, March 10-15, 2013.
16. J. R. Croy, D. Kim, K. Gallagher, M. Balasubramanian, Y. Ren, M. Thackeray, "Structural Stabilization of LMR-NMC Composite Cathodes," *U.S. DRIVE 2013,* Argonne National Laboratory, IL, 24 January, 2013.
17. J. R. Croy, S. Pol, M. Balasubramanian, D. Kim, S.-H. Kang, M. Thackeray, "High Capacity Lithium-Metal-Oxide Electrodes: Challenges and Opportunities," *John B. Goodenough Symposium,* Austin, TX, October 26, 2012.

# VI.B.2 *In situ* Solvothermal Synthesis of Novel High Capacity Cathodes (BNL)

**Feng Wang**
Brookhaven National Laboratory (BNL)

Sustainable Energy Technologies Department
Upton, NY, 11973
Phone: (631) 344-4388; Fax: (631) 344-7905
E-mail: fwang@bnl.gov

**Patrick Looney**
Brookhaven National Laboratory (BNL)
Sustainable Energy Technologies Department
Upton, NY, 11973
Phone: (631) 344-3798; Fax: (631) 344-7905
E-mail: jlooney@bnl.gov

Start Date: October 2011
Projected End Date: November 2015

## Objectives

- Develop low-cost cathode materials that offer high energy density (>660 Wh/kg) and electrochemical properties (cycle life, power density, safety) consistent with USABC goals.

## Technical Barriers

Present day Li-ion batteries are incapable of meeting the 40-mile all-electric-range within the weight and volume constraints established for PHEVs by DOE and the USABC. Higher energy density cathodes are needed for Li-ion batteries to be widely commercialized for PHEV applications.

The development of new, safer lithium batteries requires new tools to better understand the physical and chemical processes that occur during cycling and the ability to predict and ultimately control the key electrochemical properties such as capacity, durability (calendar and cycle life), abuse tolerance (safety characteristics) and cost.

## Technical Targets

- Higher energy density cathodes
- Lower cost

## Accomplishments

- Developed *in situ* reactors and time resolved XRD techniques specialized for studying hydrothermal/solvothermal, ion-exchange, and solid-state synthesis reactions.
- Determined optimal procedures for synthesis of high-capacity Cu-V-O cathodes *via in situ* studies.
- Identified lithium electrochemical reaction and degradation mechanisms of Cu-V-O cathodes *via in situ* XAS, XRD and *ex situ* TEM.
- Developed procedures for synthesis of one new class of Cu-V-O compound, using both hydrothermal and solid-state reactions.
- Demonstrated feasibility of using hydrothermal-based ion exchange to prepare polyanion-type cathodes, and explored reaction pathways of ion exchange processes using a newly developed *in situ* reactor.

✧ ✧ ✧ ✧ ✧

## Introduction

Despite considerable interest in the development of new cathodes for lithium ion batteries, only a small number of known materials show real promise for achieving significant improvement in capacity and/or a reduction in cost. The preparation of new compounds or materials with unique properties often relies on trial and error as there are a variety of synthesis parameters (precursor concentration, temperature, pressure, pH value, cation choice and reaction time) that can have a strong influence on the material properties (morphology, particle size, crystal structure) and electrochemical performance (e.g., capacity, rate capability, and durability). Most solution-based reactions are carried out in a sealed autoclave and therefore the reactor is a black box – the inputs and outputs are known, but little is known about intermediate phases and the overall reaction pathway. *In situ, real-time* probes of synthesis reactions can provide the details of reactions, elucidating intermediate phases and how temperature, pressure, time and the precursor concentrations affect the reaction pathways. The results of such studies enable strategies to optimize synthesis reactions, particularly the formation of materials of desired phases and properties. With a more fundamental understanding of

the correlation between synthesis conditions, crystallization processes, and material properties, a more rational design of advanced lithium electrode materials should emerge.

## Approach

In this effort, specialized *in situ* reactors were developed to investigate solvothermal and other solution-based synthesis reactions in real-time using synchrotron X-ray diffraction (XRD) and absorption spectroscopy (XAS) techniques, with which crystal growth and changes in chemical bonds can be monitored while leaving the reaction undisturbed. This approach provides a real-time measurement of how reaction conditions affect nucleation and crystallization, bonding, particle size, morphology and defect concentration. In addition, *in situ* measurements reveal the formation of intermediate and short-lived phases formed during the reaction without the need for quenching. These new tools and insights are being used to prepare novel high-energy cathodes.

The structural and electrochemical properties of synthesized materials are evaluated *via* synchrotron XRD combined with Rietveld refinement, and various electrochemical measurements. The structural/chemical evolution of electrodes during cycling is systematically investigated using *in situ*, *in operando* synchrotron XRD and X-ray absorption near-edge (XANES) and extended fine structure (EXAFS) and advanced TEM techniques, which help to identify the mechanism(s) responsible for the capacity fade and provide guidance to further optimizing the synthesis.

## Results

**Synthesis of high-capacity Cu-V-O cathodes**

Among the wide variety of Cu-based vanadium oxides, ε-$Cu_{0.95}V_2O_5$ (ε-CVO) is one of the few promising cathode materials with high capacities (~700 Wh/kg or above). Building on our previous work (in FY12) in which several hydrothermal approaches were identified for making ε-CVO compounds, the effort in FY13 focused on optimizing the synthesis procedures *via in situ* synthesis studies, by which the precursors, reducing agents and reaction conditions were systematically evaluated.

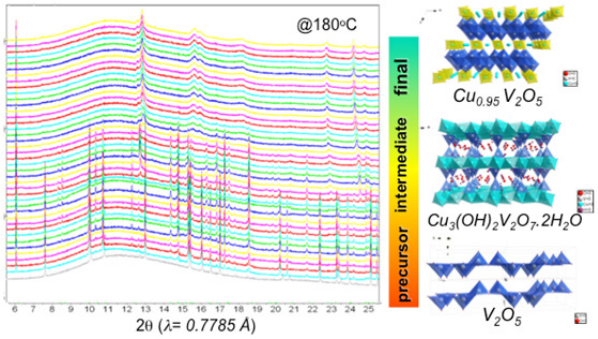


**Figure VI - 8: *Time-resolved* XRD patterns acquired during *in situ* synthesis of ε-CVO**

Figure VI - 8 shows one of the results on phase evolution during *in situ* synthesis of ε-CVO, using the procedure:

$$Cu(NO_3)_2 \cdot 3H_2O \text{ and } V_2O_5 + R.A \rightarrow Cu_xV_2O_5 \quad (1)$$

The pure ε-CVO phase in a capillary reactor was obtained by tuning the Cu/V ratio and concentration of the reducing agent (R.A.) at a temperature as low as 180°C. The intermediate phase, $Cu_3(OH)_2V_2O_7 \cdot 2H_2O$, was found to be a crucial step towards forming the desired final product. This phase was stable at low temperatures and, depending on the reaction conditions, either transformed into the pure ε-CVO phase, or a mixture with others (α-$CuV_2O_6$, Cu, …) at high temperatures. The exploration of all the possible reaction paths at real working conditions is critical for obtaining important information on optimizing synthesis and the ability to 'dial in' the desired phases.

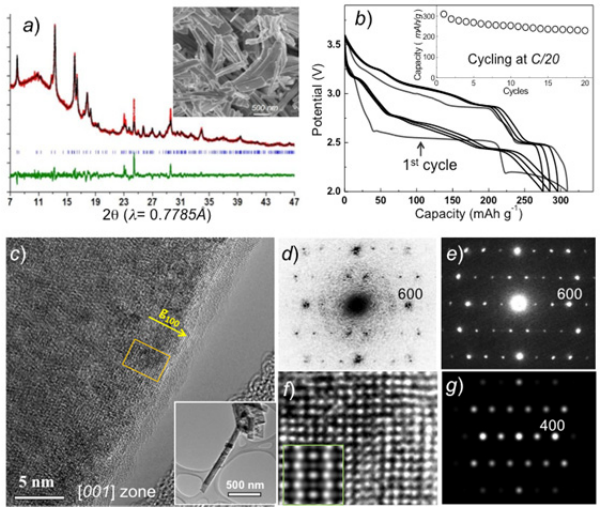


**Figure VI - 9: Structural and electrochemical properties of ε-CVO powder. (a) XRD pattern (with refinement), and morphology (by SEM; inset), (b) galvanostatic cycling profiles and cyclability (inset), (c) HRTEM imaging, (d) FFT of (c), (e) e-diffraction pattern, (f, g) simulations**

After determining the optimal reaction conditions and process, large amount of ε-CVO powder was

synthesized using an autoclave reactor, and then examined with synchrotron XRD (Figure VI - 9a). The as-synthesized material has a high degree of crystallinity and purity, and good electrochemical performance, as shown by its high capacity (~300 mAh/g) and reasonable cycling stability, (Figure VI - 9b). Detailed structural analysis of individual CVO nanorods, obtained using high-resolution TEM (HRTEM) imaging and electron diffraction (Figure VI - 9c-g), it was found that despite the good match of XRD pattern of the synthesized material to the monoclinic ε-$Cu_{0.95}V_2O_5$ phase (Figure VI - 9a), the local structural ordering is much different as a result of Cu-deficiency.

**Li reaction mechanisms in Cu-V-O.** Synchrotron XRD and TEM were used to examine the structural and morphological changes of ε-CVO as a result of lithium reaction (Figure VI - 10). With lithiation, long-range ordering in ε-CVO was lost due to the Cu extrusion, and not recovered with delithiation although the extruded Cu migrates back into the structure. This newly formed structure (after one cycle) appeared to be stabilized according to the similarity in the XRD patterns of electrodes subject to different cycles. This observation may explain the "multiple-plateau" profile in the 1st cycle, and repeatable, "slopy" curves in the following cycles (Figure VI - 9b).

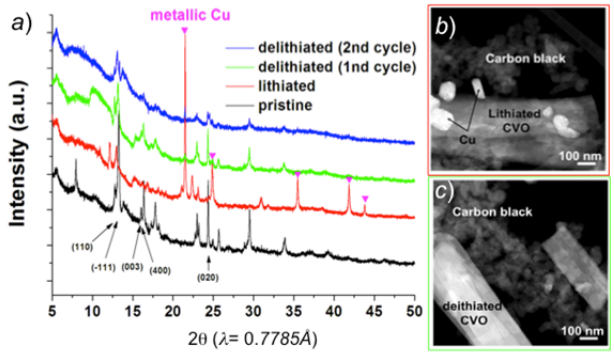


**Figure VI - 10: Structural change of ε-CVO with lithium reactions, via (a) XRD, (b, c) dark field images**

Due to the loss of long-range ordering with (de)lithiation, it is hard to determine the details of structural change in ε-CVO by XRD alone. To this end, detailed information on redox of Cu, V, and short-range ordering with Cu extrusion/insertion was obtained, *via* near-edge spectra (XANES) and extended fine structure (EXAFS); some of the results are given in Figure VI - 11. Cu and V were reduced at different lithiation stages, as illustrated in Figure VI - 11a. The $Cu^{2+/1+}$ reduction proceeds *via* solid solution, followed with displacement ($Cu^{1+/0}$), and concomitant $V^{5+/4+/3+}$ reduction. One set of V K-edge XANES spectra is given in Figure VI - 11b, in which the gradual edge shift to lower energies indicates the reduction of V with lithiation and correspondingly, the amplitude increase of V-O peak in the Fourier transform of EXAFS tells that initially distorted $VO_6$ octehedra become more symmetric due to Li insertion/Cu extrusion (Figure VI - 11c.)

The redox of Cu and V at different lithiated stages was illustrated in Figure VI - 11c started with $Cu^{2+/1+}$ reduction (*via* solid solution; state I'), followed with displacement ($Cu^{1+/0}$; II'), and $V^{5+/4+/3+}$ reduction (II, III). The $VO_6$ octahedra, initially distorted, become highly symmetric with Li insertion/Cu extrusion. Our studies also suggested the gradual Cu, V loss in ε-CVO electrodes should be the main cause of the capacity decay, which might be alleviated by surface coating.

**Synthesis of new Cu-V-O compound.** A new class Cu-V-O compound (α-CVO) was synthesized using hydrothermal (HT) reactions typically *via* the route:

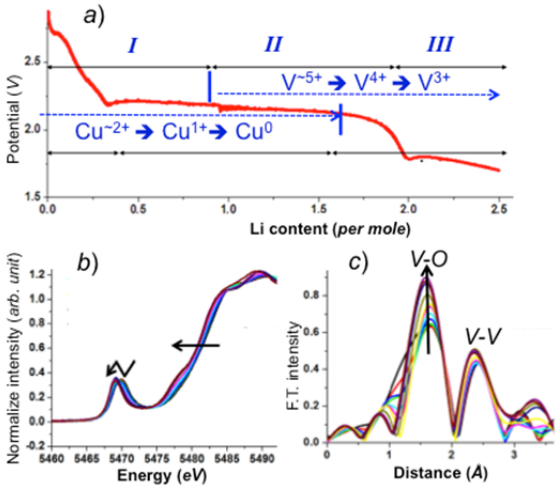


**Figure VI - 11: Redox of V, Cu, and local structural re-ordering in ε-CVO by *in situ* XAS. (a) voltage profile, (b) V K-edge XANES spectra, and (c) Fourier transform (F.T.) of the V K-edge EXAFS**

$$Cu(NO_3)_2+NH_4VO_3+R.A. \rightarrow \alpha\text{-}CuVO \quad (2)$$

The synthesis reaction at certain conditions, i.e., Cu/V ratio, pH value, and concentration of reducing agent, leads to the formation of an intermediate phase at low temperatures, and the final product of α-CVO phase at about 200°C. According to our structural analysis, this α-phase is promising for use as cathode due to its unique structure, with a 3D V-O framework and open channels for Cu-ion and Li-ion transport. The as-synthesized powder is composed of μm-sized particles, with uniform Cu, V elemental distribution across individual particles (Figure VI - 12a,b).

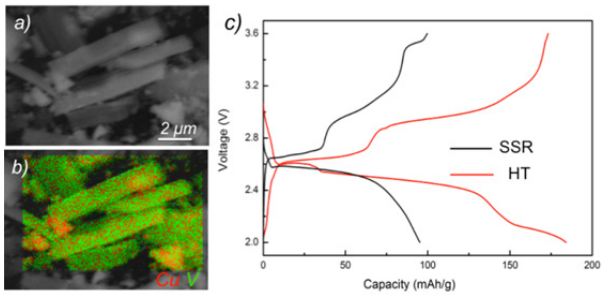


**Figure VI - 12: Morphology and electrochemical properties of α-CVO. (a, b) SEM image and EDX mapping, (c) galvanostatic voltage profiles**

Solid-state reaction (SSR) was also used to synthesize the $\alpha$-phase; this material has similar crystal structure but larger particle size. Typical voltage profiles from electrochemical tests of the synthesized powders (by HT and SSR) at C/20 are provided in Figure VI - 12c. The long single plateau observed at about 2.5 V in the discharge curves suggests that the Cu displacement reaction should be dominant. But the reaction during charging appears to be asymmetric, as indicated by two plateaus. In this preliminary electrochemical test, a moderate capacity (of ~185 mAh/g) was obtained in α-CVO grown by HT, which, however, exhibits almost 2x higher capacity than that by SSR. Further performance improvement may be achieved *via* size reduction.

**Synthesis of polyanion cathodes.** Hydrothermal based methods for preparing polyanion-type cathodes were explored, either *via* direct chemical reaction or through ion exchange *via* lithium substitution in iso-structural Na-containing precursors in an aqueous solution. Synthesis of fluorophosphates $Li_xNa_{2-x}MnPO_4F$ and $Li_xNa_{1.5-x}VPO_5F_{0.5}$ *via* ion exchange was typically performed in a sealed autoclave at elevated temperatures, using $Na_2MnPO_4F$, $Na_{1.5}VPO_5F_{0.5}$ as precursors, LiBr as Li source and 1-hexanol as solvent. The extent of exchange was maximized *via* tuning reaction conditions, such as temperature and the concentration of Li sources.

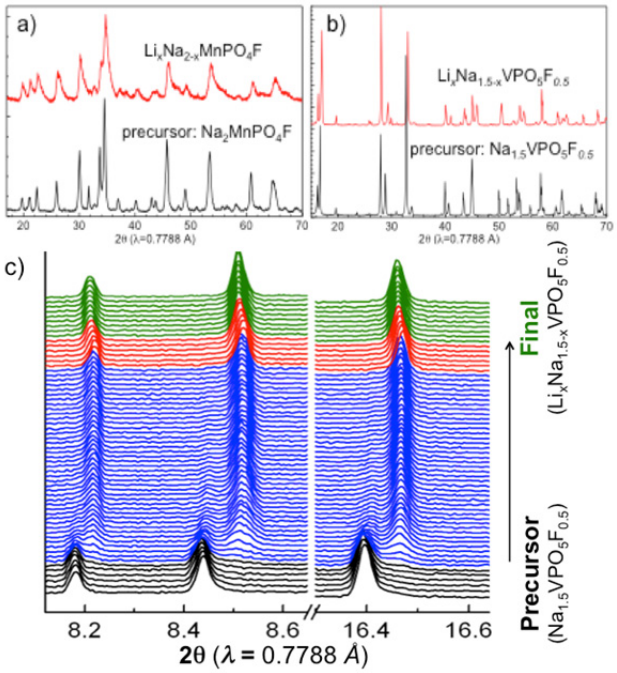


**Figure VI - 13: Structural characterization of polyanion-type materials synthesized *via* hydrothermal ion exchange. (a,b) XRD patterns of precursors and Li-exchanged final products, (c) time-resolved XRD patterns from ion exchange process in $Na_{1.5}VPO_5F_{0.5}$**

In Figure VI - 13a, the XRD patterns of synthesized $Li_xNa_{2-x}MnPO_4F$ and $Li_xNa_{1.5-x}VPO_5F_{0.5}$ exhibit similar structures as their precursors but smaller volumes. Subtle structural changes, and possibly a reduction in particle size, are suggested by the change in the relative intensity and broadening of diffraction peaks. The results demonstrate the feasibility of using ion exchange to prepare metastable phosphates which are mostly inaccessible by direct chemical reactions.

A new type of *in situ* reactor was developed for studying ion-exchange reactions and used for studies of the structural change in single-crystalline, $\mu m$-sized $Na_{1.5}VPO_5F_{0.5}$ particles throughout the entire Li exchange process. Time-resolved XRD patterns (Figure VI - 13c) show a gradual phase transformation (blue region) occurred in the early stage, followed by solid solution (red) and then stabilization of a final phase (green), which suggests a complicated reaction process with more than one phase involved. *In situ* measurements of the phase transformations and reaction kinetics during ion exchange of $Na_{1.5}VPO_5F_{0.5}$ have also been made.

## Conclusions and Future Directions

In FY13, *in situ* reactors and time resolved XRD techniques were developed and utilized for studying materials made via hydrothermal, solvothermal, ion exchange, and solid-state reactions. It was shown that *in situ* studies are crtical for understanding synthesis reaction mechanisms and developing procedures for preparing compounds of desired phases and material properties. After optimization of reaction conditions, high-quality ε-$Cu_{0.95}V_2O_5$ materials were synthesized and the structural and electrochemical properties were evaluated. Li reaction process and possible mechanisms responsible for poor cycling stability of this material were also identified. In addition, a new class of Cu-V-O compounds was synthesized, and the feasibility of synthezing polyanion cathodes *via* ion exchange was also established.

In FY14, the work on ε- $Cu_{0.95}V_2O_5$ cathodes will be completed and efforts will be extended to the second Cu-V-O phase to improve the purity and yield, and to complete the evaluation of its structural and electrochemical properties. Hydrothermal based methods will be further explored, either *via* direct chemical reaction or through ion exchange, for preparing ternary and/or quaternary Li-V-$PO_4$(-*X)* type cathodes. Also opportunities for collaborating with theory efforts will be explored, wherein kinetic and dynamic parameters measured through *in situ* synthesis studies may be compared to calculations or direct input for design of new materials.

## FY 2013 Publications/Presentations


1. "*In situ* Solvothermal Synthesis of Novel High Capacity Cathodes," *DOE Annual Peer Review Meeting*, May 13-17, 2013, Washington, DC.
2. F. Wang, Q. Wang, N.A Chernova, M.S. Whittingham, J. Graetz, "*In situ* Studies of Cathodes for Li-ion Batteries by Simultaneous Quick X-Ray Absorption/Diffraction Spectroscopy (QXAS/XRD)," *MRS Fall Meeting*, Nov. 26-30, 2012. Boston. (Oral).
3. F. Wang, X. Wang, S-W. Kim, J. Bai, J. Graetz, "Development of High-energy Cathodes *via in situ* Solvothermal Synthesis," *MRS Spring 2013 meeting*, April1-5, 2013, San Francisco. (Poster)
4. F. Wang, J. Bai, S-W. Kim, X. Wang, "Development of High-Energy Cathodes via *In situ* Solvothermal Synthesis," *ECS 223rd Meeting*, May 12 - 16, 2013, Toronto, Canada. (Oral)
5. F. Wang, S-W. Kim, J. Bai, X. Wang, L. Wu, Y. Zhu, and J. Graetz, "*In situ* studies of synthesis and lithium reaction of high-capacity electrodes for Li-ion batteries," *SPIE Meeting*, April 29 – May 3, 2013. Baltimore (Invited).

# VI.B.3 Design of High Performance, High Energy Cathode Materials (LBNL)

**Marca Doeff**
Lawrence Berkeley National Laboratory

Environmental Energy Technologies Division
Berkeley, CA 94720
Phone: (510) 486-5821
E-mail: mmdoeff@lbl.gov

Start Date: October 2011
Projected End Date: September 2015

## Objectives

- To develop high energy, high performance cathode materials based on Ti-substituted NMCs and composites of $LiNi_{0.5}Mn_{1.5}O_4$ and coated powders, using spray pyrolysis and other synthesis techniques.
- To understand surface and bulk structural properties of Ti-NMCs that lead to enhanced energy densities.

## Technical Barriers

The cost of vehicular batteries is too high and the energy density needs to be improved. Cost on a $/kWh basis will be lowered if higher energy density can be obtained without adversely affecting cycle life. However, the performance of high-energy high voltage electrode materials like $LiNi_{0.5}Mn_{1.5}O_4$ needs to be improved by reducing its reactivity with the electrolyte. Alternatively, higher utilization of NMC cathode materials could lead to higher energy density, provided cycling issues can be successfully addressed.

## Technical Targets

- Explore feasibility of increasing utilization of NMCs by partial Ti-substitution of Co and using higher voltage cutoffs during cycling.
- Understand origins of Ti-substitution effects in substituted NMCs.
- Use simple one-step synthesis procedures like spray pyrolysis to prepare cathode materials with uniform spherical particle morphologies.
- Prepare materials with protective layers on particle surfaces or composite materials consisting of a lower voltage material on surfaces of a higher voltage material, using spray pyrolysis and infiltration techniques.

## Accomplishments

- Successfully synthesized high performance $LiNi_{0.5}Mn_{1.5}O_4$ cathode materials by spray pyrolysis
- Demonstrated successful coating of $LiNi_{0.5}Mn_{1.5}O_4$ with an $Al_2O_3$ target using atomic layer deposition (ALD)
- Observed and characterized surface reconstruction in baseline and Ti-substituted NMCs as a function of electrochemical history
- Successfully transferred Ti-NMC work to the new ABR program, with goal of characterizing materials in full cells.

✧ ✧ ✧ ✧ ✧

## Introduction

Achieving DOE cost and energy goals for vehicle batteries based on Li-ion technologies requires improvement to existing cathode materials. Higher energy density can be achieved either by replacing conventional cathodes with high voltage materials such as $LiNi_{0.5}Mn_{1.5}O_4$, or by increasing the utilization of NMC ($LiNi_xMn_xCo_{1-2x}O_2$) cathodes. At present, either approach compromises the cycle life of the device, because of increased reactivity of the electrolytic solutions and/or the instability of the electrodes at high states-of-charge (particularly in the case of the NMCs). It was recently shown that partial Ti-substitution in NMCs improved the practical capacities as well as the cycling retention when cells containing the materials were repeatedly charged to 4.7V, in comparison to the baseline unsubstituted materials. The origins of this improvement are, as yet, unknown, although it was noted that Ti-substitution substantially reduced the first cycle irreversibility, resulting in improved capacity on the subsequent discharge. Work carried out this year was directed towards understanding surface and bulk structural changes occurring during high voltage cycling of NMCs using a variety of synchrotron radiation and electron microscopy techniques (in collaboration with A. Mehta, D. Nordlund and T.-C. Weng at SSRL and H. L. Xin at BNL). Experiments directed towards characterization of changes in the surface structures of baseline and Ti-substituted NMCs did not reveal substantial differences suggesting that the improvement is correlated to changes in bulk structural and electrochemical characteristics. To investigate this further, a collaboration with M. Asta (U.C. Berkeley)

was initiated this year to carry out first principles modeling on NMCs to understand these effects better.

$LiNi_{0.5}Mn_{1.5}O_4$ cycles stably in lithium half-cells, although coulombic efficiencies in the first few cycles are low. This arises from irreversible side reactions of the electrolyte and other cell components due to the high operating voltage (4.7V vs $Li^+/Li$). To ameliorate these effects, it is important to minimize the surface area of the spinel phase. Spray pyrolysis synthesis results in ideal morphologies of large, uniform spherical particles with low surface reactivity. Under some conditions, hollow particles are produced, which can be simultaneously filled and coated with a second, less reactive phase like $LiFePO_4$ by an infiltration process. Solid particles can also be coated with an ion-conducting, electronically insulating phase by a variety of techniques, including atomic layer deposition (ALD). Some effort this year was directed towards exploring the feasibility of using an $Al_2O_3$ target and an ALD process to deposit thin coatings on spray pyrolyzed $LiNi_{0.5}Mn_{1.5}O_4$ (collaboration with Chunmei Ban, NREL).

## Approach

Coprecipitation methods are used to synthesize NMC materials and spray pyrolysis is used for $LiNi_{0.5}Mn_{1.5}O_4$. For the latter, a precursor solution is sprayed through an ultrasonic nozzle into a heated furnace tube. Particle characteristics such as size, size distribution, morphology, porosity, etc. can be controlled by varying experimental conditions including nozzle frequency, type and concentration of precursors in solution, the use of additives, temperature, and post-production thermal treatments. In some cases, hollow particles are produced, which can be filled and coated simultaneously by an infiltration process. Particles are also optionally coated postproduction by atomic layer deposition using an $Al_2O_3$ target.

Electrochemical characterization is carried out in lithium half-cell configurations. A variety of physical techniques are used to characterize materials before and after electrochemical cycling. Hard and soft x-ray absorption spectroscopy (XAS) experiments carried out at SSRL are used to probe oxidation states of transition metals at particle surfaces and in the bulk as a function of their electrochemical history and *in situ* and *ex situ* synchrotron XRD experiments are performed to follow bulk structural changes as a function of state-of-charge. High-resolution transmission electron microscopy (HR-TEM) and electron energy loss spectroscopy (EELS) at the National Center for Electron Microscopy (NCEM) at LBNL is used to characterize the structure and oxidation states of particle surfaces.

## Results

**$LiNi_{0.5}Mn_{1.5}O_4$.** Either ordered (space group $P4_332$) or disordered (space group *Fd3-m*) spinels can be produced by spray pyrolysis or combustion synthesis techniques depending on details of the thermal treatments. Ordered $LiNi_{0.5}Mn_{1.5}O_4$ samples free of $Mn^{3+}$ (judging by the lack of 4V capacity) were successfully synthesized, although the cycling behavior is inferior to that of the disordered spinel containing a few percent of $Mn^{3+}$. The reason for the poorer performance is not entirely clear, but *in situ* and *ex situ* synchrotron XRD experiments show differences in the phase behaviors as a function of state-of-charge, with a much larger solid solution region observed for the *Fd3-m* spinel (Figure VI - 14).

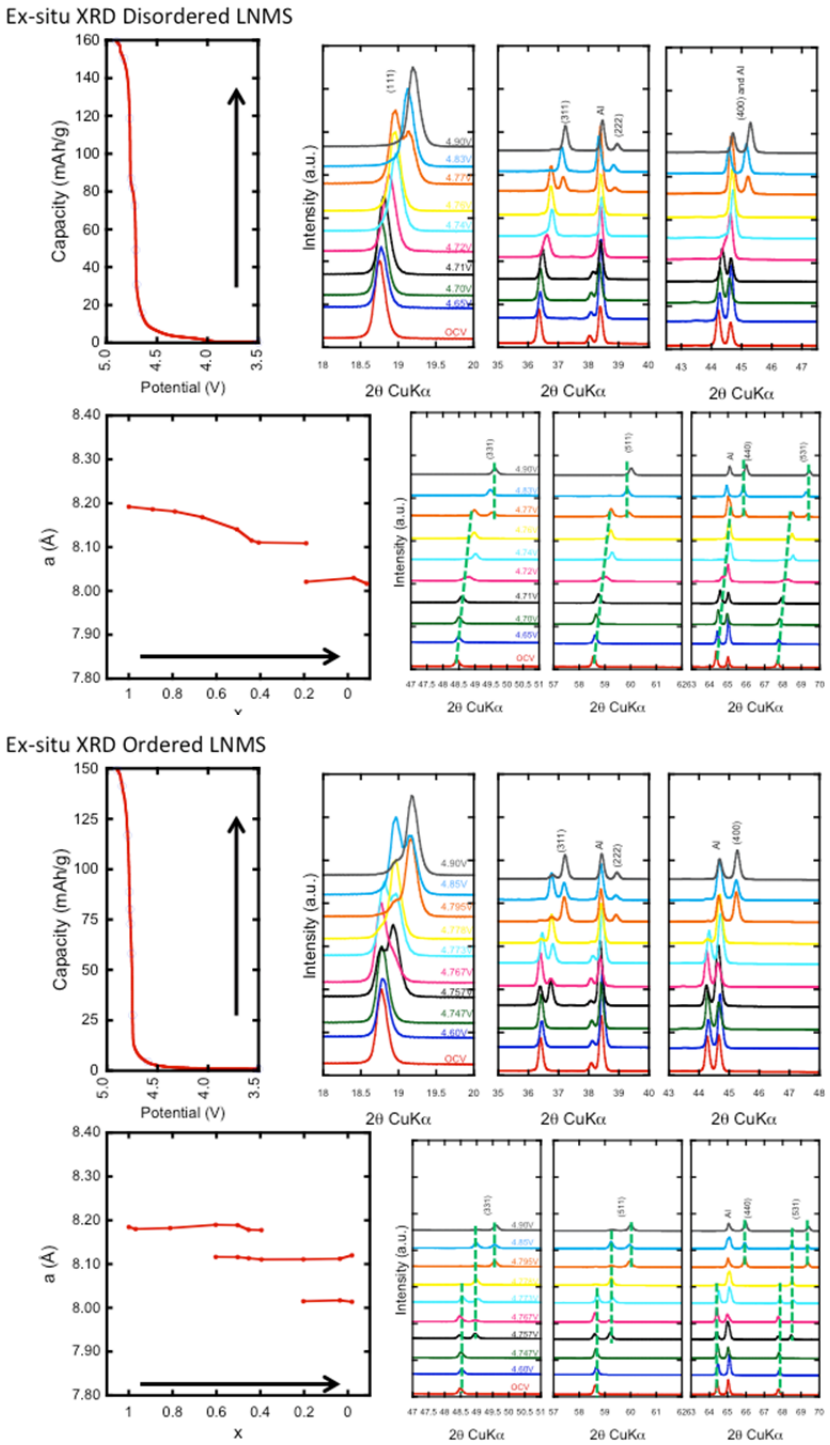


**Figure VI - 14: Charge profiles, *ex situ* synchrotron XRD patterns and lattice parameters as a function of state-of-charge of disordered (top) and ordered (bottom) $LiNi_{0.5}Mn_{1.5}O_4$ cathodes**

Figure VI - 15 shows initial results on an ALD-coated sample of $LiNi_{0.5}Mn_{1.5}O_4$ made by spray pyrolysis. An $Al_2O_3$ target was used for the deposition of the very thin (<1nm) layer on the particle surfaces. The coating does not adversely affect redox characteristics of the material although the $Mn^{3+}$ content of this spray-pyrolyzed sample is higher than desirable. Once this procedure has been optimized, cycling will be carried out on the best samples to determine if coulombic efficiencies are improved.

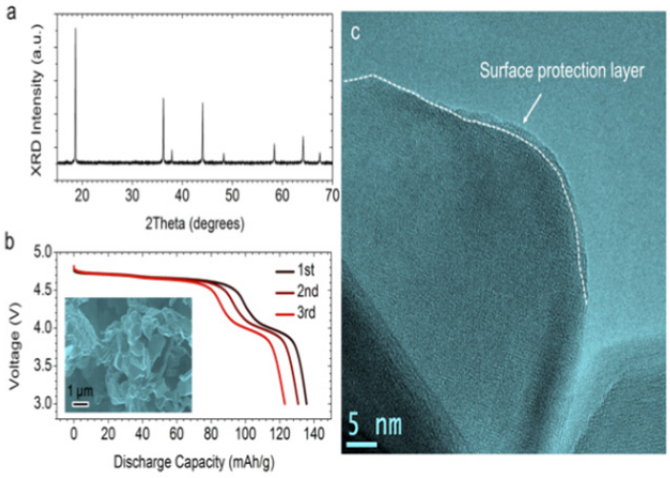


**Figure VI - 15: XRD pattern (top left), discharge profiles and SEM image (bottom left) and HR-TEM image of a spray pyrolysed $LiNi_{0.5}Mn_{1.5}O_4$ cathode material coated by an ALD process**

**NMC characterization.** Partial substitution of Ti for Co in NMCs appears to improve practical discharge capacity and cycling retention during cycling to high voltages (4.7 V) provided that the substitution level is kept below 4%, although capacity fading and impedance rise is still observed. Interestingly, impedance also increases upon extended electrolyte exposure without electrochemical cycling (Figure VI - 16).

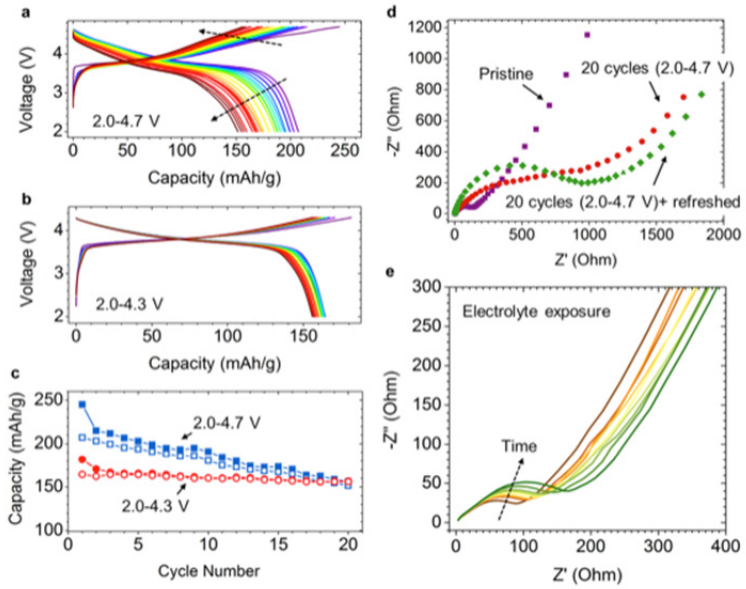


**Figure VI - 16: Cycling profiles between 2.0-4.7V (top left), 2.0-4.3V (middle left) and capacity as a function of cycle number (bottom left) for Li half-cells containing an NMC cathode. Nyquist plots show increased cell impedance upon cycling to high voltages (top right) and upon extended exposure to electrolyte (bottom right)**

Soft XAS and EELS investigations show unequivocally that a layer several nanometers thick containing reduced transition metal oxides forms on particle surfaces during high voltage cycling. Interestingly, this layer is also present on samples that have been exposed to electrolyte but have not been cycled, although it is thinner (Figure VI - 17).

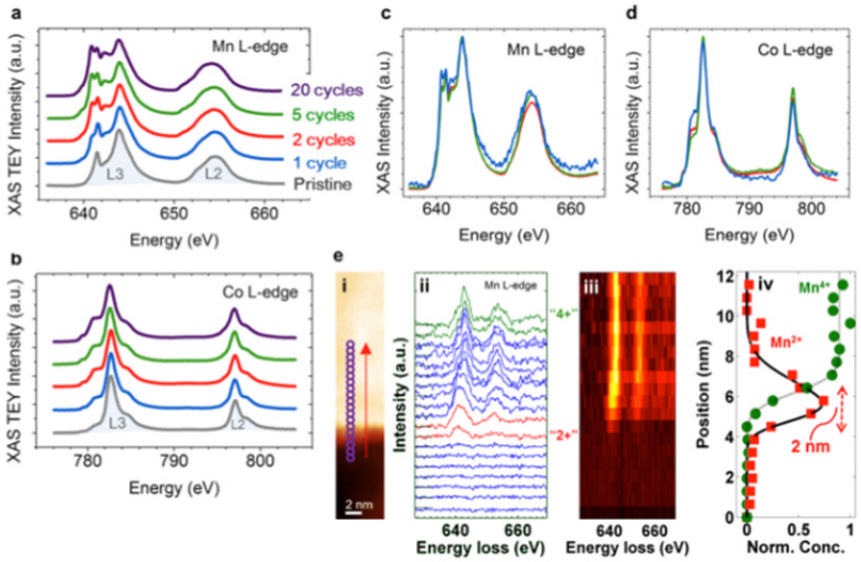


**Figure VI - 17: Surface reconstruction and chemical evolution after charge-discharge cycles. (a) Mn L-edge XAS/TEY spectra. (b) Co L-edge XAS/TEY spectra. (c) Mn L-edge XAS after 5 charge-discharge cycles. (d) Co L-edge XAS after 5 charge-discharge cycles in the AEY (blue), TEY (red) and FY (green) modes. (e) EELS line scan profile for an NMC particle along the <001> direction**

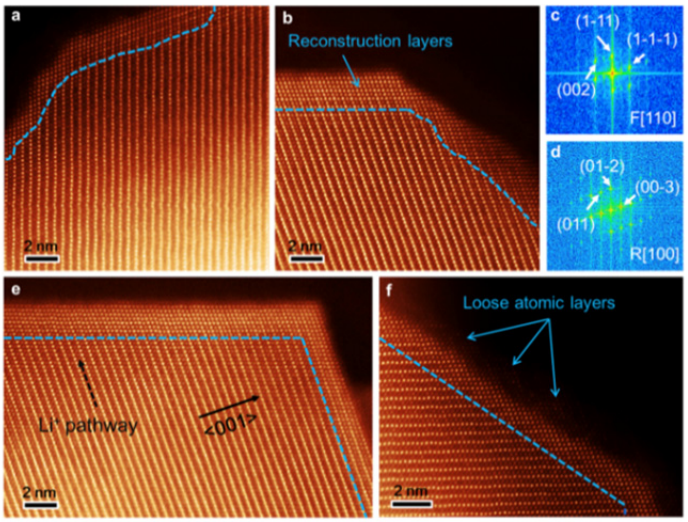


**Figure VI - 18: Atomic resolution ADF-STEM images of NMC materials with electrolyte exposure and charge-discharge cycles. (a) NMC particle after electrolyte exposure. (b) NMC particle after 1 cycle. (c and d) correspond to the FFT results of the reconstruction shell and NMC layered structure in (b), respectively. (e) Orientation effects on the surface reconstruction shell. (f) NMC particle with loose atomic layers after 1 cycle**

Atomic resolution annular dark film imaging (ADF)-STEM experiments show that the reconstructed layer on the particle surface has a rock salt structure, with a few atomic layers of spinel bridging between the surface and the bulk (Figure VI - 18). A loose atomic layer containing LiF in an organic matrix is also present on some surfaces as verified by STEM-EELS experiments (Figure VI - 19) and varies in thickness depending on the facet orientation. Surface reconstruction primarily occurs along lithium diffusion channels. This suggests that tailoring particle morphologies appropriately may minimize losses due to the surface reconstruction.

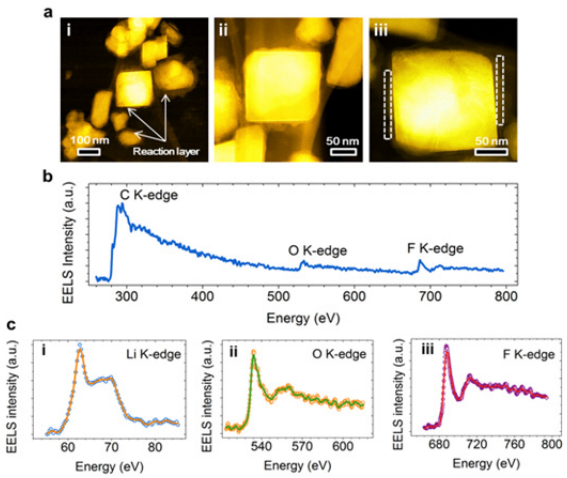


**Figure VI - 19: STEM/EELS analysis of surface reaction layer (a) STEM image. (b) Broad EELS scan. (c) Li K-edge. (d) O K-edge. (e) F K-edge**

## Conclusions and Future Directions

Surface reconstruction due to electrolyte exposure is responsible for the first cycle inefficiencies observed in NMC cells. Upon cycling, the rock salt layer becomes thicker, resulting in increased impedance and capacity loss. Although both first cycle efficiencies and capacity retention are better in Ti-substituted NMCs than in baseline materials, there appear to be no significant differences in the surface reconstruction phenomena observed in these two types of materials. This strongly suggests that bulk effects are responsible for the improved performance of the Ti-NMCs. For example, Ti-substitution results in larger initial unit cell volumes, which change less upon delithiation than the analogous bulk materials. This may be partly responsible for the improved high voltage cycling. A collaborative effort with M. Asta at UC Berkeley, involving first principles modeling of the NMCs, was initiated this year to elucidate effects of Ti substitution on bulk properties of NMCs.

Most of the experimental portion of the Ti-NMC work has been transferred to the ABR program. For this project, synthesis of the Ti-NMCs will be optimized and scaled up, and an industrial partner (Farasis Energy, Inc.) will test the materials in full cells. A variety of diagnostic techniques (including ones first developed under BATT and described in this report) will be used to assess failure modes.

Spray pyrolysis synthesis of $LiNi_{0.5}Mn_{1.5}O_4$ cathode materials will continue under the BATT program. By varying the synthesis conditions, both hollow and solid spherical particles will be produced. Hollow particles will be filled and coated with a second electro-active phase in a single infiltration step. The coating of solid particles with a protective thin layer by ALD and other processes will be optimized. These materials will be evaluated in lithium half-cells to determine whether either or both of these approaches result in improved coulombic efficiencies.

## FY 2013 Publications/Presentations

1. "Design of High Performance, High Energy Cathode Materials," *DOE Annual Peer Review Meeting*, May 13-17, 2013, Washington, DC.
2. A. Iturrondobeitia, A. Goñi, L. Lezama, C. Kim, M. M. Doeff, J. Cabana, and T. Rojo, "Effect of Si(IV) Substitution on Electrochemical, Magnetic, and Spectroscopic Performance of Nanosized $LiMn_{2-x}Si_xO_4$," *J. Mater. Chem. A,* **1**, 10857 (2013).
3. Marca M. Doeff, Guoying Chen, Jordi Cabana, Thomas J. Richardson, Apurva Mehta, Mona Shirpour, Hugues Duncan, Chunjoong Kim, Kinson Kam, and Thomas Conry, "Characterization of Electrode Materials for Lithium Ion and Sodium Ion Batteries using Synchrotron Radiation Techniques," *J. Vis. Exp.* doi:10.3791/50594 (2013).
4. Marca M. Doeff, "Batteries: Overview of Battery Cathodes" in *Springer Encyclopedia of Sustainability Science and Technology*, Springer Science + Business Media, LLC, New York, 709-739 (2012).
5. Kinson C. Kam and Marca M. Doeff, "Electrode Materials for Lithium Ion Batteries," *Materials Matters,* Aldrich Materials Science, **7**(4), 56 (2012).A. Iturrondobeitia, A. Goñi, L. Lezama, C. Kim, M. M. Doeff, J. Cabana and T. Rojo, *J. Mater. Chem. A*, **1**, 10857 (2013).

# VI.B.4 Design and Synthesis of Advanced High-Energy Cathode Materials (LBNL)

**Guoying Chen**
Lawrence Berkeley National Laboratory

Environmental Energy Technologies Division
Berkeley, CA 94720
Phone: (510) 486-5843; Fax: (510) 486-5467
E-mail: gchen@lbl.gov

Start Date: October 2012
Projected End Date: September 2016

## Objectives

- Obtain fundamental understanding on structural, chemical and morphological instabilities during Li extraction/insertion and extended cycling.
- Establish and control the interfacial chemistry between the cathode and the electrolyte at high operating potentials.
- Determine transport limitations at both material and electrode levels.
- Rationally design and develop next-generation electrode materials.

## Technical Barriers

Low energy density, low power density, poor cycle life and poor safety.

## Technical Targets

- PHEV40: 96 Wh/kg, 750 W/kg, 5,000 cycles.
- EV: 200 Wh/kg, 1,000 cycles.

## Accomplishments

- Synthesized single-crystal samples of Li-excess layered composites and Ni/Mn spinels with a variety of physical characteristics for controlled studies.
- Isolated the effect of $Mn^{3+}$ content from other variables and revealed its role in phase transformation behavior and rate capability of disordered Ni/Mn spinels.
- Utilized *in situ* XAS and scanning transmission X-ray microscopy (STXM) techniques to investigate cycling-induced structure changes at both bulk and single-particle levels.
- Illustrated the impact of particle size and morphology in the first cycle activation and the kinetic properties of Li-excess layered composite cathodes.
- Demonstrated that the side reactions between the high-voltage cathode particles and the electrolyte are surface-facet dependent.
- Developed and established the use of novel approaches to characterize the interfacial layer between the cathode and the electrolyte.

✧ ✧ ✧ ✧ ✧

## Introduction

To meet the DOE targets for Li-ion batteries for vehicular applications, electrode materials with high-energy density and high stability are needed. Critical performance issues, such as structural and morphological instabilities, side reactions with the electrolyte, and transport limitations, are sensitive to materials' chemical compositions, crystal structures, surface facets, and particle sizes. Advances in materials development, therefore, require a better understanding of the relationships between their properties and functions. This project addresses these issues by synthesizing single-crystal versions of the commercially promising yet complex electrode materials, obtaining new insights into the materials by utilizing state-of-the-art analytical techniques that are mostly inapplicable on conventional, aggregated secondary particles, and subsequently establishing the relationships between structure and function. The goal is to use these findings to rationally design and synthesize advanced electrode materials with improved performance.

## Approach

Prepare single crystals of Li-rich layered composites and high-voltage Ni/Mn spinels with well-defined physical attributes. Perform advanced diagnostic and mechanistic studies at both bulk and single crystal levels. Global properties and performance of the samples will be established from the bulk analyses, while the single-crystal-based studies will utilize time and spatial-resolved analytical techniques to probe solid-state chemistry and solid-electrolyte interfacial processes at the crystallite level.

## Results

**Synthesis of single-crystal samples.** A collection of layered oxide crystals with compositions of $Li_{1+x}(Ni_{0.33}Mn_{0.33}Co_{0.33})_{1-x}O_2$ ($x$=0 and 0.14), $Li_{1.2}Ni_{0.13}Mn_{0.54}Co_{0.13}O_2$ and $Li_{1.2}Mn_{0.6}Ni_{0.2}O_2$ were prepared in plates, needles, and polyhedrons of different sizes. Progress was also made in synthesizing large $LiMn_{1.5}Ni_{0.5}O_4$ crystals intended for single-particle measurements. The molten-salt method was modified to include an additional flux top layer that promoted crystal growth into hundreds-of-micron size. Morphology was largely influenced by the choice of the flux and the ratio between the flux and precursors (denoted as R), as shown in Figure VI - 20. XRD characterization confirmed the formation of phase-pure spinels in all cases.

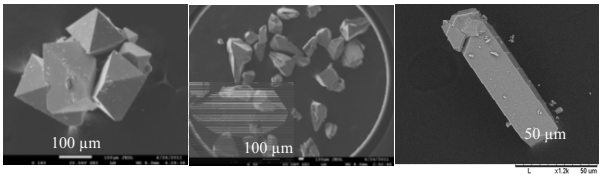


**Figure VI - 20: SEM images of Ni/Mn spinel crystals synthesized with chloride precursors in: a) LiCl and R=100, b) LiCl and R=50, and c) eutectic LiCl-KCl flux**

**Structural evolution and phase transformations in the oxide cathodes.** Previous reports have shown the importance of Ni/Mn ordering in influencing structural evolution during charge and discharge of the Ni/Mn spinels, but direct correlation was not established due to the lack of consistency in experimental results. This study intends to illustrate the importance of $Mn^{3+}$ content which is likely the culprit of these inconsistencies found in the literature. To this end, controlled studies were performed on micron-sized $LiNi_xMn_{2-x}O_4$ ($x$=0.3 and 0.5) octahedron crystals with a disordered structure, confirmed by the signature disordered features on the FTIR spectra and the same peak separation of 60 mV on the dq/dV profiles in both samples. Area integration of the broad peaks at 4.1 V estimated 5.8 and 19.3% $Mn^{3+}$ for $x$=0.3 and 0.5, respectively.

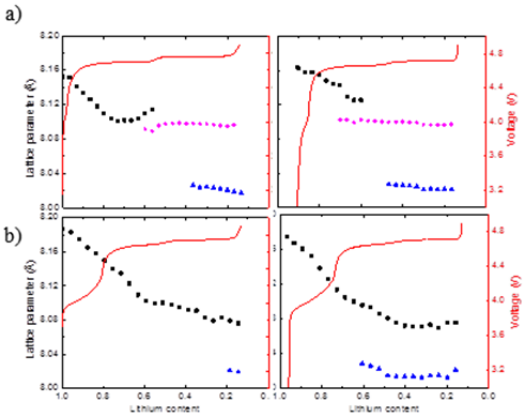


**Figure VI - 21: Phase transformation in disordered $LiNi_xMn_{2-x}O_4$ crystals: a) $x$=0.5 and b) $x$=0.3. (left) charge and (right) discharge**

Structural changes in the two crystal samples upon charge and discharge were then compared by synchrotron *in situ* XRD experiments performed at beamline 11-3 at SSRL. Figure VI - 21 shows the detailed phase composition at a given Li content obtained from structural refinement. While the crystal composite electrode with $x$=0.5 underwent two reversible two-phase transitions involving three cubic phases (Figure VI - 21a), an extensive solid-solution region with only two cubic phases were detected during the charge and discharge of $x$=0.3 (Figure VI - 21b). The latter sample also delivered enhanced rate capability. The results clearly demonstrate the intricacies in the relationships between spinel structure, phase transformation and rate capability, and the importance in optimizing physical properties in order to maximize the performance of the electrode materials.

The impact of particle size and morphology on structural evolution and the first cycle activation kinetics was demonstrated on layered $Li_{1.2}Ni_{0.13}Mn_{0.54}Co_{0.13}O_2$ crystals with four different shapes: plate, needle, large and small polyhedrons. The small polyhedron crystals prepared in a KCl flux had a particle size of 200 nm, while the other three samples had a similar size of 1-2 µm. *Ex situ* XRD experiments were performed on the samples during the first delithiation, and the results are shown in Figure VI - 22. The superlattice peaks between 20° and 34° (2θ), which are commonly used as an index for structural ordering in the transition metal layer, gradually weakened during Li extraction and eventually disappeared at a Li content of 0.5-0.3 in the plate-shaped crystals. This occurred faster in the small polyhedron sample but significantly slower in the large polyhedrons as high intensity remains even below Li=0.29. The results obtained in electrochemical cycling tests resonated this observation, where the highest and lowest rate capabilities were delivered by the small and large polyhedrons, respectively.

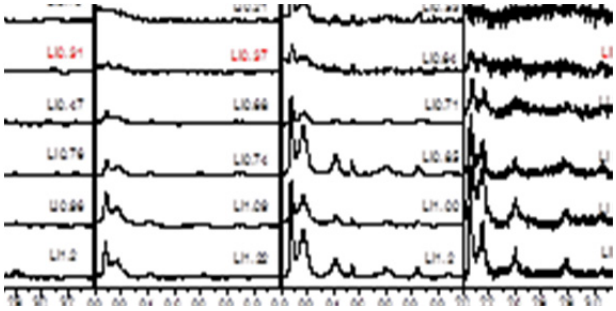

**Figure VI - 22: Evolution of the XRD superlattice peaks during the first delithiation in $Li_{1.2}Ni_{0.13}Mn_{0.54}Co_{0.13}O_2$ crystals: a) plates, b) needles, c) large and d) small polyhedrons**

Bulk structural changes in the layered oxides were further studied by soft X-ray absorption spectroscopy (XAS) at beamline 10-1 at SSRL on binder-and carbon-free electrodes containing the plate-shaped $Li_{1.2}Ni_{0.13}Mn_{0.54}Co_{0.13}O_2$ crystals. The electrodes were assembled into coin cells (with a Li metal anode) and then cycled to different states of charge in the first two cycles and then opened to recover the electrodes for analysis. Figure VI - 23 shows the Ni and Mn *L*-edge spectra in the total electron yield (TEY) mode that is surface sensitive. The Ni spectra show an increase in the oxidation state upon charge and then decreased upon discharge, consistent with the redox activity of Ni in the structure. Mn maintained at 4+ during the first charge, but a shoulder peak at 640.1 eV, which corresponds to $Mn^{3+}$, appeared upon discharge. The intensity of the shoulder peak further increased at the end of second discharge, suggesting structural irreversibility.

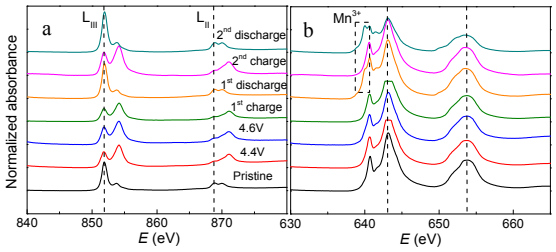


**Figure VI - 23: XAS *L*-edge spectra of $Li_{1.2}Ni_{0.13}Mn_{0.54}Co_{0.13}O_2$ electrodes at the indicated stage of cycling: a) Ni and b) Mn**

The investigation on these changes occurring at the particle-level was initiated by using scanning transmission X-ray microscopy (STXM) at beamline 11.0.2 at the Advanced Light Source (ALS), which has a high spatial resolution of 25 nm and an energy range of 95-2000 eV. In collaboration with Dr. Tolek Tyliszczak, layered $Li_{1+x}M_{1-x}O_2$ (M = Ni, Mn, Co) single crystals were chemically delithiated/relithiated or electrochemically cycled and then examined by STXM at the O *K*-edge as well as the Ni, Mn and Co *L*-edges. Figure VI - 24 shows the preliminary single-pixel (25nm x 25nm) Ni *L*-edge spectra collected on a plate-shaped $Li_{1.2}Ni_{0.13}Mn_{0.54}Co_{0.13}O_2$ crystal that was charged to 4.8 V in a binder- and carbon-free electrode. The variation of Ni oxidation state within the particle was evident as the dominate 4+ at the center of the crystal gradually lowered the oxidation state upon moving towards the edge, signaled by the increasing intensity of the peak at 853 eV (Figure VI - 24b). Since the large surfaces and the edges of the plates are composed of different surface facets, this variation may be evidence for the facet-dependent reactivity between the oxide particles and the electrolyte.

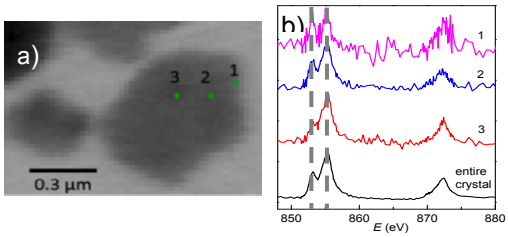


**Figure VI - 24: a) STXM image of a $Li_{1.2}Ni_{0.13}Mn_{0.54}Co_{0.13}O_2$ crystal and b) Ni *L*-edge X-ray absorption spectra collected at the indicated single-pixel as well as the entire crystal**

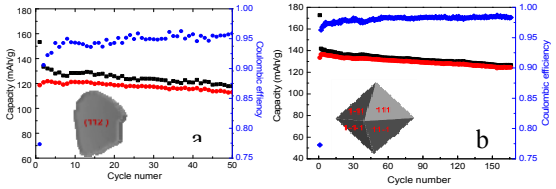


**Figure VI - 25: Half-cell cycling performance of a) plate and (b) octahedral $LiMn_{1.5}Ni_{0.5}O_4$ crystal electrodes**

**Characterization of the cathode-electrolyte interfacial reactions.** Understanding and controlling the oxidation of organic solvents, dissolution of transition metals from the cathodes, and the solid-liquid interface under high operating voltages is crucial in achieving stable cycling. To this end, the influence of crystalline orientation of particle surface on interfacial reactivity was evaluated on micron-sized spinel $LiMn_{1.5}Ni_{0.5}O_4$ single crystals with over 90% of (112) surface facets (plates) and 100% of (111) surface facets (octahedrons), respectively. Figure VI - 25 shows the extended half-cell cycling performance of the crystal composite electrodes. The octahedrons delivered a higher columbic efficiency of 99% for 170 cycles, as compared to 95% for 50 cycles in the plates. The per-cycle capacity loss was 0.05 and 0.14% for the octahedrons and plates, respectively, suggesting reduced parasitic reactions on (111) crystal facets. Selected *ac* impedance spectra at various state of charge, measured at the OCV conditions in the potential range of 4.0 to 4.85 V, are shown in Figure VI - 26a and b. Consistent with the previous reports, the spectra from both crystal electrodes are composed of a high-frequency semicircle from the surface-layer resistance ($R_{sf}$) and capacitance ($C_{sf}$), a medium-to-low-frequency semicircle from the charge transfer resistance ($R_{ct}$) and double layer capacitance ($C_{dl}$), and a low-frequency Warburg impedance ($Z_w$) due

to solid state diffusion of lithium ions within the active material. The surface-layer resistance as a function of Li content is compared in Figure VI - 26c. For both crystal samples, $R_{sf}$ increased upon initial charge and then gradually decreased to reach a steady state at low Li contents, suggesting dynamic nature of the surface layer resulting from the reactions between the cathode and the electrolyte. The resistance on the octahedrons, however, is much lower compared to those on the plates. At any given Li content, the charge transfer resistance on the octahedrons is also much lower (Figure VI - 26d), with the difference most significant at low SOCs. The results clearly demonstrate that the side reactions between the high-voltage cathodes and the electrolyte are surface-facet dependent, and it is important to design particle morphology in order to minimize these unwanted reactions.

In collaboration with Drs. Phil Ross and Zhi Liu at beamline 9.3.1 at the ALS, tender X-ray photoelectron spectroscopy (TXPS) with excellent surface sensitivity as well as the depth-profiling capability was used to non-destructively probe the atomic and chemical compositions of the species at variable sampling depth. Initial studies were performed with incident photoelectron energy between 3 and 4 keV that probes particle surfaces at a depth of 10 and 15 nm, respectively. The results from a cycled, binder-and carbon-free $LiMn_{1.5}Ni_{0.5}O_4$ electrode showed significant attenuation to Li 1*s*, Mn 3*p* and $O^{2-}$ intensities originated from $LiMn_{1.5}Ni_{0.5}O_4$, suggesting cycling leads to the deposition of solid products that suppress the detectable signals from the oxide underneath. A large amount of new carbon species with higher binding energies were revealed, and the presence of organic containing 'surface' species was further confirmed by the broadening of the higher binding energy O 1*s* peak. The chemical nature and thickness of this organic surface layer, as well as the role of particle surface features, are the topics of further investigation.

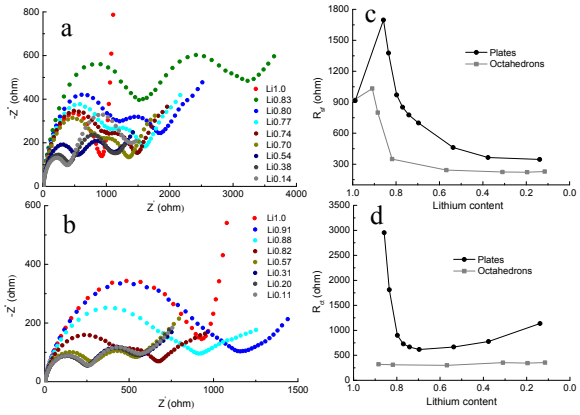


**Figure VI - 26: Nyquist plots for the $LiMn_{1.5}Ni_{0.5}O_4$ crystal electrodes at the indicated Li content: a) plates and b) octahedrons; the relationships between lithium content and c) surface-layer resistance and d) charge-transfer resistance**

## Conclusions and Future Directions

In conclusion, single-crystal samples of Li-excess layered composites and Ni/Mn spinels with specific physical characteristics suitable for controlled studies were synthesized. Structural and chemical changes resulting from Li extraction/insertion were determined and their correlation to sample physical properties established. $Mn^{3+}$ content influences the phase transformation process and the kinetic properties in Ni/Mn spinels, and particle size and morphology control is critical to the kinetics in layered oxides. Side reactions with the electrolyte were found to be dependent on the crystalline orientation of the cathode particle surfaces. Approaches were developed to obtain the details of the interfacial layer resulting from the side reactions between the cathode and the electrolyte.

Future work will focus on the examination of crystal-plane specific surface chemistries of the oxide cathodes and the stability of the interfacial layer. The chemical nature, thickness and properties of the interfacial layer, as well as the mechanism behind the role of particle surface features in side reactions will be investigated. Local structural and chemical changes as a function of lithium content and cycle number will be monitored at the single-particle level to explore the intrinsic failure mechanisms of the oxides. Synthesis conditions will be explored to produce electrode materials with properties optimized for both performance and safety.

## FY 2013 Publications/Presentations

1. M. M. Doeff, G. Chen, J. Cabana, T. J. Richardson, A. Mehta, M. Shirpour, H. Duncan, C. Kim, K. C. Kam, and T. Conry, "Characterization of Electrode

Materials for Lithium Ion and Sodium Ion Batteries Using Synchrotron Radiation Techniques," *J. Vis. Exp.*, DOI:10.3791/50594 (2013).

2. U. Boesenberg, F. Meirer, Y. Liu, R. Dell'Anna, A. K. Shukla, T. Tyliszczak, G. Chen, J. C. Andrews, T. J. Richardson, R. Kostecki, and J. Cabana, "Mesoscale Phase Distribution in Single Particles of LiFePO4 Following Lithium Deintercalation," *Chemistry of Materials*, **25**, 1664 (2013).
3. B. Hai, A. K. Shukla, H. Duncan, and G. Chen, "Effect of Particle Surface Facets on the Kinetic Properties of $LiMn_{1.5}Ni_{0.5}O_4$ Cathode Material," *Journal of Material Chemistry A*, **1**, 759 (2013).
4. "Impact of Initial Li Content on Kinetics and Stabilitis of Layered $Li_{1+x}(Ni_{0.33}Mn_{0.33}Co_{0.33})_{1-x}O_2$," G. Chen, B. Hai, A. K. Shukla, and H. Duncan, *Journal of the Electrochemical Society*, **159**, A1543 (2012).
5. "Overcharge Protection for PHEV Batteries," *DOE Annual Peer Review Meeting*, May 13-17, 2013, Washington, DC.
6. "Synthesis and Performance of $Li_{1.2}Ni_{0.13}Mn_{0.54}Co_{0.13}O_2$ Crystals," H. Duncan and G. Chen, *Berkeley Energy and Resources Collaborative Innovation Expo*, October 2013, Berkeley, CA.
7. H. Duncan, B. Hai, A. K. Shukla, and G. Chen, "Influence of Particle Morphology on Structural Evolution and Electrochemical Performance of $Li_{1+x}M_{1-x}O_2$ Cathode Materials," *CalCharge Kickoff Event*, May 2013, Berkeley, CA,.
8. S. F. Lux, A. J. Jarry, H. Duncan, N. S. Norberg, G. Chen, R. Kostecki, *"In situ* Fluorescence Spectroscopy of Interfacial Processes in High-Voltages Cathodes," *CalCharge Kickoff Event*, May 2013, Berkeley, CA.
9. G. Chen, B. Hai, and A. K. Shukla, "Impact of Particle Surface Facets on the Performance of $LiMn_{1.5}Ni_{0.5}O_4$," *The 222nd ECS Meeting*, October 2012, Honolulu, HI.

# VI.B.5 Novel and Optimized Phases for High Energy Density Batteries (LBNL)

**Jordi Cabana**
Lawrence Berkeley National Laboratory

Department of Chemistry[12]
University of Illinois at Chicago
845 W Taylor Street
Science and Engineering South (MC 111)
Chicago, IL 60607
Phone: (312) 355-4309
E-mail: jcabana@uic.edu

Start Date: October 2012
Projected End Date: July 2013

## Objectives

- Enable higher density Li-ion batteries through an increase in operation voltage and capacity of the cathode.
- Design electrode structures that maximize active material utilization and charge density.
- Understand the structure-composition-properties relationship for bulk and surface properties of electrodes.
- Identify new compounds containing non-oxide or polyanions in their crystal structure that are electrochemically active.

## Technical Barriers

Low energy-density, poor cycle life, safety.

## Technical Targets

- PHEV: 96 Wh/kg, 5,000 cycles
- EV: 200 Wh/kg; 1,000 cycles.

## Accomplishments

- The role of Mg modifications of the surface of $LiNi_{1/2}Mn_{3/2}O_4$ particles was elucidated by establishing the chemical changes during processing and cycling.
- The correlation between crystal-chemistry in $LiNi_{1/2}Mn_{3/2}O_4$, the phase transformation mechanism and electrochemical properties was fully ascertained.
- Established a low temperature synthetic method for the fluorination of lithium transition metal oxides.

✧ ✧ ✧ ✧ ✧

## Introduction

Finding Li-ion battery electrode materials that can bring about increases in energy is a critical need if their use in electric vehicles is to meet expectations. In order to fulfill this goal, the following strategies can be envisaged: i) raising the voltage of operation of the battery by using anodes and cathodes that react at very high and very low potentials, respectively, and/or ii) improving the storage capacity by switching to alternative electrode materials that can exchange a larger amount of electrons/$Li^+$ ions. Yet these changes cannot come with a penalty in terms of safety and cycle life, which implies that the mechanisms of their reaction with lithium need to be well understood in order to locate possible sources of failure.

Spinel-type $LiNi_{0.5}Mn_{1.5}O_4$ was identified by the BATT program as model material for the study of the bottlenecks of positive electrode materials reacting at very high potential. Apart from being stable, $LiNi_{0.5}Mn_{1.5}O_4$ is seriously considered by industry as an alternative to currently used materials because lithium is extracted at around 4.7 V vs. $Li^+/Li^0$. While very high rate capability has been reported in several cases, it has not been fully ascertained what the role is of the crystal-chemistry of the compound, such as metal ordering and the existence of $Mn^{3+}$ impurities in the spinel and segregated rocksalt particles. During FY2012, it was established that ordering and electrochemical proxies such as rate capability were strongly correlated, whereas $Mn^{3+}$ contents were found to have a much more marginal role. In FY2013, our goal was to ascertain the origin of these correlations

[12] Current affiliation and mailing address.

The interface between an electrode and the electrolyte is critical to extended performance. It was previously shown that large micrometric particles showed more favorable performance than nanosized ones because they minimize the surface area. However, electrolyte decomposition is still generally found to be extensive. Thus, coatings appear to be a necessary way forward. However, the rules of design for these coatings have not fully been ascertained. Modifications based on the addition of basic oxides such as MgO in the form of coatings or simple additives were chosen as a case study and a combination of electrochemistry, elemental analysis and chemical characterization at different states was used to establish such rules.

Soft X-ray spectroscopy experiments conducted in FY2012 revealed that the Ni states at the surface of $LiNi_{0.5}Mn_{1.5}O_4$ particles were more reduced than the bulk of the crystals. This was interpreted as the consequence of the increased covalence of the Ni-O bond after lithium extraction. Ultimately, this covalence can lead to irreversible destabilization of the $O^{2-}$ species toward oxygen evolution, a thermal event with negative safety consequences. Fluoride ions are less polarizable and, therefore, can provide chemical stability. In FY2013, synthetic methods for fluorinated compounds that contain redox active metals were explored, with the aim to discover new compounds that can have suitable properties.

## Approach

Employ and develop a variety of synthetic methods to produce materials with controlled purity, crystal structure and particle morphology. Use spectroscopic and diffraction techniques to monitor the reactions involved in battery electrodes. Explore chemical spaces in a search for new phases that may provide performance improvements.

## Results

All work on $LiNi_{0.5}Mn_{1.5}O_4$ was done in coordination within the Spinel Focus Group, which was concluded during FY2013.

**Phase transformations determine performance in $LiNi_{0.5}Mn_{1.5}O_4$.** The reader is referred to the FY2012 Annual Report for the study of correlations between crystal chemistry and electrochemistry, which provided motivation for this work. *Operando* X-ray diffraction experiments were conducted at beamline 11-3 at the Stanford Synchrotron Radiation Lightsource (SSRL) on $LiNi_{0.5}Mn_{1.5}O_4$ samples with different degrees of cationic ordering, as probed by nuclear magnetic resonance, neutron diffraction and electrochemical signatures. A series of reversible phase transitions were observed. The results are summarized in Figure VI - 27. The samples tested have decreasing degrees of crystallographic ordering, as follows: OO730 > OO700 > OO670 > A900. As it can be readily noticed, the difference in potential between the two faradaic electrochemical signatures smoothly traces ordering. The early stages of delithiation occur through a solid solution mechanism, followed by consecutive two-phase transitions. In contrast, the sample with the highest degree of ordering shows no discernible solid solution domains. The formation of a solid solution leads to a significant reduction in volume change between the phases involved in the first biphasic transition. It is hypothesized that such lower volume change results in smaller strain buildup in the active materials particles during this step, thereby increasing the rate of reaction that can be achieved.

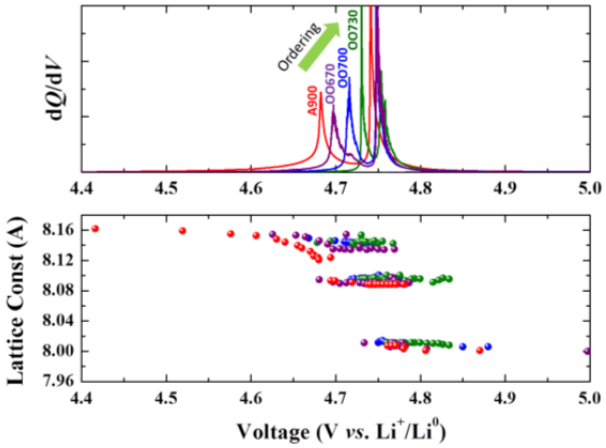


**Figure VI - 27: Summary of *operando* XRD data collected upon Li deintercalation in a series of $LiNi_{0.5}Mn_{1.5}O_4$ samples showing varying degrees of cationic ordering**

**Role of surface Mg-modifications on the chemistry and electrochemistry of $LiNi_{0.5}Mn_{1.5}O_4$.** A Mg precursor was coated on micrometric spinel particles, followed by annealing at 500 or 800°C. The results showed a rough coating with an inhomogeneous distribution of agglomerates, most likely MgO, across the surface of the material treated at 500°C. This coating was modified after treatment at 800°C, resulting in the incorporation of $Mg^{2+}$ into the spinel sub-surface (Figure VI - 28).

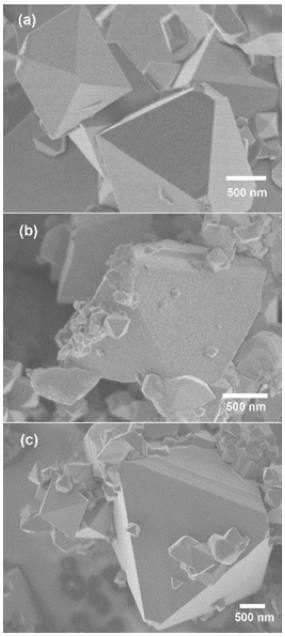


**Figure VI - 28: Scanning electron micrographs of a) baseline $LiNi_{0.5}Mn_{1.5}O_4$, and after applying a Mg-based coating, treated at b) 500 and c) 800ºC**

The electrochemical study revealed that the presence of Mg did not improve performance at room temperature, but was crucial at higher temperature. Among the two modified materials, the best results were obtained following annealing at 800°C, in terms of capacity, coulombic efficiency and rate capability at 50°C. The performance at room temperature was not severely compromised with respect to the baseline, although the presence of $Mg^{2+}$ in the spinel lattice did result in slight specific capacity losses.

In order to shed light into the difference in properties between samples and testing conditions, X-ray absorption spectroscopy data were collected at the Ni $L_{II, III}$ and O K-edges at beamline 10-1 at SSRL for all samples after a full charge to 5 V, at both room temperature and 50ºC. Spectra were acquired using a total fluorescence and total electron yield (TFY and TEY) detector simultaneously. The TEY detector provides XPS-like, surface sensitive insight, whereas experimental conditions were designed to make TFY signals representative of the bulk of the material. A comparison between a baseline sample and the correspondingly coated materials treated at 500°C and 800°C was established. The existence of broad, low energy shoulders in the pre-edge peak at 531 eV was indicative of the formation of $Ni^{4+}$-$O^{2-}$ species during Li deintercalation (Figure VI - 29). Their absence in the TEY data for the bare material is interpreted as evidence that the surface of the electrode is more reduced than the bulk. In contrast, the coated samples show pronounced shoulders, especially at 50ºC. It is hypothesized that $Mg^{2+}$ ions pin the charges of the $O^{2-}$ ions so that they cannot be polarized by the $Ni^{4+}$ ions and turn electrophilic. The result is a more stable surface toward electrolyte oxidation in coated than in bare samples.

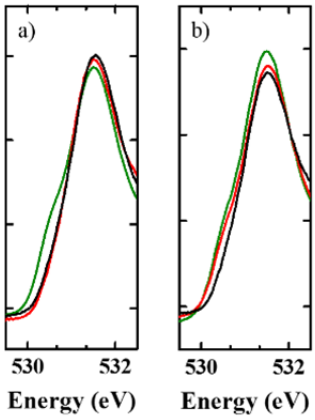


**Figure VI - 29: Zoom of the region around 531 eV in the O K-edge XAS data, highlighting the differences in intensity of the 530.2 eV shoulder depending on the sample. The data correspond to the baseline material (black), as well as after applying a Mg-based coating, treated at 500 (red) and c) 800ºC (green), which were fully oxidized in Li metal cells at a) room temperature and b) 50ºC**

The electrochemical data, together with analysis of spectra collected at the Ni $L_{II, III}$- and O K-edges, revealed two important lessons that could guide the rational design of stable high voltage materials. First, coatings that are semiconducting in nature and contain lithium are preferred to reduce charge (ion and electron) transfer losses. Second, small amounts of a redox inactive, strongly ionic species such as $Mg^{2+}$ on the surface of an active material could have a significant stabilizing effect by changing the nature of chemical bonding vis-à-vis possible redox activity with the electrolyte.

**Low temperature fluorination of oxides.** Heating lithium transition metal oxides in the presence of transition metal fluorides at temperatures as low as 250°C is sufficient to incorporate significant amounts of fluorine into the oxide lattice; up to 40 mol% fluorination was observed in certain cases. A collection of compounds containing varying rations of Mn, Ni and Fe were thus synthesized. In collaboration with the Wang group at BNL, also in the BATT program, the fluorination reactions as well as the thermal stability of the resulting oxyfluorides was evaluated by collecting X-ray diffraction patterns during heating. It was found that these phases are metastable and decompose to binary phases above 500°C. Therefore, it appears that these kinds of phases cannot be obtained at high temperature. Electrochemical testing revealed that these oxyfluorides are redox active, creating avenues for future design of new materials with unprecedented properties.

## Conclusions and Future Directions

During FY2013, work was finalized that provided new insight into the rules for the design of positive electrodes based on $LiNi_{0.5}Mn_{1.5}O_4$. It was determined that the excellent rate properties of materials with extensive Ni and Mn disorder was due to the direct dependence of the miscibility gap on such crystallographic parameter. The reduced miscibility gap is thought to lead to lower mechanical strain in the particles during cycling. At the surface, the formation of $Ni^{4+}$-$O^{2-}$ covalent bonds was found to lead to electrolyte oxidation. Such electrophilic species could be partly stabilized by the presence of $Mg^{2+}$, which tends to favor ionic bonds. Fluorine could also be a stabilizing agent. Thus, a search for new lithium transition metal oxyfluorides was initiated. A low temperature fluorination method was demonstrated. These findings have general applicability to other materials beyond $LiNi_{0.5}Mn_{1.5}O_4$ and provide natural closure to the Spinel Focus Group.

This project was closed on July 2013 due to the relocation of the Principal Investigator to the University of Illinois at Chicago. Thus, there are no future directions to be discussed.

## FY 2013 Publications/Presentations

1. "Novel and Optimized Materials Phases for High Energy Density Batteries," *DOE Annual Peer Review Meeting*, May 13-17, 2013, Washington, DC.
2. "Effect of the Crystal Chemistry of $LiNi_{0.5}Mn_{1.5}O_4$ Spinels on Electrochemical Properties," *Pacific Rim Meeting on Electrochemical and Solid State Science (PRiME) 2012*. October 7th-12th, 2012, Honolulu, HI (USA).
3. J. B. Cook, C. Kim, L. Xu and J. Cabana, J. *Electrochem. Soc.*, **160**, A46 (2013).
4. L. Xu, C. Kim, A. K. Shukla, A. Dong, T. M. Mattox, D. J. Milliron and J. Cabana, *Nano Lett.*, **13**, 1800 (2013).

# VI.B.6 Studies on High Energy Density Lithium-ion Electrodes (ORNL)

**Jagjit Nanda**
Oak Ridge National Laboratory

Material Science and Technology Division
PO Box 2008, MS 6124
Oak Ridge, TN 37831-6124
Phone: (865) 241-8361
E-mail: nandaj@ornl.gov

Postdoctoral workers:
Surendra Martha, Hui Zhou

Collaborators:
Andy Drews (Ford); Joy Andrews and Yijin Liu (Stanford Synchrotron Radiation Lightsource); Kang Xu (Army Research Lab); Andrew Callendar (Tennessee Technical Univ.)

Start Date: October 2010
Projected End Date: Continuing

## Objectives

- Investigate mechanisms behind capacity fade and voltage depression associated with high voltage Lithium-ion cathodes and provide mitigation methods.
- Improve C-rate performance and cycle life of high voltage cathodes in full cells.
- Perform *ex situ* and *in situ* micro-structural characterization to study electrodes at various states of charge (SOC) and subjected to stress cycles and correlate these to capacity fade and cycle life degradation.

## Technical Barriers

This project addresses the following technical barriers as described in the USDRIVE & USABC goals [1, 2]:

- Performance at ambient temperatures: high DC-R especially at low SOC and C-rate capability
- Materials degradation leading to cycle life loss: transition metal dissolution and structural instability against high V cycling.

## Technical Targets

- PHEV specific energy targets (pack): 3.4 (min) to 11.6 (max) kWh [1]
- EV specific energy targets (pack): 80 (min) to 200 (max) Wh/kg [2]

## Accomplishments

- Applied transmission x-ray microscopy combined with x-ray near edge absorption spectroscopy (TXM-XANES) to lithium-manganese rich NMC (LMR-NMC) high voltage cathodes to measure the chemical state changes as well as morphology in 3D.
- Performed micro-Raman imaging of LMR-NMC cathodes.
- Investigated the role of high voltage electrolyte additives on the cycle life performance of LMR-NMC cathodes.

✧ ✧ ✧ ✧ ✧

## Introduction

Current R&D efforts in lithium-ion batteries are directed towards increasing energy density with reduced cost and improved cycle-life and safety. Among other important factors, developing high energy density lithium-ion cathodes is a high priority area. Recently, there has been significant progress made on a number of high voltage cathode chemistries such as $LiMn_{1.5}Ni_{0.5}O_4$ [3] and LMR-NMC [4-5]. However, significant technical challenges still need to be addressed at the materials as well as the electrode level. These include (i) structural and phase stability under continuous high voltage cycling (>4.5 V) (ii) Mn dissolution leading to capacity fade (iii) electronic and ionic transport limitations intrinsic to the electrode material and (iv) higher first cycle irreversible capacity loss (ICL) due to interfacial issues and oxygen loss, etc. We report systematic studies on Lithium-rich NMC composite cathodes having nominal composition $Li_{1.2}Mn_{0.525}Ni_{0.175}Co_{0.1}O_2$ and address the various technical barriers mentioned above.

## Approach

High voltage LMR-NMC cathode materials having nominal composition $Li_{1.2}Mn_{0.525}Ni_{0.175}Co_{0.1}O_2$ were obtained from a pilot scale facility of Toda-Kogyo Corporation, Japan. Cathode powders were fabricated into electrodes using the slurry coating method with PVdF binder (Sigma-Aldrich) and carbon diluents (super-P, Timcal). The electrodes were assembled in the form of half cells (Li-metal as counter electrode) or full cells using

modified graphite powders obtained from Conoco-Phillips (now Phillips 66). We performed life cycle studies in both coin cell and small pouch cell format to study capacity fade at room temperature as well as at 60°C. All cells were cycled between 2.5 V and 4.9 V (vs. $Li^+/Li$) at 10 mA/g for the first cycle, and then between 2 V and 4.9 V (vs. $Li^+/Li$) at 20 mA/g using the electrolyte of 1.2 M $LiPF_6$ salt dissolved in EC: DMC (1:2) solvent. Apart from standard charge-discharge cycling, we also carried out impedance spectroscopy (EIS), cyclic voltammetry (CV) and various structural and surface spectroscopy techniques to characterize the electrodes and correlate the observed electrochemical performance with the materials degradation. Material modifications such as nanoscale surface coating and electronic filler additives were also undertaken to improve the electrochemical performance. The surface spectroscopy and structural characterization techniques used include transmission x-ray microscopy combined with x-ray near edge spectroscopy (TXM-XANES), confocal Raman imaging, x-ray diffraction and electron microscopy.

## Results

**3D Chemical Imaging & X-ray Microscopy of LMR-NMC Cathodes.** Using the TXM-XANES beam line at Stanford Synchrotron Radiation Lightsource (SSRL), we performed X-ray imaging combined with XANES [6-8] to map the chemical state and morphology of LMR-NMC electrodes at different SOC and cycle life. Changes in the Mn K-edge spectra as a function of cycle number are shown as false-color images of LMR-NMC cathode particles in Figure VI - 30.

The color maps in Figure VI - 30 are determined by fitting each of the observed spectra, ~106 per field of view (FOV) for the 200 & 50 times cycled electrode as well as the pristine electrode, which serves as the reference compound, and assigning red or green to the fraction of 200 cycle or pristine spectra, respectively. The changes observed in the Mn K edge spectra are consistent with the changes in the bulk electrochemical signature, shown by the differential capacity (dq/dv) versus voltage plot for the 1st, 50th and 200th cycle as presented recently [8]. Careful analysis of the XANES data by taking the 1st derivative spectra (not shown) shows the Mn K edge shifts from about 6553.5 eV (the pristine electrode) to 6552 eV (the 200-cycle sample), consistent with a clear change of Mn valence from 4+ to a lower valence state when the electrode material was cycled at a voltage greater than 4.5 V. The corresponding change in Ni and Co K edges under cycling are not significant.

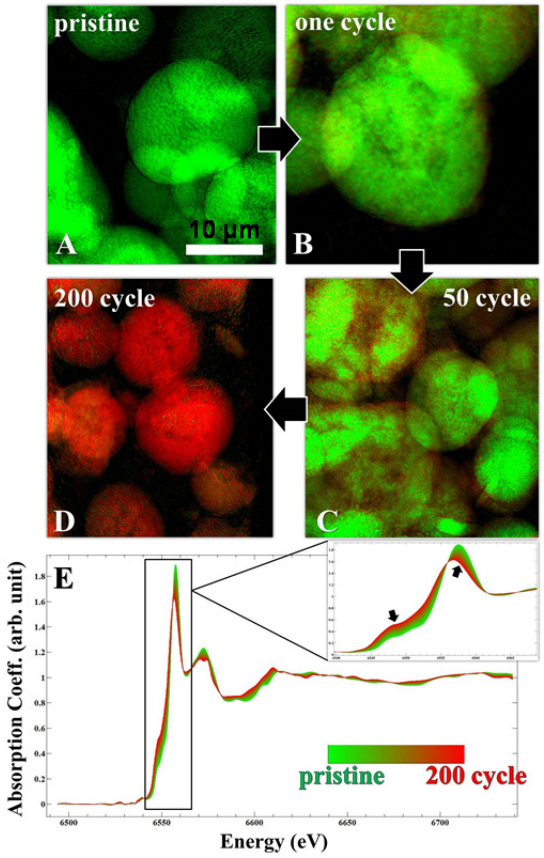


**Figure VI - 30: Panels A to D: 2D XANES chemical maps of Mn within the LRM-NMC particles, as a function of cycling. Single pixel XANES (30 nm resolution; ~ 10^6 per FOV) are assigned to green or red based on least squares fitting to the Mn K-edge spectra of pristine, 50 and 200 times cycled electrodes, respectively. (E) Evolution of the Mn K edge with cycling**

Although the 2D TXM-XANES analysis of LMR-NMC cathode materials presented above provides important information about the oxidation state evolution of Mn during repeated cycles, true 3D mapping is needed to distinguish particle heterogeneities and to quantify the transition metal (TM) cation concentration inside the bulk of the particle. Three-dimensional (3D) representations of the TM distributions within two typical particles are shown Figure VI - 31. As seen in the 3D renderings, the elemental concentrations of the particles show evidence for a difference in density near inner and outer surfaces.

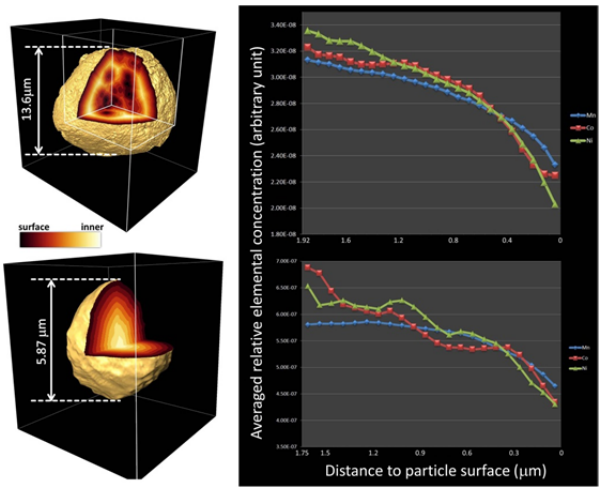


**Figure VI - 31: (Left) Tomographic reconstruction of two selected LMR-NMC cathode particles after 1 full charge-discharge cycle**

To put this observation on a firm footing, we have generated distribution plots (Figure VI - 31 right panel) to compare the shortest distance from each particle volume element, or voxel, to a particle surface (the outer surface of the particle and/or the surface of a macro pore inside the particle). In both cases there is a depletion of transition metals near the surface regions of the particles. The drop in relative concentrations of all three TMs indicates that the particles appear to be more porous at the surface even when the cathode particle undergoes only one full cycle of charge-discharge (2.5-4.9V). Specifically, we note that there is a significant drop of Co and Ni (comparing to Mn, which is the major TM in this electrode) at the layer(s) closest to the particle surface. 3D analysis of LMR-NMC cathode particles cycled for 50 and 200 cycles will reveal more information on the particle heterogeneities with cycling (analysis in progress).

**Confocal Raman Imaging of LMR-NMC Electrodes.** We carried out confocal-Raman imaging and spectral analysis of LMR-NMC electrodes at different SOC and cycle life stage. The Raman signature of LMR-NMC composition is sensitive to the lithium content in the lattice and, thus, is a good spectroscopic tool to map the variations in composition under different SOC or voltages. Further, Raman imaging provides a quantitative spectral tool for measuring spatial distribution of active materials and carbon on the electrode surface. Below we provide a summary of Raman imaging and analysis of LMR-NMC electrodes fabricated as per the procedure mentioned earlier.

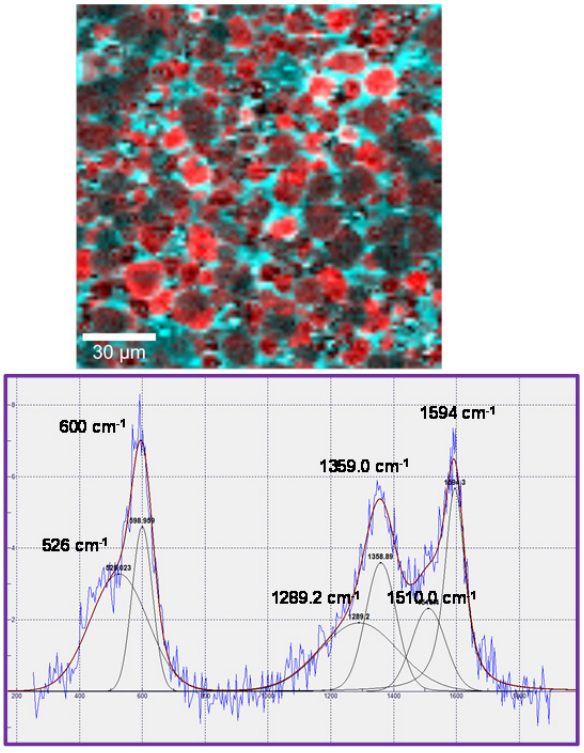


**Figure VI - 32: Raman mapping (top) and spectral analysis (bottom) of pristine LMR-NMC composite electrodes. The false color maps show carbon rich regions (red) and metal oxide (cyan); mixed colors are both carbon-LMR NMC regions**

Figure VI - 32 shows a typical Raman map of an LMR-NMC pristine electrode presenting LMR-NMC (cyan) and carbon (red) rich regions as well as a mixture of both. This map is based on the spectral component analysis as shown in the bottom figure. Typically, the fitted areal intensity is converted into a false color map as shown above. Briefly, the metal oxide Raman band is characterized by two Raman modes corresponding to Eg and A1g metal-oxide symmetric stretching modes [9] which for the given LMR-NMC particle are at around 526 and 600 $cm^{-1}$, respectively. The carbon region can be fitted with 4 components. Additionally we expect to see another Raman band at 420 $cm^{-1}$ corresponding to $Li_2MnO_3$, [10] but this relatively weaker band was not representative across all the electrode regions for the pristine sample. The peak positions at 1359 and 1594 $cm^{-1}$ correspond to D & G band of graphitic carbon while 1289 and 1510 $cm^{-1}$ are representative of the amorphous/disordered carbon. The Raman maps and their spectral behavior change as the electrodes are charged (discharged). Both spectral position and full width at half maximum (FWHM) change with the voltage (SOC) and also under continuous cycling. To further quantify the inhomegneities of the LMR-NMC electrodes, we undertake Raman analysis for cathode particles selected from different regions of electrodes charged at 3.9, 4.2, 4.5 and 4.9V and compare to a pristine electrode. Analysis

was carried out on at least 5 cathode particles and results are summarized in terms of the ratio of their Eg to A1g band areal intensities and their respective Raman band positions (Figure VI - 33). There are some interesting trends from this analysis: (i) for a given bulk electrode SOC (or voltage), the cathode particles at different electrode locations vary widely in terms of the areal ratios and band positions; and (ii) the A1g band shifts consistently to red with increased SOC with exceptions for the 4.5 V electrode. We notice more inhomogeneity for cathode particles from the electrodes charged at 4.2 and 4.9 V. Detailed analysis showing variation of the local SOC of the cathode particles will be reported shortly in a journal article.

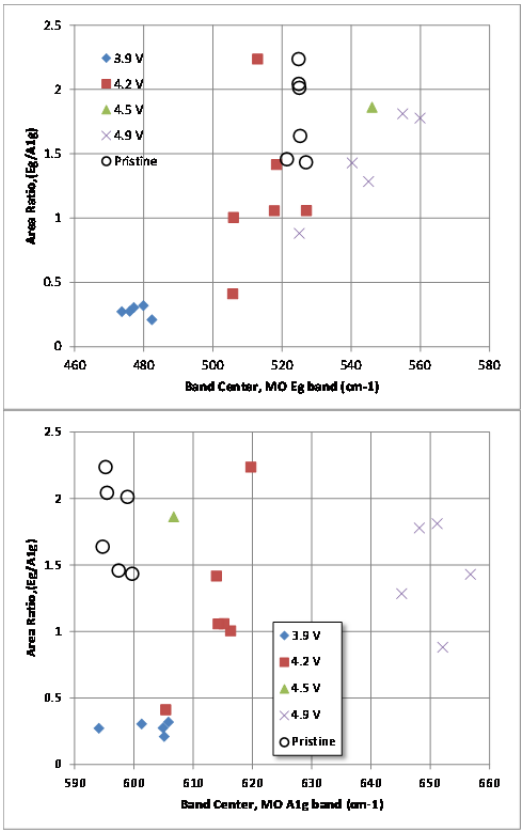


**Figure VI - 33: Ratio of the areal intensities for the Eg and A1g band plotted with respect to the band center for various LMR-NMC cathode particles maintained at different SOC**

**Role of Electrolyte additives on the performance of LMR-NMC Electrodes.** Collaborating with Dr. Kang Xu's group at Army Research Laboratory, we have tested the cycle life performance of LMR-NMC electrodes in the presence of 0.5 -1.5 wt% additives dissolved in the standard electrolyte (1.2 M $LiPF_6$ in EC-DMC 1:2 w/w). The additives are tris(hexafluoro-iso-propyl) phosphate (HFiP), aluminum substituted HFiP (AlHFiP), perfluorinated tert butoxide grafted phosphazene (PFBP), AlPFBP and PNF. HFiP has already demonstrated good cycle life benefits for high voltage spinel electrodes ($LiMn_{1.5}Ni_{0.5}O_4$) by forming a phosphate based passivation film on the cathode surface [11]. The hypothesis here is that HFiP and similar classes of compounds may also improve the cycle life performance, including 1st cycle irreversible capacity loss and columbic efficiency, for LMR-NMC high voltage cathodes. The additives were tested on several batches of electrodes (Figure VI - 34) using Argonne National Laboratory's voltage fade protocol [12].

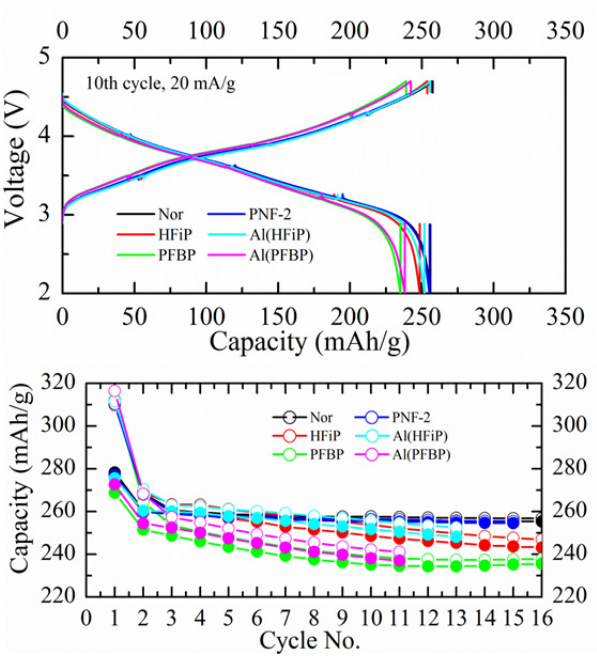


**Figure VI - 34: Impact of various electrolyte additives on the cycle life performance of LMR-NMC electrodes. (Top) Charge-discharge capacity at the 10th cycle is shown for 5 different additives**

We did not notice any improvement in the cycle life performance using any of the listed additives. Specifically, no appreciable improvement in 1st cycle irreversible capacity loss or columbic efficiency was observed as shown in Table VI - 1. In some case we even noticed a slight capacity fade when using additives such as PFBP. These data indicate that HFiP and their derivatives are most likely not forming a conductive passivation layer on the LMR-NMC cathode surface, but detailed studies are needed to investigate further. ARL will soon send purified versions of each these additives for further testing. It is likely that the presence of organic impurities in these additives can be detrimental to cycle life improvements. The overall goal of this study is to determine a suitable additive that forms a stable interphase on the LMR-NMC cathode surface to provide passivation during high voltage cycling (> 4.6 V).

**Table VI - 1: Summary of the performance of various electrolyte additives on LMR-NMC electrodes**

| Electrolyte | 1st (10 mA/g) | | | 2nd (20 mA/g) | | | 10th (20 mA/g) | | |
|---|---|---|---|---|---|---|---|---|---|
| | Charge Capacity (mAg/h) | Discharge Capacity (mAh/g) | Irreversible capacity (mAh/g) | Charge Capacity (mAg/h) | Discharge Capacity (mAh/g) | Irreversible capacity (mAh/g) | Charge Capacity (mAg/h) | Discharge Capacity (mAh/g) | Irreversible capacity (mAh/g) |
| No Additive | 311.98 | 278.23 | 33.75 (10.82%) | 268.61 | 260.51 | 8.1 (3.01%) | 257.61 | 255.93 | 1.68 (0.6%) |
| 1%HFiP | 309.82 | 276.08 | 33.74 (10.89%) | 269.12 | 259.60 | 9.52 (3.54%) | 253.74 | 248.59 | 5.15 (2.02%) |
| 1%PFBP | 312.5 | 268.76 | 43.74 (14%) | 264.46 | 251.57 | 12.89 (4.87%) | 239.00 | 235.15 | 3.85 (1.61%) |
| 1%PNF-2 | 310.37 | 277.06 | 33.31 (10.73%) | 267.96 | 259.79 | 8.17 (3.05%) | 256.47 | 255.33 | 1.14 (0.4%) |
| 1%Al(HFIP) | 311.62 | 275.60 | 36.02 (11.56%) | 270.34 | 260.31 | 10.03 (3.71%) | 255.85 | 251.73 | 4.12 (1.61%) |
| 1%Al(PFBP) | 316.40 | 272.61 | 43.79 (13.84%) | 268.20 | 254.41 | 13.79 (5.14%) | 242.24 | 238.14 | 4.1 (1.69%) |

## Conclusions and Future Directions

Using the TXM-XANES technique, we could map the Mn, Ni and Co valence state in LMR-NMC cathodes in 2D as well as 3D with a large field of view (30 microns). Tomographic reconstruction of 2D XANES images of respective TM cations on individual cathode particles provides a quantitative estimation of various TMs in terms of 3D distance maps. The surface and bulk TM concentrations will change as the cathode material undergoes repeated cycling. Raman imaging and spectral analysis of LMR-NMC electrodes showed a wide variation of the SOC of individual particles even though the bulk electrode is maintained at a particular voltage or SOC. We also tested the high voltage electrolyte additives on LMR-NMC compositions. Future work will be focused on studying other high capacity cathode compositions that are not necessarily Mn-rich. Preliminary work is in progress to stabilize high capacity cathode materials with compositions $Li_2M^IM^{II}O_2$ and $Li_2M^IM^{II}O_3$ where $M^I$ and $M^{II}$ are TMs anionically coupled to oxygen. Examples include (but are not limited to) Cu, Ni, and Fe compositions.

## FY 2013 Publications/Presentations

1. "Solid Electrolyte Coated High Voltage Layered-Layered Lithium-rich Composite Cathodes: $Li_{1.2}Mn_{0.525}Ni_{0.175}Co_{0.1}O_2$," S. K.Martha, J. Nanda, Y. Kim, R.R. Unocic, S. Pannala and N. J. Dudney, J. Mater. Chem. A 2013, 5587 (1).
2. "TXM-XANES Studies on High Voltage Lithium Rich Composite Cathodes: 3D Morphology and Phase at Nanoscale, Presented at MRS Fall Meeting," Boston, Nov 2012.
3. "Confocal Raman Imaging and Spectroscopy of High Voltage Composite Cathode for Lithium Batteries, J. Nanda, A. Callendar, H. Zhou and S. K. Martha," Confocal Raman Symposium, Ulm Germany, and September 2013 (invited presentation).
4. "Thermophysical Properties of $LiFePO_4$ Cathodes with Carbonized Pitch Coatings and Organic Binders: Experiments and First-Principles Modeling," J. Nanda et al., J. Power sources 2013 (accepted).
5. "Highly Robust Lithium-ion battery electrodes from Lignin: An Abundant Renewable and Low-cost Material," W. Tenhaeff et. al., Adv. Func. Mater., 2013.
6. Ira Bloom, Lynn Trahey, Ali Abouimrane, Ilias Belharouak, Xiaofeng Zhang, Qingliu Wu, Wenquan Lu, Daniel P. Abraham, Martin Bettge, Jeffrey W. Elam, Xiangbo Meng, Anthony K. Burrell, Chunmei Ban, Robert Tenet, Jagjit Nanda and Nancy Dudney, J. Power Sources, in press.
7. "Nanoscale X-Ray Microscopy of High Voltage Lithium-Rich MNC Composite Cathodes With 2D/3D Chemical/Elemental Sensitivity," Presented at 224th ECS Meeting, San Francisco, Oct 2013.

## References


1. Battery Test Manual For Plug-In Hybrid Electric Vehicles, Rev. 1, June 2010, INL/EXT-07-12536.
2. USABC Electric Vehicle Battery Test Manual, 2011
3. R. Santhanam, and B. Rambabu, J. Power Sources, 195 (2010) 5442–5451.
4. M. M. Thackeray, C. Johnson, J. T. Vaughey, N. Li, and S. A. Hackney, J. Mater. Chem. 15 (2005) 2257–2267.
5. S. K. Martha, J. Nanda, G. M. Veith, and N. J. Dudney, J. Power Sources, 199 (2012) 220–226.
6. F. Meirer, J. Cabana, Y. J. Liu, A. Mehta, J. C. Andrews, and P. Pianetta, J. Synchrotron Rad. 18 (2011) 773–781.
7. W. C. Chen, Y. F. Song, C. C. Wang, Y. J. Liu, D. T. Morris, P. A. Pianetta, J. C. Andrews, H. C. Wu, and N. L. Wu, J. Mater. Chem. A, 1 (2013) 10847–10856.
8. Nanoscale X-Ray Microscopy of High Voltage Lithium-Rich MNC Composite Cathodes With 2D/3D Chemical/Elemental Sensitivity, Presented at 224th ECS Meeting, San Francisco, Oct 2013
9. J. Nanda, J. Remillard, A. O'Neill, D. Bernardi, T. Ro, K. E. Nietering, J. Y. Go, and T. J. Miller, Adv. Funct. Mater. 21 (2011) 3282–3290.
10. S. K. Martha, J. Nanda, G. M. Veith, and N. J. Dudney, J. Power Sources, 216 (2012) 179–186.
11. V. Cresce, and K. Xu, J. Electrochem. Soc. 158 (2011) A337–A342.
12. M. Bettge, Y. Li, K. Gallagher, Y. Zhu, Q.Wu, W. Lu, I. Bloom, and D. P. Abraham, J. Electrochem. Soc., 160 (2013) A2046-A2055.

# VI.B.7 Lithium-bearing Mixed Polyanion (LBMP) Glasses as Cathode Materials (ORNL)

**Jim Kiggans and Andrew Kercher**
Oak Ridge National Laboratory

P.O. Box 2008; MS 6087
Oak Ridge, TN 37831-6087
Phone: (865) 574-8863; Fax: (865) 574-4357
E-mail: kiggansjojr@ornl.gov

Start Date: June 2012
Projected End Date: June 2016

## Objectives

- Model and synthesize mixed polyanion (MP) glasses for use as active cathode materials in lithium ion batteries.
- Demonstrate enhanced material properties and electrochemical performance of glass cathode materials by varying the polyanion content.
- Produce MP glass cathode materials that undergo multivalent transitions in the transition metal cations during electrochemical testing.
- Through laboratory-scale battery testing, demonstrate novel glasses with excellent overall cathode performance that are viable replacements for current cathode materials in electric vehicle applications.

## Technical Barriers

The development of MP glass cathode materials has the potential to address the key technical barriers of low energy density, poor high power performance, inadequate cycle life, safety, and high cost.

## Technical Targets

- Produce an MP glass cathode with significantly greater capacity at high discharge rates than crystalline $LiFePO_4$.
- Develop an MP glass material with at least a 25% greater specific energy than $LiFePO_4$.
- Demonstrate multivalent MP glass cathodes with specific capacities exceeding 200 mAh/g.

## Accomplishments

- Proof-of-principle of the MP glass cathode concept was demonstrated. Dramatic improvements in specific capacity and rate performance were observed with increased polyanion substitution into iron phosphate glass.
- A high-capacity 2$^{nd}$ electrochemical reaction mechanism was found to occur in polyanion glass cathodes. This 2$^{nd}$ mechanism has not been observed in polyanionic crystalline cathode materials.
- Good cycling performance has been demonstrated for an MP glass.
- Thermodynamic models of the electrochemical discharge of polyanion glass cathodes have been developed using the CALPHAD approach and have been refined by benchmarking with experimentally measured discharge curves.

✧ ✧ ✧ ✧ ✧

## Introduction

Polyanionic crystalline materials, such as $LiFePO_4$, are promising cathode materials for lithium ion batteries for electric vehicle applications because they can have excellent safety and cycling performance due to their rigid covalently bonded structure. However, many polyanionic crystalline materials with theoretically excellent energy densities, such as $LiCoPO_4$, $LiFeBO_3$, and $Li_2MnSiO_4$, have not performed well as cathodes due to low electrical conductivity and/or crystal structure changes during cycling. Oak Ridge National Laboratory has proposed that mixed polyanion (MP) glasses can be excellent high capacity cathodes that can overcome the limitations of similar polyanionic crystalline materials.

Mixed polyanion glasses have three key advantages over similar polyanionic crystalline materials. First, with the proper choice of polyanion content, MP glasses can have higher electrical conductivities than similar polyanionic crystalline materials. For example, substitutions of molybdenum oxide, tellurium oxide, and vanadium oxide for phosphate in iron phosphate glasses have demonstrated increases in room temperature electrical conductivity by orders of magnitude. Second,

the disordered covalently bonded structure of MP glasses limits the ability of the structure to rearrange, which holds the promise to prevent undesirable microstructural arrangement during cycling. Third, the polyanion content of glasses can be tailored to produce a cathode with a maximized redox potential for a given electrolyte system. Changing the polyanion content of a polyanionic cathode material has been shown to change the redox potential due to the inductive effect of the polyanion (Isono, et al., J. Power Sources, 2010, 195: 593-598). Depending on the amount and electronegativity of the polyanion substituted in the glass, the voltage of a glass cathode could be increased or decreased to the desired optimal voltage.

Most polyanionic crystalline materials are phosphates, borates, or silicates. Phosphates, borates and silicates are renowned glass formers using conventional glass processing methods. Therefore, producing these novel glass cathode materials will not likely require exotic processing methods, but could be produced by low-cost conventional glass processing methods.

## Approach

The research into MP glass cathode materials involves: (1) computational thermodynamic modeling, (2) glass processing, (3) glass structure and property characterization, and (4) electrochemical testing. Computational thermodynamic models of the electrochemical response of prospective MP glasses will be used to make decisions on the most promising glasses to pursue. Classical heat/quench glass processing has been the primary processing method. Characterization techniques are being used to confirm amorphous structure, to determine transition metal valences, and to measure fundamental glass properties. Electrochemical testing is being performed on coin cells with powdered glass cathodes produced by conventional slurry casting.

## Results

**Proof-of-principle for MP glass cathodes.** A series of iron phosphate vanadate glasses (compositions based on $Fe_4([1\text{-}x]\ P_2O_7 \bullet [x]\ V_2O_7)_3$) were produced with the polyanion content containing 0%, 30%, and 50% vanadate. Micron-scale powders of these glasses were electrochemically tested in coin cells to demonstrate the effect of mixed polyanion content on electrochemical performance. As expected, the pure iron phosphate glass showed almost no capacity (0.36% theoretical) when discharged down to 2V. However, the capacity and rate performance improved dramatically with increasing vanadate substitution in the glass (Figure VI - 35). The demonstration of dramatically improved electrochemical behavior in a glass cathode by incorporating mixed polyanion content is a proof-of-principle for the MP glass cathode concept.

Complete discharge curves of the 50% vanadate substituted iron phosphate glass showed that the electrochemical intercalation reaction during discharge yielded full iron-based theoretical capacity ($Fe^{3+}$ to $Fe^{2+}$) and some additional vanadium-based capacity ($V^{5+}$ to $V^{4+}$). X-ray absorption spectroscopy (XANES) near the iron and vanadium edges performed at the National Synchrotron Light Source at Brookhaven National Laboratory (BNL) confirmed the iron and vanadium valence changes during the intercalation stage of battery discharge.

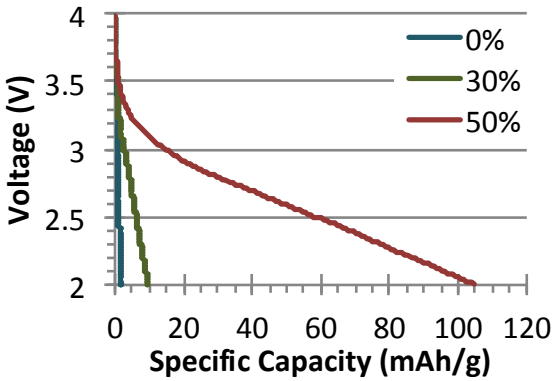


**Figure VI - 35: Iron phosphate vanadate glasses with different amounts of vanadate substitution (0%, 30%, and 50%) were battery tested at ~C/30 from 4V to 2V. The specific capacity increased dramatically with increased vanadate substitution**

**High-capacity reaction mechanism.** When discharged, cathodes of polyanionic crystalline materials undergo a lithium intercalation reaction. When MP glass cathodes were discharged down to 1V, the lithium intercalation reaction and a second lower-voltage, high-capacity reaction were observed (Figure VI - 36). Initial battery testing has suggested that both electrochemical reactions are reversible. The second electrochemical reaction has been observed in iron-bearing and manganese-bearing glasses.

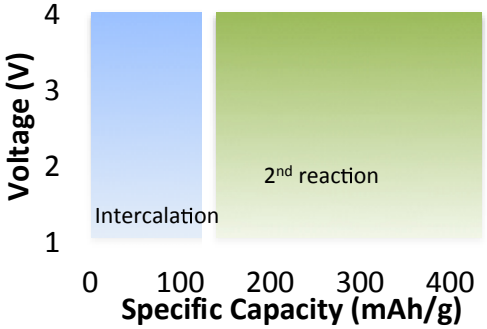


**Figure VI - 36: A high capacity 2nd electrochemical reaction was discovered to occur in polyanion glasses. A discharge curve of $Fe_4(50\%\ P_2O_7 \bullet 50\%\ V_2O_7)_3$ glass (19 mA/g) is shown**

MP glass cathodes at different electrochemical stages were analyzed by XANES at the National Synchrotron Light Source at BNL in order to study this second reaction mechanism. XANES analysis showed that, during discharge of iron phosphate vanadate glass cathodes, the iron changes from $Fe^{3+}$ to $Fe^{2+}$ during the intercalation reaction and from $Fe^{2+}$ to $Fe^{0}$ during the second reaction (Figure VI - 37). Vanadium valence was not observed to change during the second reaction. Using these insights into the second reaction mechanism, MP glasses could be designed that undergo this high-capacity reaction at higher voltages.

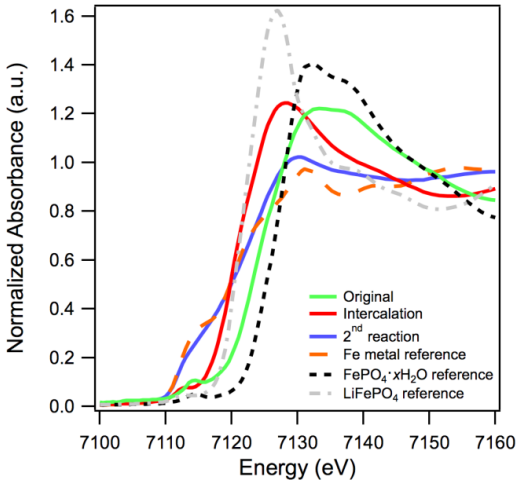


**Figure VI - 37: XANES analysis showed how iron valence changed during the discharge of iron phosphate vanadate glass**

**Cycling performance of MP glass.** Lithium iron phosphate is a polyanionic crystalline material that has excellent cycling performance. Cycle testing of MP glass cathodes was performed to determine how well polyanionic glass cathodes can cycle. Initial cycle tests have focused on the cyclability of $Fe_4(50\%\ P_2O_7 \bullet 50\%\ V_2O_7)_3$) in the intercalation reaction. The cathodes cycled well between 4V and 2V at C/10 for 100 cycles (every 20th cycle at C/50) (Figure VI - 38).

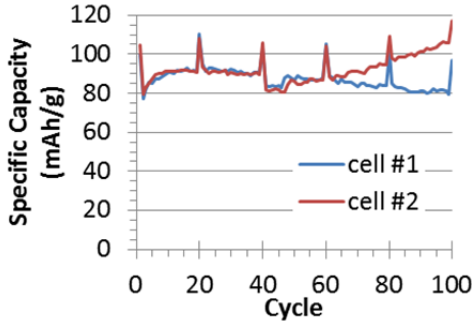


**Figure VI - 38: Cycle testing of iron phosphate vanadate glass showed good cycleability. (C/10 cycling with every 20th cycle at C/50)**

**Computational model of MP glass.** Unlike polyanionic crystalline materials, MP glasses have a large compositional flexibility and provide diverse options for prospective glass cathode compositions. Computational thermodynamic modeling using a CALPHAD (CALculation of PHAse Diagram) approach has been developed with the goal of predicting the discharge curves of MP glass concepts and guiding the project toward the most promising candidates.

Computational thermodynamic modeling has successfully reproduced the equilibrium discharge curve for crystalline lithium iron phosphate using the corresponding thermodynamic data for the constituent oxides. Since glass is inherently a non-equilibrium structure, different thermodynamic models have been developed to predict the electrochemical behavior of MP glass. The 1st generation model was based on the Gibbs free energy of the crystalline oxides of the desired composition mixed in different proportions with the Gibbs free energy of the glass melt extrapolated down to room temperature (dashed curves on Figure VI - 39). The sloped discharge curves observed in MP glasses could not be predicted based on 1st generation models. In the 2nd generation model, a symmetric sub-regular solution model was included to express non-ideality between the mixing of Li and vacancy in the dedicated sublattice. When benchmarked against experimental discharge curves for $Fe_4(50\%\ P_2O_7 \bullet 50\%\ V_2O_7)_3$), the 2nd generation model (90% solid / 10% liquid with aforementioned non-ideality) showed excellent agreement with experimental data (black solid curve on Figure VI - 39).

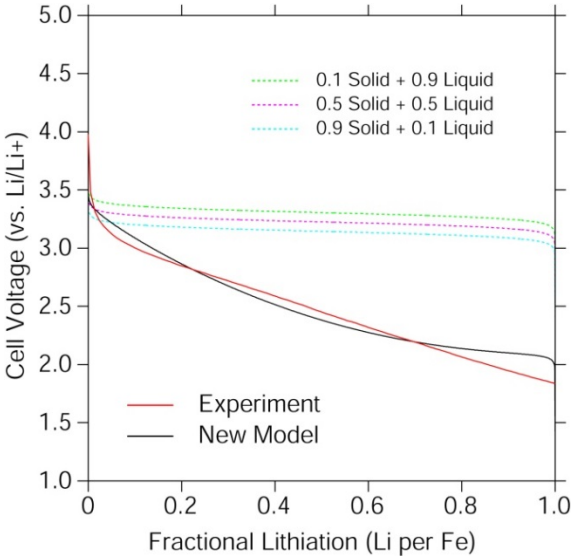


**Figure VI - 39: 1st generation (dashed lines) and 2nd generation (black line) computational thermodynamic models of the equilibrium discharge curve for an iron phosphate vanadate glass benchmarked against an experimentally measured discharge curve (red line)**

## Conclusions and Future Directions

Battery testing of iron phosphate vanadate glass cathodes provided a solid proof-of-principle for the MP glass cathode concept, demonstrating both improved capacity and rate performance with mixed polyanion content. Cyclable intercalation of iron phosphate vanadate glass has been demonstrated. The unexpected discovery of a high capacity 2$^{nd}$ electrochemical reaction suggested the possibility of a new avenue for obtaining a high capacity cathode material. The second generation of computational thermodynamic models of glass electrochemical performance showed excellent agreement with experimental discharge curves. The second generation models will predict candidate glass performance and provide guidance toward the most promising glass candidates.

Now that proof-of-principle of MP glass cathodes has been demonstrated, the project focus has been placed on glass systems with theoretical specific energies that exceed lithium iron phosphate by at least 30%. Multivalent intercalation is one route to achieve high specific energies. Transition metals of interest for multivalent intercalation in a useful voltage window include manganese, copper, and molybdenum. The 2$^{nd}$ electrochemical reaction found in MP glasses could offer another potential route to achieve high specific energies. The 2$^{nd}$ reaction appears similar to the conversion reaction found in transition metal oxides and halides. Using the voltage trends observed in conversion cathodes, future glass candidates would be chosen to potentially have these 2$^{nd}$ reactions occur at higher voltages. Cycling performance of the 2$^{nd}$ reaction will also be studied to determine long-term reversibility of the reaction.

## FY 2013 Publications/Presentations

N/A

# VI.B.8 Development of High-Energy Cathode Materials (PNNL)

**Ji-Guang Zhang**
Pacific Northwest National Laboratory

902 Battelle Boulevard
Richland, WA 99352
Phone: (509) 372-6515, Fax: (509) 375-2186
E-mail: jiguang.zhang@pnnl.gov

**Jie Xiao (co-PI)**
Pacific Northwest National Laboratory
902 Battelle Boulevard
Richland, WA 99352
Phone: (509) 375-4598, Fax: (509) 375-2186
E-mail: jie.xiao@pnnl.gov

Start Date: October 2011
Projected End Date: September 2015

## Objectives

- Develop high-energy cathode materials with improved safety.
- Develop low-cost synthesis routes for environmentally benign cathode materials with long cycle life.

## Technical Barriers

This project addresses the following technical barriers:

- High cost of materials and synthesis methods
- Limited energy density and cyclability
- Safety

## Technical Targets

- Understand the failure mechanism of Li-Mn-rich (LMR) active materials $xLi_2MnO_3 \cdot (1-x)LiMO_2$ (M = Mn, Ni, Co; $0 \leq x \leq 1$).
- Modify the synthesis methods to improve electrochemical performance of LMR cathode.
- Adjust interfacial properties between electrode and electrolyte to reduce parasitic reactions.

## Accomplishments

- Revealed corrosion and fragmentation of LMR cathode after cycling that was detrimental to cell performances.
- Investigated the electrochemical kinetics of both layered $LiNi_{0.5}Mn_{0.5}O_2$ and $Li_2MnO_3$ components in LMR during the electrochemical processes.
- Identified electrolyte additive that alleviated the side reactions between oxygen species and electrolyte at high voltages.

✧ ✧ ✧ ✧ ✧

## Introduction

LMR layered composites, for example, $Li[Li_{0.2}Ni_{0.2}Mn_{0.6}]O_2$, have attracted extensive interest because of highest energy density. The co-existence of two different components, i.e., layered $LiNi_{0.5}Mn_{0.5}O_2$ and $Li_2MnO_3$ in LMR improves the capacity of this type of layered composites. In the first few cycles, $Li_2MnO_3$ was activated and a discharge capacity of greater than 250 mAh $g^{-1}$ can be achieved. However, this activation process always is accompanied by the layered-to-spinel phase transition that releases oxygen from the lattice due to cation migration. The released oxygen reacts with the carbonate-based electrolytes, generates insulating by-products and leads to low discharge rate and capacity fade. The structure change will also lead to voltage fading with cycling. Therefore, voltage fade and low discharge rate are the main barriers preventing large scale use of LMR cathode materials.

## Approach

- Use advanced characterization technique to understand the effects caused by the oxygen release and phase transition.
- Apply knowledge gained in high voltage Li-ion battery system to study the degradation mechanism in LMR cathode.
- Explore novel electrolyte additives to control the interfacial reactions between LMR cathode and electrolyte at high voltages.

## Results

**1. LMR cathode morphology evolution during cycling.** In order to identify key factors related with the layered-to-spinel transition for LMR cathode, aberration-corrected Scanning Transmission Electron Microscopy (S/TEM) combined with Electron Energy Loss Spectroscopy (EELS) were used to probe the structure evolutions of $Li[Li_{0.2}Ni_{0.2}M_{0.6}]O_2$ during long-term cycling (Figure VI - 40). Corrosion and

fragmentation of cathode particles were identified on the cycled layered composite. Additionally, $Mn^{2+}$ species and reduced lithium content in the fragmented pieces were revealed by EELS, which were correlated with the capacity degradation mechanism.

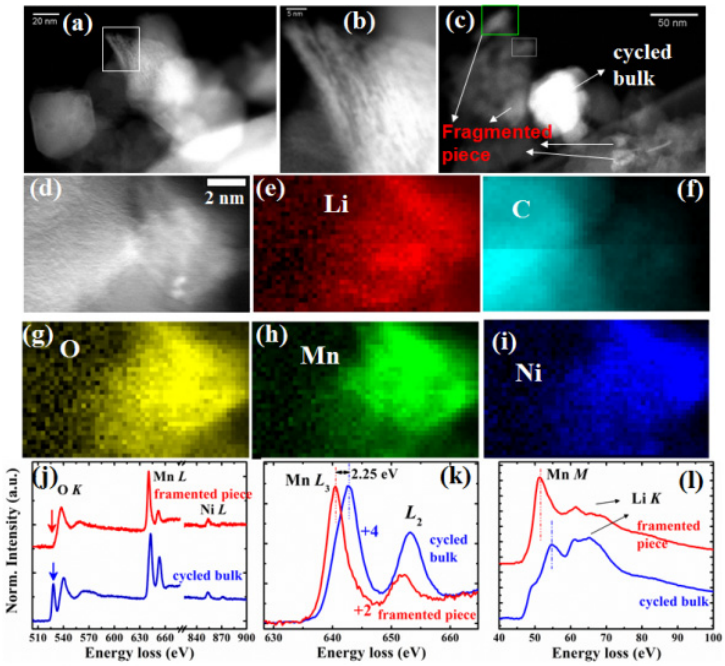


**Figure VI - 40: (a) Overview image showing the cathode nanoparticles after cycling; (b) magnified image of the region labeled by the white rectangle shown in (a); (c) Overview image of another region with fragmented pieces of cathode; (d) magnified image of the region labeled by the rectangle in (c); (e) Li map (58.25-65.5eV); (f) C map (282.25-314.75 eV); (g) O map (527.75-564eV); (h) Mn map (634.25-659eV); (i) comparison of O K, Mn L, and Ni L edges; (k) Mn L edges normalized to Mn $L_3$ peak; (l) Mn M, and Li K edge comparison of cycled bulk region and fragmented piece region**

Pristine $Li[Li_{0.2}Ni_{0.2}M_{0.6}]O_2$ was composed of crystallized particles (~200 nm) with well-defined layered structure. However, after 300 cycles, sponge-like etched surfaces were clearly observed (Figure VI - 40a-b) along with fragmented pieces (Figure VI - 40c-d). Li, C, O, Mn and Ni EELS maps (Figure VI - 40e-i) were collected from the selected region of fragmented pieces, which suggested that the fragmented pieces mixed with solid electrolyte interface (SEI) components, likely originated from the bulk particles after repeated cycling. In addition, consistent with the oxygen-deficient environment (Figure VI - 40j), Mn valence in the fragmented pieces was quantified to be $2^+$ (Figure VI - 40k), much lower than in the bulk. In addition, Li K edge peak intensity in the fragmented particle was much lower than the cycled bulk region (Figure VI - 40l), suggesting that the fragmentation probably initiated during the lithium extraction/charge process. This was consistent with the large strain generated from extensive removal of $Li^+$ and oxygen release during charge. The etched surfaces, which may evolve into fragmented pieces after cycling, were detrimental to the electrochemical properties of LMR cathode due to the loss of intimate contact with the electrode, passivation of new surface, and related increase in cell impedance.

**2. Electrochemical kinetics of LMR cathode.** To understand the poor rate performances of LMR cathode materials, the electrochemical kinetics of LMR during cycling has been investigated. It was found that the diffusion rate of $Li^+$ in LMR was mainly determined by the $Li_2MnO_3$ and its derived phase. $Li_2MnO_3$-derived phase exhibited good charge rate capability but poor discharge rate capability, which became the limiting factor at high discharge rates.

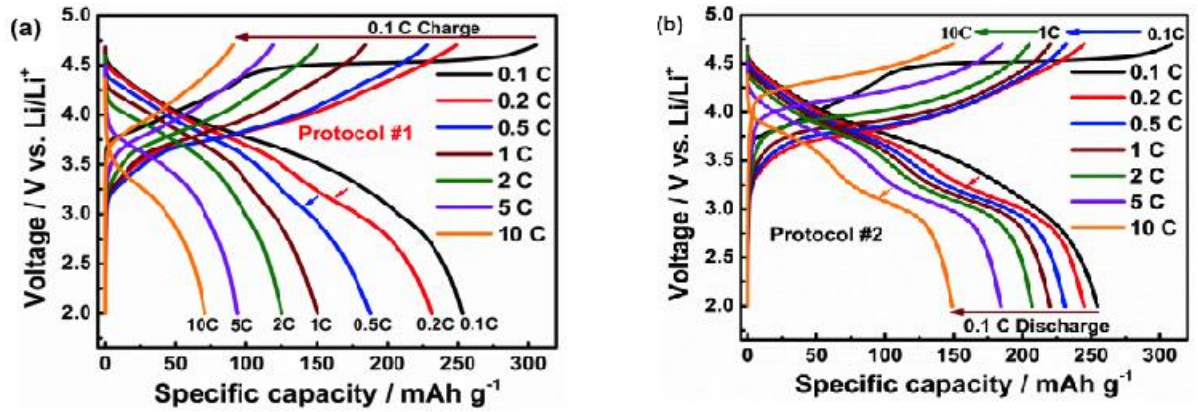


**Figure VI - 41: Voltage profiles of $Li[Li_{0.2}Ni_{0.2}Mn_{0.6}]O_2$ (a) Constant charge at 0.1 C (1C=250 mA/g) and discharged at different rates for the subsequent cycles. (b) Charged at different rates and constant discharge at 0.1 C for the following cycles**

Figure VI - 41(a) shows the voltage profiles of $Li[Li_{0.2}Ni_{0.2}M_{0.6}]O_2$ when a slow rate of 0.1C was used for all charges but different rates were applied during discharge. The voltage fading related to the spinel-phase transition (represented by a clear dent on the voltage curve at about 3.3V as shown in Figure VI - 41) was only observable at relatively slow discharge rates (≤ 2C) and completely disappeared at high rate above 2C. This result can be attributed to a poor rate capability of the $Li_2MnO_3$ component. In other words, discharge capacity delivered at 10C was dominated by the layered $LiNi_{0.5}Mn_{0.5}O_2$ component. When different charge rates were applied on the LMR cathode, followed by discharging at the same slow rates (Figure VI - 41b), the capacity retention is largely improved compared with Figure VI - 41a. In this case, the voltage fading is still seen during discharge even after charging at 10C, indicating that $Li_2MnO_3$-derived spinel phase has a good charge rate capability. It was suggested that slow discharge rate should be used to effectively capture and understand the voltage-fading phenomenon in LMR. The diffusion of $Li^+$ ions within lattice structure of $Li_2MnO_3$-derived phase had to be increased to improve the rate performances of LMR aided by the modifications of interfacial reactions, which is now under investigation.

**3. Modification of interfacial reactions by using electrolyte additives.** In order to modify the interfacial properties between the LMR cathode and electrolyte, boron-based anion receptor, tris(pentafluorophenyl) borane (TPFPB) was adopted as an electrolyte additive to limit the negative effects from oxygen species in the system. In previous works, TPFPB has been used to improve the performances of batteries containing graphite and $LiMn_2O_4$ by partially dissolving the byproducts such as LiF and $Li_2O$. Considering the strong anion coordination effect of TPFPB, the released oxygen species in the form of oxygen anions ($O_2^{2-}/O_2^-$) or radicals ($O_2^{--}/O^-$) may be trapped in the vicinity of TPFPB instead of attacking the electrolyte.

Figure VI - 42 summarizes the proposed working mechanism of TPFPB. During the activation of $Li_2MnO_3$, oxygen is extracted out of the structural lattice as highly active oxygen species, e.g., $O_2^-/O_2^{2-}$, or $O^-$, which are reactive Lewis base that could decompose the carbonate-based electrolyte. It is hypothesized that $O_2^-/O_2^{2-}$ extracted out of LMR lattice can be partially captured by boron atom located in the center of TPFPB, eliminating direct exposure to the electrolyte which would initiate parasitic reactions. Even though $O_2$ still forms, it dissolves in the presence of TPFPB since the oxygen solubility in perfluorinated compound is much higher than in carbonate solvents. The byproducts derived from the interactions between electrolyte and $O_2^-/O_2^{2-}$ were therefore substantially reduced. Other parasitic reactions such as electrolyte decomposition at high voltages also produced insulating salts such as LiF and $Li_2O$ etc., which were again soluble in the presence of TPFPB. Therefore, the intensive interfacial reactions during the first cycle as well as the continuous accumulation of passivation film on cathode surface are significantly alleviated in the presence of TPFPB, which stabilizes the electrode/electrolyte interface.

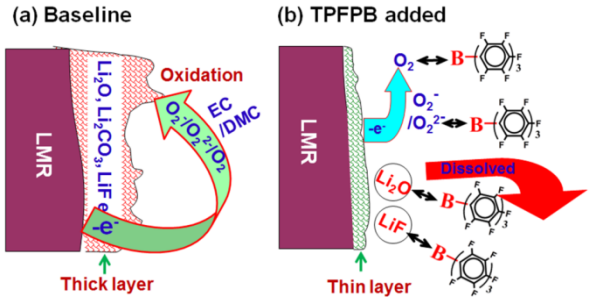


**Figure VI - 42: Scheme of the functioning mechanism of TPFPB. (a) Thick passivation layer formation in baseline electrolyte; (b) significantly reduced passivation layer formation in TPFPB added electrolyte**

Figure VI - 43a shows the initial charge/discharge curves between 2.0 and 4.7 V for $Li[Li_{0.2}Ni_{0.2}Mn_{0.6}]O_2$ cycled in electrolytes with different TPFPB concentrations. The charge/discharge profiles almost overlapped with each other for Li $[Li_{0.2}Ni_{0.2}Mn_{0.6}]O_2$ electrodes in baseline electrolyte and TPFPB containing electrolyte due to very low current density (0.1 C) used for the first three formation cycles. An irreversible voltage plateau at ca. 4.4 ~ 4.6 V was observed in all three cells caused by the irreversible loss of oxygen from the LMR electrode. After activation, the electrode materials delivered similar high discharge capacity of ca. 245 mAh $g^{-1}$ in all electrolytes (Figure VI - 43a), indicating that TPFPB additive had good compatibility with both $Li[Li_{0.2}Ni_{0.2}Mn_{0.6}]O_2$ and the electrolyte during electrochemical processes. In the subsequent cycling at C/3 (Figure VI - 43b), an initial discharge capacity of ~200 mAh $g^{-1}$ was still achieved in all cells. However, fast capacity fading was observed for $Li[Li_{0.2}Ni_{0.2}Mn_{0.6}]O_2$ in baseline electrolyte with cycling. In contrast, remarkably improved cycling stability was revealed with the addition of TPFPB. Even after 300 cycles, the discharge capacities were maintained at 157 and 161 mAh $g^{-1}$ for cathodes tested in electrolytes with 0.1 M and 0.2 M TPFPB, respectively, correspond-ding to capacity retentions of 80.6% and 81.0%. For LMR cathode, one important reason for the continuous capacity fading was the deterioration of electrode/ electrolyte interface, associated with a thick passivation layer formation and the corrosion/fragmentation of LMR cathode bulk structure. If TPFPB in the electrolyte effectively accepted oxygen anions or radicals before $O_2$ was generated, the damages of active oxygen species (including $O_2^-/O_2^{2-}$, or $O^-$) to LMR electrode surface should be much less than that without TPFPB.

The above prediction is verified by the TEM analysis of the fresh and cycled electrodes in different electrolytes (Figure VI - 44). Before cycling, a relatively smooth particle surface is observed (Figure VI - 44a). After 300 cycles, clear difference in particle surfaces was identified for electrolyte without and with TPFPB. In baseline electrolyte (Figure VI - 44b), the image revealed a distinguishable passivation layer on the surface of cycled $Li[Li_{0.2}Ni_{0.2}Mn_{0.6}]O_2$ electrode, with a thickness of 10-15 nm. In comparison, electrode cycled in the presence of TPFPB (Figure VI - 44c and d) displayed well-maintained particle morphology with smooth particle surface covered by a much thinner passivation layer. These findings substantiated our hypothesis on the capability of TPFPB in modifying the interfacial reactions through the stabilization of anions/radicals as well as dissolution of oxygen species and insulating byproducts.

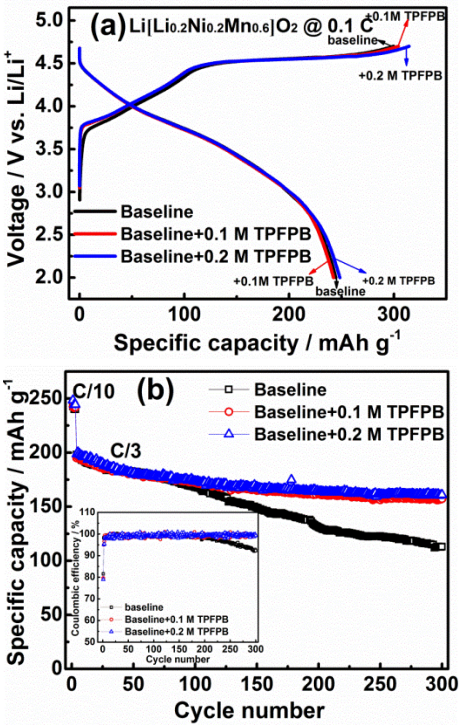


**Figure VI - 43: (a) Initial charge/discharge profiles at 0.1 C (25 mA $g^{-1}$) and (b) long-term cycling performance of cathode material $Li[Li_{0.2}Ni_{0.2}Mn_{0.6}]O_2$ at C/3 after 3 formation cycles at 0.1 C. The inset of (b) is the corresponding Coulombic efficiency during cycling**

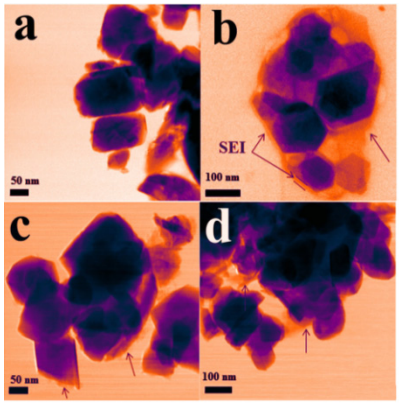


**Figure VI - 44: TEM images of fresh electrode and electrodes cycled in electrolytes without and with additive after 300 cycles at C/3 rate. (a) fresh, (b) baseline, (c) 0.1 M TPFPB, (d) 0.2 M TPFPB**

## Conclusions and Future Directions

The adverse effects of oxygen release from LMR lattice during initial activation have been systematically investigated in terms of the electrode integrity after long term cycling and the interfacial side reactions, which were then correlated to the cell failure mechanism. The

electrochemical kinetics of LMR was studied to understand the poor rate capability of LMR. It was revealed that large strain was generated from oxygen release and cation migration during charge, etching LMR surfaces into fragmented pieces during cycling. The release of active oxygen species strongly interacted with carbonate-based electrolyte solvents and produced a large amount of insulating byproducts on LMR surface and largely increased cell impedance. All of the above key-chain reactions from oxygen release partially explained the fast capacity degradation, voltage fading and poor discharge rate capabilities of LMR. TPFPB as an anion acceptor effectively coordinated with oxygen species and reduced the parasitic reactions initiating on LMR surfaces, leading to improved cycling stability. Voltage fading was also alleviated in the presence of TPFPB additive, suggesting that voltage fading is a combined effect of phase transition and surface reactions.

Future efforts include the exploration of intrinsic layered-to-spinel transition at atomic level and understanding how to mitigate/prevent this lattice change by adjusting the synthesis route. Study on the interface reactions will also be continued with an emphasis on the electrolyte modification

## FY 2013 Publications/Presentations


1. J. Zheng, M. Gu, J. Xiao, P. Zuo, C. Wang, J.-G. Zhang, "Corrosion/Fragmentation of Layered Composite Cathode and Related Capacity/Voltage Fading during Cycling Process," *Nano letters*, **13**, 3824-3830 (2013).
2. J. Xiao, X. Yu, J. Zheng, Y. Zhou, F.Gao, X. Chen, J. Bai, X.-Q. Yang, J.-G. Zhang, "Interplay between Two-Phase and Solid Solution Reactions in High Voltage Spinel Cathode Material for Lithium Ion Batteries," *J. Power Sources*, **242**,736-741 (2013).
3. J. Zheng, W. Shi, M. Gu, J. Xiao, P. Zuo, C. Wang, J.-G. Zhang, Electrochemical Kinetics and Performance of Layered Composite Cathode Material Li $[Li_{0.2}Ni_{0.2}Mn_{0.6}]O_2$, *J. Electro-chem. Soc.*, **160**, A2212-A2219 (2013).
4. J. Zheng, J. Xiao, Z. Nie, J.-G. Zhang, Lattice $Mn^{3+}$ Behaviors in $Li_4Ti_5O_{12}/LiNi_{0.5}Mn_{1.5}O_4$ Full Cells, *J. Electrochem. Soc.*, **160**, A1264-A1268 (2013).
5. J. Zheng, J. Xiao, W.Xu, X. Chen, M.Gu, X. Li, J.-G. Zhang, "Surface and structural stabilities of carbon additives in high voltage lithium ion Batteries," *J. Power Sources,* **227**, 211-217 (2013).
6. M. Gu, I. Belharouak, J. Zheng, H. Wu, J. Xiao, A. Genc, K. Amine, S. Thevuthasan, D. R. Baer, J-G. Zhang, N.D. Browning, J. Liu, and C.M. Wang, "Formation Of The Spinel Phase In The Layered Composite Cathode Used In Li-Ion Batteries," *ACS Nano* **7**(1):760-767 (2013).
7. P.V. Sushko, K.M. Rosso, J-G. Zhang, J. Liu, and M.L. Sushko, "Oxygen vacancies and ordering of d-levels control voltage suppression in oxide cathodes: the case of spinel $LiNi_{0.5}Mn_{1.5}O_{4-\delta}$," Adv. *Funct. Mater,* DOI: 10.1002/adfm.201301205 (2013).
8. J.-G. Zhang and J.Xiao, *2013 DOE BATT Program Annual Peer Review Meeting*, March 2013, Washington, DC.
9. J. Xiao, J. Zheng, X. Li, Y. Shao, and J-G. Zhang, "Hierarchically Structured Materials for Lithium Batteries," *Nanotechnology*, 24, 424004, doi:10.1088/0957-4484/24/42/424004, 2013.
10. J. Xiao, J. Zheng, X. Chen, W. Xu and J. Zhang, "High Voltage Li-ion Batteries," *222th ECS Meeting, PRiME*, 2012, Honolulu, Hawaii.
11. J.-G. Zhang, J. Xiao, and C. Wang, "Factors Affecting the Structure and Performance of High Energy Cathodes," Presented in *2013 US Drive meeting* held at ANL, Jan. 24, 2013, Chicago, IL.

# VI.B.9 Optimization of Ion Transport in High-Energy Composite Cathodes (UCSD)

**Ying Shirley Meng**
University of California San Diego

Department of Nanoengineering
9500 Gilman Dr. #0448
La Jolla, CA, 92093 – 0448
Phone: (858) 534-9553; Fax: (858) 534-9553
E-mail: shmeng@uced.edu

Start Date: October 2012
Projected End Date: September 2016

## Objectives

- Investigate the factors that affect and control Li ion transportation, transition metal (TM) migration and oxygen activity in the high-energy Li rich composite cathodes.
- Explore the relationship between electrochemistry, particle morphology, bulk compositions, and surface characteristics.
- Design new compositions for Li excess layered cathode materials that have optimum rate capability, reversible capacity and voltage stability.

## Technical Barriers

The low rate and poor voltage stability of high-energy Li rich composite cathodes.

## Technical Targets

- PHEV: 96 Wh/kg, 5,000 cycles; EV: 200 Wh/kg; 1,000 cycles (80% DoD)

## Accomplishments

- Identified dynamic structural changes and quantified voltage stability upon cycling.
- Identified at least two best Li rich layered candidate materials as focus samples.
- Demonstrated the chemical sensitivity and special resolution of the suite of surface characterization tools, including STEM/EELS, XPS and first principles computation modeling.

✧ ✧ ✧ ✧ ✧

## Introduction

Advanced diagnostics are essential to investigate performance-limiting processes in batteries. Li transport is significantly more complex in composite structures that locally integrate different crystal structures at the nano-scales. At these scales, interfaces separating different local crystal structures can play a significant role on Li transport, but precisely how is not at all understood. Some composite arrangements and spacings may promote significantly higher Li mobilities than others while some may suppress Li transport. Insights about the role of nano-scale modulations in crystal structure and chemistry are lacking but essential for the directed design of composite electrodes with significantly improved rate capabilities. Careful engineering of the surface (coating) and bulk compositions (substitution) of these nanostructured materials may lead to significant improvement on ion transport. The aim of this project is to combine a suite of diagnostic tools, including scanning transmission electron microscopy and electron energy loss spectroscopy, as well as first principles computation, to characterize new generation high-energy density lithium transition metal oxides and high capacity silicon carbon composites.

## Approach

The approach uniquely combines atomic resolution scanning transmission electron microscopy (a-STEM) & electron energy loss spectroscopy (EELS), X-ray photoelectron spectroscopy (XPS) and first principles computation to elucidate the dynamic changes in the bulk and surface of complex oxide materials during electrochemical cycling. A systematic study with powerful analytical tools is necessary to pin down surface coating mechanisms in order to determine the optimal surface characteristics of electrode materials for high rate and long life and to assist in the development of large scale synthesis methods for producing consistently high quality material.

## Results

**Materials.** Li-excess materials with and without Co substitution have been successfully synthesized using a co-precipitation method. Sol-gel, double hydroxide and carbonate syntheses routes were explored and it was found that the different secondary particle morphologies

and surface characteristics subsequently resulted in different electrochemical performances. The trials led to the conclusions that the double hydroxide method would be most suitable to consistently synthesize high quality samples for diagnostic efforts.
The electrochemical performance (i.e., discharge capacity and rate performance) of these materials has been optimized by changing the weight ratios between lithium and transitional metals as represented by the chemical formula, $xLi_2MnO_3 \bullet (1-x)LiMO_2$ (M=Ni, Mn, and Co). A typical rate profile for the optimized $Li_{1.2}Ni_{0.2}Mn_{0.6}O_2$ composition is provided in Figure VI - 45. When the sample was discharged at 2.0 C (1C = 250 mAh/g) between 2.0 V and 4.8 V, it could still provide a capacity of 170 mAh/g.

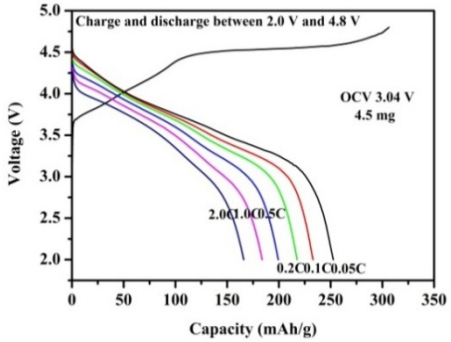


**Figure VI - 45: typical rate performance of sample $Li_{1.2}Ni_{0.2}Mn_{0.6}O_2$**

The effect that controlling $Li_{1.2}Ni_{0.2}Mn_{0.6}O_2$ sample morphology had on cyclic performance was studied. Figure VI - 46 compares the morphology of a pristine sample with no morphology control to that of a sample with morphology control. The morphologically controlled sample is composed of uniformly spherical particles with diameters in the range of 2–3µm. Although the spherical material initially exhibits a relatively smaller discharge capacity (Figure VI - 47) than the pristine sample, it cycles more stably. It was observed that morphology control improved capacity retention during cycling and partially prevented voltage fade.

**XPS and STEM/EELS diagnosis.** XPS and STEM/EELS were used to study the mechanism of voltage and capacity fade. The STEM for pristine and electrochemically cycled $Li_{1.2}Ni_{0.2}Mn_{0.6}O_2$ are shown in Figure VI - 48. After cycling, an amorphous 2–5 nm thick organic layer was observed on the surface of the material that might be related to the decomposition of electrolyte at high voltage. In addition, cation rearrangement at the surface of the particle formed a layer of the "defect spinel" phase and the amorphous outer layer was observed to increase in thickness upon further cycling.

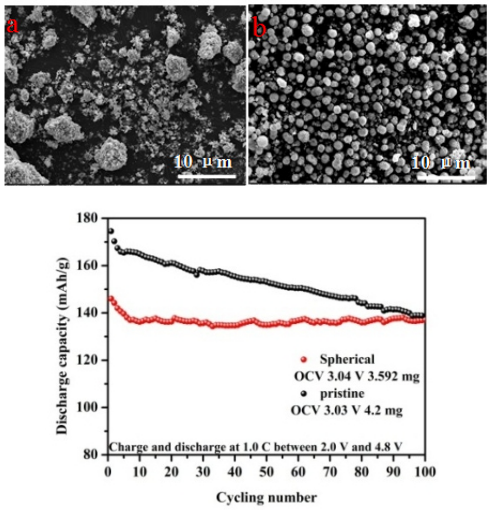


**Figure VI - 46: SEM images of $Li_{1.2}Ni_{0.2}Mn_{0.6}O_2$: (a) non spherical pristine material, and (b) homogenous spherical material, both prepared by a co-precipitation method**

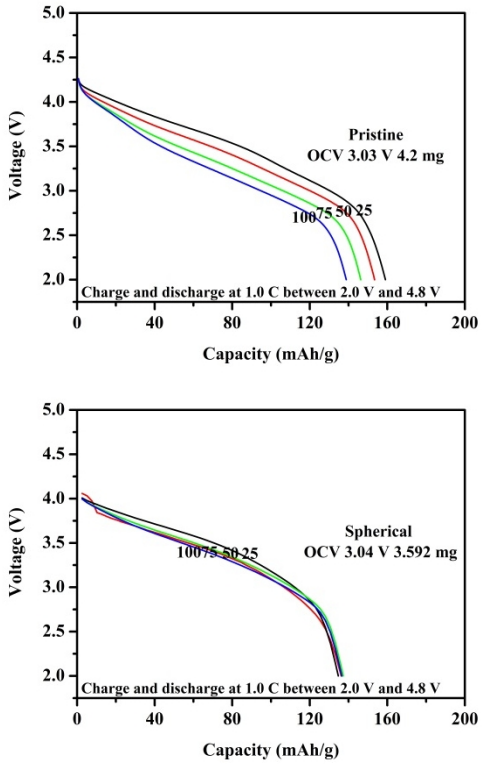


**Figure VI - 47: Comparison of cycling performance between $Li_{1.2}Ni_{0.2}Mn_{0.6}O_2$ samples with different morphologies**

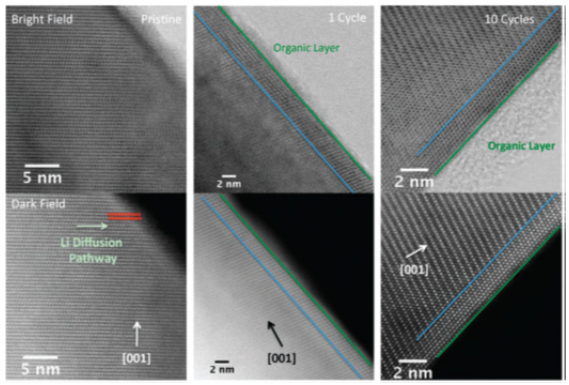


**Figure VI - 48: a-STEM images for pristine, one and ten times electrochemically cycled electrode materials with their corresponding High-Angle Annular Dark-Field (HAADF) images showing surface rearrangement occurring after cycling**

*Ex situ* surface XPS and EELS data is provided in Figure VI - 49, corresponding states of charge (SOC) are labeled A – H. In Figure VI - 49a, at SOC H, the oxygen signal did not fully recover to its original pristine state after one cycle (Figure VI - 49b). This indicated that the oxygen redox reaction was not fully reversible at the surface after the first electrochemical cycle. The XPS O1s region is provided in Figure VI - 49c. It was not until 4.45 V that the formation of a higher binding energy (535 eV) peak was observed. This peak may be associated with a superoxide species. The cause of the initial superoxide formation is believed to be the result of oxygen evolution and subsequent reaction with the electrolyte.

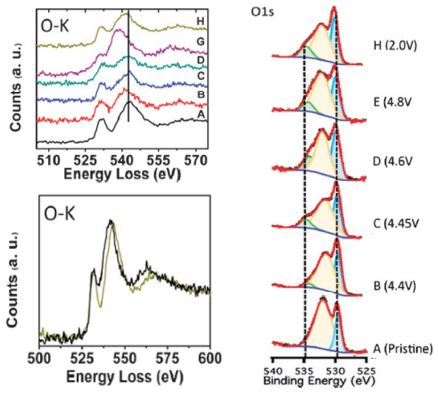


**Figure VI - 49: Surface EELS data for the (a) O–K edge spectra, (b) comparison of the pristine and the fully discharged O–K edge, and (c) XPS data for the O1s region**

The bulk EELS data are compared to the surface EELS results and are provided in Figure VI - 50. From SOC C to D, the ratio of the lower energy peak to the higher peak increased which may indicate the formation of oxygen vacancies. The ratio change may also be an indication of a local change to oxygen's local environment. After SOC C, the ratio of oxygen peaks remained constant. The ratio is larger than that for peaks in SOC A or B. A larger ratio may be a result of oxygen vacancy formation and a stronger bonding environment between oxygen and TM. The ratio shift was not reversible at the end of the first cycle.

In order to evaluate the effect of bulk substitution on the Li rich layered oxide, a series of samples with various substitutional elements were prepared. From XPS (Figure VI - 51a-b), the bonding energy shift of the Ni 3s peak identifies $Ni^{2+}/Ni^{4+}$ as the redox couple during cycling. During the 4.5V plateau region, both the Co 2p satellite relative area and the Ni 3s bonding energy results show that the oxidation states of surface Co and Ni were reduced and that oxygen vacancies may have been formed. After cycling, a defect spinel phase was visualized by high resolution STEM. Chemical differences can be identified from the EELS spectra. While the bulk spectra (red) has an oxygen pre-peak and indicates that Mn was not reduced, the oxygen pre-peak is absent in the surface spectra (blue) and surface Mn was reduced.

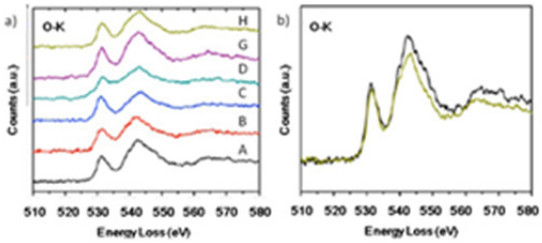


**Figure VI - 50: Bulk EELS data for the (a) O–K edge spectra, and (b) comparison of the pristine and the fully discharged O–K edge**

Based on the results above, the local environments of $Ni^{4+}$, $Mn^{4+}$, and O all simultaneously changed in the bulk and surface. Each may participate in charge compensation during the voltage plateau region, but some may not do so reversibly. Oxygen vacancies in the structure along with surface phase transformations are the two main hypotheses proposed to understand the voltage and capacity fading.

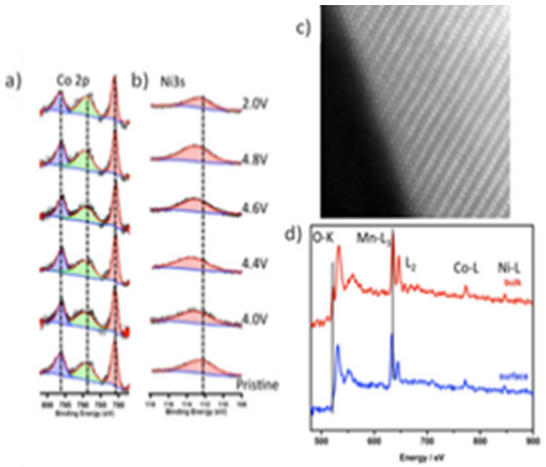


**Figure VI - 51: (a, b) XPS of surface transition metal ions oxidation status changes; (c) HRSTEM images of surface phase transformation; (d) EELS spectrum from cycled samples**

**Computational results --- oxygen vacancy assisted surface phase transformation.** From previous experimental results, it is understood that oxygen vacancies tend to form in the vicinity where phase transformation occurs. Thus, a computational study of oxygen evolution and transition metal migration barriers in Li-excess material were carried out using first principles with the Hubbard U correction on the generalized gradient approximation (GGA+U) to the density functional theory (DFT). A general trend of calculated oxygen vacancy formation energies ($E_{fov}$) versus lithium concentrations is shown in Figure VI - 52. The lithium concentration of these calculations ranges from 28/28 to 14/28. It is clear that $E_{fov}$ decreases sharply from ~2.7eV at fully lithiated state to less than 1eV for Li concentration between 20/28 to 14/28. Note that at Li concentration 10/14, the tetrahedral Li-Li dumbbells begin to form, leading to the possible formation of defect spinel phases. All the calculations were bulk calculations. In reality, it is easier to form oxygen vacancies at material surfaces or sub-surfaces than in bulk due to slow oxygen diffusion.

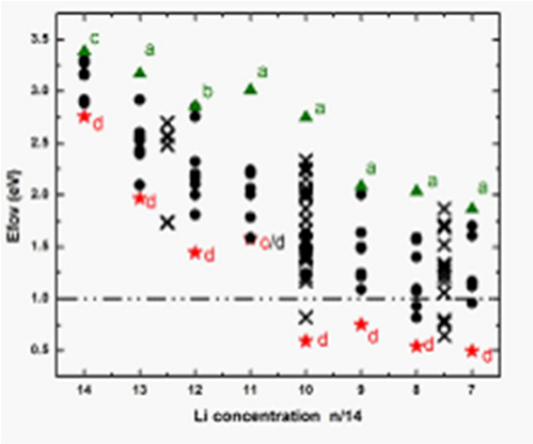


**Figure VI - 52: Oxygen formation energy at different Li concentrations**

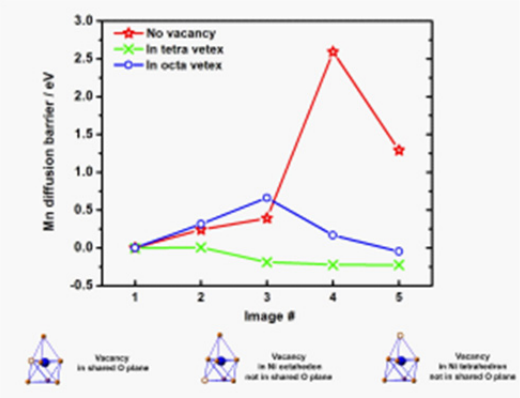


**Figure VI - 53: Mn diffusion barrier at Li concentration 20/28**

In order to investigate the migration mechanism of TM ions, the transition state theory is adopted in this work since it has been extensively utilized to describe the diffusion of cations in materials. Mn diffusion from an initial octahedral site in the TM layer to the nearest tetrahedral site in the Li layer was investigated at Li concentration $Li_{20/28}Ni_{1/4}Mn_{7/12}O_2$ where there is only one Li-Li tetrahedral dumbbell present in the cell. Oxygen vacancies, which are essential to the phase transformation process, start to form at a concentration of 20/28 in the presence of Li-Li dumbbells. Oxygen vacancies are located at three different positions in the Mn polyhedral site (shown in the footnote of Figure VI - 53): 1) in the shared oxygen plane between the octahedral site and tetrahedral site; 2) in the octahedral vertex but not in the shared oxygen plane; and 3) in the tetrahedral vertex but not in the shared oxygen plane. Although the exact values of Mn diffusion barriers are different for different configurations, the trend is consistent over all Li concentrations. Therefore results at lithium concentration 20/28 are discussed as the representative case. Figure VI - 53 shows the calculated Mn diffusion barriers at lithium concentration 20/28 with oxygen vacancies in two different locations. Generally speaking, the barrier to Mn diffusion can be reduced with the presence of an oxygen vacancy. Similarly, calculations were carried out to investigate the barrier to Ni diffusion, and it was found that the barrier can be lowered to 0.2-0.5eV by the presence of oxygen vacancies.

## Conclusions and Future Directions

Both pristine and spherically shape Li-excess materials have been successfully prepared by a co-precipitation method. These materials, which exhibit excellent rate performance and cycling performance were used as samples for advanced characterization. Based upon XPS and STEM/EELS work, two main hypotheses were proposed to understand the voltage and capacity fade. (1) Beginning at the voltage plateau region, the redox of oxygen was not fully reversible, leaving oxygen vacancies in the structure. (2) At the same time oxygen vacancies in the structure facilitate structural transformation on the surface during cycling. Additionally, a novel oxygen vacancy assisted TM diffusion mechanism is proposed for the first time to explain the near-surface phase transformation in lithium excess transition metal layered oxides. Formation of (dilute) oxygen vacancies and their roles in assisting transition metal ion diffusion were investigated using first principles calculation. In the presence of oxygen vacancies, the activation barriers for TM diffusion were drastically and consistently reduced in reasonable range for room temperature diffusion.

Using advanced characterization methods, the mechanisms of structural transformation and oxygen vacancy formation will be revealed. Various modification methods including metal doping, substitution, and surface coatings will be adopted to further improve the electrochemical performance of the $Li_{1.2}Ni_{0.2}Mn_{0.6}O_2$ Li-excess material.

## FY 2013 Publications/Presentations

1. K. J. Carroll, D. Qian, C. R. Fell, S. Calvin, G. M. Veith, M. Chi, L. Baggetto, Y. S. Meng, "Probing the electrode/electrolyte interface in the Li-excess material $Li_{1.2}Ni_{0.2}Mn_{0.6}O_2$," *Physical Chemistry Chemical Physics*, **15**, p11128-11138 (2013).
2. C. R. Fell, D. Qian, K. J. Carroll, M. Chi, J. L. Jones, Y. S. Meng, "Correlation between oxygen vacancy, microstrain, and cation distribution in Lithium-excess layered oxides during the first electrochemical cycle," *Chemistry of Materials*, **25**(9), p1621-1629 (2013).
3. D. Qian, B. Xu, M. F. Chi, and Y. S. Meng, "Uncovering the roles of oxygen vacancy on cation migration in lithium excess layered oxides," submitted and under review, 2013.

# VI.B.10 Novel Cathode Materials for High-Energy Lithium Batteries (UTA)

**Arumugam Manthiram**
University of Texas at Austin

Materials Science and Engineering Program
204 E. Dean Keeton Street, Mail Stop C2200
Austin, TX 78712
Phone: (512) 471-1791; Fax: (512) 475-8482
E-mail: manth@austin.utexas.edu

Start Date: October 2011
Projected End Date: September 2015

## Objectives

- Development of high-performance cathodes for lithium-ion batteries and a fundamental understanding of their structure-composition-performance relationships.
- Develop novel synthesis approaches for polyanion-containing cathodes such as phosphates and silicates that can offer high energy and good thermal stability.
  - Assess the factors controlling the voltages.
- Develop a fundamental understanding of the factors that control the electrochemical performances of the high-voltage spinel oxide cathodes and utilize the understanding to develop high-performance spinel compositions.
  - Assess the relative roles of morphology, cation ordering, and $Mn^{3+}$ content.

## Technical Barriers

Focusing on the cathode materials, this project addresses the following technical barriers in order for lithium-ion batteries to be employed for vehicle applications: cost, safety, cycle life, energy, and power.

## Technical Targets

- Realize high capacity through the reversible insertion/extraction of more than one lithium per transition-metal ™ ion in polyanion cathodes.
- Achieve long life and high rate with high-voltage spinel cathodes.
- Develop a fundamental understanding of the factors controlling the voltages of polyanion cathodes and the electrochemical performances of high-voltage spinel cathodes.

## Accomplishments

- Synthesis of three polymorphs of $LiVOPO_4$ by a novel microwave-assisted approach in various solvent mixtures of water and alcohols/glycols.
- Reversible extraction/insertion of more than one lithium per vanadium from/into $LiVOPO_4$.
- Optimization of the particle size of $LiVOPO_4$ by controlling the reaction time and reactant concentrations or by adding a surfactant.
- Synthesis of $Li_2MnSiO_4$ and $Li_2MnP_2O_7$ by novel template-assisted and microwave-assisted approaches.
- Accurate prediction of the voltages of polyanion cathodes based on coordination geometry and covalence of metal-oxygen bond.
- Understanding the relative roles of morphology and surface crystal planes on the electrochemical properties of high-voltage spinel cathodes in comparison to other factors.

✧ ✧ ✧ ✧ ✧

## Introduction

Cost, safety, energy, and power are the major issues that hamper the adoption of lithium-ion technology for vehicle applications. Accordingly, this project focuses on developing (i) polyanion cathodes that offer high energy while keeping the cost low and exhibiting good safety characteristics and (ii) high-voltage spinel cathodes that offer high energy and power. With polyanion cathodes, the project is specifically focused on phosphate and silicate cathodes that can facilitate the reversible extraction/insertion of more than one lithium ion per TM ion. On the other hand, the major issue in employing the high-voltage spinel is the capacity fade during cycling. Accordingly, this project is focused on understanding the relative roles of the various factors that control the electrochemical performances of $LiMn_{1.5}Ni_{0.5}O_4$ spinel cathodes: morphology, surface planes, cation ordering, $Mn^{3+}$ content, and surface reaction with electrolyte.

## Approach

Polyanion cathodes such as $LiVOPO_4$ and $Li_2MSiO_4$ (M = Mn, Fe, Co, and Ni) have the potential to cycle more than one lithium per TM ion. However, their practical capacities are limited due to the poor electronic and ionic conductivities. Synthesis and processing conditions play a critical role in realizing the full capacities of these polyanion cathodes. Accordingly, novel solution-based synthesis approaches such as microwave-assisted solvothermal and template-assisted methods that offer controlled morphologies and particle size are pursued to maximize the electrochemical performances. With the high-voltage spinel, a continuously stirred tank reactor and cation doping are utilized to obtain samples with different morphologies and surface compositions to achieve a better interface with the electrolyte. The synthesized samples are characterized by a variety of techniques including X-ray diffraction, electron microscopy (SEM, TEM, and STEM), X-ray photoelectron spectroscopy, time of flight – secondary ion mass spectroscopy, and in-depth electrochemical measurements. Based on the characterization data gathered, a fundamental understanding of the structure-composition-property-performance relationships is developed, which is then utilized to design better-performing cathodes.

## Results

**Phosphate cathodes.** Three polymorphs of $LiVOPO_4$ (α – triclinic, β – orthorhombic, and-$\alpha_1$– tetragonal) were synthesized by the microwave-assisted solvothermal process. In order to reduce the particle size, the α phase was synthesized in various solvent mixtures of water and alcohols/glycols (Figure VI - 54). The ratio of water to alcohols/glycols (3:1) was crucial to eliminate impurities at a 230°C synthesis temperature. Various solvent mixtures formed micro-flower morphology as seen in Figure VI - 54, with the smallest particle size achieved with the water/glycol mixtures.

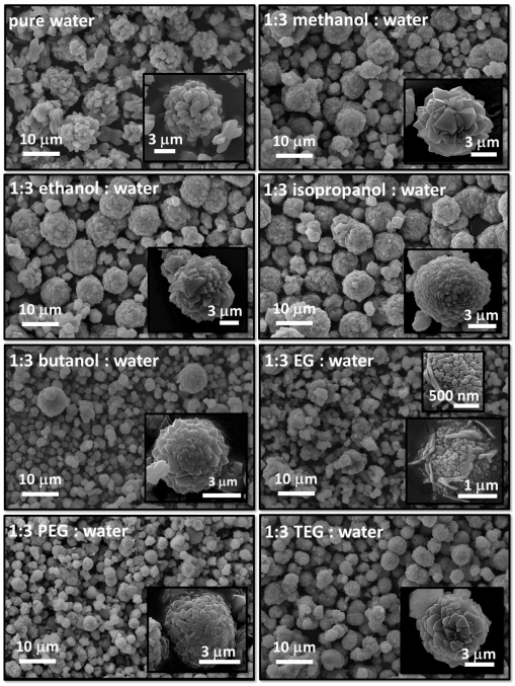


**Figure VI - 54: SEM of α-LiVOPO4 prepared in various mixed solvents at 230°C except that in water, which was held at 240°C**

Figure VI - 55 shows the electrochemical performance of each of the samples formed with the various solvent mixtures. The influence of the particle size can be seen as the highest capacities in the potential window of 3.0 – 4.5 V (indicated by dashed line in Figure VI - 55) were achieved with water/glycol mixtures, which had the smallest particle size. In addition, the importance of the solvent is apparent when comparing the electrochemical performances (Figure VI - 55) of samples with similar particle sizes. For example, the water/glycol and butanol/water samples have similar particle sizes, but the former exhibits better performance in the 3.0 – 4.5 V range. Likewise, the pure water and alcohol/water samples have similar particle sizes, but the latter exhibits a higher capacity.

The typical voltage range to cycle $LiVOPO_4$ is 3.0 and 4.5 V. Figure VI - 55 shows that by cycling to 2.0 V instead of 3.0 V, more than one lithium can be inserted/extracted by accessing the $V^{3+/4+}$ redox couple between 2.0 and 2.5 V. By increasing the voltage window, a discharge capacity of ~ 200 mAh/g was achieved.

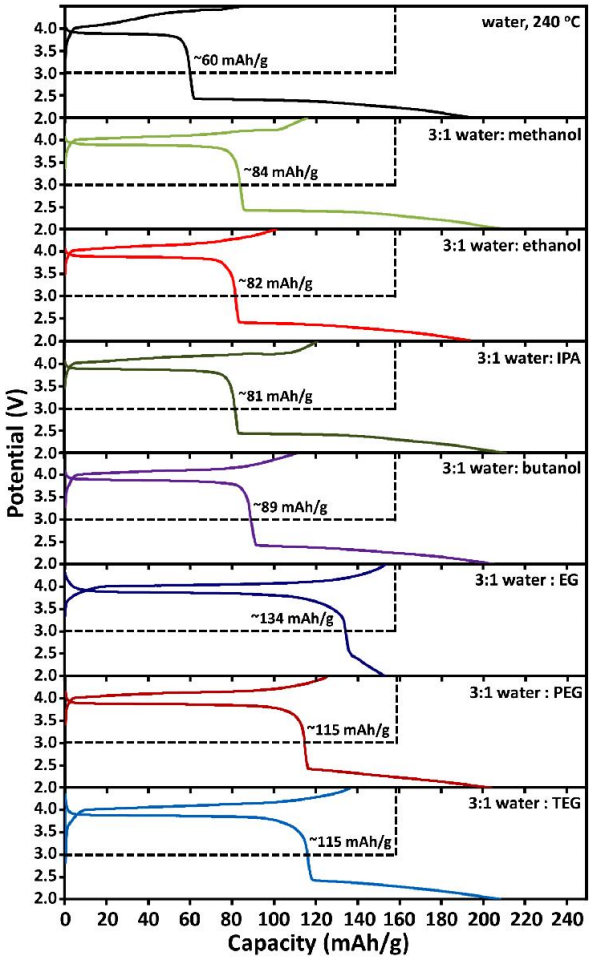


**Figure VI - 55: First charge−discharge profiles at a C/20 rate of α-LiVOPO4 prepared in various mixed solvents at 230°C except that in water, which was held at 240°C**

With a water to alcohol/glycol ratio of 3:1, we focused on optimizing the particle size further by controlling the reaction time and reactant concentrations as well as by adding cetyl trimethylammonium bromide (CTAB) to the precursor solution as shown in Figure VI - 56. Higher initial capacities were generally realized with smaller particle size when the cells were cycled in the potential window (3.0 – 4.5 V, shown by dashed box), as seen in Figure VI - 57 for the samples shown in Figure VI - 56. For instance, the initial capacity for the material with a 10 min. hold time (0.067 M in V, 0 mL CTAB) was ~ 115 mAh/g, while that for the material with a 45 min. hold time was ~ 72 mAh/g. The addition of CTAB helped to prevent particle growth and agglomeration and reduced particle size as seen in Figure VI - 56. The electrochemical performance was improved with the addition of an optimum amount of CTAB. For example, the first discharge capacity increased from ~ 82 mAh/g to ~ 124 mAh/g on going from 0 to 0.5 mL of CTAB, but decreased to ~ 90 mAh/g with further addition of CTAB (1 mL). The cycling performance was also improved by coating the particles with the conductive PEDOT:PSS.

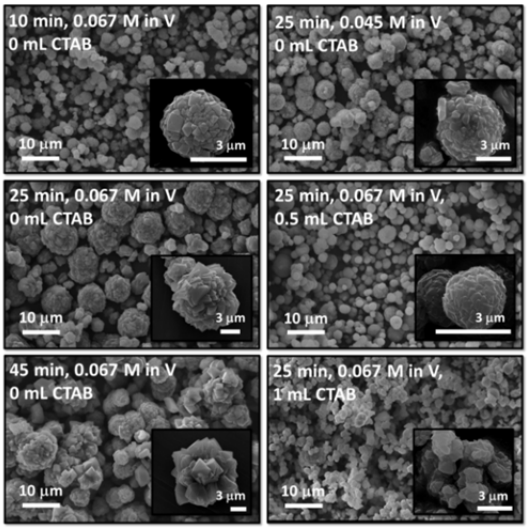


**Figure VI - 56: SEM of α-LiVOPO4 prepared with a water:ethanol ratio of 3:1 for the various indicated reaction hold times at 230°C (not including ~ 25 min ramp time to 230°C), V concentrations, and amounts of CTAB solution substituted for water**

$Li_2MnP_2O_7$ and $Li_2CoP_2O_7$ were also synthesized by the microwave-assisted solvothermal process, but their capacities were 90 – 100 mAh/g with the extraction of only 0.8 – 0.9 lithium due to a larger particle size (3 – 5 µm). Further work is needed on reducing the particle size.

**Silicate Cathodes.** $Li_2MnSiO_4$/C nanocomposite cathodes were synthesized with unique morphologies, employing poly(methyl methacrylate) (PMMA) crystals as a hard-template and the phenolic-resin polymer as the carbon source. The PMMA template decomposes to gaseous products at elevated temperatures during the synthesis without requiring any extra step to remove the template, unlike other hard-templates such as silica.

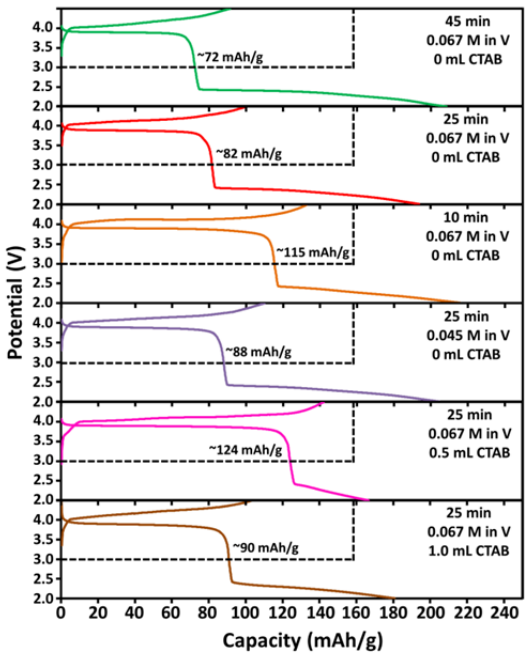


**Figure VI - 57: First charge-discharge curves at C/20 rate of α-LiVOPO$_4$ prepared with water:ethanol = 3:1 for various reaction hold times at 230°C, V concentrations, and amounts of CTAB solution substituted for water**

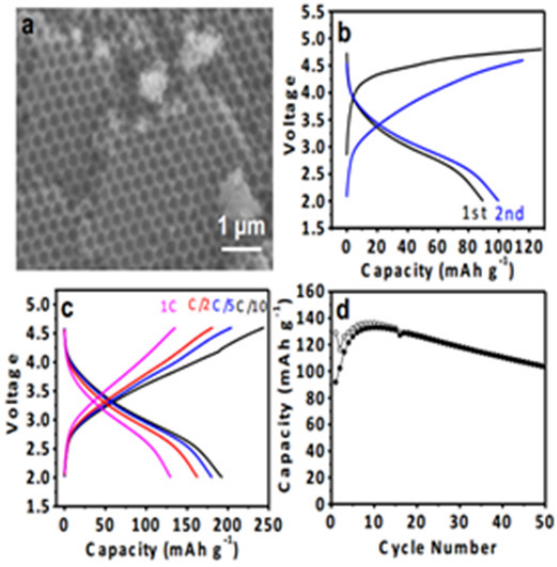


**Figure VI - 58: (a) SEM image, (b) first two charge-discharge profiles, (c) the highest capacity obtained at various rates, and (d) cycling performance at 1C rate of the Li2MnSiO4/C nanocomposite cathode material**

A long-range ordered macroporous structure resulted as seen in Figure VI - 58a due to the close-packed PMMA template. The first two charge-discharge profiles of $Li_2MnSiO_4$/C shown in Figure VI - 58b suggest a possible structural rearrangement during the first cycle. The sample exhibited a reversible capacity of ~ 200 mAh $g^{-1}$ (Figure VI - 58c) at 55°C corresponding to the extraction of 1.2 lithium per Mn. However, the cathode exhibited some capacity fade as seen in Figure VI - 58d (at a rate of 1C at 55°C) after an intial increase in capacity during the first 10 cycles. Also, $Li_2Fe_{0.9}Mn_{0.1}SiO_4$ was synthesized by a hydrothermal process at 200°C, followed by heating at 650°C, but the particle size was larger (~ 1 μm).

**Understanding the voltage variations in polyanion cathodes.** The voltage variations in polyanion cathodes have largely been explained in the past for isostructural materials. With an aim to develop a broader understanding, a crystal-chemical guide was provided for understanding how factors such as the crystal structure and covalency of the polyanion affect the M2+/3+ redox energies in polyanion cathodes having different structures. An accurate prediction of the voltage could be made based on how the coordination of the TM ion affects the covalency of the M-O bond. Additionally, a new method for assessing the covalency of the polyanion (beyond the electronegativity of the counter-cation) was presented and used to explain why the voltage delivered by Li2MP2O7 cathodes is higher than that of LiMPO4 for a given M. A comparison of the silicate and phosphate structures revealed that edge sharing between transition-metal polyhedra and other cation polyhedra has an opposite effect on the voltage delivered by these materials. It was also shown that crystal-field theory alone is not sufficient to explain the voltages of polyanion cathodes, demonstrating the necessity of considering the structural effects to fully understand the voltage trends.

**High-voltage spinel cathodes.** In order to achieve consistent performance with the high-voltage spinel cathode $LiMn_{1.5}Ni_{0.5}O_4$, a deeper understanding of the relationship among cation ordering, impurities, and particle morphology was developed. Careful chemical, structural, and electrochemical characterizations of $LiMn_{1.5}Ni_{0.5}O_4$ cathodes prepared by different methods with varying morphologies and degrees of cation ordering revealed that although an increase in the degree of cation ordering decreases the rate capability, the crystallographic planes in contact with the electrolyte have a dominant effect on the electrochemical properties. For instance, samples with octahedral morphology and {111} surface planes exhibit superior cyclability and high rate capability compared to samples with truncated {100} planes. Furthermore, doping with small amounts of certain cations was found to stabilize {111} surface planes as they segregate to the surface.

## Conclusions and Future Directions

Reversible extraction of more than one lithium per TM ion has been demonstrated with α-$LiVOPO_4$

(triclinic) and $Li_2MnSiO_4$ by employing novel synthesis approaches to control the particle size and morphology. With these polyanion cathodes, synthesis medium, reaction time, reactant concentration, and addition of surfactant were all found to play a role in controlling the morphology and particle size. Also, an accurate prediction of the voltages of the polyanion cathodes could be made based on how the coordination of the TM ion affects the covalency of the M-O bond. With the high-voltage spinel, investigation revealed that morphology and surface planes play a dominant role in controlling the performance compared to other parameters.

Future work is focused on (i) improving the performance of $LiVOPO_4$ through further tuning of the synthesis, (ii) whether or not $LiMnPO_4$ and $LiCoPO_4$ can be aliovalently doped with $V^{3+}$ and determining the doping effect on electrochemical performance, and (iii) microwave-assisted synthesis of carbonophosphates.

## FY 2013 Publications/Presentations


1. "Stabilized Spinel and Polyanion Cathodes," *DOE Annual Peer Review Meeting*, May 13-17, 2013, Washington, DC.
2. K. Chemelewski, D.W. Shin, W. Li, and A. Manthiram, "Octahedral and Truncated High-voltage Spinel Cathodes: Role of Morphology and Surface Planes on Electrochemical Properties," *Journal of Materials Chemistry,* **1**, 3347-3354 (2013).
3. K.L. Harrison and A. Manthiram, "Microwave-assisted Solvothermal Synthesis and Characterization of Various Polymorphs of $LiVOPO_4$," *Chemistry of Materials,* **25**, 1751–1760 (2013).
4. B. Pei, Z. Jiang, W. Zhang, Z. Yang, and A. Manthiram, "Nanostructured $Li_3V_2(PO_4)_3$ Cathode Supported on Reduced Graphene Oxide for Lithium-ion Batteries," *Journal of Power Sources,* **239**, 475 - 482 (2013).
5. Gutierrez and A. Manthiram, "Understanding the Effects of Cationic and Anionic Substitutions in Spinel Cathodes of Lithium-ion Batteries," *Journal of the Electrochemical Society,* **160**, A901 - A905 (2013).
6. K.R. Chemelewski and A. Manthiram, "Origin of Site Disorder and Oxygen Non-stoichiometry in $LiMn_{1.5}Ni_{0.5-x}M_xO_4$ (M = Cu and Zn) Cathodes with Divalent Dopant Ions," *Journal of Physical Chemistry C*, **117**, 12465 – 12471 (2013).
7. K.R. Chemelewski, E.-S. Lee, W. Li, and A. Manthiram, "Factors Influencing the Electrochemical Properties of High-voltage Spinel Cathodes: Relative Impact of Morphology and Cation Ordering," *Chemistry of Materials,* **25**, 2890 – 2897 (2013).

# VI.C Anode Development

## VI.C.1 Novel Anode Materials (ANL)

**Jack Vaughey**
Argonne National Laboratory

Chemical Sciences and Engineering
Building 205
9700 S Cass Avenue
Lemont, IL, 60439
Phone: (630) 252-8885; Fax: (630) 252-4176
E-mail: vaughey@anl.gov

Start Date: October 2010
Projected End Date: September 2014

### Objectives

- Design electrode architectures containing main group metal, metalloid or intermetallic components that can tolerate the volumetric expansion of the materials and provide an acceptable cycle life.
- Exploit electrochemical deposition reactions to improve the design and performance of silicon-based electrodes
- Develop methods to assess the internal changes within the electrode on cycling as a tool to improve performance.

### Technical Barriers

There are several technical barriers to the utilization of silicon as an electrode material for lithium-ion batteries – notably its high volume expansion on lithiation, reactivity with its environment, and a large kinetic resistance to lithiation are all obstacles that must be addressed before silicon can be considered as a replacement electrode material for graphitic carbons. These barriers include:

- Low energy
- Poor low temperature operation
- Abuse tolerance limitations

### Technical Targets

- 142 Wh/kg, 317 W/kg (PHEV 40 mile requirement)
- Cycle life: 5,000 cycles
- Calendar life: 15 years

### Accomplishments

- Utilized a combined synthesis, impedance spectroscopy, and MAS-NMR study to determine the types of functional groups that are at the silicon-electrolyte interface and how they can be changed as a function of synthesis.
- Discovered a new synthetic variable in the electrodeposition of electrochemically active silicon that allows some control over the crystallinity and functionality of the materials deposited.
- With Advanced Photon Source (APS) beamline scientists, micro-CT X-Ray tomography was utilized on a complex multicomponent silicon electrode to assess the role of cycling on the free space and the silicon particle size. Utilizing an element sensitive analysis technique, it was possible to differentiate the elements involved and 'see' the SEI layer grow to fill the electrode void space on cycling.
- Interactions with the EFRC – Center for Electrical Energy Storage - *Tailored Interfaces* (Argonne-Northwestern University-University of Illinois, Urbana-Champaign, were continued around the micro CT tomography effort.

✧ ✧ ✧ ✧ ✧

### Introduction

Elemental silicon has been considered the heir apparent for graphitic carbon as the negative electrode in lithium-ion batteries for many years. Among the possible main group elements with high theoretical capacities, silicon has the highest gravimetric capacity and, when combined with its high availability and low cost, it is a very desirable electrode material. Because it does not work by intercalation, it can store significantly higher energy than graphite (372 mAh/g, 818 mAh/ml), and insert lithium only a few hundred millivolts above the potential of metallic lithium. However, the limited internal void volume translates to a significant expansion on reaction and insertion of lithium as the constituent Si atoms complete their p-orbitals and become much larger anions. Although this expansion among other kinetic issues presently limits its utility, the

high potential payoff associated has made silicon a focus for the BATT-Anode program.

A major objective of our research is to understand how a silicon electrode interacts with its cell environment and how these interactions can be controlled to increase cycle life and limit capacity fade. Initial work focused on designing microporous copper host architectures that could be used to 1) simplify the lithium-ion battery electrode by combining requirements for a binder, and conductive additive and extending the current collector into the active phase, and 2) provide a sufficiently large void volume to accommodate the volumetric expansion that occurs during charging. Utilizing these electrode designs, it is possible to create a combined synthetic -diagnostic effort to understand and adapt the excellent cycling performance seen for deposited silicon electrodes to the commercially utilized laminated electrodes. Specifically, the role of synthesis on the active surface of silicon, the interfacial region with the electrolyte, and role of electrode porosity has been studied to improve the electrochemical performance of silicon-based electrodes.

## Approach

Utilizing silicon electrodeposition as a synthetic tool, the amount of silicon, its morphology, and crystallinity can be controlled to create samples that are amenable to spectroscopic studies. These electrode materials can then be evaluated to determine how their composition and surfaces interact with the electrolyte on cycling leading to capacity fade via degradation reactions. In addition, element specific microtomography techniques have been developed at the APS, to study how the electrodes are changing internally as a function of cycling.

## Results

**Tomography**. One of the biggest issues for silicon based electrodes when incorporated into lithium-ion batteries is the effect the volume expansion of the silicon has on the surrounding electrode structure. This expansion has dramatic effects on both the ability of the binder to maintain good contact with the particles and the ability to maintain good electrical contact throughout the electrode. Previous efforts (e.g., Liu, et al., *ACS Nano*, **2012**, 6(2) 1522–1531) have shown that there exists a critical particle size for silicon particles. Above approximately 150 nm, the particles are unable to withstand the stress of lithiation and degrade. Below this number they are stable.

X-Ray tomographic studies of silicon electrodes to evaluate the role of cycling on silicon particles greater than 150 nm have continued. Because most binders require the secondary particles to be on the micron scale, a standard 70% active Si/PVdF/acetylene black (AB) electrode was evaluated to establish how the particle breakdown is absorbed. The electrode was evaluated before cycling and again after 20 cycles (vs Li and with Gen2 electrolyte, [1.2 M $LiPF_6$ in EC/EMC 3:7 weight ratio]). In Figure VI - 59, the element sensitive X-Ray tomography data is shown. In Figure VI - 59a, the silicon within the electrode is shown before cycling with a typical particle size (primary) of ~20 µm. In Figure VI - 59b, the pulverization due to repeated cycling is evident with the largest particle size now in the 300-500 nm range. Additionally, another electrode level event evident in this series of experiments was the overall expansion of the entire electrode from 60 µm to 160 µm. In Figure VI - 60a, the initial pre-cycled electrode is shown, with the void volume highlighted. In Figure VI - 60b, the compactness and even distribution of pores has been altered, in part to take into account the formation (and continuous growth) of SEI within the sample. In these electrodes it can be seen that the volume expansion of the silicon has multiple effects on its surroundings, including pulverization leading to poor connectivity to the current collector, and gross changes in volume from SEI formation and inclusion within the voids of the electrodes. The effect of the void filling on performance over time is under investigation as it is probably tied to electrolyte starvation effects and capacity fade.

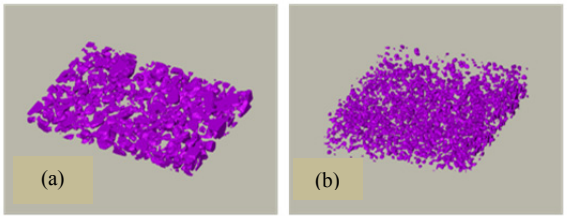


**Figure VI - 59: (a) a Si electrode of average particle size of 20 µm before cycling, (b) the same electrode after 20 cycles (vs Li)**

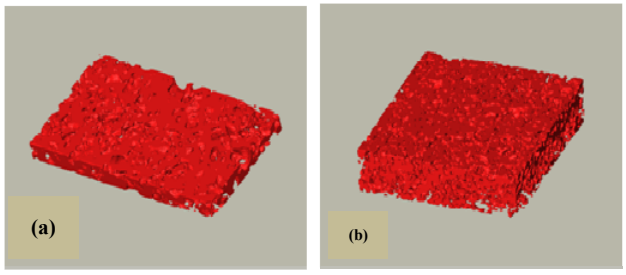


**Figure VI - 60: (a) the void volume within a Si electrode of average particle size of 20 µm before cycling, (b) the same electrode after 20 cycles (vs Li)**

**Synthesis**. In support of the goal of understanding how elemental silicon interacts with its electrochemical

cell environment, the deposition of electrochemically active elements (elemental Si or Sn) into a three-dimensional metallic foam structures was explored. This design allows us to control the amount of active material precisely while maintaining some electrode porosity. Utilizing two different porosity foam structures, the role of deposition method on morphology and cycling for a Sn on Cu three dimensional electrode was investigated. Tin was chosen as an active material initially because its air stability allows for electrode optimization outside a controlled atmosphere drybox. Previous electrodeposition work had focused on the effect of synthesis and film morphology on cycling. Testing concluded that the smoother films had more stable cycling performance. This was attributed to a variety of factors including lower surface area and possibly less of the high reactivity crystal facets being exposed to the electrolyte (Kostecki, et al., *Electrochem Comm*, 2011).

Initially an electro-less deposition process was used, optimized industrially for Sn deposition, as it has rapid turnaround and does not have 'line-of-sight' requirements.

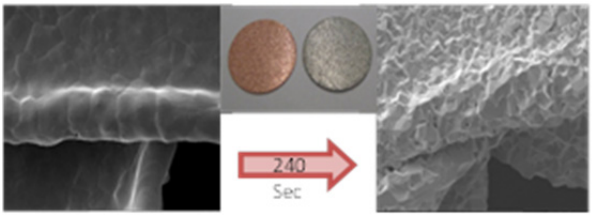


**Figure VI - 61: SEM images from the electro-less deposition of metallic Sn from a commercial plating bath on a copper-foam. Total deposition time was 240 seconds**

In Figure VI - 61, utilizing a commercial plating process, a copper substrate with tin was even coated. XRD analysis of the annealed samples at temperatures above 100°C indicated alloying to form $Cu_xSn$ phases. Of particular note is the conformal nature of the deposition throughout the substrate, a trait identified earlier as beneficial to extended cycle life. Cycling of the films showed typical capacities and plateaus expected for a tin-based anode.

Once the deposition properties of the metal foams had been established, the effort to silicon films was extended. Electrodeposition was reverted to when no electroless deposition process equivalent was reported. For silicon, silicon tetrachloride was utilized as our Si source and a supporting electrolyte of tetra-alkyl ammonium salts in propylene carbonate (PC) was used. Because a synthetic process based on electrochemical deposition is an inherently complex method, several variables were changed and we assessed the products formed and their electrochemical properties. Interestingly, it was observed that the counter-cation in the supporting electrolyte salt played a significant role on the surface chemistry and crystallinity of the silicon product. Specifically, significant changes in first cycle irreversible capacity and overall half-cell capacity were noted when supporting salts were changed.

The cycling data are shown in Figure VI - 62a and highlights the performance when using tetraethyl ammonium chloride (TEACl) as the supporting salt. The cell showed > 2000 cycles. Although both samples were synthesized and tested under the same conditions it is evident from the electrochemical curves and powder X-Ray diffraction, the measured mAh/g and >99.7% cycling efficiency over the first 125 studies, are all consistent with the deposited Si film (on Cu foam) being amorphous. Figure VI - 62b shows a similar film in terms of quantity of silicon deposited using the larger tetrabutyl ammonium chloride (TBACl) as the supporting electrolyte salt, but immediate differences, including fade rate and overall capacity are noticeable. In addition, the electrochemical curves and powder X-Ray diffraction studies are consistent with the deposited Si film (on Cu foam) being semi-crystalline.

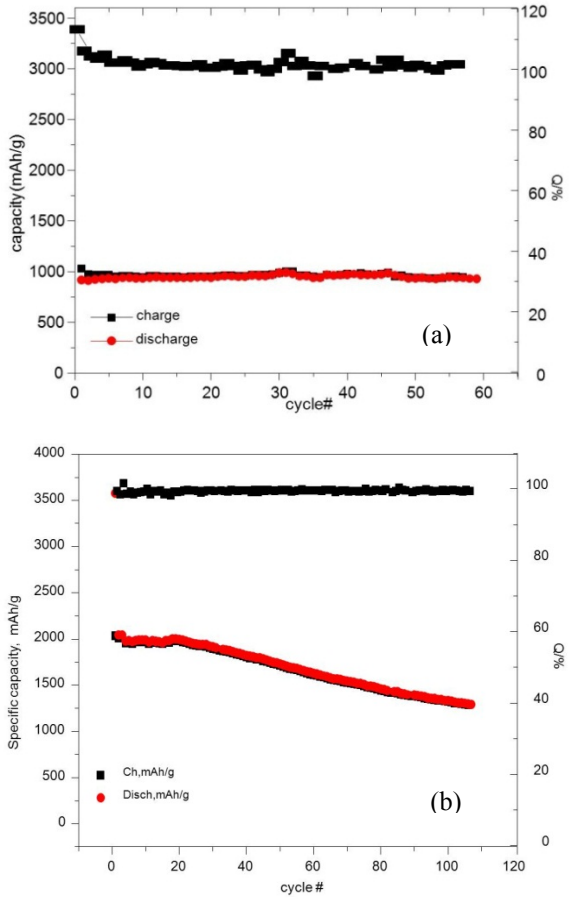


**Figure VI - 62: Cycling performance of a Si film on Cu using (a) TEACl as supporting electrolyte salt and (b) using TBACl as the supporting electrolyte salt**

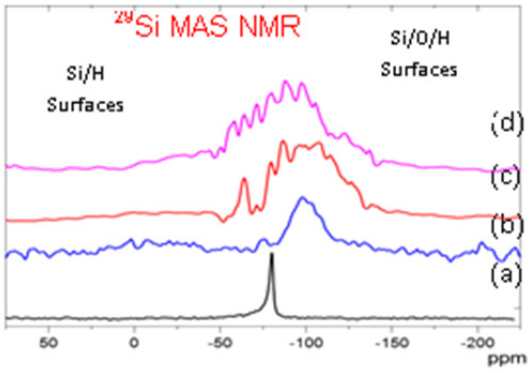


**Figure VI - 63: $^{29}$Si NMR data collected from four different types of samples is shown. Specifically, the samples are (a) uncycled bulk silicon, (b) an oxidized sample ($SiO_2$), (c) TBACl supporting electrolyte, (d) TEACl supporting electrolyte**

Utilizing spectroscopic techniques that are more surface sensitive, several differences between the samples have been identified. While XRD analysis of the bulk samples showed some particle size and crystallinity differences, the surfaces were very different. In Figure VI - 63, $^{29}$Si NMR data collected from four different types of samples is shown. Specifically, the samples are (a) uncycled bulk silicon, (b) an oxidized sample ($SiO_2$), and the two samples from the different deposition baths. From these *ex situ* experiments, the more crystalline TBACl sample electrodeposited with more oxygen as its passivation layer while the amorphous TEACl-derived sample had a passivation layer more consistent with a hydride/protonated surface. Although the exact reason why such similar cations yield such different results has yet to be determined, it has been pointed out in the electrolyte literature that the coordination requirements of the larger cations significantly reduce the availability of free solvent molecules. Such behavior has been associated with increases in ion-pairing and viscosity which may affect the deposition process.

These types of differences have implications on how the material interacts with electrolyte solvents and how the silicon attaches to binders. Since many binders are designed to work with a specific surface functionality, the ability to vary that functionality may extend electrode lifetimes.

## Conclusions and Future Directions

During these studies, the role of interfaces in silicon electrodes has been examined and the results have been extrapolated to identify underlying mechanisms that cause capacity fade and poor coulombic efficiency. Building on our initial work to design high capacity carbon-free electrodes to allow clearer interpretation of spectroscopic data, and electrodeposition as a synthetic tool to control the amount of active silicon and its surface functionality, spectroscopic tools were developed that helped identify the relationship between functionality and synthesis and how the interfaces of these electrodes with the electrolyte controls cycling performance, e.g., SEI growth and electrode side reactions. This effort has been done in tandem with an effort to develop elemental specific micro-CT as a diagnostic tool to evaluate SEI growth and electrode porosity. Future work will focus on:

- Devising model systems in conjunction with the BATT-Anode teams that better describe the surfaces and materials present in a working electrode.
- Utilizing tools, such as MAS-NMR, to understand the underlying surface-electrolyte reactions and propose strategies that decrease the losses associated with various side reactions.
- Tomography experiments on BATT-Anode baseline electrodes will be completed to compare the results to other standard electrodes and identify differences in performance related to their cycling history.

## FY 2013 Publications/Presentations

1. J.T. Vaughey, L. Trahey, F. Dogan "Novel Anode Materials: Three Dimensional Architectures," *DOE Hydrogen Program and Vehicle Technologies Program Annual Merit Review*, May 2013, Washington, DC.
2. Joyce, L. Trahey, S. Bauer, F. Dogan, J. T. Vaughey "Copper Metal Binders: the Copper-Silicon System," *J. Electrochem. Soc*., **159**, A909 (2012).
3. Fulya Dogan, Christopher Joyce, John T. Vaughey "Formation of New Silicon Local Environments upon Annealing for Silicon Anodes: A $^{29}$Si Solid State NMR Study," *J. Electrochem. Soc*, **160**, A312 (2013).
4. Lynn Trahey, Fikile R. Brushett, Zhenzhen Yang, Xianghui Xiao, Michael M. Thackeray, John T. Vaughey "Microbalance and Microtomographic Analysis of Rechargeable Battery Electrodes," *SEM 2013 Annual Conference & Exposition on Experimental and Applied Mechanics*, June 2013, Lombard, IL.
5. Dogan, D. Sanjeewa, L. Trahey, J. Vaughey "Three-Dimensional Silicon Anode Architectures via Electrodeposition on Copper Foam Current Collectors," *224$^{th}$ Meeting of the Electrochemical Society*, October 2013, San Francisco, CA.

# VI.C.2 Metal-Based High Capacity Li-Ion Anodes (Binghamton U.)

**M. Stanley Whittingham**
Binghamton University

Department of Chemistry and Materials
Vestal Parway East
Binghamton, NY 13902-6000
Phone: (607) 777-4623; Fax: (607) 777-4623
E-mail: stanwhit@binghamton.edu

Start Date: October 2010
Projected End Date: September 2014

## Objectives

- Replace the presently used carbon anodes:
  - With safer materials that will be compatible with lower-cost layered oxide and phosphate cathodes and the associated electrolyte.
  - With materials having higher volumetric energy densities, twice that of carbon.

## Technical Barriers

This project addresses the following technical barriers facing the use of lithium-ion batteries in PHEV and all-electric vehicles:

- Materials and manufacturing cost of lithium-ion batteries
- Safety of lithium-ion batteries
- Volumetric capacity limitations of lithium-ion batteries

## Technical Targets

- Determine the reaction mechanism of the nano-Sn-Fe-C system.
- Identify the cause of the first cycle excess lithium capacity and propose approaches to mitigate it.
- Identify an anode candidate having an energy density of 2 Ah/cm$^3$ for at least 100 cycles.
- Determine the electrochemistry of the leached nano-silicon material, and compare to the standard silicon.

## Accomplishments

- Several key steps in the reaction mechanism of the nano-Sn-Fe-C system have been identified. Carbon plays several key roles, including a protective covering for the active tin components and is electrochemically active contributing to the reversible capacity.
- Several causes for the excess capacity have been identified. These include reaction of the titanium oxides giving lithium titanium oxides, which are not delithiated in the charging regime used. In addition, irreversible reactions with the carbon also contribute. Some of the reaction may also be associated with SEI formation.
- The nano-Sn-Fe-C system has been identified as having the potential to double the volumetric capacity of carbon, to date for at least 50 cycles. The nano $Sn_5Fe$ phase was not found to be a suitable candidate.
- The electrochemistry of the leached nano-silicon has been determined, and compared with two samples from commercial companies. Its behavior falls between the two standard materials.

✧ ✧ ✧ ✧ ✧

## Introduction

Achieving the DOE cost and energy/power density targets will require improved anode materials that have higher volumetric energy densities than carbon, and have lower cost production methods. At the same time the material must have higher lithium diffusion rates than carbon and preferably be at a slightly higher potential to improve the safety. Replacing the present carbon anode with a Si or Sn based composite will increase the overall cell capacity.

## Approach

The anode approach is to synthesize, characterize and develop inexpensive materials that have higher volumetric energy densities than carbon. Emphasis is being placed on simple metal alloys/composites at the nano-size. The initial focus is being placed on tin, building on what we learnt from our studies of the tin-cobalt anode, the only commercial anode besides carbon. All materials will be evaluated electrochemically in a variety of cell configurations, and for thermal, kinetic and structural stability to gain an understanding of their behavior. Ideally these will have a potential slightly higher than that of carbon and above

that of pure lithium, so as to minimize risk of Li plating and thus enhance safety, whilst allowing for rapid charging.

## Results

**Reaction Mechanism of the Nano-Sn-Fe-C System.** The reaction mechanism of nano-sized Sn-Fe-C anode materials has been studied by X-ray absorption spectroscopy (XAS), which reveals it is a conversion reaction that converts tin and $Sn_2Fe$ to Li-Sn alloys. *Ex situ* samples prepared at different lithiation and delithiation states were tested. As shown in Figure VI - 64 (top) and (bottom), an obvious absorption edge energy shift can be found in the Sn K-edge X-ray absorption near edge structures (XANES), which means the oxidation state of Sn undergoes a substantial change during the lithiation/delithiation process. The XAS study of pure Sn during lithiation/delithiation is underway in order to compare and get further information of this structure evolution.

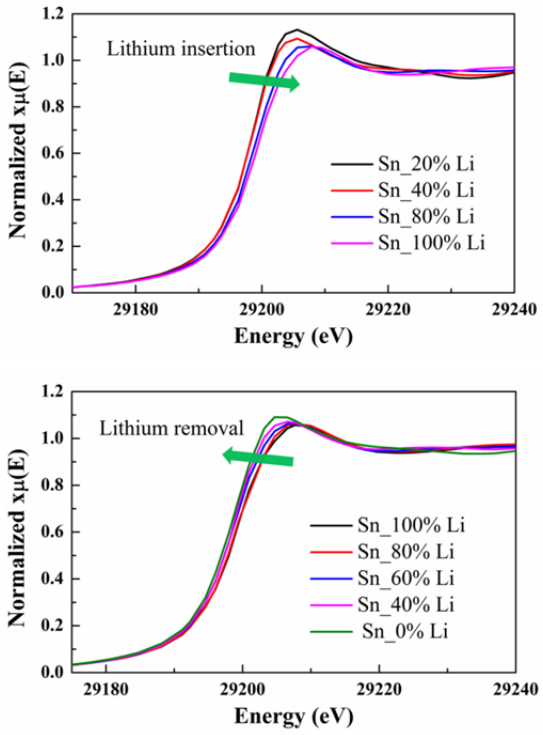


**Figure VI - 64: Sn K-edge XANES for different (top) lithiation states and (bottom) delithiation states of nano-sized Sn-Fe-C**

**First Cycle Excess Li Capacity.** The first cycle excess capacity of this material is mainly due to the formation of $LiC_2$ from the carbon; this carbon contributes significantly to the overall capacity. In addition, the existence of titanium oxides may also contribute to the first cycle excess capacity, since the lithium titanium oxide formed in the first discharge is not reversible at the charging potentials used. Further investigation is in progress to mitigate this excess capacity, including decreasing the amount of carbon and titanium used. There is close collaboration between these studies on tin and those of the BATT team on silicon, which has very similar issues.

**Identification of Anode Candidate.** The nano-Sn-Fe-C composite has been synthesized by two different techniques: mechanochemical and solvothermal. These are showing some quite different characteristics. For the mechanochemically synthesized nano-sized Sn-Fe-C anode materials it was found that Ti serves better than Al as the reducing agent for the SnO, and hard iron balls work better than soft ones. The mechanochemical reaction time is another key parameter. The XRD patterns, in Figure VI - 65 (top), show that as the reaction time increases, all the tin is converted to $Sn_2Fe$; further grinding leads to Fe metal impurities. Optimum electrochemical behavior, as shown in Figure VI - 65 (bottom), is found for 10 h reaction time, where there is still residual tin metal. Capacity retention is very good after the first few cycles.

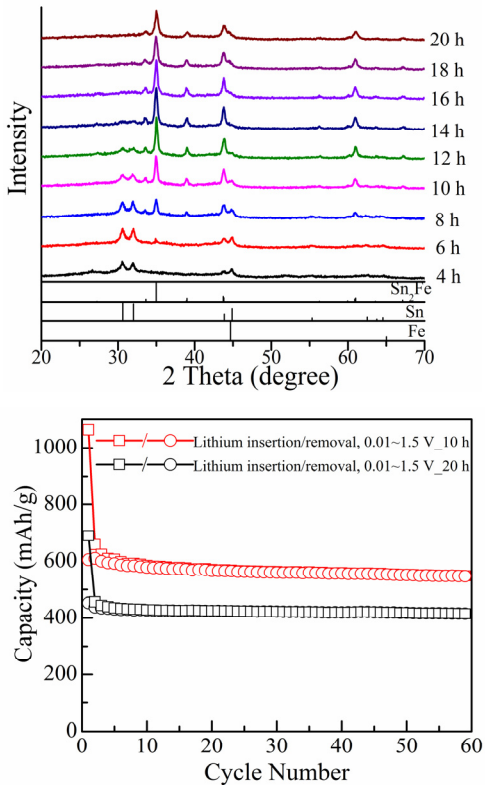


**Figure VI - 65: (Top) XRD patterns and (bottom) cycling performance of nanosized Sn-Fe-C materials**

A study of the electrochemical performances of nano-$Sn_5Fe$ material provided by our collaborators at Brookhaven National Laboratory showed that an increase in the Sn content, from $Sn_2Fe$ to $Sn_5Fe$, reduces both cyclability and rate capability (Figure VI - 66).

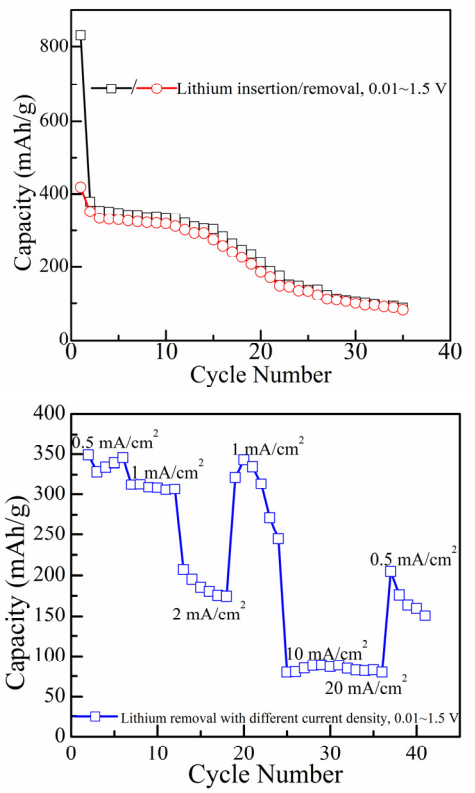


**Figure VI - 66: (Top) Electrochemical cycling and (bottom) rate capability of nano-$Sn_5Fe$**

$Sn_2Fe$ materials were also synthesized by the solvothermal method. When the initial molar ratio of Sn: Fe is increased (e.g., from 2:1 to 10:1), the product is a mixture of $Sn/Sn_2Fe$ instead of pure $Sn_2Fe$ as shown in Figure VI - 67. The capacity retention was found to fall dramatically on cycling when excess tin was present. Even for the pure $Sn_2Fe$ material the capacity faded much more rapidly than the mechanochemical $Sn_2Fe$ composite.

**Leached Nano-Silicon.** Nano-silicon anode materials have been synthesized through a novel etching approach with low-cost eutectic Al-Si alloy as the precursor. An in-depth study of the structure using Rietveld refinement of the XRD data yields a lattice parameter of a = 5.45(3) Å, V = 162.06 (6) $Å^3$ for this nano-silicon, which is larger than the standard silicon (a = 5.43Å, V = 160.15 $Å^3$), suggesting possibly a minor dissolution of other atoms in this nano-silicon material. This observation is consistent with Energy Dispersive X-ray spectroscopy (EDS) mapping, which shows that there is around 5 wt. % Al uniformly distributed in the nano-silicon particles.

The electrochemistry of leached nano-silicon has been determined, Figure VI - 68; the initial results are promising and have now been published (#3). A comparative study has been carried out on the leached nano-silicon, standard silicon and another company's silicon sample. The testing protocol is: 0.12 mA (~C/40) for the first cycle, followed by 0.5 mA (~C/10) for the remaining cycles over the potential range 0.01 V to 2 V. Among these silicon materials, the leached nano-silicon possesses a good capacity stability, which attains 1350 mAh/g after 18 cycles and is still growing. The standard silicon has a high capacity up to 2,300 mAh/g but it fades gradually. The company provided silicon behaves similarly with a capacity of 1,250 mAh/g after 17 cycles.

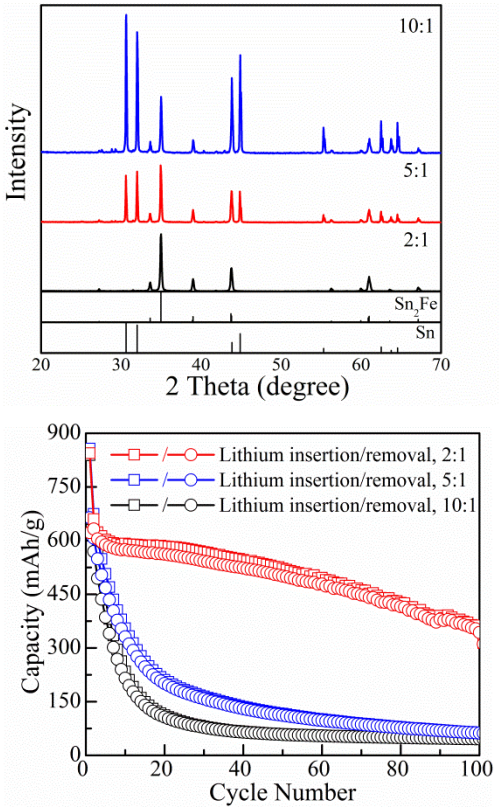


**Figure VI - 67: (top) XRD patterns and (bottom) electrochemical performance of $Sn_2Fe$ materials synthesized by the solvothermal method with different initial molar ratios of Sn:Fe**

## Conclusions and Future Directions

**Nano-Tin.** The excellent electrochemical behavior of nano-$Sn_2Fe$ has been determined, and this anode is equal to the SONY Sn-Co-C anode in capacity and rate capability. It is in a position to double the volumetric capacity of carbon. Two synthesis methods are being explored with the mechanochemical approach giving the better material, but the solvothermal approach being more amenable to scale-up. The synthesis methods will be optimized. For the mechanochemical approach, a viable source of iron for scale-up that maintains the nano-size needs to be found. In addition, the optimum

carbon and titanium content needs to be determined. For the solvothermal method, the tin metal and oxide impurity need to be eliminated and the electrochemical capacity needs increasing. A GO/NOGO decision will be made on the solvothermal approach in mid-2014. In both cases the first cycle excess capacity needs reducing. To do this a better understanding of the reaction mechanism will be achieved.

**Nano-Silicon.** Nano-silicon has been formed by two different methods - leaching an Al-Si alloy has a unique morphology and the preliminary results look promising. It was found that this contains about 5 at% Al in the Si. Nano-silicon was also formed from SiO by magnesium reduction; it had a lower capacity than the Si-Al alloy, so most effort will be placed on the former. The future effort on the nano-Si will emphasize reducing the first cycle loss and improving the cycling performance.

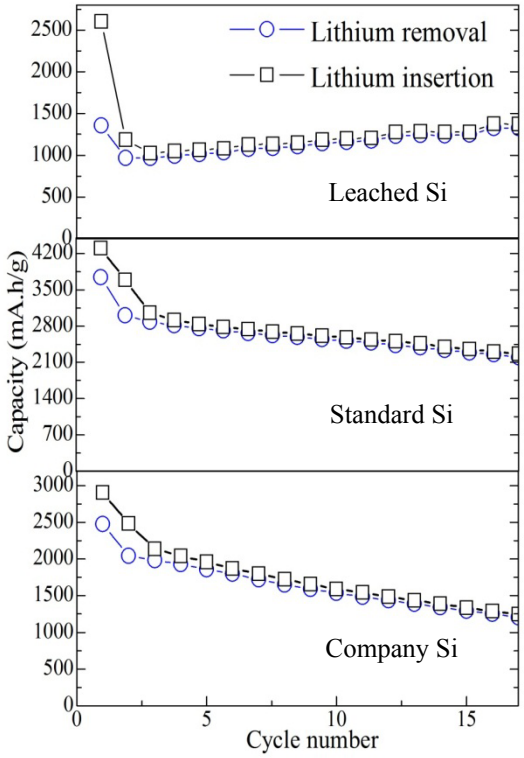


**Figure VI - 68: Electrochemical Performance of (top) leached nano-silicon, (middle) standard silicon, and (bottom) another company's silicon**

## FY 2013 Publications/Presentations

1. "Metal-Based, High-Capacity Lithium-Ion Anodes," *DOE Annual Peer Review Meeting*, May 13-17, 2013, Washington, DC.
2. 2013 DOE-BATT Anode focused Meeting presentation, May 16, 2013, Washington, DC.
3. Wenchao Zhou, Tianchan Jiang, Hui Zhou, Yuxuan Wang, Jiye Fang and M. Stanley Whittingham, "The nanostructure of the Si-Al eutectic and its use in lithium batteries," *MRS Communications*, **3**, 119-121 (2013).
4. M. Stanley Whittingham, "What are the Materials Limitations to Intercalation Batteries," *2013 KAUST,* September 25, 2013, Thuwal, Saudi Arabia.
5. W. Zhou, Z. Dong, H. Yang, F. Omenya, R. Zhang, N. A. Chernova and M. S. Whittingham, "Enhancing the Electrochemical Cycling of Si-carbon Anode with Electrolyte Additives for Lithium-ion Batteries," *Materials Research Society*, November 2012, Boston.
6. R. Zhang, W. Zhou, J., H. Zhou, Z. Dong, X. Hong and M. S. Whittingham, "Sn-Fe-C Composites as Anode Materials for Rechargeable Lithium-ion Batteries," *Materials Research Society*, November 2012, Boston.

# VI.C.3 New Layered Nanolaminates for Use in Lithium Battery Anodes (Drexel U.)

**Yury Gogotsi**
Drexel University

Department of Materials Science and Engineering
3141 Chestnut Street
Philadelphia, PA 19104
Phone: (215) 895-6446; Fax: (215) 895-1934
E-mail: gogotsi@drexel.edu

**Michel W. Barsoum (Co-PI)**
Drexel University
Department of Materials Science and Engineering
3141 Chestnut Street
Philadelphia, PA 19104
Phone: (215) 895-2338; Fax: (215) 895-6760
E-mail: barsoumw@drexel.edu

Start Date: October 2010
Projected End Date: September 2014

## Objectives

- Replace graphite with a new material selected from a group of layered (two-dimensional) binary carbides and nitrides known as MXenes, which may offer combined advantages of graphite and Si anodes with a higher capacity than the former, less expansion, longer cycle life and a lower cost than the latter.

## Technical Barriers

This project aims to address the following technical barriers facing modern lithium-ion battery (LIB) technology:

(A) short life-span of modern batteries,

(B) low charge density, and

(C) compromised safety.

## Technical Targets

- Perform the a*b initio* simulation of Li incorporation into MAX phase carbides.
- Screen electrochemical experiments on a variety of MAX phases to select the most promising ones for more detailed study.
- Study the effect of particle size on the capacity of the three best materials.
- Improve capacity by selective extraction of A atoms, to add space for the Li.
- Investigate solid electrolyte interface (SEI) formation on selected carbides.
- Optimize the material. Testing the rate capability of the anode.
- *In situ* study of charge/discharge processes and better understanding of the mechanisms of Li insertion.
- Compare powder *vs.* solids with 10-20% porosity.

## Accomplishments

- Discovered and synthesized four new materials showing potential for battery anode applications.
- Achieved reversible volumetric capacities of 820 mAh/cm$^3$ at a 1C cycling rate and 220 mAh.cm$^{-3}$ at 36C for additive-free delaminated $Ti_3C_2$ that cannot be achieved with commercial graphite electrodes.
- Conducted electrochemical testing of three new MXenes with different compositions ($Nb_2C$, $V_2C$, and $Mo_2C$) in LIBs.
- Completed a study of the effect of different binders on the performance of MXenes in Li-ion batteries.
- Achieved reversible areal capacities for additive-free $Nb_2C$ that are higher than what was reported for Si, the baseline electrode under the same conditions.

✧ ✧ ✧ ✧ ✧

## Introduction

In FY 2011 a new family of two-dimensional materials was discovered, and labeled MXenes. In FY 2012 several MXenes (such as $Ti_3C_2$, $Ti_2C$, $Ti_3(C_{0.5}N_{0.5})_2$, and $Ta_4C_3$) were successfully produced by selectively etching Al from corresponding MAX phases. As a result, it was shown that MXenes are, in fact, a family of 2-D transition metal carbides and carbonitrides with excellent potential as anode material in LIBs. In FY 2013 the main focus was on selection of the most promising MXenes for LIBs and their

optimization to maximize $Li^+$ uptake. In particular, the effect of binder additive on MXene anode performance was investigated. *In situ* study of charge/discharge processes was carried out for better understanding of the mechanism of Li insertion in order to improve the material further. The focus also shifted to lighter MXenes of $M_2X$ formulae and *additive-free* anodes.

## Approach

Since at this time the relationship between capacity and MXene phase chemistry is unknown, a rapid screening of as many MXene phases as possible is being carried out to determine the most promising chemistry, by testing their performance in LIBs. This work will also be guided by *ab initio* calculations.

## Results

**Exfoliated $Ti_3C_2$-Based anodes for LIBs**. To increase Li uptake and life-time of the anodes, the effect of different binders (polyvinylidene fluoride, poly(ethylene oxide), and alginate) on the performance of anodes was studied. $Ti_3C_2$ was used as the active material and representative for all MXenes. The carbon additive-free $Ti_3C_2$ anode with 10 wt. % of various binders delivered > 150 $mAh.g^{-1}$ at a C/3 rate after more than 50 cycles (Figure VI - 69). The increase in specific capacity was attributed to the increase in conductivity, confirmed by EIS results; the lowest charge transfer resistance ($R_{CT}$) (not shown) was obtained for a $Ti_3C_2$ with 10 wt. % alginate electrode. Combining both alginate and previously reported onion-like carbon (OLC) as the best binder and carbon additive, respectively, should result in the best performance, but it is challenging, since hydrophobic OLC does not disperse easily in alginate.

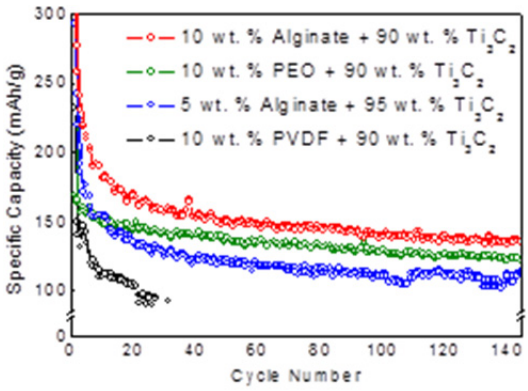


**Figure VI - 69: Effect of different binders on the capacity of exfoliated $Ti_3C_2$.**

To understand the physical changes that occur in the anodes during charging and discharging, an *in situ* dilatometric study was carried out. $Ti_3C_2$ with 10 wt.% PVDF and 10% carbon black was used as an anode. As shown in Figure VI - 70, during the first lithiation cycle, the expansion in electrode thickness, $\Delta H_{Li}/H_o$, where $H_o$ was the initial height of the electrode, was around 7%. After around 20 cycles, $\Delta H_{Li}/H_o$ was < 1%. The change in $\Delta H_{\text{delithiation}}/\Delta H_{lithiatio}$ was in a good agreement with the coulombic efficiency results (not shown). *Ex situ* XRD, however, after lithiation, showed a 21.5% increase in *c* lattice parameter during the first cycle (*c*-LP), $\Delta c_{Li}/c_o$ where $c_o$ is the *c*-LP prior to lithiation. The difference between the latter and the 7% expansion electrodes thickness can be attributed to the fact that the electrode was porous and accommodated expansion of the particles. Expansion of the MXenes upon lithiation presumably only occurs along [0001].

Furthermore, when the irreversibility of the first cycle, as measured by $\Delta H_{\text{delithiation}}/\Delta H_{lithiation}$, was compared to that estimated by comparing $\Delta c_{delithiation}/\Delta c_{Li}$, excellent agreement was found. In other words, most of the 1st cycle irreversibility is due to Li trapped between the MXene layers. More work is ongoing to further understand the lithiation and delithiation mechanisms and to minimize the 1st cycle irreversibility, e.g., by prelithiation.

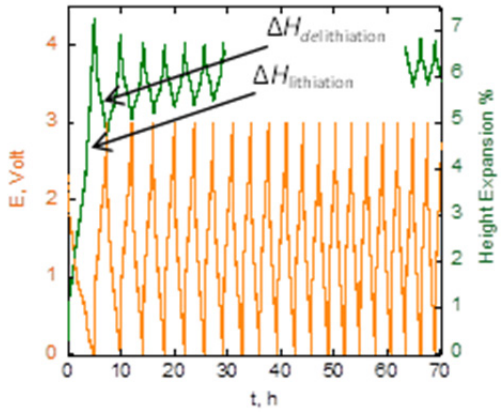


**Figure VI - 70: *In situ* dilatometry results for exfoliated $Ti_3C_2$: electrode expansion %, and voltage during lithiation and delithiation**

**Delaminated $Ti_3C_2$-Based anodes for LIBs.** In order to achieve the highest accessibility for Li and to make additives-free MXene electrodes, the possibility of layers separation by chemical intercalation and delamination was investigated. It was found that some organic compounds, such as hydrazine monohydrate, dimethylformamide, urea, dimethylsulfoxide (DMSO), can be inserted between the $Ti_3C_2$ sheets resulting in expansion along [0001]. This was confirmed by the shift of the major (0002) XRD peak to lower 2θ values. The intercalant molecules could also be de-intercalated by drying at higher temperatures, signifying that the intercalation process is reversible.

Intercalation of DMSO in $Ti_3C_2$ resulted in the largest downshift of the (0002) peak position among all intercalated composites. Further sonication of aqueous solution of DMSO intercalated material led to the delamination of $Ti_3C_2$ single flakes. By filtering the sonicated colloidal solution though a membrane, the flakes formed binder-free films or "paper" (see inset in Figure VI - 71). The volumetric capacity of the paper was 820 mAh/cm$^3$ at 1C and 220 mAh/cm$^3$ at 36C (Figure VI - 71). Such values cannot be achieved with commercial graphite electrodes. Overall, the capacity of the delaminated material was a factor of 4 higher than that of as-synthesized MXene.

**The lightest MXenes ($M_2X$) as anodes for LIBs.** In principle, $M_2X$ MXenes should have 50% higher $Li^+$ capacities as compared to their $M_3X_2$ counterpart. For this reason $Nb_2C$ and $V_2C$ were synthesized by etching Al from $Nb_2AlC$ and $V_2AlC$, respectively, and tested as electrodes for LIBs.

Cycling of $Nb_2C$ anode at 1 C yields a first cycle capacity of ~ 422 mAh/g. After 100 cycles, a reversible capacity of 170 mAh/g was obtained. Reasons for the first cycle irreversibility include SEI formation or irreversible reactions of Li with the surface groups and water molecules in the as-synthesized MXenes. The irreversibility could be minimized by controlling the surface MXene chemistry or by prelithiating the electrode material. Similarly, the first cycle capacity for $V_2C$ at 1 C was found to be ~380 mAh/g; the reversible capacity was ~ 210 mAh/g.

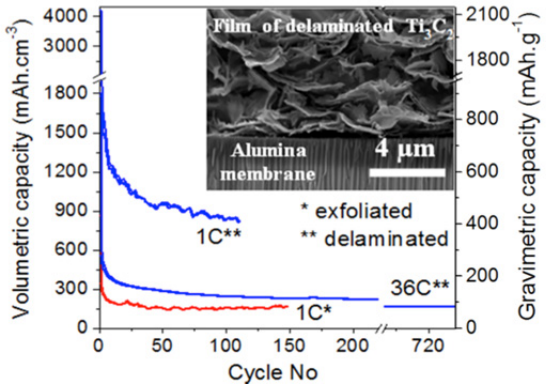


**Figure VI - 71: Volumetric and gravimetric capacities of exfoliated and delaminated $Ti_3C_2$. Inset shows SEM image of an additive-free film of delaminated $Ti_3C_2$ filtered through the membrane**

Intriguingly, the $V_2C$, produced from etching attrition milled $V_2AlC$ powders, showed > 30 % enhancement in Li uptake (Figure VI - 72) compared to $V_2C$ produced from un-milled $V_2AlC$. This can be explained by the decreased particle size, facilitating Li diffusion between the layers. A reversible capacity of 280 mAh/g was obtained instead of 210 mAh/g at the same cycling rate of 1 C.

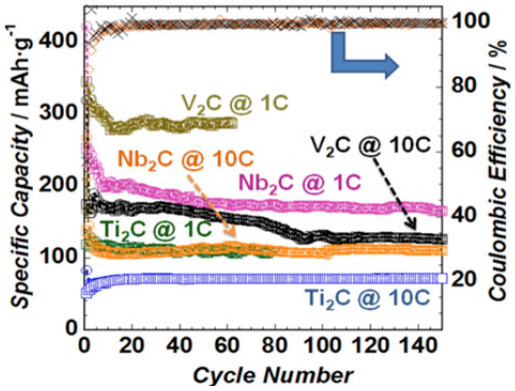


**Figure VI - 72: Electrochemical performance of $Nb_2C$ and $V_2C$ (produced by HF treatment of attrition milled $V_2AlC$) compared to what was reported previously for $Ti_2C$**

It was also observed that > 2/3 of the reversible lithiation capacity for $Nb_2C$ was below 1 V. Conversely, in the case of $V_2C$, less than 1/2 of the reversible lithiation capacity was < 1 V and more than 2/3 of the delithiation capacity of $V_2C$ was at voltages > 1.5 V. This was an important finding since it showed that each MXene had its own active voltage window. With the variety of possible MXene chemistries, selection of an optimum MXene for a required voltage window can in principle be achieved. Said otherwise, some MXenes could function better as anodes, while others could, in principle, be used as cathodes allowing for the construction in principle of an all MXene-Li-ion battery.

Figure VI - 72 further shows that capacities of 110 mAh/g for $Nb_2C$ and 125 mAh/g for $V_2C$ were obtained after 150 cycles at 10 C. These values were ≈ 50 % higher than what was reported previously for $Ti_2C$, at the same rate, and closer to the capacities obtained at 1 C. The coulombic efficiency was about 99.6% for $Nb_2C$ at 10 C. For $V_2C$ it varied between 98% and 100%.

To increase the areal capacity, $Nb_2C$ MXene powders were cold pressed into 300 µm free-standing discs without any additives under 1 GPa at room temperature (Figure VI - 73a) and tested as an anode material using the testing conditions suggested by the BATT Anode team leaders: viz. cycling between 5 mV and 1.0 V, using a lithiation current of 0.5 mA/cm$^2$ and delithiation current of 0.75 mA/cm$^2$. The areal capacity *vs.* cycle number obtained using the aforementioned conditions is shown in Figure VI - 73b for two different cells with different loadings (cell I loading was 94 mg.cm$^{-2}$; cell II loading was 136 mg.cm$^{-2}$). A reversible capacity of 3.3 mAh.cm$^{-2}$ was obtained after 60 cycles for cell I, this value is more than double that reported for the Si baseline electrode after 20 cycles tested using the same conditions. By increasing the loading to 136 mg.cm$^{-2}$, a reversible areal capacity of 7 mAh.cm$^{-2}$ was obtained after 11 cycles (cycling is still ongoing for cell II). The latter value is 5 times higher than what was reported for the Si baseline electrode after 11 cycles.

The ratio of the areal capacity for the two cells after the same number of cycles was 7:4.6 which is close to the loading ratio for the two cells: 136:94. This suggests that even higher loadings can be achieved to further increase the areal capacity without deteriorating electrode performance, a crucial consideration for practical applications. More recently a new MXene, $Mo_2C$, was synthesized from a Mo-containing MAX phase. To date the conversion process is incomplete. Etching resulted in a sample that contained only ~ 17 wt. % $Mo_2C$. Despite this low conversion, this sample exhibited a reversible capacity of 70 mAh/g after more than 500 cycles at 1C. Since in this case the unreacted MAX phase is electro-chemically inactive, the 70 mAh/g achieved was the contribution of only 17% of the electrode mass. It follows that the specific capacity of $Mo_2C$ exceeds 400 mAh/g at 1C even before delamination. Work is ongoing to make pure $Mo_2C$ and delaminate it.

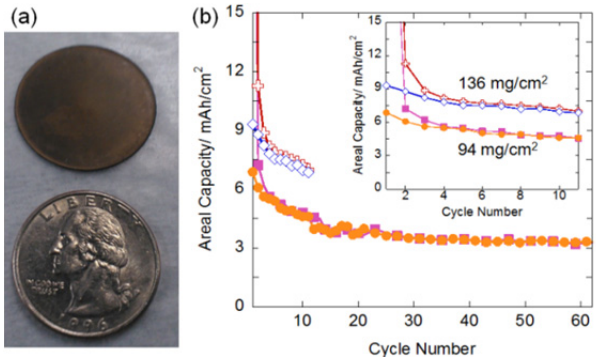


**Figure VI - 73: a) Free-standing additive-free $Nb_2C$ MXene disc. b) Areal capacity vs. cycle number for pressed additives-free $Nb_2C$. Inset zooms in on the first 11 cycles for cells with two different loadings squares and crosses are for lithiation capacities, while the circles and diamonds are for delithiation capacities for two discs with loadings of 94 and 136 mg/cm², respectively**

## Conclusions and Future Directions

During FY 2013, all our milestones were reached. The effect of binder on the performance of exfoliated $Ti_3C_2$ in LIBs was studied. The alginate was found to be the best binder showing specific capacity higher than 150 mAh/g at a C/3 rate after more than 50 cycles.

A number of chemical compounds were shown to be able to intercalate into MXene structures leading to its expansion and delamination. Totally *additive free* anodes made with delaminated $Ti_3C_2$ showed good reversible specific capacities at high rates (820 mAh/cm³ at 1C, and 220 mAh/cm³ at 36C) that cannot be achieved with graphite electrodes.

Three new MXene members ($Nb_2C$, $V_2C$ and $Mo_2C$) were synthesized by HF treatment of MAX phases at room temperature. $Nb_2C$ and $V_2C$ showed specific capacities of 110 mAh/g and 125 mAh/g, respectively, obtained at a 10 C cycling rate after 150 cycles. Reversible areal capacities of 3.3 mAh/cm² and 7 mAh/cm² were obtained after 60 and 11 cycles for cells of 94 and 136 mg/cm² loading, respectively. These values are 4 times higher than what was reported for the Si baseline electrode after the same number of cycles or less using the same conditions. $Mo_2C$ exhibited a reversible capacity of 70 mAh/g after more than 500 cycles at 1C.

It was also confirmed that the first cycle irreversibility is due to Li trapped between the MXene layers. More work is needed for complete understanding of the mechanisms involved in order to minimize it.

Future research will focus on reducing the first cycle irreversibility, doubling the areal capacity, further increasing gravimetric and volumetric capacities, and reducing the production cost of the MAX phases (the material from which MXenes are made). First, all *in situ* and *ex situ* studies of the lithiation and delithiation of MXenes will be finished in order to determine the most promising materials. To solve the first cycle irreversibility problem, chemical modification (purification) and chemical pre-lithiation will be used. Further investigation will focus on optimization and modification of the material manufacturing process to enable large-volume, low-cost production followed by optimization of the MXene electrodes to achieve a reversible areal capacity of larger than 5 mAh.cm$^{-2}$ at higher current densities.

## FY 2013 Publications/Invited Presentations

1. Naguib, M. *et al.*, "New Two-Dimensional Niobium and Vanadium Carbides as Promising Materials for Li-ion Batteries," *Journal of the American Chemical Society* (2013). DOI: 10.1021/ja405735d.
2. Naguib, M. *et al.*, "*MXenes*: A New Family of Two-Dimensional Materials," *Advanced Materials* (2013). DOI: 10.1002/adma.201304138. **Invited Paper.**
3. Lukatskaya, M.R. *et al.*, "Cation Intercalation and High Volumetric Capacitance of Two-dimensional Titanium Carbide," *Science,* **341** (6153), 1502 (2013).
4. Mashtalir, O. *et al.*, "Intercalation and Delamination of Layered Carbides and Carbonitrides," *Nature Communications,* **4**, 1716-1722 (2013).
5. Ruvinskiy, P. *et al.*, "Nano-Silicon Containing Composite Graphitic Anodes with Improved Cycling Stability for Application in High Energy

Lithium-Ion Batteries," *ECS Journal of Solid State Science and Technology*, **2** (10), M3028-M3033 (2013).

6. Mashtalir, O. *et al.*, "Kinetics of Aluminum Extraction from $Ti_3AlC_2$ in Hydrofluoric Acid," *Materials Chemistry and Physics,* **139** (1), 147-152 (2013)1.
7. N. Lane, *et al*. "Correlation Effects and Spin-orbit Interactions in Two-dimensional Hexagonal 5d Transition Metal Carbides, $Ta_{n+1}C_n$ (n = 1; 2; 3)," *European Physics Letters*, 57004 (2013).
8. "New Layered Nanolaminates for Use in Lithium Battery Anodes," *DOE Annual Peer Review Meeting*, May 13-17, 2013, Washington, DC.
9. Plenary (luncheon) presentation, International Materials Research Congress (IMRS 2013), Mexico.
10. Plenary lecture, International Conference on Advanced Capacitors (ICAC 2013), Osaka, Japan.
11. Invited talk, "Flatlands beyond Graphene," Bremen, Germany.
12. Invited talk, *37th International Conf. & Expo on Advanced Ceramics and Composites*, Daytona, FL
13. Invited talk, *Workshop at the Argonne National Lab*, Argonne, IL.
14. Invited talk, *1st International Workshop on Energy Storage at KAUST*, Saudi Arabia.
15. Invited talk, *The Minerals, Metals & Materials Society (TMS 2013)*.
16. Invited talk, *MRS* Spring Meeting 2013, Boston.
17. Invited talk, "NOVAMaking Stuff: Faster Innovation Café," *World Café Live*, Philadelphia.
18. Invited talk, *Materials Science & Technology (MS&T 2013)*, Montreal, Canada.
19. Invited talk, *Royal Swedish Academy of Engineering Sciences*, October 2013, Stockholm, Sweden.

# VI.C.4 A Combined Experimental and Modeling Approach for the Design of High Current Efficiency Si Electrodes (GM)

**Dr. Xingcheng Xiao**
General Motors LLC

Research and Development
Warren, MI 48090
Phone: (586) 947-0187
E-mail: Xingcheng.xiao@gm.com

**Dr. Yue Qi**
Michigan State University
Department of Chem. Eng. and Mat. Sci.
Engineering Building
428 S. Shaw Lane
East Lansing, MI 48824
Phone: (517) 432-1243
E-mail: yueqi@egr.msu.edu

Start Date: October 2012
Projected End Date: September 2016

## Objectives

- Combine modeling and experimental approaches to understand, design, and fabricate stabilized nano-structured Si anode with high capacity and high coulombic efficiency.

## Technical Barriers

The real challenges to developing a model that allows us to design high current efficiency Si electrodes with electrochemically and mechanically stable artificial SEI layer are: a) poor understanding of SEI failure mechanisms; b) lack of accurate mechanical properties of the SEI; and c) difficulty in validation of the model. All of these are due to the extreme challenges associated with characterizing the properties of nm thin SEI layer on lithiated Si in real battery systems. Therefore, we will first address these questions based on simpler thin film electrodes.

## Technical Targets

- Fundamentally understand the mechanical degradation of SEI (including artificial coatings) on Si electrode.
- Establish a correlation between the capacity loss (or current efficiency) and mechanical degradation of SEI on Si.
- Develop a multi-scale model to predict the stress/strain in the SEI layer on Si.
- Predict and measure the basic material properties required in the mechanics model.
- Use the model to guide the design of nanostructured Si electrode.
- Ultimately assist USABC to achieve its goal on EV energy storage: 200 Wh/kg (EV requirement); 96 Wh/kg, 316 W/kg, 5,000 cycles (PHEV 40 mile requirement). Calendar life: 15 years and improved abuse tolerance.

## Accomplishments

- Correlated the Young's modulus (E) of amorphous $Al_2O_3$ coatings with its density (which can be controlled by ALD deposition conditions and cycles), using molecular dynamics (MD) and ReaxFF.
- Successfully applied Laser Acoustic Wave system (LAWS) to characterize the mechanical properties of artificial SEI coating layers (ALD- $Al_2O_3$). The modulus of ALD- $Al_2O_3$ coating is around 150 GPa, consistent with the value reported in literature and MD simulations.
- Correlated the interfacial charge-transfer kinetics and coating thickness.
- Derived models showing that Li consumption varies with different SEI failure mechanism. This insight is being used to design new experiments to test SEI failure modes.

✧ ✧ ✧ ✧ ✧

## Introduction

Volume changes of up to ~300 vol% for Si during lithiation and delithiation lead to fracture of Si and/or loss of electrical contact with the conductive phase or the current collectors. Nano-structured Si effectively mitigates Si cracking/fracture. Unfortunately, the high surface to volume ratio in nanostructures leads to unacceptable amounts of solid-electrolyte interphase (SEI) formation, thereby lowering current efficiencies. Artificial SEI coated Si nanostructures will resolve this

issue, if the coating can be stable. Based on mechanics models we demonstrate that the SEI coating can be mechanically stable despite the volume change in Si, if the material properties, thickness of the SEI and the size/shape of Si are optimized. Engineering such a system is extremely difficult due to the large number of variables involved, especially as many are unknown.

In order to develop a validated model, it is critical to fundamentally understand the mechanical and chemical stability of SEI (hereafter, SEI refers to both naturally formed native SEI and artificial SEI coatings) in electrochemical environments, the correlation between the coulombic efficiency and the dynamic process of SEI evolution, and the structural optimization of both the SEI and the Si electrode. However, it is extremely difficult to characterize the structure and to measure the mechanical properties of SEI layers that are tens of nm thick on complicated geometries. In this project, we will take advantage of a thin-film geometry that simplifies the investigations while providing fundamental parameter values. Many measurements (e.g., AFM, indentation, XPS and TOF-SIMS depth profile) can be readily conducted with thin films, whereas similar measurements on particles or nanofibers are difficult. These thin-film electrodes can be appropriately modeled using continuum-based models, thus allowing the direct comparison of measurements with models to support model validation.

## Approach

In this project, four coherent steps will be taken: a) Develop a multi-scale model to predict the stress/strain in the SEI layer (including artificial SEI) on thin-film Si and establish a correlation between the capacity loss (or current efficiency) and mechanical degradation of SEI on Si. b) Use atomic simulations combined with experiments performed on Si-thin-films to provide critical material properties used in the continuum modeling. c) Investigate the impact of the SEI formation on the stress/strain evolution, combined with modeling to quantify the current efficiency related to a variety artificial SEI layers using *in situ* electrochemical experiments. d) Use the validated model to guide surface coating design and Si size/geometry optimizations that mitigate mechanical degradation to both SEI and Si.

## Results

**1) Determined the Mechanical property of ALD-$Al_2O_3$ coating on Si.** Using MD and ReaxFF, it has been found that the Young's modulus (E) of amorphous $Al_2O_3$ coatings decreases with its density, which can be controlled by ALD deposition conditions and cycles. To capture the main characteristics of the ALD-$Al_2O_3$ coating, the atomic structures were designed to be disordered within the film in-plane directions but to have an average layer distance of 1.1Å along the film growth direction. The predicted Young's modulus compared well with experimental measurements (listed in Table VI - 2).

Experimentally, Laser Acoustic Wave system (LAWS) has been successfully applied to characterize the mechanical properties of artificial SEI coating layer (ALD-$Al_2O_3$). The modulus of ALD-$Al_2O_3$ coating is around 150 GPa, consistent with the value reported in literature and MD simulations.

Thus, it is confirmed the LAWS is a reliable approach to measure the modulus of ultrathin coating and our ALD- $Al_2O_3$ model is accurate.

**Table VI - 2: Density and Young's modulus of various $Al_2O_3$**

| | ρ (g/cm$^3$) | E (GPa) Simulation | E (GPa) Experiment |
|---|---|---|---|
| a-$Al_2O_3$ | 2.2 ~3.3 | | 95~110 |
| ALD a-$Al_2O_3$ | 2.4±0.7 | 110 | 150 |
| a-$Al_2O_3$ | 2.8 | 135.4 | |
| a-$Al_2O_3$ | 4.0 | 268.3 | |
| Crystal $Al_2O_3$ | 3.95 | 401 | 366~410 |

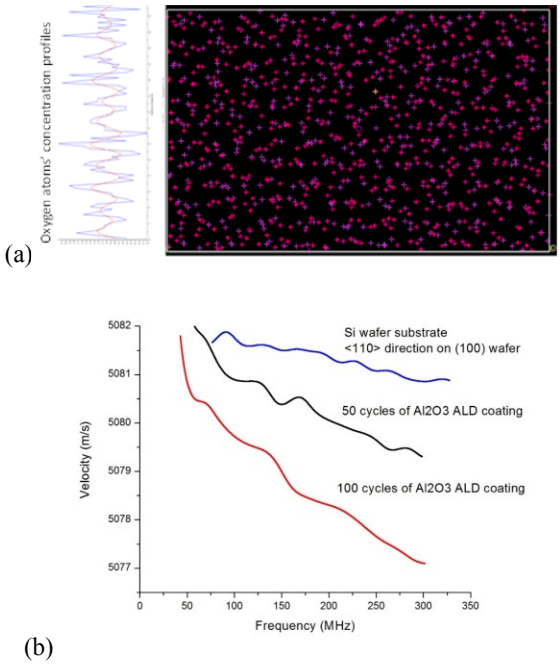


**Figure VI - 74: (a) The atomic structure of amorphous ALD-$Al_2O_3$, the concentration profile of O atoms shows 1.1Å periodicity, (c) LAWS characterization of the mechanical properties of ALD coatings**

**2) Correlated the interfacial charge-transfer kinetics and coating thickness.** The kinetics of Si thin film electrodes coated with $Al_2O_3$ by ALD was studied using a model thin film system, which provides the intrinsic properties of electrodes. Using a modified PITT measurement, the overall interfacial resistance of ALD-$Al_2O_3$ coated Si electrodes was quantified by means of a fit exchange current density. Three physicochemical parameters were extracted, including the lithium diffusion coefficient within silicon, the interfacial exchange current density, and the reaction rate constant.

The light blue curve in Figure VI - 75 portrays the trend of B vs. film thickness. The data shows the optimum surface coating thickness was identified as ~0.7nm. Thus, with five to ten atomic layers of an alumina ALD coating, the silicon electrode can deliver 2600 mAh $g^{-1}$ capacity within 3 seconds.

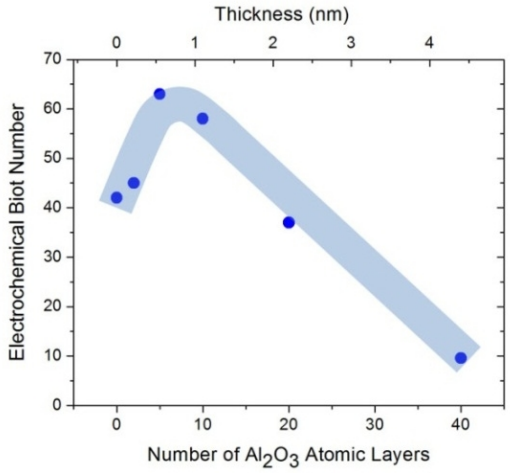


**Figure VI - 75: Electrochemical Biot number B obtained from PITT measurement**

**3) Measured and computed the chemical composition of the initial SEI formed on uncoated Si thin film electrodes at different voltages.** An uncoated Si electrode is naturally terminated by a thin layer of $SiO_2$, and the coated Si electrode considered in the 2nd quarter of the project is ALD-$Al_2O_3$ coated. Based on DFT calculations, both $SiO_2$ and $Al_2O_3$ will be lithiated at the voltage above EC decomposition (~0.8V), contributing to the initial irreversible capacity loss. Experimentally, the composition of SEI layer formed on uncoated Si at different voltages was characterized by XPS. More organic compound formed at voltage >0.4 V and more inorganic compounds formed at voltage range of 0.2V<HV<0.4V. Consequently, preliminary LAWS measurement shows the modulus of SEI layer formed at lower potential is relatively higher.

**4) Confirmed the design of patterned Si thin film.** The patterned Si thin film has been designed to evaluate the evolution of stress of the Si electrode during SEI formation and growth in *in situ* cells to inform the continuum stress model. If the Si/Cu interface is fixed, the deformation of Si will be along the film thickness direction, so only minimum strain will be applied to the SEI layer. In contrast, if the Si/Cu interface can slide and allow Si islands to expand laterally, the SEI layer will be stretched and compressed. In fact, this interface can be controlled. Using combined DFT calculations and TOF-SIM measurements, it was revealed that Li will segregate to the Si/Cu interface and cause almost frictionless interface sliding. The sliding interface will in turn change the stress developed in the Si islands.

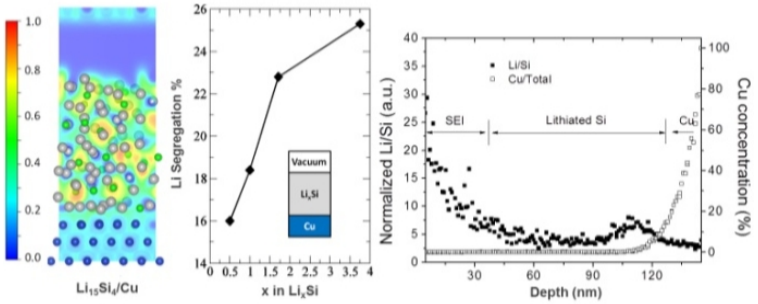


(a) (b) (c)

**Figure VI - 76: DFT results show the (a) charge transfer from Li to Cu substrate leads to (b) higher Li/Si ratio at the LixSi/Cu interface. The Li segregation behavior has also been observed in (c) SIMS depth profile**

**5) Derived that Li consumption will be different with different SEI failure mechanism.** For example if the SEI fractures, the current efficiency is lost during lithiation. If the SEI wrinkles and peels off, the current efficiency loss occurs during delithiation. This insight is used to design new experiments to test SEI failure modes.

## Conclusions and Future Directions

This project is progressing with closely integrated modeling and experiments. The experimental mechanical and electrochemical data obtained on ALD-$Al_2O_3$ coated Si show good agreement with modeling and results. This initial work validates the methods being used and demonstrates that the results are accurate. Other ALD coating samples will be sent to GM for mechanical property measurements.

The understanding of the $Li_xSi$/Cu interface allows us to design patterned Si on Cu substrate with different interface properties in order to control the deformation of Si and the mechanical strain imposed on the SEI film. The next step is to measure the stress evolution in the SEI while Si is lithiated and deliathiated. This will reveal the failure mechanism of SEI on Si and provide fundamental knowledge for constructing the mechanics models.

This team started the project in April 2013. It has already initiated collaborations with other BATT research groups. More collaboration is expected as the project continues along its path.

## FY 2013 Publications/Presentations


1. Maria E. Stournara, Xingcheng Xiao, Yue Qi*, Priya Johari, Peng Lu, Brian Sheldon, Huajian Gao*, Vivek B. Shenoy, "Lithium segregation induced structure and strength change at amorphous-Si/Cu interface," *Nano Letters*, **13** (10), 4759-4768 (2013).
2. Juchuan Li, Xingcheng Xiao*, Yang-Tse Cheng, and Mark W. Verbrugge, "Atomic Layered Coating Enabling Fast Surface Kinetics at Silicon Electrodes in Lithium Ion Batteries," *Journal of Physical Chemistry Letter*, **4**, 3387-3391 (2013).
3. Hamed Haftbaradaran, Xingcheng Xiao and Huajian Gao*, "Critical film thickness for fracture in thin film electrodes on substrate," *Modeling and Simulation in Materials Science and Engineering*, **21**, 074008 (2013).
4. Xin Su, Qingliu Wu, Juchuan Li, Xingcheng Xiao, Amber Lott, Wenquan Lu, Brian W. Sheldon, Ji Wu, "Silicon-based Nanomaterials for Lithium Ion Batteries - A Review," *Advanced Energy Materials*, DOI: 10.1002/aenm.201300882 (2013).
5. Mingyan Wu, Xingcheng Xiao, Shidi Xun, Prodip Das, Xiangyun Song, Paul Olalde-Velasco, Dongdong Wang, Adam Z. Weber, Vince Battaglia, Wanli Yang and Gao Liu, "An Ideal Polymer Binder for High-Capacity Battery Anodes," *Journal of American Chemical Society*, **135 (32)**, 12048-12056 (2013).
6. X. Xiao, "Ultrathin surface coating as artificial solid electrolyte interphase for lithium ion batteries," *246th ACS National Meeting*, Sept. 12, 2013, Indianapolis, IN (Invited).
7. X. Xiao, "High Capacity Electrode Materials for Lithium Ion Batteries: Challenges and Opportunities," *Department Seminar*, Chemical Engineering and Materials Sciences, Oct. 7, 2013, Michigan State University (Invited).
8. Y. Qi, "Predicting the transport and mechanical properties of the solid electrolyte interphase in Li-ion batteries," *Society of Engineering Science 50th Annual Meeting*, July 29, 2013, Providence, RI (Invited).
9. Y. Qi, "*Ab initio* Interface Design for Si-based electrodes," *ACS National Meeting*, April 10, 2013, New Orleans, LA (Invited).
10. B.W. Sheldon, "Chemically Induced Stresses in Li-ion Battery Electrodes," *ACS National Meeting*, April 10, 2013, New Orleans, LA (Invited).
11. B.W. Sheldon, "Lithiation Induced Stresses and Interfacial Phenomena in Li-ion Battery Electrodes," *Society of Engineering Science Annual Meeting*, July 29, 2013, Providence, RI (Invited).
12. B.W. Sheldon, "Electrochemically Induced Stresses in Energy Storage Materials," October 17, 2013, University of Wisconsin, Madison, WI (Invited).
13. Y. Cheng, "Understanding diffusion-induced-stresses and fracture, including effects of the Solid-Electrolyte-Interphase (SEI), in lithium ion battery electrodes," *Gordon Research Conference on Nano-Mechanical Interfaces*, August 4-9, 2013, Hong Kong, China (Invited).

# VI.C.5 Hierarchical Assembly of Inorganic/Organic Hybrid Si Negative Electrodes (LBNL)

**Gao Liu**
Lawrence Berkeley National Laboratory

Environmental Energy Technologies Division
1 Cyclotron Road, MS 70R108B
Berkeley, CA 94720
Phone: (510) 486-7207; Fax: (510) 486-7303
E-mail: Gliu@lbl.gov

Start Date: October 2012
Projected End Date: September 2016

## Objectives

- Develop new conductive polymer binder materials to enable large volume change lithium storage materials to be used in lithium-ion electrode.
- Explore additives to increase coulomb efficiency (CE) and stabilize capacities of Si electrode by forming a stable SEI during cycling.

## Technical Barriers

This project addresses the following technical barriers from the Energy Storage section of the Vehicle Technologies Program Multi-year Research, Development and Demonstration Plan:

- Calendar and cycle life
- Energy density

## Technical Targets

Relevant USABC goals

- EV:
  - $150/kWh.
  - 230 Wh/dm$^3$.
  - 1000, 80% capacity, discharge cycles.
  - 10-year system life.
- PHEV 40-mile:
  - $220/kWh.
  - 193 Wh/dm3.
  - 5,000 discharge cycles.
  - 15-year system life.

## Accomplishments

- Successfully developed PEFM conductive polymer binder for Si nanoparticles in lithium-ion negative electrode applications. As a modification of PFM binder, PEFM enables the Si electrode to cycle at almost full capacity.
- Successfully adapted the PFM conductive polymer binder to Sn nanoparticles for lithium-ion negative electrode applications. Optimized the composition of the Sn/PFM electrode composition. Demonstrated extended cycling of pure Sn nanoparticles with PFM binder composite electrode at 500 mAh/g-Sn capacity.
- Developed a propylene carbonate (PC) co-solvent system for lithium-ion battery, which improves the cycle life performance of lithium ion batteries.

✧ ✧ ✧ ✧ ✧

## Introduction

Achieving the DOE energy, cycle life and cost targets will require materials of higher capacity and improved coulombic efficiency or cells with higher voltage. High capacity Si or Sn alloy based anode material has the potential to fulfill the energy density requirements for EV/PHEV applications. However, full capacity cycling of the materials results in significant capacity fade due to a large volume change during Li insertion and removal. Decreasing the particle size to nanometer scale can be an effective means of accommodating the volume change. However, it is very challenging to make electric connections to all the alloy nanoparticles in the electrode by using similar size acetylene black conductive additive. The repeated volume change of the alloy nanoparticles during cycling can lead to repositioning of the particles in the electrode matrix and result in particle dislocation from the conductive matrix. This dislocation of particles causes the rapid fade of the electrode capacity during cycling. In order to address this issue, Si/conductive polymer composite electrodes were developed in this work. This new electrode can be fabricated with the current lithium-ion manufacturing processes. A new class of electric conductive binder materials was developed, which the

Lowest Unoccupied Molecular Obital (LUMO) energy is controlled to match the reduction potential of the alloy materials. The electrodes made with these binders have significantly improved cycling capability.

## Approach

Use functional polymer design and synthesis to develop new conductive polymers with proper electronic properties, strong adhesion and improved flexibility to provide electric pathways in the electrode, and to accommodate large volume change of the Si or Sn alloy active material during lithium insertion and removal. The rational design of binder is assisted with advanced diagnostic techniques such as XAS at Advance Light Sources and with advanced molecular computation at National Energy Research Scientific Computing Center – both are DOE national user facilities.

## Results

**Conductive Polymer Binder with an Ideal Structural Design for Si Alloy Materials**. Li-ion transportation in the binder system is critical for achieving the full capacity of the active materials in battery electrodes, because the binder coats the surface of the active material and may impede the Li-ion diffusion. Although ion mobility in the doped conductive polymer system has been demonstrated, strategies to further improve the ion mobility are still necessary. In our polymer system, this issue is tackled by improving the electrolyte uptake through the incorporation of the polar ethyleneoxide side chains.

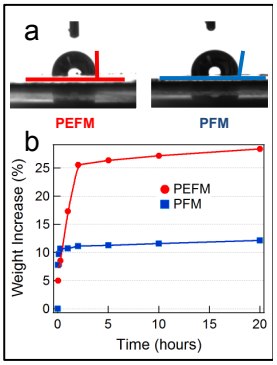


**Figure VI - 77: (a) Water contact angles on the surfaces of PEFM and PFM films. The E side chains in PEFM increase the polarity, and thus improve the swelling of the polymer. Therefore the PEFM has a lower contact angle with water. (b) The swelling tests of PEFM and PFM polymer film in the 1M LiPF6 EC/DEC (1:1) electrolyte. The electrolyte uptake in PEFM is three times higher than that in PFM, and is at the same level as that for conventional non-conductive PVDF binder**

The enhanced polarity of the PEFM polymer results in a three-fold electrolyte uptake (Figure VI - 77). The better swelling is due to the increased polarity of the polymer, which is indicated by the water contact angle measurements (Figure VI - 77a). The static contact angle is 90.9° for PEFM with the E group, versus 101.0° for PFM. The ether side chains tend to distribute uniformly in the polymer because they are chemically attached to the backbone. The uniform distribution of the ether moieties in the binder helps to improve the overall electrolyte uptake. Although PFM also swells in the electrolyte solution, the total electrolyte uptake is about 10 percent of its final weight. In swelled PEFM films, the electrolyte uptake is tripled, accounting for 30 percent of the final swelling weight (Figure VI - 77b). This number is similar to the non-conductive PVDF swelling in the electrolyte. As explained above, the enhanced electrolyte uptake is important for allowing facile Li-ion transportation through the polymer binder to the active materials.

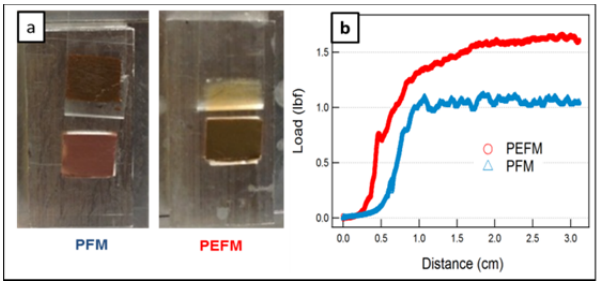


**Figure VI - 78: Peel tests comparison of the electrode laminate made with PFM and FEFM binder. (a) Peel testing photos of the two electrodes during the tests. The photo shows the PFM based electrode was peeled off (left), but PEFM based electrode remains attached to the Cu current collector with only small amount of surface materials peeled off by the tape (right). This shows that the adhesion force of the developed PEFM is too strong to be measured by such conventional method. (b) Force measured during the peel tests of PFM and PEFM based electrodes. Note again that the adhesion force of PEFM based electrode is beyond the measurement range of such method, and actually even higher than the value (1.7 lbf) showed by the red curve**

Another important benefit associated with the increased polarity of the polymer is the significantly improved adhesion force of the binder to the Si particles, and with the current collector. The photo of the peel result (Figure VI - 78) shows that almost the whole PEFM laminate persists on the current collector, while for the PFM delamination takes place between the electrode laminate and the current collector. This shows that the large adhesion force of the PEFM binder is beyond the testing range of such conventional peeling test, which is a standard technique used in the battery industry. Although the force to delaminate the PEFM-based laminate electrode is too strong to be measured,

the great improvement on adhesion among the laminate, current collector, and particles is obvious.

Figure VI - 79 shows that the cycling capacity of Si particles in the initial cycle reaches theoretical capacity (3750 mAh/g) in the PEFM/Si electrodes, indicating 100% utilization of Si material embedded in the PEFM binder. This is corresponding to 2500 mAh/g capacity of the entire laminate weight when the weight of conductive binder is included and a 1200 mAh/cm3 volumetric energy density of the electrode. In both the PF/Si and PFM/Si electrodes, the delithiation capacity of Si in the first cycle is much lower. The specific delithiation is stable and higher in PEFM/Si than that in PFM/Si electrodes over extended cycles.

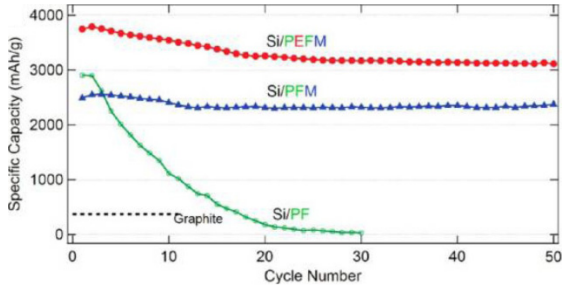


**Figure VI - 79: Cycling performance of polymer/Si composite electrodes. (The current density at C-rate is 0.92 mAh/cm$^2$)**

**Performance of Sn/Conductive Polymer Composite Electrode** Both Si and Sn work at the same potential range between 10 mV to 1 V as anode materials in the lithium-ion chemistry. A comprehensive evaluation of the conductive polymer binder with a Sn compound was performed. It is demonstrated that pure Sn nanoparticles can be stably cycled at high capacity (> 500 mAh/g) with a polyfluorene-type conductive polymer binder in composite electrodes. Crystalline Sn nanoparticles (< 150 nm) were used as anode materials in this study. The average diameter of Sn secondary particles is 270 nm, calculated based on BET surface area. The composite electrodes contain a conductive polymer binder that constitutes 2% to 10% of the material, without any conductive additives. The electrode containing 5% conductive binder showed the best cycling performance, with a reversible capacity of 510 mAh/g (Figure VI - 80a) Crystallinity of Sn particles gradually degrades during cycling, and pulverization of particles was observed after long-term cycling, leading to capacity fade. The conductive polymer binder shows advantages over other binders, such as poly(vinylidene fluoride) (PVDF) and carboxymethylcellulose (CMC) binders, because it can provide electrical conductivity and strong adhesion during Sn volume expansion (Figure VI - 80b).

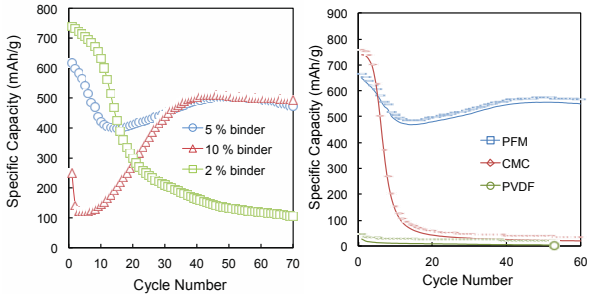


**Figure VI - 80: Pure Sn nanoparticle composite electrodes. (a) Different amount of PFM. (b) Different binders**

**New Propylene Carbonate (PC)-Based Electrolytes with High Coulombic Efficiency for Lithium-ion Batteries** Ethylene carbonate (EC) forms a stable SEI at ~0.8 V before lithium intercalation. Li+ permeable and electronically non-conductive, SEI prevents further electrolyte decomposition and allows reversible lithiation and delithiation of the graphite or Si anode. The major disadvantage of EC is its high melting point at around 34°C, which limits the use of lithium-ion batteries at low temperatures. Propylene carbonate (PC) has a wide liquid temperature range (-48.8 ~ 242.0°C) and very good low-temperature performance compared to EC. However, with only a negligible structural difference from EC, PC undergoes a detrimental solvent decomposition on the surface of graphite. This causes disintegration of the graphite electrode, usually accompanied by delamination of the active material from the current collector, and finally, cell failure.

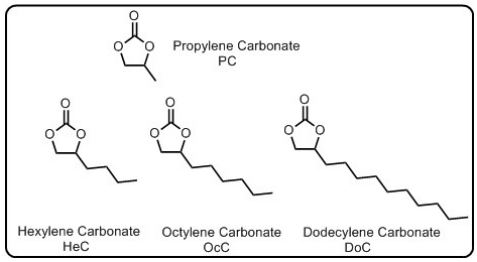


**Figure VI - 81: The structure of hexylene carbonate (HeC), octylene carbonate (OcC) and dodecylene carbonate (DoC)**

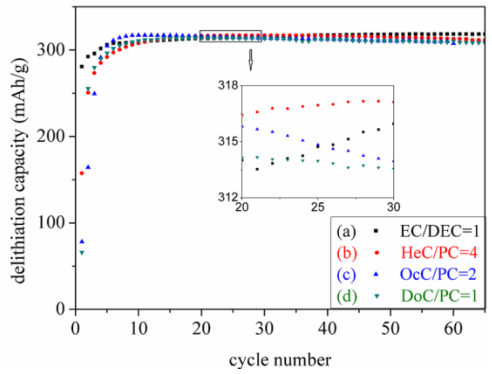


**Figure VI - 82: Cycling performances of a graphite half cell in a 1 M $LiPF_6$ solution of (a) EC/DEC=1, (b) HeC/PC=4, (c) OcC/PC=2, and (d) DoC/PC=1 (v/v) at a C/10 rate**

A homologous series of PC analogue solvents (Figure VI - 81) with increasing length of linear alkyl substitutes were synthesized and used as co-solvents with PC for graphite-based lithium-ion half cells. A graphite anode reaches a capacity of around 310 mAh/g in PC and its analogue co-solvents, with 99.95% Coulombic efficiency, similar to the values obtained with EC-based electrolytes. Figure VI - 82 shows cycling performances of graphite half cells using co-solvents of hexylene carbonate (HeC)/PC=4, octylene carbonate (OcC)/PC=2, and dodecylene carbonate (DoC)/PC=1 with 1 M $LiPF_6$. Cell capacities reach ~ 310 mAh/g in the first 10 cycles in all the electrolytes. This indicates the formation of a stable SEI on graphite surface that prevents PC exfoliation and allows reversible cycling in graphite anode. The PC co-solvents from different batches of HeC, OcC, and DoC gave the same cell performance, which indicates the consistency of the data shown in Figure VI - 82.

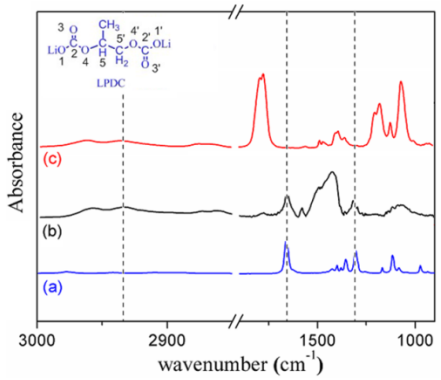


**Figure VI - 83: FTIR spectra of (a) a standard LPDC, (b) a graphite electrode cycled in a 1 M $LiPF_6$ solution of HeC/PC=4 for around 10 cycles at C/10, and (c) the electrolyte used in the cell, 1 M $LiPF_6$ in HeC/PC=4**

Figure VI - 83 shows the FTIR spectra of a graphite electrode after being cycled in HeC/PC=4 electrolyte. Besides the leftover electrolyte, the major component of SEI is lithium propylene dicarbonate (LPDC), which is the single-electron reduction product of PC. The bulky cyclic carbonate solvents compete with PC for Li solvation, which delayed the PC co-intercalation into graphene layers. PC then went through single-electron decomposition on graphite surface and formed a stable SEI.

## Conclusions and Future Directions

A modified conductive polymer, PEFM, was synthesized and characterized. Electronic, mechanical, and electrolyte-uptake properties are optimized individually without detrimental effect to each other. Full-capacity cycling of Si was accessed in this conductive polymer binder with excellent rate performance. The performance characteristics of this Sn/PFM electrode were studied and stable cycling performance was demonstrated. A homologous series of propylene carbonate (PC) analogue solvents with increasing length of linear alkyl substitutes were synthesized and used as co-solvents with PC for graphite-based lithium-ion half cells. A graphite anode reaches a capacity of 310 mAh/g in PC and its analogue co-solvents, with 99.95 percent Coulombic efficiency

[1] PFM stands for Poly(9,9-dioctylfluorene-co-fluorenone-co-methylbenzoic ester); PEFM stands for Poly(2,7-9,9-dioctylfluorene-co-2,7-9,9-(di(oxy-2,5,8-trioxadecane)) fluorine-co-2,7-fluorenone-co-2,5-1-methylbenzoic ester).

## FY 2013 Patents/Publications/Presentations

1. Gao Liu and Hui Zhao, New *in situ* elastic coating to stabilization of Si anode surface for lithium-ion rechargeable battery applications, IB-2974 disclosure filed in 2013.
2. Liu, X.; Wang, D.; Liu, G.; Srinivasan, V.; Liu, Z.; Hussain, Z.; Yang, W., "Distinct charge dynamics in battery electrodes revealed by *in situ* and *operando* soft X-ray spectroscopy," *Nature Comm.* 2013, Accepted.
3. Wu, M.; Sabisch, J. E. C.; Xun, S.; Minor, A.; Battaglia, V. S.; Liu, G., "*In situ* Formed Si Nanoparticle Network with Micronsized Si Particles for Lithium-ion Battery Anodes." *Nano Letters,* Article ASAP (2013).
4. Xun, S.; Xiang, B.; Minor, A.; Battaglia, V. S.; Liu, G., "Conductive Polymer and Silicon Composite Secondary Particles for a High Area-Loading Negative Electrode," *J. Electrochem. Soc.,* **160(6)**, A1380-A1383 (2013).
5. Xun, S.; Song, X.; Battaglia, V. S.; Liu, G., "Conductive Polymer Binder-Enabled Cycling of Pure Tin Nanoparticle Composite Anode

Electrodes for a Lithium-Ion Battery," *J. Electrochem. Soc.* **160(6)**, A849-A855 (2013).

6. Wu, M.; Xiao, X.; Vukmirovic, N.; Xun, S.; Das, P. K.; Song, X.; Olade-Velasco, P.; Wang, D.; Weber, A. Z.; Wang, L.-W.; Battaglia, V. S.; Yang, W.; Liu, G.; "Toward an Ideal Polymer Binder Design for High-Capacity Battery Anodes," *Journal of the American Chemical Society,* **132**, 12048–12056 (2013).
7. "Development of Conductive Binders for Silicon Anodes," *Advanced Automotive Battery Conference,* Feb 2013, Pasadena, CA.
8. "Development of Conductive Binders for Silicon and Tin Anodes," *10th Pacific Rim Conference on Ceramic and Glass Technology*, June 2013, San Diego, CA.
9. "Advanced Binder and Si Anode Design for High Energy Batteries," *Beyond Lithium Ion Conference,* June 2013, Boulder, CA.
10. "The Advancements of Conductive Polymer Binder for High Capacity Alloy Anode Materials," *U.S.-China Meeting*, Sept., 2013, Chengdu, China.

# VI.C.6 Electro-Deposition of Silicon and Other Metals for Li-Ion Battery Anodes (NETL)

**Dr. Manivannan Ayyakkannu**
**Contractor:** NETL/DOE

**Dr. Prashant N Kumta**
**Subcontractor:** University of Pittsburgh, Pittsburgh

Project Start Date: October 2010
Project End Date: September 2013

## Objectives

- This research is aimed at exploring electrodeposition as a low cost and scalable approach to replace graphite with metal alloy systems such as Li, Sn, Sb, etc as a high energy density anode system. The main objectives of this research are
  - Develop thin films of Si and other electroactive metal alloy systems as high capacity Li-ion anodes
  - Obtain similar or lower irreversible loss compared to graphite
  - Attain high specific capacities (>1000 mAh/g)
  - Achieve similar or better cyclability and calendar life of the developed anode systems
  - Obtain columbic efficiency close to 100%
  - Attain good rate characteristics for high load applications

## Technical Barriers

One of the major challenges of silicon based anodes is the loss of mechanical integrity and poor cyclability due to the colossal stress related problems associated with the huge volumetric changes in Si (>300%) during lithium alloying and delloying.

## Technical Targets

- Synthesize amorphous Si films for Li-ion system by cost effective electrodeposition process.
- Improve the cyclability of Si anode based system for Li-ion cell.
- Lower the first cycle irreversible loss of Si anodes.
- Application of pulse plating electrodeposition technique to control the morphology of the Si anode.

## Accomplishments

- Synthesized binder-free amorphous silicon films on copper substrate by electroreduction of Si salts from an inorganic solvent bath.
- The amorphous Si films exhibited a stable and reversible capacity of 1300 mAh/g with a columbic efficiency of 99.5% upto 100 cycles.
- Modified the morphology of the electrodeposited Si thin films using pulse plating techniques.

✧ ✧ ✧ ✧ ✧

## Introduction

Silicon, with a theoretical capacity of 4212 mAh/g, corresponding to the maximum lithiated phase of $Li_{22}Si_5$, was identified as an alternative anode which can store more than 10 times more charge than graphite. However, during alloying and dealloying of lithium, there is a very large volumetric change leading to mechanical stresses in the electrode causing cracking and consequently loss of inter – particle contact. Hence, there is delamination of the electrode layer leading to rapid capacity fade.

Nanostructured and amorphous Si synthesized by physical and chemical vapor deposition show improved performance but are not economically viable for secondary batteries. Electrodeposition is a very inexpensive process which has been widely studied and used in many industrial applications for plating metals and alloys. Electrodeposition of silicon from organic solvents and ionic liquids on metallic and graphite substrates has previously been reported in the literature. Additionally, the electrodeposition technique offers to provide the deposited films with different morphologies and functional properties by controlling the parameters such as electrolyte composition, applied voltage/current density and time of deposition.

## Approach

Silicon thin films were electrodeposited on copper substrate using galvanostatic conditions and pulse current conditions from an electrolyte of 0.5M silicon

tetrachloride ($SiCl_4$) and 0.1M tetrabutylammonium chloride (TBACL) in propylene carbonate (PC) solution in an argon environment (<0.1 ppm oxygen and <0.1 ppm water). The current density of the deposition done at constant current (galvanostatic condition) was -1mA/cm$^2$. The frequencies of negative cycle at the same deposition current density for pulse conditions were 0Hz (galvanostatic), 500Hz, 1000Hz, 2000Hz, 3000Hz, 4000Hz and 5000Hz. The current cycle had a duty cycle (active deposition time/total time) of 50%.

Electrochemical investigations were performed on the electrodeposited Si thin films on copper foil which served as the working electrode. A 2016/2025 coin cell assembly in a half cell configuration was used by employing lithium (Li) foil as counter electrode and 1 M LiPF6 in (EC:DEC = 1:2, by volume) as the electrolyte. The assembled cells were tested by cycling between 0.02 and 1.2 V employing a constant current density of 400 mA/g.

## Results

**Material Characterization.** The glancing angle X-Ray diffraction did not show any peaks corresponding to crystalline silicon. Raman spectra showed the presence of broad peak at 480 cm-1 which is indicative of the transverse optical phonon mode of amorphous silicon.

SEM analysis (Figure VI - 84) of galvanostatically deposited amorphous Si film showed islands ranging from 10–20µm with a film thickness of approximately 0.3–1µm. The EDAX indicated the presence of Si, C, O and Cu; the oxygen present was due to the surface oxidation and carbon from the residual PC and acetone.

**Electrochemical Characterization.** A first discharge and charge capacity (Figure VI - 85) of ~3400 mAh/g and ~1150 mAh/g respectively, were obtained with a first cycle irreversible loss of ~65%. This huge first cycle irreversible loss may be due to the presence of oxide layer over the Si thin film, formation of large solid electrolyte interface (SEI) layer or impurities from the electrolyte. The major alloying in the first cycle occurs near the 0.2V which is indicative of lithiation process of amorphous silicon and consistent with other literature reports.

The columbic efficiency shown in Figure VI - 85 was very close to 100%. A fade rate of ~0.016% per cycle and a capacity of ~1260 mAhg−1 were observed at the end of the 100th cycle which is an almost four fold increase over the capacities observed for graphite anode. There was no extension, modification or growth of the crack width or length in comparison to what was already prevalent in the as deposited films prior to cycling as shown in Figure VI - 84.

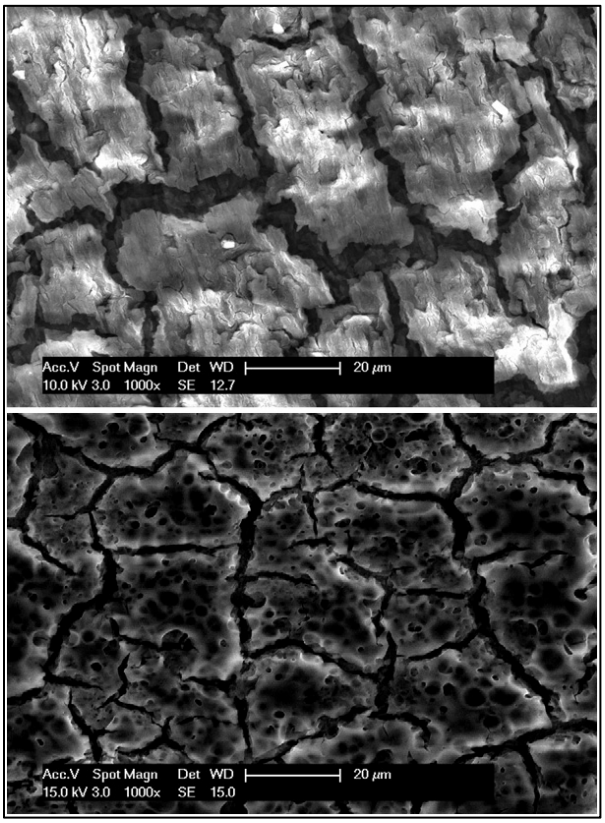


Figure VI - 84: SEM images of electrodeposited Si before cycling (top) and after 100 cycles of testing for Li/Li$^+$ battery (below)

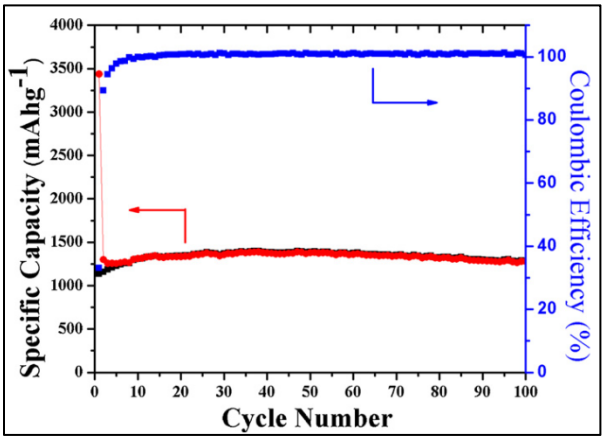


Figure VI - 85: Capacity and columbic efficiency plots cycled at 400 mA/g between 0.02 and 1.2 V for 100 cycles

**Pulse Electrodeposition Condition.** A major change in the morphology of the electrodeposited Si was observed with the change in the frequency of deposition as can be observed in Figure VI - 86. The morphology of thin films for 0Hz (galvanostatic) showed islands of Si, 500Hz showed islands of Si formed from Si particles and 1000Hz resulted in continuous thin films of Si. The formation of continuous films at high frequency

deposition can be attributed to the increased diffusion of Si4+ ions in the depletion layer close to the electrode-electrolyte interface during the relaxation time (zero current) of the deposition cycle.

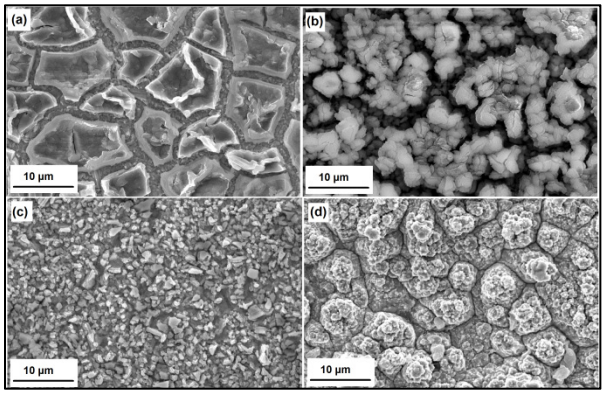


**Figure VI - 86: SEM images of electrodeposited Si films at (a) 0Hz, (b) 500Hz, (c) 1000Hz and (d) 5000Hz pulse frequency**

The electrochemical testing of these films as Li-ion anode system showed stable cycling with an improvement in the stability of the films. These films showed a decrease in the percentage loss per cycle with the increase in the frequency of the deposition cycle. The SEM analysis of the films showed that the films were stable even after 100 cycles of testing.

## Conclusions and Future Directions

Electro-reduction of $SiCl_4$ to silicon has been achieved at a cathodic potential ~−1.6 V vs. Pt.QRE on copper substrates using a PC based solvent. The electrodeposited Si films which were predominantly amorphous in nature, showed a reversible capacity of ~1300 mAh/g when cycled at a current density of 400 mA/g between 1.2 V and 0.02 V. Columbic efficiencies exceeding 99.5% and a fade rate of less than 0.016% per cycle were obtained for up to 100 cycles.

The change in frequency of electrodeposition cycle under pulse plating conditions exhibited a major change in the morphology of the Si thin films. The testing of these Si films showed stable capacity for 100 cycles and the percentage loss per cycle decreased with increase in the deposition frequency. Development of electrodeposited Si anode systems can be further carried out to decrease the first cycle irreversible loss by changing the electrolyte, post deposition heat treatment and by developing carbon/metal coatings on the Si thin films. Further multi-layer Si – (metal/carbon) system can be developed to increase the loading capacity of the active Si material on the electrode.

## FY 2013 Publications/Presentations

1. Rigved Epur, Madhumati Ramanathan, Faith R. Beck, Ayyakkannu Manivannan & Prashant N. Kumta, "*Electrodeposition of amorphous silicon anode for lithium ion batteries*"- Materials Science and Engineering: B, 2012, 177, pg:1151-1156
2. Rigved Epur, Faith Beck, Moni Kanchan Datta, Ayyakkannu Manivannan and Prashant N. Kumta, 2012 AIChE Annual Meeting, Pittsburgh, PA, USA
3. Rigved Epur, Faith R. Beck, Ayyakkannu Manivannan and Prashant N. Kumta, 221st ECS meeting at Seattle, WA – Oral presentation

## FY 2013 Patent

Silicon-Containing Compositions, Methods of Their Preparation, and Methods of Electrolytically Depositing Silicon on a Current Carrier for Use in Lithium Ion Battery Applications, U.S. Patent AppNo: 13/733992, Filed: January 4, 2013.

# VI.C.7 Atomic Layer Deposition for Stabilization of Amorphous Silicon Anodes (NREL)

**Chunmei Ban**
National Renewable Energy Laboratory

15013 Denver West Pkwy
Golden, CO, 80401
Phone: (303) 384-6504; Fax: (303) 384-6432
E-mail: Chunmei.ban@nrel.gov

**Steve M. George and Se-Hee Lee**
University of Colorado, Boulder
Department of Chemistry and Mechanical Engineering
University of Colorado Boulder
914 Broadway, Boulder, CO 80309
Phone: (303) 492-7471; Fax: (303) 492-7889
E-mail: steve.george@colorado.edu;
sehee.lee@colorado.edu

Start Date: October 2010
Projected End Date: September 2014

## Objectives

- Develop a low-cost, thick and high-capacity silicon anode with sustainable cycling performance, by advanced surface modification.
- Synthesize novel stable and elastic coatings for Si anodes using Atomic Layer Deposition (ALD) & Molecular Layer Deposition (MLD).
- Demonstrate durable cycling performance of thick Si anodes by using new ALD/MLD coatings and electrode designs.
- Investigate coating mechanism on electrochemical cycling performance via
  - Study of the mechanical properties of MLD coating materials.
  - Research on the morphology and structural evolution during lithiation/delithiation
- Explore the importance and mechanism of various coatings via the BATT Coating Group.
- Collaborate within the BATT program with the aim of developing high-rate plug-in hybrid electric (PHEV) compatible electrodes (both anodes and cathodes).

## Technical Barriers

Major barriers addressed include:

(A) Cost: Inexpensive processing techniques are employed to fabricate conventional thick electrodes.

(B) High Capacity: Silicon is predominantly being explored as a high capacity anode material. There is also a collaborative emphasis to enable high capacity cathode materials.

(C) High Rate: Both ALD coatings and nanostructured materials are being developed such that high-rate capability is demonstrated for emerging materials.

(D) Safety: The ALD coatings are targeted to improve safety for a variety of electrode materials.

## Technical Targets

- Stabilize the high-capacity silicon anodes by employing the advanced surface coating techniques, ALD and MLD
- Demonstrate the stable high-range cycling performance of Si anodes
- Relevant to USABC goals: 200Wh/kg (EV requirement); 96Wh/kg, 316W/kg, 5,000 cycles (PHEV 40 miles requirement). Calendar life: 15 years. Improved abuse tolerance

## Accomplishments

- Growth of an aluminum alkoxide polymer (alucone) film using the sequential reactions of trimethylaluminum (TMA) and ethylene glycol (EG);
- Achieved durable cycling (>100 cycles) of the MLD-engineered thick Si anodes (>15μm) using optimized MLD coating reactions and conditions;
- Demonstrated a specific capacity of ~ 900 mAh/g at the 150$^{th}$ cycle for the aulcone coated Si anodes, whereas the uncoated Si electrode undergoes the rapid degradation;
- Characterized the effect of MLD alucone coatings on the morphology and structure of silicon anodes during cycling.
- Investigated the cyclization of polyacrylonitrile (PAN) coating for Si

composite anode to address Si expansion and enable greatly improved cycling performance.

✧ ✧ ✧ ✧ ✧

## Introduction

Significant advances in both energy density and rate capability for Li-ion batteries will be critical for their implementation in next generation EVs. Due to the high theoretical capacity of Si, 3579 mAh/g for $Li_{15}Si_4$, and its natural abundance, it has attracted much attention as a promising Li-ion anode material. However, progress towards a commercially viable Si anode has been impeded by Si's rapid capacity fade caused by the large volumetric expansion. Such a massive volumetric change can result in cracking and pulverization of the Si particles, which then leads to the interruption of electronic transport pathways and the electrochemical isolation of pulverized particles. In this project, new conformal nanoscale coatings with desirable elastic properties and good conductivity are being developed via ALD and MLD, to accommodate the volumetric expansion, protect the surface from the reactive electrolytes, as well as ensure the electronic paths through the composite electrodes.

Greatly improved performance has been achieved for both ALD coated nano-$MoO_3$ anodes and cathodes. The effect of $Al_2O_3$ ALD coatings on the structure and SEI composition have been studied last year by using *in situ* synchrotron XRD and *ex situ* XPS and TOF-SIMS. It shows that ALD coatings have mitigated the side reaction on the surface of electrodes and preserved the structure during severe cycling. These past results suggest that new ALD coatings with improved mechanical properties and conductivity can help accommodate the volumetric expansion in electrodes, as well as ensure the electronic paths through the electrodes.

Both high rate and durable cycling of Si will be achieved by employing the ALD coating and new elastic (polymer-like) coatings with low elastic moduli (MLD coating). Successful completion of this project will enable the coated Si anodes to have significantly improved cycling stability and high coulombic efficiency. In the end, the development of new flexible and conductive MLD films will enable both anodes and cathodes within the BATT program achieving durable high rate capability.

## Approach

Metal-organic hybrid films have been developed and grown on the Si electrodes by using MLD, with the aim to accommodate the volumetric changes in Si particles

The growth of an aluminum alkoxide polymer (alucone) has been demonstrated using the sequential exposures of trimethylaluminum (TMA) and ethylene glycol (EG). Besides an aluminum-based precursor, other metal precursors are being used to enhance the conductivity in the MLD flexible coatings.

Chemical vapor deposition via silane decomposition on a hot filament was used to synthesize the silicon thin films with different degree of crystallinity. Recently, a Nanocrystal RF Plasma Reactor has been utilized to synthesize silicon/alloy nanocrystals with uniform size and shape. Size may be tuned from <10 to ~100 nm by varying the plasma conditions that will allow the study of how Si nanocrystal size affects the electrochemical performance. Additionally, commercial silicon particles have been used to identify the coating effects. Conventional electrodes containing active material, conductive additive and binder have been fabricated to evaluate the cycling properties.

## Results

**Develop elastic coatings by using MLD.** The new metal-organic hybrid coating, aluminum alkoxide coating (alucone), was grown based on reactions of inorganic trimethylalumium ($Al(CH_3)_3$) and organic glycerol polyols ($HOCH_2CH(OH)CH_2OH$) precursors. The sequential exposure of $Al(CH_3)_3$ and HOCH2CH(OH)CH2OH in AB cycles produces the evolution of alucone coatings with growth rates of about 3-5 Å per AB cycle at a substrate temperatures of 100-140°C.

Figure VI - 87 shows a schematic of the controlled layered chemistry structure of the aluminum alkoxide alucone polymer used in this work.

The growth of the alucone MLD coating occurs by reaction of hydroxyl groups on the alcohol with AlCH3. With more than two hydroxyl groups on the alcohol, there is greater probability that unreacted hydroxyl groups will remain after polyol reactions with AlCH3* surface species. These unreacted hydroxyl groups can produce additional crosslinking between growing polymer chains that can strengthen the alucone films and lead to higher fracture toughness.

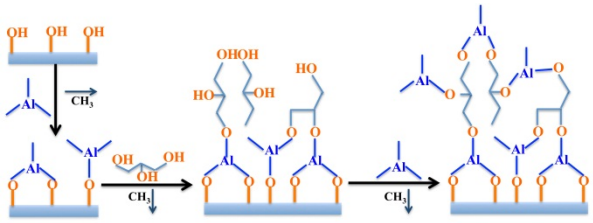


**Figure VI - 87: Schematic depicting alucone MLD reaction**

Challenges are encountered during the MLD on high-surface-area nano-Si electrodes with a tortuous

architecture. Two different reaction modes, static reactants exposure and viscous flow, were used during MLD to address the challenges in fabricating conformal coating. The static reactants exposure allows the precursor gas to reach more surfaces of the electrode, and then enhance the completion of the self-limited reaction on the surface. High angle annular dark field (HAADF) scanning transmission electron microscopy (STEM), which is highly sensitive to atomic number contrast (Z-contrast imaging), was used to further clarify the conformity of the MLD coating. HAADF-STEM image (Figure VI - 88a) shows that the alucone layer is a thin (~5 nm), dense, and conformal coating adhered to the Si particles. Electron energy loss spectroscopy (EELS) was also utilized to characterize the microstructure of the MLD coated electrodes. The conformal thin coating of the metal-alkoxide films MLD (red mapping) on the nano-Si particles (cyan mapping), as displayed in Figure VI - 88b. Note that the alucone MLD was coated on the laminated electrodes, rather than the powdery Silicon. However, the static reactants exposure facilitates the surface reactions through the entire electrode, thereby provides an intimately linked conductive network.

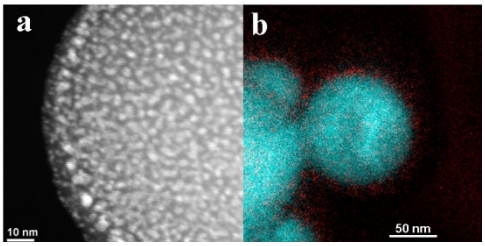


**Figure VI - 88: (a) HAADF-STEM of the alucone MLD coated particle; (b) EELS elemental mapping (Si highlighted in cyan, Al highlighted in red) confirming the conformal alucone MLD coating on the Si composite electrode**

**Improving electrochemical performance by alucone MLD coating.** Electrochemical cycling performance of the alucone coated Si electrodes has been investigated in the coin-cell configuration, with Li-metal as a counter electrode. The Si electrodes were prepared with 60% Si nanoparticles (purchased from Alfa without further treatment), 20% acetylene black and 20% PVDF binder. All of the cells were first cycled at 175 mA/g (C/20), and then cycled at 350 mA/g (C/10) in the voltage window between 0.05-1V.

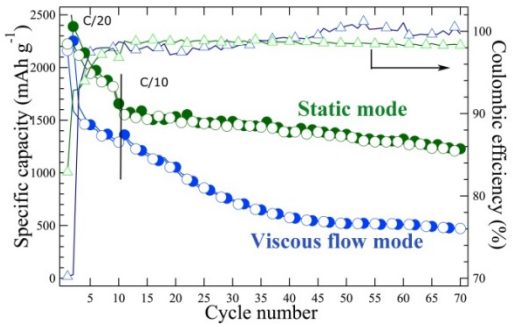


**Figure VI - 89: Cycling performance of alucone coated Si anodes by using static and viscous flow modes**

Figure VI - 89 shows the significantly improved cycling stability for the alucone MLD coated Si electrodes. The capacity obtained at a cycling rate of 0.1C has been stabilized for the static-coated Si electrode, while the slow fade in capacity is observed for the viscous-flow coated Si electrode. Besides, the static-coated Si electrode has the higher coulombic efficiency for the first cycle, which further confirms the static-coat enhancing the conformality on the tortuous electrode structure. In contrast, the bare silicon anode capacity decays to nearly zero after 28 charge-discharge cycles.

Figure VI - 90 displays the impact of different coating thicknesses on the cycling performance. The highest capacity was obtained for both thicker MLD-coated Si anodes. We expect that the better conductivity in the conformal alucone coatings may lead to the higher capacity and better cycling performance than bare electrodes.

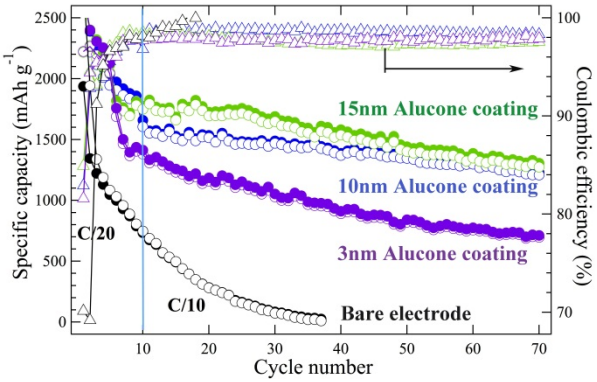


**Figure VI - 90: Cycling performance as a function of coating thickness**

Cycling stability has been demonstrated for the alucone coated Si anodes, as indicated in Figure VI - 91. Fast capacity decay was observed in the bare Si electrode. But the alucone coated Si anodes exhibit sustainable cycling over hundreds of cycles with CE in excess of 99%. The specific charge capacity of 900 mAh /g at the 150th cycle corresponds to a volumetric capacity of 569 mAh/cm$^3$ considering an initial

electrode thickness of 12.7 µm. Such good cycle life and CE for the thick electrodes is evidence that the alucone MLD coating provides favorable mechanical properties, accommodating the volumetric changes of the Si electrode and preserving the structural integrity of the electrode network throughout deep cycling.

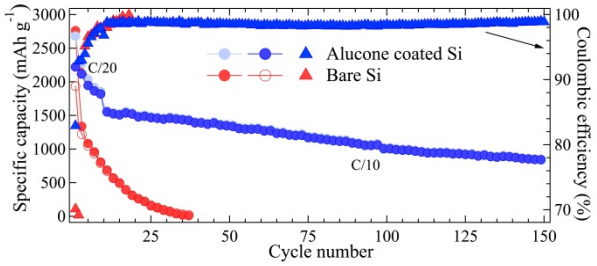


**Figure VI - 91: Greatly enhanced cycling stability in alucone MLD coating Si anodes**

**SEM characterizing the resilience of the alucone MLD coating:** The cross-section SEM images at different stages of cycling are shown in Figure VI - 92. The fresh bare and alucone coated electrodes have initial thicknesses of 12.2 µm and 12.7 µm, respectively, in Figure VI - 92b and Figure VI - 92e correspond to the first lithiation of the bare and coated electrode with the thickness of 20.3 µm and 23.0 µm. The volume expansion at the thickness direction was observed for both bare and coated electrodes. Similar volume expansion on the coated electrodes indicates that the alucone coating allows volume expansion in the coated electrodes to complete fully lithiation. The cross-sections after the 20th delithiated electrodes, as listed in Figure VI - 92c and 2f, show that the uncoated and coated electrodes have the thickness of 18.1 µm and 15.0 µm, respectively. A nearly full recovery from the massive volumetric expansion was observed for the alucone coated electrodes. On the contrary, the bare electrode remains almost fully expanded after the 20$^{th}$ delithiation. It indicates that bare electrode may lose the original electrical contact and structural integrity. The findings imply that the good resilience of the alucone coatings provides sufficient mechanical support to accommodate the major volumetric changes experienced by Si anodes, as well as to aid in the recovery and preservation of the whole composite network upon delithiation.

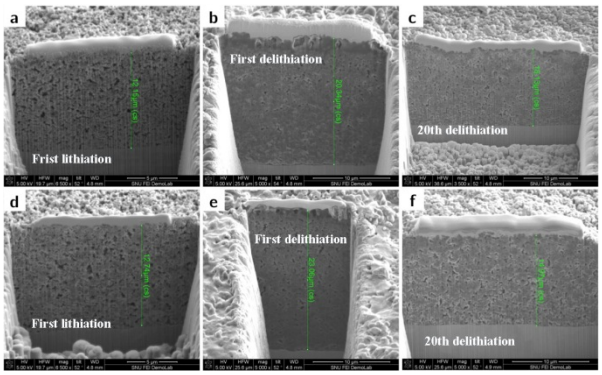


**Figure VI - 92: SEM images showing the cross-sections of the bare electrodes (a, b, c) and alucone coated electrodes (d, e, f)**

## Conclusions and Future Directions

Growth of the flexible metal-organic coatings on Si electrodes has been accomplished by using the MLD technique. Using sequential reactions of the TMA and EG precursors has coated Si electrode with the aluminum alkoxide films. To enhance the coating conformality for the tortuos electrodes, optimized static reactants exposure has been used in MLD.

The significantly-improved performance has been demonstrated for the alucone coated nano-Si electrodes. The alucone coated Si anodes exhibits sustainable cycling over hundreds of cycles with coulombic efficiency in excess of 99%. The specific charge capacity of 900 mAh/g at the 150$^{th}$ cycle corresponds to an electrode volumetric capacity of 569 mAh/cm$^3$. The thin and conformal coating, observed by advanced microscopy, accommodates the complete volume expansion during lithiation, but also helps preserve the structure integrity during delithiation.

Given the observed electrochemical and spectroscopic data, it is concluded that an alucone MLD coating provides a mechanically robust, resilient and conductive network for Si composite electrodes, allowing for a long cycle life and remarkable stability. Employment of the alucone coating on conventional nano-Si composite electrodes provides significant improvement in cycling stability, rate, and coulombic efficiency.

In FY2014, the research efforts will focus on developing the conformal elastic coatings with enhanced ionic and electronic conductivity. In order to better understand the coating effects, one of the FY2014 objectives will be to *in situ* characterize the impact of coatings on the structure and morphology evolution during cycling, and explore the importance and mechanism of various coatings via the BATT coating group.

## FY 2013 Publications/Presentations


1. M. Piper, T. A. Yersak, S-B. Son, S. C. Kim, C. S. Kang, K. H. Oh, C. Ban, A. C. Dillon, and S.H. Lee, "Conformal Coatings of Cyclized-PAN for Mechanically Resilient Si nano-Composite Anodes," *Adv. Energy Mater.* doi: 10.1002/aenm.201200850 (2013).
2. M. Piper, J. J. Travis, M. Young, S-B Son, S. C. Kim, K. H. Oh, S. M. George, C. Ban, S-H Lee, "Reversible High Capacity Si Nanocomposite Anodes enabled by Molecular Layer Deposition," *Adv. Mater.* Under review.
3. C. Ban, M. Xie, X. Sun, J. J Travis, G. Wang, H. Sun, A. C Dillon, J. Lian and S. M George, "Atomic layer deposition of amorphous TiO2 on graphene as an anode for Li-ion batteries," *Nanotechnology*, **24**, 424002, 2013, doi:10.1088/0957-4484/24/42/424002
4. I. Abdulagatov, K. E. Terauds, J. J. Travis, A. S. Cavanagh, R. Raj, and S. M. George, "Pyrolysis of titanicone molecular layer deposition films as precursors for conducting TiO2/Carbon composite films," *J. Phys. Chem. C*, **117** (34), pp 17442–17450 DOI: 10.1021/jp4051947 (2013).
5. "Atomic Layer Deposition of Al2O3 for Highly Improved Performance in Li-ion Battery Electrodes," *2012 Fall MRS*, Boston, MA, USA (Invited).
6. "Nanoscale Interface Engineering for Improved Li-ion Batteries," *2013 Spring MRS*, San Francisco, CA, USA (Invited).
7. "Atomic Layer Deposition for Stabilization of Silicon Anodes," DOE Annual Peer Review Meeting, May 13-17, 2013, Washington, DC.

# VI.C.8 Synthesis and Characterization of Si/SiOx-Graphene Nanocomposite Anodes and Polymer Binders (PSU)

**Donghai Wang**
Pennsylvania State University

Department of Mechanical and Nuclear Engineering
328 Reber Building
University Park, PA 16802
Phone: (814) 863-1287; Fax: (814) 863-4848
E-mail: dwang@psu.edu

**Michael A. Hickner**
Pennsylvania State University
Department of Materials Science and Engineering
310 Steidle Building
University Park, PA 16802
Phone: (814) 867-1847; Fax: (814) 865-2917
E-mail: hickner@matse.psu.edu

Start Date: October 2010
Projected End Date: September 2014

## Objectives

- Design, synthesize and test novel polymer binders with varying mechanical properties and surface linker groups for Si anodes
- Synthesize and characterize Si/SiOx-graphene nanocomposites,
- Identify and evaluate the electrochemical performance of the Si/SiOx-graphene nanocomposites and the polymer binder.
- Improve management of volume change characteristics of Si-based anodes, impede the capacity fading with enhanced capacity reliability, decrease initial irreversible capacity loss, and improve the specific capacity and coulombic efficiency (CE) of Si/SiOx-based anodes.

## Technical Barriers

There are several technical barriers to developing Si/SiOx-based anodes for lithium-ion batteries including:

- Poor capacity cycling.
- Large initial irreversible capacity and corresponding low CE.
- Need to add a high percentage of conductive carbon to obtain good rate (C/3) performance.

## Technical Targets

- Prepare Si nanoparticles with controlled particle size, and demonstrate Si-graphene nanocomposite anodes.
- Synthesize and evaluate novel polymer binders with controlled SiOx binding groups and Li-conducting blocks.
- Determine electrochemical properties of Si/SiOx nanoparticle, Si/SiOx-graphene nanocomposites and the polymer binders in lithium half cell.
- Achieve stable reversible capacity in excess of ~1,000 mAh/g.
- Obtain above 40% first cycle coulombic efficiency as well as 90% CE cycle to cycle.

## Accomplishments

- Synthesized SiO/$Fe_2O_3$ composite from commercially available SiO with improved capacity retention than that of SiO (capacity retention >75% after 50 cycles) and better high rate performance.
- Developed a novel type of micron-sized Si-C composites which exhibit a reversible capacity of 1459 mAh/g after 200 cycles at 1 A/g with capacity retention of 97.8%.
- Carried out fundamental studies on the influence of Si building block size, surface modification and heteroatom doping on the performance of the micron-sized Si-C composites and the results were demonstrated
- Synthesized and demonstrated crosslinking binder that achieved equivalent cycling performance to NaCMC.
- Measured binder-Si nano particle (NP) interactions and investigated factors contributing to high binder performance with commercial Si NPs.

✧ ✧ ✧ ✧ ✧

## Introduction

An increase in energy and power densities of Li-ion cells clearly depends on improvements in electrode

materials. As the commercial anode, graphite has the theoretical capacity of 372 mAh/g, which is low relative to the requirement of high-energy applications. Thus, the search for an alternative anode to replace graphite in Li-ion batteries has been underway for many years. So far, silicon has the highest theoretical capacity ($Li_{4.4}Si$ ~ 4200 mAh/g) of all known materials, and is abundant, inexpensive, and safer than graphite (it shows a slightly higher voltage plateau than that of graphite, and lithiated silicon is more stable in typical electrolytes than lithiated graphite). Unfortunately, the practical use of Si powders as anodes in Li-ion batteries is still hindered by several problems. One of the problems is severe volume changes during Li insertion/extraction, leading to loss of electric contact and poor cycling performance.

One approach to obtain a high-performance Si anode is to use silicon/carbon composites. In this project, the aim is to develop novel Si/$SiO_x$-carbon nanocomposites to improve cycling performance of Si anodes. On the other hand, many important battery characteristics, including stability and irreversible capacity losses, are critically dependent on the polymer binder's properties. High capacity electrochemically active Si particles that exhibit significant volume changes during insertion and extraction of Li require improved binder characteristics to ensure electrode integrity during use.

Inspired by these features this project seeks to mitigate the electrochemical limitations of Si-based anodes during charge/discharge by designing novel Si/$SiO_x$-carbon nanocomposite and polymer binders to tolerate volume change, improve electrode kinetics, and decrease initial irreversible capacity loss.

## Approach

Our approach is 1) to synthesize different Si-based nanocomposites and identify novel commercially available binders to tolerate volume change upon lithiation/delithiation so as to improve cycling performance; and 2) to develop novel polymer binder with controlled elastic properties, ion-conductive moieties, and SiOx surface binding functionality, in order to stabilize and bridge SiOx particles to improve cycling performance of Si-based anodes.

## Results

**Si-based anode materials.** A SiO/$Fe_2O_3$ composite, composed of SiO coated with $Fe_2O_3$ nanoparticles, was synthesized by mechanical milling and characterized by XRD, SEM, TEM, and EDS. The TEM image and corresponding EDS maps showed that the SiO particles in the composite are coated uniformly with crystalline $Fe_2O_3$ nanoparticles (Figure VI - 93A). As shown in Figure VI - 93B, both SiO and milled SiO show very poor capacity retention. The SiO/$Fe_2O_3$ composite shows considerably better cyclability than either SiO sample, with 71% charge capacity retention (1335 mAh/g) with respect to the first charge capacity after 50 cycles. The rate capability of the SiO/$Fe_2O_3$ composite is also superior to that of SiO and milled SiO. The composite still has a capacity of ~600 mAh/g at a high current density of 4.8 A/g, while the SiO can only achieve a low capacity of ~200 mAh/g at this current density. We propose that metallic Fe forms during lithiation of SiO/$Fe_2O_3$, increasing the conductivity of the composite and thereby significantly improving its performance.

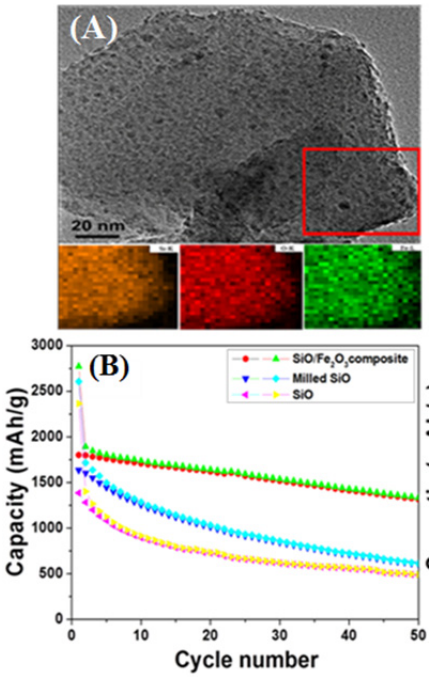


**Figure VI - 93: (A) TEM images and corresponding EDS elemental mappings of the SiO/$Fe_2O_3$ composite. (B) Cycling performance of SiO, milled SiO, and SiO/$Fe_2O_3$ composite in 50 cycles between 0.01-1.5V**

A novel micron-sized Si-C composite, which is composed of interconnected nano-scale building blocks of Si and carbon, was synthesized via a scalable and low-cost method. The composite was thoroughly characterized by a variety of methods including XRD, XPS, FT-IR, Raman, TEM and SEM. The TEM image showed that the average particle size of the composite was around 20 μm (Figure VI - 94A). The Si-C composite exhibits a reversible capacity of 1459 mAh/g after 200 cycles at 1 A/g with capacity retention of 97.8% (Figure VI - 94B) and has a high tap density of 0.78 g/$cm^3$. The first cycle CE is 77%. Capacities of 1100 and 700 mAh/g can be obtained at high current densities of 6.4 A/g and 12.8 A/g, respectively. The excellent performance is attributed to the nanoscale size of primary particles and interconnected carbon and Si

networks which can maintain internal electrical contact and sustain cycling stability.

The influence of Si nanoscale building block size and carbon coating on the electrochemical performance of the microsized Si–C composites was then further investigated. Four primary Si building sizes (10nm, 15nm, 30nm, and 50nm) were obtained by adjusting the heat treatment temperature. It was found that the critical Si building block size was 15 nm, which enables a high capacity without compromising the cycling stability (Figure VI - 95A).

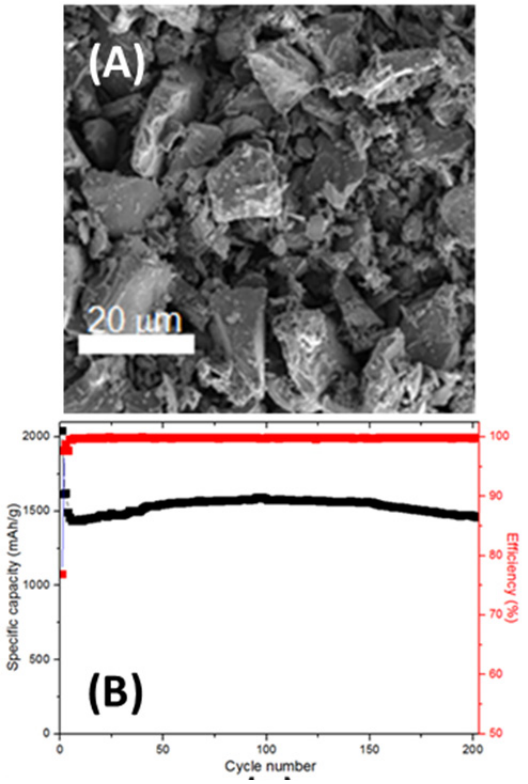


**Figure VI - 94: (A) SEM image of the micro-sized Si-C composite. (B) Cycling performance of the Si-C composite in 200 cycles between 0.01-1.5V**

It is also confirmed that carbon coating at higher temperature improves the first cycle CE and the rate capability. At elevated temperature, the carbon source gas help reduce the surface oxides, which was examined by Raman and XPS spectroscopy. A better graphitic carbon layer was also achieved at higher temperature. An optimized coating temperature of 800°C was confirmed according to experimental results (Figure VI - 95B).

The influence of further boron doping on the electrochemical performance of the micro-sized Si–C composites was also investigated. Boron doping was achieved by simply introducing dopant precursors ($B_2O_3$) during thermal disproportionation of SiO. Compared to undoped Si-C, the XRD peaks of B-doped Si-C shift to higher angles due to the replacement of Si atoms by smaller B atoms, which leads to a smaller lattice constant. This result, combined with the absence of Si-B alloy peaks, indicates the successful doping of B into Si. The Si Raman peak shifts from 510 $cm^{-1}$ for undoped Si to 494 $cm^{-1}$ for B-doped Si due to disorder in the Si structure caused by the stress developed in the surrounding Si atomic network after B doping, which is consistent with the XRD results (Figure VI - 96A). B in carbon was not detected as shifting of C peaks is not observed, which is due to the moderate carbon coating temperature, thus. Only Si was doped with B in the composite. The B-doped Si-C composite shows much improved rate capability, delivering a capacity of 575 mAh/g at 6.4 A/g without any external carbon additive, 80% higher than that of undoped composite (Figure VI - 96B).

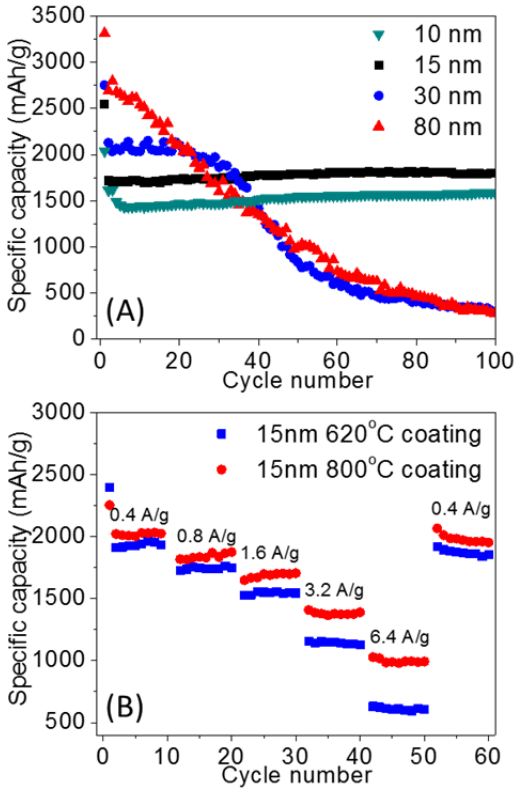


**Figure VI - 95: (A) Cycling performances of micro-sized Si-C composites with different building block sizes. (B) Rate performance of Si-C composite Si-15nm with different C coating temperatures**

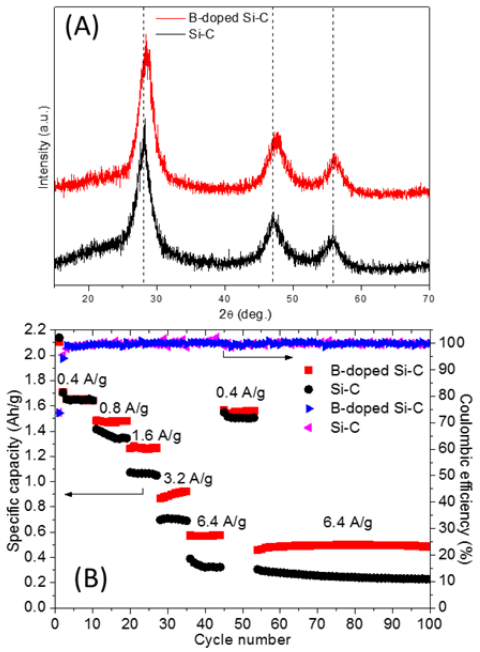


**Figure VI - 96: (A) XRD patterns of B-doped Si-C and Si-C composites. (B) Rate performance comparison of B-doped Si-C and Si-C composites**

The B-doped Si-C composite also exhibits better cycling stability at high rates. In contrast to the obvious capacity fading of Si-C, the capacity of B-doped Si-C was stable for about 50 cycles at 6.4 A/g. The improved rate capability and cycling stability are attributed to lower charge transfer resistance of B-doped Si-C.

**Synthesis and Evaluation of Polymer Binders.** A number of ionic polymer binders based on stiff backbones have been synthesized. Figure VI - 97 shows the capacity retiontion of anodes based on commercial Si NPs with NaCMC and experimental binders.

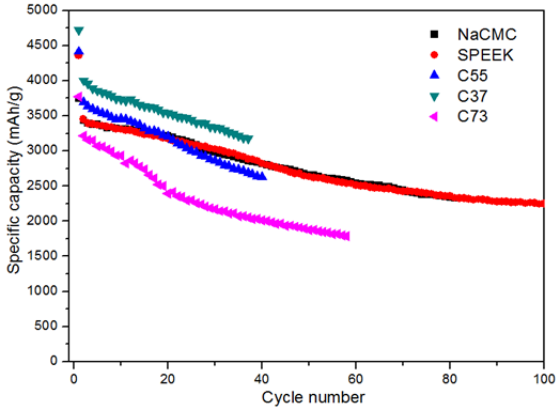


**Figure VI - 97: Cycling performance of commercial Si NP anodes with a range of ion-containing polymer binders**

By examining a range of binder compositions and looking at ionic forms of the binders in Na, H, and Li forms, the capacity fade performance was correlated to the interaction of the bonder with the Si-NP surface. Swelling of the binder in electrolyte was combatted with crosslinking of the binder by poly(acrylic acid). Optimized crosslinking showed binder performance that matched or exceeded the commercial NaCMC standard material. Higher cycling rates at equivalent capacity fade were observed with the experimental binders due to their electrolyte uptake and ionic conductivity.

## Conclusions and Future Directions

A novel $SiO/Fe_2O_3$ composite from commercially available SiO has been developed, synthesized and characterized. The composite showed improved capacity retention than that of SiO (capacity retention >75% after 50 cycles) and better high rate performance (~600 mAh/g at 4.8 A/g). A proposed mechanism that metallic Fe forms during lithiation of $SiO/Fe_2O_3$, increasing the conductivity of the composite and thereby significantly improving its performance has been made according to the experiment result and literature. A series of micro-sized Si-C composites has been synthesized and characterized. The overall particle size is micrometer range with a primary building block size of ~10 nm crystalline Si. The Si-C composite exhibits a reversible capacity of 1459 mAh/g after 200 cycles at 1 A/g with capacity retention of 97.8%. A further study on the influence of building block size and C-coating condition showed an optimized primary particle size of 15nm and a C-coating temperature of 800°C, which provide the best electrochemical performance as well as long cycling ability. In addition, boron doping was found to help increase the conductivity of the Si-C composite. The B-doped Si-C composite shows much improved rate capability, delivering a capacity of 575 mAh/g at 6.4 A/g without any external carbon additive, 80% higher than that of undoped composite.

Binder properties were shown to influence the performance of commercial Si-NP based anodes. The capacity fade was controlled by the interaction between the binder and the NPs and could be modulated based on the chemistry of the binder and crosslinking.

During the remainder of the project period, future work will focus on: 1) Introducing Si alloy with different forms (e.g., surface coating, alloy) to further improve the performance of previous reported Si-based materials. 2) Electrochemical characterization of the modified Si-based anode materials with improved mass loading. 3) Synthesis and optimization of semiconducting polymer binders with strong surface-bonding groups.

## FY 2013 Publications/Presentations


1. "Development of High Energy Density Lithium-Sulfur Cells," *DOE Annual Peer Review Meeting*, May 13-17, 2013, Washington, DC.
2. Wang, D. H., "In Symposium of Nanostructured Materials for Lithium Ion Batteries and for Supercapacitors," *TMS Annual Meeting & Exhibition*, San Antonio, TX, March 2013.
3. Yi, R., Dai, F., Gordin, M. L., Chen, S., Wang, D., *Advanced Energy Materials* **3**, 295-300 (2013).
4. Yi, R., Dai, F., Gordin, M. L., Sohn, H., Wang, D., *Advanced Energy Materials,* DOI:10.1002/aenm.201300496 (2013).
5. Yi, R., Zai, J., Dai, F., Gordin, M. L., Wang, D. *Electrochem. Communications,* **36**, 29-32 (2013).
6. Zhou, M., Gordin, M. L., Chen, S., Xu, T., Song, J., Lv, D., Wang, D. *Electrochem. Communication*s, **28**, 79-82 (2013).

# VI.C.9 Development of Silicon-based High Capacity Anodes (PNNL)

**Ji-Guang Zhang**
Pacific Northwest National Laboratory

902 Battelle Boulevard, Mail Stop K2-44
Richland, WA, 99352
Phone: (509) 372-6515; Fax: (509) 375-2186
E-mail: Jiguang.Zhang@pnnl.gov

**Jun Liu**
Pacific Northwest National Laboratory
902 Battelle Boulevard, Mail Stop K2-01
Richland, WA, 99352
Phone: (509) 375-4443; Fax: (509) 351-6242
E-mail: Jun.Liu@pnnl.gov

Start Date: October 2010
Projected End Date: September 2014

## Objectives

- Develop Si-based anodes with high capacities, high cycle stabilities and high rate capabilities.
- Develop low-cost synthesis routes for Si-based anodes.
- Advance the fundamental understanding on the electrolyte additive effect, stress and volume expansion effect, and degradation mechanism of Si-based anodes.

## Technical Barriers

Low energy density, limited cycle life, and high cost.

## Technical Targets

- Identify the main failure mechanisms of Si-based anodes.
- Develop low-cost and scalable approaches to synthesize Si-based nanocomposite materials with improved performance (a capacity retention of >700 mAh/g over 250 cycles).
- Demonstrate good cyclability of thick electrodes.

## Accomplishments

- Developed high-capacity stable Si anodes using a scalable anodization method. Porous Si synthesized by the electrochemical etching process has demonstrated excellent cycling performance with a high capacity of up to ~750 mAh/g (based on the full electrode including the carbon additive and binder) and >80% capacity retention over 1000 cycles.
- Developed pre-lithiation treatment of anode and reduced the first cycle irreversible capacity loss of the porous Si anode to <10%.
- Demonstrated good cycling stability of thick porous Si anodes with a high areal specific capacity of ~1.5 mAh/cm$^2$ and a capacity retention of >95% over 200 cycles.
- Identified the fundamental mechanism on how FEC additive affects the formation of solid electrolyte interphase (SEI) film on Si anode: 1) FEC is reduced through the opening of the five-member ring leading to the formation of lithium poly(vinyl carbonate), LiF and some dimers; 2) The FEC-derived lithium poly(vinyl carbonate), which has good mechanical flexibility, leads to enhanced the stability of the SEI film.

✧ ✧ ✧ ✧ ✧

## Introduction

Si has very high theoretical capacity of ~4200 mAh/g and has a good potential to be used as an anode for next generation Li-ion batteries. However, large volume expansion during the lithiation process usually leads to a fast capacity fade hindering its practical applications. Several nanostructured Si materials have demonstrated good performance, but most of them work best only in low loading conditions and their performance degrade quickly with increasing capacity loading required by practical applications. Another barrier in this field is that most of high capacity Si based electrodes have to be prepared by high cost processes that are difficult to scale up. Therefore, to pave the road for practical applications, a cost effective and scalable approach needs to be developed to prepare Si based anodes which can retain good performance at high loading conditions.

## Approach

Two approaches have been developed for a highly stable, high-capacity anode based on silicon composite. First, the meso-porous sponge-like Si particles (MSS) with nano size pores and high porosity are synthesized

by a scalable anodization method. The etched material was then coated with a thin layer of carbon using chemical vapor deposition to improve its electronic conductivity. Although the etched samples exhibit a size of >20 μm, they were not pulverized even after thousands of charge/discharge cycles. This is a significant improvement as compared to those of the conventional large silicon particles. The large volume expansion of MSS during lithiation/de-lithiation was mainly accommodated by the inner pores so only ~30% expansion of the whole particle was observed. The large irreversible capacity loss in the as prepared anode was minimized by pre-lithiation of Si anodes using a controlled amount of stabilized Li metal powder (SLMP™, FMC Lithium) on the electrode.

In another effort, the cost-effective and scalable ball-milling method was further optimized to improve the cycling stability and rate performance of the core-shell structured Si/$B_4C$/graphite composite with high area specific capacity. In this composite, conductive $B_4C$ with high Mohs hardness serves not only as micro-/nano-millers in a high energy ball-milling process to break down micron-sized Si, it also improves the electronic conductivity of the composite. A low energy ball milling process was then used to coat a thin layer of conductive carbon to further enhance the conductivity of the composite.

The volume expansion effect and the electrolyte additive effect on the formation of the SEI film was investigated using advanced characterization techniques such as *in situ* TEM, $^6$Li nuclear magnetic resonance (NMR), and x-ray photoelectron spectroscopy.

## Results

**1. Mesoporous Silicon Sponge (MSS): An anti-pulverization structure for high-performance Lithium-ion anodes.** Porous Si with large pore sizes of ~50 nm has most of the volume change accommodated by the inner channels. Therefore, large Si particles (>20 μm) with such large pore sizes exhibit only ~30% volume expansion in their outside dimension and can be charged/discharged more than 1000 cycles without pulverization. Figure VI - 98 shows the *in situ* TEM result of the lithiation process of a porous Si particle. The dimension and crystallinity change at different lithiation states are monitored. Porous Si became amorphous during lithiation and the expansion along <01 1> is only 7.8%. The overall volume expansion of the whole particle is ~30%, much less than 300% observed in the fully lithiated conventional Si particles.

Porous Si anode showed excellent cycling stability with a high initial capacity (based on the whole electrode weight including binder and conductive carbon) of up to ~750 mAh/g. By tuning the weight ratio of the MSS in electrodes, the capacity and the cycling stability of the anode can be fine-tuned for different applications. Figure VI - 99a shows the representative results of an electrode with ~46 wt% MSS. It exhibits a specific capacity of ~640 mAh/g and ~81% capacity retention over 1000 cycles. Figure VI - 99b is the long term cycling data of a battery with ~40 wt% MSS in the electrode. A capacity of ~570 mAh/g and ~87% capacity retention over 1000 cycles were obtained.

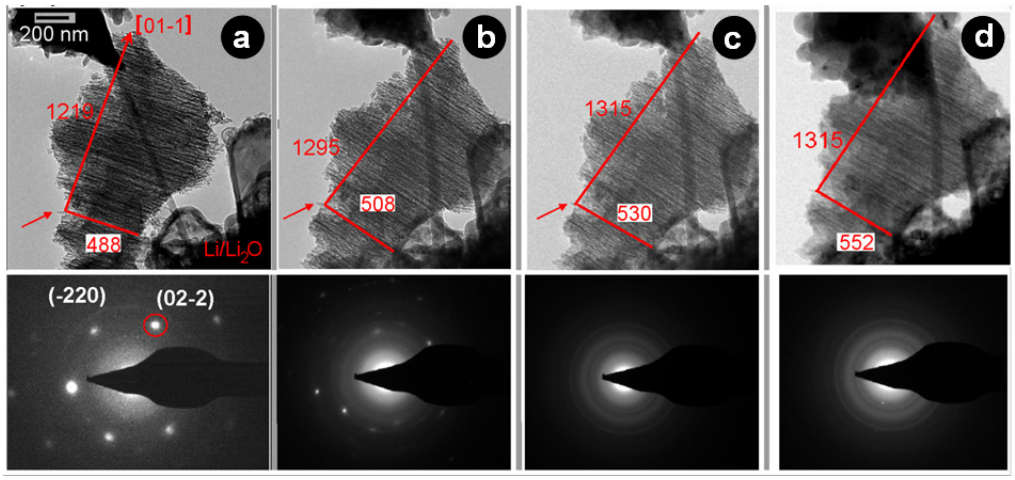


**Figure VI - 98: *In situ* TEM observation of the lithiation process of an MSS particle. a) -d) TEM images and selected area electron diffraction patterns of the MSS particle at different lithiation states: a) before lithiation; b) 22 min of lithiation; c) 40 min of lithiation; d) 160 min of lithiation. Note that the scale bar in b) applies to b-d)**

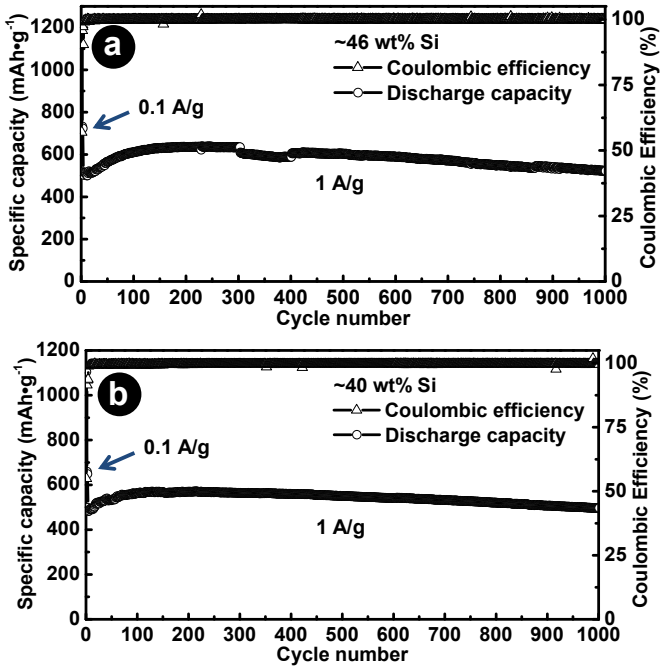


**Figure VI - 99: Long-term cycling of the MSS electrode with a) 46 wt% and b) 40 wt% Si loading**

With the pulverization eliminated and particle volume expansion limited to ~30%, MSS allows good cycling stability for electrodes with high Si loading per unit area. A high area specific discharge capacity of ~1.5 mAh/cm$^2$ at 0.5 mA/cm$^2$ discharge and 0.75 mA/cm$^2$ charge current density has been demonstrated (Figure VI - 100). The sample has demonstrated excellent cycling stability with ~95% capacity retention over 200 cycles.

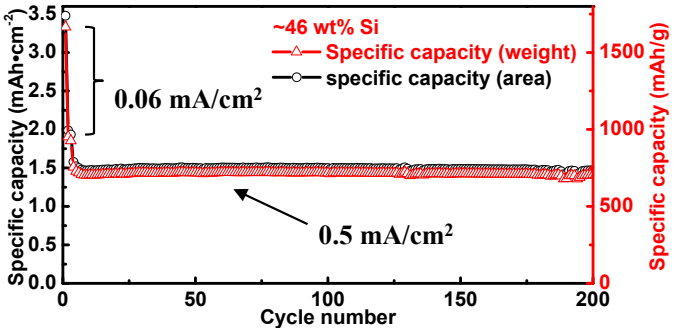


**Figure VI - 100: Cycling stability of the porous Si anode with a high areal discharge capacity of ~1.5 mAh/cm$^2$**

**2. Improved Si/$B_4C$/graphite (SBG) composites.** The SBG composite shows improved cycling stability after further modification. Figure VI - 101 shows the modified SBG material with a high areal specific capacity of ~1.25 mAh/cm$^2$ with >95% capacity retention over 100 cycles. The area specific capacity of the electrodes can be tuned by adjusting the ratio of the electrode and electrolyte additives.

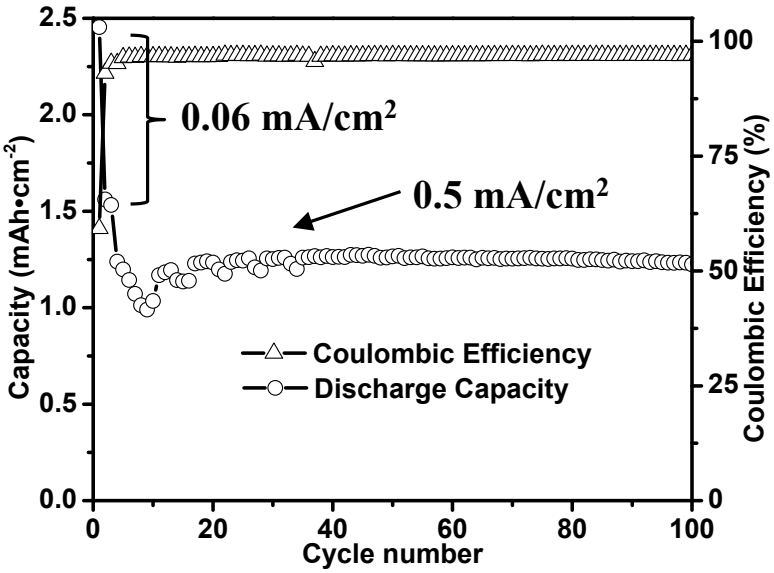


Figure VI - 101: Cycling performance of the modified SBG composite with ~12.8 wt% additive

**3. Pre-lithiation treatment of Si anodes.** The pre-lithiation of Si anodes was done by adding an appropriate amount of SLMP™, from FMC Lithium, on the electrodes. The irreversible capacity loss of Si based anode in the first cycle was greatly reduced after pre-lithiation treatment. Figure VI - 102a shows the cycling performance of a modified SBG electrode after pre-lithiation. It has a high areal specific capacity of ~1.5 mAh/cm$^2$ and ~88% capacity retention after 50 cycles. Figure VI - 102b and c are the cycling performance of pre-lithiated MSS electrodes of different thickness. For thin electrodes, it has a capacity of ~740 mAh/g and the capacity retention is ~96% over 300 cycles (Figure VI - 102b). For thick electrodes, it has ~95% capacity retention over 200 cycles even with a high area specific capacity of ~1.5 mAh/cm$^2$ (Figure VI - 102c).

**4. The fundamental mechanism on FEC effects.** The fundamental mechanism on how FEC additive affects the formation of the SEI film on Si anode has been investigated. Based on the SEM morphology and $^6$Li NMR investigations, it was found that the SEI film formed in the FEC-free electrolyte grows much faster than in the electrolyte with FEC. The results of x-ray photoelectron spectroscopy study (Table VI - 3) indicates that Li/F ratio in SEI film formed in FEC containing electrolyte is much larger than that which is predicted by the previous SEI formation mechanisms. Based on these results, a molecular-level mechanism (Figure VI - 103) was proposed on how FEC affects the formation of the SEI film: 1) FEC is reduced through the opening of the five-member ring leading to the formation of lithium poly(vinyl carbonate), LiF and some dimers; 2) The FEC-derived lithium poly(vinyl carbonate) would enhance the stability of the SEI film. The proposed reduction mechanism opens a new path to explore new electrolyte additives that can improve the cycling stability of silicon-based electrodes.

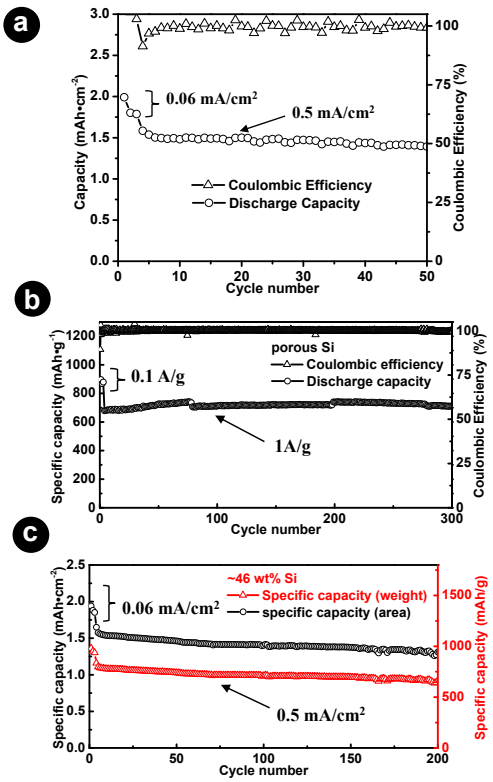


Figure VI - 102: Cycling stability of pre-lithiated Si anodes. a) Modified SBG composite electrode with a high area specific capacity of ~1.5 mAh/cm$^2$. b) Thin MSS electrode. c) Thick MSS anode with a high area specific capacity of ~1.5 mAh/cm$^2$

**Table VI - 3: The percentage of Li, C, O and F in the SEI films in electrolytes. a) 1M $LiPF_6$ in EC/DMC (1:2 in vol.); b) 1M $LiPF_6$ in EC/DMC (1:2 in vol.) with 10 wt% FEC; c) 1M $LiClO_4$ in pure FEC**

| Table 1. The ratio of Li, C, O and F in the SEI films in electrolytes (a) 1M $LiPF_6$ in EC/DMC (1:2 in vol.), (b) 1M $LiPF_6$ in EC/DMC (1:2 in vol.) with 10% FEC and (c) 1M $LiClO_4$ in pure FEC | | | | | |
|---|---|---|---|---|---|
| Samples \ Elements | Li | C | O | F | Li/F ratio |
| Electrolyte (a), 2 cycles | 27.7 | 23.3 | 24.1 | 24.9 | 1.11 |
| Electrolyte (a), 35 cycles | 22.7 | 31.3 | 37.6 | 8.4 | 2.70 |
| Electrolyte (b), 2 cycles | 22.9 | 32.5 | 32.1 | 12.5 | 1.83 |
| Electrolyte (b), 100 cycles | 21 | 33.8 | 31.9 | 13.3 | 1.58 |
| Electrolyte (c), 2 cycles | 21.1 | 34.7 | 32.2 | 12 | 1.76 |

**5. Optimization of binder.** Several different binders including PVDF, CMC, sodium alginate, PEO, and CMC-SBR have been investigated to further improve the cyclability and Coulombic efficiency of the SBG composite electrode. A mixture of CMC-SBR (10 wt%-10 wt%) binder is found to be the best choice for electrodes with high area specific capacity. Figure VI - 104 shows the typical cycling performance of a thick SBG electrode with the capacity of ~1.4 mAh/g. The capacity retention is 78% after 95 cycles.

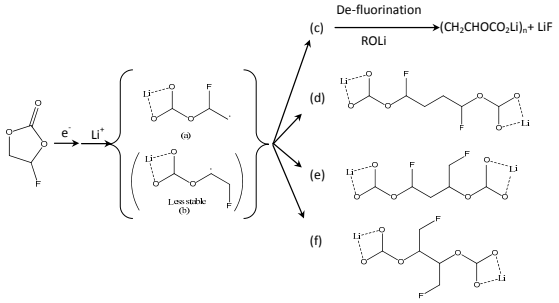


**Figure VI - 103: A proposed decomposition mechanism of FEC**

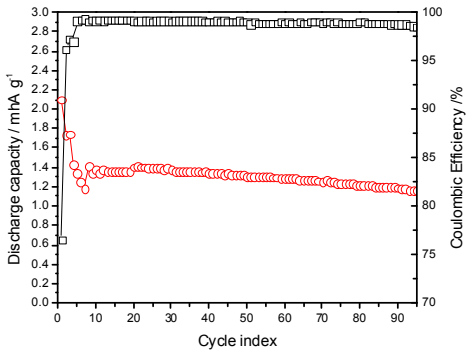


**Figure VI - 104: Cycling stability of the SBG electrode with CMC-SBR binder**

## Conclusions and Future Directions

Micron sized Mesoporous silicon sponge was synthesized by the electrochemical etching process. It exhibits only ~30% overall volume expansion during full charge process so a large MSS particles (>20 μm) can be cycled without pulvurization. The thin electrode prepared with MSS demonstrated excellent cycling performance with a high capacity of ~750 mAh/g (based on the full electrode including the carbon additive and binder) and >80% capacity retention over 1000 cycles. The thick electrodes with a high area specific capacity of ~1.5 $mAh/cm^2$ also demonstrated a capacity retention of >95% over 200 cycles. The SBG composite was further optimized to improve their cycling stability especially for thick electrodes. The modified SBG material demonstrated good cycling stability with > 95% capacity retention over 100 cycles even at a high area specific capacity of ~ 1.25 $mAh/cm^2$. Pre-lithiation treatment was developed to reduce the first cycle irreversible capacity loss. By adding Li powder to Si electrodes, the first cycle irreversible loss can be reduced to <10% while the capacity and cycling stability almost remain the same. At last, the fundamental mechanism on how FEC additive affects the formation of the SEI film on Si anode has been identified. This will open a new path to explore electrolyte additives that can improve the cycling stability of silicon anodes.

Future work will focus on the following areas:

- Develop new approaches and electrode structures to enable electrodes with high Si mass loading without compromising the long-term cycling stability.
- Optimize porosity of porous Si and the architecture of rigid skeleton supported Si composites to further investigate the stress and volume effect to the capacity fading.
- Develop new electrolyte additives and binders to improve stability of the SEI layer and stability of the thick Si-based anode.
- Develop a more cost-effective method to synthesize porous Si.

## FY 2013 Publications/Presentations

1. Xilin Chen, Xiaolin Li, Donghai Mei, Ju Feng, Mary Y Hu, Jianzhi Hu, Mark Engelhard, Jianming Zheng, Wu Xu, Jie Xiao, Jun Liu, Ji-Guang Zhang, "Reduction and polymerization of fluoroethylene carbonate for stable SEI via alternative ring opening mechanism," *Chem Sus Chem.* In press.
2. Cong-Min Wang, Xiaolin Li, Zhiguo Wang,Wu Xu, Jun Liu, Fei Gao, Libor Kovarik, Ji-Guang Zhang, Jane Howe, David J. Burton, Zhongyi Liu, Xingcheng Xiao, Suntharampillai Thevuthasan, and

Donald R. Baer, "*In situ* TEM Investigation of Congruent Phase Transition and Structural Evolution of Nanostructured Silicon/Carbon Anode for Lithium Ion Batteries," *Nano Letters,* **12**(3):1624–1632.

3. Meng Gu, Ying Li, Xiaolin Li, Shenyang Hu, Xiangwu Zhang, Wu Xu, Suntharampillai Thevuthasan, Donald R. Baer, Ji-Guang Zhang, Jun Liu, and Chongmin Wang, "*In situ* TEM Study Of Lithiation Behavior Of Silicon Nanoparticles Attached to and Embedded in a Carbon Matrix," *ACS Nan,* **6**(9):84398447.
4. "Development of Si-based High Capacity Anodes," *DOE Annual Peer Review Meeting*, May 13-17, 2013, Washington, DC.
5. Xiaolin Li, et al., "Porous structured silicon-based nanocomposites as high performance Li-ion battery anodes," *2013 MRS Spring Meeting*, San Francisco, CA.
6. Xiaolin Li, et al., "Porous Si as high performance Li-ion battery anodes," *246th ACS Meeting*, 2013, Indianapolis, IN (Invited).
7. Ji-Guang Zhang et al., "Meso-Porous Silicon Sponge as High Performance Li-ion Battery Anodes," *8th China-U.S. EV and Battery Technology Workshop*, Sep. 21, 2013, Chengdu, China.
8. Ji-Guang Zhang, "Next Generation of energy storage systems," Naval Postgraduate School-Defense Energy Seminar, August 7, 2013, Monterey, CA.

# VI.C.10 Wiring up Silicon Nanoparticles for High Performance Lithium Ion Battery Anodes (Stanford U.)

**Yi Cui**
Stanford University.

Department of Material Science and Engineering
476 Lomita Mall, McCullough 343
Stanford, CA 94305
Phone: (650) 723-4613; Fax: (650) 725-4034
E-mail: yicui@stanford.edu

Start Date: October 2010
Projected End Date: September 2014

## Objectives

- Go beyond the charge capacity limitation of conventional carbon anodes by designing nano-architectured silicon electrodes.
- Design, synthesize and characterize Si nanostructure-based anodes to overcome the volume change-induced materials challenges and to realize high performance.
- Understand the fundamental structure-property relationship on electrode materials with large structure and volume changes.
- Develop low-cost materials processing methods.

## Technical Barriers

The large structure and volume changes of Si during cycling causes multiple materials challenges: 1) mechanical breaking; 2) unstable solid electrolyte interface (SEI); 3) difficulties in maintaining good electrical connections. These fundamental challenges result in the following technical barriers to good battery performance:

- Large first cycle irreversible capacity loss
- Poor cycle life
- Inadequate coulombic efficiencies

## Technical Targets

- Develop fundamental materials guidelines through structure and property correlations and nanostructured Si anodes with these features to address the material challenges outlined above.
- Develop synthesis techniques to produce the designed nanostructured Si anodes.
- Develop low-cost materials processing methods.

## Accomplishments

- Used *in situ* transmission electron microscopy (TEM) to examine critical size and rate for fracture of crystalline, polycrystalline and amorphous Si nanostructures
- Developed a synthesis strategy to make Si nanoparticles from rice husks, an abundant and cheap source
- Developed an *in situ* polymerization method to incorporate conducting hydrogel into Si nanoparticle anodes
- Developed a variety of carbon templates from crab shells to make Si-C nanocomposites with controllable morphology

✧ ✧ ✧ ✧ ✧

## Introduction

Next generation high capacity electrode materials are needed in order to generate high energy battery technology to meet the demands of the transportation sector. Silicon is an exciting and promising anode material for replacing carbon in Li-ion batteries due to: 1) a high gravimetric capacity of ~4200 mAh/g, ten times higher than graphite (~370 mAh/g); 2) a high volume capacity; 3) its relatively low working potential (~0.5 V Vs $Li/Li^+$), which makes it suitable as an anode; 4) the abundance and environmentally friendly nature of Si; and 5) the ability to leverage the fundamental and manufacturing knowledge that has been established in the Si semiconductor and solar industries. However, there exist several scientific and technical challenges for silicon anodes: 1) Mechanical fracture caused by large volume changes. The electrochemical alloying reaction of Li with Si involves volume expansion of up to 300% and significant contraction during lithium extraction. The stress induced by the large volume changes causes cracking and pulverization of silicon, which leads to loss of electrical contact and eventual capacity fading. 2) Unstable SEI. The repetitive volume expansion/contraction causes the continuous movement of the interface between Si and organic electrolyte, which makes it challenging to form a stable SEI layer, resulting in low coulombic efficiency and capacity loss during cycling. 3) It is challenging to maintain good

electrical contact between Si materials and the current collector. Even though mechanical fracture does not take place in Si nanostructures below critical sizes, large volume changes can still cause the movement of Si nanostructures and their detachment from the conducting framework during long-term battery cycling. 4) Challenges associated with generating Si materials to address the above three challenges with low-cost and scalable processing.

The goal of this project is to study the fundamental principles related to alloy anodes, to design nanostructured Si anodes to solve the three fundamental challenges and to develop low-cost and scalable processing for these materials.

## Approach

This project takes a two-pronged approach to solving these problems. First, *ex situ* and *in situ* observation techniques are developed and used to uncover the fundamental nature of the Li-Si reaction and volume changes. Insight gained from this fundamental study is used as the framework for designing new nanostructured anodes that feature minimal structural damages and dimensionally stable surface/electrolyte interface regions. A focal point of the project is to also develop low-cost and scalable methods to synthesize these designed nanostructured Si anodes.

## Results

**Unexpected two-phase lithiation in amorphous Si.** Amorphous hydrogenated Si spheres were fabricated via decomposition of trisilane in supercritical n-hexane at high temperature. The *in situ* TEM set-up is shown in Figure VI - 105a. When a negative bias was applied to the amorphous Si electrode, Li diffused into the Si and it became lithiated, as shown in Figure VI - 105b-e.

The sharp contrast between the core and shell regions in Figure VI - 105c, d during lithiation is unexpected, because this indicates that there is a reaction front that sweeps through the particle. The lithiation mechanism is important to understand because it affects fracture behavior and reaction kinetics. Analysis of the TEM images showed that this contrast difference could not be caused by conventional diffusion. Previously, it was thought that amorphous Si is lithiated via a single-phase reaction because of its sloping potential profile in electrochemical experiments, but these TEM experiments show that it is a two-phase reaction. Further experiments showed that this two-phase behavior was limited to the first lithiation – later lithiation cycles did not show a reaction front. The two-phase reaction is attributed to the activation energy required to break up the Si-Si bonds in the amorphous Si phase, which is actually similar to crystalline Si lithiation. The single-phase reaction on later cycles may occur because of lingering damage (dangling bonds) in the amorphous Si or perhaps even trapped Li in the structure. This study shows that the first lithiation of amorphous and crystalline Si is more similar than previously thought. However, there are some important differences: 1) amorphous Si particles up to 800 nm in diameter did not fracture upon lithiation, whereas crystalline Si particles >~200 nm did fracture, and 2) the amorphous Si particles show better kinetics (there is not reaction front slowing, as in crystalline Si). These features suggest that amorphous Si may be more advantageous in real Si electrodes.

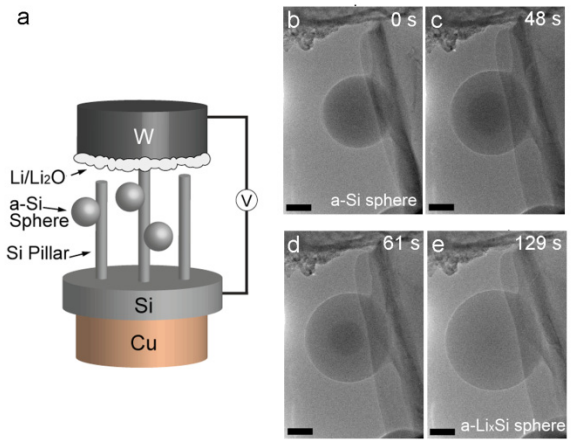


**Figure VI - 105: (a) Schematic of *in situ* device. (b-e) Time series of amorphous Si sphere during lithiation**

**Si nanoparticles from abundant and cheap sources for Li battery anodes.** Si is an abundant element in nature, but the electronic-grade Si that is commonly used to synthesize nanomaterials is quite expensive. Cheap methods to easily synthesize large quantities of lower-purity Si are needed. We have developed a method to synthesize Si nanoparticles for Si batteries directly from agricultural waste products. Specifically, we use rice husks, which are extremely cheap (~$18 per ton) and naturally contain up to 20 wt% $SiO_2$. We first convert the rice husks to pure silica by burning in air and then we reduce the silica to silicon. This results in an interconnected network of nanoparticles, as shown by the SEM images in Figure VI - 106a. The particles are agglomerated and are physically interconnected, but the void space between the particles should allow for accommodation of volume expansion during lithiation. The synthesis process results in a 5 wt% yield of Si when considering the weight of the initial rice husks. The Si nanoparticles were made into slurry-type electrodes and tested in half cells vs. Li metal. Galvanostatic curves are shown in Figure VI - 106b. The initial discharge capacity is ~4,100 mAh/g at C/50. After this, the rate is increased to

C/2, and a stable capacity of about 1,750 mAh/g is exhibited over 300 cycles.

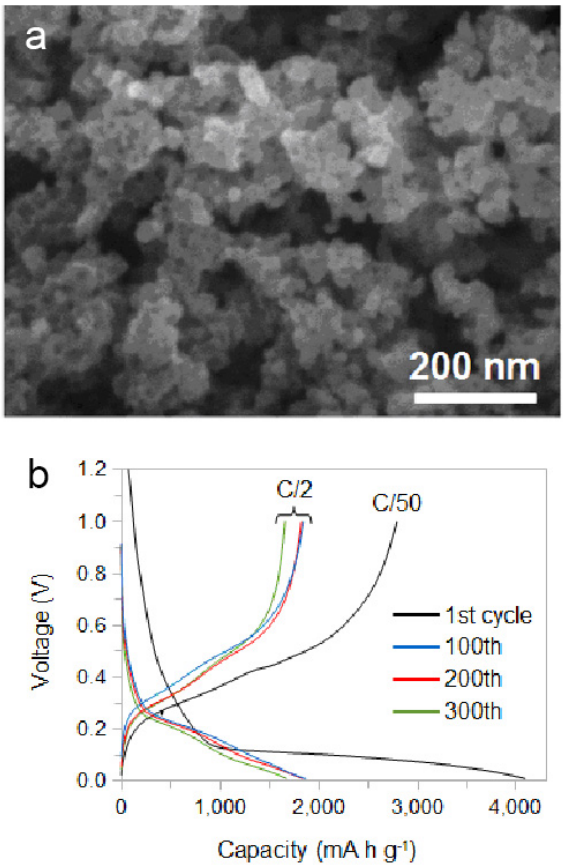


**Figure VI - 106: (a) SEM images of the Si nanoparticles. (b) Galvanostatic cycling of the Si nanoparticle electrode**

**Incorporation of conducting hydrogel into Si nanoparticle anodes.** A high-performance Li-ion battery anode has been fabricated by encapsulating Si nanoparticles in a 3D porous conductive polymer hydrogel framework. Typically, Si nanoparticles are mixed with monomer and crosslinker in the solution first, and then initiator was added to start the polymerization. This unique *in situ* polymerization fabrication technique results in a well-connected 3D network structure consisting of Si nanoparticles conformally coated by the conducting polymer (Figure VI - 107a). Such hierarchical hydrogel framework combines multiple advantageous features. First, the continuous electrically conductive PANi network provides fast electronic and ionic transfer channels. Second, strong interactions were introduced between Si nanoparticles and PANi hydrogel to make the framework more stable. Third, the porous hydrogel network provides enough free space for Si volume change during lithiation/delithiation process. With this anode, we successfully achieved high capacity and extremely stable electrochemical cycling. The electrode demonstrates a cycle life of 5,000 cycles with over 90% capacity retention at current density of 6.0A/g (Figure VI - 107b). The solution synthesis and electrode fabrication process are highly scalable and compatible with existing slurry coating battery manufacturing technology. This will potentially allow for the high-performance composite electrode to be scaled up for manufacturing the next generation of high-energy Li-ion batteries.

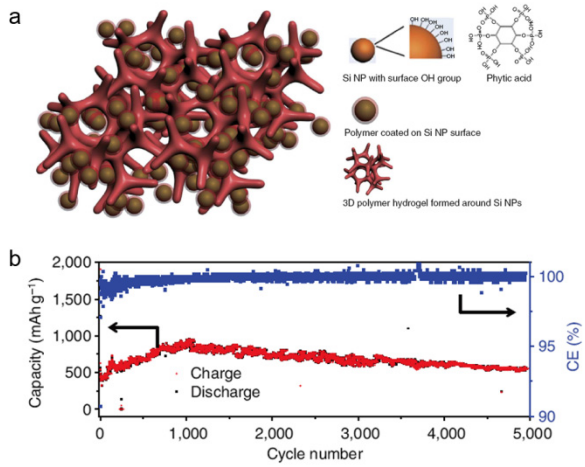


**Figure VI - 107: (a) Schematic illustration of 3D porous SiNP/conductive hydrogel composite electrodes. (b) Lithiation/delithiation capacity and CE of Si-PANi electrode cycled at current density of 6.0 A/g for 5000 cycles**

**Crab shells as sustainable templates from nature for Li-ion battery anodes.** Crab shells with the unique Bouligand structure consisting of highly mineralized chitin-protein fibers can be used as biotemplates to fabricate hollow carbon nanofibers. Typically, crab shell was calcined in the air to remove the chitin-protein organic to form pure $CaCO_3$ frameworks containing twisted hollow channels with ~60 nm inner diameter. As illustrated in Figure VI - 108b, a carbon thin layer was then coated on the whole surface of the frameworks, followed by silicon deposition into the carbon channels. Final Si encapsulated carbon fibers was obtained after removing $CaCO_3$ with HCl solution. The resulting nanostructured Si/C electrodes show high specific capacities (3060 mAh/g) and excellent cycling performance (up to 200 cycles with 95% capacity retention). The coulombic efficiencies of the cells over 200 cycles are ~98.6% at C/2 and ~98.9% at 1C (Figure VI - 108c). All these results indicate the high stability of crab shell-templated Si/C anode materials. Since crab shells are readily available due to the 0.5 million tons produced annually as a by-product of crab consumption, this waste-recycling preparation process is cheap and scalable for advanced rechargeable lithium ion batteries.

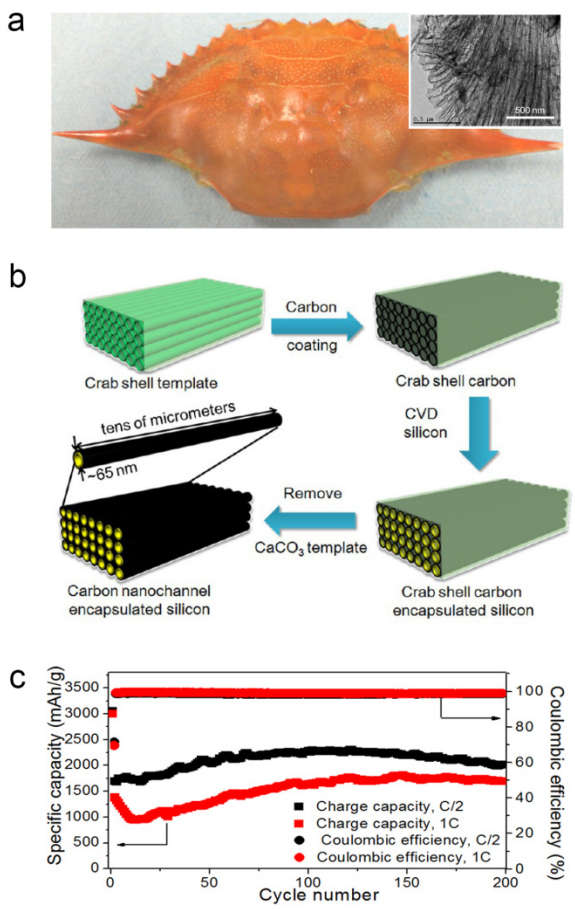


**Figure VI - 108: (a) Photo of a crab shell. The inset is TEM image of final carbon nano-channel arrays from crab shell. (b) Schematic illustration of the fabrication procedure for hollow carbon nanofiber arrays encapsulating silicon. Lithiation/delithiation capacity and CE of Si encapsulated crab shell-templated carbon channel**

## Conclusions and Future Directions

Much progress has been made on these projects this year. A variety of *in situ* and *ex situ* microscopy techniques have been used to determine the effect of nanostructure size, shape, and crystallinity on volume expansion/contraction and structural changes. Based on these fundamental studies, tailored nanostructured anodes were designed and fabricated that showed high capacity, high coulombic efficiency, and good cycle life. *In situ* polymerization of conducting hydrogel on Si nanoparticles makes a 3D porous Li-ion anode. By taking advantage of the conducting polymer matrix, as well as free space for Si volume changes, we successfully achieved high capacity and extremely stable electrochemical cycling. In addition, we developed various strategies to obtain Si nanostructures from sustainable sources, such as rice husks and crab shells. This green, cost-effective, and scalable synthesis will open a new avenue for producing nanostructured electrode materials from low-cost sustainable sources.

Future directions include: 1) further developing and exploring conducting polymer additives, coatings, and binder to improve the connectedness of the Si electrode framework during cycling. This includes the use of viscous polymers for a self-healing effect. In addition, the use of micron-scale Si particles will be explored in conjunction with polymer coatings. 2) *In situ* TEM and *ex situ* SEM study of two or multiple Si nanostructures during lithiation/delithiation will be started to understand how neighboring particles affect each other as volume changes. 3) Other conducting coating materials will be evaluated to increase the coulombic efficiency and cycling stability. 4) Finally, prelithiation of Si structures will be used to increase the first cycle coulombic efficiency.

## FY 2013 Publications/Presentations

1. N. Liu, K. Huo, M.T. McDowell, J. Zhao, Y. Cui, "Rice husks as a sustainable source of nanostructured silicon for high performance Li-ion battery anodes." *Scientific Reports*, **3**, May 2013.
2. M.T. McDowell, S.W. Lee, J.T. Harris, B.A. Korgel, C. Wang, W.D. Nix, Y. Cui, (2013). "*In situ* TEM of Two-Phase Lithiation of Amorphous Silicon Nanospheres." *Nano Letters*, **13**, 2, 758-764 January 2013.
3. M.T. McDowell, S.W. Lee, W.D. Nix, Y. Cui, "25th Anniversary Article: Understanding the Lithiation of Silicon and Other Alloying Anodes for Lithium-Ion Batteries." *Advanced Materials*, **25**, 36, 4966-4985 August 2013.
4. H. Wu, G. Yu, L. Pan, N. Liu, M.T. McDowell, Z. Bao, Y. Cui, "Stable Li-ion battery anodes by *in situ* polymerization of conducting hydrogel to conformally coat silicon nanoparticles." *Nature Communications*, **4**, June 2013.
5. H. Yao, G. Zheng, W. Li, M.T. McDowell, Z. Seh, N. Liu, Z. Lu, Y. Cui, "Crab Shells as Sustainable Templates from Nature for Nanostructured Battery Electrodes." *Nano Letters*, **13**, 7, 3385-3390, June 2013.

# VI.C.11 Synthesis and Characterization of Silicon Clathrates for Anode Applications in Lithium-ion Batteries (SwRI)

**Kwai S. Chan**
Southwest Research Institute

Department of Materials Engineering
Mechanical Engineering Division
6220 Culebra Road
San Antonio, TX 78238
Phone: (210) 522-2053; Fax: (210) 522-6965
E-mail: kchan@swri.org

**Michael A. Miller**
Southwest Research Institute
Department of Materials Engineering
Mechanical Engineering Division
6220 Culebra Road
San Antonio, TX 78238
Phone: (210) 522-2189; Fax: (210) 522-6220
E-mail: mmiller@swri.org

Start Date: October 2010
Projected End Date: September 2014

## Objectives

- Develop scalable synthesis methods for producing empty and substituted silicon clathrates
- Design, synthesize, and characterize silicon clathrate compounds for anode applications in Li-ion batteries
- Fabricate and characterize prototype silicon clathrate anodes designed to exhibit small volume expansion during lithiation, high specific energy density, while avoiding capacity fading and improving battery life and abuse tolerance

## Technical Barriers

This project addresses the following technical barriers of the lithium-ion battery technology, especially focusing on the development of silicon clathrate compositions as anode materials:

- Low energy density
- Low power density
- Short calendar and cycle lives

## Technical Targets

Develop silicon clathrate anodes to meet PHEV and EV goals by exceeding current benchmarks (Conoco Phillips CPG-8 Graphite/1 M $LiPF_6$+EC:DEC (1:2)/ Toda High-energy layered (NMC) in the following metrics:

- Energy density
- Power density
- Calendar and cycle lives

## Accomplishments

- Synthesized 20 mg of empty silicon clathrate ($Si_{46}$) via a Hofmann-type elimination-oxidation reaction scheme done in solution
- Constructed and evaluated several electrochemical half-cells using $Ba_8Al_8Si_{38}$ synthesized as anodes combined with best-case additives and electrolyte formulations
- Characterized electrochemical properties of silicon clathrate anodes and achieved an initial capacity of 300 mAh/g (active material basis) on the 4$^{th}$ cycle which decayed gradually to 54 mAh/g at near steady-state conditions after 200 cycles with a coulombic efficiency of 98.79±0.14%. at C/2 for $Ba_8Al_8Si_{38}$
- Identified structural and mechanical states of silicon clathrate anodes during lithiation and delithiation processes and validated against theoretical calculations

✧ ✧ ✧ ✧ ✧

## Introduction

Low-cost advanced anode materials with high-energy density, high-power density, and longer calendar and cycle lives are needed to achieve DOE's performance targets for PHEV and EV applications. In an effort to address these needs, this project explores the viability of silicon clathrates (Type I) as an anode material for potential applications in PHEV and EV Li-ion batteries, and focuses efforts on the development of scalable synthetic methods, complete characterization of electrochemical performance, and the design and fabrication of prototype anodes for evaluation.

Silicon clathrate, a polymorph of silicon, is an emerging anode material that is composed of $sp^3$ bonded

silicon atoms arranged in cage-structures. It consists of crystalline Si with a regular arrangement of 20- and 24-atom cages fused together through five atom pentagonal rings (Type I clathrate) (see Figure VI - 109). It has a simple cubic structure with a lattice parameter of 10.335 Å and 46 Si atoms per unit cell ($Si_{46}$). The crystal structure (Space Group $Pm\bar{3}n$ ) of the $Si_{46}$ clathrate is different from the common form of crystalline Si (c-Si), which is diamond cubic (Space Group $Fd\bar{3}m$ ) with a lattice parameter of about 5.456 Å.

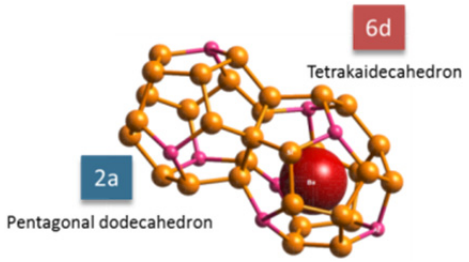


**Figure VI - 109: Silicon calthrate crystal structure**

First-principles computations performed at SwRI® have revealed that significant amounts of Li ions can be inserted into and extracted from the cage structure of silicon clathrates without substantial volume changes or pulverization of the cage structure. Theoretical predictions of the total, occupyable, and accessible volumes within Type I silicon clathrate structures indicate that the empty spaces within the cage structures are accessible to Li and amenable to Li intercalation through electrochemical means, while overcoming the usual problems of irreversible volume expansion encountered in *d*-Si-based anodes. On this basis, silicon clathrates are attractive as anode materials for Li-ion battery applications.

## Approach

SwRI is working with LBNL to develop silicon clathrate anodes for PHEV and EV applications. The approach is to synthesize guest-free Type I silicon clathrate ($Si_{46}$) using a number of high-temperature processing methods, while concurrently exploring an investigational low-temperature route for direct synthesis of guest-free clathrate. *Ab initio* and classical molecular dynamics (MD) computations are being carried-out to predict the lattice energies of pure-silicon and intermetallic (substitutional) clathrate structures, and to identify the lithiation pathways involved as these structures are intercalated with lithium atoms. Silicon clathrates will be utilized in combination with the appropriate or best-case additive to fabricate prototype anodes. Electrochemical characterization will be performed to evaluate and improve, if necessary, anode performance including cyclic stability. The final year of the program will be directed at the design, assembly, and characterization of a complete small-scale, prototype battery suitable for concept demonstration.

## Results

**Batch Synthesis via Soft Oxidation of $Na_4Si_4$.** The conditions for the phase transformation of fuel-grade sodium silicide ($NaSi_2$) were optimized to yield the highest purity of the Zintl phase $Na_4Si_4$ possible by varying excess additions of NaH combined with the silicide. XRD analyses of the thermal transformation products (Figure VI - 110) showed that new reflections emerge at or near the positions theoretically computed for the Zintl phase, and with similar relative intensities, when 10% excess NaH was combined with the silicide during thermal processing. Higher additions of NaH did not manifest the required XRD reflections for the Zintl phase. Using these process conditions, about 10 g of $Na_4Si_4$ was synthesized for subsequent use in the batch synthesis of $Si_{46}$.

After successful scale-up of $Na_4Si_4$, this Zintl compound was employed in combination with a previously-synthesized alkylammonium-$AlCl_3$ ionic liquid (IL) to synthesize empty silicon clathrate ($Si_{46}$) in batch quantity via a Hofmann-type elimination-oxidation reaction scheme done in solution. The XRD analysis (Figure VI - 111) of the reaction product indicated that the desired Type I clathrate was formed along with unreacted Zintl compound and the reaction by-products. The product will be further purified for subsequent electrochemical measurements as an anode material.

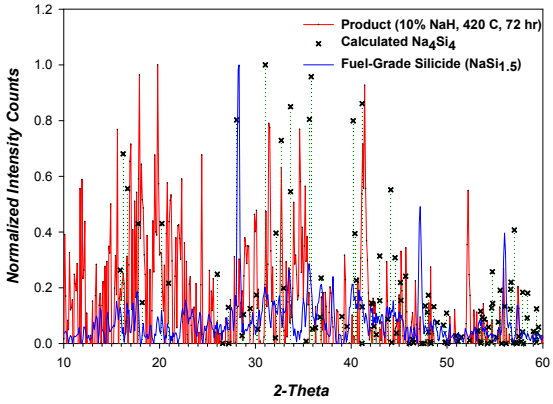


**Figure VI - 110: Overlay of powder XRD patterns for the fuel-grade silicide and transformation product, compared with the calculated reflections for the Zintl phase (Na4Si4)**

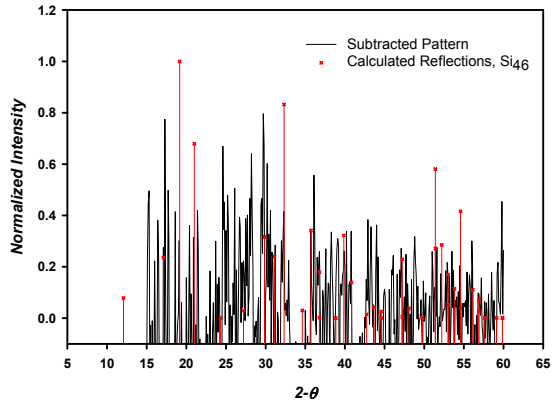


**Figure VI - 111: Overlay of powder XRD patterns for the synthesis product and the calculated reflections of empty clathrate (Si46), after subtraction of impurity phases**

**Molecular Modeling of Silicon Clathrates.** The lithiation pathways for Na-stabilized $Si_{46}$ were identifying by first-principles computations and the results are evaluated against those of Ba-stabilized and empty $Si_{46}$ clathrates by comparing the lattice constant and energy change as a function of the number of Li atom in Figure VI - 112. For all cases, insertion of Li causes expansion of the cage structure when the number of Li atoms inserted exceeds about 20 to 24 (Figure VI - 112a), depending on the number of Na or Ba guest atoms residing within the cage structure but not on the number of Al substituted atoms on the framework. The energy charge associated with Na- and Ba-stabilized silicon clathrates is comparable to those for lithiated silicides (Figure VI - 112b).

**Prototype Silicon Clathrate Anode Fabrication.** **Several** different additive and binder combinations were attempted in the fabrication of silicon clathrate anodes. The framework-substituted Type I clathrate, $Ba_8Al_8Si_{38}$, synthesized in bulk (200g) in the previous year, was processed via ball milling and sequential particle sizing to produce sub-micron particles (Figure VI - 113). The milled product was combined with a conductive additive to make a slurry. The conductive additive used included (1) 0.2 to 4 wt. % Graphenol®, (2) 10 wt.% Super P carbon, and (3) 20 wt.% Super P carbon. The resulting slurries were then used to cast thin-film anodes for electrochemical half-cell evaluation.

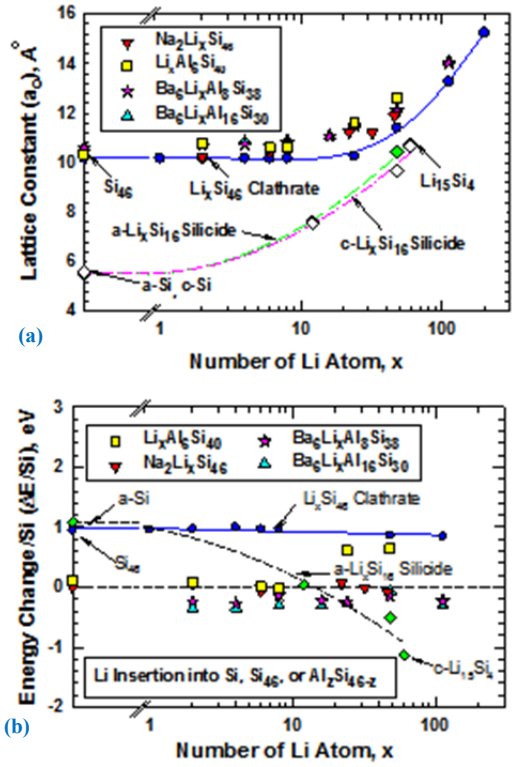


**Figure VI - 112: Lattice constant expansion and energy change associated with lithium insertion in Na- and Ba-stabilized clathrates against those for empty silicon clathrates: (a) lattice constant expansion, (b) energy change**

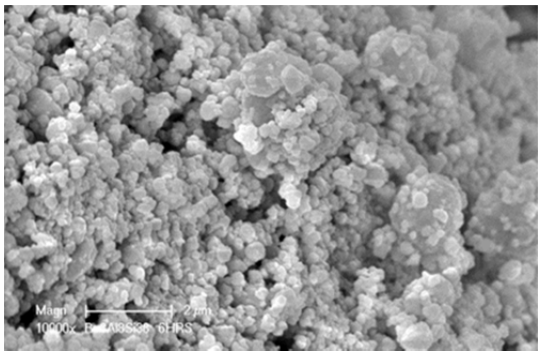

**Figure VI - 113: Particle morphology of processed $Ba_8Al_8Si_{38}$ milled powder for prototype anode**

**Half-Cell Electrochemical Characterization**. Half-cell charge/discharge cyclic tests were performed on an anode composed of the intermetallic clathrate, $Ba_8Al_8Si_{38}$, combined with Super-P carbon (10 wt.%) and EC/DEC/FEC electrolyte. The specific capacity and coulombic efficiency were recorded out to 200 cycles at C/2, allowing the half-cell to rest at OCP for ~ 8 hrs at the end of the 50th and 100th cycle (Figure VI - 114). These results showed an initial capacity of 300 mAh/g (active material basis) on the 4th cycle which decays to 54 mAh/g at near steady-state conditions upon reaching the 200th cycle. The average steady-state coulombic efficiency was 98.79±0.14%. Peak capacities much greater than the theoretical value (259 mAh/g for invariant lattice constant), along with marked improvements in the capacity fade, are expected from the use of higher than present carbon loadings.

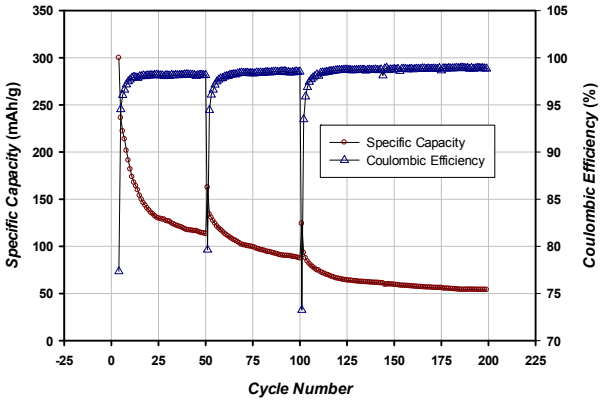


**Figure VI - 114: Long-term cyclic capacity and coulombic efficiency profiles measured for Ba8Al8Si38 anode (10 wt.% Super P + 10 wt.% PVDF) using ED/DEC/FEC (45:45:10). Cell was allowed to rest at OCP for ~8 hrs at end of 50th and 100th cycles before resuming test**

A suite of *ex situ* techniques was employed to map the structural and mechanical state of the clathrate anodes as a function of lithiation/delithiation cycles. Structural and compositional analysis of $Ba_8Al_8Si_{38}$ was done using high-resolution magic angle spinning nuclear magnetic resonance (MAS-NMR), and neutron diffraction measurements (facilitated through ORNL).

In the case of NMR, the chemical shift environments of $^{29}Si$ and $^{27}Al$ along with that of the $^{7}Li$ were probed to study the effects of lithium intercalation on structural parameters and local interactions. Notably, the $^{27}Al$-NMR spectra acquired for the unlithiated and lithiated clathrate (Figure VI - 115) show three distinct magnetic environments, most likely associated with the three known framework substitution sites in the dodecahedron and tetrakaidecahedron cages of the Type I clathrate structure. Upon lithiation, only the 16i framework sites near 80 ppm appear to be affected by the presence of $Li^+$, but only with respect to relative amplitude when comparing the integration ratios for the three lines. No significant change in chemical shift was observed, suggesting that $Li^+$ interactions with Al framework atoms are weak and the structural order of the framework remains intact. Only the spin-lattice ($T_1$) relaxation times are influenced by the local structuring of $Li^+$ near the 16i framework sites giving rise to a change in relative amplitude after lithiation. Additionally, the near-baseline resolution of the NMR lines corresponding to the three framework sites is remarkable from the viewpoint of substitutional order. This result indicates that Al substitution of framework atoms during synthesis does not occur randomly, but rather prefers ordered substitution for the bulk material. By contrast, random substitution would otherwise result in one broad peak due to the superposition of all site-substitution combinations.

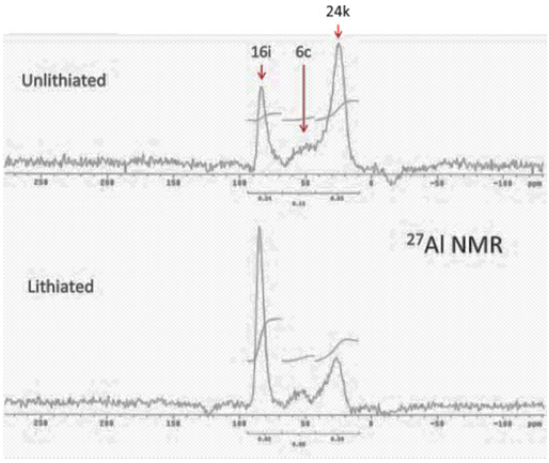


**Figure VI - 115: Solid-state $^{27}Al$ NMR spectra acquired for unlithiated ($Ba_8Al_8Si_{38}$) and lithiated ($Li_xBa_8Al_8Si_{38}$) clathrate anode material. The results show near-baseline resolution of the three known and magnetically-distinct framework substitution sites for a Type I structure: 6c, 16i, and 24k**

Neutron diffraction measurements (Figure VI - 116) were used to verify against first principles computations that the lattice constants for the clathrate alloy ($Ba_8Al_ySi_{46-y}$) do not change as a function of lithium intercalation up to the theoretical capacity (259 mAh/g for invariant lattice constant). Figure VI - 116 shows that the neutron diffraction patterns for the unlithiated (blue) and lithiated $Ba_8Al_8Si_{38}$ anodes exhibit the same intact structure and lattice constant. Additional diffraction measurements are needed to determine the extent to which the clathrate framework can be lithiated reversibly beyond its theoretical capacity.

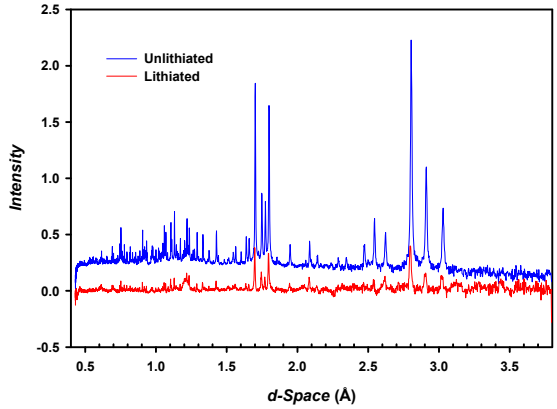


**Figure VI - 116: Neutron diffraction patterns obtained for Ba8Al8Si38 before (blue) and after lithiation (red), providing evidence that the clathrate framework remains structurally intact up to its theoretical capacity**

## Conclusions and Future Directions

A solution synthesis method based on the Hofmann-elimination oxidation reaction scheme was successful in producing empty $Si_{46}$. Future work will be to prepare half-cells with $Si_{46}$ anodes and demonstrate a cyclability of 50 cycles at C/2 and a capacity of 750 mAh/g.

Half-cells with a $Ba_8Al_8Si_{38}$ anode were successfully cycled for 200 cycles at C/2 with an initial capacity of 300 mAh/g and an average steady-state coulombic efficiency of 98.79±0.14%. Future work will be to prepare half-cells of $Ba_8Al_8Si_{38}$ with higher conductor contents and demonstrate a cyclability of 50 cycles at C/2 and a capacity of 1500 mAh/g.

A suite of *ex situ* techniques will be employed to map the structural and mechanical state of the clathrate anodes as a function of lithiation/delithiation cycles for both $Si_{46}$ and $Ba_8Al_8Si_{38}$ anodes. The experimental data will be evaluated against theoretical predictions based on first-principle computations.

## FY 2013 Publications/Presentations

1. "Synthesis and Characterization of Silicon Clathrates for Anode Applications in Lithium-Ion Batteries," *DOE Annual Peer Review Meeting*, May 13-17, 2013, Washington, DC.
2. M.A Miller, K.S. Chan, W. Liang, and C.K. Chan, "Clathrate Allotropes for Rechargeable Batteries," U.S. 2012/0295160 A1, Nov. 22, 2012.
3. C. K. Chan, M. A. Miller, and K. S. Chan, "Alloys of Clathrate Allotropes for Rechargeable Batteries," U.S. Patent Application No. 13/452,403 (pending).

# VI.C.12 First Principles Modeling of SEI Formation on Bare and Surface/Additive Modified Silicon Anode (TAMU)

**Perla Balbuena**
Texas A&M University

Department of Chemical Engineering
3122 TAMU
College Station, TX 77843
Phone: (979) 845-3375; Fax: (979) 845-6446
E-mail: balbuena@tamu.edu

**Jorge Seminario (co-PI)**
Department of Chemical Engineering
3122 TAMU
College Station, TX 77843
Phone: (979) 845-3301; Fax: (979) 845-3301
E-mail: seminario@tamu.edu

Start Date: October 2012
Projected End Date: September 2016

## Objectives

- Develop fundamental understanding of the molecular processes that lead to the formation of a solid electrolyte interphase (SEI) layer due to electrolyte decomposition on Si anodes.
- Develop a rational selection of additives and/or coatings.

## Technical Barriers

Description of the electrode surface chemistry; characterization of the electron transfer rate through the SEI layer; description of the SEI layer structure and its evolution as well as that of the electrode during cycling.

## Technical Targets

- Elucidate solvent and additive reduction mechanisms on Si surfaces as a function of degree of lithiation and nature of the exposed facet.
- Develop a method for evaluating electron transfer through solid surfaces and apply it to model SEI layers of various thicknesses on Si surfaces.
- Understand solvent and additive reduction mechanisms on surfaces covered with oxides.

## Accomplishments

- Effects of degree of lithiation and nature of the exposed surface on EC and FEC reductions were fully characterized and the most probable reduction mechanisms identified.
- Reactivity of oxide surfaces $Li_4SiO_4$ and $Li_2Si_2O_5$ were evaluated.
- Electron transfer through simple models of SEI layers on model electrodes (LiF and $Li_2O$ between EC and $Li_xSi_y$) was assessed.

✧ ✧ ✧ ✧ ✧

## Introduction

Investigation of the formation/growth mechanisms of the SEI layer on bare surfaces requires incorporation of effects from surface structure and chemical states: the presence of functional groups, surface oxidation, nature of exposed facets, and electrolyte composition including additive species. Finding the correspondence between additive molecular properties and SEI formation mechanism, structure, and properties will allow identification of new/improved additives. Including the state of lithiation of the surface is also a key factor to determine possible changes in the electrolyte reduction mechanism and/or nature of the products. Finally, it is crucial to understand how the electron transfer from the electrode to the electrolyte is modified by deposition of the initial SEI intermediates or products of the SEI formation reaction.

## Approach

A comprehensive first-principles computational approach employed in this work includes density functional theory (DFT), *ab initio* molecular dynamics (MD), and *ab initio*-Green's function theory. Static DFT is utilized within two approaches: cluster models are used to investigate electrolyte reduction on model Si surfaces with ultra-low state of lithiation, whereas periodic surfaces represent both quasi-amorphous low lithiated surfaces and well-characterized crystalline $Si_xLi_y$ alloys. Adsorption of solvent (EC) and additives ( FEC and VC) on the surface and the potential energy surfaces including activation barriers for their decomposition are studied with these methods. Models of periodic surfaces in contact with liquid electrolyte

mixtures are also utilized to investigate mechanisms of electrolyte reduction using *ab initio* MD (AIMD). Electron transport through the composite material (electrode/ SEI layer/electrolyte molecule) is determined using *ab initio* Green's functions calculations.

The procedure consists of separate DFT optimizations of the electrode (bare or coated), electrolyte, and "extended molecule" including all the components present in the interfacial region. These optimizations yield the Hamiltonian and overlap matrices needed to create the transition matrix used to evaluate the rate of electron transfer.

## Results

**Mechanisms of EC and FEC reductions on ultra-low lithiated surfaces.** EC and FEC reactions on $LiSi_{15}H_{16}$ clusters representing Si (001) surfaces were employed to model reduction on surfaces with an ultra-low degree of lithiation using DFT. For adsorbed EC, the barrier for ring opening via one $e^-$ transfer (1.08 eV) was found higher than that in gas phase or solution. A 2nd $e^-$ transfer to the adsorbed opened molecule yielded adsorbed $CO_3$ and $C_2H_4$. Two oxygen atoms bound on the Si(001) surface, leading to significant charge transfer from the Si cluster to $CO_3$. Alternatively, a 2nd electron may be transferred instead to the intact adsorbed molecule which then dissociates with a comparable barrier of 1.18 eV yielding adsorbed $CO_3$ and $C_2H_4$. Reaction energies were calculated for the subsequent association and reaction steps to form 5 different products. In general, the surface reactions have more favorable reaction energy compared to those taking place in the gas phase. In the presence of another EC molecule, both pathways (single and double $e^-$ transfer) are possible. However, a much lower energy barrier (0.24 eV) for the single electron transfer pathway suggested that this may be the favorable mechanism in very low lithiation stages at high EC concentrations.

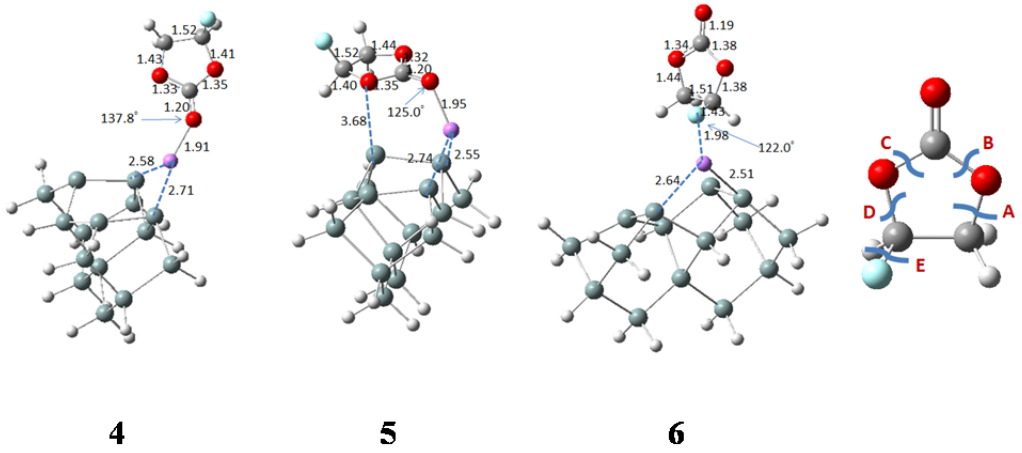


**Figure VI - 117: Calculated geometries of adsorbed FEC configurations on a low-lithiated Si (001) surface after 1 or 2 $e^-$ transfer processes. Image of FEC illustrates bond breaking pathways**

The FEC adsorbed system (FEC-$Li^+$-$Si_{15}H_{16}$) may receive one or two $e^-$ before the decomposition reactions take place. Figure VI - 117 illustrates the most stable configurations found. The most stable obtained via 1$e^-$ transfer is **4**, and **5** is the most stable after transfer of 2$e^-$. To understand the bond-breaking in FEC on the ultra-low lithiated Si surface, the first step of bond dissociation was examined for both mechanisms. Bond dissociation via 1 and 2 $e^-$ transfers was found plausible via C-O bond breaking (carbonyl $C_C$ or ethereal $C_E$ may be involved) and in some cases simultaneous breaking of two C-O bonds was found. The bond-breaking positions, A, B, C, D and E, are denoted in Figure VI - 117. For the 1 $e^-$ mechanism, bond cleavage occurs at A, B, C, D, and B/D. Bond-breaking at E was not found. It is deduced that the C-F breaking may not be viable for the 1 $e^-$ mechanism. The corresponding reaction energies and energy barriers are listed in Table VI - 4. $C_E$-O bond-breakings were thermodynamically favorable for the 1 $e^-$ mechanism, but kinetically unfavorable due to a high energy barrier (1.14-1.57 eV). The lowest energy barrier (0.43 eV) was found for the $C_c$-O cleavage. The intermediates had more binding site(s) on the Si surface, via O and $C_E$ atoms.

**Table VI - 4: First step for the reduction of FEC on Li-$Si_{15}H_{16}$ cluster. (Structure 4, Figure VI - 117). Reaction energies ($E_{reac}$) and energy barriers (E*) are in eV. Route refers to Figure VI - 117**

| Reactant | Product | Route | $E_{reac}$ | $E^*$ |
|---|---|---|---|---|
| **4** | •$CH_2$-CHF-$CO_3$-Li($Si_{cluster}$) | A | -0.48 | 1.14 |
| **4** | •$OCH_2$-CHF-OCO-Li($Si_{cluster}$) | B | 0.68 | 1.24 |
| **4** | •OCHF-$CH_2$-OCO-Li($Si_{cluster}$) | C | 0.35 | 0.43 |
| **4** | •FCH-$CH_2$-$OCO_2$ -Li($Si_{cluster}$) | D | -0.36 | 1.57 |
| **4** | •CHF-$CH_2$-O-Li($Si_{cluster}$)-$CO_2$ | B, D | -0.15 | 1.24 |

$C_C$-O bond breakings via the 2 $e^-$ mechanism were found both thermodynamically and kinetically favorable in agreement with AIMD simulations (Table VI - 5).

**Table VI - 5: First step for reaction of FEC-Li-$Si_{15}H_{16}^-$. Reaction energies ($E_{reac}$) and energy barriers (E*) are in eV. Route refers to Figure VI - 117**

| Reactant | Product | Route | $E_{reac}$ | $E^*$ |
|---|---|---|---|---|
| **5** | $^{\bullet}OCO_2$ -($Si_{cluster}$)$^-$ + $CH_2$=CHF | A, D | -2.85 | 1.24 |
| **5** | $^{\bullet}$O-$CH_2$-CHF-OCO-Li($Si_{cluster}$)$^-$ | B | -2.38 | 0.11 |
| **5** | $^{\bullet}$O-CHF-$CH_2$-OCO-Li($Si_{cluster}$)$^-$ | C | -1.86 | 0.28 |
| **6** | $^{\bullet}$EC-($Si_{cluster}$)-LiF | E | -2.06 | 0.72 |

**Effects of degree of lithiation and nature of exposed surfaces on EC and FEC reduction mechanisms.** Low, intermediate, and high stages of lithiation were represented by quasi-amorphous $LiSi_4$ and $LiSi_2$, and crystalline LiSi, and $Li_{13}Si_4$ respectively. The (100) surface was predicted to be the most stable low-index surface of the LiSi phase, with a surface energy of 0.039 eV/Å$^2$. For $Li_{13}Si_4$, the two most stable low-index surfaces were (100) and (010), with surface energies of 0.356 and 0.371 eV/Å$^2$, respectively. Reactivities of the minimum energy surfaces were investigated with O, OH, and H functionalizations. Results from AIMD simulations showed two different 2 $e^-$ EC reduction mechanisms (simultaneous vs. sequential) at intermediate lithiation (LiSi) surfaces independently of surface functionalization or nature of exposed facets. The surface is able to start reducing EC molecules once they are located at a critical distance where they form a C-Si bond (Figure VI - 118) and the carbonyl O interacts strongly with Li, inducing ring opening via $C_c$-O cleavage. This simultaneous 2 $e^-$ mechanism yields a radical anion $O(C_2H_4)OCO^{2-}$ adsorbed species. On the other hand, a sequential 2 $e^-$ reduction was also observed, where initially a single electron is transferred from the surface to a lithium-coordinated EC molecule, causing a $C_E$-O bond breaking. Subsequently, a second electron is transferred to the $EC^-$ anion, breaking a second $C_E$-O bond and generating $C_2H_4$ + $CO_3^{2-}$.

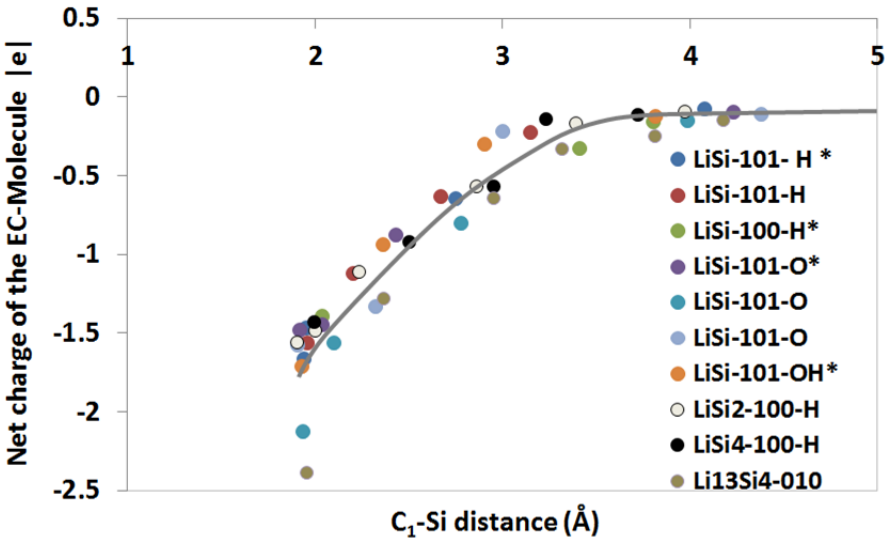


**Figure VI - 118: Evolution of the EC charge (in e$^-$) as a function of the C-Si distance for various surface facets and terminations**

On less lithiated surfaces (quasi-amorphous $LiSi_4$ and $LiSi_2$) the simultaneous 2 $e^-$ reduction was more frequently found. Strongly lithiated $Li_{13}Si_4$ surfaces were found to be highly reactive. Reduction of adsorbed EC molecules occurred via a 4 $e^-$ mechanism (Figure VI - 119) yielding as reduction products adsorbed $CO^{2-}$ and $O(C_2H_4)O^{2-}$ usually in the liquid phase. Direct transfer of 2 $e^-$ to EC molecules in liquid phase was also found, resulting in $O(C_2H_4)OCO^{2-}$ anions that remained in the liquid phase possibly ready for further reaction.

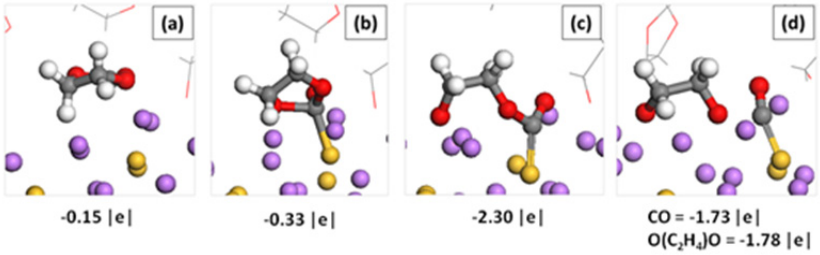


**Figure VI - 119: EC decomposition on the $Li_{13}Si_4$-(010) surface. The sequence shows charge transfer to EC and reaction products**

FEC was much more reactive and very fast processes involving sequential 4 or 5 $e^-$ were found independently of surface functionalization or degree of lithiation. Bonds were broken in the order CO/CF/CH/CO (Figure VI - 120) yielding $CO^{2-}$ and $C_2O_2H_2^{2-}$, or $CO_2^{2-}$ and $C_2OH_3^{2-}$, with F and H adsorbed. In the first case, the sequence of events includes (see Figure VI - 120 for atom nomenclature): 1) $C_{33}$-$O_{41}$ breaking during its adsorption on the surface corresponding to the reaction FEC + 2$e^-$ → $(C_3O_3H_3F)^{2-}$(ads); 2) $C_{32}$-$F_1$ bond breaks and F adsorbs: $(C_3O_3H_3F)^{2-}$(ads) → $(C_3O_3H_3)^-$(ads) + $F^-$(ads); 3) $C_{31}$-$H_{42}$ bond breaks and H may adsorb: $(C_3O_3H_3)^-$(ads) + 1 $e^-$ → $(C_3O_3H_2)^{2-}$(ads) + H(ads); 4) $C_{33}$-$O_{40}$ bond breaks resulting in the final products: $(C_3O_3H_2)^{2-}$ (ads)+ 2 $e^-$ → $(CO)^{2-}$(ads) + $(C_2O_2H_2)^{2-}$

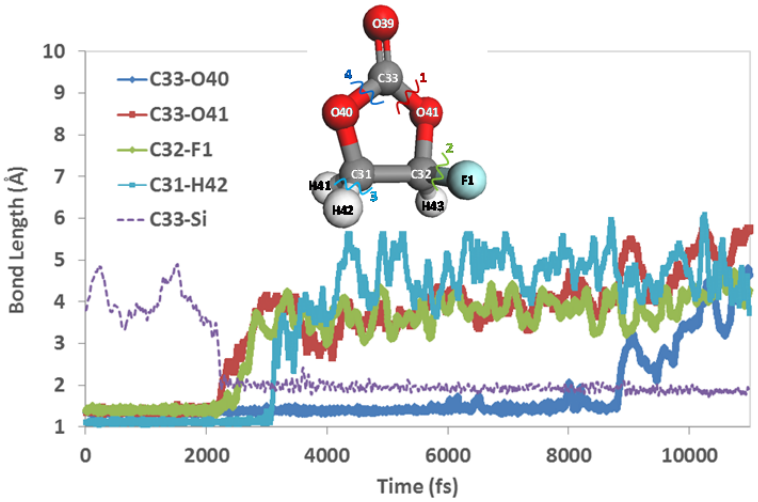


**Figure VI - 120: FEC decomposition on the $Li_{13}Si_4$-(010) surface. As the molecule gets adsorbed on the surface (C-Si bond forms), there is a sequential bond breaking illustrated by the time evolution of the respective bond distances**

An alternative FEC reduction mechanism takes place with the same initial steps yielding adsorbed $(C_3O_3H_3F)^{2-}$ that decomposes into $(C_3O_3H_3)^-$(ads) + $F^-$ (ads). However, the last step is different, where the $C_{31}$-$O_{40}$ bond breaks, resulting in the final products according to the reaction $(C_3O_3H_3)^-$ (ads) + 2 $e^-$ → $(CO_2)^{2-}$(ads) + $(C_2OH_3)^-$.

VC reduction mechanisms were found similar to those of EC (although yielding double-bonded products).

**Electron transfer through model electrode/SEI/EC interfaces.** Electron transfer was calculated through electrode/SEI/EC interfaces.

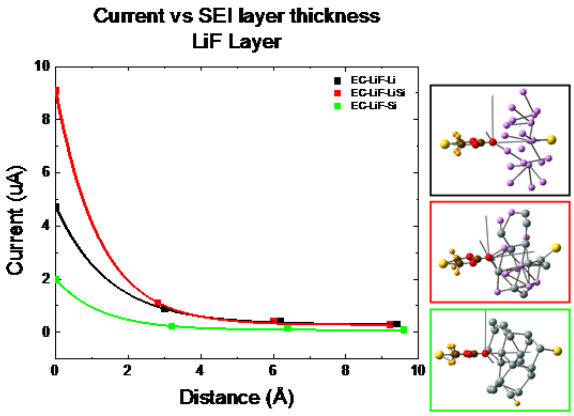


**Figure VI - 121: Decay of electron transfer from the electrode to an EC molecule through a model SEI layer as a function of SEI thickness. Three model electrodes represent degrees of lithiation of the Si anode**

SEI layers were represented by a composite cluster model of one component ($Li_2O$ or LiF) and the electrode modeled by Si, LiSi, and Li clusters respectively (Figure VI - 121). Calculations were done for variable thicknesses and configurations of the SEI layer. Gold tips were attached at each end of the interfacial system and a bias voltage was applied to evaluate electron transfer using a DFT/Green's function method. It was found that the rate of electron transfer followed the expected trend depending on the type of electrode (Li > LiSi > Si) and both model SEI layers showed similar degrees of electron transfer resistance. At constant applied voltage (2V), the electron current was found to decay exponentially by ~94% at SEI thicknesses of ~10 Å (Figure VI - 121). However, both for Li and LiSi electrodes, a non-zero constant current was still detected (although very low) suggesting that the system may be able to sustain a low-rate growth at even larger thicknesses.

**Reactivity of oxide surfaces.** A preliminary attempt was made at modeling 1 $e^-$ attacks on FEC in the presence of a $Li_{13}Si_4$ electrode, with each surface coated with a 7 Å thick $Li_4SiO_4$ layer so that FEC liquid is no longer in contact with $Li_{13}Si_4$ surfaces. FEC is found to decompose in picosecond time scales. Despite the expectation that the oxide should slow down electron transfer and enhance 1-$e^-$ attack on FEC over 2 $e^-$ reduction, Bader charge decomposition analysis showed that the products are still consistent with 2 $e^-$-induced reactions. However, EC and FEC reductions tested on slabs of pure $Li_4SiO_4$ and $Li_2Si_2O_5$ were found not possible. These results suggested a critical role of the oxide thickness on surface reactivity.

## Conclusions and Future Directions

At very early stages of lithiation (Li/Si ratio 1:15), the presence of adsorbed Li on the Si surface is able to generate EC reduction via a single electron transfer to the adsorbed molecule. When EC is surrounded by other EC molecules this single $e^-$ transfer is more favorable than the 2 $e^-$ transfer. At slightly higher Li/Si ratios (1:4, 1:2 and 1:1) the 2 $e^-$ mechanism is favored by the large proportion of Li on the surface able to interact with EC molecules. The reaction starts by formation of a C-Si bond and a strong O-Li interaction sustained by charge transfer from the surface which favors ring opening. Two types of 2 $e^-$ mechanisms were found: simultaneous and sequential, yielding different charged or neutral fragments either adsorbed or in the liquid phase. Strongly lithiated surfaces are very reactive and 4 $e^-$ transfer reactions were detected.

FEC was found much more reactive than EC and its reaction mechanisms were found to be independent of the degree of lithiation, type of exposed surface and/or details of surface functionalization. DFT calculated barriers at the lowest Li/Si ratio (1:15) indicated that the 2 $e^-$ transfer via $C_c$-O cleavage is the most favorable, in agreement with the AIMD results which illustrate the complete sequence of bond breakings involving 4 or 5 $e^-$ mechanisms. The products include adsorbed F and sometimes H, as well as charged CO or $CO_2$ and other radical anions.

VC reduction mechanisms were found similar to those of EC (although yielding double-bonded products).

Initial studies of electron transfer done in model systems including electrode/SEI layer/EC showed how the resistance of the film increases with its thickness. The SEI layer was represented by LiF or $LiO_2$. For the case of LiF the current from Li or LiSi electrodes was found to decrease exponentially and decay to very low constant values (but not completely zero) at about 1 nm thickness, suggesting that a low-rate SEI growth may subsist at larger SEI thicknesses.

Preliminary studies were conducted to investigate the role of surface oxides. AIMD simulations resulted on 2 $e^-$ transfers from a composite surface ($Li_{13}Si_4$ coated with $Li_4SiO_4$) to FEC and EC molecules similar to those found in bare $Li_xSi_y$ electrodes. However, AIMD simulations in slabs of $Li_4SiO_4$ and $Li_2Si_2O_5$ showed no FEC reductions. Thus, it is not clear if the results are a consequence of DFT inaccuracies to treat the oxide systems or if indeed a very thin film of the oxide may allow $e^-$ transfer.

Future work will address: 1) Comparisons of reduction behavior between additives (FEC vs. VC) and their consequences on the SEI layer composition; 2) Product aggregation and SEI layer growth from the initial fragments; 3) Further characterization of the role of surface oxides; 4) Growth on SEI layers deposited on the $Li_xSi_y$ or $Li_xSi_y$ coated with oxides; 4) Further clarification on the electron transfer mechanisms, identification of electron channels and electron-blocking regions, tests of additional SEI products and "mosaic" model films.

## FY 2013 Publications/Presentations


1. J. M. Martinez de la Hoz, Y. Ma, and P. B. Balbuena, "Solvent reduction on Si anodes of Li-ion batteries," *2013 ACS Fall National Meeting*, Sept. 2013, Indianapolis, IN.
2. P. B. Balbuena, J. M. Martinez de la Hoz, Y. Ma, L. Espinoza, and J. M. Seminario, "SEI layer formation on Si anodes of Li-ion batteries," *64th Annual ISE Meeting*, Sept. 2013, Queretaro, Mexico.
3. P. B. Balbuena, J. M. Martinez de la Hoz, Y. Ma, L. Espinoza, and J. M. Seminario, "SEI layer formation on Si anodes," *2013 ECS Fall Meeting*, Oct. 2013, San Francisco, CA.
4. K. Leung, S. B. Rempe, M. E. Foster, Y. Ma, J. M. Martinez de la Hoz, N. Sai, and P. B. Balbuena, "Modeling Electrochemical Decomposition of FluoroEthylene Carbonate on Silicon Anode Surfaces in Lithium Ion Batteries," submitted.
5. J. M. Martinez de la Hoz, K. Leung, and P. B. Balbuena, "Reduction Mechanisms of Ethylene Carbonate on Si Anodes of Lithium-Ion Batteries: Effects of Degree of Lithiation and Nature of Exposed Surface," submitted.

# VI.C.13 Analysis of Film Formation Chemistry on Silicon Anodes by Advanced *In situ* and *Operando* Vibrational Spectroscopy (UCB)

**Gabor Somorjai**
University of California, Berkeley

Department of Chemistry
Berkeley CA 94720
Phone: (510) 642-4053; Fax: (510) 643-9668
E-mail: somorjai@berkeley.edu

**Philip Ross**
Lawrence Berkeley National Laboratory
Materials Sciences Division
Berkeley CA 94720
Phone: (510) 486-5821
E-mail: pnross@lbl.gov

Start Date: October 2012
Projected End Date: September 2015

## Objectives

- Understand the composition, structure, and formation/degradation mechanisms of the solid electrolyte interface (SEI) on the surfaces of Si anodes during charge/discharge cycles by applying advanced *in situ* vibrational spectroscopies.
- Determine how the properties of the SEI contribute to failure of Si anodes in Li-ion batteries in vehicular applications. Use this understanding to develop electrolyte additives and/or surface modification methods to improve Si anode capacity loss and cycling behavior.

## Technical Barriers

High energy density Si anodes have large irreversible capacity and are not able to cycle. These failures are due in part to loss of electrolyte by reduction and a SEI that is not stable on the surface with repeated cycling.

## Technical Targets

- EV: > 200 wh/kg with > 1,000 cycles to 80 % depth of discharge.

## Accomplishments

- A novel *in situ* ATR-FTIR spectroelectrochemical cell was developed that provided unprecedented tuning of the depth of probing the vibrational spectra of molecules near the electrode surface.
- Two alternative anode materials were studied, Si and Sn, with Au used as a contrasting "inert" metallic electrode.
- It was determined that with Si and Sn reduction of electrolyte solvent, mostly the alkyl carbonate co-solvent formed soluble products via alkyl and alkoxide radicals, the main products observed (in EC:DEC) being lithium propionate and diethyl 2,5 dioxohexane dicarboxylate (DEDOHC).
- In contrast, electrolyte reduction on Au produces different products, more like those observed with graphite anodes, insoluble compounds such as lithium ethylene dicarbonate (LiEDC) and lithium oxalate. The precipitation of these compounds on the gold surface passivates the surface to further electrolyte reduction.
- Since soluble lithium propionate is the primary reduction product observed in lithiated Si, passivation does not occur, electrolyte reduction is continuous.

## Introduction

Major efforts are under way to develop novel materials that provide higher battery capacity for increased driving distances of electric vehicles. A high capacity alternative to graphitic carbon anodes is Si, which stores 3.75 Li per Si versus 1 Li per 6 C yielding a theoretical capacity of 4008 mAh/g vs. 372 mAh/g for C. Unfortunately, this high capacity comes at a cost: the Si anodes exhibit excessive irreversible capacity loss and short cycling lifetime. The irreversible capacity loss is believed to be caused by lattice expansion accompanying lithiation that is followed by particle cracking, continued reduction of electrolyte and formation of SEI on freshly exposed surface. Detachment of the SEI from the Si surface occurs even when the potential region of cycling is restricted to

produce a degree of expansion similar to that of graphite. These observations suggest that the SEI on Si is not intrinsically passivating and that the chemistry of the SEI on the Si surface is different from that of the SEI on graphite. Nonetheless, there are no studies to date suggesting that the SEI on Si is significantly different than that on graphite.

Studies of the electrolyte reduction products (i.e., SEI) have been performed on both inert (Au, Ni, or Cu) and electroactive (Li or graphite) materials where many properties of the SEI including its chemical composition, electrical resistance, and Li+ ion conductivity have been determined. The SEI is considered to contain organic and inorganic components that are comprised of lithium carbonates (e.g., $(CH_2OCO_2Li)_2$, $ROCO_2Li$, $Li_2CO_3$, polycarbonates), oxalate and alkoxides (e.g., $Li_2C_2O_4$, ROLi, HCOLi) and inorganic materials (e.g., LiF, $Li_2O$, LiOH). The formation mechanism of the interphase on anodes is still under debate, yet there are some properties that are generally agreed upon. Formation is suggested to occur in two voltage stages: at 1.5-0.8 V vs. Li/Li+ a porous, resistive, and dimensionally unstable phase is formed by electrochemical reduction of electrolyte components; a second stage of reduction occurs concomitantly with intercalation or lithium deposition forming a compact phase that prevents further electrolyte reduction, i.e., passivation, yet allows Li ion conduction, i.e., the solid electrolyte interphase. While lithium diethylcarbonate (LEDC) is considered to be a primary product from the one electron reduction of EC in the first stage, the overall composition of the inhomogeneous compact passivating SEI layer remains unclear. It is not known whether the SEI on graphite is unique to that electrode material, or that the cyclability of graphite is due entirely to the relatively small lattice change accompanying lithiation/delithiation.

The uncertainty regarding composition, structure, and formation and degradation mechanisms of the SEI is in general due to the poor interfacial sensitivity obtained using conventional spectroscopies. These issues will be addressed with a development of advanced *in situ* vibrational spectroscopies, sum frequency generation (SFG) and a new type of attenuated total reflection (ATR) Fourier transform infrared spectroscopy. Using these new tools, the focus will be on determining the failure modes of an operating Si/Li electrochemical system for vehicular applications. These results will lead to an improved an understanding of the:

- chemical composition and structure of the SEI at the Si/electrolyte interface, including
  - which electrolyte components are involved,
  - how lithium ion solvation is involved;
- formation mechanisms as a function of potential, time, and number of cycles;
- degree of SEI inhomogeneity across Si electrodes;
- stability of the SEI with respect to
  - the physical changes of Si that incur with lithiation and delithiation,
  - the crystal size, structure, and orientation of Si
  - doped or undoped Si,
  - electrolyte composition.

This knowledge will be used to develop and tailor SEI films for Si anodes that reduce irreversible capacity loss, improve long-term stability and cyclability for vehicular applications.

## Approach

Model Si anode materials including single crystals, e-beam deposited polycrystalline films, and nanostructures are studied using baseline electrolyte and promising electrolyte variations. A combination of *in situ* and *operando* Fourier Transform Infrared (FTIR), Sum Frequency Generation (SFG), and UV-Raman vibrational spectroscopies are used to directly monitor the composition and structure of electrolyte reduction compounds formed on the Si anodes. Pre-natal and post-mortem chemical composition is identified using X-ray photoelectron spectroscopy. The Si films and nanostructures are imaged using scanning and transmission electron microscopies.

## Results

A new design for an *in situ* ATR-FTIR cell to analyze the chemistry of the electrolyte reduction at the surface of a p-type Si(100) single crystal (doped) *in operando* was developed. This design is shown in Figure VI - 122, which made it possible to vary the penetration depth of the IR radiation and analyze both near-surface (< 1 μm) and boundary layer (> 10 μm) regions, thus analyzing for both dissolved and precipitated products. This cell was used to compare the chemistry of reduction on Si versus Au and Sn surfaces obtained earlier by conventional *in situ* reflection absorption infrared spectroscopy (RAIRS) and *ex situ* ATR-FTIR.

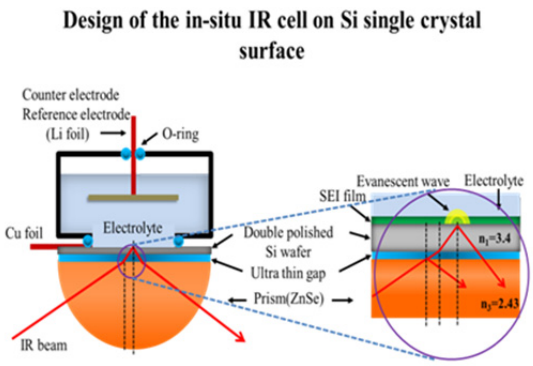


**Figure VI - 122: The use of an index matching dielectric liquid in the thin gap between the Si crystal and the ZnSe optic enables tuning of the position of the evanescent wave from the surface of the Si into the bulk**

The *in situ* spectra from the near surface region changed when the potential was applied to the electrode. Two strong peaks appeared above the electrolyte features which could be attributed to diethyl 2,5 dioxohexane dicarboxylate (DEDOHC) by comparison to the spectrum of the pure compound synthesized in this work. The spectrum of DEDOHC is very similar to that of the co-solvent DEC, diethylcarbonate, but the effect of solvation with the Li ion (or ion-pair) shifts the frequency of DEC enough for resolution of the two. The relative intensities of the vibrations are also significantly different to resolve the two molecules. The amount of DEDOHC was time-potential-depth dependent. Briefly summarizing numerous measurements, it was concluded that the DEDOHC appears over a large potential window beginning at around 1.5 V vs. Li/Li+, but not increased by stepping to lower potentials. The DEDOHC diffuses away from the surface quickly and the concentration in the bulk is very low. The reaction appeared to be self-limiting, possibly due to a parallel reaction forming an insoluble product, i.e., passivation. The passivating product appeared to be lithium propionate, seen only *ex situ*. There were also experiments that indicated that the reaction to form DEDOHC is a surface reaction with oxide on the surface of the Si. Similar results were observed with Sn.

By varying the penetration depth of the IR radiation, analysis of both near-surface (<1 µm) and boundary layer (>10 µm) regions of the Si electrode was possible. The wide wave number range (4000-800 $cm^{-1}$) allows us to correlate the stretching vibration of $PF_6^-$ anion near 840 $cm^{-1}$ with new features appearing near 1600-1700 $cm^{-1}$ that indicate a change in the Li ion solvation state commensurate with solvent reduction. It was discovered that with different depth into the electrolyte, the $PF_6^-$ vibration peak shifts without correlation to solvent reduction. Interpretation of these shifts in terms of solvation states will require quantum chemical modeling.

The electrochemical properties of Si (100), Si (110), Si (111), both doped and undoped wafers (450 microns thickness), were characterized during the charging-discharging cycles, using primarily cyclic voltammetry (at 0.1 mV/s equivalent to ca. 4 hr. constant current cycling). The kinetics of Li diffusion was observed to be dependent on crystal orientation and more importantly changes in depth of lithiation with number of cycles was also orientation dependent. Typically, the charge for delithiation increased progressively in the first few cycles, and achieved a quasi-equilibrium value (after about 30 cycles) as a result of the competition between Li diffusion rate and potential scanning rate. The level and type of dopant (n or p) strongly affected the bulk electrical conductivity and also the Li capacity of the Si wafers - increasing n-type dopant concentration decreased capacity, while p-type dopant density demonstrated the opposite trend. These results are consistent with some reports in the literature, e.g., *J. Phys. Chem. C*, 2011, **115**, 18916–18921. The correlation between the electrochemical properties of model Si wafers and real world Si may therefore be problematic, as the nature of the bulk impurities is typically unknown and/or uncontrolled. Perhaps a better model electrode of Si would be thin films fabricated from commercial bulk Si material vs. the doped Si single crystals often employed in spectroelectrochemistry.

At the recommendation of the Anode Focus Group in September 2013, fluoroethylene carbonate (FEC) has been chosen, the monofluorinated version of ethylene carbonate, as the additive for future study by SFG and ATR-FTIR.

## Conclusions and Future Directions

- Here it was determined that on Si electrodes reduction of electrolyte solvent, mostly the alkyl carbonate co-solvent, formed soluble products via alkyl and alkoxide radicals, the main products observed (in EC:DEC) being lithium propionate and diethyl 2,5 dioxohexane dicarboxylate (DEDOHC).
- In contrast, electrolyte reduction on gold produces different products, more like those observed with graphite anodes, insoluble compounds such as lithium ethylene dicarbonate (LiEDC) and lithium oxalate. The precipitation of these compounds on the gold surface passivates the surface to further electrolyte reduction.
- Since soluble lithium propionate is the primary reduction product observed in lithiated Si,

passivation does not occur, electrolyte reduction is continuous. This appears to be the primary problem with cycle life of Si anodes. A change in electrolyte composition from the conventional Li-ion electrolyte is therefore needed.

- It is recommended that co-solvents other than DMC or DEC be employed with EC.
- Fluorinated ethylene carbonate (FEC) was selected as an additive for future studies by SFG and ATR-FTIR.
- Selectively directing the solvent reduction reactions pathways by surface modification of the Si will also be a future direction of study.

## FY 2013 Publications/Presentations

1. Feifei Shi and Kyriakos Komvopoulos (Mechanical Engineering Department, U.C. Berkeley, Berkeley, CA, United States), Philip N Ross (Materials Sciences Division, LBNL, Berkeley, CA, United States), and Gabor Somorjai (Chemistry Department, U.C. Berkeley, Berkeley, CA, United States), "Li-Ion Battery Solid Electrolyte Interface (SEI) Investigation With *In situ* Attenuated Total Reflection-Infrared (ATR-IR) Spectroscopy," *224th Electrochemical Society Meeting*, October 27 – November 1, 2013, San Francisco CA.

# VI.C.14 Nanoscale Composite Hetero-structures and Thermoplastic Resin Binders: Novel Li-ion Anode Systems (U. Pittsburgh)

**Prashant N. Kumta**
University of Pittsburgh

Department of Bioengineering, Chemical and Petroleum Engineering, Mechanical Engineering and Materials Science
Pittsburgh, PA 15261
Phone: (412) 648-0223; Fax: (412) 624-8069
E-mail: pkumta@pitt.edu

Start Date: October 2010
Projected End Date: September 2014

## Objectives

- Identify new alternative nanostructured anodes to replace synthetic graphite providing higher gravimetric and volumetric energy densities.
- Similar or lower irreversible loss (≤15%) in comparison to synthetic graphite.
- Similar or better coulombic efficiency (>99.9%) in comparison to synthetic graphite.
- Similar or better cyclability and calendar life in comparison to synthetic graphite.
- Improve the coulombic efficiency, available energy density, rate capability and cycle life of high specific capacity Si based electrodes.
- Investigate nano-structured (*nc*-Si) and amorphous Si (*a*-Si) based composite or hybrid heterostructured anode.

## Technical Barriers

The important technical barriers of alternative anodes for lithium ion batteries (LIBs) to be used in electrical vehicles or plug in hybrid electrical vehicles are following:

(A) Low energy density
(B) Large first cycle irreversible loss (>25-40%)
(C) Inadequate coulombic efficiencies
(D) Poor cycle life
(D) Poor rate capability
(E) Low charge/discharge rates

## Technical Targets

- Synthesize nano-structured (*nc*-Si) and amorphous Si (*a*-Si) based composite or hybrid structured anodes using cost effective processing techniques.
- Achieve reversible capacity of ≥ 1200 mAh/g.
- Reduce first cycle irreversible loss to less than ~15%.
- Improve coulombic efficiencies higher than 99.7%.
- Improve the rate capability.
- Characterize the nano-scale hetero-structures for structure and composition using electron microscopy techniques such as SEM, TEM and HREM.

## Accomplishments

- Developed a scalable approach to generate hollow silicon nanotubes (SiNTs) using a low cost and high throughput sacrificial inorganic nanowire (INW) template.
- Binder-free and slurry based SiNTs were fabricated with capacities >2500 mAh/g.
- Specific capacities >1000 mAh/g were obtained for SiNTs after 400 cycles with a fade rate 0.067 % loss per cycle and a high coloumbic efficiency ~99.9%.
- Reversible capacities around ~1000 mAh/g were achieved on the SiNTs using DOE-BATT test conditions for over 100 cycles.
- Novel high strength and elastomeric natural and modified polymer binders, GG and MAB were identified and developed which exhibited comparable first cycle irreversible loss and better capacity retention (0.08% loss per cycle) compared to the commercial PVDF and CMC based binder (0.37% loss per cycle).

✧ ✧ ✧ ✧ ✧

## Introduction

In the earlier quarterly and annual reports, several novel approaches have been explored to achieve DOE-BATT technical targets for Si based anodes: high specific capacity (>1200 mAh/g), lower first cycle irreversible loss (<15%), high coloumbic efficiency (>99.9%), good cyclability and rate capability. These approaches involved the development of nano-scale heterostructures of vertically aligned carbon nanotube (VACNT) forests coated with nanocrystalline/

amorphous silicon films/droplets, thin films of interface control agent (ICA), thin films of electrodeposited amorphous silicon and high strength thermoplastic binders. The VACNT-Si composites exhibited capacities >2800 mAh/g with a very low irreversible loss (~12%) with moderate cyclability. Addition of a thin layer of ICA between the VACNT and Si improved the adhesion of Si film resulting in better cyclability and capacity retention. Electrodeposition of amorphous silicon films also showed excellent cyclability with a capacity of 1300 mAh/g over 100 cycles.

Hollow silicon nanostructures such as silicon nanotubes (*h*SiNTs) have been shown to offer mechanical strain relaxation during the colossal volume expansion of silicon occurring in the lithiation process, thus preventing mechanical failure (decrepitation of electrode) and hence improving the cyclability of the electrode for hundreds of cycles. The current known methods for synthesizing SiNTs involve a sacrificial template (anodized alumina and electrospun carbon fibers) made by expensive precursors onto which silicon was deposited by decomposing silane ($SiH_4$) and then removing the underlying template either by etching or by heat treatment resulting in a low yield of SiNTs. In the current work, scalable quantities of smooth and long nanowire templates were generated using inexpensive precursors and equipment. Reaction parameters including pH of the precursor solution and heat treatment conditions were further optimized to produce uniform and smooth inorganic nanowires (INWs) with high aspect ratio.

Currently, PVDF is the accepted commerical binder for anodes and cathodes. However, the large volume expansion of Si results in a significant stress field in the PVDF binder matrix leading to mechanical failure of the electrode. A high fracture strength binder is hence necessary to accommodate the volume strain that arises due to the large related Si volume expansion. In this report, results obtained on the electrochemical properties of Si/C composite with our newly developed modified natural polymer binders, named GG and MAB are discussed.

## Approach

For the hollow silicon nanotube (*h*SiNTs) synthesis, a sacrificial one dimensional inorganic nanowire template (INW) was first synthesized in an autoclave reactor under hydrothermal conditions (Figure VI - 123). Surfactants comprising long chain ampiphilic molecules were added to improve the dispersibility of the nanowires. The effect of other parameters such as pH of the precursor solution and heat treatment were studied and optimized to generate smooth and long sacrificial nanowire templates with very high aspect ratio. A thin layer of amorphous silicon was then deposited on the surface of these nanowires either by RF magnetron sputtering at 50W or by thermal cracking of silane gas ($SiH_4$) in a low pressure CVD reactor resulting in a core-shell (INW/Si) structure. This composite structure was dispersed in a mineral acid to dissolve the nanowire template to generate the hollow silicon nanotubes (*h*SiNTs).

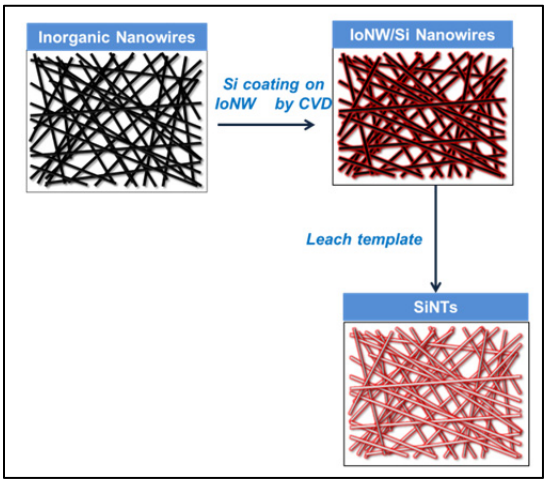


**Figure VI - 123: Schematic of *h*SiNT synthesis using inorganic nanowire (INW) template**

The newly identified water soluble natural and modified elastomeric binders (GG & MAB) were tested against a high energy mechanical milling (HEMM) derived high specific capacity Si/C system. The modified binders were synthesized using alkylation method of natural polymer AB. In this method, sodium monochloroacetate has been used as a crosslinking agent to AB polymer in order to improve the mechanical properties such as fracture strength.

## Results

**Hollow Silicon Nanotubes (*h*SiNTs):** The morphology of the hollow silicon nanotubes is largely dependent on the morphology of the INW template since the silicon deposited via sputtering or CVD assumes the nanowire morphology and hence a smooth, un-agglomerated and high aspect ratio nanowire of the inorganic template is desired. The inorganic nanowire (INW) template synthesis was optimized by controlling several parameters such as use of surfactants, pH and heat treatment conditions. The use of long chain amphiphilic molecules greatly enhanced the dispersibility of the nanowires that also proved essential for obtaining a uniform coating of silicon in the next step. Increasing the pH of the initial precursor solution further improved the surface smoothness of the INWs. In the first approach, the INWs drop casted onto the copper foils were used as the substrate onto which silicon was deposited by RF sputtering at 50W for one

hour. Hollow silicon nanotubes were generated after the Si coated INWs were dispersed in mineral acid to dissolve the INW template. The binder-less *h*SiNT electrode exhibited a very high first discharge capacity (~ 4100 mAh/g) close to the theoretical capacity of silicon when cycled with a current density of 100 mA/g in a voltage range 0.02V to 1.2 V vs. $Li^+/Li$. These smooth *h*SiNTs also exhibit good cyclability with a capacity retention of 89% at the end of 50 cycles.

In order to make slurry derived electrodes, scalable quantities of *h*SiNTs are required and hence a low pressure CVD technique was employed wherein large quantities of the INWs were used as the template onto which silicon was deposited by thermal cracking of silane gas ($SiH_4$) at 500°C. Similar to the earlier approach, the INW/Si core-shell structure was dispersed in mineral acid to remove the INW template thus generating scalable quantities of *h*SiNTs which were used to make slurry along with binder and conductive additives.

SEM, HRTEM and EDAX spectra of the resultant *h*SiNTs are shown in Figure VI - 124. The length of the INWs varied from 5µm to 100µm while the diameters were in the range 0.6µm to 1µm. The wall thickness of the *h*SiNTs was estimated to be in the 60 nm to 100 nm range. Both the SEM and HRTEM images (Figure VI - 124b and c) show the open eneded hollow structures of SiNTs. The EDAX spectra shows that the final product obtained contained only Si with some amount of surface oxidation. Raman spectra of the SiNTs showed a broad peak around 480 $cm^{-1}$ clearly validating that the Si formed is amorphous.

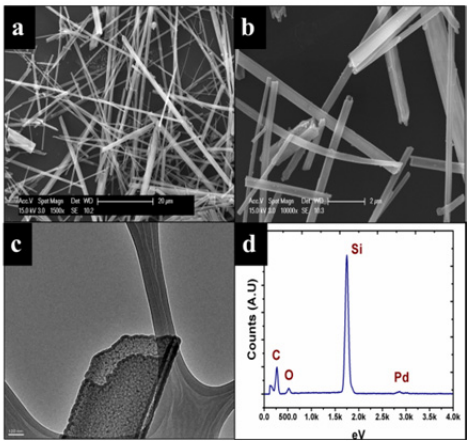


**Figure VI - 124: SEM images of (a) INW template, (b) *h*SiNTs after acid leaching, (c) HRTEM image of an open ended *h*SiNT & (d) EDAX spectra of *h*SiNTs**

A medium current density of 300 mA/g was employed between the voltage range 0.01 and 1 V vs. $Li^+/Li$ for the first cycle and a high current of 2A/g was applied for subsequent cycles to determine the cycling and long term stability. The charge-discharge characteristics of *h*SiNTs are shown in Figure VI - 125. A specific capacity of 2615 mAh/g and 1960 mAh/g were obtained for the first cycle discharge and charge capacity, respectively. A first cycle irreversible loss of ~25% was observed for these *h*SiNTs which may be due to the SEI layer formation on the surface of the SiNTs. At 2A/g, the SiNTs show excellent cycling stability over hundreds of cycles. Specific capacities in excess of 1000 mAh/g were obtained after 400 cycles corresponding to a fade rate of 0.067% loss/cycle (for 400 cycles) and a coulombic efficiency in the range of 99.9% was achieved.

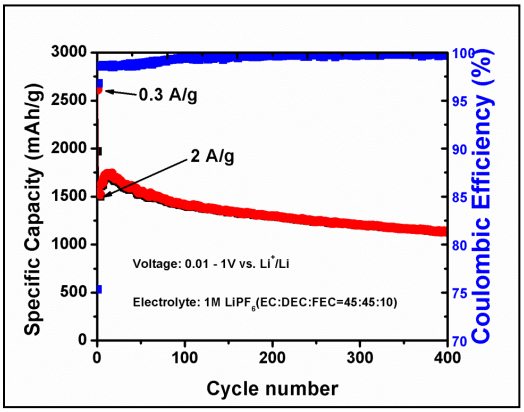


**Figure VI - 125: Long term cycling of *h*SiNTs performed at 2A/g (1st cycle at 0.3 A/g)**

The *h*SiNTs were also cycled using the DOE-BATT recommended protocol at a current density of 0.02 $mA/cm^2$ between the voltage range 0.005 to 1 V vs. $Li^+/Li$ for the first 3 cycles (to form a stable SEI layer). A first discharge and charge capacity of 2810 mAh/g and 2035 mAh/g were oberved resulting in a first cycle irreversible loss of 27%. Current densities of 0.5 $mA/cm^2$ and 0.75 $mA/cm^2$ were applied for the lithiation and de-lithiation processes, respectively as shown in Figure VI - 126. A stable and reversible capacity around ~1500 mAh/g was obtained for 100 cycles and the coloumbic efficiency close to 99.5% was achieved when cycled with current densities of 0.5 $mA/cm^2$ and 0.75 $mA/cm^2$ for lithiation and de-lithiation processes, respectively. This translates to a capacity retention of 93.2% and a fade rate of 0.07% loss per cycle (for 100 cycles). The *h*SiNTs also showed good rate capability when cycled from a curent density of 0.5 A/g to 4 A/g. Capacities close to 1200 to 1500 mAh/g were obtained at high current densities of 4 A/g.

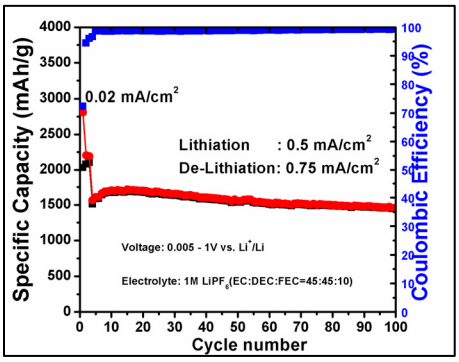


**Figure VI - 126: Electrochemical cycling of *h*SiNTs using DOE recommended test conditions**

**High strength and elastomeric binders:** As shown in Figure VI - 127, the Si/C nanocomposite with GG binder (3mg/cm$^2$) loading shows a 1$^{st}$ cycle discharge (~1179mAh/g) and charge capacity (~960mAh/g) with an irreversible loss ~18%, while the Si/C composite with PVDF binder (3mg/cm$^2$ laoding) exhibited an irreversible loss (IR) of ~17%, indicating that the newly developed GG binder has no negative effect on the 1$^{st}$ cycle IR loss. The long term cycling of Si/C composite cycled at 160mA/g (C/6) shows that the GG binder exhibits better cycling stability (0.08% loss per cycle) in contrast to the commercial PVDF (0.37% loss per cycle). However, significant chemical modification of the GG binder reflecting improvements in the mechanical strength is necessary for achieving excellent cycling stability (0.01% loss per cycle).

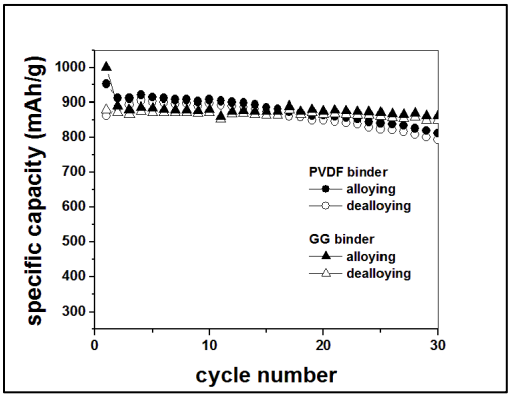


**Figure VI - 127: Variation of specific capacity vs. cycle number of Si/C composite with PVDF and GG binder**

Recently, a modified water soluble amine based binder (MAB) has been identified which shows excellent cyclability even when tested with high specific capacity Si/C based anode (~1000mAh/g) synthesized by high energy mechanical milling (Figure VI - 128). Si/C composite with MAB shows 21% 1$^{st}$ cycle irrversible loss and excellent capacity retention of specific capacity ~800mAh/g when cycled at a rate of 300mA/g and 3mg/cm$^2$ total loading.

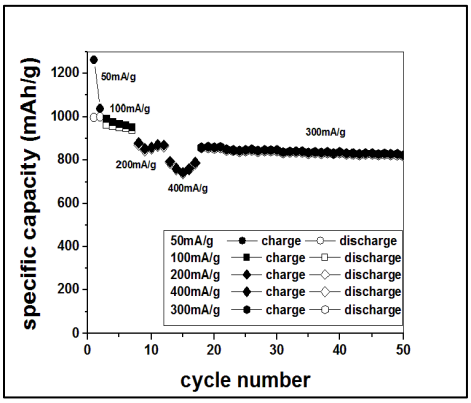


**Figure VI - 128: Charge-discharge characteristics of Si/C composite with MAB binder**

## Conclusions and Future Directions

A cost effective and scalable approach has been developed to generate *h*SiNTs using a sacrificial inorganic nanowire template. The silicon obtained was identified to be amorphous (from Raman spectra) and the SEM and HRTEM images showed the hollow tubular structure of *h*SiNTs. These *h*SiNTs were used in both binder-free and slurry based electrode systems delivering capacities >2600 mAh/g. Slurry based *h*SiNTs exhibited excellent cycle life and capacities >1000 were obtained after 400 cycles. This corresponds to a fade rate of 0.067% loss/ cycle. High strength water soluble elastomeric polymers, GG and amine based MAB binder were identified and chemically modified to achieve excellent capacity retention (fade rate of <0.08% loss/cycle) compared to the commercially available PVDF (~0.35% loss/cycle).

Future work will be directed to study the SEI layer formed on the surface of *h*SiNTs, perform rate capability studies and use HRSEM tools to investigate the morphological changes that may occur at the end of extended cycling (>500 cycles). Impedance studies will also be performed on the *h*SiNTs to study the interface and charge transfer characteristics. To further lower the cost of synthesizing *h*SiNTs, regeneration of the nanowire template will be explored where the dissolved INW templates to produce *h*SiNTs will be recovered again by a cost effective solution based chemical approach. The aforementioned efforts will enable us to comprehensively investigate and understand the chemical, materials and electrochemical characteristics of *h*SiNTs and further advocate their commercial viability as a replacement for graphite anodes in the next generation lithium ion batteries (LIBs).

## FY 2013 Publications/Presentations


1. R. Epur, M. K. Datta & P. N. Kumta, *Electrochim. Acta*, **85**, (2012) 680-684.
2. R. Epur, M. Ramanathan, F. R. Beck, A. Manivannan and P. N. Kumta, *MSEB*, 177, **14**, (2012) 1157-1162.
3. R. Epur, M. K. Datta & P. N. Kumta, J. *Solid State Chem.* (2013) http://dx.doi.org/10.1016/j.jssc.2013.09.002.
4. M. K. Datta, R. Epur, P. Saha, K. Kadakia, S. K. Park & P. N. Kumta, *J. Power Sources*, 225, **1**, (2013) 316-322.
5. S. Pal, S. S. Damle, P. N. Kumta & S. Maiti, *Computational Materials Science*, **79**, (2013) 877-887.
6. S. Pal, S. S. Damle, S. H. Patel, M. K. Datta, P. N. Kumta & S. Maiti, *J. Power Sources*, **246**, 149-159 (2013).
7. L. Minardi, R.Epur & P. N. Kumta, *2012 AIChE Annual Meeting*, Pittsburgh, PA USA.


.

# VI.D Electrolyte Development

## VI.D.1 Advanced Electrolytes and Electrolyte Additives (ANL)

**Khalil Amine**
Argonne National Laboratory

Chemical Sciences and Engineering Division
Argonne, IL 60439
Phone: (630) 252-3838; Fax: (630) 252-4672
E-mail: amine@anl.gov

**Larry Curtiss**
Argonne National Laboratory
Material Science Division
Argonne, IL 60439
Phone: (630) 252-7380; Fax: (630) 252-5999
E-mail: curtiss@anl.gov

Start Date: October 2009
Projected End Date: September 2013

### Objectives

- Use advanced quantum chemical (QC) models to predict electrolyte additives that can (1) act as redox shuttles for overcharge protection and (2) form stable Solid Electrolyte Interphases (SEI) on electrode interfaces
- Use the model to predict how additives interact with the surface of the anode and cathode to form good protective films.
- Synthesize suitable additives predicted by the modeling, characterize them, and carry out extensive cycle and calendar life tests.

### Technical Barriers

This project addresses the following technical barriers in lithium-ion battery technology (a) Cycle/calendar life (b) Abuse tolerance

### Technical Targets

- New additives that exhibit stable film formation on anodes and cathodes
- Increased cycle life
- Improved safety

### Accomplishments

- The database of potential additives for SEI formation and overcharge protection has been added to by using QC models for screening of reduction and oxidation potentials. The database now has over 500 additive molecules.
- Density functional methods were used to examine the oxidation potential and other properties of a potential redox shuttle F3-DDB. This molecule has less symmetry compared to previously studied shuttles DDB and F6-DDB. The F3-DDB compound was synthesized and tested as a redox shuttle and found to perform well.
- Density functional methods were used to examine the oxidation potential and decomposition reactions of a new fused ring shuttle OFDDB. Ortho methoxy groups make the shuttle more polar. Two decomposition pathways also were examined using density functional theory (DFT) and found to be stable. Experimentally, the fused ring structure and increased dipole moment significantly improves the solubility and provides a promising new platform for a variety of new shuttles.
- The stability of a potential redox shuttle, quaterphenyl, was investigated using DFT, which indicates that it should have high oxidative stability and is potentially a viable redox shuttle candidate. Substituted quaterphenyls are also predicted to be stable and possible redox shuttle candidates.
- DFTs were used to examine one and two electron reduction reactions of maleic, citraconic and dimethylmaleic anhydrides. They have good reduction potentials and have reaction pathways that are likely to lead to anionic polymerization following one electron reduction. Experimentally, the performance of citraconic anhydride has been examined, and it exhibits excellent performance.

✧ ✧ ✧ ✧ ✧

## Introduction

The development of advanced electrolytes with functional additives that provide for stabilization of the interfaces of lithium-ion batteries to prevent detrimental degradation is important for enhancing their cycle life and safety. In addition, electrolyte additives can provide protection against overcharge at the cathode. This project involves the use of high level QC methods for accurate energy assessments to screen for electrolyte additives that can be added to the electrolyte and form a protective SEI during the initial charging to prevent the conventional passivation film from forming first. Similar QC methods are being used to screen for new additives for redox shuttles to provide for overcharge protection in Li-ion batteries.

## Approach

This is a joint theoretical/experimental approach for the design and discovery of new electrolyte additives that act during cell operation to prevent detrimental decomposition of cell components. QC screening based on DFT and wave-function based methods are used to predict accurate oxidation and reduction potentials. In addition, these methods are used to investigate decomposition pathways of the additives that will result in a protective layer on the anode as well as to find stable additives for overcharge protection. Synthesis and testing of the new additives is done to determine the cycle life of the batteries followed by characterization.

## Results

**Electrolyte additives for SEI formation.** Calculations are being used to screen for additives for protective film formation on anodes with some being studied experimentally. Following are results for some of the additives that have been investigated.

**Anhydrides**. DFT were used to examine one and two electron reduction reactions of maleic, citraconic and dimethylmaleic anhydrides shown in Figure VI - 129. The calculated reduction potentials are all greater than 2 V vs. Li/Li+ due to conjugation but decrease as more electron releasing methyl groups are attached. There are various reaction pathways for decomposition after reduction including anionic polymerization following one electron reduction, formation of $Li_2CO_3$ after two electron reduction, and reaction with EC after one electron reduction. The first pathway (polymerization) has been examined in detail and was found to be favorable.

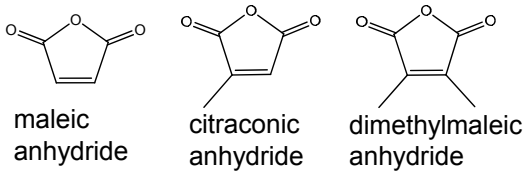


**Figure VI - 129: Structures of the three anhydrides**

Experimentally, the performance of citraconic anhydride has been examined, and it exhibits excellent performance. The citraconic anhydride additive (1%) was added to the electrolyte of a cell having the following components: $LiNi_{1/3}Co_{1/3}Mn_{1/3}O_2$ //1.2M $LiPF_6$ EC/EMC//MCMB. It is found that the citraconic anhydride can be easily reduced consistent with the theoretical predictions. It also results in improved cycling performance compared to the electrolyte without the additive as shown in Figure VI - 130.

**Redox shuttle screening.** Calculations are being used to screen for redox shuttles for overcharge protection with promising ones being studied experimentally. Following are results for some of the shuttles that have been investigated.

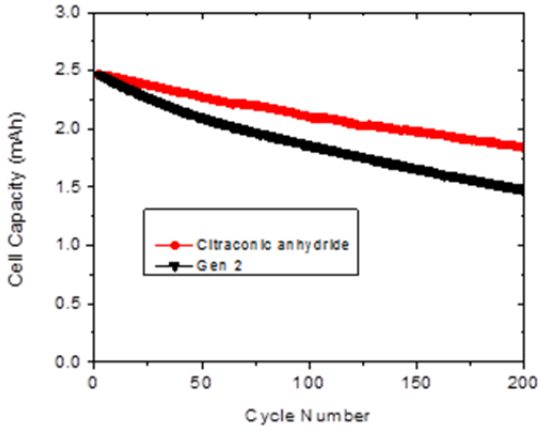


**Figure VI - 130: Cell performance for citraconic acid showing improved cycling**

**Ortho-6,7-dimethoxy-1,1,4,4-tetramethyl-1,2,3,4-tetrahydronaphthalene.** DFT methods were used to examine the oxidation potential and decomposition reactions of a new fused ring shuttle ortho-6,7-dimethoxy-1,1,4,4-tetramethyl-1,2,3,4-tetrahydronaphthalene (OFDDB). Ortho methoxy groups make the shuttle more polar. Steric repulsion between methoxy groups causes a higher oxidation potential than DDB because one methoxy group is rotated out of the plane of the ring and cannot contribute electrons to the ring via resonance, whereas both methoxy groups are coplanar in DDB. The methoxy groups of both shuttles are coplanar with the ring in the cation radical.

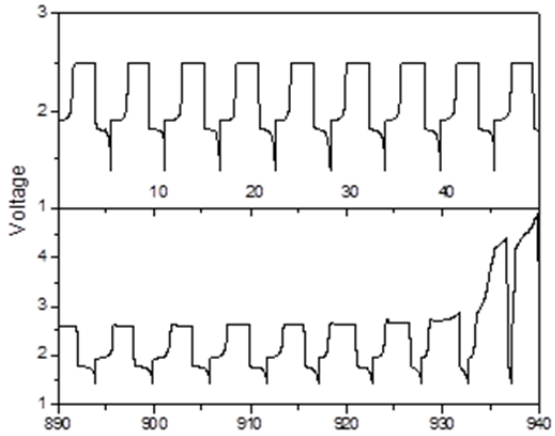


**Figure VI - 131: Voltage profile as a function of time (in hours) of LiFePo4/LTO cell at 100% overcharge condition (electrolyte containing 0.4 M OFDDB in the Gen2 electrolyte)**

Experimentally, the redox potential of OFDDB is in agreement with theory. The negative voltage sweep does not show any significant peaks indicating good stability of the redox shuttle on the low voltage range. The fused ring structure and increased dipole moment significantly improve the solubility of the shuttle compound. The OFDDB can survive over 150 overcharge cycles (100% overcharge; more than 900 hours) as shown in Figure VI - 131 at a relatively high charge rate for a $LiFePO_4$ based cathode materials. The OFDDB shuttle provides a promising new platform for a variety of new shuttles by simple molecular engineering. Replacement of the electron-rich methoxy groups with other electron-poor functional groups can tune the oxidation potential to create new shuttles for overcharge protection of high voltage cathode materials.

**1-(2,2,2-trifluoroethoxy)-4-methoxy-2,5-di-tert-butylbenzene.** DFT methods were used to examine the oxidation potential and other properties of a potential redox shuttle 1-(2,2,2-trifluoroethoxy)-4-methoxy-2,5-di-tert-butylbenzene (F3-DDB). This molecule has less symmetry compared to the previously studied shuttles DDB (1,4-di-t-butyl-2,5-dimethoxybenzene) and F6-DDB (bis-(2,2,2-trifluoroethoxy)-2,5-di-tert-butylbenzene). The structures are illustrated in Figure VI - 132. The calculated oxidation potential of F3-DDB is 4.02 V in good agreement with the experimental value of 4.09 V measured as part of this study. Calculated spin densities suggest that the less symmetric F3-DDB is slightly more prone to radical attack than the symmetric DDB and F6-DDB. Decomposition pathways were also examined. F3-DDB has three exergonic side arm reactions, F6-DDB has two and parent DDB has one. All investigated have large activation barriers so they are unlikely to decompose. However, decomposition could be catalyzed by transition metal sites on the electrode surface.

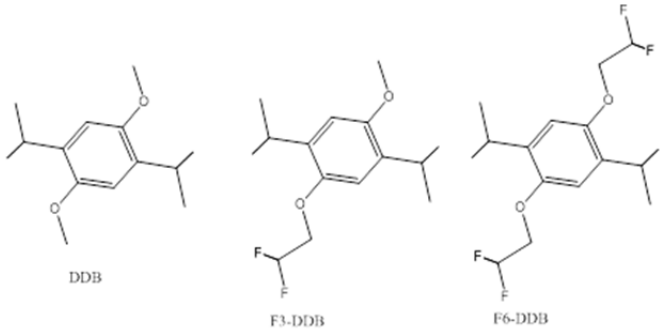


**Figure VI - 132: DDB and fluorine modified DDB redox shuttles**

The F3-DDB compound was synthesized using a commercially available precursor for testing as a redox shuttle. The introduction of –OCH2CF3 group increase the oxidation potential compared to DDB. The compound was characterized using NMR. F3-DDB also showed improved solubility in carbonate-based electrolytes due to the introduction of the fluorinated alkoxy group.

**Quaterphenyl: The stability of another candidate.** Quaterphenyl was investigated using DFT. Quaterphenyl can undergo anodic polymerization in which two cation radicals bond to form a "sigma" dication dimer followed by slow loss of two H+ ions to form octaphenyl. From theory the free energy change for 2 quaterphenyl cation radicals to form a dication dimer is uphill by 1.3 eV. The oxidation potential of octaphenyl is slightly lower than that of quaterphenyl which means that octaphenyl can oxidize more easily and attack another cation radical and continue the polymerization process. However, octaphenyl cation radical has decreased spin on external carbons making it less reactive. From theory, if H radicals are available, it is thermodynamically favorable for quaterphenyl to break down into biphenyl and benzene. The quaterphenyl cation radical can also form an adduct with EC, but the free energy change is uphill by about 2.4 eV. The dication dimer can also form an adduct with EC, but this leads to fragmentation into two quaterphenyl species, one of which is bonded to EC. Quaterphenyl cation radicals can break down into cation and radical fragments or cation radical and benzyne fragments. In the absence of additional radicals, quaterphenyl is expected to have high oxidative stability and could potentially be a viable redox shuttle candidate.

## Conclusions and Future Directions

The results obtained during the past year have shown how advanced QC methods can be used to successfully screen molecules as candidates for additives for advanced electrolytes in Li-ion batteries. Some of these candidate molecules that have been identified in these studies have been explored experimentally for their performance in Li-ion batteries. The calculations have been used to calculate the reduction and oxidation potentials of potential additives and to calculate decomposition pathways. This information has been used to help screen the new additives for optimal reduction/oxidation potentials and for needed stability or favorable protective SEI film formation. The development of electrolyte additives for SEI formation and overcharge protective is important for improving the safety and lifetime of Li-ion batteries.

## FY 2013 Publications/Presentations

1. "Electrolytes - Advanced Electrolyte and Electrolyte Additives," *DOE Annual Peer Review Meeting*, May 13-17, 2013, Washington, DC.
2. W. Weng, Y. T. Tao, Z. Zhengcheng, Paul C. Redfern, L. A. Curtiss, K. Amine, "Asymmetric Form of Redox Shuttle Based on 1,4-Di-tert-butyl-2,5-dimethoxybenzene," *J. Electrochem. Soc.,* **160**, A1711-A1715 (2013).
3. Z. C. Zhang, L. B. Hu, H. M. Wu, W. Weng, M. Koh, P. C. Redfern, L. A. Curtiss, K. Amine, "Fluorinated electrolytes for 5 V lithium-ion battery chemistry," *Energy and Environmental Science,* **6**, 1806-1810 (2013).
4. Z. C. Zhang, L. B. Hu, H. M. Wu, W. Weng, M. Koh, P. C. Redfern, L. A. Curtiss, K. Amine, "Fluorinated electrolytes for 5 V lithium-ion battery chemistry," *Energy and Environmental Science*, **6**, 1806-1810 (2013).

# VI.D.2 Sulfone Liquids and Sulfate/Triflate Solids for High Voltage Electrolytes (ASU)

**C. Austen Angell**
Arizona State University

Department of Chemistry and Biochemistry
Tempe, AZ 85287
Phone: (480) 965-7217; Fax: (480) 965-2747
E-mail: caa@asu.edu

Start Date: May 2010
Projected End Date: December 2013

## Objectives

- To complete study of sulfone and sulfone-carbonate based electrolytes for high voltage cathode cells.
- To demonstrate the possibility of alternative electrolytes that are less likely to have capacity- limiting side reactions
- Complete the development of amorphous metal organic frameworks (MOF) nanoporous membrancs as electrolyte supports.

## Technical Barriers

Technical barriers to development of sulfone electrolytes stable to high voltage cathodes lie in the unexpected inability of all-sulfone solutions to withstand high voltage cathodes, indicated by preliminary cyclic voltammetry (CV) studies on in-house fabricated LNMO cathodes. It appeared to be due to an inability to establish a suitable SEI between cathode material and the solution. Intrinsic oxidative stability, which seemed so high at the manganate cathode, and platinum cathode, had not been found at LNMO spinel cathode. For success, it seemed SEI-forming additives need to be developed.

Concerning the alternative solvent-free electrolytes that were to be investigated, the barriers were mainly those of synthesis of new concept inorganic plastic crystals with high alkali cation mobility. The preliminary indications were that these might have high enough conductivities to replace the liquid electrolytes. However, problems of purity and validation of conductance mechanism, remain to be solved.

For amorphous and glassy MOF studies, there are technical barriers to be overcome in measuring accurately the available internal surface areas, and in changing the compositions so as to generate high conductivities and, in particular, to obtain single alkali ion conductivities of favorable magnitudes.

## Technical Targets

- Finding suitable co-solvents and additives for sulfone based liquid electrolytes, and executing half-cell tests to evaluate their performances.
- Finding novel physical systems for electrolytes in which mobile species are the alkali cations, targeting inorganic ionic liquid and plastic crystal systems.
- For glassy MOFs, finding the conditions for reducing the mechanical fragility of the monolithic glassy films, and finding the conditions for optimizing the alkali ion conductivity.

## Accomplishments

- With new battery cycler equipment, half-cell tests have been made on cathodes using BATT Program- supplied LNMO cathode sheets. Excellent cycle life (2.9 mAh/g loss over 100 cycles) with 99% coulombic efficiencies have been obtained using a mixed sulfone (EMS)-carbonate (DMC) solvent with $LiPF_6$ electrolyte. Furthermore, similar or better performance has been demonstrated at the high power LTO cathode. However, *all*-sulfone solvents have been eliminated as candidates.
- For plastic crystals alkali ion conductors, where problems with completeness of reactions have been encountered, completely revamped synthetic procedures have been developed.
- For glassy MOFs, compositions that are analogs of sodium ion conducting minerals have been developed, but conductivities have been disappointing. High conductivities of tetrahedrally linked small chain polyethers containing LiTFSI have been recorded.

✧ ✧ ✧ ✧ ✧

## Introduction

**Electrolytes for high voltage cells.** The original objectives of this project emphasized a search for

electrolytes that might be able to avoid the side reactions that afflict the current generations of lithium batteries that incorporate high voltage cathodes, such as the high rate-capable LNMO spinel cathode. Electrolytes based on molecular solvents that were believed to be the most resistant to oxidation of all, were being investigated. These were the sulfones, the known high oxidative stability of which was attributed to the character of the dipolar group of the molecule (the sulfone group). However, after finding an all-sulfone solvent electrolyte that seemed to behave very well at the graphite anode, apparently intractable problems with stability at the cathode were encountered. The cathode half-cells could not be charged beyond the first stage, and evidence of gaseous products was found. This implied that the alkyl groups comprising the remainder of the molecules were being attacked, and so implied that a favorable SEI (that must be invoked to explain the success of the intrinsically more oxidizable carbonate solvent based electrolytes) was not being formed. Success in improving cycle life of high voltage cathodes by incorporation of phosphite additives, had been reported from by Xu at ARL, indicating that the only route to success for sulfones would be through the use of additives. This was deemed contrary to the research group strengths, and a new approach, seeking a quite different solution based on removing all oxidizable elements and focusing on single ion conductors, such as those bringing limited success (at expense of high current) to glassy electrolyte technologies, was substituted, perhaps prematurely.

This lead to the development of a quite new class of solid electrolytes that, in principle, could provide the answer to many of the problems that are currently afflicting the field of high voltage cathode electrochemistry. These were reported on in some detail in the 2012 annual report, and remain in focus.

However, the perceived failure of the original aims of the proposal (to develop high voltage sulfone solvent-based electrolytes) was not fully accepted, and new equipment for cell testing, purchased for new system evaluation, was available in this third year for their further investigation, using cathode material supplied under the BATT program. The favorable outcome of these further studies is reported on in detail in the present report.

## Approach

**Electrolytes. (i) sulfone-based electrolytes.** Sulfone electrolytes both of all-sulfone and sulfone-carbonate hybrid varieties, which had seemed to have failing behavior from the initial CV studies, have been resurrected after the performance of half-cell studies using a new battery tester purchased early in the current year. Half-cell charge/discharge cycles are performed using both types (all sulfone, and sulfone- carbonate [EMS-DMC]) of electrolytes, over 100 cycles. These compare well with the same tests using the ($LiPF_6$ in EC:DMC 1:1) electrolyte, over 100 cycles (see below).

In view of new, favorable, results with the ASU hybrid electrolyte, in half-cells with the newly-provided LNMO cathode sheets (from Hydro-Quebec under arrangement with the BATT Program), further tests of half-cells using graphite electrodes, also supplied by Hydro-Quebec, were suggested. Finally, half-cell 100 cycle tests need to be extended to the 1.5 V "safe" LTO anodes.

Then tests of 100 cycle performance at LMNO cathode need to be made for the EMS-DMC -based electrolyte containing molecular and ionic additives, in part provided by collaborating laboratory personnel (Kang Xu at ARL).

**(ii) New generation solid state alkali cation conducting electrolytes.** As an alternative to using liquid electrolytes with oxidizable carbon-containing groups, all-inorganic materials in which alkali cations are the least strongly bound elements, have been sought. Alternative to alkali-metal conducting glasses, systems with low melting inorganic salts, or systems in which there is rapid ion rotation within a crystal lattice (rather than alkali cation migration alone), have been sought.

**(iii) Nanoporous electrolyte supports.** A successful approach to synthesizing nanoporous network glasses, developed in the 2012 period, is further developed by varying choice of strut and linker, including compositions to mimic ceramic alkali ion conductors. Evaluation of reliable conductivities has been problematic because of the poor mechanical strength of the glasses. Much effort is invested in improving mechanical properties.

## Results

Results for each of the three components of the Technical Targets section are reported but most attention is devoted to results from the successful electrolytes for high voltage cathode and high power anode findings.

**Electrolytes. (i) sulfone-based electrolytes.** The electrochemical window for the sulfone-carbonate with $LiPF_6$ (1M) solute is shown in Figure VI - 133, where it is seen to be a clean 6.0 V wide when allowance is made for the scan rate.

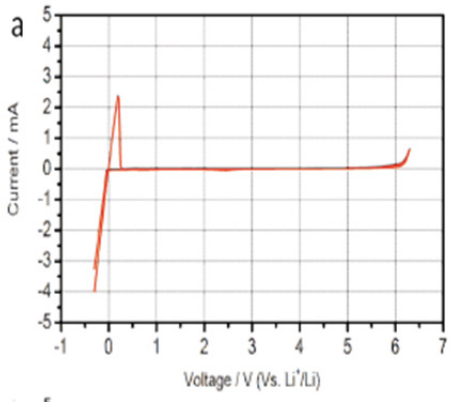


**Figure VI - 133: Electrochemical window for EMS:DMC ($LiPF_6$ 1M)**

The derivative dQ/dV for the half-cell with the LNMO cathode with reference Li+/Li is shown in Figure VI - 134. The two stages of the oxidation, and reduction on the negative sweep are clearly differentiated. The coulombic efficiency is shown in the lower panel of Figure VI - 134, and is seen to reach ~100% after about 20 cycles.

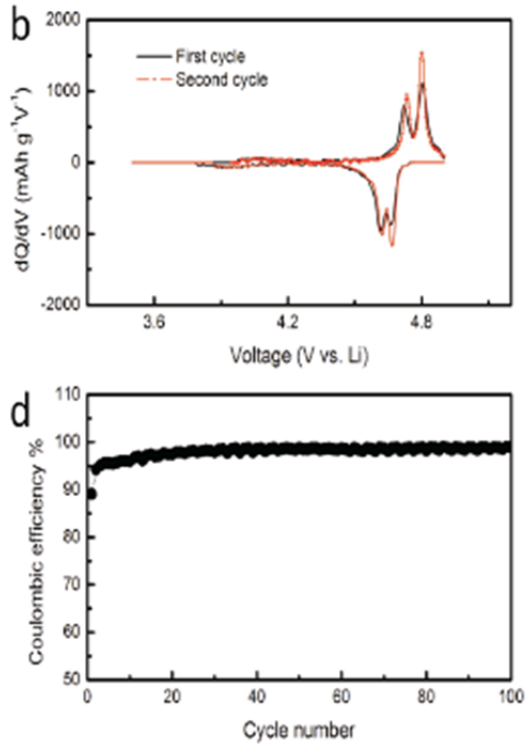


**Figure VI - 134: (Upper) dQ/dV for LNMO high voltage cathode vs. Li+/Li, (Lower) Coulombic efficiency vs. cycle number showing ideal behavior after 20 cycles**

Capacity retention in the half-cell with EMS-DMC/1M $LiPF_6$ as an electrolyte, is almost the equal of the half-cell with the standard electrolyte, while offering greater protection against thermal runaway in event of battery failure. The oscillatory behavior of the charge/discharge capacity in four cycle repeats is shown in the blow-ups to Figure VI - 135. The excursions appear to be increasing with increasing cycle number.

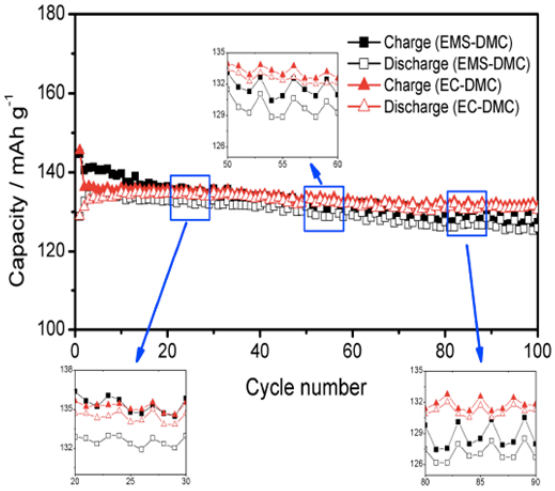


**Figure VI - 135: Superposition (on expanded scale) of capacity retention plots for LNMO half cell with EMS:DMC($LiPF_6$ 1M) electrolyte and with standard EC:DMC($LiPF_6$ 1M) electrolyte**

**Studies at the anode.** For successful cells, the cathode quality needs to be matched with anode quality. Figure VI - 136 shows the almost ideal behavior of the highly conducting LTO anode with the present electrolyte which would enable 3.5 V cells. To realize a full 4.7 V battery, the success with the LNMO and LTO electrodes has to be matched by success at the Graphite (or equivalent) anode.

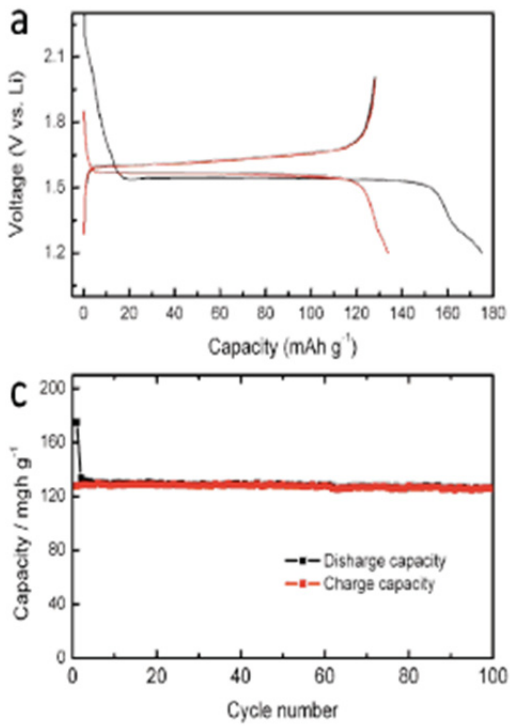


**Figure VI - 136: Half-cell tests at LTO anode: (Upper) Half-cell voltage profiles for charge and discharge vs state of charge for LTO high power anodes Li+/Li, (Upper) Charge and discharge capacities in relation to cycle number, showing almost ideal behavior**

Unlike the standard EC-DMC electrolyte, the sulfone-carbonate does not form a stable SEI at the graphite electrode, without additives. A vinyl carbonate (VC) additive was found, in earlier work with sulfones, to provide a stable SEI but, to date, VC has not been tested with the present electrolyte.

**(ii) New generation solid state alkali cation conducting electrolytes.** In order to reduce the risk of errors due to traces of unreacted acid (detected by NMR) in plastic crystal formulations of novel lithium ion conductors (2012 annual report), a complete revision of the preparative procedures has been undertaken. New findings will be reported in future publications.

**(iii) Nanoporous electrolyte supports.** Some new results on alkali metal salt conductivities in tetrahedral nets containing flexible struts and showing ionic conductivities comparable with the best linear "salt in polymer" solid electrolytes of Armand and co-workers, (red dashed line for 100ºC) are shown in Figure VI - 137.

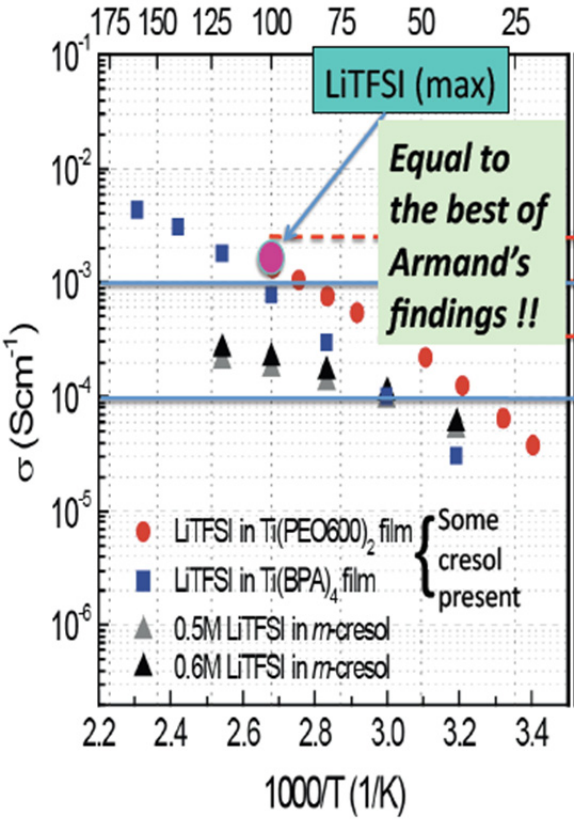


**Figure VI - 137: Conductivity of new semi-flexible tetrahedral net, using PEO 600 struts and containing LiTFSi in the interstices. Comparison is made with findings of Armand and co-workers on LiTFSI in high MW linear PEO polymers**

## Conclusions and Future Direction

It is evident, from Figure VI - 134, Figure VI - 135 and Figure VI - 136, that with the high quality of LNMO cathode material presently available to the BATT Program investigators, the 3.5 V high safety battery can be implemented with both standard carbonate and the new sulfone-carbonate electrolytes, with anticipation of less than 5% capacity loss over 100 cycles, and (in view of recent 500 cycle studies by Batelle NW lab), probably less than 20% capacity loss over 1000 cycles. Both sulfone-carbonate and all-carbonate-based cells have substantial conductivity and cost advantages over the recently reported fluorinated carbonate type electrolyte cells from the Amine group at Argonne. The sulfone-based system has a safety advantage due to diminished thermal runaway propensity.

In future work, this group will explore half-cells with variants of the present sulfone-based electrolyte incorporating 15 mol% of the smaller but higher-melting dimethyl sulfone DMS; earlier work showed

that it forms a low-melting eutectic with EMS. This should lead to increased protection against low temperature crystallization, coupled with some increase in conductivity at the same weight fraction of co-solvent carbonate.

Explorations of crystallization resistance and effect of increased co-solvent content and changes of carbonate co-solvent formula from DMC to the asymmetric ethylmethyl carbonate will also be investigated. Finally to be included will be studies with additional SEI-forming co-solvents that are not to be disclosed here.

## FY 2013 Publications/Presentations

1. C. Austen Angell, "Electrolytes and separators for high voltage Li-ion cells," *2012 DOE Annual Peer Review Meeting*, May 13-17. 2013, Washington, DC.
2. Seung-Yul Lee, Kazuhide Ueno, and C. Austen Angell, "Lithium salt solutions in mixed sulfone, and sulfone-carbonate, solvents: a Walden plot analysis of the maximally conductive compositions," *J. Phys. Chem. C*, **116**, 23915-23920 (2012).
3. Leigang Xue, Kazuhide Ueno, S.-Y. Lee and C. Austen Angell, "Performance of sulfone, and sulfone-containing, solvents at lithium ion battery electrodes, including the LiNiMnO high voltage cathode," *J. Electrochem. Soc.* (submitted).

# VI.D.3 Bifunctional Electrolytes for Lithium-ion Batteries (CWRU)

**Daniel Scherson**
Case Western Reserve Univ ersity

Department of Chemistry
10900 Euclid Avenue
Cleveland, OH 44106
Phone: (216) 368-5186
E-mail: dxs16@case.edu

**John Protasiewicz**
Case Western Reserve University
Department of Chemistry
10900 Euclid Avenue
Cleveland, OH 44106
Phone: (216) 368-5060
E-mail: jdp5@case.edu

Start Date: October 2009
Projected End Date: September 2013

## Objectives

- Design, synthesize, and characterize physical, electrochemical, and interfacial characteristics of functionalized Li-salt anions containing phosphorus moieties known to impart materials with flame retardant properties (Flame Retardant Ions or FRIONs) and additional functional redox active groups capable of providing overcharge protection (FROPs).
- Develop and implement ATR-FTIR spectroscopic methods for monitoring *in situ* the nature of products generated at Li-ion battery anodes under highly controlled conditions

## Technical Barriers

This project addresses the abuse tolerance barriers from the BATT program.

## Technical Targets

- Demonstrate superior abuse characteristics compared to a baseline cell: Conoco Philips CPG-8 Graphite/1 M LiPF6+EC:DEC (1:2)/Toda High energy layered (NMC)

## Accomplishments

- Several new FRION salts of two different classes were prepared and characterized
- A select number of these FRIONs were analyzed by TGA showing excellent thermal stability and minimal mass loss.
- Precursors to other potential FRIONs were also prepared.
- The electrochemical properties of new FRIONs were examined by cyclic voltammetry (CV) over a wide potential range using Ni working electrodes and differences were noted in their behavior.
- A new approach was developed to gain insight into the structure and composition of the solid electrolyte interphase (SEI) in electrolytes of relevance to lithium ion batteries

✧ ✧ ✧ ✧ ✧

## Introduction

The main objectives of this project are to develop rational guidelines for the design and synthesis of new classes of Li-based salts endowed with flame retardant properties. In addition, such bifunctional electrolytes should be weakly coordinating and of low molecular weight, exhibit low toxicity, promote formation of low impedance SEIs and from an economic viewpoint be relatively inexpensive.

## Approach

The strategy being implemented involves the chemical functionalization of anions of Li salts known to improve the performance of Li-ion batteries with covalently linked groups displaying flame retardant and/or overcharge protection attributes. The ultimate goal is to establish guidelines for the rational design and synthesis of optimized FRIONs and FROPs based on the analysis of results of testing in actual Li-ion batteries. Spectroscopic characterization of the products generated at Li-ion battery anodes and of the SEIs formed therein is pursued using *in situ* ATR-FTIR.

## Results

**Synthesis**. Two categories of precursors have been synthesized during this year, namely: diphosphinato

catechol (DPC) and 2,3-dihydroxy-1,4-diphosphinato napthalene (DPN). These two classes of compounds are based upon the use of an organo-phosphorus containing di-anionic bidentate ligand which chelates to either a boron or phosphorus atom center. Scale up of the previously reported FRION Li[B(DPC)(oxalato)] (Figure VI - 138, middle) has been completed by Argonne National Laboratory based on this procedure.

New DPC based FRIONs synthesized and characterized include $Li[B(DPC)F_2]$ (Figure VI - 138, top) and $Li[P(DPC)_3]$ (Figure VI - 138, bottom). $Li[B(DPC)F_2]$ contains two units of organophosphorus per anion. It is prepared using one molar equivalent of DPC and $LiBF_4$. The FRION $Li[P(DPC)_3]$ was synthesized by reacting three molar equivalents of DPC with $PCl_5$ in the presence of a lithium source. The $Li[P(DPC)_3]$ possesses a negatively charged phosphorus atom center, which is analogous to the atom center of $LiPF_6$. $Li[P(DPC)_3]$ contains six units of organophosphorus per anion. The DPN based FRION $Li[B(DPN)_2]$ was synthesized from DPN and boric acid in the presence of a lithium source (Figure VI - 140). The $Li[B(DPN)_2]$ contains four units of organophosphorus per anion.

The structure of $Li[P(DPC)_3]$ was determined using single crystal X-ray diffraction (XRD) methods and is shown in Figure VI - 139. As expected, the phosphorus atom center is octahedral. The DPC ligands bind to the phosphorus atom center in a bidentate fashion. The lithium atom center is tetrahedral and coordinates to four phosphoryl (P=O) oxygen atoms. The negative charge formally located on the phosphorus atom should be delocalized via resonance on the aromatic ring. This effect should be enhanced due to the electron withdrawing nature of the phosphoryl group attached to the benzene ring.

Thermogravimetric Analysis (TGA) was performed on $Li[B(DPC)F_2]$ and $Li[P(DPC)_3]$ and the results are shown in Figure VI - 141. Both salts are stable at the normal operating temperatures of Li-ion batteries. The $Li[P(DPC)_3]$ is thermally stable at temperatures below 150°C. When exposed to higher temperatures, the salt maintains approximately 60% of its original mass after decomposition. The $Li[B(DPC)F_2]$ is stable at temperatures below 270°C, and maintains 67% of its original mass.

Although attempts to prepare other types of FRIONs were unsuccessful, new precursors were obtained in the process. These include phosphonic acid incorporating both H and isopropyl groups to reduce symmetry and thus impart the resulting FRIONs increased solubility and also novel phosphorus containing biphenol precursors.

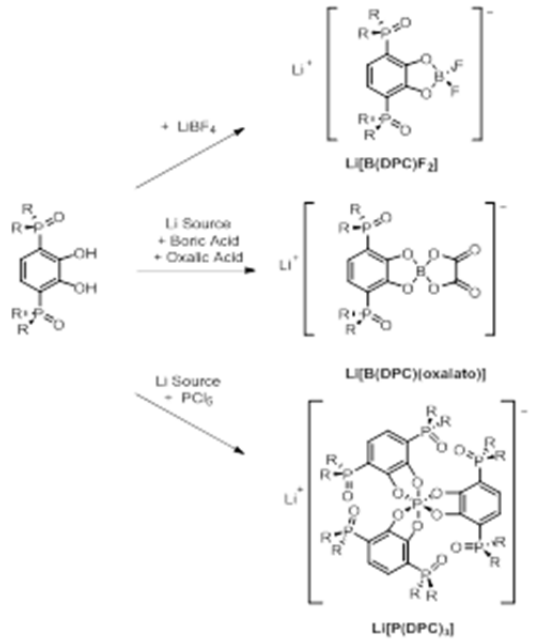


**Figure VI - 138: Synthesis of $Li[B(DPC)F_2$, $Li[B(DPC)(oxalato)]$ and $Li[P(DPC)_3]$**

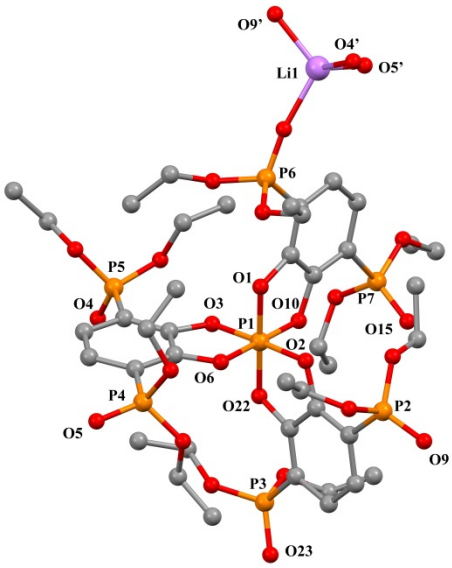


**Figure VI - 139: Single Crystal X-Ray Structure of $Li[P(DPC)_3]$**

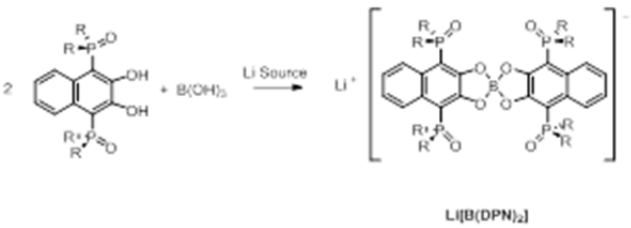


**Figure VI - 140: Synthesis of Li[(DPN)2]**

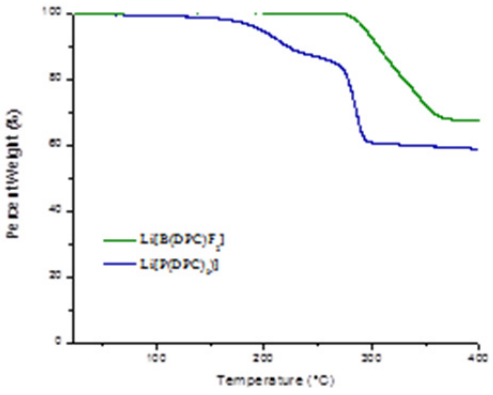


Figure VI - 141: TGA of FRION Salts

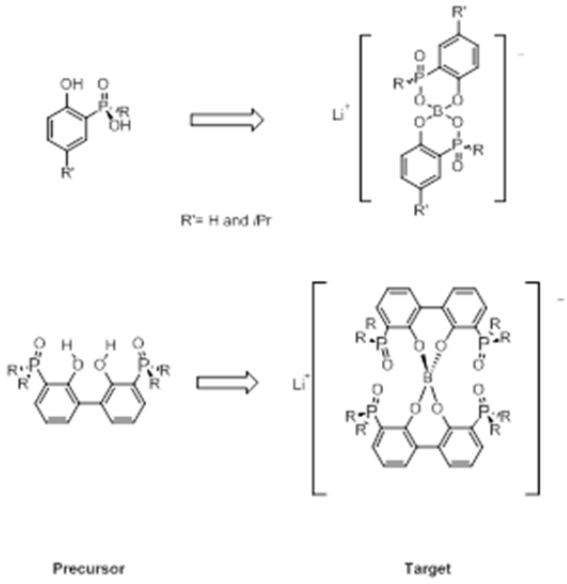


Figure VI - 142: Synthesized Novel Precursors with Target Frions

**Electrochemistry.** At present there exists no rational guidelines for correlating the properties of the SEI formed at the anode-solution interface during the initial charge discharge cycles of Li-ion batteries with those of both the solvent and the anion of the Li salt dissolved therein. The strategy that has been implemented toward unveiling such correlations involves systematic studies of structurally related materials using CV as a diagnostic tool. To this end, measurements were performed with some of the newly synthesized materials in deareated EC/EMC(50/50 by volume) using a Ni wire as the working electrode and a piece of metallic Li as the counter-reference electrode. In all cases, the materials were dissolved to saturation. The voltammetric curves shown in Figure VI - 143, recorded as a scan rate of 10 mV/s, illustrate some of the changes induced by the structure of the material. In particular, the B-containing materials (see panels B and C, Figure VI - 143) display features reminiscent of those obtained in the standard 1M $LiPF_6$ in the same solvent mixture (see Panel A in this figure). In stark contrast, the response of the phosphorous analogue yielded a resistive type behavior (see panel D, Figure VI - 143) over a wide potential range, which is indicative of the formation of a different film on the Ni electrode derived from the reduction of the anion.

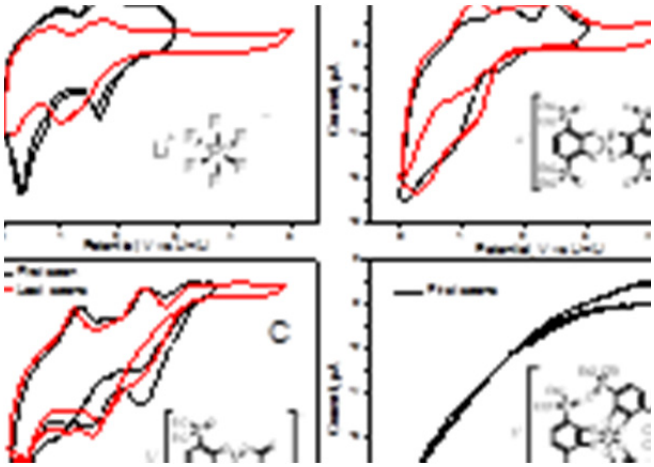

Figure VI - 143: Cyclic voltammetric curves recorded with a Ni wire electrode in EC/EMC(50/50 by volume) solutions at a scan rate of 10 mV/s, for solutions containing the materials shown in the insets

***In situ* spectroscopy**. Analyses of numerous experiments aimed at acquiring *in situ* FTIR data of the film formed upon electrodeposition and stripping of Li on an inert substrate surface both in the attenuated total reflection (ATR) and internal reflection absorption (IRAS) modes, failed to reveal the presence of spectral features attributable to species other than those of the solvent mixture employed. It may be concluded on this basis that: i. the products of the reaction are not IR active and/or ii. the sensitivity of the techniques are not sufficient to detect otherwise IR active products due to their very small cross sections. A new approach is being currently pursued involving deposition of a very thin boron doped diamond layer on top of the diamond window of the ATR-FTIR cell designed under this program which will serve as the electrode onto which metallic Li will be deposited. As evidenced by the CV data collected for B doped diamond films supported on glass, shown in Figure VI - 144, this inert surface can promote the reversible deposition and stripping of Li metal.

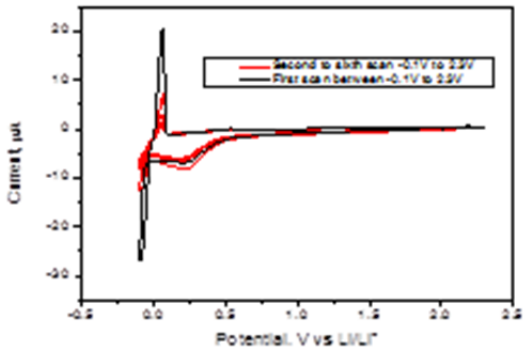


**Figure VI - 144: Series of cyclic voltammetric curves of a boron-doped diamond film supported on glass in 1 M LiPF6 in EC/EMC(50/50 by volume) using Li metal as counter reference electrode, recorded at a scan rate of 10mV/s**

## Conclusions and Future Directions

Novel DPC and DPN FRIONs containing multiple units of organophosphorus per anion have been synthesized and characterized. This expanded library of compounds features FRION salts that incorporate either a negatively charged boron or phosphorus atom as the anion center. The structure of $Li[P(DPC)_3]$ was determined using single crystal XRD. $Li[B(DPC)F_2]$ and $Li[P(DPC)_3]$ were analyzed by TGA and found to be stable at normal operating temperatures of lithium-ion battery and to maintain a high percentage of their original weight after being exposed to high temperatures. Details regarding the synthesis of the most promising FRION prepared to date were made available to scientists at Argonne National Laboratories who scaled up the procedure to hundreds of grams to be made the material available to other agencies for testing.

Future directions include optimizing electrochemical and flame retardant performance of FRION salts, as well as maximizing the solubility of FRIONs. Arrangements will be made with ANL and LBNL for these new compounds to be thoroughly evaluated in coin cells or other formats. The electrochemical and thermal properties of possible FRION decomposition products will be analyzed to better understand the fate of FRIONs in a battery system. As always attention will be paid to structure-function relationships.

Vendors have been contacted for the design and construction of a novel ATR-FTIR optical attachment compatible with the *in situ* spectroscopic cell now available in our laboratories to conduct measurements of a boron-doped diamond electrode. This configuration may be regarded as ideal to detect the elusive spectral properties of the passive film formed on nascent Li metal in contact with electrolytes of relevance to Li-ion batteries.

## FY 2013 Publications/Presentations

1. "Bifunctional Electrolytes for Lithium-ion Batteries," *DOE Annual Peer Review Meeting*, May 13-17, 2013, Washington, DC.
2. Rectenwald, M.F.; D. Scherson; and J. Protasiewicz, "Bifunctional Electrolytes for Lithium-Ion Batteries," *Research ShowCASE*, April 13, 2013, Cleveland, OH.
3. Rectenwald, M.F.; Shaffer, A. R.; and J. Protasiewicz, "Bifunctional Electrolytes for Lithium-Ion Batteries," *American Chemical Society Meeting in Miniature*, March 13, 2013, Cleveland, OH.
4. Michael Rectenwald, Andrew R. Shaffer, Joshua Gaffen, Nihal Deligonul, Daniel A. Scherson, and John D. Protasiewicz "FRIONs: Flame Retardant Ions for Safer Lithium Ion Batteries," *National ACS Meeting*, Sept. 11, 2013, Indianapolis, IN.

# VI.D.4 Interfacial and Bulk Properties and Stability (LBNL)

**John B. Kerr**
Lawrence Berkeley National Laboratory

Environmental Energy Technologies Division
1 Cyclotron Road, MS 62R0203
Berkeley, CA 94720
Phone: (510) 486-6279; Fax: (510) 486-4995
E-mail: jbkerr@lbl.gov

Start Date: October 2009
Projected End Date: September 2013

## Objectives

- Determine the role of electrolyte structure upon bulk transport and intrinsic electro-chemical kinetics and how it contributes to cell impedance (Energy/power density).
- Determine chemical and electrochemical stability of electrolyte materials to allow elucidation of the structure of and the design of passivating layers, e.g., solid polymer electrolyte (SEI).

## Technical Barriers

This project addresses the following technical barriers:

- Low power and energy densities, including fast charge capability.
- Poor cycle and calendar life.
- High manufacturing cost.
- Safety

## Technical Targets

- Determine the contribution to the interfacial impedance of the salt structure in terms of reactivity versus intrinsic electrode kinetics.
- Determine the contribution to the interfacial impedance of the solvent or polymer structure in terms of reactivity versus intrinsic electrode kinetics.
- Determine the contribution to the interfacial impedance of the physical properties of the electrolyte – liquid vs. gel. vs. SEI.

## Accomplishments

- Scaled up polysulfone single ion conductor (SIC) synthesis to 20g scale.
- Improved degree of functionalization of polysulfone synthesis to allow wider variation of ion exchange capacity in SICs.
- Scaled up polyether synthesis procedures to 20g scale.
- Scaled up functionalization of carbon to 20g levels.
- Prepared and tested $TiO_2$ nanocable anode materials as test of surface functionalization methods.
- Material preparation methods improved to a level of reproducibility that allows optimization of electrode fabrication to proceed.

✧ ✧ ✧ ✧ ✧

## Introduction

The choice of electrolyte used in lithium ion batteries presents significant challenges from the point of view of charge transport as well as electrochemical and chemical stability. The impedances introduced by the electrolyte are frequently the major source of failure of the battery and consist of the bulk ohmic resistance (conductivity), concentration polarization (transport properties) and interfacial impedance (intrinsic electrochemical kinetics of charge transfer at the electrodes). Most of the attention of electrolyte researchers over the years has focused upon the ohmic resistance (conductivity) of the bulk electrolyte yet this impedance is usually smaller than that due to concentration polarization (especially in composite electrodes) and much smaller than that of the interface. Both interfacial and concentration polarization impedances are critical barriers to the deployment of lithium ion batteries in traction vehicles. In fact, without a solution to the concentration polarization issue, a rapid charge of a high energy battery with a composite electrode will be impossible.

Single-ion polyelectrolyte lithium conductors possess the solution for many of the problems with present electrolytes. They can be used with no liquid solvent thereby reducing the safety problem. They can be prepared and deployed in ways that avoid many of the reactivity issues both in the bulk of the electrolytes

and at the interfaces and hence offer a solution to the lifetime problem. Because they possess a unity transference number, there is no concentration polarization through the composite electrodes. Thus, provided the conductivity is in excess of $10^{-4}$ S/cm, the SICs can facilitate the use of thicker composite electrodes thereby leading to higher energy and power densities. Without such a capability, rapid charging is not possible for high energy batteries suitable for vehicular use. They further appear to have application to the operation of large volume expansion electrodes where concentration gradients have a considerable negative effect on cycling.

In past years this group has demonstrated that SIC materials, both dry and as gels, possess the transport properties required both in the bulk separator and in the composite electrodes. However, the interfacial impedance has presented a particular challenge which has been at least partially overcome in the last two years of the project. The progress has been sufficiently encouraging to warrant scale up of the polymer synthesis and composite electrode fabrication to more practical levels that allow for synthesis of sufficient materials to conduct optimization studies of the composite electrodes. This is a necessary requirement for practical application of the materials to practical systems.

## Approach

The work involves use of model compounds as well as synthesis of new materials to test hypotheses which may explain battery behavior. Examples include:

- SIC polyelectrolytes (dry polymers and gels) as separators and binders in composite electrodes.
  - Measure transport, chemical and mechanical properties of polyelectrolytes as bulk separators.
  - Measure transport, chemical and mechanical properties of electrode coating inks and coated electrodes
- Different solvents and single ion salts, including polymer gels and solid polymer electrolytes.
- Functionalized surfaces for electrode components to control interfacial impedances
- Use electrode materials with different reaction potentials to determine electrochemical stability.
- Measure thermal and inherent chemical stability of electrolytes.
- Develop chemical analysis methods to assist in improvements in stability and lifetime.

Figure VI - 145 illustrates the types of polymers and functionalized materials that are under study and how they are deployed in practical batty systems. The goal is to provide electrolytes that allow the electrodes to be made as thick as possible in order to maximize the energy density of the cell while also allowing the rates to be maximized.

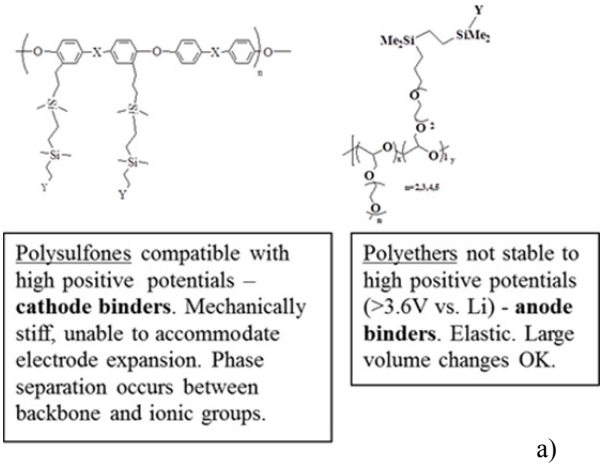


**Figure VI - 145: Methods of immobilizing electrolyte anions in lithium ion batteries. (a) Polyelectrolyte ionomers for use as separators and binders; (b) surface modified carbons for incorporation into composite electrodes to control lithium ion concentration**

## Results

**Preparation of Polymer Backbones.** Commercially available polysulfone (Udel) material is chemically modified to provide the backbone for gel SICs. The reaction is shown in Figure VI - 146 and the optimization processes are shown in Table VI - 6.

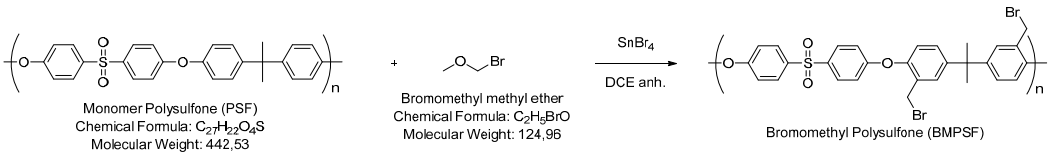


Monomer Polysulfone (PSF)
Chemical Formula: $C_{27}H_{22}O_4S$
Molecular Weight: 442,53

Bromomethyl methyl ether
Chemical Formula: $C_2H_5BrO$
Molecular Weight: 124,96

Bromomethyl Polysulfone (BMPSF)

| PSF | Bromomethyl methyl ether | Tin(IV) Bromide | 1,2-Dichloroethane anhydrous |
|---|---|---|---|
| 20 g | 20.0 ml | 6.0 ml | 250 ml |
| 45.19 mmol | 220.5 mmol | 45.19 mmol | 50 °C |
| | (4.9 eq) | (1 eq) | 24h |

**Figure VI - 146: Functionalization of Polysulfone polymer backbone**

**Table VI - 6: Optimization of polymer functionalization conditions**

| *Ref* | $CH_3O$-$CH_2Br$ | Tin (IV) | Temp. | time | Subs. Rate | Mn[1] | Comment |
|---|---|---|---|---|---|---|---|
| SG5 | 5 eq | 1 eq | 40°C | 21h | ~168% | ~55 kDa | |
| SG7#1 | 5 eq | 1 eq | Reflux[2] | 24h | ~199% | ~86 kDa | Cross linking |
| SG7#2 | 5 eq | 1 eq | Reflux[2] | 48h | ~208% | ~94 kDa | Cross linking & burned |
| SG10 | 5 eq | 1 eq | 80°C | 24h | ~179% | | Cross linking |
| SG12 | 10 eq | 2 eq | 60°C | 66h | ~188% | | |
| SG13 | 5 eq | 1 eq | 60°C | 6h | ~129% | | Mixed[3] |
| SG14 | 5 eq | 1 eq | 60°C | 14h | ~172% | | Trace of monomer |
| SG19 | 5 eq | 1 eq | 60°C | 24h | ~193% | | Part of insoluble or cross linking |
| SG22 | 5 eq | 1 eq | 40°C | 24h | ~161% | | |
| SG27 | 5 eq | 1 eq | 50°C | 24h | ~189% | ~75 kDa | |

[1] Calculated with kaleïdagraph; $Mn_{PSF}$ ~152 kDa. [2] oil bath at 100°C. [3] large mix of substituted and non-substituted monomer

Table VI - 6 illustrates the issue with polymer synthesis involving cross-linking and overreaction that leads to unusable product. Such problems tend to increase as the process is scaled up and hence considerable effort has been expended on optimizing the reaction as is illustrated by Table VI - 6. The resulting bromomethyl substituted polymer is converted to the SIC by the reactions shown in Figure VI - 147, which shows to synthesis of a fluorosulfonate. The resulting material has good film-forming properties and Figure VI - 148 shows the results of small angle x-ray scattering (SAXS) for such a membrane compared with the SAXS for Nafion®. The SAXS data for PSF-Li shows only small activity as the material has much less fluorine content.

The purpose of the SAXS experiments is to detect signs of phase separation which might account for the better conductivity and interfacial performance observed before when the SIC polymer was prepared as a gel with carbonate solvents. However, it was noted that the polymer dissolved in the usual EC/EMC solvents and hence cross-linking of the polymer is required. This creates a complication in preparation of composite electrodes that will require extensive further study. However, the availability of large amounts of reproducible polymer makes such as study possible where it was not practical before.

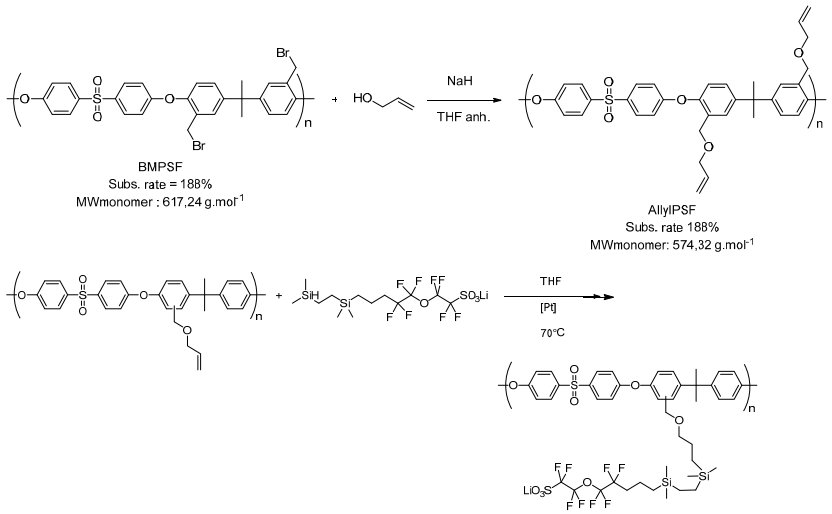


**Figure VI - 147: Preparation of Polysulfone substituted with fluorosulfonate groups**

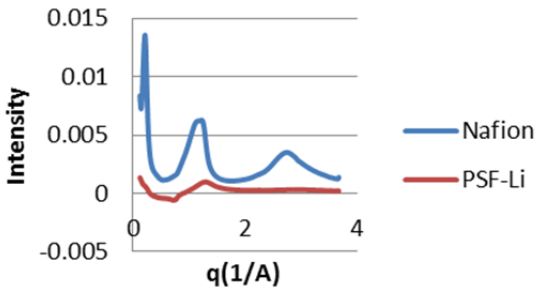


**Figure VI - 148: Background subtracted SAXS data for Nafion® and fluoroalkylsulfonate-substituted polysulfone**

Similar progress on preparation of the polyether backbones shown in Figure VI - 145 has also uncovered issues. The molecular weight that is achievable with long chain combs is quite low and this is inherent to the polymerization of such materials due to chain transfer in the reaction. This again will require considerable optimization of crosslinking conditions to achieve the mechanical properties desired in both the separator and the composite electrodes.

**Surface Modification of Conducting Carbon Components in Composite Electrodes.** In an effort to increase the local concentration of ions at the electrode surface, carbon conducting elements have been functionalized by a number of methods. Figure VI - 149 illustrates the concept of functional carbon which is substituted with allyl groups. This can be carried out on a variety of carbon substrates but the best results have been obtained with multiwalled carbon nanotubes (MWCNT). The functionalization step has been scaled up to 30g batches which is more than adequate to allow detailed optimization studies. This process has been monitored closely by means of TGA and FTIR. Figure VI - 149 shows how the allyl groups are used to attach fluorocarbonsufonylimide groups which have been shown to provide the best interfacial behavior. The fluorosulfonate groups can be similarly attached for use in fuel cell electrodes.

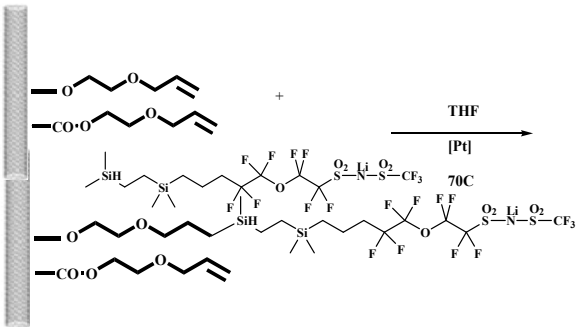


**Figure VI - 149: Preparation of carbon modified with fluorosulfonylimide groups**

The procedures for preparation of the carbons have been used to prepare new composite electrodes that overcome some of the conductivity limitations of some electrode materials.

Figure VI - 150 shows the synthesis of MWCNT nanocables with $TiO_2$ and some of the electrochemical properties of these composite electrodes are shown on Figure VI - 151.

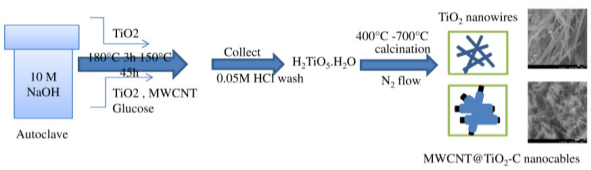


**Figure VI - 150: Synthesis of MWCNT@$TiO_2$ nanocables**

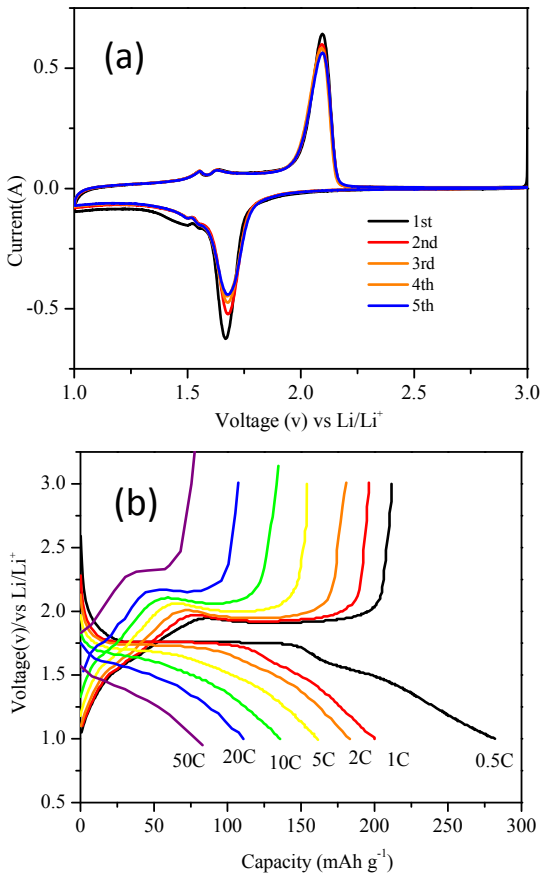


**Figure VI - 151: (a) Voltammograms of the CNT@$TiO_2$-C nanocable electrode at a scan rate of 0.1 mV s-1; (b) The first charge-discharge voltage profiles at different current rates**

## Conclusions and Future Directions

Generation of electrochemical performance data has been delayed in order to produce sufficient materials of reproducible quality to allow a meaningful optimization study to be carried out. The activities described in this report detail the achievement of this objective. The final year of the project will now involve optimization of composite electrodes with single ion conductor electrolytes to fully demonstrate the advantages of this approach.

## FY 2013 Publications/Presentations

1. John B. Kerr, Li Yang, Jianli Cheng and Peter Driscoll, “Electrolytes - R&D for Advanced Lithium Batteries. Interfacial and Bulk Properties,” 2012 *DOE Annual Peer Review Meeting*, May 17, 2013, Washington, DC.

# VI.D.5 Development of Electrolytes for Lithium-Ion Batteries (URI)

**Brett Lucht**
University of Rhode Island

Department of Chemistry
51 Lower College ROAD, Pastore
Kingston, RI 02881
Phone: (401) 874-5071; Fax: (401) 874-5072
E-mail: blucht@chm.uri.edu

Start Date: April 2009
Projected End Date: December 2014

## Objectives

- Develop novel electrolytes with superior performance to state of the art (SOA) ($LiPF_6$ in carbonates).
- Develop an understanding of the source of performance fade in graphite/$LiNi_{0.5}Mn_{1.5}O_4$ cells cycled to high voltage (4.8 V vs Li).
- Develop an electrolyte formulation that allows for superior performance of graphite/$LiNi_{0.5}Mn_{1.5}O_4$ cells.
- Synthesize and characterize novel non-fluorinated lithium salts for lithium battery electrolytes.

## Technical Barriers

This project addresses the following technical barriers from the Batteries for Advanced Transportation Technologies Research, Development Plan regarding electrolytes: Improving the cell performance, cell life, and cost; Improving the calendar life of lithium ion batteries; Expanding the survival temperature range.

## Technical Targets

- Cell performance, life, cost: Calendar life: 40°C, 15 years.
- Survival Temperature Range: -46 to +66°C
- Unassisted Operating & Charging Temperature Range, -30 to + 52°C.

## Accomplishments

- Developed an understanding of the role of electrolyte in capacity fade for graphite/ $LiNi_{0.5}Mn_{1.5}O_4$ full cells cycled at moderately elevated temperature (55 °C).
- Designed electrolyte formulations to decrease cell inefficiency (50 % of SOA) and decrease capacity fade (50 % of SOA) for graphite/$LiNi_{0.5}Mn_{1.5}O_4$ full cells.
- Attemmpted to synthesize and characterize novel non-fluorinated lithium salts and test novel electrolytes in graphite/$LiNi_xCo_{1-2x}Mn_xO_2$ cells.
- Completed electrochemical cycling of Si nano-particle electrodes with electrolytes containing added VC or FEC.

✧ ✧ ✧ ✧ ✧

## Introduction

While commercial lithium-ion batteries (LIBs) perform well for most home electronic applications, currently available LIB technology does not satisfy some of the performance goals for Plug-in Hybrid Electric Vehicles (PHEV). In particular, currently available LIB technology struggles to meet the 15 year calendar life requirement and suffers rapid fade at elevated voltage (>4.5V) and temperature.

The most extensively used LIB electrolytes are composed of $LiPF_6$ dissolved in organic carbonates. However, $LiPF_6$ based electrolytes have poor thermal stability and performance when cycled to high voltage. Significant energy fading occurs after several years at room temperature and over only a few months at the moderately elevated survival temperature of 66°C. While there are several different factors that limit the thermal stability, calendar life and voltage window of LIBs, the reactions of the electrolyte with the surface of the electrode materials are frequently reported to be the most important.

## Approach

Investigate the surface of cathodes and anodes cycled with novel electrolytes, with or without additives, to develop a mechanistic understanding of interface formation and degradation. Develop additives for high voltage (~4.8 V) cathode materials which inhibit performance fade via reduction of Mn dissolution or cathode surface passivation. Use novel synthetic methods to prepare non-fluorinated lithium salts for lithium ion battery electrolytes. Conduct electrochemical cycling of Si-nanoparticle cells with electrolytes containing various quantities of commonly used additives, such as vinylene carbonate (VC) and/or

fluoroethylene carbonate (FEC), to determine optimal electrolyte formulation for silicon anodes.

## Results

**Capacity fade of graphite/$LiNi_{0.5}Mn_{1.5}O_4$ cells.** Due to significant differences in the observed capacity retention and efficiency of Li/$LiNi_{0.5}Mn_{1.5}O_4$ cells compared to graphite/$LiNi_{0.5}Mn_{1.5}O_4$ cells, a detailed analysis of the capacity retention and cycling efficiency of graphite/$LiNi_{0.5}Mn_{1.5}O_4$ cells cycled to high voltage at moderately elevated temperature has been conducted. The cycling performance of graphite/$LiNi_{0.5}Mn_{1.5}O_4$ cells at 25°C is good, but capacity decreases dramatically upon cycling at 55°C, see Figure VI - 152. Independent electrochemical analysis of anodes and cathodes extracted from cells cycled at 55°C suggest that both electrodes have significant capacity loss, although the cathode capacity can be recovered with longer charging times consistent with a significant increase of impedance on the cathode.

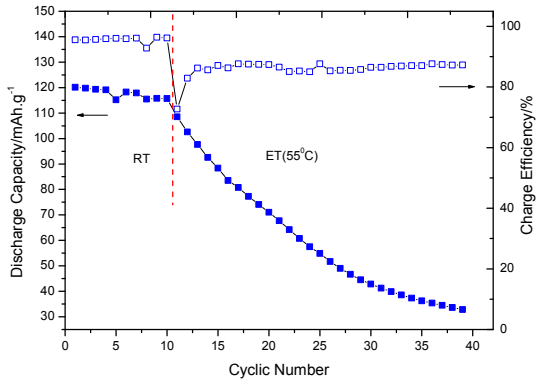


**Figure VI - 152: Cycling performance of graphite /$LiNi_{0.5}Mn_{1.5}O_4$ cell at 25°C (RT) and 55°C (ET)**

Capacity loss on the graphite anode is typically reported to be due to continuous dissolution/reformation of SEI film during cycling at 55°C. Surface analysis of the graphite anodes after cycling suggests that the anode SEI is changing and becoming thicker, but the changes to the graphite SEI do not explain the significantly poorer performance of graphite/ $LiNi_{0.5}Mn_{1.5}O_4$ cells cycled to 55°C than graphite/$LiCoO_2$ cells. Anodes extracted from graphite/$LiNi_{0.5}Mn_{1.5}O_4$ cells cycled at 55°C and analyzed by ICP-MS, contain 0.06 mg Mn which is approximately 1% of the available Mn from cathode, while fresh anodes and anodes cycled at 25°C contain two orders of magnitude lower concentrations of Mn. The deposited Mn may result in damage to the graphite SEI contributing to the capacity fade of the cell.

Analysis of the cathodes by XPS after cycling at 55°C reveal that the intensity of the Mn 2p peaks are decreased, consistent with Mn dissolution, but C 1s, O 1s, F 1s, and P 2p spectra are very similar (Figure VI - 153), consistent with small changes to the thin cathode surface film composed of electrolyte decomposition products including lithium alkyl carbonates, polyethylene carbonate, and lithium flouride. Changes to the XPS spectra of the PVDF binder are also observed. The C1s peak at 290.4 eV is diminished and the F1s peak is shifted from 687.6 eV to slightly lower binding energy (~ 687 eV), suggesting that the PVDF may be decomposing.

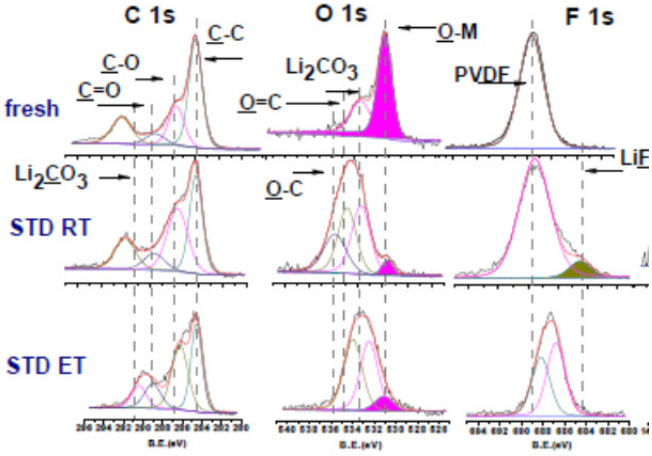


**Figure VI - 153: XPS spectra of LiNi0.5Mn1.5O4, fresh and after cycling at 25°C and 55°C**

*Ex situ* surface analysis of the cathode with SEM reveals that the bulk cathode particles and the cathode laminate are retained. Cross-sectional SEM images clearly indicate that the graphite electrode is delaminating from the Cu current collector. The increased performance loss of the graphite anode is likely related to Mn dissolution and reduction on the anode which may be damaging the anode SEI and contributing to anode delamination. The results suggest that both the anode and the cathode contribute to performance loss in graphite/$LiNi_{0.5}Mn_{1.5}O_4$ cells.

**Additives which improve the performance of graphite/$LiNi_{0.5}Mn_{1.5}O_4$ cells.** Novel additives have been prepared which improve the performance of graphite/ $LiNi_{0.5}Mn_{1.5}O_4$ cells cycled to 4.8 V (vs Li) with $LiPF_6$ in EC/EMC at 55°C. Figure VI - 154 shows the cycling performance of the graphite/$LiNi_{0.5}Mn_{1.5}O_4$ cells with baseline electrolyte and electrolyte containing the additive at RT, ET (55°C) and RT. The initial discharge capacity of the cells with 1.5% and 2.5% (lithium bis(oxalato) borate, LiBOB) are slightly lower than the cells with baseline electrolyte at RT. This difference is ascribed to the irreversible decomposition of the additive on the electrode surface. However, after 30 cycles at 55°C, the cell with baseline electrolyte suffered significant capacity loss, only delivering 24 % of the original capacity. The cells with 1.5% and 2.5%

additive showed improved cycling stability upon cycling at 55°C, 63 and 69 % capacity retention, respectively. After cycling at 55°C the cells were cycled at RT. The cell with baseline electrolyte had continued capacity fade; while the cells with additive exhibited much better cycling stability. In addition to the improved capacity retention, the cells containing the additive have better columbic efficiency while cycling at 55°C.

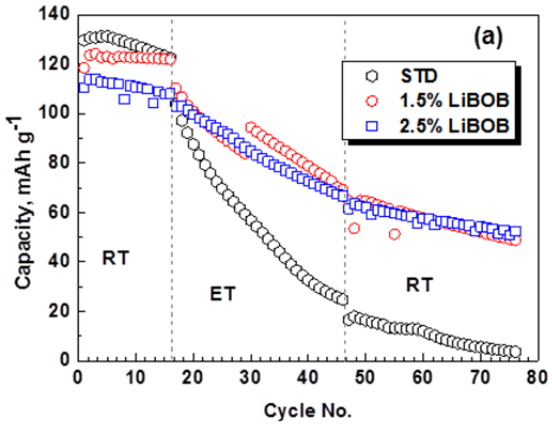


**Figure VI - 154: Cycling performance of graphite/ LiNi0.5Mn1.5O4 cells with STD and LiBOB containing electrolyte at RT, ET (55°C), and RT**

*Ex situ* surface analysis of both the anode and the cathode extracted from graphite/$LiNi_{0.5}Mn_{1.5}O_4$ cells was conducted via a combination of XPS, SEM, TEM with EDX, and ICP-MS to develop a better understanding of the role of the additive in capacity retention upon cycling at elevated temperature. Incorporation of the additive results in the generation of a thin cathode surface film. The cathode surface film inhibits the deposition of poly(ethylene carbonate) and dissolution of Mn and Ni at the cathode surface during cycling at 55°C. The additive also inhibits damage to the anode surface. The presence of the additive results in less Mn and Ni deposition on the anode surface and less damage to the anode SEI. Incorporation of the novel additives to graphite/ $LiNi_{0.5}Mn_{1.5}O_4$ cells cycled to 4.8 V (vs Li) results in improved capacity retention and efficiency. The improved cycling performance can be attributed the inhibition of electrolyte decomposition at the electrode surfaces and inhibition of Mn and Ni dissolution from the cathode and deposition on the anode. Second generation additives which further improve the performance of graphite-$LiNi_{0.5}Mn_{1.5}O_4$ cells have been developed. A patent is being filed and the results will be published in the future.

**Preparation and investigation of novel non-flourinated salts.** Synthetic methods to prepare novel salts were attempted. Two different novel salts were targeted, however, significant difficulties were experienced during the development of the synthetic methods. The project goals were realligned to support the new Silicon Focus Group within the BATT program.

**Investigation of electrolyte additives on the performance of silicon anodes.** Developing an understanding of the role of common additives, such as VC and FEC, on the capacity retention of silicon nano-particle electrodes is being conducted. Li/silicon nano-particle cells were prepared with seven different electrolyte formulations. The baseline electrolyte was 1.2 M $LiPF_6$ in EC/DEC (1:1). The other electrolyte formulations included 3 and 6 % VC and 5, 10, 15, and 25 % FEC (wt %). The cycling performance of the different electrolytes is provided in Figure VI - 155. The best capacity retention was observed for cells containing 10 and 15 % of FEC. Interestingly, the electrolytes with a lower concentration (5 %) and a higher concentration (25 %) of FEC have inferior capacity retention. In addition, the cells with 3 and 6 % VC had comparable cycling performance to the baseline electrolyte. *Ex situ* analysis of the silicon-nano-particle electrodes with XPS, SEM, and FT-IR is currently being conducted and will be presented in FY 14 reports.

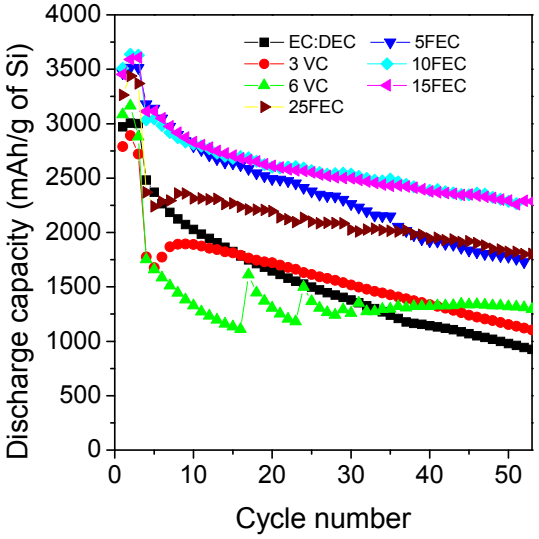


**Figure VI - 155: Capacity retention of Li/silicon nano-particle cells cycled with different electrolytes**

## Conclusions and Future Directions

The failure mechanism of graphite/$LiNi_{0.5}Mn_{1.5}O_4$ cells cycled at 25°C and 55°C have been analyzed by electrochemical methods and *ex situ* surface analysis of the electrodes. Graphite / $LiNi_{0.5}Mn_{1.5}O_4$ cells cycle well at 25°C, but have rapid capacity fade upon cycling at 55°C. Independent electrochemical analysis of anodes and cathodes extracted from cells cycled at 55°C suggest that both electrodes have significant capacity loss, although the cathode capacity can be recovered

with longer charging times. *Ex situ* surface analysis of the cathode with SEM reveals that the bulk cathode particles and the cathode laminate are retained while XPS confirms the presence of a cathode electrolyte interface composed of the decomposition products of the electrolyte. *Ex situ* analysis of the anode reveals a thick anode SEI, anode delamination, and the presence of Mn. The results suggest that both the anode and the cathode contribute to performance loss in graphite/ LiNi0.5Mn1.5O4 cells.

The performance of the graphite/ $LiNi_{0.5}Mn_{1.5}O_4$ cells cycled to 4.8 V (vs Li/Li+) with 1.0 M $LiPF_6$ in EC/EMC (3/7, v/v) with and without added LiBOB (1.5 and 2.5 % (wt)) at 25 and 55°C has been investigated. The initial discharge capacity of the cells with added LiBOB is slightly lower than the cells without added LiBOB. However, after 30 cycles at 55°C, the cells with standard electrolyte suffer poor capacity retention (20 %). The cells with 1.5% or 2.5% LiBOB have improved cycling stability at 55°C with 63 and 69 % capacity retention, respectively, after 30 cycles. The cells containing added LiBOB also have better coulombic efficiency and lower impedance after cycling at 55°C. *Ex situ* surface analysis of both the anode and the cathode extracted from graphite/ $LiNi_{0.5}Mn_{1.5}O_4$ cells was conducted via a combination of XPS, SEM, TEM with EDX, and ICP-MS. The improved cycling performance with added LiBOB can be attributed to the inhibition of electrolyte decomposition at the electrode surfaces and inhibition of Mn and Ni dissolution from the cathode and deposition on the anode upon cycling at high voltage and elevated temperature. Additional novel additives which provide superior performance of graphite/$LiNi_{0.5}Mn_{1.5}O_4$ cells are currently being developed.

The future direction of the project is to develop an understanding of the mechanism of improved capacity retention for Si nano-particle electrodes in the presence of electrolyte additives FEC and/or VC. A direct comparison of the cycling performance of electrolytes with different concentrations of added FEC and/or VC will be conducted and the results will allow the determination of an optimized electrolyte for use with Si nano-particle electrodes. This formulation will be suggested as a standard formulation for BATT researchers to allow for better cross comparison of electrochemical cycling data for different novel Si anode materials. After cycling Si-nanoparticle electrodes with different electrolyte formulations, the electrodes will be extracted and *ex situ* surface analysis will be conducted. The surface analysis and cycling data will be used to develop a mechanism for capacity retention enhancement via addition of FEC or VC.

## FY 2013 Publications/Presentations


1. "Development of Electrolytes for Lithium Batteries," *DOE Annual Peer Review Meeting*, May 13-17, 2013, Washington, DC.
2. "Effect of electrolyte and additives on performance of $LiNi_{0.5}Mn_{1.5}O_4$," *Pacific Rim Meeting on Electrochemistry and Solid State Sciences*, Honolulu, HI, October 2012.
3. "Effect of electrolyte and additives on performance of $LiNi_{0.5}Mn_{1.5}O_4$," *NAAT Batt Annual Meeting and Symposium*, Austin, TX, January 2013.
4. "Role of Electrolyte in interface formation and cycling performance in Lithium Ion Batteries," *IBA Meeting*, Barcelona, Spain, March 2013.
5. 2010 DOE Annual Peer Review Meeting Presentation, May 2013.
6. "Improved performance of graphite/ Li $Ni_{0.5}Mn_{1.5}O_4$ cells with electrolyte additives," *6th International Conference on Advanced Lithium Batteries for Automotive Applications*, Argonne IL, September 2013.
7. L. Zhou, M. Xu, B. L. Lucht, "Performance of lithium tetrafluorooxalatophosphate in methyl butyrate electrolytes," *J. Appl. Electrochem.* 43, 497-505, 2013.
8. M. Nie, D. Chalasani, D. P. Abraham, Y. Chen, A. Bose, B. L. Lucht, "Failure Mechanism of Graphite/$LiNi_{0.5}Mn_{1.5}O_4$ Cells at High Voltage and Elevated Temperature," *J. Electrochem. Soc.* 160, A3138-A3143, 2013.
9. M. Xu, L. Zhou, Y. Dong, Y. Chen, A. Garsuch, B. L. Lucht, "Improving the Performance of Graphite/ $LiNi_{0.5}Mn_{1.5}O_4$ Cells at High Voltage and Elevated Temperature with added Lithium bis(oxalato) borate (LiBOB)," *J. Electrochem. Soc*. **2013**, *160*, A2005-A2013.

# VI.E Cell Analysis, Modeling, and Fabrication

## VI.E.1 Predicting Microstructure and Performance for Optimal Cell Fabrication (BYU)

**Dean Wheeler**
Brigham Young University

Department of Chemical Engineering
350 Clyde Building
Provo, UT 84602
Phone: (801) 422-4126
E-mail: dean_wheeler@byu.edu

**Brian Mazzeo**
Brigham Young University
Department of Electrical and Computer Engineering
459 Clyde Building
Provo, UT 84602
Phone: (801) 422-1240; Fax: (801) 422-0201
E-mail: bmazzeo@ee.byu.edu

Start Date: October 2012
Projected End Date: September 2016

### Objectives

- Develop rapid, reliable, and standardized methods for measuring electronic and ionic conductivities in porous electrodes.
- Determine and predict microstructures for porous electrodes.
- Understand tradeoffs and relationships between fabrication parameters and electrode performance.

### Technical Barriers

One main technical barrier to improved battery performance is to understand electrode conductivity and spatial variability. Within a cell there are inhomogeneities on multiple length scales, from sub-particle size up to hundreds of microns and across the width of full rolls of commercially-prepared electrode films. New approaches must be devised to quantify and better understand these variations. Additionally, while, x-ray tomography (nano-CT) and SEM/FIB can be used to determine a few Li-ion electrode microstructures at very fine resolution, a 3D microstructure prediction model needs to be developed to routinely generate structures for new materials and fabrication conditions, especially over much larger length scales. Because electronic and ionic transport take place in different phases that cannot occupy the same volume, new experimental and modeling techniques are needed to bring greater clarity to the relationships between electrode composition and morphology.

### Technical Targets

- Fabricate micro-four-line probes to determine bulk electronic conductivity in non-delaminated battery films.
- Develop mathematical-model inversion technique to determine current collector contact resistance from film measurements.

### Accomplishments

- Cleanroom procedure established to fabricate the first generation micro-four-line probe.
- Utility of the micro-four-line measurement technique was demonstrated on laboratory-prepared and commercial films.
- Mathematical inversion technique was used to provide first-order estimates of bulk conductivity.

✧ ✧ ✧ ✧ ✧

### Introduction

A great deal of effort is expended by battery researchers and battery manufacturers worldwide to develop improved materials for Li-ion storage batteries; yet a greater understanding of how best to turn those materials into composite porous electrodes with optimized and uniform performance is needed. A lack of fundamental understanding about the relationships between fabrication parameters, microstructure, and performance prevents appropriate feedback and hurts the development of next-generation battery materials and process improvement in battery manufacturing.

Either experimental measurements or predictive models can be used to make the processing-structure-property connection for battery electrodes. In this project, both are used. The effort on this project is

intended to be general and system agnostic, but must of necessity focus on a few key materials in a validation and test environment. For this reason, synergistic collaborations with other researchers, for example, at Argonne National Laboratory (ANL) and A123 Systems, is an important part of this work.

## Approach

The general approach of this project is to use particle-based microstructural modeling, coupled with extensive experimental validation and diagnostics, to understand relationships between fabrication processes, microstructure, and corresponding electron and ion transport in composite electrodes. The fabricated probes will be used to assess electronic and ionic conductivities of porous electrodes attached to current collectors, including local heterogeneities and anisotropic effects, through the use of newly designed instrumentation. The measurements will be used to validate and parameterize the particle model using experimental microstructural and macroscopic properties. Then, these modeling and diagnostic tools will be used to suggest processing conditions that will improve cell performance.

## Results

**Materials.** BYU has received three batches of electrode materials for testing, one from ANL, and two from A123, including commercial $LiFePO_4$ and NCM films from production runs. Additionally, a graphite anode sample from A123 was obtained, as was a batch of $LiCoO_2$ electrode films from Saft America that were calendared to different porosities. Not all of these materials were tested in FY2013, and more complete testing is part of FY2014 milestones.

**Fabrication of four-line-probe.** Planar probes allow the surface of the probe to be placed directly upon electrode materials and thus allow an even pressure to be applied to the films while remaining mechanically robust. As shown in Figure VI - 156, a micro-four-line probe was fabricated in the BYU Cleanroom with inner conducting lines spaced 10 microns apart. The base material is nickel and gold was electrodeposited onto this nickel layer to provide good electrical contact to the electrode films. Because the spacing of the contacts is on the order of the cathode material thickness, a significant amount of the current passing through the battery electrode sample bypasses the current collector. This allows the probe to sample the bulk cathode conductivity without being unduly influenced by the stray current passing through the current collector metal film.

**Construction of automated measurement apparatus.** To be able to consistently make measurements with the fabricated four-line-probe, an apparatus was constructed to make automated measurements. As shown in Figure VI - 157, the electrode material was mounted on an X-Y stage with a force gauge under the target position. Then, the wafer probe was clamped in an inverted configuration to a Z-axis stage that descended on the electrode material. The entire measurement procedure with current source and multimeters was controlled using a computer control and data logging interface.

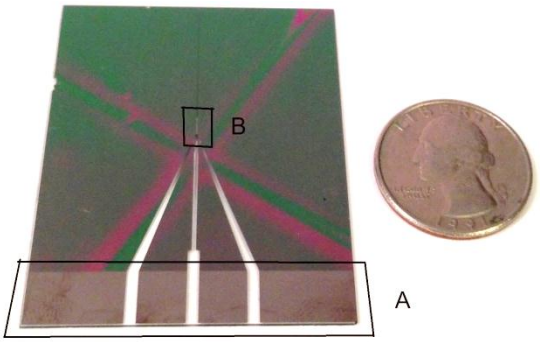


**Figure VI - 156: Completed micro-four-line-probe wafer showing: (A) exposed connection pads, and (B) window for exposing the four contact lines**

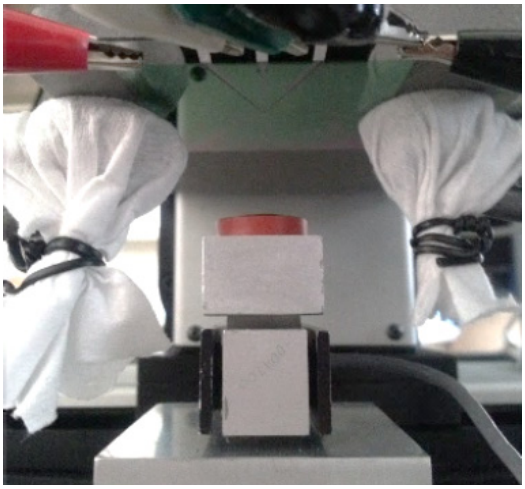

**Figure VI - 157: Measurement apparatus for electronic conductivity measurements. The probe wafer is gently clamped in an inverted orientation to an aluminum block that descends upon the electrode target. Electrical connections are made to the exposed connection pads. The electrode film target is mounted on a disc that is attached to a force gauge to measure and allow the control of the applied pressure**

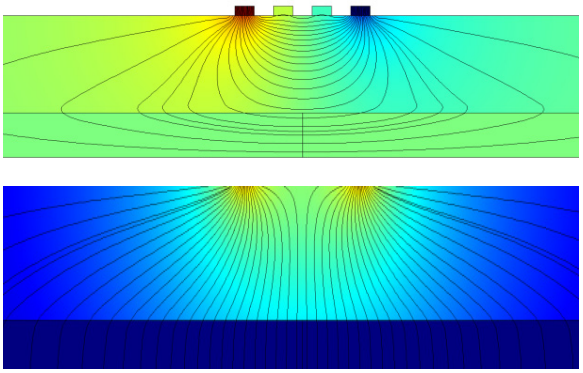

Figure VI - 158: Simulations of current and potential distributions for two orthogonal electrical measurements of an intact electrode using the four-line probe procedure

**Numerical inversion procedure.** To be able to properly interpret the micro-four-line probe measurements, a numerical inversion procedure was developed using simulations of the electrode conductivity as well as the current collector-cathode interface resistance. Examples of the COMSOL simulations of these properties are shown in Figure VI - 158. The simulations show different measurement configurations for determining bulk conductivity of the composite electrode and bulk-to-current-collector interface resistance.

**Demonstration on commercial film.** As shown in Figure VI - 159, conductivity variations were assessed for an NCM cathode film of thickness 70 μm. The repeatability of measurements at single locations was very high. On other hand, there was significant condsuctivity variability at different locations on the film (each separated by a few mm). A more complete study of such spatial variations is planned in FY2014.

In another test, the two experiments illustrated in Figure VI - 158 were carried out on a single location of an NCM electrode. The bulk conductivity at this location was determined to be 58.7 mS/cm. The contact resistance to the current collector was determined to be 9.8 mΩ $cm^2$. This preliminary measurement satisfies our "proof of concept" technical target or milestone; further validation of these measurements is planned in FY2014.

A


B

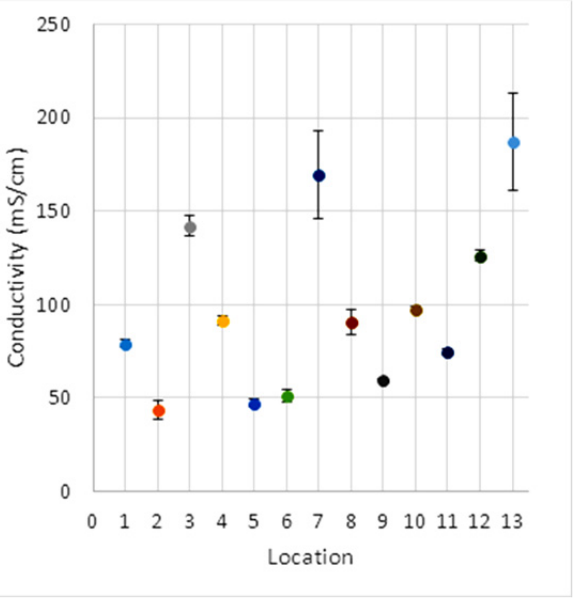


Figure VI - 159: (A) Relative locations of repeated electrical sampling on 17-mm-diameter circular electrode. (B) Location mean conductivities with 95% confidence intervals, showing significant spatial variability of the sample electrode compared to probe variability

## Conclusions and Future Directions

This was the first (partial) year of a new contract and so the above results constitute completion of the expected technical targets or milestones for FY2013. Micro-four-line probes were successfully fabricated and the utility of the measurement technique was demonstrated on laboratory-prepared and commercial films, including those obtained from ANL and A123. Multiple iterations of the probe device and associated computer model took place during the year. Each iteration led to improvement in the robustness and utility of the design.

Significant improvements are expected over the coming contract year that will increase the reliability as well as the durability of the probes that are used to measure these important conductivity properties of the

electrode films. This will feed into the modeling efforts to understand the relationship between the electrode processing conditions and the electronic film conductivity.

This year did not include any milestones explicitly dealing with the particle-based microstructure model. Activities to build the model were carried out and will be reported in FY2014 as part of model-associated milestones.

## FY 2013 Publications/Presentations

1. B. Lanterman, J. Flygare, A. Cutler, B. A. Mazzeo, D. R. Wheeler. "Development of a micro four-line probe for the measurement of thin-film battery electrode conductivity," *224th ECS meeting*, The Electrochemical Society, Oct. 2013, San Francisco, CA.
2. B. A. Mazzeo, B. Lanterman, J. Flygare, A. Cutler, N. Gates, D. R. Wheeler. "Conductivity measurements of thin-film battery films," *3rd SHPE Engineering Research Symposium*, Nov. 2013, Indianapolis, IN.
3. L. Zielke,T. Hutzenlaub, D. R. Wheeler, I. Manke, A. Tobias, N. Paust, R. Zengerle, S. Thiele, "A Synthesis of X-ray Tomography and Carbon Binder Modeling - Reconstructing the Three Phases of $LiCoO_2$ Li-ion Battery Cathodes," *Advanced Energy Materials*, submitted, 2013.

# VI.E.2 Assembly of Battery Materials and Electrodes (HydroQuebec - IREQ)

**Karim Zaghib**
Hydro-Québec (IREQ).

IREQ, Hydro-Quebec
1800 Lionel Boulet
Varennes, QC J3X 1S1, Canada
Phone: (450) 652-8019; Fax: (450) 652-8204
E-mail: Zaghib.Karim@ireq.ca

Start Date: October 2012
Projected End Date: September 2016

## Objectives

- Develop high-capacity, low-cost electrodes with good cycle stability and rate capability to replace graphite anodes in Li-ion batteries.
  - Identify an optimized silicon-carbon-binder electrode composition
  - Use *in situ* SEM methods to determine the failure mode of Si-based anodes.

## Technical Barriers

The challenge is to overcome the electrochemical capacity limitations (both gravimetric and volumetric) of conventional carbon anodes by developing low-cost electrode architectures based on silicon. One of the biggest challenges of this anode material is related to its volume expansion and structural changes which lead to capacity fade and shorten the cycle life.

## Technical Targets

- Identify Si-based anode materials that can achieve a capacity of 1200 mAh/g.
- Produce Si nano powder and supply a 1 kg batch as a baseline material for BATT PIs.
- Supply laminate Si-based electrodes to BATT PIs.

## Accomplishments

- Identified an optimized silicon-carbon-binder electrode composition with an appropriate mixing method.
- Demonstrated a Si-anode composition with 1600 mAh/g and more than 100 cycles with 100% capacity retention.
- Successfully synthesized a new Si material as an alternative source for BATT PIs.

✧ ✧ ✧ ✧ ✧

## Introduction

The BATT Program is looking for the next-generation systems for high-energy batteries. Thus, identifying new anode and cathode materials is necessary. One of the BATT recommendations was the spinel $LiMn_{1.5}Ni_{0.5}O_4$ as cathode and Si-based alloy as anode materials. Thus, the Hydro-Quebec (HQ) project was directly affected with these changes, which were made to better integrate with the other DOE programs. This modification has oriented HQ to work on Si-anode materials.

HQ proposed a strategy to design the architecture of the Si-anode material that can tolerate the volumetric expansion and provide acceptable cycle life with low capacity fade. The particle size, binder type and the electrode composition are the main parameters to define the formulation of the Si-anode. The porosity of the electrode has a direct impact on the performance, and therefore should be optimized by investigating various mixing methods.

To further improve the comprehension of the failure mode of the Si-based anode material, *in situ* SEM was used to monitor the anode during cycling. In this case, a dry polymer was used as the binder to avoid electrolyte evaporation inside the SEM.

## Approach

To address and overcome the electrochemical capacity limitations (both gravimetric and volumetric) of conventional carbon anodes, low-cost electrode architectures based on silicon that can tolerate volumetric expansion and provide an acceptable cycle life with low capacity fade were proposed. Volume expansion, which is a common problem with Si-based electrode materials, will be addressed by: i) tortuosity/porosity optimization and ii) improved current collector technology.

## Results

**Electrode Preparation.** To prepare useful Si-based electrodes, optimizing the process formulation is

necessary. The Si (Umicore) material recommended as a reference anode material by the BATT Program was used. This Si material consists of 25-100 µm agglomerates composed of primary spherical particles of 20-150 nm diameter. In order to minimize the stress on these anode materials, it is important to redesign the anode architecture.

The first step is to develop an appropriate method for mixing the Si composite. Different mixing methods were explored such as jar mill, ball mill (Spex), planetary mixer (Thinky) and their combinations. The initial study utilized acetylene black and alginate binder in the electrode composition, which was compared at low and high loadings of Si and carbon contents. Two composition ratios (Si: binder: carbon black) were identified; (83:15:2) and (50:25:25), one with high Si content and the second with high carbon content. The difference in electrode composition and mixing method will help to better understand the electrode behavior and also identify the appropriate conditions to make a preformed anode. The cells were formed at C/24 with a cut-off voltage at 5 mV and 1 V. The reversible capacity (Figure VI - 160) was 3500, 3810 and 4380 mAh/g, respectively, for the mixing methods; Jar mill (JM), Jar mill + thinky (JMT) and Jar mill + Spex (JMS). The 1st and 2nd cycle coulombic efficiencies of these cells were; (88, 97), (85, 97) and (88, 98), respectively. AC impedance spectroscopy was used to compare the electrodes prepared by different mixing methods. Figure VI - 160 shows the interface resistance (Ri) before and after formation cycles; higher Ri was found with (JMS) followed by (JMT) then JM. But, this trend cannot explain the capacity fade during cycling (Figure VI - 161).

The highest capacity, at C/6, was obtained with JMS (4280 mAh/g), followed by JMT (3710 mAh/g) then JM (3300m Ah/g). The capacity fade after 70 cycles was 48%, 34% and 65%, respectively. These results indicate that JM alone is not effective as a mixing method.

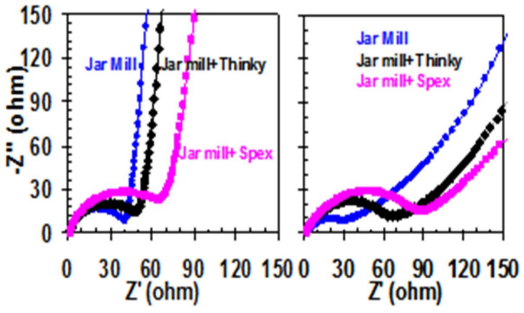


Figure VI - 160: AC impedance before and after formation cycles of Li/EC-DEC-LiPF$_6$/Si cells

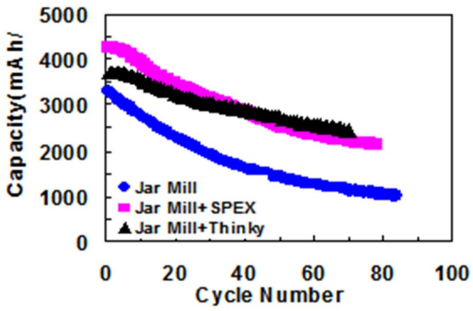


Figure VI - 161: Cycling life of Li/EC-DEC-LiPF$_6$/Si cells at C/6

**Loading Effect.** HQ focused on optimizing the Si-anode formulation and electrode architecture using the reference material provided by Umicore. The studies identified the best anode composition and the appropriate method for mixing the Si composite. By using the appropriate mixing method of jar-mill followed by planetary mixing, two Si loadings were evaluated 50% and 83%. As expected, Ri in Figure VI - 162.a is low in electrodes with more carbon and low Si. The high carbon content played an important role in producing an appropriate anode structure and higher cycle life. The carbon facilitated improved electric contact between particles, hence high capacity was obtained and cycle life with 48% fading after 80 cycles compared to 72% for the low loading anode (Figure VI - 162).

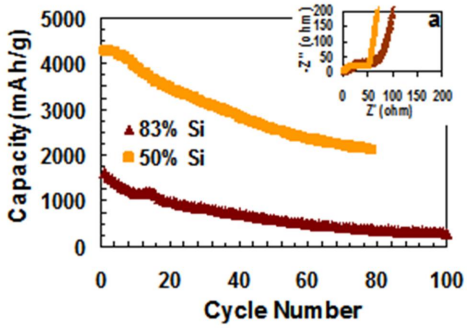


Figure VI - 162: AC Impedance before cycling and cycling life of Li/EC-DEC-LiPF$_6$/Si cells with different loading

The porosity of the electrode, which is strongly influenced by the electrode composition, is a major parameter affecting the electrode performance. A high carbon content and low Si ratio in the anode composition yielded significantly better performance.

The studies identified that the optimal range of the anode composition (Si:binder:carbon) is between (50:25:25) and (60:20:20). By increasing the Si content to 70%, the specific capacity fades faster than when the Si content is lower. The porosity and tortuosity of the electrode, which are strongly influenced by the electrode composition, are major parameters affecting electrode performance. The porosity varied from 0.5 to

0.4, respectively, in anodes with 50% and 70% Si content, and the influence on capacity is shown in Figure VI - 163. The capacity fade is more pronounced when the Si content is higher and porosity is lower. This implies that with the current mixing technique, the composition should be limited to 60% Si material in the electrode. In another study, a Cu current collector with rougher surface showed lower impedance compared to a standard one; but it does not appear to improve the cycling stability.

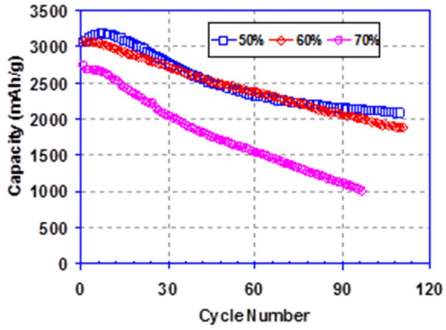


**Figure VI - 163: Cycle life of Li/EC-DEC-LiPF$_6$/Si cells at C/6 with anodes having different loading**

**Cycling Conditions**. An electrode with the composition (50%:25%:25%) was selected for investigations of different cycling conditions.

Cells were cycled at C/6 and 1C rates to determine the effect of stress on the particles after prolonged cycling, Figure VI - 164 shows that the capacity fade is more pronounced when the rate is higher. The Si particles suffers more stress at high rate (1C), which induces a fade of 85% of the initial capacity compared to 56% at C/6.

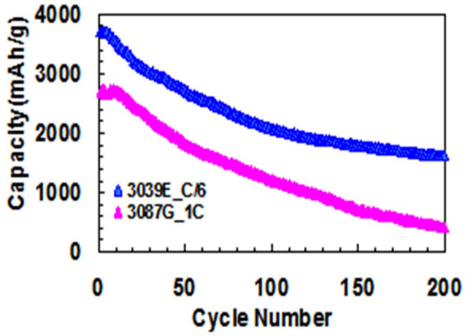


**Figure VI - 164: Cycle life of Li/EC-DEC-LiPF$_6$/Si cells at 1C and C/6 rates**

Studies at various depth of discharge (DoD) were used to monitor the stress on Si particles and its effect on the cycling performance. The stress level was controlled by varying DoD. At low DoD, the Si particles in the anode will experience minimum stress. Figure VI - 165 shows clearly the effect of DoD on the cycling stability at C/6. Capacity fade is severe when Si is cycled at high DoD, and the particles suffer from high stress that induces cracks. At DoD higher than 50% (2000 mA/g capacity), the cells show capacity fade that ultimately degrade in the same trend. At 40% DoD, an acceptable reversible capacity of 1670 mAh/g with good stability after 100 cycles is obtained.

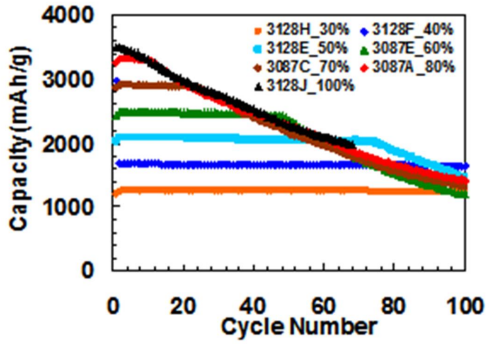


**Figure VI - 165: Cycle life at C/6 of of Li/EC-DEC-LiPF$_6$/Si cells at different DoD**

***In situ* Analysis.** The stress on the Si particles during charge and discharge will spread throughout the electrode, and thus destroy the integrity of the anode, as observed by *in situ* SEM. The *in situ* study (Figure VI - 166) was performed on the electrode using Umicore Si with composition 50%:25%:25%.

The results of the *in situ* analysis revealed an increase in the electrode thickness during discharge to 5 mV, resulting from lithium insertion in the host structure of the Si particles.

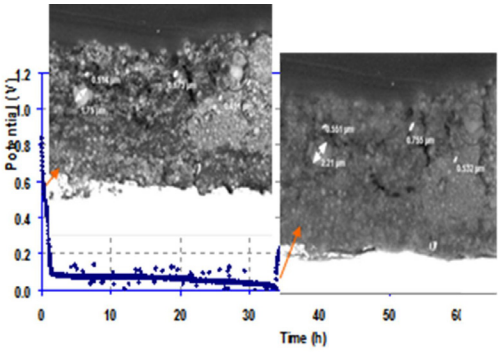


**Figure VI - 166: *In situ* analysis of Li/polymer_LiTFSI/Si cell in polymer matrix**

The average electrode expansion was about 58%. The volume expansion also depends on the electrode composition; a different value was obtained with different electrode compositions. An increase in the primary particle size was noted, with an important morphology change in the electrode (Figure VI - 166). Less cracks in the particles were observed with this material and only few larger particles break down during lithium de-insertion and insertion. Several

fractures in the electrode were observed during the 1st charge. These fractures could be a consequence of electrode densification.

## Conclusions and Future Directions

The *in situ* analysis and cycling studies on the Si anode materials indicate that controlling the rated capacity by limiting %DoD is beneficial to reduce stress and to maintain the mechanical integrity of the particles. Thus, sacrificing some capacity could be an acceptable compromise to obtain a useful Li-ion cell with longer cycle life.

HQ proposes to continue development of the Si-nano material as an improved anode for the BATT PIs, and to continue using *in situ* methods to better understand the failure mechanism of this material.

## FY 2013 Publications/Presentations

1. K. Zaghib, A. Guerfi, P. Hovington, A. Vijh, M. Trudeau, A. Mauger, J.B. Goodenough, C.M. Julien "Review and analysis of nanostructured olivine-based lithium rechargeable batteries: Status and trends," *Journal of Power Sources*, **232**, 357-369 (15 June 2013).
2. "Facile dry synthesis of sulfur core-shell composite for the scalable fabrication of lithium/sulfur batteries," Chi-Su Kim,*6th International Conference on Advanced Lithium Batteries for Automobile Applications*, September 9-11, 2013, Argonne Advanced Photon Source Conference Center Argonne, IL.

# VI.E.3 Model-Experimental Studies on Next-generation Li-ion Battery Materials (LBNL)

**Venkat Srinivasan**
Lawrence Berkeley National Laboratory

Environmental Energy Technologies Division
1 Cyclotron Road, MS 70R0108B
Berkeley, CA 94720
Phone: (510) 495-2679; Fax: (510) 486-4260
E-mail: vsrinivasan@lbl.gov

Start Date: October 2012
Projected End Date: September 2016

## Objectives

- Quantify the usefulness of alloy anodes for use in PHEVs.
- Understand the mechanical degradation in electrodes used in EVs and PHEVs.
- Model reaction distribution in battery electrodes.

## Technical Barriers

Low energy efficiency; low calendar/cycle life; high cost.

## Technical Targets

- Available energy: 56 Wh/kg (10 mile) and 96 Wh/kg (40 mile).
- 10-s discharge power: 750 W/kg (10 mile) and 316 W/kg (40 mile).

## Accomplishments

- Modeled NMC electrode behavior with a systematic approach of finding parameters used in the model. Final model has no fitting parameters.
- Created general-purpose software package capable of solving systems of nonlinear discretized equations on two-dimensional grids.
- Simulated lithium insertion and extraction for model particle-binder systems. Model reveals conditions under which binder, silicon, or interface fails and is how failure is related to mechanical properties.
- Experimentally determined concentration dependent transport properties for $LiPF_6$ in EC:DEC (1:1)

✧ ✧ ✧ ✧ ✧

## Introduction

**Modeling porous electrodes with layered $LiNi_{1/3}Co_{1/3}Mn_{1/3}O_2$ (NMC) active material**. High energy density and long cycle life are critical for reducing the cost of rechargeable Li-ion batteries. Thick porous electrodes result in large energy densities; however, transport limitations can decrease power capability. The primary goal of this project is to develop mathematical models for candidate Li-ion chemistries with little to no adjustable parameters. The layered $LiNi_{1/3}Co_{1/3}Mn_{1/3}O_2$ (NMC) cathode material has been selected as the baseline system to study rate performance associated with the transport limitations in solid and electrolyte phases.

Over the past year, work has been focused on developing mathematical models for porous electrodes with the aim of predicting electrode behavior. When charging/discharging at high rates, electrode performance is limited in solution phase of the porous electrode. Therefore, it is important to understand mass transport in tortuous pores of the electrode. The effective transport properties are associated with electrode structure, i.e., porosity and tortuosity, and bulk properties of the electrolyte. While porosity is a measureable parameter, tortuosity is non-measurable and is usually estimated from porosity through the Bruggeman relation. Literature studies have measured electrode tortuosity and bulk electrolyte properties.

An accurate model prediction requires correct estimate of effective transport properties. In the present model, both electrode tortuosity and electrolyte properties are taken from literature to show a preliminary prediction of experimental data and understand limitations in the NMC electrode. Separate experiments were performed to measure the electrolyte properties for use in the model in future work.

**Estimating electrolyte transport properties.** In order to predict the cell performance under a variety of cycling conditions, reasonable estimates of the concentration dependent transport properties in the electrolyte becomes imperative. The electrolyte used in this project is $LiPF_6$ in EC:DEC (1:1 by weight) which is also the baseline electrolyte for the BATT program.

According to Onsager reciprocal relations, there are *n(n-1)/2* independent transport properties, where *n* is the number of species in the electrolyte. If the solvent mixture (EC and DEC) is treated as a single species, the number of transport properties become three: (a) conductivity; (b) salt diffusion coefficient; (c) transference number. In addition to these three properties, the salt activity coefficient (which is a thermodynamic property) also needs to be measured.

**Stress and strain in silicon electrodes.** The high capacity of silicon for inserted lithium is associated with large volume changes and large stresses. In a porous electrode, the material surrounding silicon particles is also subjected to stress. Stresses can cause material damage and reduce battery capacity. In order to understand the conditions under which binders must operate, and to determine the qualities that binders should possess in order to better tolerate these conditions, a mathematical model was developed.

## Approach

**Rate limitations in NMC electrode.** A systematic approach has been applied to find the kinetic parameters needed for the model for studying limitations in NMC cathode. The rate constant associated with Li anode in 1M $LiPF_6$ in EC:DEC (1:1) was obtained from the rate experiment data of Li-Li symmetric cells in coin-cell configuration. At each applied current, the corresponding potential was measured and plotted as a function of current. The I-V curve was fitted using the Butler-Volmer equation and the exchange current density was obtained from the Tafel slope.

The rate constant associated with NMC electrode was obtained from a NMC-Li coin cell. The electrode was made thin, so the mass transport in the electrolyte phase was minimized. An open circuit relaxation experiment was used with a model to extract diffusion coefficient as a function of the state of charge (SOC) for this cathode. In addition, the experimental potentials can be fitted to the model. The discharge potential at each rate was calculated with a correction for the potential drop at Li anode. The exchange current density of NMC cathode was then obtained by fitting the model with experimental data.

**Transport properties.** The diffusion coefficient as a function of concentration was measured using the restricted diffusion method. In this technique free standing $LiPF_6$ in EC:DEC (1:1 by weight) was placed between Li-Li electrodes. Constant current was passed for a certain time to build up a concentration gradient. The current was then stopped and the cell potential monitored during this open-circuit relaxation period. Chapman and Newman (1980) have shown that at long relaxation times the slope of ln V vs. time curve is a straight line, which is proportional to the salt diffusion coefficient at that particular electrolyte concentration. The procedure was repeated for different electrolyte concentrations and at different polarization times to check for reproducibility. The functionality of the salt activity coefficient and transference number as a function of concentration was obtained using a concentration cell. The cell consisted of two separate chambers that were separated by a glass frit to prevent rapid mixing of the electrolyte. The concentration in one of the chambers was kept constant at 2M whereas in the other chamber it was varied in between 0.2M to 2M. The open circuit voltage was measured for each concentration and lithium metal was used as the electrode in the experiments. The conductivity of the electrolyte as a function of concentration was measured using a conductivity meter.

**Stress and strain in silicon electrodes.** In order to capture important mechanical behavior in a relatively simple model, the finite-deformation graphite model of Christensen and Newman (2006) was adopted, modified, and cast into set of two-dimensional equations on an axisymmetric cylinder. Binder regions were attached to the active material region and coupled through stress and displacement.

Working in two spatial dimensions introduces significant complications relative to a one-dimensional model, but supplies a wealth of additional information. The resulting model equations proved to be difficult to solve with available software packages, so a new general-purpose package was written in order to provide the necessary flexibility.

The model equations were solved over lithium insertion/extraction cycles and stresses were computed throughout the model systems. Calculated stress values and strain energies are comparable to published yield stresses and adhesion energies.

## Results

**Rate limitations in NMC electrode.** The model-experiment comparison of NMC electrode at different rates is shown in Figure VI - 167 using kinetic parameters obtained from experiments and electrode tortuosity and transport properties taken from literature studies of $LiPF_6$ in EC:DEC or similar electrolyte. The electrode behavior is well predicted at rates smaller than 1C. For rates larger than 1C, the model is able to predict the electrode potential at the beginning of discharge, but not the capacity loss near the end of discharge. This is because electrolyte concentration increases at the Li anode and extrapolating the literature values might not reflect the real electrolyte properties towards the end of discharge.

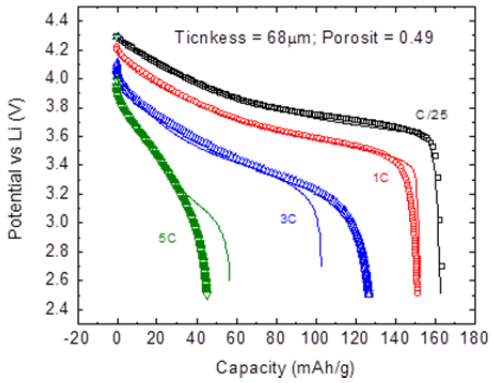


**Figure VI - 167: Model-experiment comparison of NMC electrode discharge at different rates**

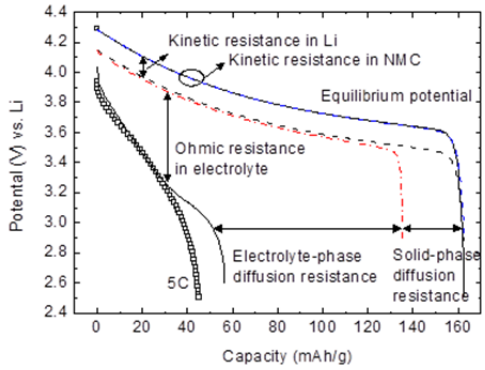


**Figure VI - 168: Potential drop estimation of NMC electrode at 5C**

Figure VI - 168 shows the estimate of potential drops in NMC electrode at 5C. While some potential drops are due to kinetic resistances at Li anode and NMC cathode and some capacity loss is due to solid-phase diffusion resistance, most of the potential drops and capacity loss come from ohmic resistance and diffusion resistance in the electrolyte. This is evidence that the electrode performance is limited in the electrolyte phase of the porous electrode. Therefore, understanding the effective transport properties is important to improve battery design and model predictions, especially at high rates.

**Transport properties – diffusion coefficient.** The diffusion coefficient at different salt concentrations was measured using the restricted diffusion method. Figure VI - 169 shows the experimental data points and model fit for the diffusion coefficient at different salt concentrations for $LiPF_6$ in EC:DEC (1:1).

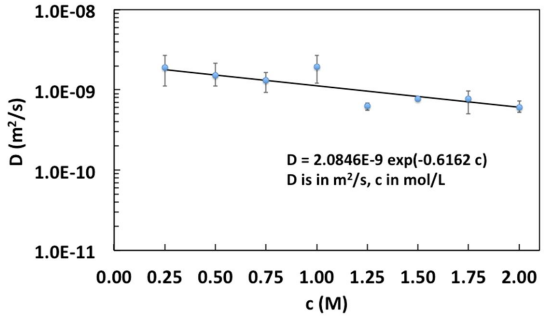


**Figure VI - 169: Diffusion Coeffcient as a function of concentration for LiPF6 in EC:DEC (1:1) measured using Restricted Diffusion method**

**Transference number and salt activity coefficient.** Concentrated solution theory suggests that the open – circuit voltage ($U$) measured from a concentration cell at different salt concentrations ($c$) is related to transference number ($t_+$) and thermodynamic factor $\left(1+\frac{dlnf}{dlnc}\right)$ by the relationship: $\frac{dU}{dlnc}=\frac{2RT}{F}(1-t_+)\left(1+\frac{dlnf}{dlnc}\right)$, where $R$ is ideal gas constant, $T$ is temperature and $F$ is Faraday's constant. The variation of $(1-t_+)\left(1+\frac{dlnf}{dlnc}\right)$ with concentration is shown in Figure VI - 170. At infinite dilution, the curve approaches $(1-t_+)$ as $\left(1+\frac{dlnf}{dlnc}\right)$ approaches unity. The value of transference number at infinite dilution was found to be 0.38.

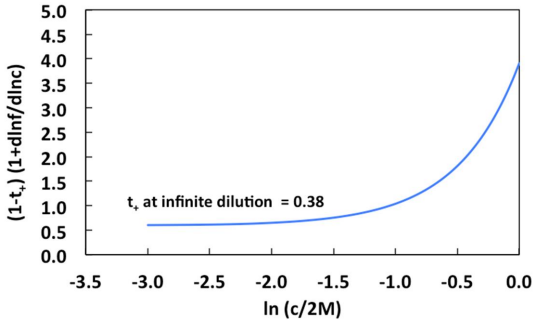


**Figure VI - 170: Variation of $(1-t_+)\left(1+\frac{dlnf}{dlnc}\right)$ with concentration for LiPF6 in EC: DEC (1:1)**

**Conductivity.** Figure VI - 171 shows the experimental data and model fit for the conductivity of the electrolyte as a function of concentration.

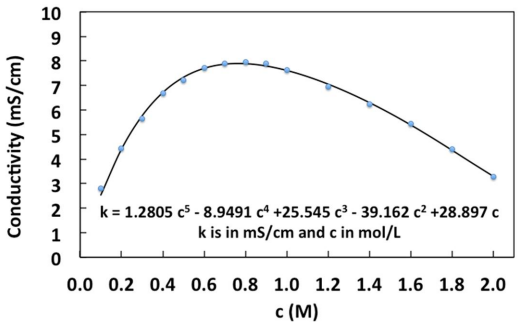


**Figure VI - 171: Conductivity as a function of concentration for $LiPF_6$ in EC:DEC (1:1)**

**Stress and strain in silicon electrodes:** Solutions to the model equations were calculated as spatial distributions of inserted lithium and material displacement throughout the active material domain, as well as displacement in the binder region. From this information, stresses are calculated throughout the entire system, and available strain energy is calculated from auxiliary relaxation simulations.

Figure VI - 172 shows visualization from a typical simulation, near the end of lithium insertion. The vertical axis is the cylinder's axis of symmetry, and the horizontal axis is a plane of symmetry. Colors reflect the mole fraction of lithium-occupied sites, and the binder region is drawn as a wireframe. All material is shown in its "present" deformed location. The binder has been given the material properties of PVdF.

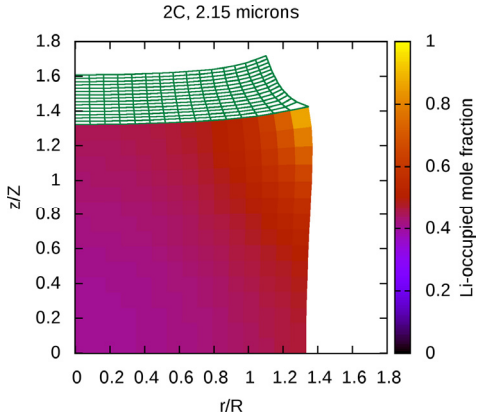


**Figure VI - 172: Lithium-occupied mole fraction near end of lithium insertion for active material cylinder sandwiched between binder layers**

The von Mises yield criterion and definition for equivalent tensile stress has been adopted because it is simple and common and provides a qualitative understanding of the stress distribution. This is shown in Figure VI - 173 for the same situation shown in Figure VI - 172. Unfortunately, a quantitatively-correct theory of yielding does not seem to exist for lithiated silicon or typical binder materials.

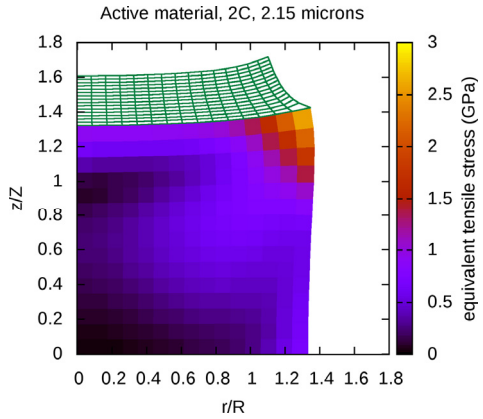


**Figure VI - 173: von Mises equivalent stress throughout the active material region**

Figure VI - 174 shows the maximum equivalent stress in the active material domain for different particle sizes. The particle size relative to the diffusion length scale determines the degree of uniformity in lithium distribution and material displacement for a given system. The maximum stress increases with particle size, which is qualitatively consistent with reports from many other researchers. A reported yield stress for the lithium-silicon system is shown on the plot in order to demonstrate that computed results are in reasonable and physically-significant range.

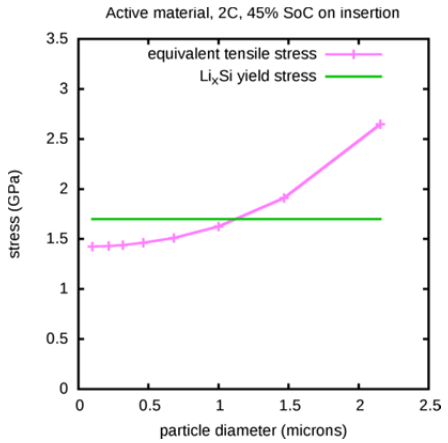


**Figure VI - 174: Maximum equivalent stress in active material as a function of particle size, compared with reported yield stress**

## Conclusions and Future Directions

The analysis of potential drops of NMC electrode showed that most of the potential drops and capacity loss come from resistances in the electrolyte phase. Accurate model predictions require correct estimate of effective transport properties in the porous electrode. Therefore, future studies will focus on investigating electrode structure and electrolyte transport properties to improve electrode performance.

Simulations of lithium insertion and removal in model systems produced qualitative trends that are generally in agreement with the findings of other researchers. However, in order for the simulations to have predictive power, they require the input of much more comprehensive experimental data, as well as additional, quantitatively-correct theories of material behavior.

In order to address, in part, this lack of experimental data, fabrication of material samples and measurements of mechanical properties are now being trialed. Once reliable parameter values are obtained, they will be incorporated into the simulations in order to improve predictive power.

## FY 2013 Publications/Presentations

1. Shao-Ling Wu, Venkat Srinivasan, "Understanding Limitations in $LiNi_{1/3}Mn_{1/3}Co_{1/3}O2$ Electrode," *224th ECS Meeting of The Electrochemical Society*, Oct. 27- Nov. 1, 2013, San Francisco, CA.
2. Amal Mehrotra, Sunil Mair, Venkat Srinivasan, "Transport Property Measurements for $LiPF_6$ in EC:DEC (1:1)," *224th ECS Meeting of The Electrochemical Society*, Oct. 27- Nov. 1, 2013, San Francisco, CA.
3. Kenneth Higa, Venkat Srinivasan, "Stress and Strain in Silicon Electrode Models," *224th ECS Meeting of The Electrochemical Society*, Oct. 27- Nov. 1, 2013, San Francisco, CA.

# VI.E.4 Predicting and Understanding Novel Electrode Materials from First-Principles (LBNL)

**Kristin Persson**
Lawrence Berkeley National Laboratoty.

Energy and Environmental Technologies Division
1 Cyclotron Road
Berkeley, CA 94563
Phone: (510) 486-7218
E-mail: kapersson@lbl.gov

Start Date: October 2012
Projected End Date: September 2016

## Objectives

- Model and predict the behavior of electrode materials from first-principles.
- Understand the atomistic interactions underlying the behavior and performance of the high-capacity lithium excess and related composite cathode materials.
- Predict new materials using the recently developed Materials Project high-throughput computational capabilities at LBNL.

## Technical Barriers

Investigating electrode materials with atomistic modeling require rigorous bench marking as well as insight into the materials chemistry and its effect on electrode performance. In the case of the Li-excess materials, it is challenging, as there are an increased number of variables associated with the unknowns regarding possible composite or solid solution structure of the material, the amounts of each phase, synthesis procedure, etc.

## Technical Targets

- Elucidate the phase space of the layered $Li_2MnO_3$, and associated defect spinel phases that can form as a function of different Mn and Li sites and migration patterns.
- Understand the charging mechanism in $Li_2MnO_3$.
- Chart out and elucidate the transformation paths in $Li_2MnO_3$ as a function of charge.
- Increase the number of predicted battery compounds available on the Materials Project.

✧ ✧ ✧ ✧ ✧

## Introduction

There is increasing evidence that many of the performance limiting processes present in electrode materials are highly complex reactions occurring on the atomic level. The Persson BATT effort at LBNL is studying these processes using first-principles density-functional theory modeling tools. By understanding the underlying reasons for the electrode materials working performance, improvements or design schemes can be directed at the root cause of the process.

The composite cathode materials show great promise for high voltage and high capacity, however, they also present voltage fade, structural degradation and safety concerns. The voltage and capacity fade of the composite cathode materials are due to possible 1) dissolution of the transition metal ions and 2) structural transformation reactions as a function of rate and cycling. There are safety concerns relating to oxygen loss and electrolyte breakdown. All these aspects will in turn be addressed in this project and during the first year the main focus was to understand the structural and chemical changes in the layered $Li_2MnO_3$ structure which is a key material to explain the high capacity in layer-layer or layer-spinel composite electrode materials. Layered $Li_2MnO_3$ has been assumed to be largely electrochemically inactive due to the high oxidation state of Mn (4+ in the discharged state). Additions of $Li_2MnO_3$ to other spinel and/or layered materials have been used to increase the structural stability of the composite materials and allow more Li extraction than for the layered or spinel materials alone. However, many recent experimental studies have shown that the $Li_2MnO_3$ component is actually electrochemically active, which demands a re-examination of the conventional belief on the structural and chemical behavior of $Li_2MnO_3$ and the existing explanation of the origin of high capacity in the composite materials.

Furthermore, the last results for the $LiNi_{0.5}Mn_{1.5}O_4$ (LNMO) project are reported. For many systems, nano-scaling of electrode materials is frequently used in battery applications to enhance performance, particularly concerning rate capability. However, for the high-voltage spinel, LNMO, conflicting results have been reported on the effectiveness of nano-scaling to enhance its rate performance.

## Approach

The Persson group uses atomistic modeling to study the relevant thermodynamic and kinetic processes. The calculations are performed at NERSC and on the Lawrencium cluster at LBNL. To elucidate the atomistic interactions, first-principles zero-temperature calculations are employed and coupled with the cluster expansion technique to examine the structural and chemical space, establish ground states, and resulting electrochemical signature of the materials. To examine temperature-induced properties, statistical mechanics and kinetic Monte Carlo methodologies are utilized.

## Results

**Transformation mechanisms of $Li_2MnO_3$.** Layered-layered composites containing $Li_2MnO_3$ show a large 'activation' capacity (about 350 mAh/g) for the first charge, but then for the 1st discharge and later charge/discharge cycles it exhibits lower capacity. This is believed to be due to partial phase transformation to the spinel structure. A cluster expansion model of the ionic interactions in $Li_xMnO_3$ (0<=x<=2) was employed to predict the ground states as a function of Li. Hundreds of Li/Mn arrangements within the $Li_2MnO_3$ structure (see Figure VI - 175) were computed within GGA+U and used to fit the cluster expansion to arrive at a converged model of the coupled ionic interactions.

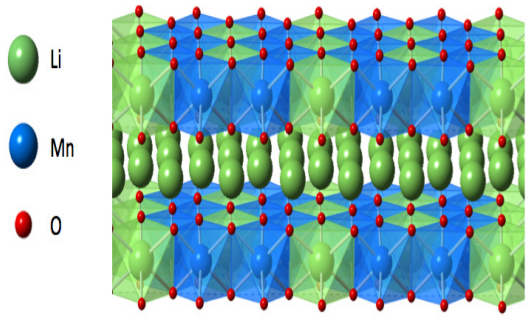


**Figure VI - 175: The crystal structure of Li2MnO3 where the Li layer is shown without local coordination spheres but the combined Li/Mn layers shows the octahedrally coordinated Mn (blue) and Li (green) ions**

In combination with the cluster expansion, possible phase transformations in the $Li_2MnO_3$ structure and their driving mechanisms are investigated. In Figure VI - 176, the formation energies ('stability') of a large number of $Li_xMnO_3$ structures are presented, including a large number of Mn/Li defect phases. The blue points signify compounds which retain the overall $Li_2MnO_3$ structure and the red points correspond to compounds which exhibit large structural deformations from the parent $Li_2MnO_3$ compound. As can be seen in Figure VI - 176, the structural deviations significantly increase with the amount of Li extracted from the compound, especially at $x_{Li} < 1$. Furthermore, in cases of large deformation, there exist a significant driving force for Mn ions to migrate from the Mn-layer into the Li-layer. The Mn migration results in spinel-like structures, as the major difference between the layered structure and the spinel is the existence of Mn tetrahedrons formation spanning the Mn-layer and Li-layer. The degree of Mn migration is determined by thermodynamic as well as kinetic factors, which means that the migration could be slow enough for material to retain its original structure during fast Li-extraction even if the structure is thermodynamically unstable.

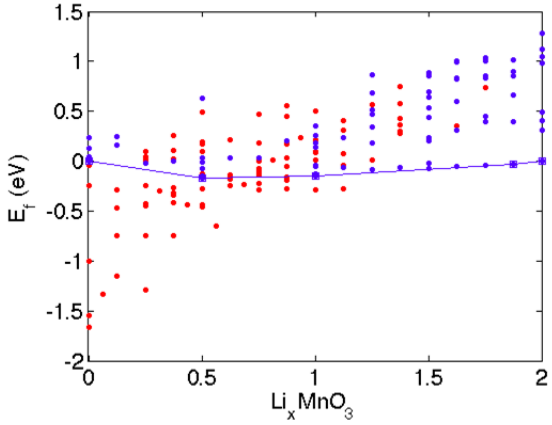


**Figure VI - 176: Calculated formation energies of LixMnO3 structures with Li/vacancy defects spanning both the Li and the Mn layer. The blue points signify structures that retain the overall Li2MnO3 structure but the red points correspond to structures with a large deformation and defect formations compared to the parent structure**

Analyzing the chemical and structural arrangements of the defect structures (red points) provides evidence of the thermodynamic stable states and driving force towards structural transformations in the $Li_2MnO_3$ compound. Hence, further calculations of the energy barriers of Mn migration were performed. The elastic band method was employed for several different hypothesized Mn migration paths at three different Li content, x = 0, 0.5, and 1. For low Li content, a favorable Mn migration path was found which implies a correlation between high charge, and increased spinel transformation.

**Surface morphology effects in high-voltage spinel $LiMn_{1.5}Ni_{0.5}O_2$ (LNMO).** To investigate the effect of nano-scaling on LNMO, specifically focusing on the role of surface stability and cation ordering, the surface energy for the low index facets (100), (110), and (111) was calculated. It was found that the most stable facet is dependent on the cation ordering at the surface layer. For a uniformly disordered structure (the most highly occurring local ordering in the disordered spinel with random cation arrangements), the (111) facet has the

lowest surface energy among the investigated facets, which agrees with several existing experimental observations.

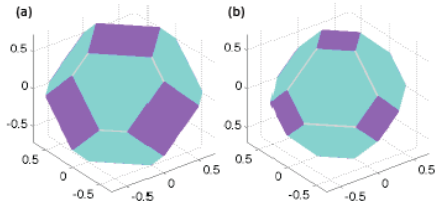


**Figure VI - 177: The equilibrium shape of (a) the ordered spinel structure with a local inverse spinel surface structure and (b) the disordered spinel structure. The (100), (110) and (111) facets are colored violet, grey and turquoise, respectively**

For the ordered structure, however, using only the atomic rearrangement required to remove the dipole moment and routine cell relaxations, the (100) facet with the Li/Mn/Ni/O-termination is predicted to be most stable, which contrasts with experimental observations. The surface reconstruction previously found successful for the $LiMnO_2$ spinel [4] was applied, where the (111) facet can be drastically lowered if a targeted surface reconstruction is employed where the Mn ions on the surface are locally swapped with the Li ions in the next available layer leading to an inverse spinel structure near the surface. This reconstruction successfully rendered the (111) facet the most stable for the LMNO ordered system, as expected for the spinel structure.

## Conclusions and Future Directions

Through extensive calculations and analyses of the layered-spinel $Li_xMnO_3$ phase space, it has been found that the original structure of $Li_2MnO_3$ is thermodynamically unstable towards transformation and deformation to spinel-like domains, especially at low Li content. For low Li content, a favorable Mn migration path is found which implies a correlation between high charge, and increased spinel transformation. Future studies involve analysis of the charge and positions of the oxygen around each path which will provide further understanding on the phase transformation mechanism. Further studies also include oxygen migration.

For the LMNO surface project, the calculations predict that the (111) facet is the most stable surface facet (followed by the (100) and the (110) facets) for both the ordered as well as the disordered LMNO materials, resulting in the equilibrium cubo-octahedral particle morphology. The surface reconstruction in the ordered material results in a deviation from the ideal ordered surface cation arrangement, which will likely result in an enhanced accessibility to the Li-vacancy solid-solution region close to the surface.

## FY 2013 Publications/Presentations

1. Anubhav Jain, Shyue Ping Ong, Geoffroy Hautier, Wei Chen, William Davidson Richards, Stephen Dacek, Shreyas Cholia, Dan Gunter, David Skinner, Gerbrand Ceder, Kristin A Persson, "Commentary: The Materials Project: A materials genome approach to accelerating materials innovation," *APL Mater.,* **1**, 011002 (2013).
2. Nadeem Tahir, Altaf Karim, Kristin A. Persson, Syed Tajammul Hussain, Alejandro Gabriel Cruz Gonzalez, Muhammad Usman, Muhammad Naeem, Ruimin Qiao, Wanli Yang, Yi-De Chuang, Zahid Hussain, "Surface Defects: Possible Source of Room Temperature Ferromagnetism in Co Doped ZnO Nanorods," *J. Phys. Chem. C*, **117** (17), pp 8968–8973 (2013).
3. Eunseok Lee and Kristin A Persson, "First-principles study of the nano-scaling effect on the electrochemical behavior in LiNi0.5Mn1.5O4," *Nanotechnology*, **24**, 424007, 2013 doi:10.1088/0957-4484/24/42/424007.
4. Altaf Karim, Sonia Fosse and Kristin A. Persson, "Surface structure and equilibrium particle shape of the LiMn2O4 spinel from first-principles calculations," *Phys Rev. B*, **87** (7), 075322 (2013) DOI: 10.1103/PhysRevB.87.075322.
5. Dan Gunter, Shreyas Cholia, Anubhav Jain, Michael Kocher, Kristin Persson, Lavanya Ramakrishnan, Shyue Ping Ong, Gerbrand Ceder, *5th Workshop on Many-Task Computing on Grids and Supercomputers (MTAGS) 2012*, Conference proceedings.
6. Shyue Ping Ong, William Davidson Richard, Gerbrand Ceder, Anubhav Jain, Michael Kocher, Shreyas Cholia, Daniel Gunter, Kristin A. Persson, Geoffroy Hautier, and Vincent L. Chevrier, "Python Materials Genomics (pymatgen): A Robust, Open-Source Python Library for Materials Analysis," *Computational Materials Science*, **68**. 314–319 (2013).

# VI.E.5 Electrode Fabrication and Materials Benchmarking (LBNL)

**Vincent Battaglia**
Lawrence Berkeley National Laboratory

Environmental Energy Technologies Division
1 Cyclotron Road
Berkeley, CA 94960
Phone: (510) 486-7172; Fax: (510) 486-4260
E-mail: vsbattaglia@lbl.gov

Start Date: October 2012
Projected End Date: September 2016

## Objectives

- Make good cells for testing experimental chemistries
- Optimize the electrode fabrication processes
- Bring fundamental understanding to the processes
- Test materials developed in the BATT Program
- Test for initial performace.
- Test for cycling performance
- Identify limitations and failure modes

## Technical Barriers

Energy density and cycle life are critical to the realization of electric vehicles.

## Technical Targets

- Energy Density: 200 Wh/kg
- Cycle Life: 1000 full discharge cycles

## Accomplishments

- High speed shearing and long mixing times lead to electrodes with more uniform carbon distribution and higher electronic conductivities.
- When mixing components, there is a peak in the viscosity of the slurry.
- The viscosity after peaking the viscosity drops to a steady level at *ca*. 80 minutes of mixing.
- A new FRION from Scherson's Group shows a drop in reversible capacity but no negative impact on cyclability.

✧ ✧ ✧ ✧ ✧

## Introduction

The BATT Program positions itself as a fundamental research program focused on applied problems. As such, 50% of the program is dedicated to finding new materials. The talented investigators that make up this portion of the program train their efforts on materials synthesis and pay less attention to the application. A good material does not a good electrode make. Our responsibility in the program is to develop the ability to make good electrodes with a limited amount of material. For this reason, electrode preparation procedures are constantly being investigated in order to gain greater insight into the steps used to fabricate a good electrode and cell.

This year the group is focused on mixing. Specifically, investigating the time and speed of mixing to help us understand what mixing step is most critical and what is not so critical and to determine whether there is an optimum condition for mixing that may be overshot as a result of over mixing.

The group is also responsible for providing facilities for other LBNL investigators to make electrodes and cells, to provide baseline laminates to investigators with expertise in diagnostics, to support Focus Groups with baseline performance data, and to provide a venue for other BATT PIs to send materials for testing in well made electrode and cells. This report discusses some of those efforts.

## Approach

All BATT PIs are made aware of the facilities here at LBNL for providing laminates and testing of materials. Once a year, a call is issued to investigators who are either half-way through their funding or just about finished their funding to send us materials for evaluation. Once materials arrive, they go through a series of physical characterization tests, including BET measurement, particle size analysis, and SEM. This data is used by the electrode fabrication team to decide how much conductive additive and binder is needed in the electrode. The Group has been successful at making quality electrodes of cathode materials with a secondary particle size greater than 1 micron. The present effort is focused on optimizing some of the levers available for making electrodes such that the electrodes are as good as possible and that any deterioration that one may see during testing can be attributed to the material being tested and not the electrode formulation.

## Results

**Priority of mixing steps.** Mixing of materials is a critical step in the making of a quality electrode. The fractional composition and order of mixing of the components that make up an electrode was investigated. Part of this year's effort is the investigation of mixing time. In making an electrode, the active material and conductive carbon are interspersed in N-methylpyrrolidone (NMP) with a high speed mixer. Once combined, the binder is added and the components are sheared together for a second mixing time. The initial research of this process involves the investigation of the length of the first mixing time, the shear rate during the first mixing time, and the length of the second mixing time. The table below was followed in the development of nine laminates.

**Table VI - 7: Mixing Conditions**

| 1st mixing(NMC 94%wt+AB 2%wt)(min) | Speed I (krpm) | 2nd mixing (PVDF 4%) (min) |
|---|---|---|
| 4 | 2.5 | 10 |
| 30 | 2.5 | 10 |
| 30 | 10 | 10 |
| 4 | 10 | 10 |
| 4 | 2.5 | 120 |
| 30 | 2.5 | 120 |
| 30 | 10 | 120 |
| 4 | 10 | 120 |
| 17 | 5.5 | 65 |

The results of conductivity measurements of cast laminates are provided in the Table VI - 8. The numbers in the first column correspond with the order of experiments listed in Table VI - 7.

These results indicate that the longest total mixing time combined with the highest shear rate results in a laminate with the highest conductivity. The data also indicate that the length of time of the second mixing step is the most important of the three parameters.

**Table VI - 8: Electronic conductivity of laminates prepared by mixing conditions (in Table VI - 7)**

| Laminate | Average conductivity (S $cm^{-1}$) |
|---|---|
| 1 | 0.0107 |
| 2 | 0.0120 |
| 3 | 0.0154 |
| 4 | 0.0170 |
| 5 | 0.0209 |
| 6 | 0.0224 |
| 7 | 0.0310 |
| 8 | 0.0234 |
| 9 | 0.0185 |

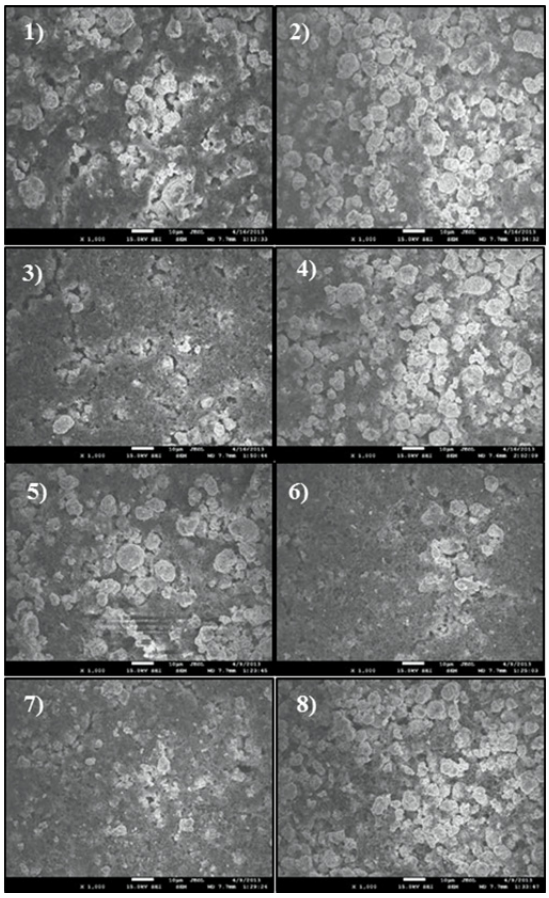


**Figure VI - 178: SEMs provided in order of first 8 mixing conditions as listed in the tables above**

The SEMs of the laminates that resulted from the first eight mixing conditions are provided in Figure VI - 178.

Careful inspection of these SEMs reveals that the laminate with the highest conductivity, #7, is also the laminate with the most uniform distribution of carbon black.

**Viscosity*versus* mixing time.** An investigation of mixing time on slurry properties was also conducted. The objective of this study was to understand the effects of the mixing process on cell performance, where performance includes reversible capacity, rate capability, and long-term cyclability. Thus, a more refined analysis was undertaken to investigate the effect of the second mixing step on slurry properties, specifically, viscosity.

A more in-depth analysis of the second mixing step was conducted. In this experiment, NCM (Micro MX6) and carbon black (Super P) were combined at a ratio of 94:2 in NMP at a ratio of 5:4 solids to liquids. The materials were mixed with a homogenizer at 10,000 rpm for twenty minutes. This was followed by the addition of PVDF 1100 at twice the concentration as that of the carbon additive for nearly two hours with the same homogenizer at 2500 rpm. The viscosity was measured every 10 minutes at different shear rates. The results are presented in Figure VI - 179. As expected, the slurry is shear thinning, thus, at higher shear rates, the proportionality constant between shear rate and shear force, i.e., the viscosity, is lower. It is also evident from the figure that there is a maximum in the viscosity at around 50 minutes into the mixing. It is believed that the first 50 minutes is a reflection of the macro mixing of the solids mix with the polymer. Once the two materials are uniformly distributed in the jar, the mixture of solids, and in particular, the high-surface area carbon additive which begins highly agglomerated starts to breakdown and the solution shows a lower viscosity. After 80 minutes, the viscosity of the solution begins to level off with time.

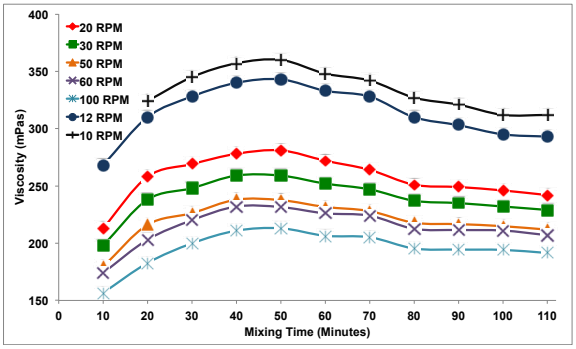


**Figure VI - 179: Viscosity *versus* mixing time at different shear rates**

**Testing BATT materials**. Two LNMO materials were received from Prof. Manthiram. These materials were based on findings in half-cells by the High-voltage Focus Group. However, as shown in previous reports, the biggest problems identified for this class of materials is the high first-cycle-irreversible-capacity loss in a full cell, additional capacity loss as a result of impedance rise in the cell, and rapid capacity fade at 55°C. These problems are believed to be a result of interactions with the graphite anode, which were not considered by the Focus Group. As might be expected, the materials from Manthiram did not improve upon these limitations in cells cycled against graphite.

Prof. Scherson sent a second FRION for testing. The results of full-cell testing are provided in the Figure VI - 180. In Figure VI - 180a, the cycling of a Graphite/NCM cell with baseline electrolyte 1M $LiPF_6$ in EC:DEC 1:2, and in Figure VI - 180b is the same chemistry plus 1 wt% FRION. These graphs demonstrate that the cyclability of the cell is not adversely affected by the presence of the salt and actually shows less capacity fade than the cell without the FRION. Rate performance, not shown, was not affected to a C-rate of 1C. However, there are some differences between the two cells. For one, the first cycle loss is worse for the cell with the FRION; second, the cell with the FRION shows less coulombic efficiency. In fact, the coulombic inefficiency is 15 times worse with the FRION than without it, yet shows better cyclability. At this stage it is not evident that this coulombic inefficiency will lead to a faster loss of electrolyte and therefore fewer overall cycles before catastrophic cell failure. If the FRION does not adversely affect long-term cycle life, it is possible that addition of more FRION may lead to a protective shuttle.

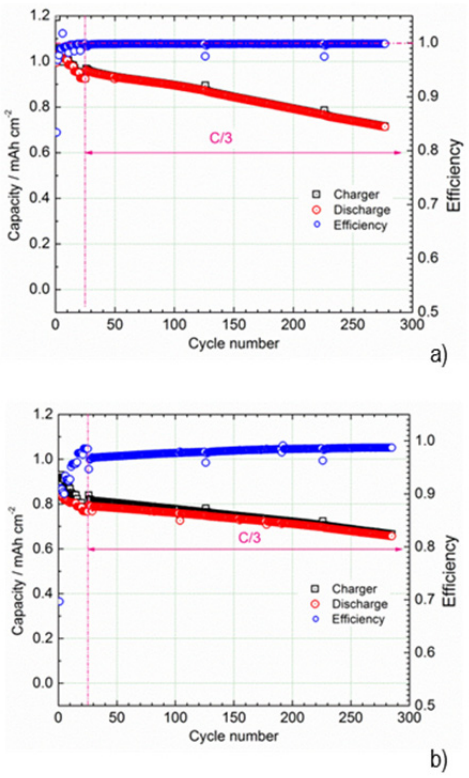


**Figure VI - 180: Cycling and coulombic efficiency data for a Graphite/NCM cell, a), without FRION and b), with FRION**

## Conclusions and Future Directions

The degree of mixing clearly has an effect on the dispersion of the materials and the conductivity of the laminates, however, the effect on cycle life and all the other factors that dictate electrode performance is not clear. Cells need to be prepared from these laminates and tested for rate capability, adhesion to the current collector, and cyclability. This work will occur in 2014.

As the SEM images only the surface of an electrode, cross sections of electrodes will be made to determine if the distribution is the same through the electrode as it is across the electrode surface. Results will be reported in the next fiscal year.

From the viscosity measurements it appears that the mixing is nearly complete after 80 minutes. In the next stage of this experiment, electrodes and cells will be fabricated from the 80$^{th}$ minute and the two hour limit to determine if the time after 80 minutes shows any performance improvements. Also, extended mixing will be performed to see how long this constant viscosity interval lasts. There is a presumption in the electrode fabrication community that a slurry can be over mixed. The goal is to try to reach such a point and to understand what occurs in the slurry beyond this point.

The latest FRION from Scherson was tested. Unlike the first material sent, this did not require the addition of vinyl carbonate. Since testing of the first FRION, ANL has scaled it up and just sent us some material to re-test. Hopefully some of this material will make its way to SNL and they will be able to put it into 18650s to see if the FRION improves the response to abuse.

## FY 2013 Publications/Presentations

1. "Scale-up and Testing of Advanced Materials from the BATT Program," *DOE Annual Peer Review Meeting*, May 13-17, 2013, Washington, DC.

# VI.E.6 Cell Failure: Electrochemical Diagnostics (LBNL)

**Vincent Battaglia**
Lawrence Berkeley National Laboratory

Environmental Energy Technologies Division
1 Cyclotron Road
Berkeley, CA 94960
Phone: (510) 486-7172; Fax: (510) 486-4260
E-mail: vsbattaglia@lbl.gov

Start Date: October 2012
Projected End Date: September 2016

## Objectives

- Develop tools to assess performance limitations
- Develop a means of measuring the gas composition in a Li-ion cell
- Interpret 3-electrode impedance data.
- Assess failure of cells and electrodes

## Technical Barriers

Energy density and cycle life are critical to the realization of electric vehicles.

## Technical Targets

- Energy Density: 200 Wh/kg
- Cycle Life: 1,000 full discharge cycles

## Accomplishments

- Established the abilty to sample gas from a coin cell.
- Able to interpret impedance data of an electrode *versus* a reference electrode in a 3-electrode coin cell.
- Benchmark a $LiFePO_4$ electrode.
- Estalish that the electrode suffers from a side reaction and impedance rise.

✧ ✧ ✧ ✧ ✧

## Introduction

The BATT Program consists of six major groupings: Cathode, Anode, Electrolyte, Diagnostics, Modeling, and Electrode Architecture. This project falls under the last category. The goal of this project is to test materials developed under the cathode, anode, and electrolyte projects. To perform this task appropriately, requires the ability to fabricate quality electrodes of active materials and to build quality cells. These capabilities have been developed over the past years. With this established, the next step is to develop better tools to assess performance. This year the ability to assess the gas formed in a coin cell was developed and the understanding of 3-electrode impedance data was acquired.

This group also contributes to Focus Groups when it can. This year the BATT Program is focused on understanding the issues that limit the use of Si-based materials as the anode in high energy cells. Several investigators have started to report coulombic efficiencies of Si greater than 99% in half-cells. Our group will investigate the performance of Si in a full cell. $LiFePO_4$ was selected as the cathode against which a Si-baseline electrode will be tested. The immediate focus is the development of this nanomaterial based cathode.

✧ ✧ ✧ ✧ ✧

## Approach

The approach is to identify the most likely problem facing a technology of interest and then develop a tool that will bring greater insight and isolate that problem. Last year the main technology of interest was the high-voltage $LiNi_{1/2}Mn_{3/2}O_4$ material. Electrochemical evaluation suggested that a gas was formed in the cell that delayed the first charge *via* a shuttle. It was also clear that there was quite a bit of capacity fade in the cell as a result of side reactions and impedance rise. What was not known was the quantity or composition of the gas and the electrode where most of the impedance rise was occurring. For this reason, the focus was on developing the capability of analyzing gas in a coin cell and analyzing impedance data in a three electrode coin cell.

It is well known that many of the transition metal based oxide cathodes considered for Li-ion batteries lose metal into the electrolyte during operation and the metal then interferes with the performance of the anode. In testing Si in a full cell, the goal is to avoid issues unrelated to the Si itself. For this reason, the iron phosphate material was chosen for the cathode.

## Results

**An apparatus was designed to sample gas from a coin cell.** Modifications were made to an apparatus designed to sample gas from a coin cell, specifically, hardware was selected with minimal void volume. A half-cell of high-voltage Ni-spinel and Li metal was assembled. The cell was connected to the mass spec through a thin tube and a valve that entered the cell behind the cathode.

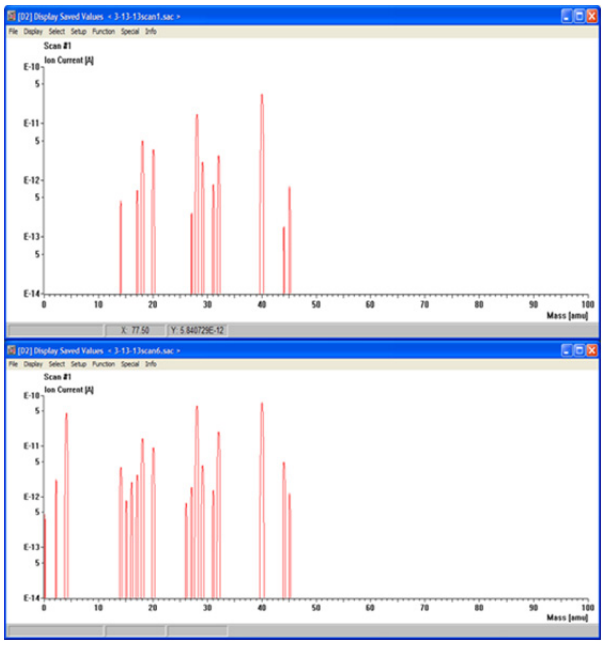


**Figure VI - 181: Mass spectrograph of the vapor in a coin cell 2 hours into a 10 hour charge (top) and 4 hours into the first charge (bottom). The spikes to the far left on the bottom graph suggest the pressure of hydrogen**

The cell was charged at a 10-hour rate and after 2 hours of testing the valve was opened briefly and the mass spec pulled a small vacuum on the cell. Only a background gas was detected which was indicative of the vapor pressure of the carbonate electrolyte. Two hours later the valve was opened for a second time and this time hydrogen was detected, as indicated by the differences in the graphs shown in Figure VI - 181. This was somewhat unexpected and still needs to be confirmed.

**Three electrode cell.** A visiting researcher in Srinivasan's Group used Comsol to see if he could duplicate the "inductance" loops seen experimentally by researchers that use three-electrode cells. To be clear, instead of the 2-D geometry in cylindrical coordinates, he solved the 2-D problem in Cartesian coordinates. However, we are certain that the results cross over these two geometries. He solved Laplace's equation for the potential distribution with linear kinetics as boundary conditions and ignored mass transfer effects (secondary current distribution). In so doing, he could reproduce the inductance loops. The impedance data for a full cell looks like what most others find when they perform ac-impedance on 2-electrode cells. In addition, one can show that the impedance data from one electrode *versus* the reference can be added to the data of the other electrode *versus* the reference electrode to give the 2-electrode cell data. However, the 3-electrode cell data typically contains "inductance" loops. It appears that the source of the loops in the individual cell data comes from geometries where the reference electrode is placed close to a region where the anode and cathode are not perfectly aligned. Simulations of different electrode alignments and reference electrode placements indicates that anything short of perfectly aligned electrodes leads to loops in one set of the reference electrode data. However, the simulations suggest that one should still be able to use the reference electrode impedance data to distinguish the contributions from the anode and the cathode in the 2-electrode cell data. In the figure below is an example of two electrode data, upper left; three electrode data of ref/cathode and ref./anode, middle right; and the sum of the ref/anode and ref./cathode, on the lower left. [In this example, the reference electrode is under the cathode and a small hole has been punched through the cathode.] One can see that the two electrode data is indistinguishable from the sum of the data from each electrode *versus* the reference. According to the modeling, impedance associated with the cathode is being captured by the impedance data measured on the ref./anode couple.

This would clearly lead to a false interpretation of what is happening in the cell.

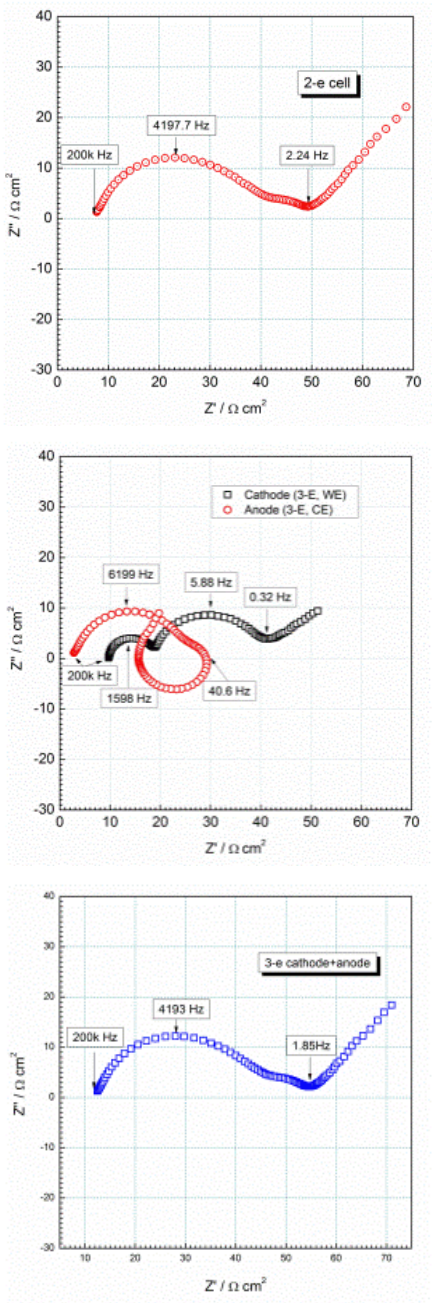


**Figure VI - 182. Upper, Nyquist plot of two-electrode impedance; middle, Nyquist plot of each electrode versus a Li ref. electrode; lower, sum of the reference electrode data**

**Cathode for Si Focus Group.** As part of the BATT Program, this group contributes to Focus Groups, in particular this group will investigate the performance of a Si-based anode in a full cell. The Liu Group will supply the Si anode, our group will develop the cathode. Since many of the oxide cathodes are known to lose transition metals during cell cycling, this group decided to use $LiFePO_4$ for the cathode. This material is considered to perform well with regard to cycling, although our group has little experience in making a cycleable electrode from this material. An SEM of the material is provided in Figure VI - 183. The sample is a distribution of particles from 100 nm to 700 nm. 7.5 wt% PVDF and an equal amount of Super-P. Li was added to the active material and mixed in NMP. Half-cells of the electrodes were tested at different discharge

rates and for cyclability. The results of the cyclability are provided in Figure VI - 184.

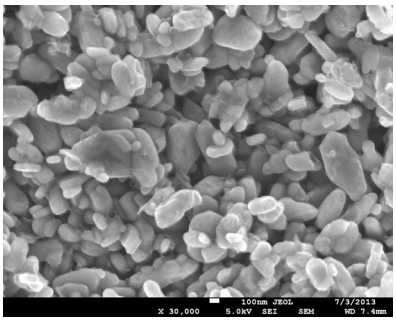

Figure VI - 183: SEM of LFP powder

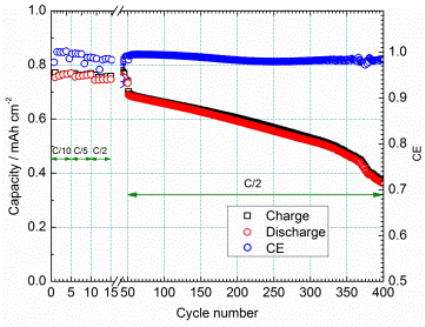


Figure VI - 184: Capacity versus cycle number for an LFP electrode

The cycling results are not acceptable at this point. A more in-depth analysis shows that there is a side reaction and an impedance rise with cycling. There are several possible reasons for the sub-optimum performance. First, this is our initial experience with this material and our typical electrode formulation was applied.

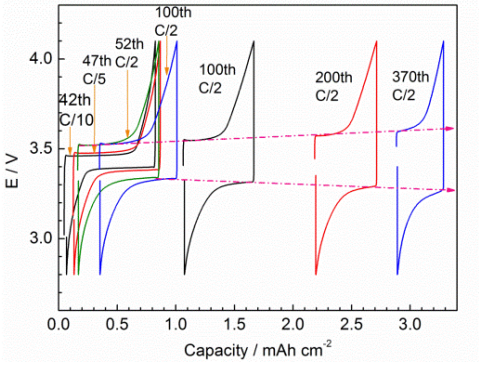


Figure VI - 185: Voltage versus capacity plotted sequentially. Certain cycles are displayed to high light motion due to side reactions and impedance rise in the cell with time

## Conclusions and Future Directions

Although the electrochemical data suggested that gas in a Li/NMO cell was responsible for a delay in charging the cell, it was difficult to measure it in a coin cell. For this reason, pouch cells with this chemistry will be fabricated in an attempt to measure the quantity of gas produced. The gas collection apparatus will also be modified such that a pouch cell can be sampled instead of just coin cells. This work will be expanded to a full cell of graphite and Ni-spinel and to a pouch cell. If the result turns out to be significant, the chemistry responsible for the gas will be sought.

With regard to the impedance data, it appears one can *a priori* determine which contribution of impedance is due to which electrode. In the next year, the experiment will be repeated but with several electrode geometries to demonstrate that the impedance data for each electrode can be unequivocally identified and the rate of growth appropriately measured.

With regard to the LFP electrode, since this is a sub-micron material, it is possible that the standard formulation does not contain enough carbon conductive additive to ensure particle-to-particle connectivity from cycle to cycle. It is also possible, given the large number of particles per gram for this material, that the time of mixing as recommended in the standard formulation protocol is not long enough to lead to complete dispersion of the materials. Also, the cells with these electrodes were cycled between 2.8 and 4.1 V. Shifting the cycling regime to 2.1 to 3.8 V may reduce the side reactions. Together with Hydro-Quebec, the hope is to get to low capacity loss electrodes early in the next fiscal year.

## FY 2013 Publications/Presentations

1. "Scale-up and Testing of Advanced Materials from the BATT Program," *DOE Annual Peer Review Meeting*, May 13-17, 2013, Washington, DC.

# VI.E.7 First Principles Calculations of Existing and Novel Electrode Materials (MIT)

**Gerbrand Ceder**
Massachusetts Institute of Technology

Department of Materials Science and Engineering
77 Massachusetts Avenue
Cambridge, MA 02139
Phone: (617) 253-1581
E-mail: gceder@mit.edu

Start Date: May 2013
Projected End Date: Dec 2016

## Objectives

- Develop more stable high capacity Li-excess layered cathodes.
  - Identify the structure of layered cathodes that leads to high capacity.
  - Clarify the role of the initial structure as well as structural changes upon first charge and discharge.
- Give insight into the factors that control the capacity and rate of Na-intercalation electrodes, and make suggestions for novel Na-intercalation cathode materials.
- Generate insight into the behavior of alkali-intercalating electrode materials.

## Technical Barriers

- Low rate capabilities
- High cost
- Poor stability
- Low energy-density

## Accomplishments

- Investigated the relation between voltage and thermal stability of materials.
- Indicated that most poly-anion cathodes are unlikely to be competitive with layered oxides
- Identified diffusion mechanism of Na in P2 layered oxides.
- Obtained high capacity $LiMn(BO_3)$

✧ ✧ ✧ ✧ ✧

## Introduction

Improving cathode performance is an important component towards higher energy density batteries. Currently, the BATT Program has multiple new cathode materials under investigation, including several high voltage materials, as well as the high capacity layered materials. First principles modeling can provide insight into how these materials function and what their limitations are. There are now many cathode properties which can be modeled fairly accurately using first principles methods. This includes voltage, ion mobility, electron mobility, cation ordering and phase diagrams, and aspects of thermal stability. In addition to using these methods on individual materials, some of these computational techniques can also be scaled to scan through hundreds of materials.

This BATT Program project is a systematic approach towards higher energy density. To achieve high energy density one needs either high voltage or high capacity. High *voltage* tends to correlate with strong oxidation strength of the charged cathode, and hence degradation and lack of safety. As part of this BATT project, the relation between voltage and safety of the cathode material is being investigated. This is done through the computational screening of hundreds of compounds in order to obtain good statistics on this relation. Specific focus is on the oxidation chemical potential and decomposition reaction pathways of some high voltage materials that are being studied in this BATT project: $LiCoPO_4$, $Li_2MnP_2O_7$, $Li_2FeP_2O_7$, and $Li(Ni_{0.5}Mn_{1.5})O_4$.

To achieve large specific and volumetric *capacity* requires a large amount of Li to be cycled in and out of a compact and light crystal structure. The relation between theoretical and practical capacity and chemistry is being investigated in this program. Previous findings under the BATT Program indicate that there are very few useful two-electron couples in polyanion systems, as many redox couples are moved to very high voltage due to the inductive effect of the polyanion, which is why this program is focused on understanding better the high-capacity layered oxides (Li-excess materials) (together with Persson and others in the BATT Program).

In addition, a limited exploration of layered Na-intercalation materials is performed to understand better if high energy density Na-intercalation battery systems are possible.

## Approach

First principles computations are being used to evaluate existing and novel materials. Voltages and intercalation curves are calculated with GGA+U, and if highly accurate results are required HSE methods are used. Phase diagrams are calculated with the Materials Project infrastructure. Configurational disorder for elevated temperature and off-stoichiometry is modeled with either point defect models (when off-stoichiometry is small) or with the cluster expansion for larger disorder. Ion mobility is evaluated with the Nudged Elastic Band Method or with direct Molecular Dynamics Simulations. Thermal stability is investigated with the approach developed previously under this program. Some of the computational work is performed in collaboration with Persson and with the Materials Project. Work on Li-excess layered materials is done in coordination with Persson (computational) and with the experimental efforts in the BATT Program (e.g., Thackeray, Grey).

## Results

**General Analysis:** Figure VI - 186 shows the best specific capacity that can be obtained with a single electron reaction for a 3d transition metal and a specific anion chemistry. The results indicate that most polyanion chemistries are not competitive with today's layered oxides. Only borates, fluorides, and oxy-fluorides can achieve competitive specific capacities.

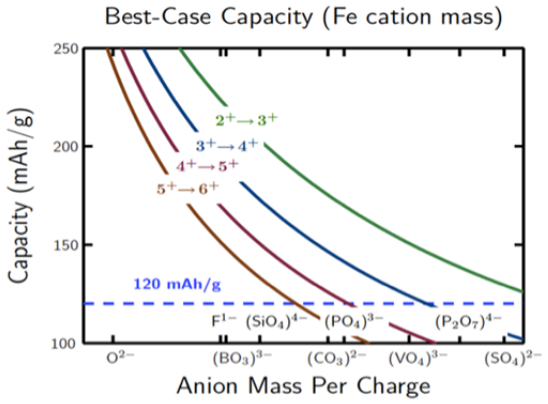


**Figure VI - 186: Best case capacity for single electron redox couples for each anion chemistry**

**Borates.** As borates are the only polyanion systems that combine good safety with competitive specific capacity, the $LiMnBO_3$ system was investigated extensively. Previous work indicated potential transport limitations. For this reason, the particle size dependence of the Li transport in this system was investigated. The monoclinic $LiMnBO_3$ is another example of a one-dimensional Li-ion conductor. In such a case, Li transport can be impeded by antisite defects which block the migration path (Mn in Li sites). In addition, assuming homogeneous distribution of the defects, this clogging of the channel becomes more serious in large particles than in small ones since Li will have a higher probability to encounter the defect as the particle becomes larger.

The experimentally achieved capacity (100 mAh/g) of $LiMnBO_3$ so far has been limited to 50% of its theoretical value (222 mAh/g). Considering both Mn and Li sites are trigonal-bipyramidal with similar ionic radii in $LiMnBO_3$, a fair amount of antisites are expected. Indeed, a refined XRD pattern of the as-synthesized $LiMnBO_3$ revealed that more than 4% Mn occupy the Li sites (Figure VI - 187). After firing at 500°C, the average particle size of $LiMnBO_3$ was 100 nm with a wide distribution ranging from 20 to 230 nm.

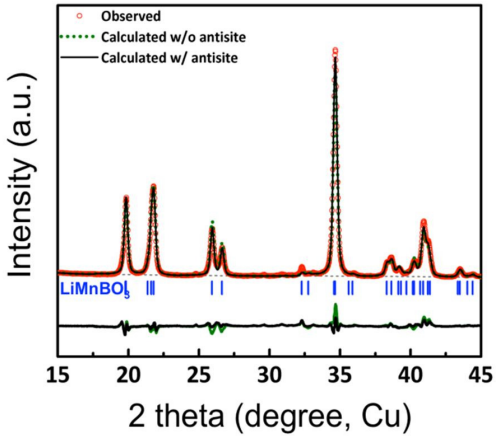


**Figure VI - 187: Profile matching of XRD pattern of monoclinic $LiMnBO_3$ with and without considering antisite defects in the unit cell**

Small particles (less than 50 nm) are not likely to be affected by the channel blockage, but its portion to the overall volume is insignificant. On the other hand, particles larger than 150 nm may not contribute to the Li intercalation reaction at all because almost all of the diffusion channels will be effectively shut off by the antisite defects. In the particles with intermediate sizes, Li migration can occur even if the migration path is blocked since there is a chance for Li to detour the blockage via neighboring channels. Although possible, however, this rate is estimated to be very low. All in all, the limited capacity of monoclinic $LiMnBO_3$ results from the size dependency of Li transport rooted in the channel blockage in large particles due to the antisite defects.

Work is continuing to gauge the actual diffusivity values of $LiMnBO_3$ by using standard diffusion analysis (Figure VI - 188).

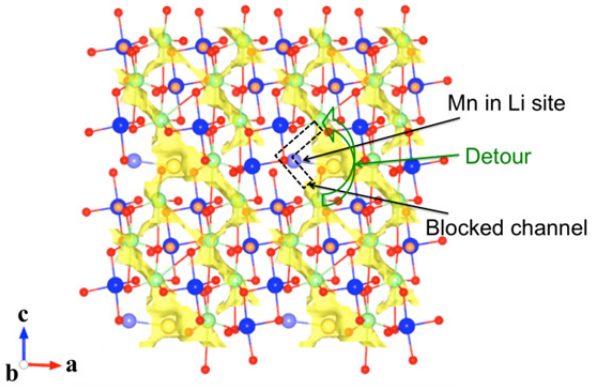


**Figure VI - 188: Li trajectory as calculated by ab initio computation**

**Li-excess layered oxides.** This is a newly initiated program. Progress is currently mainly on the algorithm side, with limited technical results to report. Algorithms have been constructed to enumerate possible atomic arrangements for layered and spinel structures in the Li-Co-Mn-O system. These structures will be queued up and computed in order to give us information on the phase diagram of this system. Once a reliable set of ground states is obtained, the phase diagram construction will be initiated.

Work on the Li transport in Li-excess materials has been initiated to understand the effect of Li-excess on Li diffusion. Exciting initial results have been obtained and will be further refined in the coming year.

**Na layered oxides.** Work on Na-ion intercalating layered oxides has begun with aims to design high energy density Na-ion battery cathodes and understand the effects of structure (P2 or O3) on their functional properties. First principles work has included the calculation of voltage curves for both structure types and the determination of the Na-ion diffusion mechanisms for the O3 and P2 versions of these structures. *Ab initio* molecular dynamics work has been initiated to calculate the diffusion mechanisms in both the O3 and P2 type structures to examine how they differ (Figure VI - 189).

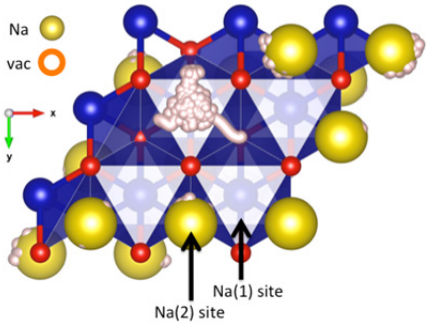


**Figure VI - 189: Sodium trajectory as calculated by AIMD simulation**

These calculations have so far determined that the di-vacancy diffusion mechanism present in O3 type structures is absent in P2 type structures. Work is continuing on how these contribute to Na-ion mobility and diffusion rates.

## Conclusions and Future Directions

An initial conclusion is that very few poly-anion compounds can be competitive with layered oxides in terms of specific capacity. Only borates can combine reasonable theoretical capacities with high voltage and good safety.

As this new program was only started a few months ago, there are no clear conclusions on the Li-excess layered materials and Na-intercalation compounds.

Future work will focus on the phase diagram of Li-excess materials, diffusion of transition metals and lithium in these materials, and the role of the overcharge. In Na materials, the focus will be on the role of crystal structure on Na diffusion.

## FY 2013 Publications/Presentations

1. H. Chen, Q. Hao, O. Zivkovic, G. Hautier, L-S Du, Y. Tang, Y-Y Hu, X. Ma, C.P. Grey, G. Ceder, "Sidorenkite ($Na_3MnPO_4CO_3$): A New Intercalation Cathode Material for Na-Ion Batteries," *Chem. Mater.*, **25**(14), 2777-2786 (2013).
2. G. Hautier, A. Jain, T. Mueller, C. Moore, S.P. Ong, G. Ceder, "Designing Multielectron Lithium-Ion Phosphate Cathodes by Mixing Transition Metals," *Chemistry of Materials*, **25**(10), 2064-2074 (2013).
3. S.P. Ong, Y. Mo, W. D. Richards, L. Miara, H.S. Lee, G. Ceder, "Phase Stability, Electrochemical Stability and Ionic Conductivity of the Li10 +/-1MP2X12 (M = Ge, Si, Sn, Al or P, and X = O, S or Se) Family of Superionic Conductors," *Energy & Environmental Science,* (**6**), 1, 148-156 (2013).
4. H. Chen, G. Hautier, G. Ceder, "Synthesis, Computed Stability, and Crystal Structure of a New Family of Inorganic Compounds: Carbonophosphates," *Journal of the American Chemical Society*, **134**(48), 19619–19627 (2012).

# VI.E.8 Design and Scalable Assembly of High Density Low Tortuosity Electrodes (MIT)

**Yet-Ming Chiang**
Massachusetts Institute of Technology

Department of Materials Science and Engineering
77 Massachusetts Avenue
Cambridge, MA 02139
Phone: (617)-253-6471, Fax: (617)-253-6201
E-mail: ychiang@mit.edu

**Antoni P. Tomsia, Collaborator**
Lawrence Berkeley National Laboratory
Materials Science Division
1 Cyclotron Road
Berkeley, CA 94720
Phone: (510) 486-4918; Fax: (510) 486-4761
E-mail: APTomsia@lbl.gov

Start Date: October 2012
Projected End Date: September 2016

## Objectives

- Develop scalable high density binder-free low-tortuosity electrode designs and fabrication processes to enable increased cell-level energy density compared to conventional Li-ion technology.
- Characterize electronic and ionic transport as a function of state-of-charge (SOC) in relevant systems including Li(Ni,Co,Al)$O_2$ (NCA), $Li_2MnO_3$-Li$MO_2$ and high-voltage spinels $LiM_xMn_{2-x}O_4$ and iron doped $LiMn_{1.5}Ni_{0.5-x}Fe_xO_4$.

## Technical Barriers

Achieving sufficient electronic conductivity, avoiding mechanical failure upon cycling, meeting automotive duty cycles, lowering cost.

## Technical Targets

- Identify high energy density cathode compositions with electronic transference number >0.5 across the SOC range for use in directional freeze-casting processing.
- Fabricate conductive additive free sintered cathodes with controlled pore volume fraction and topology yielding tortuosity values less than 2.
- Increase cell-level specific energy and energy density, and lower inactive materials cost, by achieving area capacity of 10 mAh/cm$^2$ at C-rates or current densities commensurate with operating conditions for PHEV and EV.

## Accomplishments

- Measured electronic and ionic conductivity and diffusivity of NCA as a function of temperature and lithium content.
- Measured electronic conductivity of sintered Fe-doped $LiMn_{1.5}Ni_{0.5-x}Fe_xO_4$ (x = 0.00, 0.08, 0.10, 0.50) as a function of lithium content *x*.
- Fabricated NCA cathodes by directional freeze casting and sintering.

✧ ✧ ✧ ✧ ✧

## Introduction

This project aims to develop alternative electrode architectures and scalable fabrication methods that result in thick, high density electrodes with low tortuosity porosity oriented normal to the electrode plane, using electrode actives of interest for future EV battery systems. Previously, it was shown that sintered $LiCoO_2$ cathodes with aligned, low tortuosity porosity fabricated by co-extrusion or directional freeze-casting could reach area capacities of 7.5-9.5 mAh/cm$^2$ at 1C rate and 6.5-7.5 mAh/cm$^2$ at 2C rate (Figure VI - 190). Here, a key technical performance target is to achieve at least triple the capacity per unit area at 1C-2C rate (e.g., >10 mAh/cm$^2$) that the same active materials can deliver in a conventional calendared electrode, and in cathodes of interest for next-generation lithium ion batteries. The electrode density and thickness at which the discharge energy and discharge power are optimized for PHEV and EV applications critically depends on the pore topology of the sintered electrodes. Data on capacity per unit area and tortuosity of conventional calendared electrodes is available from literature and prior work under BATT. The baseline approach for the current project is pressureless sintering of cathode compounds. The open porosity of sintered electrodes allows for electrolyte infusion and ion transport with a low tortuosity compared to that in conventional calendared electrode technology. However, in order to maximize the density and thickness of electrodes at which the desired utilization can be achieved, it is desirable to

introduce lower tortuosity porosity into the dense sintered electrodes.

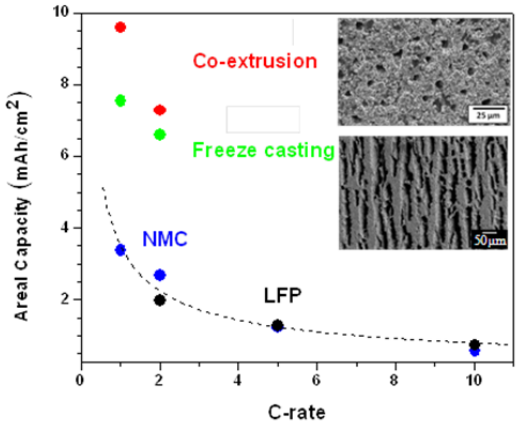


**Figure VI - 190: Area capacity vs C-rate of sintered $LiCoO_2$ with oriented mesocale porosity prepared by two methods, compared to conventional calendared Li-ion electrodes (H. Zheng, J. Li, X. Song, G. Liu, V.S. Battaglia, *Electrochimica Acta* 2012, *71*, 258)**

## Approach

Since the current program began in May 2013, efforts have been, firstly, focused towards identifying cathode compositions with sufficiently high electronic conductivity that conductive additives need not be incorporated. Secondly, the bulk lithium transport of candidate cathodes has been characterized in order to define the microstructural scale that is necessary to achieve the target performance without solid-state transport being rate-limiting. Thirdly, NCA electrodes have been fabricated by directional freeze-casting and sintering, and electrochemical characterization to identify rate-limiting mechanisms has been conducted.

## Results

**Electronic and ionic conductivity and diffusivity of $Li_{1-x}Ni_{0.8}Co_{0.15}Al_{0.05}O_2$.** Despite its widespread use in current Li-ion technology, there is a paucity of transport data for NCA. Here, electronic conductivity was measured in sintered dense $Li_{1-x}Ni_{0.8}Co_{0.15}Al_{0.05}O_2$ (NCA) plate as a function of temperatures and lithium content. Measurements were performed on additive-free, sintered NCA, and therefore reflect pure phase conductivity. Samples were fired at 850°C for 12h and cooled at 5°/min, resulting in samples of 96% sintered density. Electrochemical delithiation was conducted to obtain a range of $x$ values. Ag paste electrodes were used as ion-blocking electrodes for the measurement of electronic conductivity (Ag/NCA/Ag). DC polarization technique as well as AC impedance measurement was performed to obtain the electronic conductivity. Representative results are shown Figure VI - 191. The electronic conductivity of the fully lithiated phase increases monotonically with increasing $x$, with a sudden enhancement of conductivity occurring at 60% delithiation. NCA is semiconducting over the range of lithium concentrations measured. The values of activation energy calculated using the Arrhenius law varies from 0.22 eV to 0.14 eV as shown in Figure VI - 191a, similar to literature values for $Li_xNi_{0.8}Co_{0.2}O_2$ and typical for the small polaron migration process generally observed in mixed-valence systems. The electronic configuration for $Ni^{3+}$, $Co^{3+}$ and $Ni^{4+}$ has the ($t_2$) orbitals filled, with electron delocalization being less probable. The increase in electronic conductivity with delithiation is attributed to hole formation in the narrow ($Ni^{4+}/Ni^{3+}$) band. The sudden increase in conductivity at ~60% delithiation (Figure VI - 191b) may be due to the onset of $Co^{3+}$ oxidization.

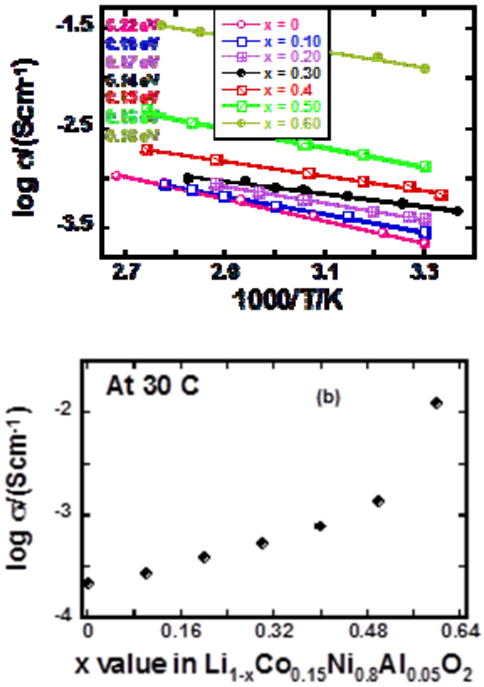


**Figure VI - 191: (a) Electronic conductivity of NCA as a function of temperature and (b) lithium content**

To measure ionic conductivity, ion conducting/electron blocking electrodes of polyethylene oxide (PEO) with 1% lithium iodide salt were used in the configuration: Li/PEO/NCA/PEO/Li. The DC polarization technique as well as AC impedance measurements were performed to obtain the ionic conductivity and diffusivity (Figure VI - 192), with good agreement between the two methods. Activation

energies are almost the same for ionic conductivity (1.15 eV) and diffusivity (1.20 eV) (within±0.20 *eV* error) as shown in Figure VI - 192b. Despite the extensive commercial use of NCA and its long research history, this is, to our knowledge, the first report of such data.

The lithium ion diffusivity as a function of lithium concentration *x* was also measured using GITT and depolarization techniques. The diffusivity was found to vary strongly with x, being nearly $10^2$ lower for x<0.5 than for *x*>0.5. While the lithium concentration dependence is complex, the absolute value of diffusivity is high enough that it can be concluded that for micron-scale particles and at practical C-rates, solid-state transport in NCA is not rate-limiting in lithium ion cells.

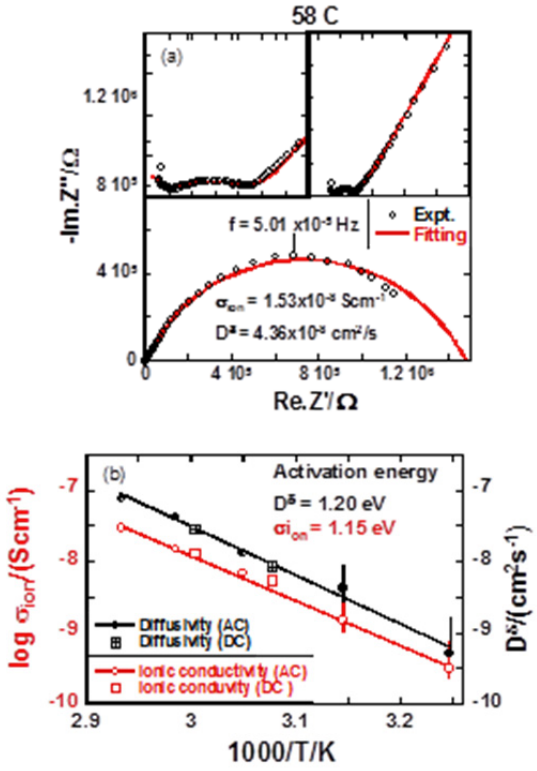


**Figure VI - 192: (a) AC impedance spectra obtained from electron-blocking cell at 58°C and fitted with equivalent circuit, (b) lithium ionic conductivity and diffusivity as a function of temperature**

**Electronic conductivity of $LiMn_{1.5}Ni_{0.5-x}Fe_xO_4$.** $LiMn_{1.5}Ni_{0.5-x}Fe_xO_4$ (x = 0.00, 0.08, 0.10, 0.50) powder was synthesized by solid state reaction, producing an octahedral crystallite morphology (Figure VI - 193), and sintered for electronic conductivity measurements. The ordered phase was obtained by heating the pellet at 950°C for 24h followed by annealing at 650°C for 48h and cooling to room temperature (1°C/min). The disordered phase was obtained by heating the pellet at 950°C for 24h and cooling to room temperature at 10°C/min.

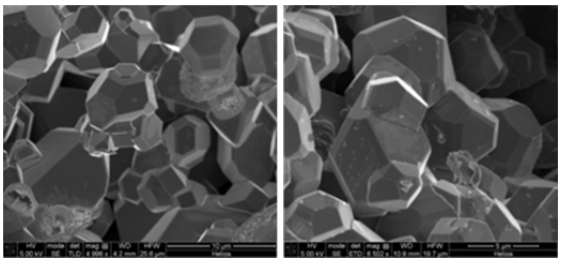

**Figure VI - 193: Microstructure of ordered (a) $LiMn_{1.5}Ni_{0.5}O_4$, (b) $LiMn_{1.5}Ni_{0.42}Fe_{0.08}O_4$**

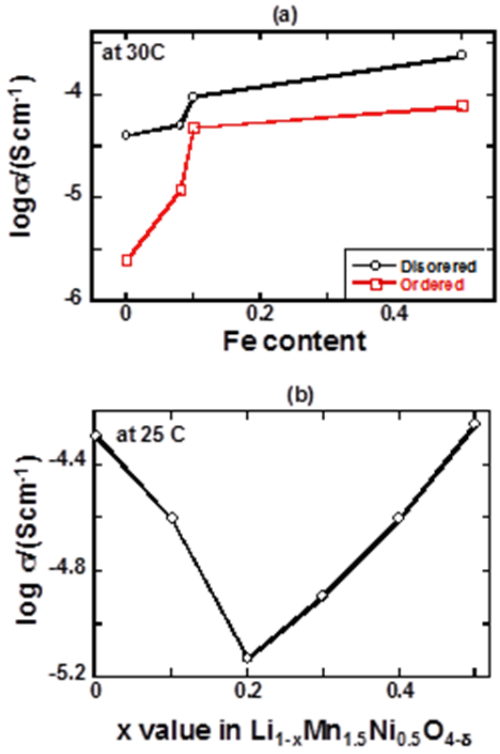


**Figure VI - 194: The electronic conductivity of ordered and disordered $LiMn_{1.5}Ni_{0.5-x}Fe_xO_4$ (x = 0.00, 0.08, 0.10, 0.50) as a function of Fe content at 30°C (a) and the electronic conductivity of disordered $LiMn_{1.5}Ni_{0.42}Fe_{0.08}O_4$ as a function of lithium content at 25°C (b)**

The electronic conductivity was measured by AC and DC techniques as a function of temperature using the symmetrical cell configuration (Ag/LMNO/Ag). Figure VI - 194 (a) shows the electronic conductivity at 30°C for both ordered and disordered phases increases as a function of Fe content. The electronic conductivity of partially electrochemically delithiated disordered $LiMn_{1.5}Ni_{0.42}Fe_{0.08}O_4$ as a function of lithium content is shown in Figure VI - 194 (b). This behavior is similar to that seen previously for undoped LMNO: the electronic conductivity decreases until the end of the 4V

intercalation plateau (complete oxidation of $Mn^{3+}$ to $Mn^{4+}$) and inceases thereafter.

## Conclusions and Future Directions

- Both NCA and Fe-doped LMNO have sufficient electronic conductivity for use as additive free sintered cathodes.
- The measured lithium transport coefficients allow a maximum microstructural length scale to be defined in fabricated microstructures such that solid state transport is not rate-limiting.
- In the coming year, directionally-freeze cast NCA electrodes (already fabricated) will be characterized, and Fe-doped LMNO electrodes will be fabricated.
- At very high area capacity, pulse power performance may differ substantially from conventional electrodes. This behavior will be characterized using PHEV- and EV-specific "drive cycles."

## FY 2013 Publications/Presentations

1. **"**Studies on the transport properties of ordered and disordered high voltage cathode," *International Conference on Energy Harvesting, and Storage: Materials, Device and Application*, 29-30th April, 2013, Baltimore, USA.
2. "Transport properties of high voltage spinel cathode lithium ion battery," *ECS 223th Meeting,* 12-16th May, 2013, Toronto, Canada.
3. "Investigation of transport properties of $LiNi_{0.8}Co_{0.15}Al_{0.05}O_2$ (NCA)," *ECS 224th Meeting,* 27th Oct-1st Nov, 2013, San Francisco, California.

# VI.F Diagnostics

## VI.F.1 Energy Storage Materials Research using DOE's User Facilities (ANL)

**Michael Thackeray**
Argonne National Laboratory

9700 South Cass Avenue
Argonne, IL 60439
Phone: (630) 252-9184; Fax: (630) 252-4176
E-mail: thackeray@anl.gov

Collaborators
ANL: Jason Croy, Brandon Long, Paul Fenter, Tim Fister
Advanced Photon Source, ANL: Mali Balasubramanian, Matthew Suchomel
Electron Microscopy Center, ANL: Dean Miller
Northwestern University: Michael Bedzyk, Xiao Chen
Rutherford Appleton Laboratory, UK: Bill David

Start Date: October 2012
Projected End Date: September 2015

### Objectives

- The primary objective of this project is to broaden the scope of studies of electrode materials relevant to the BATT program, using DOE and international user facilities through collaborative efforts.
- More specifically, the goal is to use a range of x-ray spectroscopic techniques, including *in situ* methods, such as X-ray diffraction (XRD), X-ray absorption (XAS), and X-ray reflectivity (XR) at the Advanced Photon Source (APS); high-resolution transmission electron microscopy (HRTEM) at Argonne's Electron Microscopy Center (EMC); and neutron scattering at the ISIS facility, Rutherford Appleton Laboratory (RAL), UK and/or ORNL's Spallation Neutron Source (SNS).

### Technical Barriers

- Low energy density
- Poor low temperature operation
- Abuse tolerance limitations

### Technical Targets

- 142 Wh/kg, 317 W/kg (PHEV 40 mile requirement)
- Cycle life: 5,000 cycles
- Calendar life: 15 years

### Accomplishments

- High resolution XRD and XAS data were collected at the APS to examine and unravel the complex structural features of high capacity, composite electrode structures.
- HRTEM data of composite electrode structures were collected to monitor differences in the domain structures of quenched and slow cooled samples.
- XRD analyses of $LiMn_2O_4$ (LMO) spinel and Ge anode thin films were undertaken as an exploratory study to probe electrochemical reactions at lithium-metal oxide (cathode) and lithium-alloy (anode) surfaces.
- A proposal to conduct neutron diffraction studies of high capacity composite electrode structures at ISIS in the UK was submitted.
- Two papers in preparation. One presentation.

✧ ✧ ✧ ✧ ✧

### Introduction

Bulk and interfacial electrochemical processes are of fundamental scientific interest as well as of technological importance. The performance of energy storage and power supply systems is largely dependent on these processes, which can occur at an electrode-electrolyte interface or in the bulk of the electrode. In this project, the structural features, ionic transport phenomena and charge-transfer reactions at the electrode/electrolyte interface of lithium battery electrode materials, notably high potential metal oxide cathodes, are studied.

This project is relevant to Argonne's BATT research on electrodes with integrated 'composite' structures, which has highlighted the possibility of designing new, high-potential and high capacity electrodes with

$Li_2MnO_3$ as a stabilizing component; in particular, the project complements and supports the BATT project *'Novel Cathode Materials and Processing Methods (VI.B.1)'*. It has been demonstrated that it is possible to integrate $Li_2MnO_3$ with layered $LiMO_2$- or spinel $LiM_2O_4$ components (e.g., M=Mn, Ni, Co) at the atomic level, and that these composite materials can provide a very high capacity (250 mAh/g), which is significantly higher than the capacity offered by conventional layered $LiCoO_2$, spinel $LiMn_2O_4$ and olivine $LiFePO_4$ electrodes. These lithium- and manganese-rich composite materials have extremely complex structures which are surprisingly stable when delithiated at high potentials (~5 V). Despite the enhanced stability of these electrode materials, it is still necessary to passivate the electrode surface to prevent electrode/electrolyte reactions, and to improve lithium-ion transport at the surface, thereby enhancing the power capability. In this respect, several coating techniques and passivating agents, such as metal oxides ($Al_2O_3$, $ZrO_2$), fluorides ($AlF_3$) and phosphates ($AlPO_4$) have been shown to improve the surface stability and rate capability of electrodes, but little is known about surface structures, or the mechanisms by which lithium-ion transport occurs at the electrode surface.

## Approach

Important analytical techniques for probing the structure-electrochemical property relationships of lithium battery electrode materials, notably at electrode surfaces, include neutron scattering, XAS, photoelectron spectroscopy, nuclear magnetic resonance, Raman spectroscopy, Fourier transform infrared spectroscopy, and electron microscopy. Over the past year, analytical efforts have focused predominantly on x-ray techniques, including "*in situ"* experiments, and high-resolution electron microscopy. Major facilities are available at Argonne to conduct these experiments, notably at the APS and the EMC. In addition, new initiatives using X-ray reflectivity and neutron scattering techniques were initiated.

Surface-protected 'coated' cathode materials to be studied include those with integrated 'composite' structures in which the coating contains specific 3d/4d transition metals that are not present in the core structure. Coatings are applied by various techniques, for example, from solution by standard sol-gel methods or by atomic layer deposition (ALD). *"In situ"* synchrotron hard x-ray spectroscopic techniques including XAS, resonant and non-resonant x-ray emission spectroscopy (XES) and x-ray Raman scattering (XRS) are useful techniques for monitoring reactions at the electrode-electrolyte interface. A comparison of the electrochemical properties of uncoated and coated electrodes will be made. It is envisioned that these studies will provide important information about the structure of coatings at the molecular level, the mechanism of lithium-transport at the electrode-electrolyte interface and an insight into degradation mechanisms. Another aspect to be investigated is the effect of the coating on the bulk structure of the composite material itself, particularly on deintercalation at high voltages, for example 4.6 V, during the initial charge. Recent XAS studies of uncoated composite materials have shown convincing evidence of oxygen loss during the first charge. The exact mechanism for oxygen loss and the accompanying reactions are not yet known. Detailed studies of the local structure within the bulk are likely to provide key insights on structure-property relationships of coated materials. In addition to the studies of composite cathode structures, investigations of well defined electrode surfaces will be undertaken using spectroscopic and microbeam methods. Such studies will utilize the property of total external reflection of x-rays at small incident angles, which minimizes the contribution from the bulk of the material, thereby providing interface sensitivity without sacrificing the "*in situ*" capability of hard x-rays.

## Results

A novel technique to synthesize composite electrode structures was recently devised at Argonne. Specifically, layered $Li_2MnO_3$ is used as a precursor template. The precursor is treated in an acidic solution in the presence of soluble transition metal cations of interest, for example, $Ni^{2+}$. In the process, lithium and oxygen can be leached from the $Li_2MnO_3$ precursor with concomitant ion-exchange of lithium with the desired cations. On subsequent annealing, the exchanged cations are driven into the manganese layers to form the composite structure. The technique is extremely versatile and can produce a wide range of integrated, composite structures including 'layered-layered', 'layered-layered-spinel', and 'layered-layered-rocksalt' configurations. Furthermore, it was discovered that elements and compounds of interest for surface stabilization (e.g. fluorides, phosphates, Al, etc.) can be added to the initial acidic solution to yield products with modified surfaces and bulk structures.

Figure VI - 195 shows cycling data from a $Li/0.5Li_2MnO_3 \bullet 0.5LiMn_{0.5}Ni_{0.5}O_2$ electrode synthesized from a $Li_2MnO_3$ precursor with the addition of 2.5% F. Cells were cycled at room temperature at 15 mA/g. The first 20 cycles were between 4.6 – 2.0 V where the electrodes delivered a stable 250 mAh/g. Starting with cycle 21 the upper voltage cut-off was increased to 5.0 V. The electrode delivered a steady capacity of 275 mAh/g for the remaining 30 cycles on test. The inset of Figure VI - 195 shows that these electrodes

achieve ~200 mAh/g discharge capacity at close to C rates.

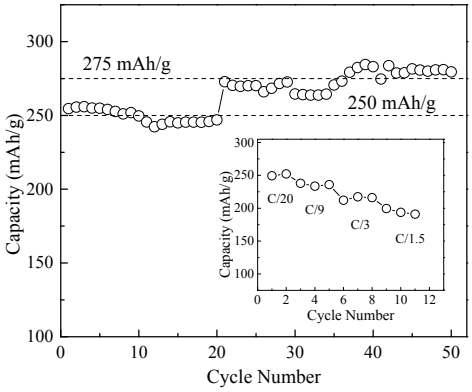


**Figure VI - 195. Li/0.5$Li_2MnO_3$•0.5$LiMn_{0.5}Ni_{0.5}O_2$ electrodes cycled between 4.6-2.0 V (cycles 1-20) and 5.0-2.0 V (cycles 30-50) at 15 mA/g. The inset shows rate data**

*XAS (APS)*

In order to probe the structures of these fluorinated electrodes XANES and EXAFS were carried out on fresh (MnNiF_fresh) and cycled (MnNiF_cycled) as well as un-fluorinated (MnNi_fresh) electrodes at the APS. Figure VI - 196a shows Mn K-edge XANES data of all samples along with $Li_2MnO_3$, a $Mn^{4+}$ standard reference. It was observed that all uncycled, fresh samples had an average Mn oxidation state of 4+, in agreement with $Li_2MnO_3$. Figure VI - 196b shows Mn K-edge EXAFS data of the samples in Figure VI - 196a. Again, all of the fresh materials are similar and reveal that fluorination has not altered the bulk, local structure and, therefore, likely resides predominantly at the surface. For the cycled materials, Figure VI - 196a and Figure VI - 196b reveal clear changes that are associated with the local manganese environment including significant disorder, which is evident from the increased intensity of the pre-edge peaks in Figure VI - 196a. Figure VI - 196b also reveals a significant reduction of the first shell Mn-O correlations at ~1.5 Å (not corrected for photoelectron wave shift) as well as longer range correlations between ~4-6 Å. These changes to the local manganese environment are similar to those observed in the Mn K-edge data of all lithium-rich x$Li_2MnO_3$•0(1-x)$LiMO_2$ (M=Mn, Ni, Co) electrodes after activation and high-voltage cycling. These changes are directly linked to the voltage fade phenomenon triggered by processes (e.g. oxygen loss) occurring along the first cycle, activation plateau.

These data reiterate the importance of surface modifications to produce desirable electrochemical performance in high-voltage systems; they also highlight the inherent, bulk nature of performance degradation (e.g., voltage fade) with cycling.

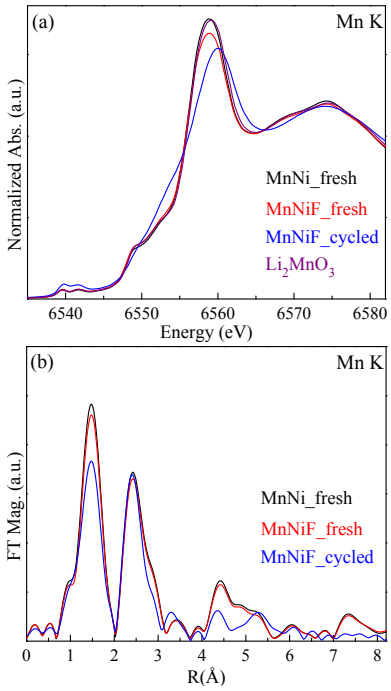


**Figure VI - 196: Mn K-edge XANES (a) and EXAFS (b) of fresh and cycled 0.5$Li_2MnO_3$•0.5$LiMn_{0.5}Ni_{0.5}O_2$ electrodes. (a) Includes a $Li_2MnO_3$, $Mn^{4+}$ reference**

*XRD (APS) and HRTEM (ECM)*

High resolution XRD data of 0.5$Li_2MnO_3$•0.5$LiCoO_2$ electrode samples that had been annealed at 850°C followed by slow cooling, quenching and intermediate (programmed) protocols were collected at the APS (Beamline 11). The XRD patterns of all the samples (not shown here to save space) were virtually identical – irrespective of the cooling protocol. The HRTEM images of the 0.5$Li_2MnO_3$•0.5$LiCoO_2$ samples that had been slow cooled and quenched are shown in Figure VI - 197a and Figure VI - 197b, respectively. In this case, it is clear that slow cooling increases the $Li_2MnO_3$ and $LiCoO_2$ domain size and the degree of order, as illustrated in Figure VI - 197 by the 213 domains of $Li_2MnO_3$ (blue) and 112 domains of $LiCoO_2$ (red). These structural differences impact the electrochemical behavior of the electrodes, thereby highlighting the critical need to control synthesis parameters and procedures in order to fabricate optimized compositions and structures in a reproducible manner.

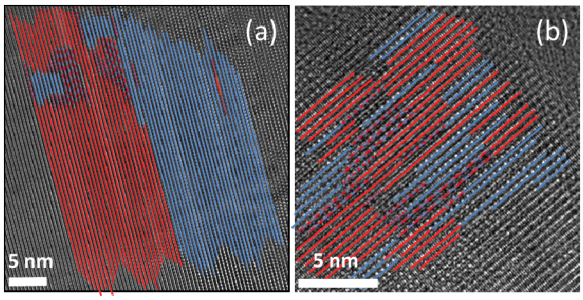


**Figure VI - 197: Transmission electron microscopy images of $0.5Li_2MnO_3 \cdot 0.5LiCoO_2$ annealed at 850°C followed by (a) slow cooling and (b) quenching**

*XR (APS)*

A project to prepare and characterize model thin-film electrode structures for high resolution *in situ* studies of charge/discharge processes was initiated in FY2013. This project is a collaborative effort between staff at the APS from Argonne (Paul Fenter and Tim Fister) and Northwestern University (Michael Bedzyk and Xiao Chen). The goal is to obtain a mechanistic understanding of the changes to electrode and electrode-electrolyte structures as a function of applied potential, through direct, *in situ* and real-time observations. Efforts have focused on developing and studying two model thin film electrode systems: a germanium (Ge) film as a model anode, and lithium manganese oxide (LMO) spinel thin film as a model cathode. The films were grown by sputter deposition. The film structures were characterized and studied by X-ray reflectivity (XR) at the APS. Ge films were found to have a controlled morphology with a uniform thickness of a few nanometers. Preliminary *in situ* XR studies have shown that these films can be reversibly lithiated with associated changes to film thickness and density. The growth of laterally uniform LMO films has been a greater challenge. It was found that LMO films grow in a complex 3d morphology when deposited on $Al_2O_3$ or MgO substrates, which is not ideal for XR studies. The use of an interfacial coating (e.g., TiN films) on the substrate prior to the growth of the electrode to control the LMO film morphology and to provide an electronic collector layer is being explored (see Figure VI - 198.)

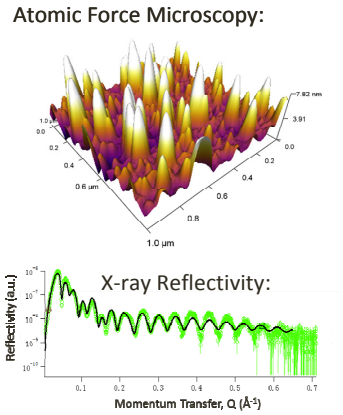


**Figure VI - 198: (Top) AFM image and (bottom) X-ray reflectivity data of $LiMn_2O_4$/TiN/MgO(001) films grown by RF-sputtering. The LMO film is crystallographically aligned with the substrate, but is rougher than optimal**

*NS – ISIS, UK*

A proposal was submitted to ISIS, UK for beamtime on POLARIS to undertake a preliminary neutron study of the structure and nanostructure of 'layered-layered' cathode materials that contain both Mn and Ni as active redox sites using PDF and Rietveld analyses. In combination with electron microcopy and electrochemical measurements undertaken at ANL, these measurements will enable an assessment of the efficacy of neutron powder diffraction to gather an understanding of complex structure-electrochemical property relationships in Mn and Ni-containing electrode materials. A longer range goal is to undertake *in situ* studies of cycled electrodes and use isotopically labeled (e.g. $^{62}Ni$) materials. The main objectives of this task are to:

- Gather detailed information about the structures of 'layered-layered' and 'layered-layered-spinel' composite electrode materials, structure-electrochemical property relationships, electrochemical activation processes, and degradation mechanisms.
- Identify structural configurations associated with voltage fade and hysteresis phenomena.

## Conclusions and Future Directions

*Conclusions*

This project is a work in progress. An approach has been adopted to use a wide variety of analytical methods, notably with DOE's user facilities, to probe electrode materials of interest to the BATT program. A novel synthesis method is being exploited to tailor and optimize the composition and the surface and bulk structures of lithium- and manganese-rich composite electrodes. Electrochemical and XAS data have revealed

that surface modifications with fluorine result in enhanced electrochemical stability, delivering 275 mAh/g when cycled over a wide voltage window, 5.0-2.0 V. HRTEM images have highlighted that the domain structure of composite electrodes depends on processing conditions, impacting electrochemical performance. Efforts to conduct neutron diffraction experiments to determine structure-property relationships have been initiated to broaden the scope of research on these complex materials. X-ray reflectivity techniques at the APS have been introduced to probe surface structures of lithium transition metal oxide and lithium-alloy anodes.

*Future Work*

This work reiterates the importance of engineering and controlling surface reactivity of high-voltage systems, and combating inherent degradation mechanisms. At the core of both surface and bulk phenomena in lithium- and manganese-rich composite electrode materials is the incorporation and utilization of the $Li_2MnO_3$ component. Significant advances are only likely to be made with a full understanding of structure-electrochemical property relationships using a full suite of characterization techniques. Studies will focus on understanding the $Li_2MnO_3$ activation process and the influence of domain size on electrochemical performance. Optimization of composite electrodes will be investigated by studying cation-substituted materials of interest (e.g., Mg, Zn), before and after cycling. The analytical studies will be extended to include high-voltage spinels.

## FY 2013 Publications/Patents/Presentations

**Publications**

1. J. R. Croy, B. Long, M. Balasubramanian and M. M. Thackeray, *An Electrochemical and Structural Study of Substituted $xLi_2MnO_3 \bullet (1-x)LiMO_2$ Composite Electrodes Prepared from an $Li_2MnO_3$ Precursor* (2013). In preparation.
2. J. R. Croy, B. Long, M. Suchomel, D. Miller and M. Balasubramanian, *Cooling Effects on the Domain Structure of $xLi_2MnO_3 \bullet (1-x)LiCoO_2$ Electrode Materials* (2013). In preparation.

**Presentations**

1. 2013 DOE Annual Peer Review Meeting Presentation, Arlington, VA.

# VI.F.2 Advanced *in situ* Diagnostic Techniques for Battery Materials (BNL)

**Xiao-Qing Yang**
Brookhaven National Laboratory

Chemistry Department
Building 555, Brookhaven National Laboratory
Upton, NY 11973
Phone: (631) 344-3663; Fax: (631) 344-5815
E-mail: xyang@bnl.gov

**Kyung-Wan Nam**
Brookhaven National Laboratory
Chemistry Department
Building 555, Brookhaven National Laboratory
Upton, NY 11973
Phone: (631) 344-3202; Fax: (631) 344-5815
E-mail: knam@bnl.gov

Start Date: October 2012
Projected End Date: September 2016

## Objectives

- To determine the contributions of electrode material changes, interfacial phenomena, and electrolyte decomposition on cell capacity and power decline.
- To develop and apply synchrotron based *in situ* X-ray techniques such as X-ray diffraction (XRD) and X-ray absorption spectroscopy (XAS) to study materials in an environment that is close to the real operating conditions.
- To perform diagnostic studies of the potentially low cost and high energy density cathode materials such as spinel structured $LiNi_xMn_{2-x}O_4$.
- To perform diagnostic studies of the Si-based high energy density anode materials.
- To develop new diagnostic tools for battery studies.
- To alleviate the chemical interaction between superoxide ($O_2^{\cdot-}$) and electrolyte.
- To enhance the rechargability of lithium-air batteries.

## Technical Barriers

- Li-ion and Li-metal batteries with long calendar and cycle life
- Li-ion and Li-metal batteries with superior abuse tolerance
- To reduce the production cost of a PHEV batteries

## Technical Targets

- Complete the *in situ* time resolved XRD studies of $LiMn_{2-x}Ni_xO_4$ cathode material with ordered ($P4_332$) spinel structure during heating.
- Complete the XAS studies of $LiMn_{2-x}Ni_xO_4$ cathode material with ordered ($P4_332$) spinel structure during heating.
- Complete the *in situ* time resolved XRD studies of $LiMn_{2-x}Ni_xO_4$ cathode material with disordered ($Fd$-3m) spinel structure during heating.
- Complete the XAS studies of $LiMn_{2-x}Ni_xO_4$ cathode material with disordered ($Fd$-3m) spinel structure during heating.
- Complete the *ex situ* Si K-edge XAS studies of Si-based high energy density anode materials after cycling.

## Accomplishments

- Developed new "quick XAS" technique to do kinetic studies on cathode materials for Li-ion batteries during electrochemical delithiation at constant voltage.
- Carried out thermal stability studies of high voltage cathode material $LiMn_{1.5}Ni_{0.5}O_4$ with spinel structure (both ordered $P4_332$ and disordered $Fd$-3$m$ structures) using time resolved XRD combined with mass spectroscopy during heating.
- Carried out thermal stability studies of high voltage cathode material $LiMn_{1.5}Ni_{0.5}O_4$ with spinel structure (both ordered $P4_332$ and disordered $Fd$-3$m$ structures) using XAS during heating.
- Carried out studies on electronic structure changes of high energy density Si anode using Si K-edge X-ray absorption near edge structure (XANES) spectroscopy during lithiation-delithiation cycling.
- Developed a boron containing Lewis acid which could catalyze rapid disproportionation of the superoxide ions to prevent their reaction with electrolytes.

- $Li_2O_2$ can be dissolved and soluble complex $O_2^{2-}$ can be electrochemically oxidized on carbon electrode.

✧ ✧ ✧ ✧ ✧

## Introduction

4V-spinel $LiMn_2O_4$ is one of the important cathode materials for lithium-ion batteries (LIBs) as the power sources of electric vehicles due to high ionic- and electronic- conductivity, excellent thermal stability, and low cost. Recently, one of its derivatives, $LiNi_xMn_{2-x}O_4$, denoted as LNMO, (where x is around 0.5) has attracted research attention as a promising high-energy density cathode material with higher operating voltage at ~4.7V. On the other hand, the poor cycle and calendar life of LNMO, especially at elevated temperatures, still needs to be improved. Heat treatment procedure is very important since LNMO is formed in two different kinds of structures, depending on the annealing procedure adopted after the 900°C solid-state reaction. Reportedly, spinel-structured LNMO, formed through the solid-state reaction, loses oxygen between 700°C and 900°C, causing the partial transformation of a spinel phase to a rock-salt phase. The majority of the rock-salt structure can be transformed back to a spinel structure during cooling by regaining oxygen below 700°C. However, if the cooling is not slow enough, the amount of oxygen regained is low and a significant amount of the rock-salt impurity phase will be retained. Under such conditions, the disordered phase is formed, in which $Mn^{4+}$ and $Ni^{2+}$ cations are randomly distributed in the transition metal layer, with the space group *Fd*-3*m* (to be referred as *d*-LNMO). On the other hand, if the cooling of the material is slow enough (in some cases, a constant temperature-annealing duration below 700°C is used), the re-incorporation of oxygen is almost complete, and the rock-salt impurity residues will be negligible. Under the latter conditions, the ordered phase is formed in which $Mn^{4+}$ and $Ni^{2+}$ cations are located at certain different sites in the crystal lattice with the space group $P4_332$ (to be referred as *o*-LNMO). Although most researchers presently believe that the cycling performance of the disordered *d*-LNMO is better than that of the ordered *o*-LNMO, there are more and more reports demonstrating that the *o*-LNMO can display a satisfactory cycling performance, while preserving other properties like higher average operating voltage and larger capacity than those of the *d*-LNMO. The thermal stability of LNMO, which could greatly impact the safety of LIBs, has received little attention. This lack of interest probably could be attributed to the assumption that the excellent thermal stability of the delithiated LNMO can be naturally inherited from its parent material $LiMn_2O_4$, for which only a subtle structural rearrangement takes place without the oxygen release up to 500°C in the fully delithiated state. Therefore, $Li_xMn_2O_4$ has been regarded as a thermally safer cathode material than layered materials. However, for LNMO, what was overlooked at is that when a quarter of the Mn is replaced by Ni, the thermodynamics of the material inevitably changes yielding a very different thermal stability than its parent $LiMn_2O_4$. Unfortunately, little research has been published on the thermal stability of LNMO materials and their doped derivatives. There are very few studies correlating thermal stability either with structural differences (ordered or disordered) or with oxygen-releasing structure changes during heating for LNMO. The systematic studies reported here are aimed to explore these correlations.

Electrochemical reduction of molecular $O_2$ is known to form superoxide ions ($O_2^-$), which can react with organic solvents and specifically carbonate solvents. The decomposition of the solvents induced by $O_2^-$ consumes the electrolyte as well as forming undesired side-products (e.g. $Li_2CO_3$), which are difficult to re-oxidize during the recharge process. We hypothesize that the chemical interaction between the superoxide ions and the electrolyte is one of a few competing parallel reactions that $O_2^-$ may undergo. Other reactions may also include the disproportionation and further reduction of $O_2^-$. To alleviate the problems associated with the $O_2^-$/electrolyte reactions, we have attempted to facilitate the disproportionation and further reduction of $O_2^-$, while hindering its chemical interaction with the electrolyte.

One of the major problems for Li-air battery is the precipitation of $Li_2O_2$ on the surface of the porous electrode as when the pores in the GDE are filled up, the electrode will cease functioning. In order to unlock the potential of Li-air chemistry, it is crucial to increase the solubility dramatically for these reaction products formed in charge-discharge cycling for Li-air batteries.

## Approach

Use both time resolved XRD and mass spectroscopy to study the structural changes of high voltage cathode material $LiMn_{2-x}Ni_xO_4$ with spinel structure (both ordered $P4_332$ and disordered *Fd-3m* structures) during heating.

Use *in situ* XAS, both XANES and EXAFS to study the structural changes of high voltage cathode material $LiMn_{2-x}Ni_xO_4$ with spinel structure (both ordered $P4_332$ and disordered *Fd-3m* structures) during heating.

Investing a Lewis acid compound to dissolve solid $Li_2O_2$ and catalyze superoxide disproportionation.

## Results

*In situ* TR-XRD combined with mass spectroscopy TR-XRD/MS were used to study both charged *d*- and *o*-LNMO during heating up to 375°C as shown in Figure VI - 199 and Figure VI - 200. The phase transitions and accompanying oxygen release can be tracked

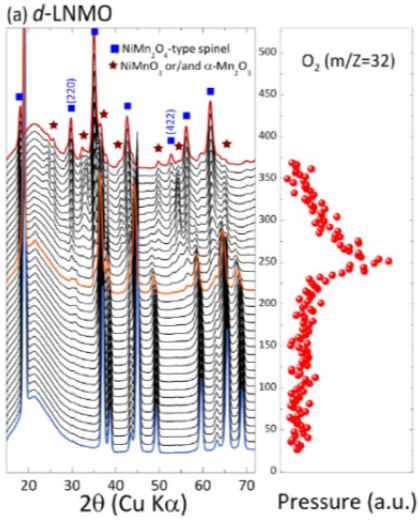


**Figure VI - 199: *In situ* XRD pattern combined with simultaneously measured mass spectroscopy (MS) data that trace oxygen gas release of fully charged disordered LNMO during heating up to 370°C**

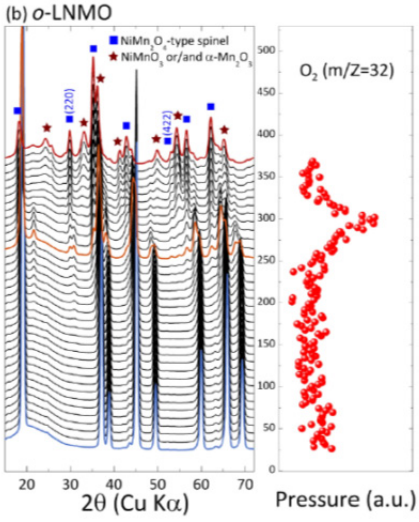


**Figure VI - 200: *In situ* XRD pattern combined with simultaneously measured mass spectroscopy (MS) data that trace oxygen gas release of fully charged ordered LNMO during heating up to 370°C**

closely during heating. There was clear evidence of thermal-decomposition-related phase transitions accompanied with noticeable oxygen release below 250°C for both *d*-LNMO and *o*-LNMO. These results are in sharp contrast to the conventional spinel $Li_xMn_2O_4$ at the fully charged (x = ~0.0) state, where no oxygen-release peak was observed below 375°C. This tells us that when 25% of the Mn in conventional spinel $LiMn_2O_4$ is replaced by Ni, the thermal stability of this high voltage LNMO is greatly changed for both *d*-LNMO and *o*-LNMO. Also it was found that the thermal stability *o*-LNMO is better than *d*-LNMO.

***In situ* X-ray Absorption Spectroscopy (XAS).** XAS can provide information about the changes in local- and electronic-structure surrounding the absorbing atoms in an elemental-selective way. This is very helpful in identifying which element is mainly responsible for thermal instability. Ni K-edge XANES data for delithiated *d*- and *o*-LNMO during heating up to 370°C are shown in Figure VI - 201. The most notable change in Ni K-edge XANES spectra is the inhomogeneous edge-shifting to lower energy (i.e., the decrease in average oxidation state of Ni); this sudden jump of edge shift divides the series of spectra into two parts. It occurs at some temperature between 220°C and 270°C for the charged *d*-LNMO, and between 270°C and 320°C in the charged *o*-LNMO. This feature is clearly shown in the Figure VI - 201 where the changes in edge position are plotted as a function of temperature.

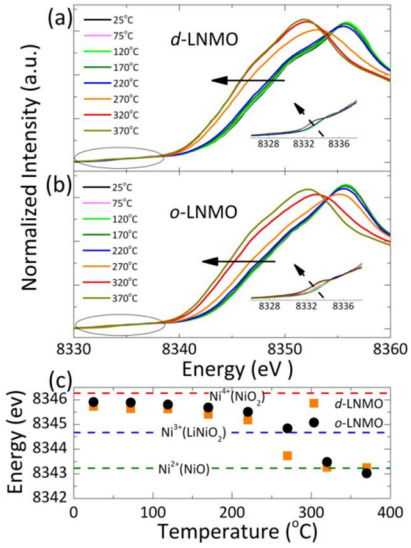


**Figure VI - 201: *In situ* Ni K-edge XANES spectra of fully charged a) *d*-LNMO and b) *o*-LNMO during heating up to 370°C. Insets show the detailed feature of pre-edge region. c) Variations of the Ni-K edge positions (defined as the energy at half height of the energy step at main edge)**

The Mn K-edge XANES results depicted in Figure VI - 202 showed only a moderated edge shift to lower energy for both samples, even during oxygen release, compared with the Ni K-edge results. The Mn reduction commenced at higher temperatures and ended with

lesser change than did the Ni reduction, demonstrating the structural-stabilizing role of Mn. At 370°C, after major oxygen release, the average oxidation state of Mn in both charged *d*- and *o*-LNMO only fell to somewhere between $Mn^{3+}$ and $Mn^{4+}$, while that for Ni was reduced to close to $Ni^{2+}$. This finding suggests that the release of oxygen was initiated by the $Ni^{4+}$ to $Ni^{2+}$ reduction for LNMO upon heating resulting in highly disordered and defective structures and decomposition compounds, which, in turn, triggered the reduction of $Mn^{4+}$ ions. Figure VI - 202 shows that the charged *o*-LNMO has higher average oxidation state of Mn than the charged *d*-LNMO at 370°C confirming the better thermal stability of the former than the latter in the charged state.

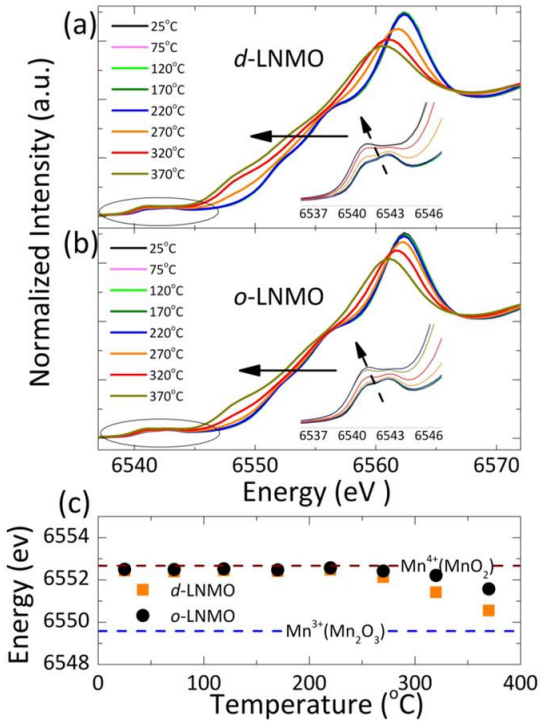


**Figure VI - 202: *In situ* Mn K-edge XANES spectra of fully charged a) d-LNMO and b) o-LNMO during heating up to 370°C. Insets show the detailed feature of pre-edge region. c) Variations of the Mn-K edge positions (defined as the energy at half height of the energy step at main edge)**

**Si K-edge XANES study.** The electronic structure changes of Si anode were studied during the first cycle as shown in Figure VI - 203. During lithiation, the spectra showed continuous edge shift to lower energy side probably due to the expansion of Si-Si bonds. The intensity of the 1s → 2p transition peak (A) also decreased during lithiation, revealing increased local structural disordering around Si. The evolution of peak B was found to originate from the formation $Li_xSi$ alloy using DFT calculation. After the 1st cycle, the XANES feature changed back to nearly its pristine spectrum but not completely, showing the irreversible lithiation/delithiation behavior of the Si anode studied in this work.

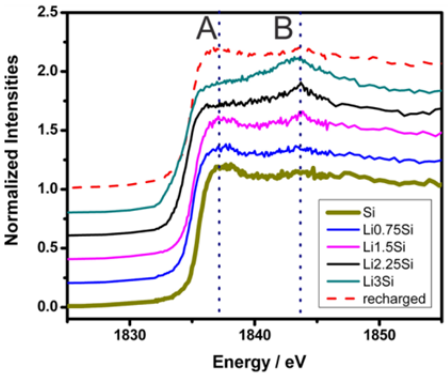


**Figure VI - 203: Si K-edge XANES spectra of Si anode at different states of lithiation and delithiation**

**Li-air batteries.** A boron containing Lewis acid compound can increase the solubility of $Li_2O_2$ and the complexed peroxide ion can be re-oxided electrochemically (see Figure VI - 204).

The negative impact of the reaction between the electrolyte and $O_2^-$ produced by the $O_2$ reduction is minimized by a rapidly catalyzed superoxide disproportionation. The pseudo 2-electron $O_2$ reduction reaction due to the replenishment of $O_2$ at the electrode surface. This discovery could lead to a new avenue for the development of high capacity, high rate, rechargeable Li-Air batteries (see Figure VI - 205).

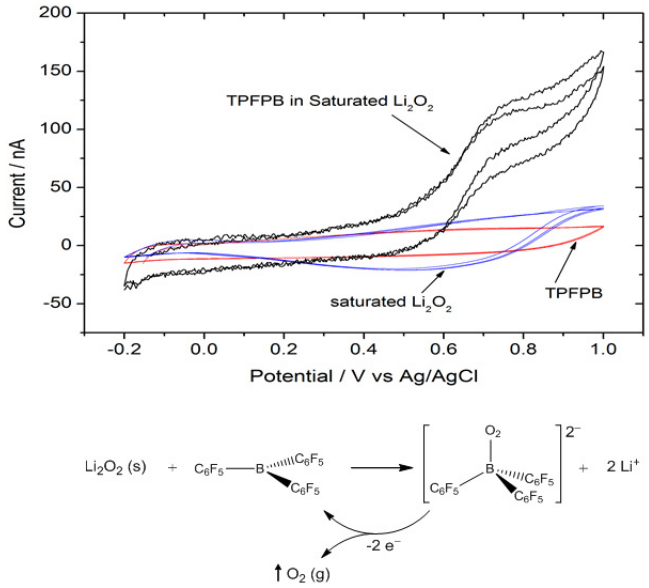


**Figure VI - 204: Comparison of the cyclic voltammetry for the powder microelectrode of the same carbon material in $Li_2O_2$ saturated PC/ACN electrolyte and supporting electrolyte (0.5 M $LiPF_6$), PC/ACN electrolyte containing only TPFPB and supporting electrolyte (0.5 M $LiPF_6$) and $Li_2O_2$ saturated PC/ACN solution with 0.5 wt% TPFPB. Scan rate: 1mV/sec**

## Conclusions and Future Directions

New findings on the thermal-stability are discovered for the high-voltage spinel LNMO with ordered (*o*-) and disordered (*d*-) structures at fully delithiated state were obtained using a combination of *in situ* TR-XRD coupled with mass spectroscopy (MS) and XAS during heating: Both *o*- and *d*-LNMO at their fully charged states start oxygen-releasing structural changes at temperatures below 300°C, which is in sharp contrast to the good thermal stability of the 4V-spinel $Li_xMn_2O_4$. In addition, charged *o*-LNMO shows better thermal stability than the *d*-LNMO counterpart.

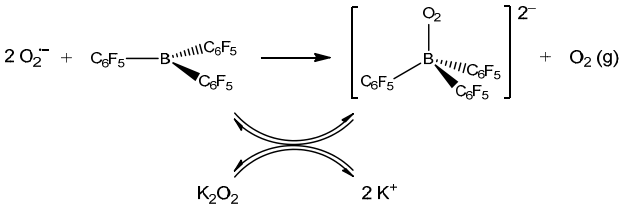


**Figure VI - 205: Mechanism for the catalyzed superoxide disproportionation**

The solubility of solid $Li_2O_2$ can be dramatically increased through the Lewis acid-base interaction between boron and peroxide. The solube $O_2^{2-}$ ion can be re-oxided electrochemically. Rapid superoxide disproportionation can be catalyzed by tris(penftafluorophenyl) borane additive.

In the future more *in situ* XRD and XAS studies of Fe substituted high voltage spinel cathodes during charge-discharge cycling will be performed.

In the future study, more Lewis acid compounds will be syntheized and tested. A unique flow lithium air cell design is being tested

## FY 2013 Publications/Presentations

1. Jianming Zheng, Jie Xiao, Xiqian Yu, Libor Kovarik, Meng Gu, Frederick Omenya, Xilin Chen, Xiao-Qing Yang, Jun Liu, Gordon L. Graff, Stanley M. Whittingham, Ji-Guang Zhang, "Enhanced $Li^+$ ion transport in $LiNi_{0.5}Mn_{1.5}O_4$ through control of site disorder," *Physical Chemistry Chemical Physics*, **14**, 13515-13521 (2012).
2. Jie Xiao, Xiqian Yu, Jianming Zheng, Yungang Zhou, Fei Gao, Xilin Chen, Jianming Bai, Xiao-Qing Yang, Ji-Guang Zhang, "Interplay between two-phase and solid solution reaction in high voltage spinel cathode material for lithium ion batteries," *Journal of Power Sources*, **242,** 736-741 (2013).
3. Huilin Pan, Xia Lu, Xiqian Yu, Yong-Sheng Hu, Hong Li, Xiao-Qing Yang, Liquan Chen, "Sodium storage and transport properties in layered $Na_2Ti_3O_7$ for room-temperature sodium-ion batteries," *Advanced Energy Materials*, **3**, 1186-1194 (2013).
4. Yuesheng Wang, Xiqian Yu, Shuyin Xu, Jianming Bai, Ruijuan Xiao, Yong-Sheng Hu, Hong Li, Xiao-

Qing Yang, Liquan Chen, Xuejie Huang, "A zero-strain layered metal oxide as the negative electrode for long-life sodium-ion batteries," *Nature Communications*, **4,** 2365 (2013).

5. J.J. Ding, Y.N. Zhou, Q. Sun, X.Q. Yu, X.Q. Yang, Z.W. Fu, "Electrochemical properties of $P_2$-phase $Na_{0.74}CoO_2$ compounds as cathode material for rechargeable sodium-ion batteries," *Electrochimica Acta,* **87**, 388-393 (2013).
6. Yong-Ning Zhou, Jing-Jing Ding, Kyung-Wan Nam, Xiqian Yu, Seong-Min Bak, Enyuan Hu, Jue Liu, Jianming Bai, Hong Li, Zheng-Wen Fu* and Xiao-Qing Yang*, "Phase transition behavior of $NaCrO_2$ during sodium extraction studied by synchrotron-based X-ray diffraction and absorption spectroscopy," *A Journal of Materials Chemistry*, **1**, 11130 (2013).
7. Zheng, H-S Lee, X.Q. Yang, D.Y. Qu, "Electrochemical Oxidation of Solid $Li_2O_2$ in Non-aqueous Electrolyte Using Peroxide Complexing Additives for Lithium-Air Batteries," *Electrochemistry Communications*, **28**, 17-19 (2013).
8. "Diagnostic Studies to Improve Abuse Tolerance and Life of Li-ion Batteries," *DOE Annual Peer Review Meeting*, May 13-17, 2013, Washington, DC.
9. Xiqian Yu, Hung-Sui Lee, Xiao-Qing Yang, Kyung-Wan Nam, and Yongning. Zhou, Hong Li, Xuejie Huang, Liquan Chen, Kan Xu and Arthur von Cresce, "Studies on the formation and stability of solid electrolyte interphase on the surface of anode and cathode of lithium-ion batteries," *222nd Meeting of the Electrochemical Society*, October, 8-12, 2012, Honolulu, Hawaii, USA, **Invited.**
10. Xiqian Yu, Kyung-Wan Nam, Chao Ma, Hong Li, and Xiao-Qing Yang, "Investigation on Si anode materials for Lithium-ion batteries using X-ray absorption spectroscopy," *222nd Meeting of the Electrochemical Society*, October, 8-12, 2012, Honolulu, Hawaii, USA.
11. Xiqian Yu, Kyung-Wan Nam, Xiao-Qing Yang, Yongning Zhou, Enyuan Hu, Yingchuan Lv Hong Li, Daniel Abraham, Huiming Wu, and Khalil Amine "Structure Evolution and Its Relation to the Voltage Fading Behavior In Li-Rich Layered $Li_{1.2}Ni_{0.15}Co_{0.1}Mn_{0.55}O_2$ Cathode Material During Cycling: X-Ray Diffraction And Absorption Spectroscopy Study," *Advanced Electrochemical Energy Symposium and Shanghai Jiao Tong University-Sinopoly Battery Technology Forum (2012 AEES)*, December 22, 2012, Shanghai, China. **Invited.**

# VI.F.3 Interfacial Processes (LBNL)

**Robert Kostecki**
Lawrence Berkeley National Laboratory

Environmental Energy Technologies Division
1 Cyclotron Road, MS 90-3026D
Berkeley, CA 94720
Phone: (510) 486-6002; Fax: (510) 486-5454
E-mail: r_kostecki@lbl.gov

Start Date: October 2012
Projected End Date: September 2016

## Objectives

- Establish direct correlations between electrochemical performance of high-energy Li-ion composite cathodes, and surface chemistry, morphology, topology and interfacial phenomena
- Improve the capacity and cycle life limitations of $Li_xSi$ anodes
  - Determine physico-chemical properties of the SEI, i.e., chemical composition, reaction kinetics, morphology, ionic/electronic conductivity etc.
  - Investigate electrocatalytic behavior of intermetallic anodes in organic electrolytes
  - Provide remedies to interface instability e.g., new alloys and/or structures, electrolyte additives, codeposition of other metals etc.
  - Characterize degradation modes, improve SEI long-term stability in high-energy Li-ion systems
  - Evaluate the effect of surface composition and architecture on electrochemical behavior of the electrode

## Technical Barriers

This project addresses the following technical barriers related to the battery technology development effort of the DOE Office of Vehicle Technologies:

- Inadequate Li-ion battery energy (related to cost)
- Poor lithium battery calendar/cycle lifetime for PHEVand EV applications
- High electrode impedance that limits power density
- Need for new advanced battery materials and composite electrodes with acceptable specific energy, durability, cost, and safety characteristics.

## Technical Targets

- Cycle life: 5,000 (deep) and 300,000 (shallow) cycles
- Available energy: 200 Wh/kg ·
- Calendar life: 15 years

## Accomplishments

- Determined the mechanism of interfacial processes on $LiNi_{0.5}Mn_{1.5}O_4$
  - Inorganic and organic fluorescent electrolyte decomposition products form at the cathode and anode
  - Mn and/or Ni dissolution leads to formation of soluble fluorescent species, which diffuse toward the anode and interfere with the anode (SEI Mn/Ni poisoning?)
  - Insoluble electrolyte decomposition products form electronic and ionic barriers in composite cathodes and contribute to the impedance rise in Li-ion cells
- Pioneered the use of near-field IR spectroscopy and microscopy to study electrochemical interfaces in Li-ion systems
  - New technique and experimental methodology was developed under the BES-funded NECCES (Energy Frontier Research Center)
  - Preliminary measurements carried out on a model Sn-foil anode revealed non-uniform distribution of electrolyte decomposition products at nanometer scale

✧ ✧ ✧ ✧ ✧

## Introduction

A primary aim of this project is to develop and use advanced diagnostic techniques and experimental methodologies to characterize basic physico-chemical properties and function of Li-ion electrode active and passive components that are being developed for use in PHEV and EV applications. The main objective of this task is to apply novel far- and near-field optical multifunctional probes to obtain detailed insight into the

dynamic behavior of molecules, atoms, and electrons at electrode/electrolyte interfaces of intermetallic anodes (Si) and high voltage Ni/Mn-based materials at a spatial resolution that corresponds to the size of basic chemical or structural building blocks. The goal of these studies is to unveil the structure and reactivity at hidden or buried interfaces and interphases that determine battery performance and failure modes. A better understanding of the underlying principles that govern these phenomena is inextricably linked with successful implementation of high energy density materials such as Si and high voltage cathodes in Li-ion cells for PHEVs and EVs.

## Approach

Design and employ novel and sophisticated *in situ* analytical methods to address the key problems of the BATT baseline chemistries. The proposed experimental strategies combine imaging with spectroscopy aimed at probing electrodes at an atomic, molecular, or nanoparticulate level to unveil structure and reactivity at hidden or buried interfaces and determine electrode performance and failure modes in baseline $Li_xSi$-anodes and high-voltage LMNO cathodes. The proposed methodologies include *in situ* and *ex situ* Raman, FTIR and laser induced breakdown spectroscopy (LIBS) far- and near-field spectroscopy/microscopy, scanning probe microscopy (SPM), spectroscopic ellipsometry, electron microscopy (SEM, HRTEM), and standard electrochemical techniques and model single particle and/or monocrystal model electrodes to probe and characterize bulk and surface processes in Si anodes, and high-energy cathodes.

## Results

Fluorescence spectroscopy/imaging investigations of interfacial phenomena that occur at different crystal facets/orientations of $LiNi_{0.5}Mn_{1.5}O_4$ single microcrystals, namely <112> and <111> in EC:DEC 1:2, 1M $LiPF_6$ electrolyte between 3.5 and 5.0 V vs. $Li/Li^+$ revealed that the fluorescence intensity at the electrode interface always rises at the beginning of the nickel oxidation and then slowly vanishes upon relithiation. In fact, the fluorescence response of the model $LiNi_{0.5}Mn_{1.5}O_4$ single crystal electrodes was somewhat similar to the signal observed for a regular polycrystalline material. Insoluble products of the electrolyte oxidation tend to accumulate at the surface of the electrode contributing to a gradual increase of the fluorescence background signal whereas soluble compounds diffuse away into the electrolyte (Figure VI - 206).

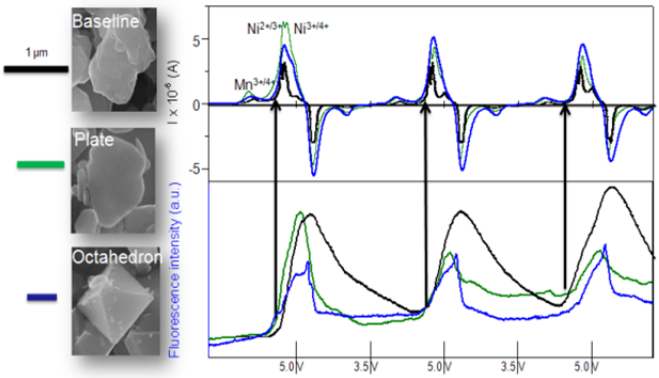


**Figure VI - 206: SEM images (left) (courtesy of Guoying Chen, LBNL), Electrochemical data (right-top), corresponding integrated fluorescence intensity (right-bottom) of $LiNi_{0.5}Mn_{1.5}O_4$ baseline (black), <112> platelet (green) and <111> octahedron (blue) particles in EC:DEC 1:2 1M $LiPF_6$**

Both model electrodes showed a steady increase of the fluorescence background with cycling. However, for the octahedrons the intensity of the fluorescence background remains unchanged after the first cycle whereas fluorescence on the platelets seem to keep growing after every cycle. These compounds that formed on $LiNi_{0.5}Mn_{1.5}O_4$ octahedrons tend to passivate the material better during the initial charge/discharge cycles. This may indicate quite radical differences in surface activity of $LiNi_{0.5}Mn_{1.5}O_4$ depending on material surface orientation. In other words, the steady fluorescence signal from the octahedrons can be associated with the formation of a more stable surface layer on this crystal facet. Further investigations will focus on identification of the fluorescence compounds, their formation mechanism and possible implications for Li-ion battery systems.

Interfacial phenomena occurring on Si (100), (110) and (111) single crystal electrodes in organic electrolytes showed that electrochemical response upon polarization depends on surface crystal orientation of silicon. The (111) crystal facet displays higher current

density and lower decomposition potential. Chemical composition of the SEI layer varied strongly on the different crystal orientations of Si and included $LiPF_6$ salt and EC and DEC solvents decomposition products. On (100) facets, the SEI contains more carbonate and salt decomposition products and appears to be less stable. At potentials below 0.5 V, the SEI undergoes reformation due to Si cracking and structural transition from crystalline to amorphous Si upon alloying with lithium. This results in similar SEI chemical composition for the three different crystal orientations. A lower potential induces an increase in decomposition products, e.g., LiF, P-O-C and P-F.

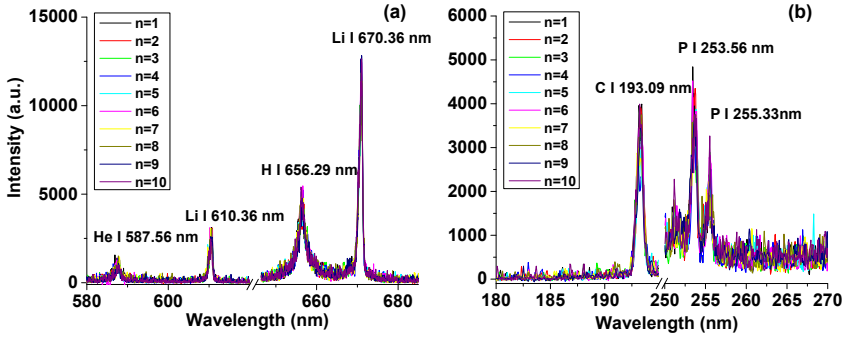


**Figure VI - 207: Ultrafast LIBS emission intensity from the Si electrode/organic electrolyte system as a function of wavelength in the (a) 580-685nm and (b) 180-270 nm spectral region**

Figure VI - 207 depicts the ultrafast LIBS spectral emission originating from a 1M $LiPF_6$ EC:DEC [1:1] electrolyte in contact with a Si wafer with (100) crystal orientation. All major elements of interest (C, P, Li, H) were successfully detected from the electrolyte for the first 10 laser pulses. Subsequent experiments involved optimization of laser parameters including laser energy/pulse and laser repetition rate as well as organic electrolyte thickness above the working electrode to control the contribution of the electrolyte in the emission signal. It was found that higher repetition rates can contribute significantly towards improvement of the Si signal-to-noise ratio, a phenomenon associated with cavitation in the electrolyte due to the laser material interaction in the examined laser energy regime.

Clear correlation between surface activity, SEI composition and stability and crystal facets has been highlighted. Those results point out the critical role of Si crystal orientation in achieving longer Li battery lifetime and its impact on electrochemical performance.

Preliminary *ex situ* near-field IR (NF-IR) imaging of an SEI layer on Sn-foil model electrode was successfully carried out. NF-IR images of the Sn electrode (Figure VI - 208) wavelengths display local spectral variance, which indicates non-uniform distribution of SEI layer basic building blocks at the nanometer level. These new results are consistent with earlier far-field spectroscopy observations.

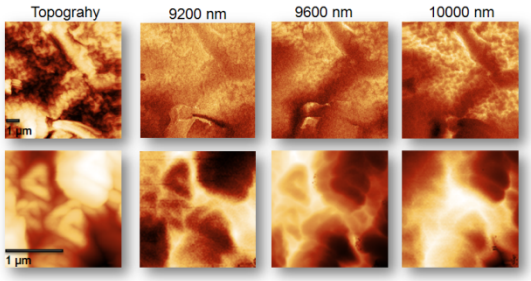


**Figure VI - 208: *Ex situ* near-field IR and topography images of the SEI layer on Sn at 0.8V (top) and $Li_xSn$ at 0.1V (bottom)**

## Conclusions and Future Directions

- Inorganic and organic fluorescent electrolyte decomposition products form at the LNMO cathode and dissolve in the electrolyte
  - Fluorescence rise correlates with the beginning of the $Ni^{2+}$ oxidation.
  - Ni and possibly Mn ions constitute flourophore centers in fluorescence compounds formed on LMNO positive electrodes.
  - Solvent oxidation at LMNO leads to formation of soluble fluorescent species, which diffuse toward the anode and interfere with the SEI (Mn/Ni poisoning?).
  - Well-designed particle morphology is critical in achieving optimal rate capability and stability of the high-voltage LMNO spinel.

- Insoluble electrolyte decomposition products form electronic and ionic barriers in composite cathodes and contribute to the impedance rise in Li-ion cells.
- Electrolyte additives and surface coatings could be effective strategies to reduce surface reactivity of high-voltage cathodes.
- Preliminary *ex situ* near-field IR imaging of an SEI layer on Sn-foil model electrode was successfully carried out.
- Near-Field IR images reveal chemical complexity of the SEI layer and its functionality at nanometer level.
- These new experimental results are in concert with earlier far-field spectroscopy observations and provide new insight into the mechanism of interfacial processes on intermetallic anodes.
- Need to work with model samples of similar dimensions of functional electrode materials.

Near-field optical techniques constitute a class of emerging analytical tools with unprecedented analytical capabilities toward electrical energy materials and systems. With this underpinning knowledge, wholly new concepts in materials design can be developed for producing materials that are capable of storing higher energy densities and have long cycle lifetimes.

- Develop and apply novel innovative experimental methodologies to study and understand the basic function and mechanism of operation of materials, composite electrodes, and Li-ion battery systems for PHEV and EV applications.
- Apply novel far- and near-field optical multifunctional probes to obtain detailed insight into the dynamic behavior of molecules, atoms, and electrons at electrode/electrolyte interfaces of intermetallic anodes (Si) and high voltage Ni/Mn-based materials at a spatial resolution that corresponds to the size of basic chemical or structural building blocks.
- Unveil the structure and reactivity at hidden or buried interfaces and interphases that determine battery performance and failure modes.
- Understanding of the underlying principles that govern these phenomena is inextricably linked with successful implementation of high energy density materials such as Si and high voltage cathodes in Li-ion cells for PHEVs and EVs.
- Cooperate with the BATT Task Groups "SEI on Alloys," "High-Voltage Cathodes" and industrial partners (3M, Dow Chemical) to investigate the effect of material structure, morphology on formation of the SEI layer

## FY 2013 Publications/Presentations


1. Boesenberg, Ulrike; Meirer, Floria; Liu, Yijin; Shukla, Alpesh; Dell'Anna, Rossana; Tyliszczak, Tolek; Chen, Guoying; Andrews, Joy; Richardson, Thomas; Kostecki, Robert; Cabana, Jordi, "Mesoscale phase distribution in single particles of $LiFePO_4$ following lithium deintercalation," *Chemistry of Materials,* in press. DOI: 10.1021/cm400106k.
2. Addy, S. E. A.; Gadgil, A.; Srinivasan, V.; Kowolik, K.; Muller, M.; Huang, J.; Kostecki, R., "Arsenic removal from groundwater using iron electrocoagulation: Effect of charge dosage rate," *Journal of Environmental Science and Health***,** in press.
3. Chunjoong Kim, Nick S. Norberg, Caleb T. Alexander, Robert Kostecki, Jordi Cabana, "Mechanism of phase propagation during lithiation in carbon-free $Li_4Ti_5O_{12}$ battery electrode," *Adv. Funct. Mater.* 2013, **23**, 1214–1222 (DOI:10.1002/adfm.201201684) (2013).
4. Nick S. Norberg, Robert Kostecki, "The Degradation Mechanism of a Composite $LiMnPO_4$ Cathode," *J. Electrochem. Soc.* **159(9)**: A1431-A1434; doi:10.1149/2.018209jes (2012).
5. Vassilia Zorba, Jaroslaw Syzdek, Xianglei Mao, Richard E. Russo and Robert Kostecki, "Ultrafast laser induced breakdown spectroscopy (LIBS) of electrode/electrolyte interfaces," *Applied Physics Letters*, **100**, 234101 (2012).
6. Nick S. Norberg and Robert Kostecki, "Interfacial Phenomena at a Composite $LiMnPO_4$ Cathode," *J. Electrochem. Soc.* **159(7)**: A1091-A1094; doi:10.1149/2.076207jes (2012).
7. S.F. Lux, I.T. Lucas, E. Pollak, S. Passerini, M. Winter and R. Kostecki, "The mechanism of HF formation in $LiPF_6$ based organic carbonate electrolytes," *Electrochemistry Communications*, **14**, 47–50, (2012).
8. "Interfacial Processes in EES Systems Advanced Diagnostics," *DOE Annual Peer Review Meeting*, May 13-17, 2013, Washington, DC.
9. Kostecki, Nick Norberg, "*In situ* Studies of Interfacial Phenomena at a $LiMn_{0.5}Ni_{0.5}O_2$ cathode in organic carbonate Electrolyte," *International Battery Association 2013 Meeting*, March 11-15, 2013, Barcelona, Spain. (invited lecture)
10. Robert Kostecki, Jaroslaw Syzdek, Ivan Lucas, "Near Field Optical Imaging of Interfaces and Interphases in Battery Materials," *Special*

*Symposium to honor Michael Thackeray*, March 10th 2013, Casa de Convalescència, Barcelona. (invited lecture)

11. Robert Kostecki, “Characterization of Interfaces and Interphases in Li-ion Systems with Far- and Near-Field Optical Probes,” *FIRST International Symposium Innovation of Energy Storage Device by Interdisciplinary Synergy*, January 17-18, 2013 Tokyo, Japan. (invited lecture)
12. Syzdek, V. Zorba, X. Mao, R. Russo, and R. Kostecki, "Ultrafast Laser Spectroscopy of Electrode/Electrolyte Interfaces," *PRiME 2012*, October 7-12, 2012, Honolulu, Hawaii.
13. Norberg, S. Lux, I. Lucas, J. Syzdek, and R. Kostecki, "*In situ* Fluorescence Spectroscopy of Interfacial Processes in High-Energy Li-ion Batteries," *PRiME 2012,* October 7-12, 2012, Honolulu, Hawaii.
14. Kim, C. Alexander, N. Norberg, R. Kostecki, and J. Cabana, “Study of the Factors that Enable Carbon-Free Insulating Li-Ion Battery Electrodes,” *PRiME 2012,* October 7-12, 2012, Honolulu, Hawaii.
15. Kostecki, I. Lucas, N. Norberg, and J. Syzdek, “Materials and Interfaces Degradation in High-Energy Cathodes for Li-ion Batteries,” *PRiME 2012,* October 7-12, 2012, Honolulu, Hawaii. (invited lecture)
16. S. Lux, I. Lucas, J. Chevalier, T. Richardson, and R. Kostecki, “Time-Dependent Determination of HF Formation in $LiPF_6$-Containing Electrolytes by Spectroscopic Ellipsometry,” *PRiME 2012,* October 7-12, 2012, Honolulu, Hawaii.
17. I. Lucas, J. Syzdek, S. Lux, N. Norberg, A. McLeod, Z. Fei, D. Basov, and R. Kostecki, “Scanning Near-Field Infrared Microscopy of a $Li_xFePO_4$ Single Particle,” *PRiME 2012,* October 7-12, 2012, Honolulu, Hawaii.

# VI.F.4 *In situ* Electron Microscopy of Electrical Energy Storage Materials (ORNL)

**Raymond R. Unocic**
Oak Ridge National Laboratory

Center for Nanophase Materials Sciences
One Bethel Valley Road
PO Box 2008, MS-6064
Oak Ridge, TN 37831
Phone: (865) 574-0096; Fax: (865) 576-5413
E-mail: unocicrr@ornl.gov

Start Date: January 2010
Projected End Date: September 2013

## Objectives

- The primary objective of this research is to develop the tools and methodology to conduct *in situ* electron microscopy studies of electrical energy storage materials using a microfluidic electrochemical cell and the transmission electron microscope (TEM) as the experimental platform.
- The key benefits of this characterization method include the ability to: 1) wholly contain and image through volatile organic liquid electrolytes; 2) perform controlled nanoscale electrochemistry experiments within the high vacuum environment of the TEM column; and 3) image electrochemical processes at high spatial and temporal resolution.

## Technical Barriers

- The technical barrier is the present lack of advanced electron microscopy based materials characterization methods that allow for the direct visualization of electrochemical processes during electrochemical charge-discharge cycling.

## Technical Targets

- Develop *in situ* characterization technique and methodology to investigate dynamically evolving electrochemical reaction mechanisms. Use this method to perform detailed *in situ* TEM experiments on the following subjects:
  - Investigate the dynamics of solid electrolyte interphase (SEI) formation mechanisms in relevant electrode/electrolyte systems.
  - Investigate dendrite nucleation and growth mechanisms.
  - Fabricate thin film electrodes of relevant electrode materials and perform electrochemical cycling feasibility studies.

## Accomplishments

With the development of a microfluidic electrochemical liquid cell for *in situ* TEM, we have gained insight into:

- The dynamics of SEI formation mechanisms, including tracking the growth of the SEI at the natural graphite anodes and organic liquid electrolyte interfaces during cell discharge.
- The nucleation and growth mechanisms of lithium dendrites during electrodeposition conditions.
- The electrochemical cycling behavior of thin film electodes deposited on small-scale electrochemical microchip devices.

✧ ✧ ✧ ✧ ✧

## Introduction

The direct visualization of electrochemical reactions that occur in Li-ion batteries necessitates the development of alternative *in situ* characterization methodologies and is absolutely critical if we are to further our fundamental understanding into a range of transport phenomena that occur within batteries. TEM, combined with diffraction and spectroscopic capabilities is a characterization technique that enables the unmatched ability to image and analyze the structure and chemistry of materials at multiple length scales. Recently, *in situ* TEM methods have been developed and used for Li-ion battery research to study the structural evolution in nanowire electrodes during Li intercalation. These experiments were facilitated by the use of TEM vacuum-compatible, ionic liquid-based electrolytes as a medium for Li-ion transport in an open cell configuration. Most commercial Li-ion battery electrolytes have a high vapor pressure and would rapidly evaporate when placed into the high vacuum environment of the TEM column if used in the same experimental setup; therefore, the main experimental

challenge for simultaneously conducting quantitative electrochemical measurements and imaging the resultant reactions depends upon the ability to image through highly volatile Li-ion battery liquid electrolyte while testing under realistic electrochemical conditions. This is the ultimate goal of this project.

## Approach

In this program, we have developed an electrochemical liquid cell for *in situ* TEM studies of electrochemical reactions that take place in electrical energy storage systems. The core challenge of preventing the evaporation of volatile organic liquid electrolytes is overcome by sealing the liquid electrolyte between thin electron transparent viewing membranes. The general concept for conducting *in situ* TEM characterization is as follows: MEMS based silicon microchip devices containing a central thin electron transparent silicon nitride ($SiN_x$) viewing membrane are stacked upon one another and placed withing the tip of a precision-machined TEM holder. Liquid electrolyte is delivered through the TEM holder with a microfluidic delivery system to fill the gap between the $SiN_x$ membranes. Gold or platinum biasing contacts that are deposited onto the lower chip/window of the cell serve as a platform for attaching battery electrodes and for interfacing with an external potentiostat for electrochemical testing. A 500nm thick spacer material patterned on the upper chip controls the thickness of the liquid electrolyte layer in the cell.

## Results

***In situ* environmental cell (ec)-TEM Characterization of the SEI.** The *in situ* electrochemical cell was used to visualize the dynamics of SEI formation. Natural graphite was used as the anode and lithium metal as the counter electrode. Figure VI - 209A shows an image of the natural graphite within the electrochemical cell, imaged without any electrolyte. Figure VI - 209B shows the same region of the graphite electrode when 1M $LiPF_6$ EC:DEC is present in the cell during discharge to 1.75V. Here we observe the dynamics of SEI formation and growth.

***In situ* ec-TEM Characterization of Dendrite Nucleation and Growth Mechanisms.** Understanding the mechanisms of dendrite formation in lithium ion batteries is critical. We utilize the *in situ* electrochemical cell to image dendrite nucleation and growth and quantitatively measure dendrite growth kinetics. Figure VI - 210A – Figure VI - 210B are false-colored bright-field TEM micrographs depicting dendrite growth from a gold working electrode. The dendrites were grown by electrodeposition using cyclic voltammetry in a 1.2M $LiPF_6$ EC:DMC electrolyte.

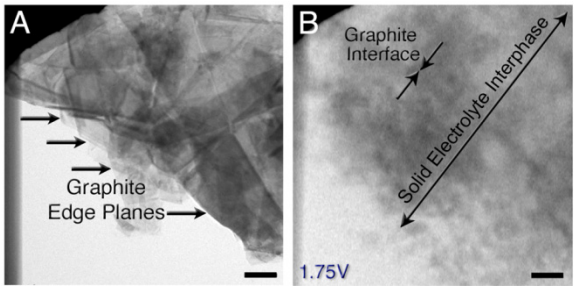


**Figure VI - 209: A) Bright-field TEM image of natural graphite anode between two electron transparent SiN membranes within the electrochemical cell. B) Extracted frame-shot of the same region showing SEI growth**

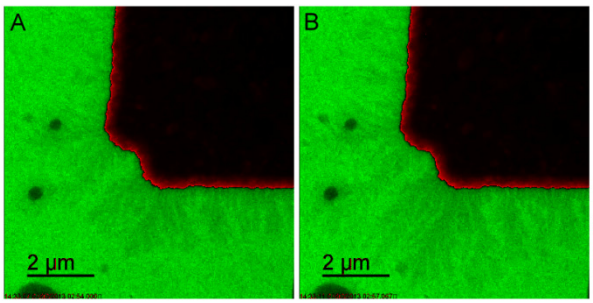


**Figure VI - 210: *In situ* observations of dendrite nucleation and growth from a gold working electrode in a 1M $LiPF_6$ EC:DMC electrolyte**

**Thin Film Device Fabrication and Electrochemical Cycling.** RF Magnetron sputtering techniques have been used to deposit thin film electrode materials directly on the microfabricated electrochemical microchip devices. Figure VI - 211A shows the size scale of the electrochemical microchip with the top portion covered with a thin layer Cu-Sb anode material. Figure VI - 211C – Figure VI - 211D shows bright-field TEM image and selected area electron diffraction pattern from the $SiN_x$ viewing region of the cell and shows that the sputtered thin films are nanocrystalline in nature. Figure VI - 211E is the electrochemical discharge-charge profile of the "on-chip" microbattery. Continued research in this direction has demonstrated the feasibility to deposit thin film electrode materials for a wide range of anode and cathode chemistries ($Li_4Ti_5O_{12}$, $LiMn_2O_4$, $LiMn_{1.5}Ni_{0.5}O_4$, etc) directly on the microchip device for *in situ* experimentation.

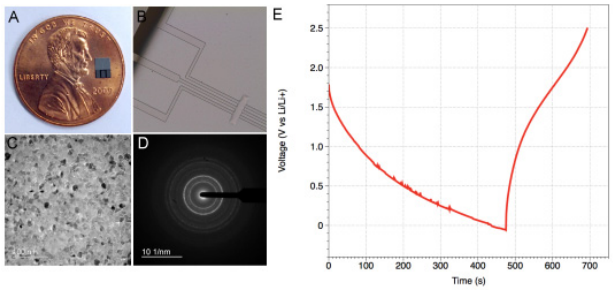


**Figure VI - 211: *In situ* observations of dendrite nucleation and growth from a gold working electrode in a 1M $LiPF_6$ EC:DMC electrolyte**

## Conclusions and Future Directions

The *in situ* electrochemical liquid cell microscopy technique is a versatile characterization method that is useful for characterizing dynamically evolving electrochemical processes in battery grade liquid electrolytes. With this method, it is possible to visualize the dynamics of electrochemical proceses such as SEI formation, dendrite nucleation and growth and degradation mechanisms in electrode materials. In future work, this system will be used to study the influence of electrolyte additives on SEI formation and dendrites and the lithiation/delithiation behavior of relevant electrode materials.

## FY 2013 Publications/Presentations

1. Unocic RR, Baggetto L, Sacci RL, Veith GM, Dudney NJ, More KL, "*In situ* Electron Micrscopy of Electrical Energy Storage Materials," DOE VTO Annual Merit Review and Peer Evaluation Meeting, Arlington, VA, May 2013.
2. Unocic RR, Sacci RL, Dudney NJ, More KL, "Quantitative *In situ* Electrochemical Liquid Cell Characterization of SEI Formation in Lithium Ion Batteries." Microscopy and Microanalysis Annual Meeting, Indianapolis, IN, August 2013.
3. Unocic RR, "Development and Application of *In situ* Electrochemical Cell TEM Methods for Electrical Energy Storage Research," Electron Microscopy Laboratory and the Hitachi Electron Microscopy (HEMIC) Product Development Centre at the National Institute for Nanotechnology, Edmonton, Canada, June 2013.

**Submitted Publications:**

1. Unocic RR, Sun XG, Adamczyk LA, Alsem DH, Salmon NJ, Dai S, Dudney NJ, More KL, "Visualizing SEI Formation in Li-ion Batteries with *In situ* ec-TEM," (2013).
2. Sacci RL, Dudney NJ, Veith GM, More KL, Browning ND, Unocic RR, "Direct Visualization of Dendrite Nucleation and Growth Kinetics with *in situ* ec-TEM," (2013).
3. Unocic RR, Baggetto L, Unocic KA, Veith GM, Dudney NJ, More KL, " Probing Materials Chemistry in Liquid Enviornments with *In situ* Liquid Electron Energy Loss Spectroscopy," (2013).

# VI.F.5 Microscopy Investigation on the Fading Mechanism of Electrode Materials (PNNL)

**Chong-Min Wang**
Pacific Northwest National Laboratory

Environmental Molecular Sciences Laboratory
902 Battelle Boulevard, Mail Stop K8-93
Richland, WA 99352
Phone: (509) 371-6268; Fax: (509) 371-7866
E-mail: Chongmin.wang@pnnl.gov

Start Date: July 1, 2013
Projected End Date: September 30, 2016

## Objectives

- Develop *ex situ*, *in situ*, and *operando* high-resolution transmission electron microscopy (TEM) and spectroscopy to probe the fading mechanism of electrode materials
- Probe the structural and chemical evolution of interfaces between the electrode and electrolyte
- Directly correlate structural and chemical evolution with battery performance to guide the design of new materials.

## Technical Barriers

- Capacity and voltage fading of Li-ion batteries
- Materials with a theoretical high capacity that cannot be fully extracted in practical use.

## Technical Targets

- Develop new *ex situ*, *in situ, and operando* TEM diagnostic techniques for directly probing the structural evolution of electrode and interfaces
- Identify the quantitative correlation of the structural and chemical change with the fading and failure of Li-ion batteries

## Accomplishments

- Use *in situ* TEM to study mesoscale structure change of silicon nanoparticles wrapped by conductive polymer
- Discovered that capacity/voltage fading of $Li_{1.2}Ni_{0.2}Mn_{0.6}O_2$ cathode is closely related to the corrosion and fragmentation of material
- Discovered that Ni segregation in the $Li_{1.2}Ni_{0.2}Mn_{0.6}O_2$ is directly related to the capacity and voltage fading.

## Introduction

Most previous microscopic investigations on the structural/chemical evolution of electrode materials and the solid-electrolyte interphase (SEI) layer formation have been either *ex situ* studies or used low-vapor-pressure/solid electrolytes for *in situ* TEM studies. Therefore, these results do not reveal fully detailed dynamic information under practical conditions. It is necessary to develop new *operando* characterization tools to characterize the structural/chemical evolution of electrode and SEI formation and electrode/electrolyte interaction using a practical electrolyte. This will be critical for making new breakthroughs in this field. The success of this work will increase the energy density of Li-ion batteries and accelerate market acceptance of electrical vehicles (EV) and plug-in hybrid electrical vehicles (PHEV) as described by the *EV Everywhere* Grand Challenge proposed by DOE/EERE.

## Approach

Extend and enhance the unique *ex situ* and *in situ* TEM methods for probing the structure of Li-ion batteries, especially for developing a biasing liquid electrochemical cell that uses a real electrolyte in a nano-battery configuration. Use various microscopic techniques, including *ex situ*, *in situ*, and especially the *operando* TEM system, to study the fading mechanism of electrode materials in batteries. This project will be closely integrated with other research and development efforts on high-capacity cathode and anode projects in the BATT Program to 1) discover the origins of voltage and capacity fading in high-capacity layered cathodes and 2) provide guidance for overcoming barriers to long cycle stability of silicon (Si)-based anode materials.

## Results

**1. Mesoscale *in situ* TEM study of Si nanoparticles wrapped in a conductive polymer.** In this study, we studied the lithiation characteristics of two types of Si-nanoparticle (Si-NP)-based electrodes at the mesoscale using *in situ* TEM. The functional composite unit well represents structural changes of the whole electrode

during cycling as shown in Figure VI - 212. The Si-NP conductive polymer composite anode exhibits excellent electrochemical cycling stability and high energy density, which are attributed to a good and sustained electrical contact between the Si-NP and the surrounding conductive polymer because of the resilient bonding between the two. On the other hand, a conventional Si-NP based anode is obviously not good at establishing and maintaining good electrical contact between the Si-NPs and the additives. Typically, Si-NPs that are not in contact with the acetylene black additive carbon cannot be lithiated during cycling. *In situ* TEM observations directly pinpoint the failure mechanism of the conventional Si composite as compared with Si-NP conductive polymer composite anode, which agrees well with available electrochemical performance data. The present results serve as an excellent example for linking mesoscale phenomenon with the properties of the real device.

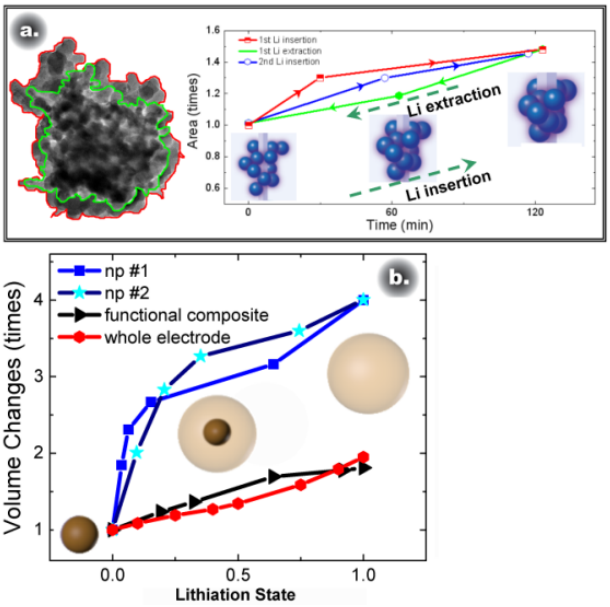


**Figure VI - 212: (a) Comparison of the starting fresh state and lithiated state of the SCP anode and plot of the measured areas of the anode in the TEM image acquired at different times (b) Comparison of the volume expansion of the whole electrode, functional composite, and single NP. The inset drawing in panel (b) shows structure changes of the single Si-NP during the lithiation process**

**2. Capacity/voltage fading of $Li_{1.2}Ni_{0.2}Mn_{0.6}O_2$ cathode is closely related to the corrosion and fragmentation of material.** The Li- and Mn-rich (LMR) layered cathode materials exhibit very high discharge capacities that exceed 250 mAh/g and are very promising cathodes. However, significant barriers, such as voltage fade and low rate capability, still need to be overcome before these materials can be used in practical applications. A detailed study of the mechanisms of voltage/capacity fading will be beneficial for further tailoring the electrode structure and, thus, improving the electrochemical performance of these layered cathodes. Detailed studies of structural changes of the LMR layered cathode $Li[Li_{1.2}Ni_{0.2}Mn_{0.6}O_2]O_2$ after long-term cycling were undertaken using aberration-corrected scanning transmission electron microscopy (STEM) and electron energy loss spectroscopy (EELS). The results are shown in Figure VI - 213. The fundamental findings provide new insights into the mechanisms of capacity/voltage fading of Li[Li0.2Ni0.2Mn0.6]O2. A sponge-like structure and fragmented pieces were found on the surface of the cathode after extended cycling. Formation of $Mn^{2+}$ species and reduced Li content in the fragments leads to the significant capacity loss during cycling. These results also imply the functional mechanism of surface coatings; for example, $AlF_3$, which can protect the electrode from etching by acidic species in the electrolyte, suppress cathode corrosion/fragmentation, and thus improve long-term cycling stability

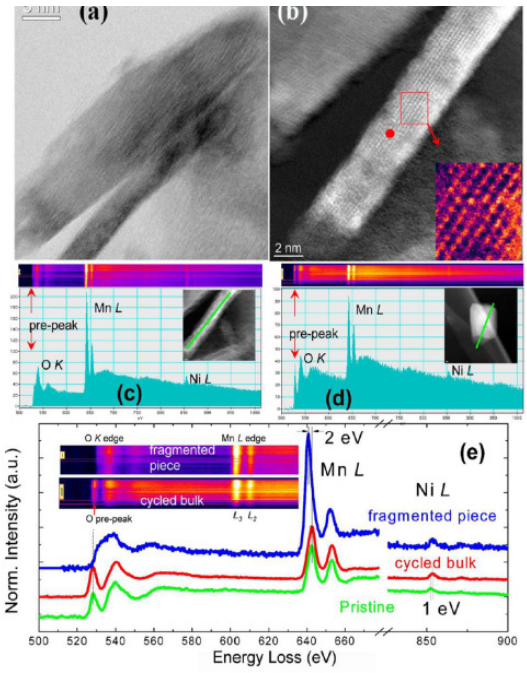


**Figure VI - 213: (a) Bright-field image showing lattice fringes in this region. (b) Z-contrast image showing the destroyed electrode structure (the inset shows a magnified view of the region within the red rectangle. 2D map and EELS spectra of the core edges of O K, Mn L, and Ni L by EELS line scan from (c) fragmented piece and (d) cycled bulk. (e) Comparison of the O-K, Mn-L, and Ni-L edges of the fragmented piece, and the cycled bulk and pristine materials**

**3. Direct correlation of Ni segregation in $Li_{1.2}Ni_{0.2}Mn_{0.6}O_2$ to the capacity and voltage fading.** State-of-the-art energy dispersive x-ray spectroscopy (EDS) in aberration corrected STEM was used to map the spatial distribution of chemical species in the $Li[Li_{0.2}Ni_{0.2}M_{0.6}]O_2$ cathode. A direct correlation of Ni segregation with the capacity fading characteristics of the battery has been established as illustrated in Figure VI - 214. Collective experimental evidence has indicated that, for the LMR layered composite cathode materials, local cation ordering and distribution play key roles in the battery performance. However a direct demonstration of the correlation of cation distribution with the electrochemical performance has not been established. In this task, a newly developed x-ray energy dispersive spectroscopy (XEDS) system, aberration-corrected STEM), and EELS were used to investigate the effects of cation distribution and local crystal structure on the performance of a typical LMR cathode (i.e., $Li[Li_{0.2}Ni_{0.2}M_{0.6}]O_2$) prepared by different approaches. The uniqueness of the new EDS system is high collection efficiency (~10 times more efficient than the traditional one), which enables direct observation of trace elemental segregation. The results reveal that materials prepared by co-precipitation and sol-gel approaches exhibit obvious Ni segregation at certain crystallographic surface and grain boundaries of the particles. Materials with Ni segregated show poor rate capability and fast capacity degradation, which is attributed to the bulk structural instability and deteriorated electrode/electrolyte interface that result from side reactions between highly active $Ni^{4+}$ at the particle surface and the electrolyte at high voltage. On the other hand, the material prepared by the hydrothermal assisted approach shows significantly improved Ni/Mn cation uniformity and reduced Ni segregation, which could explain its excellent cycling performance and enhanced rate capability.

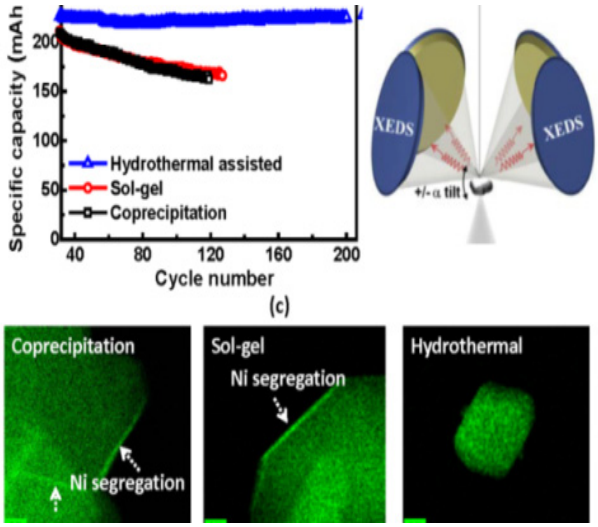


**Figure VI - 214. Direct correlation of capacity fading of the $Li[Li_{0.2}Ni_{0.2}M_{0.6}]O_2$ cathode with the Ni distribution. (a) Specific capacity as a function of cycle numbers for $Li[Li_{0.2}Ni_{0.2}M_{0.6}]O_2$ prepared by three different methods. (b) Schematic drawing showing the newly developed 4-detector system in a TEM, which enables efficient collection of the EDS signal. (c) EDS mapping showing Ni segregation in $Li[Li_{0.2}Ni_{0.2}M_{0.6}]O_2$ prepared by different methods. The work is done in collaboration with FEI Company in Hillsboro, Oregon**

## Conclusions and Future Directions

A combination of *ex situ* and *in situ* TEM and STEM techniques were used to study the structural and chemical evolution of both anode and cathode materials for Li-ion batteries, such as Si nanoparticle wrapped in a conductive polymers for the anode and $Li(Ni_{0.2}Mn_{0.6}Li_{0.2})O_2$ for the cathode.

Lithium insertion into Si is an interface-controlled process. Transformation of a-$Li_xSi$ to c-$Li_{15}Si_4$ is a congruent process that is solely controlled by Li concentration and is not accompanied by large-scale atomic migration and phase separation. Formation of c-$Li_{15}Si_4$ is favored because the electronic structures of c-$Li_{15}Si_4$ and a-$Li_{3.75}Si$ are similar. The conductive polymer deforms consonantly to accommodate the volume change of the Si-NPs, resulting in the excellent cycling capability of the material. We discovered that dopant may selectively segregate in $Li(Ni_{0.2}Mn_{0.6}Li_{0.2})O_2$, which will affect the Li-ion transport; and, therefore, the charge/discharge rate of battery. The layer to spinel phase transformation, corrosion, and segmentation are the main factors that contribute to the capacity and voltage fading of the cathode. Furthermore, the capacity/voltage fading of the cathode also is closely related to the distribution of Ni, typically Ni surface segregation leads to fast capacity/voltage fading.

Future work will focus on: (1) Investigate the fundamental characteristics of the SEI layer on a Si anode and its correlation with the chemistry of electrolyte as well as the battery fading mechanism. Different types of Si-based materials will be studied. (2) Investigate the cathode electrolyte interface structure and phase stability of $Li(Ni_{0.2}Mn_{0.6}Li_{0.2})O_2$). *In situ* TEM will be used to directly observe the characteristics of $Li(Ni_{0.2}Mn_{0.6}Li_{0.2})O_2$-electrolyte interface structures with respect to different electrolyte additives and surface coatings. The future work will intend to answer questions such as: What is the structure between the cathode particle and the electrolyte, and how does this structure evolve during Li-ion transport? How does the phase transformation happen? How does electrolyte additive affect the phase stability and the interface structure and their correlation with the voltage and capacity stability?

## FY 2013 Publications/Presentations

1. Jianming Zheng, Meng Gu, Jie Xiao, Pengjian Zuo, Chong-Min Wang, and Ji-Guang Zhang, "Corrosion/Fragmentation of Layered Composite Cathode and Related Capacity/Voltage Fading during Cycling Process," Nano Lett. 13, 3824−3830 (2013).
2. Meng Gu, Xing-Cheng Xiao, Gao Liu, Suntharampillai Thevuthasan, Donald R. Baer, Ji-Guang Zhang, Jun Liu, Nigel D. Browning, and Chong-Min Wang, "Mesoscale Origin of the Enhanced Cycling-Stability of the Si-Conductive Polymer Anode for Li-ion Batteries," Sci. Rep., 2013, in press.
3. M Gu, B Li, W Wang, V Sprenkle, CM Wang, "*In situ* Analytical Electron Microscopy Study of the Lithiation of TiO2 Nanowires Used in Li-Ion Batteries Microscopy and Microanalysis 19 (S2), 1102-1103 (2013).

4. CM Wang, M Gu, Z Wang, F Gao, JG Zhang, DR Baer, S Thevuthasan, N Browning, J Liu, "*In situ* TEM Study of Lithiation of Si and Phase Transformation," Microscopy and Microanalysis 19 (S2), 1468-1469 (2013)

# VI.F.6 NMR and Pulse Field Gradient Studies of SEI and Electrode Structure (Cambridge U.)

**Clare Grey**
Cambridge University

Department of Chemistry
Lensfield Road
Cambridge, CB2 8BJ
Phone: +44(1223)336509; Fax: +44(1223)336362
E-mail: cpg27@cam.ac.uk

Start Date: October 2012
Projected End Date: September 2016

## Objectives

- Identify major solid electrolyte interphase (SEI) components, and their spatial proximity, and how this changes with cycling.
- Contrast SEI formation on Si vs. graphite and high voltage cathodes.
- Correlate $Li^+$ diffusivity in particles and composite electrodes with rate.
- Investigate local structural changes of high voltage/high capacity electrodes on cycling.

## Technical Barriers

Capacity fade due to significant SEI formation (focusing on Si); Reduced rate performance due to SEI formation; High energy density; High power

## Technical Targets

- Specific power 300 W/kg,
- 10 year life,
- < 20% capacity fade

## Accomplishments

- Used solid state nuclear magnetic resonance (NMR) spectroscopy to determine the extent of ordering in high voltage $Li(Ni_{0.5}Mn_{1.5})O_4$ spinels and correlated this with performance
- Used NMR and diffraction based methods to investigate layered oxides within the $Na_xNi_{x/2}Mn_{1-x/2}O_2$ ($2/3 \leq x \leq 1$) system to determine cation ordering and the nature of stacking.
- *In situ* $^7Li$ and $^6Li$ NMR studies of working batteries have been performed to investigate paramagnetic cathode materials. Initial studies have focused on $Li_{1.08}Mn_{1.92}O_4$ and have shown that the method can be used to detect changes of lithium transport within the electrode, *in situ.* Variable temperature *in situ* NMR studies have been used to examine the effect of temperature on Li dynamics and Mn dissolution.
- Established protocol for investigating SEI in Si with multinuclear NMR spectroscopy

✧ ✧ ✧ ✧ ✧

## Introduction

The formation of a stable SEI is critical to the long-term performance of a battery, since the continued growth of the SEI on cycling/aging results in capacity fade (due to Li consumption) and reduced rate performance due to increased interfacial resistance. Although arguably a (largely) solved problem with graphitic anodes/lower voltage cathodes, this is not the case for newer, much higher capacity anodes such as silicon, which suffer from large volume expansions on lithiation, and for cathodes operating above 4.3 V. Thus it is essential to identify how to design a stable SEI. The SEI study will be complemented by investigations of local structural changes of high voltage/high capacity electrodes on cycling focusing on new *in situ* NMR methodologies and methods developed to study paramagnetic materials.

## Approach

- Multinuclear NMR of local structure.
- *In situ* and *ex situ* NMR studies of $Li^+$ transport and structural changes
- Pulse Field Gradient (PFG) measurements of electrolyte diffusivity and tortuosity
- SIMS and XPS of SEI composition

## Results

**1. Ordering in layered $Na_xNi_{x/2}Mn_{1-x/2}O_2$ ($2/3 \leq x \leq 1$):** A series of layered cathode materials within the $Na_xNi_{x/2}Mn_{1-x/2}O_2$ ($2/3 \leq x \leq 1$) system were synthesized by solid-state methods and their long and short-range structure was investigated by combining X-ray diffraction (XRD) and NMR spectroscopy.[1] A transition

from P2 to O3 stacking was observed at $x$>0.8 when samples were made at 900°C, which was accompanied by disordering of ions in the transition metal layer. This cation order/disorder could be clearly observed via the $^{23}$Na NMR spectra of these materials (Figure VI - 215), a very broad $^{23}$Na signal being observed for the O3 materials.

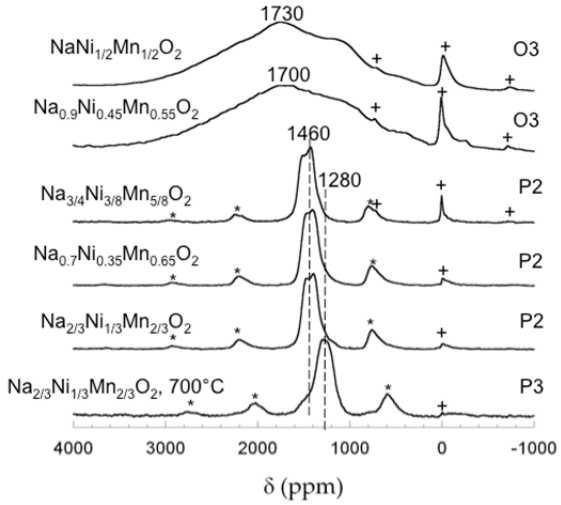


**Figure VI - 215: 23Na MAS NMR spectra of the NaxNix/2Mn1-x/2O2 series. All the samples were prepared at 900°C unless noted**

At $x$=2/3, both the P2 and a P3 structures were observed, depending on the synthesis temperature. Na/Li exchange led to structures with octahedral or tetrahedral coordination of the alkali metal. The transition from alkali metal prismatic coordination to octahedral/tetrahedral involves $[TMO_6]_\infty$ layer shearing that induces structural disorder through the formation of stacking faults. These results help the understanding of how these materials operate as Na and Li-ion batteries. This project was performed in collaboration with BATT PI's J. Cabana and M. S. Whittingham. Studies are currently being performed on related materials with BATT PI Y. S. Meng. $^{23}$Na NMR studies on the new battery material sidorenkite were performed in collaboration with BATT PI G. Ceder.[2]

**2. Application of *In situ* NMR studies to study lithium-ion mobility in paramagnetic cathode materials – application to Li.** A new NMR methodology has been applied to study the cathode, $Li_{1+x}Mn_{2-x}O_4$ (chosen as a model cathode material to develop the technique).[3] This is challenging primarily due to three factors: (1) The resonance lines are broadened severely; (2) spectral analysis is made more complicated by bulk magnetic susceptibility (BMS) effects, which depend on the orientation and shape of the object under investigation; (3) the difficulty in untangling the BMS effects induced by the paramagnetic and metallic components on other (often diamagnetic) components in the system. In an important finding, the BMS induced shift was minimized by orienting the cell at an angle of 54.7°, facilitating the interpretation of the *in situ* NMR spectra of a working battery containing paramagnetic electrodes. Importantly, the NMR spectra (Figure VI - 216) were shown to be highly sensitive to changes of Li dynamics and cation ordering as the battery was cycled, and two-phase reactions vs. solid solutions could be separated in this system. The method is now being used to examine how dynamics varies as a function of temperature.

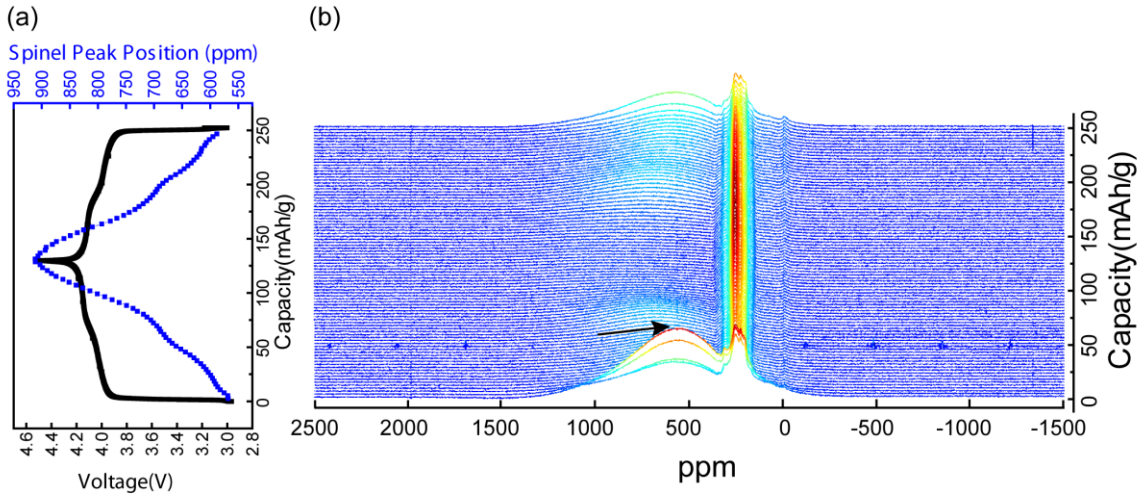


**Figure VI - 216: *In situ* 7Li static NMR spectra for the first cycle of an Li1.08Mn1.92O4 vs. Li/Li+ bag cell. (a) Voltage profiles and Li1.08Mn1.92O4 isotropic shifts vs. capacity plots. (b) Stacked plot of the 7Li spectra. The *in situ* cell was cycled galvanostatically with a C/50 rate between 3.0 and 4.5 V during the spectral acquisition. Note the increase of intensity following 50% Li extraction (at the end of the 1st process) consistent with cation ordering**

**3. Silicon and its SEI** Work has focused on the development of a new approach to allow *in situ* NMR spectroscopy of Si nanomaterials to be performed. The method allowed multiple cycles to be performed, which had not been possible in previous work, allowing the processes that occur in the 2nd cycle involving the amorphous phase to be explored.

A second focus was to develop a robust NMR methodology with which to monitor SEI formation. To this end $^{13}C$ experiments have been performed with $^{13}C$ enriched electrodes DMC and EC. Finally, PFG methods have been performed during diffusion through the electrodes, with a long-term goal to extract tortuosity as a function of cycle number.

The $^{13}C$ NMR studies of the enriched carbonate electrodes have been initiated. Since the focus has been on establishing a protocol and identifying key SEI components, studies with FEC and VC have not yet been initiated. These will be commenced in the next quarter. The work to determine the voltage at which key breakdown products are formed will continue, along with comparison studies with FEC and VC additives. The effect of cycle number on reversible capacity will continue to be explored. New Si coatings have been explored electrochemically and with NMR studies.

## Conclusions and Future Directions

The work described here has established and applied new NMR methodologies that are sensitive to cation dynamics (Li and Na) of a battery while cycling. Cation arrangements and their implications for the electrochemical cycling of layered materials have been investigated.

Major products in the Si SEI have been identified and the focus is now on identifying all the different components, when they are formed and whether they are stable on cycling. Future work will include an investigation of additives and Si coatings.

## FY 2013 Publications/Presentations

1. J. Cabana, N. A. Chernova, K. A. Aldi, J. Xiao, M. Roppolo, M. S. Whittingham and C. P. Grey, "Study of the Transition Metal Ordering in Layered $Na_xNi_{x/2}Mn_{1-x/2}O_2$ (2/3 <= x <= 1) and Consequences of Na/Li Exchange," *Inorganic Chem.istry*, **15**, 8540 – 8550 (2013).
2. H. -L. Chen, Q. Hao, O. Zivkovic, G. Hautier, L. -S. Du, Y.-Z. Tang, Y. –Y. Hu, X. –H. Ma, C. P. Grey, G. Ceder, "Sidorenkite ($Na_3MnPO_4CO_3$): A New Intercalation Cathode Material for Na-Ion Batteries," *Chem. Mater*., **25**, 2777-2786 (2013).
3. L. Zhou, M. Leskes, A. J. llott, N. M. Trease, and C. P. Grey, "Paramagnetic electrodes and bulk magnetic susceptibility effects in the *in situ* NMR studies of batteries: Application to $Li_{1.08}Mn_{1.92}O_4$ spinels," *J. Magn. Reson.,* **234**, 44 – 57 (2013).

# VI.F.7 Chemical and Structural Gradients in Composite Electrodes (LBNL)

**Jordi Cabana**
Lawrence Berkeley National Laboratory.

Department of Chemistry[13]
University of Illinois at Chicago
845 W Taylor Street
Science and Engineering South (MC 111)
Chicago, IL 60607
Phone: (312) 355-4309
E-mail: jcabana@uic.edu

Start Date: September 2011
Projected End Date: July 2013

## Objectives

- Enable higher energy density Li-ion batteries by informing the design of optimized electrode architectures that maximize active material utilization and charge density.
- Establish correlations between inhomogeneities in local states of charge (SOC), pore structure and inactive component distribution in commercially relevant electrodes.
- Understand the role of phase transformations within active materials vis-à-vis utilization and durability.

## Technical Barriers

Low energy-density, poor cycle life, safety.

## Technical Targets

- PHEV: 96 Wh/kg, 5,000 cycles
- EV: 200 Wh/kg; 1,000 cycles.

## Accomplishments

- Establish the validity of using *operando* bulk X-ray diffraction (XRD) to study the formation of chemical gradients in thick NMC composite electrodes.
- The first maps of local SOCs in commercially relevant materials were produced.
- Determined changes during delithiation of new fluoride phases using *operando* bulk XRD.

✧ ✧ ✧ ✧ ✧

## Introduction

The quest for gains in energy density that fulfill cost and safety requirements constitutes a major thrust in Li-ion battery research. These gains can be brought about through a reduction of the dead weight in the battery by optimizing the architecture of the system. This approach is attractive from the technological perspective because it involves engineering changes within the current material space. Thus, in principle, it is also free of the time constraints that occur from materials discovery to implementation.

In Li-ion batteries, the dual transport of electrons and ions required to complete an electrochemical reaction is achieved with a 50-100 μm thick, porous composite of the redox active material, a conductive additive and a polymeric binder. The energy density of the device can be raised by increasing the mass loading of active material per unit area in the electrode, either by reducing the ratio of support components or by reducing electrode porosity through calendaring methodologies (or both). Thick, additive-free electrodes in the form of sintered pellets have reportedly been cycled successfully, albeit at low to moderate rates. However, what appear to be trivial changes actually constitute a significant challenge. Reducing the amount of carbon and binder can lead to structures that have lower mechanical stability against the continued particle volume changes that occur during cycling. In turn, thick electrodes and/or low porosity result in depletion of ionic carriers within the composite structure. The reason is that the paths for electrolyte wetting become longer due to the effect of pore tortuosity. As a result, the gains in energy density are offset by significant losses in the power capability of the electrode. Indeed, a few studies have demonstrated that the active materials currently considered have inherently higher rate capabilities than

[13] Current affiliation and mailing address.

when employed in "real life" electrodes, clearly pointing at a bottleneck that goes beyond individual components.

While the limitations observed in current electrode designs are macroscopically well described, their origin needs to be clearly defined at multiple length scales (from nano to macro) if they are to be overcome. Differences in behavior between electrodes of different thickness must be related to disparate utilization with respect to the distance from the supply of ions (electrolyte) and electrons (current collector). Likewise, failure could be defined as the extent of disconnected regions and component shuffling. Both these effects lead to electrode inhomogeneity. Mathematical models of porous composite electrodes have been employed in order to explain macroscopic observations and predict long term behavior. These models are based on the simulation of the reaction distribution, i.e., the location of the electrode fractions that have undergone a redox transformation, for which little experimental observation exists. Therefore, experimental validation of this aspect in the models is not yet possible. This gap is particularly important when considering that currently available models fail to account precisely for the poor behavior of thick electrodes. Apart from the impossibility of visualizing local SOCs in an electrode, another factor in this discrepancy is the difficulty of experimentally quantifying pore size, distribution and tortuosity in order to provide input parameters for the models. In their absence, these parameters are fit during the simulations, or a semi-empirical value is introduced. However, this approach can lead to serious deviations between predictions and macroscopic observations. As 3D models of porous composite electrodes are being developed, the need for experimental data will be accentuated.

This project aims to provide input for models that accurately predict battery degradation, as well as inform electrochemical engineers in their optimization of designs that increase energy storage while preserving power performance. Changes in porosity, component distribution and utilization with manufacturing procedures (e.g., calendaring, mixing protocols) will be revealed. Further, our work will identify modes of failure associated with processes that occur in buried regions, such as the creation of internal isolated portions.

## Approach

Use spectroscopic and diffraction techniques to monitor the reactions involved in battery electrodes. Use synchrotron-based spectromicroscopy tools to probe porous composite electrodes at high chemical and spatial resolution, in 2D and 3D. Develop methodologies that rely on less sophisticated techniques to probe inhomogeneities in battery electrodes. Correlate chemical and morphological information.

## Results

**Validation of *operando* XRD as a tool to probe in-depth gradient formation in NMC electrodes.** In collaboration with the Battaglia and Srinivasan groups in BATT at LBNL, a baseline cathode material of relevance to battery engineering was identified as the system of study for this project. The choice was $LiNi_{1/3}Co_{1/3}Mn_{1/3}O_2$ (NCM333, hereafter); electrodes of different thickness were provided by the Battaglia group. The electrochemical properties of these electrodes are being evaluated both experimentally and computationally by the Battaglia and Srinivasan groups.

*Operando* XRD was performed on a series of NCM333 electrodes of different thickness (from 50 to 150 μm). The experiments were performed at beamline 11-3 at the Stanford Synchrotron Radiation Lightsource (SSRL), at SLAC National Accelerator Laboratory. Data were acquired after the X-ray beam was transmitted through the electrochemical cell, which consists of a standard coin cell with a very small window (~1 mm diameter) that is covered with conductive tape. The small size of the window minimizes concerns over pressure gradients. Consequently, to a first approximation, the collected patterns represent an average of the composition of the composite cathode in depth. These data are, thus, amenable to comparison and fit using continuum models pioneered by the Srinivasan group. In the case of a material undergoing a second-order phase transformation (i.e., solid solution mechanism) such as NCM, a continuous shift of the XRD peaks, with no new reflections appearing, is expected.

Figure VI - 217 shows the electrochemical profile of the *operando* cell using a 150 μm NCM333 electrode, together with selected XRD patterns at relevant points of the reaction. After an initial charge to 4.3 V at 1C rate, the cell was relaxed for 100 min. XRD patterns were collected every 2 minutes during these processes. As expected, a smooth shift of the peaks, indicative of a solid solution mechanism of Li deintercalation, was observed during charge. However, such shift was accompanied by a significant increase in peak width, indicative of the formation of compositional in-homogeneities in the electrode. This observation appears to be in contradiction with the fact that a homogeneous electrochemical potential is expected throughout the electrode when the reaction follows such mechanism. More importantly, an evolution of the peak width and position was observed during cell rest, indicating that compositional relaxation was occurring in the electrodes.

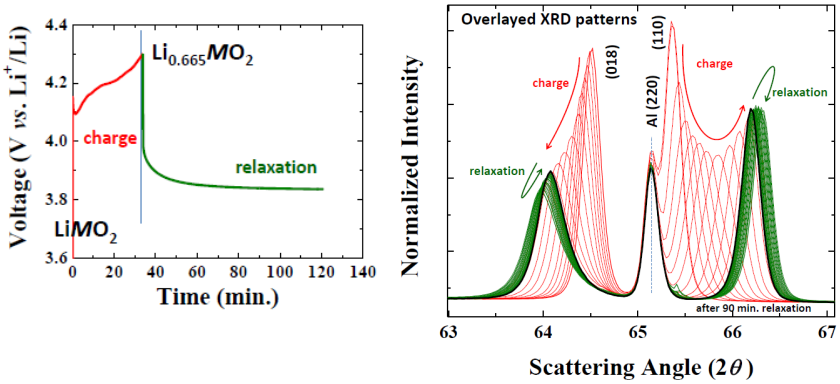


**Figure VI - 217: (Left) Voltage vs. time trace of an operando XRD cell with Li metal and NCM333 electrodes. (Right) Selected patterns taken during operation of the cell**

The study of 150 µm thick NCM333 electrodes was complemented by comparing the data in Figure VI - 217 with a different set collected at C/10, instead. While a continuous evolution of the XRD peaks was observed during relaxation after the 1C charge, the peaks remained unchanged during relaxation after a charge at C/10. This observation provides further support to the conclusion that a fast charge in such thick composite electrodes results in the buildup of in depth chemical gradients due to kinetic limitations imposed by inhomogeneous carrier transport. When thinner (50 µm) electrodes with very low porosity were used instead, the gradients became so significant that peak splitting, mimicking what would occur in a first order transition, were observed. They are indicative of areas that are not supplied with a sufficiently high concentration of ions to let the reaction proceed.

**Detection of reaction homogeneities in NCM333 using microprobe spectroscopy.** The electrode SOC based on transition metals can be obtained by measuring the oxidation state of these metals using X-ray absorption spectroscopy (XAS). Through the use of a beamline like 2-3 at SSRL, the X-ray probe can be focused down to 2 µm, so that spectra can be collected at many points within a composite electrode. This methodology can thus be used to build chemical maps of local SOCs. Figure VI - 218, top, shows an *ex situ* chemical map of the cross section of a 150 µm thick NCM333 electrode harvested after a charge to 4.3 V at 3C. The current collector was located at the bottom in the image. This map was produced by collecting µ-XAS at the Ni K edge. The energy of the beam was set at a discrete number of energies in the vicinity of the edge, at values where the spectroscopic difference between pristine and oxidized material is largest. The intensity at these points was normalized by collecting maps above and below the edge. Separately, full spectra were collected at selected points (Figure VI - 218, bottom right) to confirm the trends in the map. The results indicated the existence of areas in the electrode that did not charge (oxidize, red) as effectively as the rest. Contrary to what would be expected based on porous electrode theory of materials reacting through solid solutions, such as NCM333, there is no homogenization of the composition when the electrochemical potential is removed. This effect could be an indication of poor electrical connection of the domain, an early sign of a possible source of failure upon extended cycling.

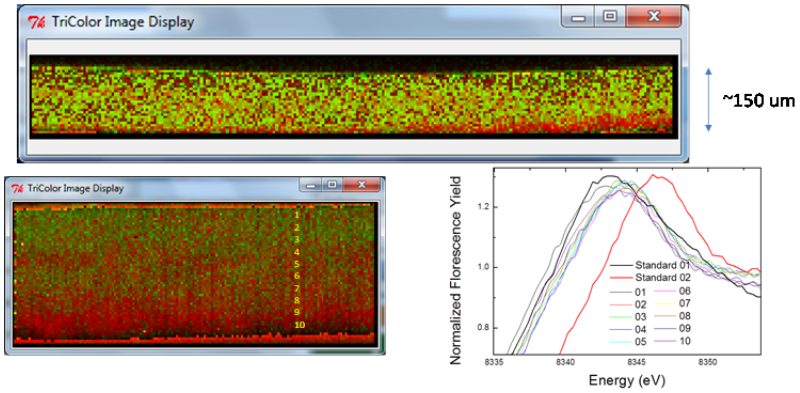


**Figure VI - 218: (Top) Ni K edge µ-XAS of the cross-section of a NMC333 electrode charged to 4.3 V at 3C. (Bottom) Zoom-in of the top image, indicating the points where individual full spectra were collected (right)**

***Operando* XRD study of new fluoride phases synthesized in the Cathode effort.** The goal in this sub-task was to provide characterization insights into new compounds identified under a separate Cathode task by the same PI. Following the general theme of the task, the role of the phase transformations occurring upon delithiation will be tied to the properties of the materials and their durability in composite electrodes.

During FY2013, electrodes based on of alkali metal iron fluorides such as $KFeF_3$ (Figure VI - 219) were evaluated. Despite the low crystallinity of the material due to the need to aggressively mill with carbon to achieve electrochemical activity, it was possible to observe a shift to lower angles of the peaks during charging. This shift was indicative of removal of $K^+$ through a solid solution mechanism. This removal was found to be reversible.

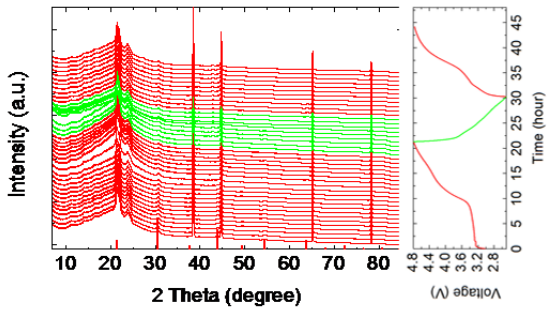


**Figure VI - 219: Operando XRD data of a Li metal cell with a KFeF3 working electrode**

## Conclusions and Future Directions

During FY2013, proof of concept was established of the value of simple *operando* XRD experiments to detect the generation of gradients in SOC of commercially relevant NCM333 electrodes. These gradients were found to aggravate with cycling rate. Using μ-XAS, their localization could be ascertained. It was found that they form in close proximity of the current collector and do not always homogenize when the circuit is open, indicative of poor ionic connectivities. In parallel to this tool development effort, characterization of the phase transformations of alkali metal transition metal fluorides synthesized by the same group under a Cathode project was undertaken. Electroactivity was confirmed for a variety of phases, such as $KFeF_3$.

This project was closed on July 2013 due to the relocation of the Principle Investigator to the University of Illinois at Chicago. Thus, there are no future directions to be discussed.

## FY 2013 Publications/Presentations

1. "High resolution chemical imaging of phase transformations during intercalation reactions," *Pacific Rim Meeting on Electrochemical and Solid State Science (PRiME) 2012,* October 7th-12th, 2012, Honolulu, HI (USA).
2. "Multiscale phase transformations in battery electrodes: visualization and consequences," *ALS-CXRO Seminar,* Lawrence Berkeley National Laboratory, February 27th, 2013, Berkeley, CA (USA).
3. "Study of the factors that enable carbon-free insulating Li-ion battery electrodes," *International Battery Association Meeting: IBA2013*, March 10th-15th, 2013, Barcelona (Spain).
4. "High resolution chemical imaging of phase transformations during electrochemical reactions," *2013 MRS Spring Meeting*, April 1st-5th, 2013, San Francisco, CA (USA).
5. Kim, N. S. Norberg, C. T. Alexander, R. Kostecki and J. Cabana, *Adv. Funct. Mater.*, **23**, 1214 (2013).
6. C. Kim, R. Buonsanti, R. Yaylian, D. J. Milliron and J. Cabana, *Adv. Energy Mater.*, **3**, 1286, (2013).
7. P. F. Teh, S. S. Pramana, C. Kim, C.-M. Chen, C. H. Chuang, Y. Sharma, J. Cabana and M. Srinivasan, *J. Phys. Chem. C*, 2013, Just Accepted, DOI: 10.1021/jp408762v.

# VI.G Beyond Lithium-Ion Battery Technologies

## VI.G.1 Novel Chemistry: Lithium Selenium and Selenium Sulfur Couple (ANL)

**Khalil Amine and Ali Abouimrane**
Argonne National Laboratory

Chemical Sciences and Engineering Division
9700 S. Cass Avenue, Building 205
Argonne, IL 60439-4837
Phone: (630) 252-3838; Fax: (630) 972-4440
E-mail: amine@anl.gov; Abouimrane@anl.gov

Start Date: October 2010
Projected End Date: September 2013

### Objectives

The proposed work has the following objectives:

- Solve the problems facing the new Li/Se battery system, such as low efficiency, high polarization, and poor cyclability through component optimization.
- Develop new battery design based on an improved mechanistic understanding and use of
  - enriched Se phases such as alpha-, beta-, or gamma-monoclinic or gamma trigonal phase and
  - $Se_xS_y$ compounds that decrease the battery cost and increase the capacity.
- Design an effective electrode structure to allow for full capacity utilization:
  - Prepare different carbon-$Se_xS_y$ composites to optimize the electrochemical performance
  - Develop a method for morphology control of Se-containing cathode material, for example, nanotube or nanowire
- Optimize Na battery analogue.

### Technical Barriers

This project addresses the following technical barriers from the Energy Storage section of the Vehicle Technologies Program Multi-year Research, Development and Demonstration Plan:

- Cycle and calendar life performance: good cyclability with high coulombic efficiency is needed to meet the automotive requirement.
- Cost: High energy can significantly reduce cost.

### Technical Targets

USABC goals for electric vehicle: \$150/kWh, 230 Wh/dm$^3$, 1000 cycles with 80% capacity retention, and 10-year system life.

USABC goals for 40-mile plug-in hybrid vehicle: \$220/kWh, 193 Wh/dm$^3$, 5,000 discharge cycles with 75% capacity retention, and 15-year system life.

### Accomplishments

- Gained mechanistic understanding through advanced materials characterization techniques: *in situ* synchrotron high-energy X-ray diffraction (XRD) that monitors the crystalline phase changes during the electrochemical process.
- Adopted new electrolytes, such as ether-based electrolyte, instead of carbonate-based electrolyte to enable this new system.
- Tested different carbons (nanotubes, graphene, etc.) and different binders, such as PVDF, polytetrafluoroethylene (PTFE), or conductive polymer binders to improve cycle life.

✧ ✧ ✧ ✧ ✧

### Introduction

A new class of cathode materials based on selenium has been discovered for both lithium and sodium batteries Notably, unlike the existing Na/S batteries that only operate at high temperatures, these new Se-based electrodes are capable of cycling against Na at room temperature. The choice of selenium, which is a *d*-electron-containing member of Group 16 in the periodic table, is due to its higher electrical conductivity compared to sulfur, as well as its high theoretical capacity (678 mAh/g) and volumetric capacity (3268 mAh/cm$^3$). However, as a new battery system, some fundamental issues still need to be clarified. For example, the charge and discharge voltages evolve in

the Li/Se system during the initial cycles. Significant polarization occurs once the charge and dicharge voltages are stabilized after 5 cycles, which leads to a low roundtrip efficiency. In addition, the coulombic efficiency is quite low during the first 20 cycles. The mechanisms or underlying reasons for this unsatisfactory performance are still not well understood due to inadequate characterization on the battery materials during electrochemical cycling. In particular, the effects of organic electrolytes on both lithiation and delithiation of the Li/$SeS_x$ cells, if any, are still not clear, nor are the effects of the sulfur content in $SeS_x$. As the selenium-sulfur system has a rich phase diagram, we have found in the literature many selenium-sulfur composites, such as $Se_5S$, $Se_5S_2$, $Se_5S_4$, SeS, $Se_3S_5$, $SeS_2$ (commercially available), $SeS_7$, and $Se_{1.5}S_{10.5}$. These materials offer a capacity between 675 and 1550 mAh $g^{-1}$. Not only does the Se electrode show promising electrochemical performance with Li anodes, but the additional potential for mixed $Se_xS_y$ systems allows for tunable electrodes, combining the high capacities of S-rich systems with the high electrical conductivity of the d-electron-containing Se. Unlike the widely studied Li/S system, both Se and $Se_xS_y$ can be cycled to high voltages (up to 4.6 V) without failure in the GEN 2 electrolyte (1.2 M $LiPF_6$ dissolved in EC/EMC in 3:7 weight ratio). Their high densities and voltage output offer greater volumetric energy densities than S-based batteries, opening possibilities for new energy storage systems that can enable EVs and smart grids.

## Results

In this work we show that Se and Se-S represent an attractive new class of cathode materials capable of reacting with lithium ions with promising electrochemical performance. Furthermore and unlike existing Na-S batteries that operate only at high temperature, these new electrodes can cycle well in a Na battery system at room temperature. This is the first report of room temperature rechargeable lithium or sodium coupled with Se and Se-S systems. Not only does Se provide opportunities for developing new high performance batteries, including mixed chalcogenide-systems, but has the potential to enhance our fundamental understanding of batteries. The Se-C composite was used as the cathode material for cycling against lithium and Na. Elemental Se and multiwalled carbon nanotubes were combined (mass ratio 7 to 3) and mixed for one hour using high-energy ball miller. The mixture was pressed into a pellet and heated at 260ºC for 12 hours under an oxygen atmosphere. The weight loss was below 1% due to the low pressure vapor of selenium above its melting point (~10-2 torr at 260ºC). The Se-C composite had an electronic conductivity of 6.2 S•$cm^{-1}$.

The Li/Se-C cell was cycled between 0.8 V and 4.2 V at 50 mA/g, and its electrochemical behavior was found to differ from that of the Li/S system. If the latter system is charged to only 3.9 V, the voltage drops to 2 V, and the cell cannot cycle again. Figure VI - 220 and Figure VI - 221 show the capacity retention over 100 cycles and the voltage profiles for the 25th of the Li/Se-C system. A capacity of more than 300 $mAhg^{-1}$ was sustained for one-hundred cycles, with charge discharge efficiency higher than 99% (see Figure VI - 220). Inductively coupled plasma spectroscopy showed no variation in the amount of Se in the cathode with cycling from the 20th cycle.

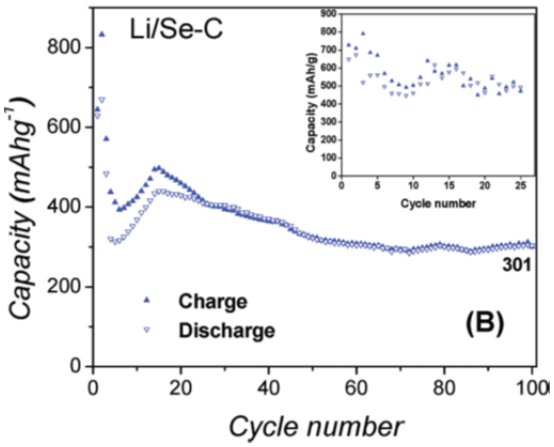


**Figure VI - 220: Cyclability of Li/Se−C system showing more than 300 $mAhg^{-1}$ as capacity**

These results can be explained by the fact that no further polyselenide dissolution in the electrolyte has happened. Furthermore, with regard to the reversibility of Li/Se-C system, we noticed, from the 50th cycle, essentially no variation in the charge/discharge capacities (Figure VI - 220) or in the cell voltage profile (Figure VI - 221). Even though the theoretical capacity of the Li /Se system based on the formation of $Li_2Se$ is only 675 mAh/g, much lower than that of the Li/S system (1675 mAh/g). However, the high density of Se (4.82 g/$cm^3$) versus S (2.07 g/$cm^3$) makes the volumetric capacity of these materials very close (~3,253 Ah/l for Se and ~3,467 Ah/l for S). Furthermore, we found that the Li/Se system delivers an output voltage at least 0.5 V higher than Li/S (Figure VI - 221) and thus could surpass the Li/S system in terms of volumetric energy density.

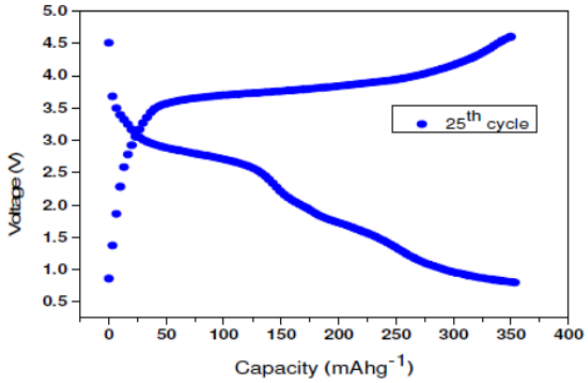


Figure VI - 221: Voltage profile of Li/Se–C system

To understand what happens during the lithium insertion and de-insertion in selenium, we performed pair density function (PDF) and *ex situ* x-ray diffraction (XRD) measurements for various states of discharge and charge at a low current rate of 10 mAh/g. During the Se reduction, one voltage plateau appears at 1.9 V. At 0.8 V, the capacity was about 650 mAh/g, which corresponds to 90% of the theoretical capacity based on the formation of $Li_2Se$ and traces of selenium being present, as observed by XRD and PDF measurement (Figure VI - 222).

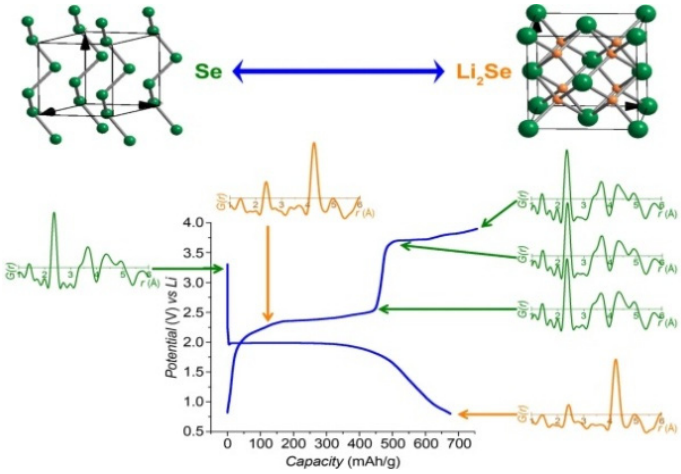


Figure VI - 222: PDFs for the pristine Se–C electrode and upon recovery from various states of discharge/charge. Structural representations of the Se and $Li_2Se$ (antifluorite) phases are shown at top

The PDF provides local and long-range structural information as a histogram of all atom-atom distances within a system, independent of crystallinity. Unlike conventional diffraction methods, it allows phases to be identified regardless of any changes in particle size (including nanoscale), particle morphology or structural order. PDFs for the pristine and recovered Li/Se materials are shown in Figure VI - 222. Refinement of a structure against the data obtained for pristine Se confirmed the tetragonal structure, with chains of Se atoms linked by Se-Se bonds of 2.36Å. For the Li/Se system, PDF results reveal that during the discharge (1.99V~240 mAh/g), $Li_2Se$ and Se are present.

Organic electrolytes are known to be important in $Li/O_2$ and Li/S batteries. We tested an ether-based electrolyte with our Li/Se system, as it has proven to be superior to the carbonate-based electrolyte. The results demonstrated that cell performance is significantly improved in terms of voltage profile and coulombic efficiency. The voltage profiles of these cells indicate that complete lithiation of Se to $Li_2Se$ is occurring through the formation of intermediate phases, i.e., $Li_2Se_n$ (Figure VI - 223). This behavior differs from the single-phase transition in the carbonate-based electrolyte, as reported earlier. This result clearly suggests that cell performance highly depends on the nature of the electrolyte. To better understand the relationship between the formation of the intermediate phases and voltage profile of the cells with the ether-based electrolyte, we performed an in-depth study by different characterization techniques, including high-energy X-ray diffraction (HEXRD) and X-ray absorption spectroscopy (XAS). The powerful capability of *in situ* HEXRD and XAS, available at the Advanced Photon Source (APS) at ANL, allowed us to monitor instantly the phase transition, the intermediate phases, and their oxidation states during cycling. We have proposed a mechanism behind the (de)lithiation processes for $Li/SeS_x$ cells, based on the results obtained from *in situ* X-ray absorption near edge structure (XANES) probes (Figure VI - 224). This work has helped us to better understand and correlate the formation of intermediate phases with the electrochemical performance of $Li/SeS_x$ cells, and shines new light on how to improve the cell

performance by tuning the electrolyte composition. Detailed analysis demonstrated that lithium polyselenides are formed during the charge and discharge process, and the formation and existence of the polyselenides in the electrolyte were further proved by end-product solubility tests.

During lithiation, the critical points (at 2.04 and 1.67 V) of the electrochemical process are well-correlated with the evolution of the XANES spectra. For example, the inflection point at 2.04V in the voltage profile coincides with the shift of the XANES spectrum to lower energy. The precipitous voltage drop at around 6-hour of discharging corresponds to the sudden appearance of the Se K-edge of $Li_2Se$. Generally, the energy position of the edge is determined as the maximum at the lowest energy of the first derivative of the XANES spectra. To determine the edge positions, we show the first derivatives of the XANES spectra in Figure VI - 224c. This plot shows that the Se edges are shifted significantly with (de)lithiation. When the cell is first discharged through the inflection point at 2.04 V, the edge shifts from 12,657.9 eV to 12,656.7 eV. In the following 3 hr (more than 300 mAh/g capacity), the edge positions do not change much and are accompanied by the voltage plateau around 2 V. When the cell is discharged to 1.67 V, the Se K-edge jumps to 12,660 eV, suggesting the formation of $Li_2Se$. During charge, the Se edges slowly shift back to lower energy. These observations indicate that polyselenides might have formed during the cycling, but in a non-crystalline state; hence, they are not detected by XRD.

In addition, excellent performance was demonstrated with the ether-based electrolyte in cell tests for 50 cycles (Figure VI - 225).

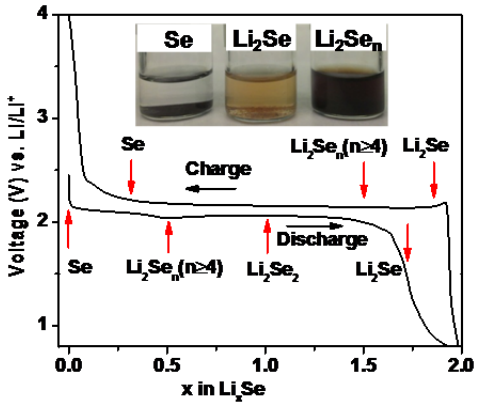


**Figure VI - 223: Representation of cathode phase evolution during charge and discharge of a Li/Se cell with an ether-based electrolyte**

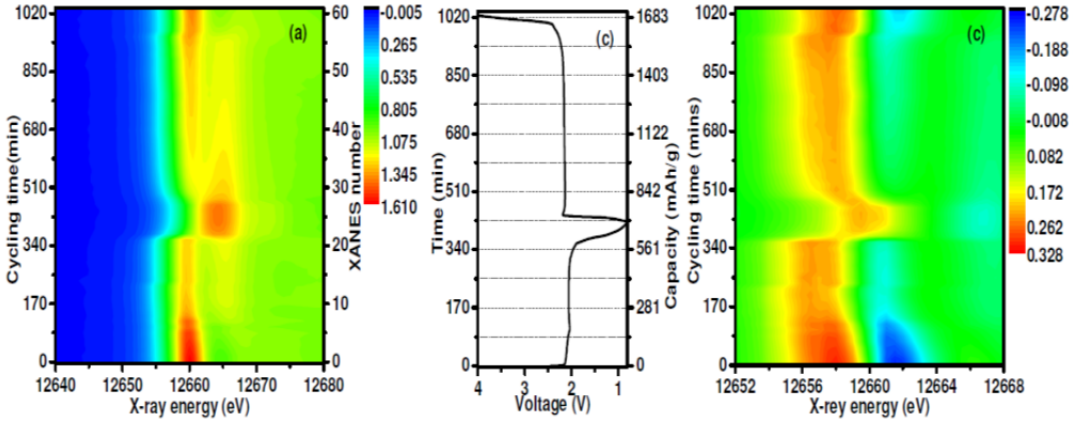


**Figure VI - 224: (a) Normalized XANES spectra of Li/Se cell during cycling, (b) battery voltage profile, and (c) derivative of normalized XANES spectra of Li/Se cell during cycling**

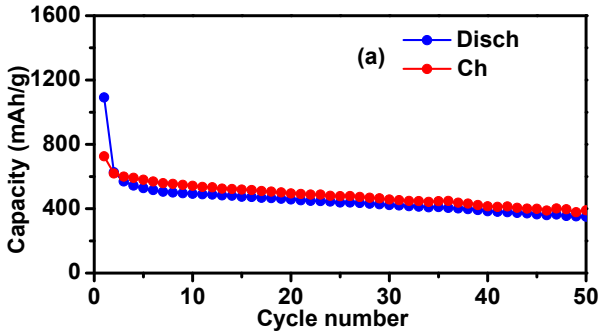


**Figure VI - 225: Cycle performance of Li/Se cell in ether-based electrolyte**

## Conclusions and Future Directions

In this project we demonstrated that Se-containing materials are promising cathode materials for high-energy-density battery applications, while system optimization is still needed. *In situ* XANES provided valuable information on the oxidation states of crystalline and amorphous phases, including intermediate species dissolved in the electrolyte. A mechanism for lithiation/(de)lithiation was obtained on the basis of a combination of *in situ* synchrotron X-ray techniques and electrochemical methods. We intend to adopt several strategies to prove that the Se-S/Li or Na system can exhibit long cycle life and be cost competitive with sulfur batteries. Our first strategy is to design a $SeS_2$ /carbon composite where carbon conductive matrix is closely linked to the $SeS_2$ particle to ensure continuous good electronic conductivity. We will also develop an electrode processing technology that allow for maximizing the $SeS_2$ active material in the electrode. Unlike S where over 65% of electrode is made of high surface area carbon and binder which are inactive, $SeS_2$ has high conductivity and therefore the inactive element in the electrode will be reduced and the energy at the electrode level will increase significantly.

## FY 2013 Publications/Presentations

1. Y. Cui, A. Abouimrane, J. Lu, T. Bolin, Y. Ren, W. Weng, C. Sun, V. A. Maroni, S. M. Heald, and K. Amine, J. Am. Chem. Soc. 2013, 135 (21), 8047.
2. Abouimrane, D. Dambournet, K.W. Chapman, P.J. Chupas, W. Weng, and K. Amine, J. Am. Chem. Soc. 2012, 134, 4505.
3. Y. Cui, A. Abouimrane, J. Lu, T. Bolin, Y. Ren, W. Weng, C. Sun, V. A. Maroni, S. M. Heald, and K. Amine, "(De)Lithiation Mechanism of Se-based Lithium Batteries Determined by *In situ* Synchrotron X-ray Probe," Extended Abstract #520, 224th Meeting of Electrochemical Society, San Francisco, CA, U.S., Oct. 27- Nov. 01, (2013).
4. Abouimrane, Y. Cui, and K. Amine, "Electrochemical Mechanism Study of Selenium-Based Rechargeable Lithium Battery," 6th International Conference on Advanced Lithium Batteries for Automobile Applications, Argonne, IL, September 9-11, (2013).
5. Abouimrane, D. Dambournet, K. W. Chapman, P. J. Chupas, W. Weng, Y. Cui, H. El Tayeb, and K. Amine, "Selenium and Selenium Sulfide − A New Class of Positive Electrode Material for Room Temperature Lithium and Sodium Rechargeable Batteries," Extended Abstract #335, 222nd Meeting of Electrochemical Society, Honolulu, Hawaii, U.S., October 7-12, (2012).

# VI.G.2 Development of Novel Electrolyte for Lithium Air (ANL)

**Khalil Amine and Jun Lu**
Argonne National Laboratory
Chemical Sciences and Engineering Division

9700 S. Cass Avenue, Building 205
Argonne, IL 60439-4837
Phone: (630) 252-3838; Fax: (630) 972-4440
E-mail: amine@anl.gov and junlu@anl.gov

**Larry Curtiss**
Argonne National Laboratory
Material Science Division
9700 S. Cass Avenue, Building 200
Argonne, IL 60439-4837
Phone: (630) 252-7380
E-mail: curtiss@anl.gov

Start Date: October 2010
Projected End Date: September 2013

## Objectives

- Develop stable electrolytes and new cathode architectures in lithium air batteries to lower the charge overpotential, improve the cell efficiency and cycle life.
- Understand the oxygen crossover effect at the anode on the electrochemical performance of Li-air battery.

## Technical Barriers

This project addresses the following technical barriers from the Energy Storage section of the Vehicle Technologies Program Multi-year Research, Development and Deomnstration Plan.

- **Unstable electrolytes**: electrolyte decomposition (in particular the carbonate-based electrolyte) in the presence of the reduced oxygen species, especially superoxide anion ($O_2^-$).
- **Inefficient cathode structure and catalysis**: Commonly used carbons and cathode catalysts do not access the full capacity of the oxygen electrode and cause significant charge overpotentials. This lowers power capability.
- **Lithium electrode poisoning** due to oxygen crossover and reaction with the electrolyte. This degrades cycle life.

## Technical Targets

The goal of this project is to enable Li-air battery for automotive applications. The targets are to achieve 300 cycles and an energy density of 600~700 Wh/kg. This will provide the necessary breakthroughs and a firm basis for follow-on optimization and incremental improvements.

## Accomplishments

- Enabled a new stable silicon-containing oligo(ethylene oxide) solvent 1NM3 for Li-air battery
- Developed a new nanostructured cathode architecture utilizing atomic layer deposition (ALD) technique to lower the charge overpotential and improve the efficiency of the Li-air cell.
- Investigated oxygen crossover effect at the anode of a Li-air battery from density functional studies and *in situ*/*ex situ* measurements.

✧ ✧ ✧ ✧ ✧

## Introduction

Li-air batteries can be considered the 'holy grail' of lithium batteries because they offer, in principle, at least ten times the energy density of conventional lithium-ion systems. The lithium-ion cell chemistry, the best to date, would provide a theoretical specific energy of ~900 Wh/kg if the calculation is based on the masses of the anode and cathode materials alone; in practice, 150-200 Wh/kg has been accomplished at the cell level. In contrast, a lithium-air cell, when discharged to $Li_2O_2$ at an average 3.1 V would provide a theoretical specific energy of 3623 Wh/kg, or when discharged to $Li_2O$ at the same voltage, 5204 Wh/kg. Note that gasoline (octane) offers a theoretical energy of ~13,000 Wh/kg if the mass of the injected oxygen is not considered in the calculation because it is supplied externally and combusted within, and exhausted from, the engine. By the same token, a lithium-air cell would offer a specific energy of ~11,000 Wh/kg if the 'free' oxygen supplied during discharge and released during charge is ignored in the calculation.

While the inherent energy potential of Li-air approaches that of gasoline, today's battery manufacturers have not yet been able to unlock this

potential. While today's lithium-ion batteries may provide acceptable power for hybrid electric vehicles (HEVs) and all-electric vehicles (EVs), they do not provide sufficient energy for an acceptable driving distance. This range limitation and the absence of a battery charging infrastructure have limited public interest in EVs. A breakthrough in Li-air battery technology would significantly increase the possibility of extending the electric range of these vehicles with the added advantages of reducing battery cost and weight.

This Li-air battery technology is still in its infancy and, no doubt, will require significant research efforts in a variety of fields to unlock its full potential. The successful implementation of non-aqueous Li-air cells has been hampered because of severe materials problems that have limited electrochemical performance: (1) the non-aqueous electrolytes are unstable at high potentials and are easily oxidized by the oxygen released during charge, thereby seriously limiting cycle life; (2) during discharge, the solid and insoluble $Li_2O_2$ and/or $Li_2O$ products are deposited on the surface or within the pores of the carbon cathode, thereby clogging the pores and restricting oxygen flow; (3) poisoning of the lithium electrode due to oxygen crossover destroys the integrity and functioning of the cell; and (4) commonly used cathode catalysts, such as $MnO_2$ or Mn metal, do not access the full capacity of the oxygen electrode or enable sufficiently high rates.

This team is working on problems that limit the electrochemical performance of the Li-air battery, including the stability of the organic electrolyte, cathode catalysts and structures, and stability of the lithium anode under oxygen-crossover conditions. This effort will lead to the development of a reversible lithium air battery that provides 10 times the energy density of the state-of-the-art lithium ion battery for powering EVs. The technology, if successful, can also benefit many military applications that require very high energy density such as satellite, military vehicles for silent watch and operation.

## Approach

This project addresses the current limitations of Li-air batteries through: (a) New electrolytes, based on siloxanes and ethers, that will be more stable than incumbent carbonates, (b) Catalytic activated carbons with an optimal pore size distribution that will create the maximum volumetric density of triple-phase boundaries, (c) Metal/metal oxide cluster catalysts, incorporated onto carbon support, that will promote formation of electronically-conductive superoxide species, and (d) Protected lithium, through a coated lithium powder anode and/or ceramic protection layer for a lithium foil anode that will reduce dendrite formation.

The experimental designs to create advanced electrolytes, carbons, catalysts, cathodes, and anodes was guided by theory and modeling and the experimental results were thoroughly analyzed with very sophisticated analytical techniques that were used to fine-tune the computational studies.

## Results

**Stable electrolytes for Li-air cells:** There is a wealth of experimental and theoretical evidence that the organic carbonates, e.g., propylene carbonate (PC), ethylene carbonate, and dimethyl carbonate, commonly used in Li-ion batteries are not stable toward the oxygen reduction products formed during Li-air discharge. It has been reported that, during discharge, in addition to formation of the desired lithium peroxide, propylene carbonate is decomposed, resulting in the formation of lithium carbonate and other organic species. Another challenge beside the decomposition of the electrolyte is the large overpotential observed in lithium air cell which affects both power and cycle life.

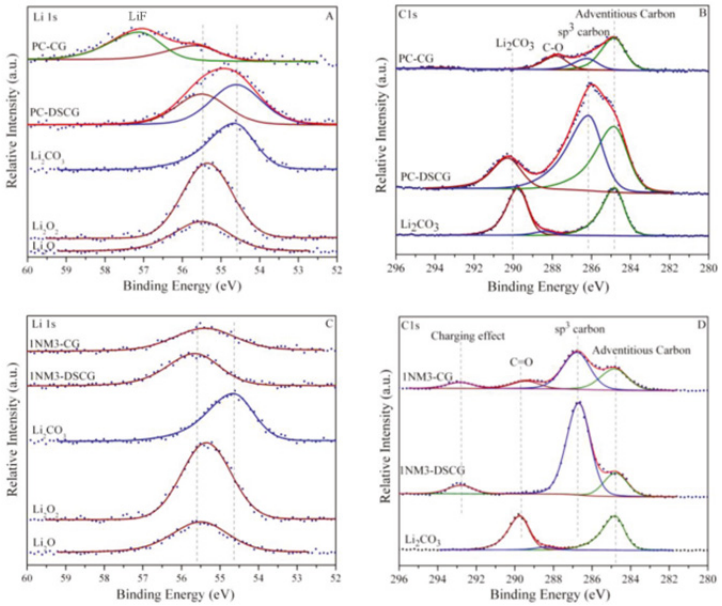


**Figure VI - 226: XPS spectra of Li 1s and C 1s core peaks of the cathode carbon electrodes after discharge and charge when using PC or 1NM3 as solvent in the electrolyte**

In order to understand the source of the large polarization observed in Li-air cell, we carried out a detailed investigation of the charge and discharge products formed in systems employing the PC based electrolyte. In this work we employed XPS as a primary tool to characterize the charge and discharge products, as shown in Figure VI - 226. The results indicated that $Li_2CO_3$ was the major product formed during discharge with only minor amounts of lithium oxides being formed. During the first charge cycle the $Li_2CO_3$ was decomposed based on the XPS data and is believed to be the primary cause of the large charge overpotential required for charging. This is due to the need to oxidize the carbonate or other materials rather than the formation of desired $Li_2O_2$. Density functional (DFT) calculations confirmed that PC is unstable to oxygen reduction species. As it stands, the cells based upon PC cannot be considered viable as the overall reaction appears to be oxidation of PC to $CO_2$.

In contrast, the silicon-containing oligo(ethylene oxide) compound 1NM3 was shown by DFT calculations to be more stable to the highly active oxygen reduction species when compared to PC. When 1NM3 is used in place of PC, the XPS data collected after single discharge (see Figure VI - 226c and Figure VI - 226d) show that only lithium oxides are formed and moreover they are partially decomposed upon charging. The increased stability of the 1NM3 solvent results in a significantly lower overpotential for the Li-air cell as shown in Figure VI - 227. We have to confirm that the product from charging in the 1NM3 is oxygen, but the lower overpotential could be due to the fact that oxidation of lithium oxides is easier that the oxidation of carbonate which is formed in the PC cells. Clearly, the electrolyte solvent stability plays a key role in the performance of Li-air batteries and will be a key factor in improving their efficiencies.

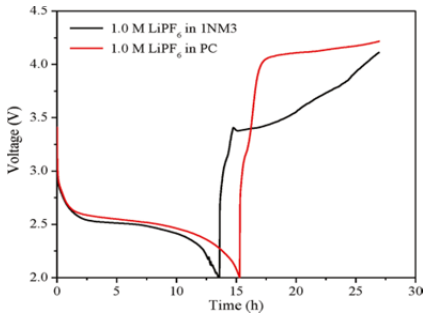


**Figure VI - 227: First charge and discharge cycles or a Li-air cell with propylene carbonate (PC) as and polylethylene oxide siloxane (1NM3) showing the reduced charge overpotential due to the stability of 1NM3 to oxygen reduction products**

While the stability during discharge found for the 1NM3 electrolyte is a key result, electrolytes that provide stability during charge as well as discharge are needed as well as ones that aid in reversibility of the reactions. Further work is underway to improve the reversibility of the system in the presence of this new electrolyte. However, one should comsider other factors that affect cycleability and charge overpotential before optimizing the full cell system. For instance we have found that the oxygen cross over can significantly degrade the lithium anode and affect the cycle life. We also found that the cathode structure can impact the efficiency of the cell.

**Nanostructured Cathode Architecture for Low Charge Overpotential in Li-$O_2$ Batteries:** There may be a number of other contributing factors for the large charge overpotentials other than the lack of an effective electrocatalyst. Poor electronic conductivity of $Li_2O_2$ may limit the charge process. Contaminants in the $Li_2O_2$ discharge product from electrolyte decomposition such as $Li_2CO_3$ may also cause a higher charge potential. The electrolyte decomposition may result from reaction of the electrolyte with defects on the carbon surface. Therefore, it may be possible to significantly lower the charge potential if solutions to the above problems can be discovered. We are able to demonstrate a conceptually new approach as illustrated in Figure VI - 228 based on a new cathode architecture for the Li-$O_2$ cells that shows promising results for solving the charge overpotential problem. The cathode architecture addresses the electrolyte decomposition problem with a porous carbon passivated by a protective $Al_2O_3$ coating applied by ALD. Very small Pd nanoparticles attached to the surface by ALD act as effective electrocatalysts (Figure VI - 229) and seem to promote formation of a nanocrystalline form of $Li_2O_2$ that provides good electronic transport.

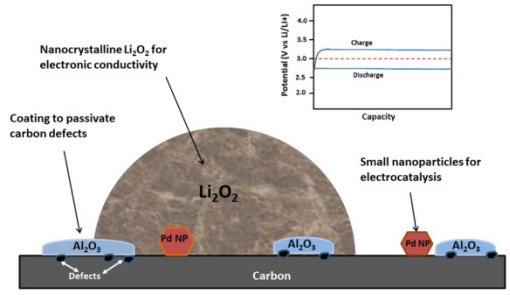


**Figure VI - 228: Schematic of the nanostructured cathode architecture shows the $Al_2O_3$ coating, the palladium nanoparticles and the nanocrystalline lithium peroxide, all of which contribute to lowering the overpotential. The inset shows a hypothetical charge/discharge voltage profile vs. capacity**

The resulting low charge overpotential is about 0.2 V, as shown in Figure VI - 230. The formation of lithium peroxide was confirmed by XRD and SEM as well as High Resolution Transmission Electron Microscopy (HRTEM) techniques. Computational modeling was used to provide insight into the role of the $Al_2O_3$ protective coating and the Pd nanoparticles for preventing electrolyte decomposition and catalyzing the lithium peroxide decomposition, respectively.

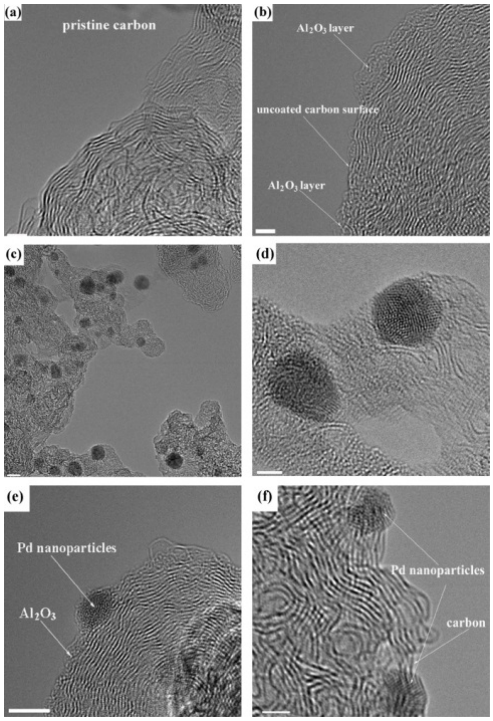


**Figure VI - 229: HRTEM of the cathode structure: (a) pristine Super P carbon (scale bar, 2nm); (b) carbon surface coated with 3 ALD cycles of $Al_2O_3$, (scale bar, 2nm); (c)-(f) carbon + 3 ALD cycles $Al_2O_3$ + 3 ALD cycles Pd nanoparticles, (scale bar for (c)-(f), 5nm, 2nm, 4nm, and 2nm respectively)**

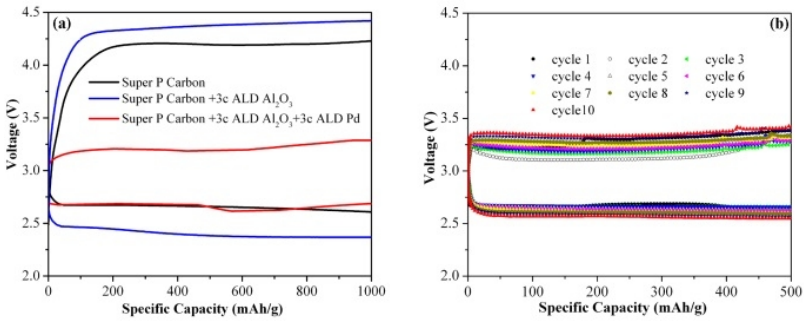


**Figure VI - 230: (a) Voltage profile during discharge-charge of cells (to 1000 mAh/g) based on super P carbon; super P carbon coated with $Al_2O_3$; and $Al_2O_3$ coated super P carbon further coated with Pd nanoparticles. (b) Voltage profile during discharge-charge of cells (to 500 mAh/g) based on $Al_2O_3$ coated super P carbon further coated with Pd nanoparticles. The electrolyte used is TEGDME-$LiCF_3SO_3$**

**Investigation of oxygen crossover effect at the anode:** The electrolyte chemistry occurring at the Li-anode in the presence of an oxygen crossover may play an important role in the cyclability and capacity of the Li-$O_2$ cells. It is of interest to investigate possible electrolyte decomposition mechanisms at the lithium anode especially in the presence of $O_2$ crossing over from the cathode and the possible effects on the performance of the Li-$O_2$ cell. In this work, the reductive stability of an ether-based electrolyte (tetraglyme) and subsequent reactions in an $O_2$ environment is addressed using *in situ*/*ex situ* high-energy X-ray diffraction (HE-XRD), and *ex situ* FT-IR techniques.

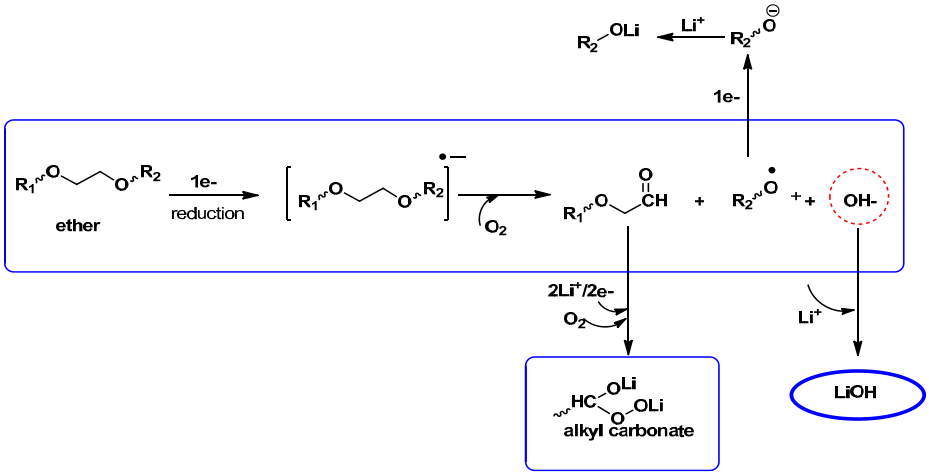


**Figure VI - 231: Scheme 1 Possible reaction mechanisms of decomposition of ethers to form LiOH and alkyl carbonates at the anode surface upon electron attachment and oxygen crossover**

In order to investigate potential products that are formed at the anode in a Li-air battery such as proposed in Scheme I (see Figure VI - 231), we have carried out a detailed characterization study of the anode in a Li-air cell during various stages of discharge and charge using a TEGDME-$LiCF_3SO_3$ electrolyte. Figure VI - 232b shows the charge and discharge profile for the cell for 4 cycles. The *in situ* XRD data is shown in Figure VI - 232a for the Li anode during the first four charge and discharge cycles. The peaks in the XRD spectra clearly show the formation of LiOH and a decrease in the Li (peak 110) metal on cycling. This suggests that an electrolyte decomposition reaction is occurring during charge at the electrolyte/Li surface with the hydrogen coming from the ether-based electrolyte and Li from the anode (which results in depletion of the Li metal). The *ex situ* XRD patterns in Figure VI - 233b for the anode after the first and tenth cycles provide clear evidence that the accumulation of LiOH is occurring on the anode and also the severe consumption of Li anode was taking place (evidenced by the absence of the (110) peak at the 10th cycle). This was further confirmed by FT-IR results from the anode after 10 cycles in Figure VI - 233a, which show an OH peak.

It is necessary to consider other possible sources of the species found on the anode. Another potential source of electrolyte decomposition could be the carbon cathode defect sites or by lithium peroxide surface. This could lead to the formation of LiOH or $Li_2CO_3$ on the

cathode. However, these solid species would not move across the membrane to the anode. Therefore the formation of LiOH at the anode is probably predominantly due to the oxygen crossover effect (a small percentage of LiOH may be from small amounts of water contaminants from the TEGDME or $LiCF_3SO_3$ salt). It is also noted that the TEGDME decomposition may lead to soluble products that could react further on the cathode or anode involving other reaction mechanisms.

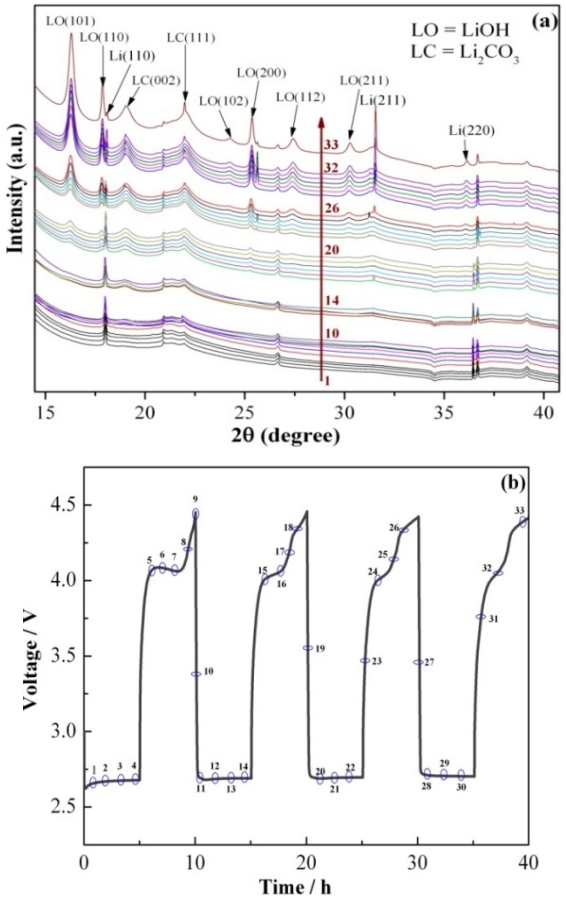


**Figure VI - 232: a) *In situ* XRD patterns of Li anode and LiOH formation during the operations conditions, and (b) corresponding voltage vs time profile. Numbers on XRD data correspond to those on voltage profile**

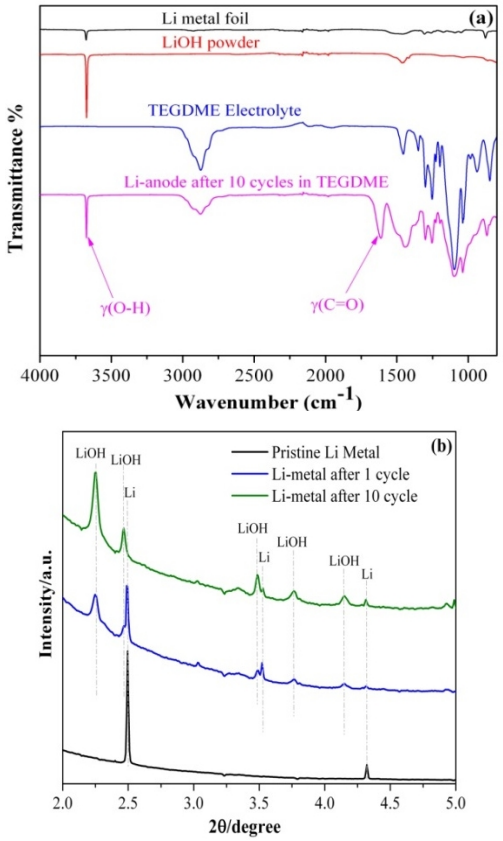


**Figure VI - 233: *Ex situ* FT-IR spectra of Li anode after 10 cycles and (b) HE-XRD patterns of the Li-anode after being cycled for 1 and 10 cycles. For the FT-IR spectra, we have included the standard Li metal, LiOH powder and TEGDME electrolyte for comparison**

## Conclusions and Future Directions

In this project, several approaches were developed to address the technical barriers for non-aqueous Li-air battery.

- New silicon-containing oligo(ethylene oxide) solvent 1NM3 was developed to lower the charge overpotential of the Li-air cell.
- New cathode utilizing palladium nanoparticles on a carbon surface with an alumina ALD coating for passivation of carbon defect sites was developed to lower the charge overpotential and improve the efficiency of the Li-air cell.
- Demonstrate that the crossover of $O_2$ from the cathode to the anode in Li-air cells will result in different decomposition reactions occurring at the Li-anode than occur in at a lithium anode in a Li batteries. The evidence indicates formation of LiOH as well as carbonates at the anode in a Li-$O_2$ battery with a tetraglyme-

based electrolyte. Thus, controlling reactions of ethers at the lithium anode through suitable membranes or passivation films will be essential for achieving good performance of Li-$O_2$ cells based on ether electrolytes

Future research will focus on further developing new electrolytes and novel catalysts to lower the charge overpotential and increasing the cycle life of the Li-air battery. We will also develop model systems to understand the mechanism of formation and dissociation of lithium peroxide using size-selective metal cluster catalyst.

## FY 2013 Publications/Presentations


1. Jun Lu, Yu Lei, Kah Chun Lau, Xiangyi Luo, Peng Du, Jianguo Wen, Rajeev S. Assary, Ujjal Das, Dean Miller, Jeffrey W. Elam, Hassan M. Albishri, D. Abd El-Hady, Yang-Kook Sun, Larry A. Curtiss, Khalil Amine, "A Novel Nanoscale Cathode Architecture for Low Charge Overpotentials in Li-$O_2$ Batteries," *Nature Commun. 4*, 2383, **2013**.
2. Jun Lu, Yan Qin, Peng Du, Zonghai Chen, Yang Ren, Tianpin Wu, Jeffery T. Miller, Jianguo Wen, Dean J. Miller, Zhengcheng Zhang and Khalil Amine, "*In situ* fabrication of porous-carbon-supported α-$MnO_2$ nanorods at room temperature: application for rechargeable Li–O2 batteries" *Energy and Environmental Science*, 6, 519-531**,** **2013**.
3. Jun Lu, Rajeev S. Assary, Peng Du, Xiangyi Luo, Xiaoyi Zhang, Yang Ren, Larry A. Curtiss and Khalil Amine, "The Effect of Oxygen Crossover on the Anode of a Li–$O_2$ Battery using an Ether-Based Solvent: Insights from Experimental and Computational Studies" *ChemSusChem*, *6(1)*, 51-55, **2013**.
4. Jun Lu, Peng Du, Kah Chun Lau, Xiangyi Luo, Javier Bareño, Xiaoyi Zhang, Yang Ren, Zhengcheng Zhang, Larry A. Curtiss, Yang-Kook Sun and Khalil Amine "Compatibility of lithium salts with solvent of the non-aqueous electrolyte in Li–$O_2$ batteries" *Phys. Chem. Chem. Phys., 15*, 5572-5581, **2013**.
5. Jun Lu, Hun-Ji Jung, Kah Chun Lau, Zhengcheng Zhang, John A. Schlueter, Peng, Du, Rajeev S. Assary, Jeffrey Greeley, Glen A. Ferguson, Hsien-Hau Wang, Jusef Hassoun, Hakim Iddir, Jigang Zhang, Lucia Zuin, Yongfeng Hu, Yang-Kook Sun, Bruno Scrosati, Larry A. Curtiss, and Khalil Amine, Evidence for Magnetism in Lithium–$O_2$ Discharge Product. *ChemSusChem.*, *6(7)*, 1196-1202, **2013**.
6. Jun Lu, Yan Qin, Peng Du, Xiangyi Luo, Tianpin Wu, Yang Ren, Jianguo Wen, Dean J. Miller, Jeffrey Miller and Khalil Amine, "Synthesis and Characterization of Uniformly Dispersed $Fe_3O_4$/Fe Nanocomposite on Porous Carbon: Application for Rechargeable Li-$O_2$ Batteries" *RCS Adv.*, 3, 8276-8285, **2013**, (DOI: 10.1039/C3RA40451J)
7. Jun Lu, Yu Lei, Xiangyi Luo, Tianpin Wu, Yang Ren, Jeffery T. Miller, Jeffery Elam and Khalil Amine, "Synthesis of Porous Carbon Supported Pd/PdO Nanoparticles by Atomic Layer Deposition: Application for Rechargeable Li-air Battery" *Nano Letter*, 13 (9), 4182-4189, **2013**.
8. Jun Lu, "*In situ* Fabrication of Porous-carbon-supported α-$MnO_2$ Nanorods at Room Temperature: Application for Rechargeable Li-O2 Battery," 2013 APS/CNM/EMC Users Meeting, Argonne National Laboratory, IL, May 6-9, 2013. (Invited Talk)
9. Jun Lu, "Metal Oxide Prepared by a Wet-Chemistry Approach: Application for Rechargeable Li-$O_2$ Battery," 7th U.S.-China Electric Vehicle and Battery Technology Workshop, Lawrence Berkeley National Laboratory, Berkeley, California, April 4-5, 2013. (Invited Talk)

# VI.G.3 Integrated Lab-Industry Research Project. (LBNL, ANL)

**Marca Doeff[1], Jordi Cabana[1], John T. Vaughey[2]**
Lawrence Berkeley National Laboratory

[1]Environmental Energy Technologies Division
1 Cyclotron Road, MS62R0203
Berkeley, CA 94720-8168
E-mail: mmdoeff@lbl.gov

[2]Chemical Sciences and Engineering Division
9700 S Cass Avenue
Argonne National Laboratory
Lemont, IL 60439
E-mail: vaughey@anl.gov

Participants:
Guoying Chen, Tom Richardson, Robert Kostecki, Marca Doeff, Gao Liu, John Kerr, Vince Battaglia, Nitash Balsara, Robert Kostecki, Vassilia Zorba, Brian Ingram, Aude Hubaud, D. Schroeder (NIU)

Start Date: August 2010
Projected End Date: September 2013

## Objectives

- Design, synthesize and characterize solid lithium ion conductors that enhance the cycle life of lithium metal based anodes.
- Search for phases with high Li-ion conductivity that are stable against lithium.
- Improve the mechanical properties of the prospective layers using ceramic composites.

## Technical Barriers

Energy density, poor cycle life (incompatibility with electrolyte, dendrite formation) and safety.

## Technical Targets

- PHEV: 96 Wh/kg, 5,000 cycles.
- EV: 200 Wh/kg; 1,000 cycles.

## Accomplishments

- Sintered cubic LLZO ($Li_7La_3Zr_2O_{12}$) to a relative density of 94% at a considerably lower temperature than previously reported.
- Established that the processing conditions strongly affect the morphology and impurity formation in the sintered pellets. These properties, in turn, have a significant impact on the electrochemical properties.
- Determined the mechanism of Al(III) doping of LLZ via a combination of $^{27}Al$ MAS-NMR and high resolution XRD.
- Isolated and determined the ionic conductivity of the low temperature cubic polymorph of LLZ.
- Determined processing conditions for $Li_{1.3}Ti_{1.7}Al_{0.3}(PO_4)_3$ that alter the grain boundary phases and increase the conductivity by an order of magnitude.

✧ ✧ ✧ ✧ ✧

## Introduction

One important challenge to the development of rechargeable batteries for large format applications such as electric vehicles is to increase their practical energy density. Successful use of lithium metal as the negative electrode would enable a very high energy density device, especially when coupled with a high capacity positive electrode such as air or sulfur. There are, however, serious safety concerns due to the extreme reactivity of metallic lithium with most liquid electrolytes. The use of a solid electrolyte is considered one way to enable a metallic lithium electrode, provided that the criteria of high conductivity and chemical stability are met. Among the ceramic electrolytes that have been studied, the garnet $Li_7La_3Zr_2O_{12}$ (LLZO) is promising due to its fast ion transport and purported good chemical stability against metallic lithium. Two polymorphs of this material have been described. The high temperature cubic phase is reported to have an ionic conductivity two orders of magnitude higher than that of the tetragonal phase, but high temperature synthesis (above about 1000ºC) and the presence of small amounts of Al are generally required to form it.

A key factor for any application is controlling the microstructure of the solid conductor because it defines the overall mechanical integrity. Sintered densities below 90% can result in a lower total conductivity and risk the penetration of lithium dendrites through the pores during cycling, which may lead to an electrical short or fracturing of the pellet. In polycrystalline ceramics, large grains are desirable because they also minimize the grain-boundary resistance. But long sintering times and high sintering temperature often result in impurity phases due to lithium migration and loss. The stringent processing requirements, together

with reported difficulties controlling the chemistry of the Al-substituted compounds provided motivation for the work in this program. During FY2013, the effects of processing conditions on formation, grain size and impurity formation during sintering of an Al-substituted cubic LLZO were systematically studied.

## Approach

Explore the existence of conductive crystalline and glassy phases in phase diagrams of candidate lithium-ion conducting ceramic systems. Deposite complex ionic conductors using physical methods. Measure the ionic conductivity of ceramic layers. Evaluate the compatibility of the ceramic layers with lithium metal.

## Results

**Sintering of LLZO pellets and the influence of processing on impurity formation and interfacial chemistry.** A powder mixture of precursors containing the right stoichiometry to form Al-substituted LLZO was fired at 1000°C. The resulting oxide showed the cubic structure, as expected. Part of this fresh LLZO powder was milled and used for compacting pellets, while the rest was used to cover the pellets during sintering. The influence of the history of the powder bed was explored by comparing fresh powders with those employed after having been annealed at 1100°C for either 6 h or 12 h during pellet processing.

Differences in the morphologies of pellets sintered with different powder covers were observed (Figure VI - 234). The pellets under fresh powder cover were successfully densified to 94% at only 1100°C, more than 100°C lower than previously reported for conventional methods. A thin pellet that was only a single grain (~150 μm) thick was also prepared by these means. The pellet prepared using the powder annealed for 6h was also well sintered. However, there appeared to be a phase preferentially segregated at grain boundaries on the surface, which show a darker contrast than that the bulk of the grains. SEM-EDS spectral imaging revealed that the grain boundaries were rich in Al but low in La and Zr, pointing at a $LiAlO_2$ impurity. Finally, the pellet sintered in the powder annealed for 12h was porous, with a particle size of only 1-2 μm. The electrochemical properties of this pellet were not studied. Thus, the powder cover can dramatically affect the morphology of sintered pellets, depending on its thermal history. Given that all three powder covers consisted of cubic LLZO (with slight lattice parameter variations) and had similar particle sizes (10 μm), this phenomenon must be attributable to the differences in the chemical compositions, in particular, Li and Al contents.

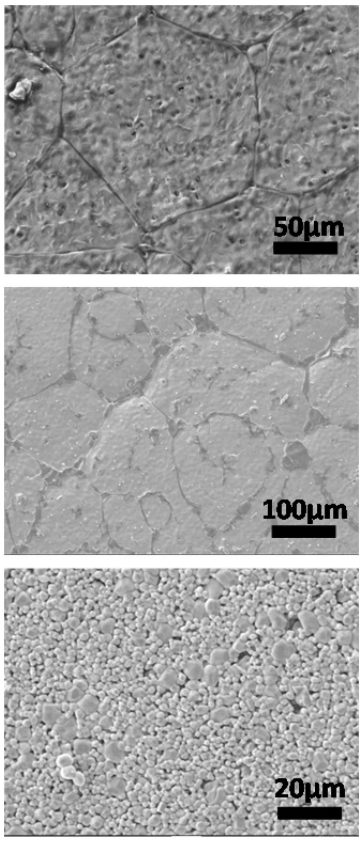


**Figure VI - 234: SEM images of pellets sintered in fresh (top), 6h annealed (middle) 12h annealed (bottom) LLZO powder covers**

Elemental atomic ratio maps of major (Li, La, Zr) and minor element (Al) distribution were obtained using femtosecond laser induced breakdown spectroscopy (LIBS, Figure VI - 235), a tool that is highly depth sensitive and, thus, can lead to insight into the variation of chemistry in the pellet. In the case of the pellet sintered in the fresh powder, a constant Al/La atomic ratio of 0.1 was measured from near the surface to 35 μm deep. In contrast, Al enrichment appeared to occur at greater depths for the pellet sintered with the powder cover annealed for 6h. The Al/La atomic ratio was highest at the surface and gradually decreased with pellet depth, and only at a depth of 20 μm did the ratio approach the expected value of 0.1. In contrast, the two pellets both had a consistent Zr/La ratio throughout the material. The atomic ratios of Li/La, Zr/La and Al/La were plotted in the form of 2D cross-sections (Figure VI - 235). Plots of total ionic conductivities vs. temperature revealed the LLZO film that is a single grain thick (Figure VI - 236) had the highest total ionic conductivity of $5.2\times10^{-4}$S/cm at 25°C, and the activation energy was 0.29 eV.

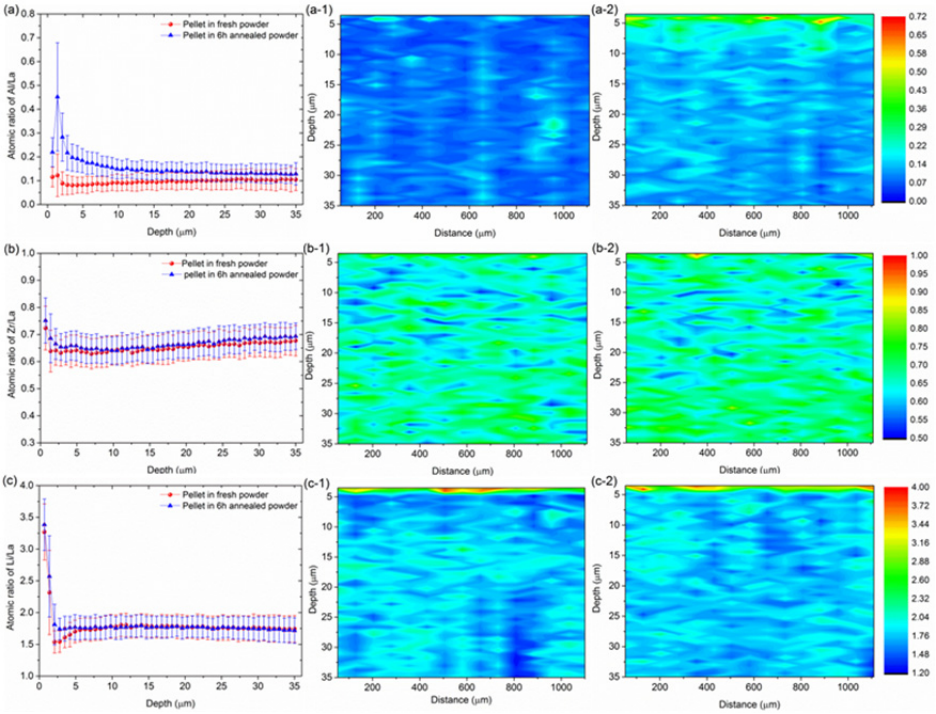


**Figure VI - 235: LIBS depth profiles (a, b, c) and cross-section imaging (a-1, a-2, b-1, b-2, c-1, and c-2) of Al/La (a, a-1, and a-2), Zr/La (b, b-1, and b-2) and Li/La atomic ratios (c, c-1, and c-2) of pellets made in fresh powder (middle column) and the powder annealed for 6h (right column)**

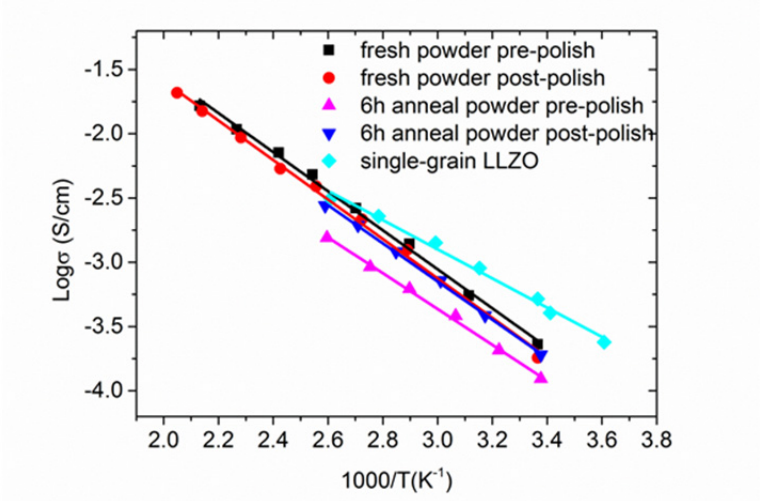


**Figure VI - 236: Total ionic conductivities of pellets prepared in fresh powders or those annealed for 6 h**

At the same temperature, the total ionic conductivity and the activation energy of the thick pellet sintered in fresh powder prior to polishing were $2.3\times10^{-4}$S/cm and 0.37 eV, respectively. This strongly implies that the room temperature ionic conductivity and activation energy of the bulk is higher than it is in the grain-boundaries, because the concentration of grain boundaries is much lower in the thin sample than in the thick pellet. The room temperature conductivities varied somewhat with the conditions used to process the pellets. The room temperature total ionic conductivity of the pellet processed in the annealed powder was only half the value of that of the pellet processed in fresh powder but it increased to $1.9\times10^{-4}$ S/cm after the surface impurity layer was polished away, indicating that this layer has some influence on the total ionic conductivity depending on its chemical composition.

Symmetrical Li/LLZO/Li cells were assembled and subjected to galvanostatic charge and discharge, using a thick pellet processed in fresh powder without polishing. No increase in voltage or other significant change in the response was seen over 10 cycles, indicating that LLZO is reasonably stable against lithium metal under these conditions.

**Deposition of LLZO thin films and interfacial chemistry.** The LLZO sintered pellets were used as the targets for pulsed laser deposition (PLD) of the thin films. A Lambda Physik 248nm KrF excimer laser with 350mJ at the source was used for ablating the target in 0.3mtorr background oxygen gas environments in the deposition chamber. The films were found to be dense and ~200 nm thick. In order to assess the stability of these films to lithium metal, X-ray photoelectron spectroscopy (XPS) experiments were carried out on LLZO films in contact with lithium foil for 15 hours at 90ºC. For comparison, an Ohara LATP glass-ceramic plate was treated the same way. As expected, the glass-ceramic darkened in contact with the lithium, and the XPS results showed clearly that some of the $Ti^{4+}$ was reduced to $Ti^{3+}$, as is known to occur for this material. In contrast, the LLZO film did not appear to change (Figure VI - 237).

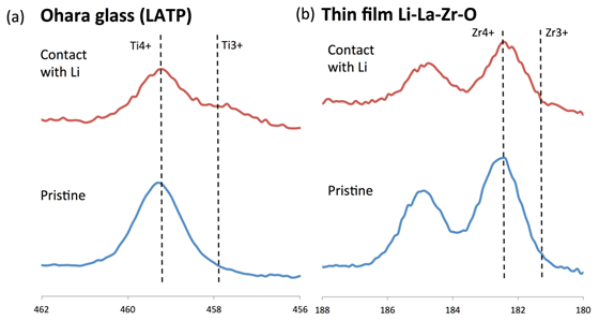


**Figure VI - 237: XPS spectra of (a) Ti in Ohara glass-ceramic and (b) Zr in thin film amorphous LLZO, before and after contact with lithium metal at 90°C**

**Low Temperature Cubic LLZO.** There are two known stable polymorphs of LLZ as noted previously. However, it has been reported that a lower temperature cubic phase can exist in a small temperature window as long as aluminum cations are present. Seeing it as a secondary phase in several samples, the synthetic conditions under which it forms were investigated. Specifically, we sought to determine the mechanism of the Al cation incorporation into the LLZO structure and the eventual formation of the cubic LLZO phase. The movement of Al(III) cations at 850°C was tracked by a combined powder X-ray diffraction (XRD), $^{27}Al$ and $^{7}Li$ MAS NMR, seen in Figure VI - 238, and high-resolution XRD (HRXRD) effort. Analysis shows that initially, the Al cations are mainly in the phase $Li_5AlO_4$, a phase that forms quickly in this $Li_2O$ rich environment. This phase then acts as the highly mobile source of Al(III) cations and gets incorporated into the garnet via reaction with tetragonal LLZO, where it migrates to the Li(1) site and gradually transforms the overall garnet to a cubic LLZO.

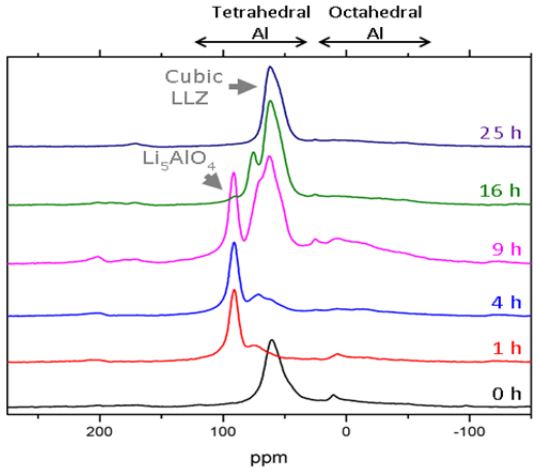


**Figure VI - 238: 27Al MAS NMR spectra of LLZO powders annealed at 850°C over time**

This transformation, driven by both aluminum and lithium cation movement, was tracked using $^{27}Al$ MAS-NMR and using high resolution XRD at the APS. Under the conditions which were used, the Al(III) continues to equilibrate forming a series of phases differentiated by small differences in Al content and cell parameters. After 24h at temperature (850°C) Al(III) incorporation has not reached equilibrium positions (*24d* site). The low temperature cubic phase, stable from 750-850°C, appears to result from the disorder created on the garnets tetrahedral site as Al displaces lithium from the structure. In order to compare how the structure affects conductivity, the ionic conductivity of the low temperature cubic phase (estimated from $^{7}Li$ MAS-NMR) was compared to the other two LLZO phases. The low temperature cubic phase was found to have a conductivity of $10^{-5}$ S/cm, approximately in between the values reported for the tetragonal and high temperature cubic phases.

## Conclusions and Future Directions

Pellets of cubic Al-substituted LLZO were successfully sintered to a relative density of 94% at 1100 ºC, the lowest temperature reported using conventional ceramic processing techniques. The microstructure, composition, and distribution of minor impurities in the pellets were strongly influenced by the thermal history of the powder cover used for processing. These factors, in turn, impacted the total conductivity and interfacial behavior of the pellets in contact with lithium electrodes. The best results were obtained on samples which were heated for 12 hours in a fresh

LLZO powder bed. Using the same processing conditions, it was also possible to fabricate a freestanding thin film only a single grain thick (~150 μm). This sample exhibited the highest total conductivity ($5.2\times10^{-4}$S/cm at 25°C) because fewer grain boundaries were present than in the thicker pellets. AC and DC experiments are consistent with the interpretation that LLZO is a single ion conductor and that it has negligible electronic conductivity. Symmetrical cells with lithium electrodes and a thick LLZO pellet as electrolyte could be cycled without noticeable deterioration in performance over 10 cycles for 20 hours, suggesting good stability of LLZO against lithium. This project was finalized on September 2013. Thus, there are no future directions to be discussed.

## FY 2013 Publications/Presentations


1. "Protective layers for the lithium electrode based on ceramic phases." *Pacific Rim Meeting on Electrochemical and Solid State Science (PRiME) 2012.* October 7th-12th, 2012, Honolulu, HI (USA).
2. "Thin film lithium ion conducting electrolyte for Li metal cells." *Pacific Rim Meeting on Electrochemical and Solid State Science (PRiME) 2012.* October 7th-12th, 2012, Honolulu, HI (USA).
3. "Study of the sintering of $Li_7La_2Zr_3O_{12}$ as an electrolyte for Li metal cells." *Pacific Rim Meeting on Electrochemical and Solid State Science (PRiME) 2012.* October 7th-12th, 2012, Honolulu, HI (USA).
4. "Aluminum Migration During Deposition of $Li_7La_2Zr_3O_{12}$ Thin Films on Aluminum Oxide Substrates." *223rd Electrochemical Society Meeting,* May 12th-16th, 2013, Toronto (Canada).
5. J. H. Park, W.-S. Hong, J. S. Park, L. Cheng, J. Cabana, G. Chen, M. M. Doeff, Y. Li, T. J. Richardson and J.-W. Son, *ECS Trans.*, **53**, 1 (2013).
6. I. Gurevitch, R. Buonsanti, A. A. Teran, B. Gludovatz, R. O. Ritchie, J. Cabana and N. P. Balsara, *J. Electrochem. Soc.*, **160**, A1611 (2013).
7. L. Cheng, J. S. Park, H. Hou, V. Zorba, G. Chen, T. J. Richardson, J. Cabana, R. Russo and M. M. Doeff, *J. Mater. Chem. A*, In press.
8. A. Hubaud, B, Ingram, B. Key, D. Schroeder, J. Vaughey, "Role of Al Substitution in Stabilizing the Structure of the Solid Lithium-Ion Conductor $Li_{7-x}Al_xLa_3Zr_2O_{12}$," *J. Mat Chem. A*, **1**, 8813 (2013).
9. D. J. Schroeder, A. A. Hubaud, J. T. Vaughey, "Stability of the Solid Electrolyte $Li_3OBr$ in Non-Aqueous Solvents," *Mat. Res. Bulletin,* in press.
10. "Understanding the Formation of Solid Lithium-Ion Conductors," *Beyond Lithium VI*, June 2013, Boulder, Colorado.
11. "Protection of a Lithium Metal Anode with a Conductive Solid Ceramic Electrolyte," *Beyond Lithium VI*, June 2013, Boulder, Colorado.
12. "Protection of a Lithium Metal Anode with a Conductive Solid Ceramic Electrolyte*," 6th International Conference on Advanced Lithium Batteries for Automobile Applications*, September 2013, Argonne, IL.

# VI.G.4 Integrated Lab-Industry Research Project (LBNL, ANL, FMC, Saft)

**Gao Liu, Vince Battaglia and Venkat Srinivasan**
Lawrence Berkeley National Laboratory

Environmental Energy Technologies Division
1 Cyclotron Road, MS 70R108B
Berkeley, CA 94720
Phone: (510) 486-7207; Fax: (510) 486-7303
E-mail: gliu@lbl.gov; vsbattaglia@lbl.gov; vsrinivasan@lbl.gov

**Zhengcheng Zhang and Khalil Amine**
Argonne National Laboratory
Chemical Sciences and Engineering Division
9700 S. Cass Avenue, Building 205
Argonne, IL 60439-4837
Phone: (630) 252-7868; Fax: (630) 972-4440
E-mail: zzhang@anl.gov,amine@anl.gov

**Marina Yakovleva**
FMC Corporation
Lithium Division
2801 Yorkmont Road, Suite 300
Charlotte, NC 28208
Phone: (704) 426-5391; Fax: (704) 426-5387
E-mail: marina.yakovleva@fmc.com

**Bridget Deveney**
Saft America, Inc.
Space and Defense Division – U.S.
107 Beaver Court
Cockeysville, MD 21030
Phone (410) 568-6415; Fax (410) 771-0234
E-mail: bridget.deveney@saftbatteries.com

Start Date: October 2010
Projected End Date: September 2013

## Objectives

- Apply Stabilized Lithium Metal Powder (SLMP) in lithium ion batteries to achieve lower cost and high energy density.
  - Reduce the high cost associated with formation process.
  - Improve the cycle life of the high energy density lithium ion battery for electrify vehicles (EVs).

## Technical Barriers

This project addresses the following technical barriers from the Energy Storage section of the Vehicle Technologies Program Multi-year Research, Development and Demonstration Plan:

- Performance: High first-cycle irreversible capacity loss (ICL), low coulombic efficiency, and poor cycle life.
- Life: Poor calendar life.
- Cost: High manufacture cost.

## Technical Targets

- DOE/USABC goals (EV): \$150/KWh, 230 $Wh/dm^3$, 1,000 cycles with 80% capacity retention, and 10-year system life.
- DOE/USABC goals (PHEV, 40-miles): \$220/KWh, 193 $Wh/dm^3$, 5,000 discharge cycles, and 15-year system life.

## Accomplishments

- Enabled the application of SLMP to lithium ion battery electrode during the slurry making process by developing SLMP-compatible solvents and polymer binders.
- Developed new process to activate the SLMP particles in the negative electrodes.
- Investigated the impact of the SEI layer formed by the incorporated SLMP and the cell cycling performance with the new SLMP incorporation and activation process.

✧ ✧ ✧ ✧ ✧

## Introduction

To meet the requirement for applications in EVs and plug-in hybrid electric vehicles (PHEV), it is desirable to develop high energy density and low cost materials. With current Li-ion technology, the lithium source in the cell is limited to that from the cathode material, e.g., $LiCoO_2$, and electrolyte. Solid-Electrolyte Interphase (SEI) formation on the surface of the anode during the initial cycles consumes lithium and results in partial capacity loss irreversibly. The incorporation of Stabilized Lithium Metal Powder (SLMP), developed by FMC Corporation, into graphite has been suggested to help overcome the ICL, and increase the capacity by 5~10% in lithium-ion cells. A recent study on

prelithiation of silicone-carbon nanotube (Si-CNT) anodes in lithium-ion batteries by using SLMP showed that the 20-40% first cycle ICL could be eliminated. This implies that anode materials inside commercial lithium ion cells can be chosen from other promising anode materials such as Si and Sn, which have very high capacity but large first cycle ICL and thus cannot be used in current lithium-ion batteries. Moreover, some non-lithiated materials with high specific capacities such as Reduced Graphene Oxide/$Fe_2O_3$ composite and $V_6O_{13}$ can be used as cathode materials if coupled with pre-lithiated anodes. Using this prelithiation strategy, the full cell energy density can be significantly improved and meet requirements for EV batteries in the future.

There is a trend in the battery and ultracapacitor industry of experimenting with SLMP® to address ICL and other issues. However, these efforts are not coordinated and lack a focus on fundamental understanding of the SLMP material properties, and their impact on long-term performance. ILIRP is aimed to solve the fundamental issues in order to apply SLMP in the lithium-ion battery. The success of this material will have a broad impact to the lithium-ion industry.

SLMP is an air stable surface-coated lithium metal powder material manufactured by FMC-Lithium (Figure VI - 239). The product consists of spheres of lithium metal with an average particle diameter of 40-50 µm with a coating consisting primarily of a 100 nm layer of $Li_2CO_3$. The lithium metal content is over 98% by weight. Initially developed as an easy-to-handle reducing agent for synthetic organic chemists, FMC-Lithium has also explored potential applications of SLMP as a lithium source in primary and secondary lithium-ion batteries. Initial work has demonstrated its utility as an additive in the battery manufacturing process.

LBNL and ANL are teaming with FMC-Lithium and lithium battery manufacturer Saft America to work on problems that impede or prevent the SLMP from being used as a performance enhancing additive in the negative electrode in commercial lithium ion batteries. This effort will lead to commercialization of batteries with lower ICL (leading to higher energy densities) and allow for a wider range of cathode materials to be utilized for transportation applications.

## Approach

Three issues have been identified that limit SLMP's widespread acceptance with battery manufacturers: (1) chemical incompatibility between the SLMP and common solvents used to formulate electrode slurries; (2) lack of practical activation of SLMP; and (3) unknown long-term stability of the direct SEI formation by SLMP. With these identified limitations, SLMP has achieved only limited marketplace penetration.

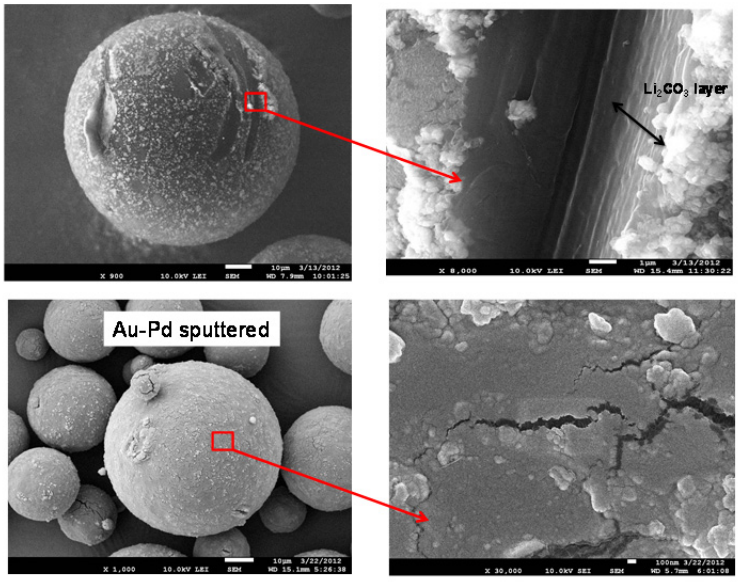


Surface scratches and cracks were observed on the pristine and the sputtered SLMP-$Li_2CO_3$ particles with 20nm Au/Pd coating: intrinsic surface morphology or due to Au/Pd surface tension.

**Figure VI - 239: Particle morphology of pristine SLMP (top) and Au-Pd surface sputtered SLMP (bottom) analyzed by SEM**

In this project, corresponding approaches were developed jointly at LBNL and ANL. The first issue is the chemical incompatibility between the SLMP and conventional slurry-making solvent NMP. To increase acceptance, new solvents, new polymer binders and new solvent/binder compositions that are chemically stable towards SLMP have been synthesized and evaluated. The second issue is related to the activation of SLMP in

the electrode. The $Li_2CO_3$ coating on SLMP is very robust and the activation to expose the active lithium metal is typically done using compression to physically break the coating. The coating chemistry and the effect of compression on the SLMP particles have been investigated. New activation processes are being developed and investigated. The third issue is that SLMP can be used as an additive in the negative electrode to accelerate the formation of the SEI. The long-term stability of the direct SEI formation by SLMP is not well understood and is therefore investigated here.

## Results

**New solvent/binder combinations for SLMP.** A large number of solvent/polymer combinations and their reactivity with SLMP were investigated. A variety of organic solvents were selected and their chemical reactivity with SLMP was evaluated by the amount of the remaining active lithium after long term mixing. The stable solvents were chosen for the polymer solubility test. The first feasible combination is toluene/SBR and the process of incorporation and activation of SLMP is illustrated in Figure VI - 240.

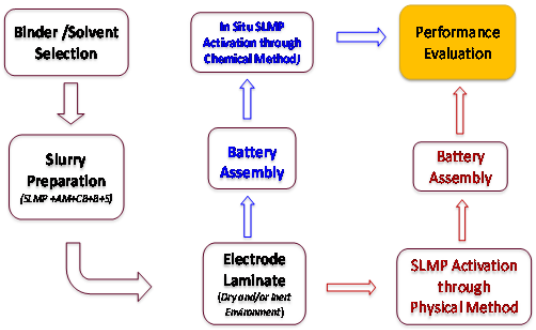


**Figure VI - 240: Flow chart of application of SLMP to electrode including incorporation and activation of SLMP particle through electrode slurry-making process**

SBR/toluene as a binder solution mixed with SLMP and graphite powder can form a uniform slurry, and can be coated into uniform electrode laminate. However, SBR covered graphite particles tend to have degraded rate performance compared to the PVDF based electrode. To solve the lithium-ion transport issue at the binder particle interface, a thin layer of PVDF or cross-linked PEO (1-2% by weigh) is coated on the surface of graphite to improve the electrolyte transport. This has led to significantly enhanced rate and cycling performance of the SBR/toluene processed SBR/graphite electrode, as shown in Figure VI - 241.

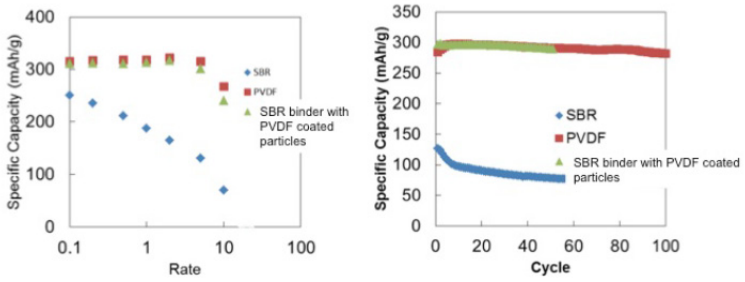


**Figure VI - 241: C-rate (left) and cycling performance (right) for the Li/graphite cell using SBR/toluene combination when the graphite is coated with 2% of PVDF**

Another new polymer binder poly(phenylene oxide) (PPO) suitable with SLMP and a solvent (dichlorobenzene) (DCB), compatible with both SLMP and the binder have been developed. A graphite anode was fabricated using the solvent of dichlorobenzene and with the binder poly(phenylene oxide). In the screening test, DCB showed the highest chemical stability towards SLMP among all the selected solvents (cyclohexylbenzene, anisole, DCB, chlorobenzene, DMSO). A mixture of MCMB (84 wt%), carbon black (4 wt%), PPO (5-10 wt%) dissolved in DCB and SLMP (2 wt%) were added to a container inside an argon-filled glovebox, an appropriate amount of dichlorobenezene was added to adjust the viscosity of the slurry. The slurry was coated onto a copper foil using a Dr. Blade coater, and dried in the oven at 75°C for 0.5 hour to 3 hours, then further dried in vacuum oven under dynamic vacuum for overnight. The electrode was activated by conventional compression method and high first cycle coulombic efficiency (99.1%) and cycling stability was achieved as shown in Figure VI - 242.

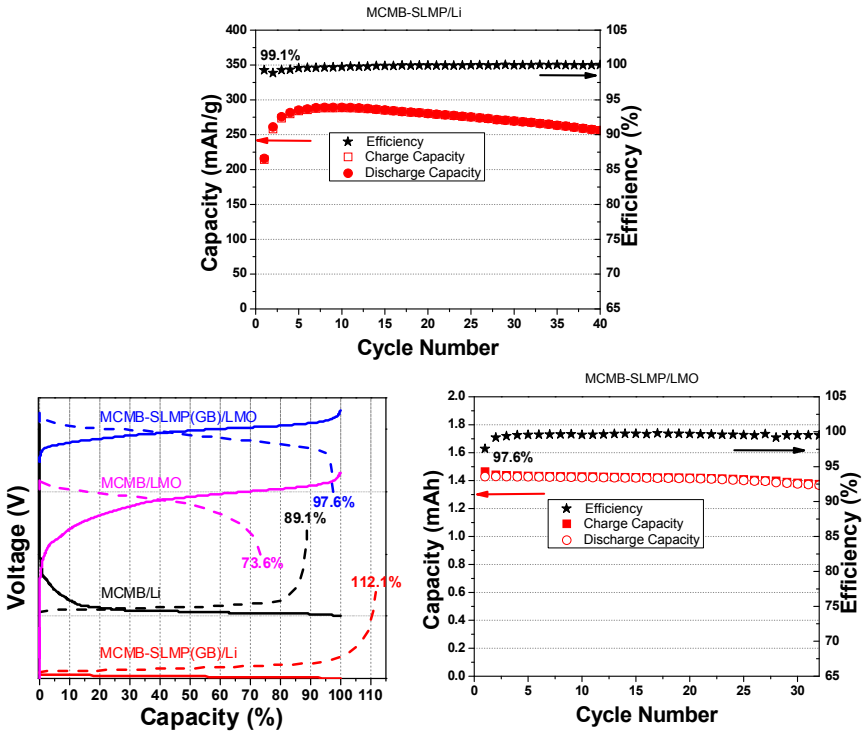


**Figure VI - 242: Li/MCMB-SLMP half-cell cycling data (top) and $LiMn_2O_4$/MCMB-SLMP full cell voltage profiles (left, bottom) and capacity retention and coulombic efficiency (right, bottom)**

**Demonstration of the activation of SLMP in the electrode laminate.** A compression method to activate the SLMP has been demonstrated in previous research. When the electrode went through a compression/calendaring process, the SLMP particles were broken to expose lithium metal, which made intimate contact with the graphite particles. In the past year, a new activation method was developed by thermal treatment and its activation mechanism is illustrated in Figure VI - 243. The aforementioned activated laminates were cut into certain size suitable as anode. The anode electrodes were then placed in an appropriate heating source to heat at 180-200°C for 10-30 minutes to activate the lithium inside the SLMP.

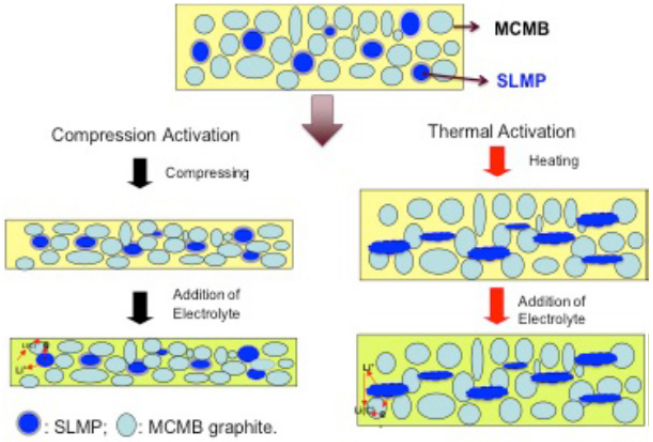


**Figure VI - 243: MCMB-SLMP electrode activated by compression method and new thermal treatment method**

After the SLMP was activated through the thermal treatment method, the anode electrodes were used to assemble the half-cell and the full cell. Upon addition of Gen 2 electrolyte (1.2 M $LiPF_6$ in EC/EMC (3/7), the graphite anodes will be lithiated *in situ* by the activated SLMP. An illustration of the mechanism of lithiation

process is shown in Figure VI - 243. An MCMB-SLMP electrode was thermally treated and assembled into a coin cell battery with LMO cathode and Gen 2 electrolyte. The charge discharge profiles of these batteries indicated that first cycle ICL could be greatly reduced as shown in Figure VI - 244. When heated to 180-190°C, the surface coatings were broken and the active lithium was released. When the electrolyte was added, the prelithiation occurred without electrically charging the electrode. The cycle performance of MCMB-SLMP/LMO cell is shown in Figure VI - 244, indicating that the thermal-activation is as effective as the conventional compression activation method.

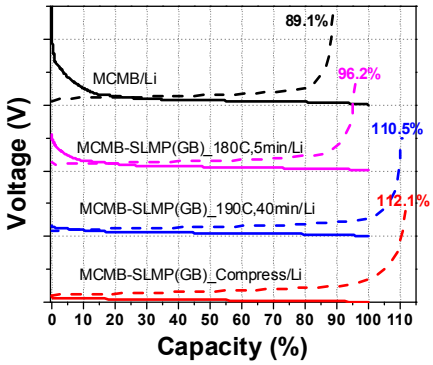


**Figure VI - 244: The first voltage profiles of half-cells using MCMB-SLMP (2%) electrodes activated by thermal treatment at 180°C and 190°C**

**Electrode performance improvement.** The first cycle voltage profiles of the two graphite-SLMP/Li cells starting with C/3 cycle rate are shown in Figure VI - 245A. First, the plateau at 0.6-0.7V is absent; suggesting development of SEI is already completed by the SLMP during the rest period. The first cycle coulombic efficiency of this cell is about 100%, showing that 1.2% of SLMP is enough to provide a full compensation to the capacity loss in this system, and therefore its charge capacity was not sacrificed. For the first regular cell without SLMP (no formation), its first discharge and charge capacities at C/3 current rate only reach 297 and 276 mAh/g, respectively (Figure VI - 245A), but the coloumbic efficiency does not vary much (about 93%). Cycle performance and Coulombic efficiency of these two cells as well as one graphite/Li cell after formation are compared and results are shown in Figure VI - 245B. Specific capacity of the cell without SLMP and without formation reaches only around 280 mAh/g, while both the cell with SLMP and the one without SLMP but with formation process reach capacity of around 320 mAh/g when the cells cycling capacities are stabilized (Figure VI - 245B). The cell with SLMP has an even better cycle performance than the cell without SLMP but with formation (Figure VI - 245B), indicating SEI formed in the cell with SLMP is as effective as, or better than that formed in the regular cell during low current (e.g., C/25 or C/10) formation process. The coulombic efficiencies of all three cells are comparable. These results confirm the effective prelithiation of anode by SLMP, and SLMP induced SEI formation on graphite electrode surface.

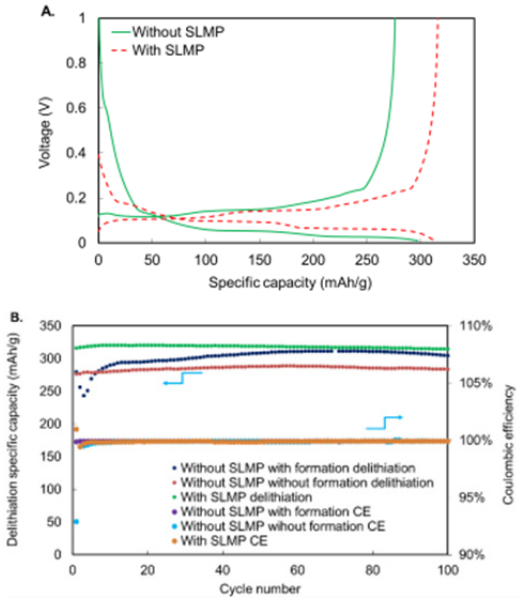


**Figure VI - 245: (A) The first cycle voltage profiles for graphite half-cells with 1.2% wt SLMP (red line) and without SLMP (green line) at C/3 rate. The cell with SLMP was rested under open circuit for four days before cycling and the cell without SLMP was cycled at C/3 after assembling; (B) The cycle performance and coulombic efficiency for graphite half-cells with (green symbols) and without SLMP (blue and red symbols) at C/3 rate. The cell without SLMP with formation (blue symbols) was cycled at C/25 for two cycles, followed by C/10 for five cycles, then cycled at C/3 rate. The cell without SLMP without formation (red symbols) was cycled at C/3**

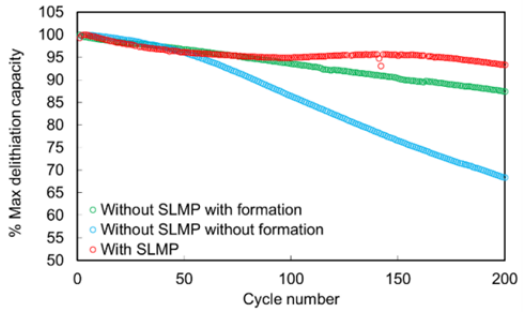


**Figure VI - 246: Cycle performance for graphite/NMC full cells with (red symbols) and without SLMP (green and blue symbols) at C/3 rate. The cell with SLMP was rested at open circuit for four days before cycling. The cell without SLMP with formation (green symbols) was cycled at C/25 for five cycles, followed by C/10 for ten cycles, then cycled at C/3 rate. The cell without SLMP without formation (blue symbols) was cycled at C/3 after assembling**

Cycle performance for the first 200 cycles of the graphite/NMC cells are shown in Figure VI - 246. As expected, the cell without SLMP and without formation decays the fastest, most likely due to the poor quality of formed SEI. After 200 cycles, the capacity decays to only 68.2% of its initial value. Meanwhile, capacity retention of the cell with SLMP and the one without SLMP but with formation was 93.2% and 87.3%, respectively. Among these three cells, SLMP-contained cell displays the highest capacity retention upon cycling. These results indicate that SEI formation in the SLMP prelithiated cell occurred during its resting time and the quality of the developed SEI is the same or even better than that developed in the regular cell upon low current formation.

This study, therefore, has provided direct evidence that SLMP can effectively help SEI formation. Particularly, after the cell with SLMP prelithiated anode is assembled, it could be rested at open circuit and the SEI formation occurred spontaneously. It is possible to skip the external current driven formation process to reduce lithium battery manufacturing cost by applying this strategy.

## Conclusions and Future Directions

In this project, corresponding approaches were developed jointly at LBNL and ANL to address the technical barriers of application of SLMP to the battery industry. New polymer binders and new compatible solvents were developed to enable the incorporation of SLMP through the slurry-making process. A new activation method has developed and the long-term effect of the SEI formed by the SLMP was thoroughly studied. Future research will focus on the validation of new materials in the large format lithium ion battery.

## FY 2013 Publications/Presentations


1. Jung-Je Woo, Zhengcheng Zhang, and Khalil Amine, "Separator/Electrode Assembly for Safe Lithium-ion Battery," *Adv. Energ. Mater.*, (2013), in press.
2. Jung-Je Woo, Zhengcheng Zhang, Nancy L. Dietz Rago, Wenquan Lu and Khalil Amine, "A high performance separator with improved thermal stability for Li-ion batteries," *J. Mater. Chem. A*, **1**, 8538-8540, (2013).
3. Z. Xue, Z. Zhang, L. Hu, K. Amine, "Polysiloxane-epoxide as cross-linkable binders for lithium-ion Batteries," *J. Electrochem. Soc*., **160**(10), A1819-A1823, **(2013)**.
4. Z. Xue, Z. Zhang, K. Amine, "Cross-linkable urethane acrylate oligomers as binders for lithium-ion battery," *Electrochem. Commun.,* **34**, 86-89, (2013).
5. Xiang, B.; Wang, L.; Liu, G.; Minor, A. M., "Electromechanical Probing of Li/Li2CO3 Core/Shell Particles in a TEM," *J. Electrochem. Soc.,* **160** (3), A415-A419, (2013).
6. Wu, M.; Xiao, X.; Vukmirovic, N.; Xun, S.; Das, P. K.; Song, X.; Olalde-Velasco, P.; Wang, D.; Weber, A. Z.; Wang, L.-W.; Battaglia, V. S.; Yang, W.; Liu, G., "Toward an Ideal Polymer Binder Design for High-Capacity Battery Anodes," *J. Am. Chem. Soc.*, **135** (32), 12048-12056, (2013).
7. Wang, L.; Fu, Y.; Battaglia, V. S.; Liu, G., "SBR-PVDF based binder for the application of SLMP in graphite anodes," *Rsc Advances*, **3** (35), 15022-15027, (2013).
8. Chong, J.; Xun, S.; Song, X.; Liu, G.; Battaglia, V. S., "Surface stabilized $LiNi_{0.5}Mn_{1.5}O_4$ cathode materials with high-rate capability and long cycle life for lithium ion batteries," *Nano Energy,* **2** (2), 283-293, (2013).
9. Jung-Je Woo, Zhengcheng Zhang, Nancy L. Dietz Rago, Wenquan Lu and Khalil Amine, "A thermally stable separator for improved safety and cycle life of lithium ion batteries," *6th International Conference on Advanced Lithium Batteries for Automobile Applications*, Sep. 9-11, 2013, Argonne National Laboratory, Lemont, IL.
10. Z. Xue, Z. Zhang,* L. Hu, K. Amine, "Cross-linkable urethane acrylate oligomers as binders for lithium-ion battery," *6th International Conference on Advanced Lithium Batteries for Automobile Applications*, Sept. 9-11, 2013, Argonne National Laboratory, Lemont, IL.
11. Shengwen Yuan, Zhengcheng Zhang, Khalil Amine, "Application of SLMP in Lithium ion battery," *DOE Integrated Laboratory and Industry Research Program Review Meeting*, July 16, 2013, Berkeley, CA.
12. Shengwen Yuan, Zhengcheng Zhang, Khalil Amine, "Application of SLMP in Lithium ion battery," Meeting with FMC, Sep. 10, 2013, Argonne National Laboratory, Lemont, IL.
13. Lei Wang, Vincent S. Battaglia, and Gao Liu, "Prelithiated Graphite Anode SEI Formation by Stabilized Lithium Metal Powder in Li-Ion Batteries," Abstract 1010*, 222nd meeting of The Electrochemical Society, PRiME*, Oct 7-11, 2012, Honolulu HI.
14. Zhihui Wang, Lei Wang, Vince Battaglia, Gao Liu, "Applications of Stabilized Lithium Metal Powder (SLMP) in Lithium-ion Batteries," *2013 MRS Spring Meeting*, Apr. 3, 2013, San Francisco, CA.

15. Zhihui Wang, Vince Battaglia1, Gao Liu, Marina Yakovleva, "Applications of Stabilized Lithium Metal Powder (SLMP®) in Lithium-ion Batteries," *2013 The 6th International Conference on Advanced Lithium Batteries for Automobile Applications (ABAA6)*, Sep 9-11, 2013, Argonne National Laboratory, Lemont, IL.
16. Gao Liu, Vince Battaglia, and Lei Wang, Lithium Metal Doped Electrodes for Lithium-ion Rechargeable Chemistry, WO/2013/052916, International applications No. PCT/US2012/059127.
17. Zhengcheng Zhang, Shengwen Yuan, Khalil Amine, Electroactive compositions with poly(arylene oxide) and stabilized lithium metal particles, ANL-IN-12-027.

# VI.G.5 Developing Materials for Lithium-Sulfur Batteries (ORNL)

**Chengdu Liang**
Oak Ridge National Laboratory

Center for Nanophase Materials Sciences
Building 8610 MS 6493
Oak Ridge, TN 37831-6493
Phone: (865) 456-9185; Fax: (865) 574-1753
E-mail: liangcn@ornl.gov

Collaborators:
Nancy J. Dudney (ORNL)

Start Date: June 2010
Projected End Date: September 2014

## Objectives

- Overcome the technical hurdles for the longevity of lithium-sulfur (Li-S) batteries through innovative design of solid-state battery configuration.
- Identify key problems for cycling solid state Li-S batteries.
- Develop enabling materials for solid-state Li-S batteries.

## Technical Barriers

Among known battery chemistries, lithium-sulfur (Li-S) holds the greatest promise for high-energy batteries. However, the development of Li-S batteries has been impeded by the intrinsically low electronic and ionic conductivities of the sulfur cathode and the poor cyclability of the metallic lithium anode. To enable the cycling of the sulfur cathode in a conventional Li-S battery, a liquid electrolyte that has a high solubility of polysulfides is required in order to overcome the poor ionic conductivities of the solid sulfur species. As a result of the dissolution of polysulfides in the liquid electrolyte, the diffusion of polysulfides from the cathode to the anode during battery cycling leads to intrinsically short cycle-life. In addition to the problems with the sulfur cathode, the dendritic growth of lithium metal in liquid electrolytes and the ever growing solid electrolyte interphase on the anode surface shorten the cycle life of Li-S batteries and also cause safety concerns.

## Technical Targets

- Derive the relationship of ionic conductivity of Li-S cathode materials with their electrochemical cyclability.
- Achieve long-term cyclability of Li-S batteries without polysulfide shuttle.

## Accomplishments

- Developed solid-state Li-S batteries through a simple cold pressing procedure.
- Unraveled the relationship of ionic conductivity of cathode material with their cycling conditions
- Developed composite electrolytes for achieving high conductivity.
- Explored the possibility of using air-stable sulfide-based solid electrolytes for Li-S batteries.

✧ ✧ ✧ ✧ ✧

## Introduction

The electrification of vehicle transportation requires electrical energy storage technologies that have high energy density, low cost, and enhanced safety. The Li-S battery, which uses elemental sulfur as the cathode material, is expected to meet the needs for electric vehicles (EV). However, conventional Li-S batteries have a short cycle-life because of the intrinsic polysulfide shuttle phenomenon. The use of a liquid electrolyte inside the electrochemical cell enables the polysulfide shuttle. ORNL proposed to develop solid-state Li-S batteries that completely eliminate the polysulfide shuttle phenomenon. The solid electrolytes do not dissolve the polysulfide formed during discharge of Li-S batteries. Therefore, solid-state Li-S batteries exclude the migration of sulfur species that is caused by the polysulfide shuttle mechanism. In addition to the prevention of polysulfide migration, the solid electrolyte addresses the challenges of cycling the metallic lithium anode. Solid-state Li-S batteries are expected to have long cycle-life.

Although solid-state Li-S batteries are an enticing solution to the growing demand for inherently safe and higher capacity energy storage devices, there are still hurdles for the deployment of solid-state Li-S batteries. Selecting a suitable solid state electrolyte is critical to

the success of solid-state batteries. Few solid electrolyte materials are available for battery applications, and none of them satisfies all desirable characteristics. While some electrolytes have high Li-ion conductivity at room temperature, they lack the chemical and electrochemical stability to be practical in real-world devices. Where stability is present, conductivity is not as high, or material processing is difficult. Besides the challenges of solid electrolytes, the extremely low ionic conductivity of sulfur and its discharge products precludes the direct cycling of solid-state sulfur. Facilitation of ionic transport at the electrode and across the solid electrolyte is of paramount importance to enabling the function of solid-state Li-S batteries.

## Approach

ORNL is working on the development of solid-state Li-S batteries to completely eliminate the polysulfide shuttle. A sulfide-based solid electrolyte has been used to achieve compatibility with the cathode and anode. Stoichiometric lithium thiophosphate ($Li_3PS_4$) is known for its excellent stability with metallic lithium among all sulfide-based solid electrolytes. The high conductivity beta phase has been stabilized through nanostructures. Using β-$Li_3PS_4$ as the platform, ORNL developed a series of solid-state Li-S batteries. In FY13, a core-shell nanostructure of $Li_2S@Li_3PS_4$ was developed as a cathode material. A comparison of this new material with the lithium polysulfidophosphate (LPSP) developed during FY12 illustrated the positive correlation of ionic conductivity of the cathode materials with their electrochemical cyclability. The research validated that these solid-state Li-S batteries completely blocked the polysulfide shuttle. Long term cyclability has been achieved. To enable the solid-state Li-S battery for EVs, further research efforts have been focused on the following directions: (1) improve the ionic conductivity of the solid electrolyte to achieve high power; (2) enhance the mechanical strength and flexibility of the solid electrolyte membrane by forming polymer-ceramic composites through addition of a polymer mesh in the membrane; and (3) explore cost reductions through use of air-stable solid electrolytes.

## Results

**Relationship of ionic conductivity of the cathode materials and their electrochemical performance.** In the previous fiscal year, the lithium polysulfidophosphate (LPSP) was developed as an excellent cathode material for solid-state Li-S batteries. A salient characteristic of LPSP is its high conduction of lithium ions. A basic question regarding this new material is how the ionic conductivity affects the electrochemical cycling performance of the cathode material. To this end, two additional new materials were developed to investigate the effect of ionic conductivity of the sulfur cathode on cycling performance: nanoparticles of $Li_2S$ and core-shell structured $Li_2S@Li_3PS_4$. Among these three samples, the LPSP showed the best cycling performance with a stable capacity over 100 cycles and showed no sign of degradation after 100 cycles. Both the $Li_2S$ nanoparticles and the core-shell structured $Li_2S@Li_3PS_4$ samples had significant capacity decay after 100 cycles. The $Li_2S@Li_3PS_4$ cathode retained a capacity of 581 mAh/g while the $Li_2S$ nanoparticles retained a capacity of 381 mAh/g. The room temperature ionic conductivity of these materials followed the same trend as their cyclability: LPSP ($8.2\times10^{-5}$ S/cm) > $Li_2S@Li_3PS_4$ ($4.5\times10^{-6}$ S/cm) > $Li_2S$ nanoparticles ($2.1\times10^{-11}$ S/cm). It is obvious that the ionic conductivity has a positive correlation with the electrochemical cycling performance of the cathode. The charge capacities of all samples are equal to or less than the discharge capacity. Therefore, the solid-state batteries do not have problem associated with the polysulfide shuttle, which causes the charge capacity to be much higher than the discharge capacity.

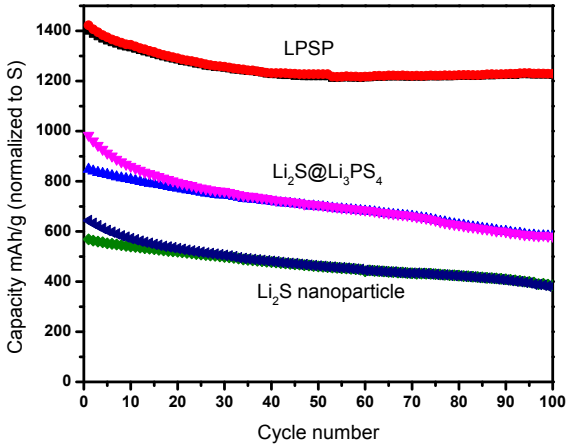


**Figure VI - 247: Comparison of cycling performance of LPSP, $Li_2S@Li_3PS_4$ and $Li_2S$ nanoparticles**

**Composite of oxide and sulfide electrolytes for high conduction of lithium ions**. Lithium thiophosphate ($Li_3PS_4$) was used in our previous development because it meets the basic requirements of good compatibility with both the metallic lithium anode and the sulfur cathode. However, the ionic conductivity of $Li_3PS_4$ is only $2.0\times10^{-4}$ S/cm at room temperature. To improve the ionic conductivity of solid electrolytes for Li-S batteries, lithium lanthanum zirconium oxide $Li_7La_3Zr_2O_{12}$ (LLZO), a garnet structure, has been used as a filler with $Li_3PS_4$ to enhance the ionic conductivity and mechanical and chemical properties of the solid electrolyte. It is known that LLZO has good ionic conductivity (>$10^{-4}$ S/ cm) with excellent

electrochemical stability and mechanical properties. However, it has a high interfacial resistance with metallic lithium. LLZO is difficult to press at room temperature. Compression at 1100°C is needed to get a solid electrolyte membrane. In stark contrast to LLZO, $Li_3PS_4$ is a much softer material that can be cold pressed. In addition, $Li_3PS_4$ has a very low interfacial resistance with metallic lithium. From the aforementioned properties, it can be observed that the LLZO and $Li_3PS_4$ are complementary to each other, making them interesting candidates for a composite electrolyte material.

Mechanical mixing of LLZO and $Li_3PS_4$ was done under mild ball-milling conditions. Shown in Figure VI - 248 are the trends of ionic conductivity and activation energy as a function of weight fraction of LLZO in the composites. The maximum Li-ion conductivity for the nanocrystalline $Li_3PS_4$ composites was observed at the 30:70 (LLZO:$Li_3PS_4$) composition as 9.12 $\times 10^{-4}$ S/cm, which is greater than the parent $Li_3PS_4$ electrolyte. There were no chemical reactions between LLZO and $Li_3PS_4$. Therefore the enhanced conductivity is attributed to the interfacial conduction.

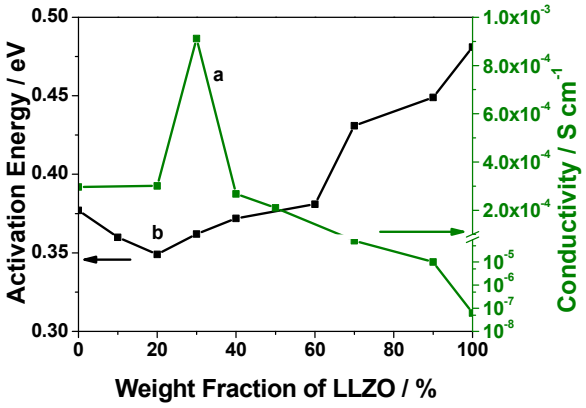


**Figure VI - 248: Ionic conductivity (right y-axis) and activation energy (left y-axis) as a function of the weight fraction of LLZO**

**Polymer mesh enhanced solid-electrolyte membranes.** One of the key impediments for the use of a fragile ceramic membrane in a mobile battery is its poor mechanical strength. To overcome this problem, a polypropylene (PP) mesh has been used to enhance the mechanical strength and impart flexibility to the solid electrolyte membrane. The PP is 100 microns thick with 90% open porosity. Taking advantage of the ductility of the β-$Li_3PS_4$, a composite of PP mesh and solid electrolyte membrane was prepared by dry-pressing the powder and the mesh together at room temperature. Figure VI - 249 shows photos of the PP mesh (left) and the mesh enhanced membrane (right). The composite membrane is intact and flexible.

**Figure VI - 249: Photos of polymer mesh (left) and mesh enhanced β-$Li_3PS_4$ membrane (right). The thickness of the membrane is 100 µm**

**Development of high-conductivity air-stable sulfide-based solid electrolytes for Li-S batteries.** Although lithium thiophosphate ($Li_3PS_4$) meets the basic requirements of all-solid-state Li-S batteries, the hypersensitivity of $Li_3PS_4$ to air and moisture requires sophisticated handling under a dry inert gas atmosphere, which increases the processing cost. A new series of arsenic-doped lithium tin sulfide solid electrolytes have been developed to replace $Li_3PS_4$. Figure VI - 250 shows the effect of arsenic doping on the ionic conductivity. The highest conductivity achieved is $1.39\times10^{-3}$ $Scm^{-1}$ at 25°C with the composition $Li_{3.833}Sn_{0.833}As_{0.166}S_4$. Considering $Li^+$ as the only mobile species in the solid electrolyte, the conduction of $Li^+$ in the solide electrolyte is comparable to that of current carbonate-based liquid electrolytes. It is worth noting that the activation energy versus the concentration of As substitution shows an inverse relationship to the conductivity (Figure VI - 251). The lowest activation energy (0.21 eV) was observed in the composition that had the highest ionic conductivity ($Li_{3.833}Sn_{0.833}As_{0.166}S_4$). Such low activation energy ensures a flat conductivity curve in a broad temperature range.

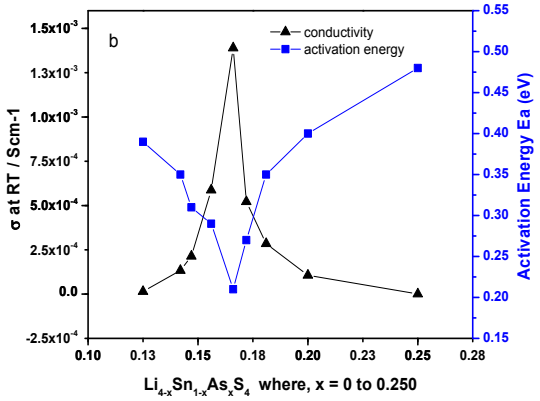


**Figure VI - 250: Ionic conductivity (right y-axis) and activation energy (left y-axis) as a function of As concentration doped in $Li_4SnS_4$**

An important goal of this research is to achieve air stability of sulfide-based solid electrolytes. To test the air stability, a representative sample of $Li_{3.833}Sn_{0.833}As_{0.166}S_4$ was shaken in ambient air for over

48 h. For comparison purposes, a sample of β-$Li_3PS_4$ was synthesized and shaken in ambient air at identical conditions. The ionic conductivities of the pristine and air-exposed samples were measured by ac impedance. Figure VI - 251 presents the temperature dependencies of the conductivity of $Li_{3.833}Sn_{0.833}As_{0.166}S_4$ and β-$Li_3PS_4$ before and after exposure to air. The room-temperature ionic conductivities of $Li_{3.833}Sn_{0.833}As_{0.166}S_4$ before and after air exposure were $1.39\times10^{-3}$ $Scm^{-1}$ and $9.95\times10^{-4}$ $Scm^{-1}$, respectively. There was only a very minor change in conductivity, which may be due to a very small amount of moisture uptake or to variance in sample preparation. In stark contrast to the stable $Li_{3.833}Sn_{0.833}As_{0.166}S_4$ phase, the β-$Li_3PS_4$ showed more than an order of magnitude drop in ionic conductivity after air exposure.

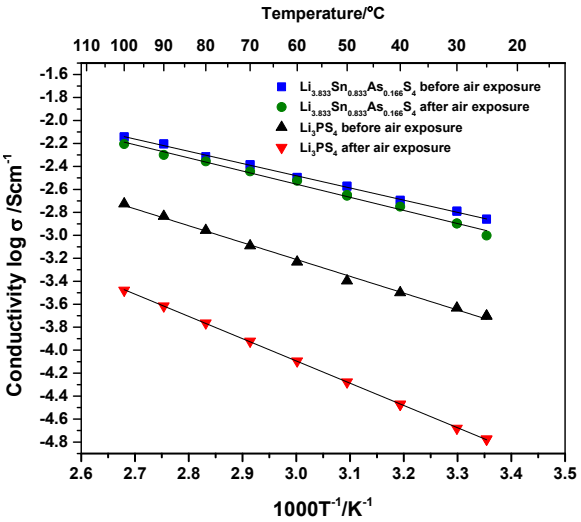


**Figure VI - 251: Comparative Arrhenius plots for $Li_{3.833}Sn_{0.833}As_{0.166}S_4$ and β-$Li_3PS_4$ before and after air exposure**

## Conclusions and Future Directions

Solid-state Li-S batteries overcome the problems caused by the polysulfide shuttle. The ionic conductivity is crucial for the cycling performance of the cathode. In order to use ceramic membranes for mobile batteries, two problems must be overcome: the relatively low ionic conductivity and the fragility of the membrane. Sulfide-based solid electrolytes hold great promise for high conduction at room temperature. When LLZO is used as the filler for Li3PS4, the ionic conductivity is significantly improved. The mechanical properties of sulfide-based solid electrolytes can be improved using a polymer mesh as a scaffold. Air-stable high conduction sulfide-based electrolytes provide an avenue for processing the Li-S batteries in a dry-room. Air-stable battery components would significantly reduce the cost of material handling and battery assembly.

Future efforts will focus on the use of these newly developed solid electrolytes in the assembly of Li-S batteries and the complete evaluation of solid-state Li-S batteries.

## FY 2013 Publications/Presentations

1. Z. Lin, Z. Liu, N. Dudney, and C. Liang "A Lithium Superionic Sulfide Cathode for All-Solid Lithium-Sulfur Batteries," ACS Nano, 2013 7, 2829-2833.
2. "High-Energy All-Solid Li-S Batteries," DOE-VTO Annual Merit Review and Peer Evaluation Meeting, Arlington, VA, May 2013.
3. "New Materials for All-Solid-State Lithium-Sulfur Batteries," Beyond Lithium-ion Symposium VI, Boulder, CO, June 6, 2013.
4. "Material Challenges for All-Solid Lithium-Sulfur Batteries," The 10th Pacific Rim Conference on Ceramic and Glass Technology including GOMD 2013, San Diego, CA, June 4, 2013.
5. "New Directions for Li-S Batteries," DOE BATT program Li-S focus group symposium, July 17, 2013
6. "Li-S cathode Materials," Energy Storage Solutions Industrial Symposium, Oak Ridge, TN, Sept. 4, 2013
7. "Li-ion Conducting Sulfur-Rich Compounds for All-Solid Lithium-Sulfur Batteries," 2013 Fall ECS meeting, San Francisco, CA, Oct 27, 2013
8. "Aliovalent Doping of Tetra Lithium Ortho-sulfidostannate Li4SnS4 as Air Stable Solid Electrolyte with High Ionic Conductivity," C. Liang, G. Sahu, and N. Dudney; (2013 invention disclosure)
9. "A High Conducting Oxide – Sulfide Composite Lithium Superionic Conductor," C. Liang, E. Rangasamy, J. K. Keum, A. J. Rondinone, N. J. Dudney; (2013 invention disclosure)

# VI.G.6 Composite Electrolyte to Stabilize Metallic Lithium Anodes (ORNL)

**Nancy Dudney**
Oak Ridge National Laboratory

Material Science and Technology Division
PO Box 2008, MS 6124
Oak Ridge, TN 37831-6124
Phone: (865) 576-4874
E-mail: dudneynj@ornl.gov

Start Date: October 2011
Projected End Date: September 2016

## Objectives

- Understand $Li^+$ transport at the interface between two dissimilar solid electrolytes, e.g. ceramic/polymer.
- Develop composites of electrolyte materials with the requisite electrochemical and mechanical properties as guided by simulation.
- Fabricate thin membranes and demonstrate stability upon cycling of a thin metallic lithium anode with good power performance and long cycle life.
- Identify design rules that can be generally applied to composites of other solid electrolyte materials.

## Technical Barriers

Advanced lithium batteries, including Li-air and Li-S, require robust protection of the metallic lithium anode to maintain a mechanically and chemically stable lithium anode. Any reaction or roughening of the lithium will result in loss of capacity, degradation of performance and may also compromise safety. A robust solid electrolyte to protect the lithium while ensuring rapid cycling is the clear solution, yet fabricating such an electrolyte with the required ionic transport, electrochemical stability, and mechanical strength is a technical challenge. The electrolyte must be very thin and light, and cost effective for manufacturing. To provide a lithium anode with significantly higher energy density than current Li-ion anodes, all components of the anode including the packaging, current collector, protective electrolyte, and indeed the lithium itself, must be minimized.

## Technical Targets

- Develop a solid electrolyte membrane that stabilizes the long-term, safe, and efficient cycling of lithium metal anodes to enable high energy density batteries.
- Provide an electrolyte protected anode to promote the equivalent electric range of 40 miles (PHEV) and 200-300 miles (EV).
- Enable battery anodes for very high energy Li-S Battery (500 Wh/kg) by 2020 and Li-Air Battery (700 Wh/kg) by 2030.

## Accomplishments

- Results show that many polymer-ceramic interfaces have similar behavior, possibly related to PEO conformation. Even a small interface resistance will alter $Li^+$ path through a composite.
- Vapor deposited lithium contacts are generally less resistive than pressure contacts to lithium foil, but may cause premature failure of ceramic electrolytes.
- Simulation shows that formation of sintered necks between ceramic particles greatly enhances both conduction and stiffness of the dispersed particle electrolyte composites.
- Grain boundaries contribute only a small increase in resistance for dense sintered garnet electrolytes.
- When equilibrated, composites with ~50vol.% submicron ceramic powder demonstrate that $Li^+$ ion path accesses both ceramic and polymer phases. The thin 100-200μm membranes are pliable and robust.

✧ ✧ ✧ ✧ ✧

## Introduction

This program is based on the observation that no single solid electrolyte, either polymer, ceramic, or glass, can currently meet all of the requirements for a stable interface with the active lithium anode. Many inorganic materials are not stable in contact with lithium metal and also suffer from being too brittle when thinned to a light weight membrane. Polymer electrolytes, even those with rigid block co-polymer structures, gradually roughen with lithium cycling and

are too resistive for room temperature operation. Formation of a composite polymer-ceramic structure offers a pragmatic approach to optimizing the electrolyte properties. Using the wealth of known solid electrolyte materials, this program is addressing the fabrication and testing of such composites, both experimentally and through simulation. A critical aspect of such a composite is the properties of the interface formed between two different electrolytes, which must offer mechanical integrity while not impeding the transport of lithium ions. Characterizing and modifying these interfaces is a primary focus of this program.

## Approach

**Material selection.** Although new solid electrolytes are being reported, only well understood and relatively stable electrolytes are chosen from different classes of electrolyte materials for this study. The intent is to identify design rules that can later by applied to composites of alternative and perhaps more conductive electrolyte materials. Representative materials from different classes of electrolytes include: sputter deposited Lipon glass film; dry PEO polymer-based electrolytes having either LiTFSI or $LiCF_3SO_3$ salts; powders and sintered ceramic plates of Al-doped $Li_7La_3ZrO_{12}$ garnet (LLZO) from Prof. Sakamoto (Michigan State Univ.) and of phosphate electrolytes from Ohara and nGimat Corps.; and block co-polymer electrolytes from Prof. Balsara (UC Berkeley).

**Preparation and electrochemical characterization of bi-layer interfaces.** Following earlier work, bi-layer structures create a simple planar interface with which to characterize the resistance for lithium ion transport from one material to another. Bilayers include pairs of dissimilar solid electrolytes, principally ceramic and polymer couples, and also the interface formed with vapor deposited lithium films onto various solid electrolytes. Care is taken to prepare clean and adherent interfaces for these studies. A high-vacuum chamber is used for thermal evaporation of the lithium thin films directly onto clean electrolyte surfaces. Ceramic electrolyte pellets are carefully polished and dried. Only dry processing of the polymer electrolytes is used to eliminate all solvent effects. Electrochemical impedance spectroscopy (EIS) and DC transport are used to extract the impedance of the interface from the series summation of the individual components. An interfacial impedance that is significant in magnitude relative to the bulk resistance can be readily resolved. Results from these investigations provide the interface resistance used in simulations of the composite properties.

**Simulation of ion transport and mechanical stability of composite structures.** Codes were developed in our earlier work to predict both ion transport and also elastic modulus of various composite electrolyte structures including dispersed particle composites and ordered laminar structures. Comsol tools were developed to evaluate how variation in the interfacial resistivity alters the overall ionic conduction path and the uniformity of current through the composite electrolyte. In the current year, a new approach was developed for high volume loading of dispersed particles with varying extents of the contact area (necks) assumed between ceramic particles.

**Fabrication and characterization of electrolyte composites for conduction and mechanical properties.** Based on results of bilayer and simulation studies, selected materials are prepared as dispersed composites. Using EIS, ion transport measurements are compared against the simulations to evaluate the influence of the interfaces to block or direct the ionic current. Promising composite electrolytes are also prepared with metallic lithium contacts to evaluate the dc transport, transference number and electrochemical stability with Li. As work progresses, alternative fabrication methods and materials will be investigated to improve performance. This may require highly aligned or partially sintered network structures with high volume fractions of the hard ceramic phase.

## Results

**Studies of bi-layer electrolyte laminates and polycrystalline electrolytes.** Results for interface impedance between a variety of polymer and ceramic electrolytes were compared. Many follow the Arrhenius temperature dependence; it is noteworthy that the activation energies are quite similar (see Table VI - 9), although the specific area resistance varies by orders of magnitude. This may reflect the conformation of the polymer at the interface.

**Table VI - 9: Bilayer and activation energy of the interface resistance**

| | |
|---|---|
| Lipon\PMMA-$EO_{10}$:$LiClO_4$ | 106 kJ/mol |
| Lipon\PS-$EO_{10}$:$LiClO_4$ | 104 kJ/mol |
| LLZO\$PEO_{10}$:LiTFSI (laminated film) | 95 kJ/mol |
| LLT\$PEO_{20}$:$LiCF_3SO_3$ (Abe,et.al, *J. Electrochem. S.* (2005) | 96 kJ/mol |

For the relatively conductive interfaces, it is harder to accurately extract the small resistance and its temperature dependence using EIS of the bilayer. More sensitive characterization methods will be developed as needed. Examples of these results, where the area specific resistance is only a few ohms, both positive and negative, are shown in Figure VI - 252.

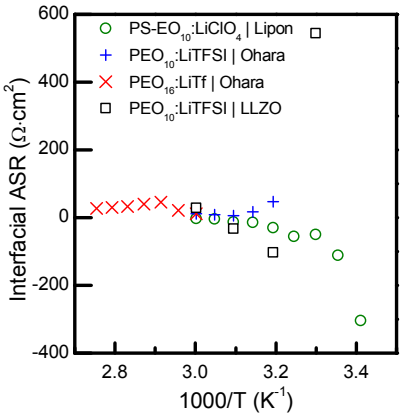


**Figure VI - 252: Area specific resistance for the interface between polymer and inorganic electrolytes. Values were determined from impedance of the bilayer compared to individual components as a function of the temperature**

Similarly, EIS approaches are used to characterize the interface resistance of vapor deposited Li onto various solid electrolytes. In general, this interface is less resistive than those formed by hot-pressing lithium foil against the solid electrolyte.

**Simulation of dispersed particle composites.** Our prior work demonstrated that a very high volume fraction (~60%) of dispersed ceramic particles is needed for mechanical stability and good ionic conduction, assuming a well adhered and conductive interface is formed between the phases. To accurately address the complex contacts between dispersed particles, we developed software and methods to simulate microstructures with varying extents of neck formation between the ceramic particles. The contact area (necks) is assumed to be perfectly adhered and conductive. Calculations were conducted with material properties typical for PEO-based electrolytes and a garnet ceramic electrolyte. Figure VI - 253 shows that a reasonably effective Li ion conductivity can be achieved even for a poorly conductive polymer electrolyte. The size of the necks between particles is a key variable. Similarly, the mechanical stability of a composite improves with necks at the particle contacts and the ceramic loading needed for a high bulk modulus is somewhat reduced. Because of these predictions, efforts are underway to develop a fabrication method that allows for partial sintering and percolation of the ceramic phase as a 3D network.

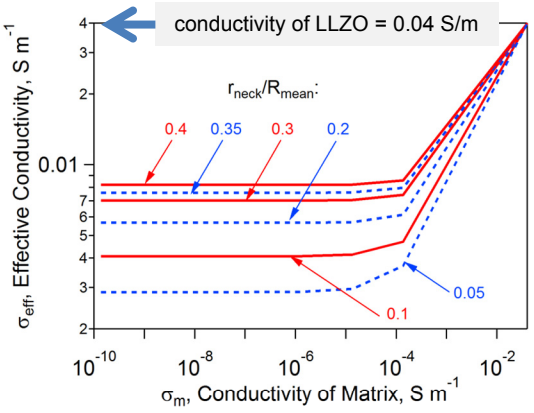


**Figure VI - 253: Effective conductivity for 50 vol.% loading of randomly dispersed LLZO particles in a polymer matrix. Conductive necks are assumed to form at contacts between the ceramic particles**

**Grain boundary conductivity.** The effect of grain boundaries on the ionic conductivity of garnet ceramic electrolytes was unknown, with conflicting reports appearing in the literature. This is important to resolve as grain boundaries likely form at sintered necks. Using very dense hot-pressed pellets from Prof. Sakamoto (Michigan State University), impedance analysis over an extended temperature and frequency window was used to carefully extract the grain boundary contribution, such as shown in Figure VI - 254. From this work, grain boundaries are expected to add only a small resistance at ambient temperatures to the composites if the boundary is pure and dense.

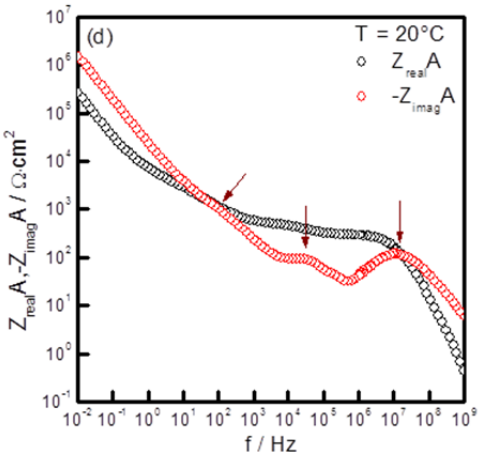


**Figure VI - 254: Example of extended impedance scan showing dispersion attributed to the grain boundary resistance**

**Dispersed particle composites.** Composites with promising mechanical and ion transport properties have been prepared using submicron ceramic powder in several different polymer-salt matrices. The fabrication approach is critical to ensure good adhesion and contact

between the phases, as earlier attempts resulted in a highly resistive ceramic-polymer interface and hence a suppression of the conductivity of the composite relative to the pure polymer phase. An example is shown in Figure VI - 255 where the conductivity of the composite falls between that of the pure sintered ceramic (Ohara Corp.) and the pure polymer, a melt cast sheet of PEO with lithium triflate salt. Interestingly, initial measures of the conductivity with blocking electrodes gave values that were quite resistive, less than or equal to that of the polymer matrix, but the conductivity equilibrated to values within an order of magnitude of the dense ceramic. This is consistent with the simulation shown in Figure VI - 253 for a minimal neck radius. Ongoing studies will probe the equilibration process and form composites containing the garnet ceramic. The garnet is proving to be chemically stable with lithium metal, and the larger micron-size particles of the garnet ceramic will minimize the number of interfaces across the membrane that add resistance.

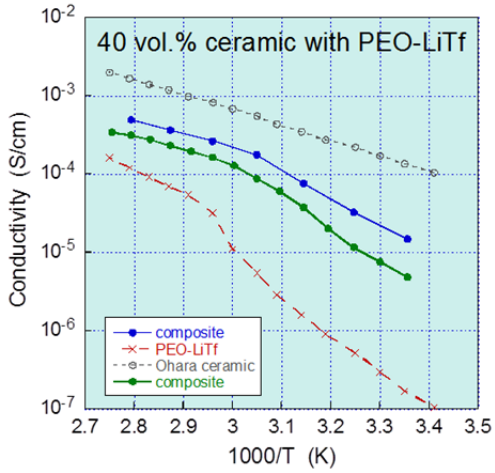


**Figure VI - 255: Conductivity of dispersed ceramic polymer composite electrolyte compared to those of the pure and dense phases**

## Conclusions and Future Directions

Bilayer results demonstrate that, with optimized fabrication, the interface resistances of grain boundaries, lithium metal contacts, and polymer electrolyte to ceramic electrolyte boundaries can be minimized. Simulation results indicate that composites where the hard ceramic phase forms an interconnected skeleton, preferably with sizeable necks, will compensate for a polymer electrolyte that has a low bulk modulus and high resistivity. Successful composites that are conductive and mechanically robust have been prepared using submicron powders of the Ohara phosphate electrolyte in several polymer electrolyte matrices. Future work will seek similarly promising composites with the stable garnet electrolyte.

## FY 2013 Publications/Presentations

1. N.J. Dudney, W.E. Tenhaeff, S. Kalnaus, K.A. Perry, “Composite Electrolyte to Stabilize Metallic Lithium Anodes,” DOE-VTO Annual Merit Review and Peer Evaluation Meeting, Arlington, VA, May 2013.
2. W. E. Tenhaeff, K. A. Perry, S. Kalnaus, N. J. Dudney, “Tough Solid Composite Electrolytes to Enable Lithium Metal Anodes,” Prime Pacific Rim Meeting on Electrochemical and Solid-State Science. Honolulu, HI, Oct. 2012.
3. Wyatt E. Tenhaeff, Nancy J. Dudney*, Sergiy Kalnaus, Kelly Perry, Erik G. Herbert, Ezhiylmurugan Rangasamy, Jeff Sakamoto, “Transport and Mechanical Properties of Bilayer and Composite Electrolytes for Li-metal Batteries,” Fall MRS, Boston, MA Nov. 29, 2012 (invited).
4. W.E. Tenhaeff, K.A. Perry, N.J. Dudney, “Impedance characterization of Li ion transport at the interface between laminated ceramic and polymeric electrolytes,” J. Electrochem. Soc, 159 [12] (2012) A2118-2123.
5. Sergiy Kalnaus, Wyatt E. Tenhaeff, Jeffrey Sakamoto, Adrian S. Sabau, Claus Daniel, Nancy J. Dudney, “Analysis of composite electrolytes with sintered reinforcement structure for energy storage applications,” J Power Sources 241 (2013) 178-185.
6. Wyatt E. Tenhaeff, Ezhiyl Rangasamy, Yangyang Wang, Alexei P. Sokolov, Jeff Wolfenstine, Jeffrey Sakamoto, Nancy J. Dudney, “Resolving the grain boundary and lattice impedance of hot pressed $Li_7La_3Zr_2O_{12}$ garnet electrolytes,” in press, ChemElectroChem.

# VI.G.7 Lithium Dendrite Prevention for Lithium-Ion Batteries (PNNL)

**Wu Xu**
Pacific Northwest National Laboratory

Energy and Environment Directorate
902 Battelle Boulevard
Richland, WA 99354
Phone: (509) 375-6934; Fax: (509) 375-2186
E-mail: wu.xu@pnnl.gov

**Ji-Guang Zhang (Co-PI)**
Energy and Environment Directorate
902 Battelle Boulevard
Richland, WA 99354
Phone: (509) 372-6515; Fax: (509) 375-2186
E-mail: jiguang.zhang@pnnl.gov

Start Date: October 1, 2011
Projected End Date: September 30, 2015

## Objectives

- Prevent Li dendrite growth and improve the safety of Li-ion batteries during overcharging and low-temperature operating conditions
- Enable Li metal as an anode material for rechargeable Li-battery applications.

## Technical Barriers

Li dendrite growth and low Li Coulombic efficiency are the two major problems hindering the application of Li metal as an anode material in rechargeable Li batteries. Li dendrite growth on carbonaceous anodes in Li-ion batteries also has been a serious safety issue during abusive charging conditions, such as overcharging, charging at high rates, and charging at low temperatures. All of these barriers have hindered commercialization of rechargeable Li-metal batteries as well as state-of-the-art Li-ion batteries for use in plug-in hybrid electric vehicles and pure electric vehicles.

## Technical Targets

- Optimize electrolyte compositions to effectively prevent Li dendrite growth on Li-metal anode.
- Identify appropriate electrolyte formulations to minimize the formation of Li dendrite growth on carbonaceous anodes.
- Identify optimal electrolyte formulations to extend the cycle life of Li-metal batteries without internal shorting.

## Accomplishments

- Significantly improved Li Coulombic efficiency by using appropriate EC-based electrolytes and adding SEI film formation additives.
- Demonstrated dendrite-free Li morphologies on Li and carbon anodes by adding small amount of a cesium (Cs) additive.
- Successfully prevented Li plating or dendrite formation on a hard carbon anode during the overcharging process.
- Successfully demonstrated that the addition of a Cs additive does not affect the rate capability and long-term cycling stability of a Li-metal anode, a hard-carbon anode, and cathode materials.

✧ ✧ ✧ ✧ ✧

## Introduction

Li-metal batteries have been called the “holy grail” of energy storage systems because the Li metal anode has an ultra-high theoretical specific capacity, low density, and the lowest negative electrochemical potential. They have been extensively investigated over the last 40 years but two major problems—Li dendrite growth and low Li Coulombic efficiency—hinder its commercial applications. For a Li-ion battery, Li plating and Li dendrite formation during overcharging or fast charging, or charging at low temperatures also is a serious problem to be solved. It has been found that Li dendrite formation is related to the non-uniformity of the passivation layer at the electrode/electrolyte interface, which results in fluctuation of the current density across the anode surface and in turn causes different Li deposition rates at different sites, resulting in the formation of dendrites. A rough or dendritic Li film generated at the anode surface is an intrinsic characteristic and a self-accelerated process. The formation of Li dendrites may lead to internal short circuiting of the battery and result in a shortened battery cycle life or even more serious safety problems such as thermal runaway, fire, and explosion. A general solution to the dendrite growth problem will not only enable a series of Li-metal based energy storage systems, but also significantly improve the safety of Li-ion batteries.

## Approach

The PNNL approach is to develop appropriate electrolyte solvents and additives to prevent Li dendrite growth on the Li-metal and the carbon anode surface during repeated charging/discharging cycles and overcharging processes of Li-metal and Li-ion batteries by the self-healing electrostatic shield (SHES) mechanism recently developed at PNNL. Electrolyte solvents, Li salts, and self-healing additives will be investigated to minimize or even eliminate Li dendrite formation that is detrimental to the safety of Li-ion batteries. The surface smoothing electrolytes proposed in this work are expected to significantly improve the safety of Li-ion batteries and ultimately enable application of Li metal batteries.

## Results

**1. Effects of solvents and salts on Li Coulombic efficiency.** The average Columbic efficiency of Li deposition and the morphologies of deposited Li film in the electrolytes of different organic solvents and Li salts were studied by using the Li|Cu cell configuration and modified Aurbach's method. The Li Coulombic efficiency in electrolytes containing EC-PC mixtures (EC:PC = 0 to 100) shown in Figure VI - 256 indicates that Li Columbic efficiency is significantly improved by adding EC into the PC electrolyte, and the efficiency increases with EC content in the EC-PC mixtures. For example, Li Columbic efficiency is increased from 76% to 93% when the EC:PC ratio is increased from 0 to 80%. Without the $CsPF_6$ additive, significant dendrites were observed on the Li film deposited in an electrolyte of 1-M $LiPF_6$/EC-PC mixture, which is similar to that using 1-M $LiPF_6$/PC electrolyte. When 0.05-M $CsPF_6$ is added to the electrolytes, Li films exhibit a metallic shining surface without dendrite growth. However, no significant difference in the Columbic efficiency of Li deposition was found among the electrolytes either with or without Cs additives (represented by the red dots in Figure VI - 256).

In addition to $CsPF_6$, another two Cs-based additives, CsTFSI and $CsClO_4$, also were studied in PC-based electrolytes to investigate the effect of anions on Li deposition morphology and Columbic efficiency. Both Cs additives can significantly improve the Li deposition morphology, but they significantly affect the Columbic efficiency of Li deposition. For CsTFSI, the efficiency slightly increased from 70.4% to 72.3% with addition of 0.01- to 0.1-M CsTFSI. For $CsClO_4$, the efficiency slightly decreased from 72.1% to 70.7% (67.4%) with addition of 0.01-M (0.05-M) $CsClO_4$.

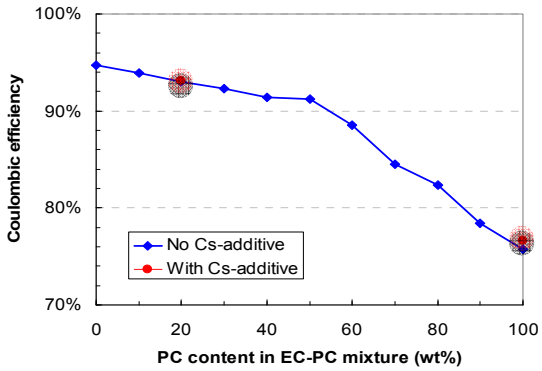


**Figure VI - 256: Li Columbic efficiency of $LiPF_6$/EC-PC electrolytes**

The average Coulombic efficiency of Li deposition in electrolytes containing different carbonate and ether solvents is summarized in Table VI - 10 and Table VI - 11. It is seen from both tables that the cyclic carbonate and ether solvents give much higher Columbic efficiency than the linear solvents. FEC, VEC, and VC (these are the carbonate solvents often used as SEI formation additives in Li-ion battery electrolytes) give even higher Li Coulombic efficiencies (above 97%) than EC. Therefore, these chemicals can be added as co-solvents or additives to protect Li-metal anodes and to further increase the Coulombic efficiency of the anode. As for ether-based solvents, DOL gives the highest Coulombic efficiency among other tested solvents. The average Coulombic efficiency is over 90% depending on the Li salt used. With the combination of $LiAsF_6$ in DOL, the Li Coulombic efficiency is greater than 99%. However, addition of $CsPF_6$ in the DOL solvent leads to gelation, and the dendrite still appear when Li deposits in $LiAsF_6$ in the DOL.

**Table VI - 10: Summary of average Li Coulombic efficiency in 1-M $LiPF_6$-based electrolytes**

| Carbonate solvent | Average Li Coulombic efficiency | |
|---|---|---|
| | Without $CsPF_6$ | 0.05M $CsPF_6$ |
| PC | 75.7% | 76.6% |
| EC | 94.8% | |
| EC-PC (8:2 wt) | 93.1% | 93.1% |
| DMC | 23.6% | |
| EMC | 7.3% | |
| VC | 97.1% | |
| FEC | 97.6% | |
| VEC | 98.2% | |

It is also seen from the results in the two tables that the addition of Cs-additives into the electrolytes has negligible effects on the Coulombic efficiency of Li deposition. In ether-based electrolytes, the salt significantly affects the Li deposition morphology. LiTFSI and $LiClO_4$ lead to very poor Li deposition with low coverage on copper (Cu). Even with the addition of CsTFSI into LiTFSI electrolytes, the morphology is not improved. On the other hand, $LiAsF_6$ gives good coverage and morphology of Li film deposited on Cu. It can be concluded that the nature of the organic solvent has a significant effect on the Coulombic efficiency and morphology of lithium deposition. The selection of lithium salts also plays an important role.

**Table VI - 11: Summary of average Li Coulombic efficiency in 1-M ether-based electrolytes**

| Solvent | Salt | Ave. Li Coulombic efficiency | | |
|---|---|---|---|---|
| | | No CsTFSI | 0.01M CsTFSI | 0.05M CsTFSI |
| DME | LiTFSI | 61.1% | | |
| Diglyme | LiTFSI | 36.8% | | |
| Triglyme | LiTFSI | 54.1% | | |
| Tetraglyme | LiTFSI | 42.0% | | |
| THF | LiTFSI | 78.8% | 80.2% | 79.2% |
| DOL | LiTFSI | 94.0% | 93.0% | 93.7% |
| DOL | LiTFSI | 94.0% | | |
| DOL | $LiClO_4$ | 90.6% | | |
| DOL | $LiAsF_6$ | 99.1% | | |

**2. Effect of additives on Li Coulombic efficiency.** The average Li Coulombic efficiency of control electrolytes can be improved by adding SEI formation additives, even at 2% addition by weight (see Table VI - 12). The high Coulombic efficiency of 97% and good morphology for Li deposition is obtained for an electrolyte of 1-M $LiPF_6$ in EC/PC (8:2 by wt.) with 0.05-M $CsPF_6$ and 2% VC.

**Table VI - 12: Summary of average Li Coulombic efficiency in carbonate-based electrolytes with different additives**

| | No | VC | FEC | $LiAsF_6$ | LiBOB | LiDFOB |
|---|---|---|---|---|---|---|
| 1 | 73.2% | 93.3% | 93.7% | 77.4% | 80.0% | 80.3% |
| 2 | 74.7% | 91.7% | | 80.9% | | |
| 3 | 94.4% | | | 98.2% | | |
| 4 | | 96.6% | | | | |

Notes:
1 = 1M $LiPF_6$ in PC
2 = 1M $LiPF_6$ in PC + 0.05M $CsPF_6$
3 = 1M $LiPF_6$ in EC/PC (8:2 wt)
4 = 1M $LiPF_6$ in EC/PC (8:2 wt) + 0.05M $CsPF_6$

**3. Effect of Cs-additive on hard carbon electrodes.** First, the effect of the Cs additive on the Li deposition morphology on a carbonaceous surface during overcharge was studied. The carbon electrode was prepared using hard carbon/SP/PVDF at 8:1:1 by weight. The overcharging test was conducted inside an argon-filled glove box in a beaker cell, where the carbon electrode was used as the working electrode, a Li plate as the counter electrode, and 1.0-M $LiPF_6$ in PC with 0.05-M $CsPF_6$ as the electrolyte. The theoretical capacity of the hard carbon was selected as 500 mAh/g. After two formation cycles between 0.01 V and 1.5 V at a C/4 rate, the carbon electrode was charged to a capacity three times its theoretical capacity (i.e., 200% charged over the theoretical capacity). The scanning electron microscopy images in Figure VI - 257 shows that Li dendrites formed during overcharging in the control electrolyte that did not contain an additive (Figure VI - 257a), while only small spherical Li particles were formed in the Cs-containing electrolyte (Figure VI - 257b). When overcharging was 100%, a large amount of silver colored Li dendrites were formed on the carbon electrode surface in the control electrolyte that did not contain $CsPF_6$ (Figure VI - 258a), while no Li dendrites are found on the carbon surface from the Cs-containing electrolyte (Figure VI - 258b). This demonstrated that the $CsPF_6$ additive can prevent Li dendrite formation on a carbon surface during overcharging, which should improve the safety of Li-ion batteries during abuse conditions.

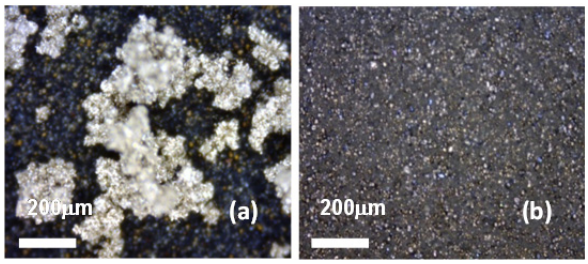


**Figure VI - 257: Scanning electron microscopy images of surface morphologies of hard carbon electrodes after 200% overcharging in the control electrolyte (a) and the electrolyte with 0.05 M $CsPF_6$ as additive (b)**

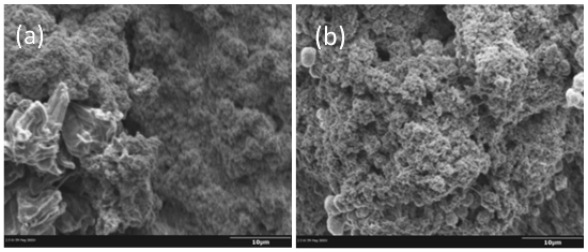


**Figure VI - 258: Optical images of surface morphologies of hard carbon electrodes after 100% overcharging in (a) control electrolyte of 1.0-M $LiPF_6$ in PC and (b) the electrolyte with 0.05-M $CsPF_6$**

The effect of the Cs-additive on the rate capability and long-term cycling stability of the hard carbon electrodes was examined. Figure VI - 259a and Figure VI - 259b show that the addition of $CsPF_6$ into the electrolyte does not affect the rate capability (up to 10 C rate) and the cycling stability of the hard carbon electrode, respectively, in more than 250 cycles. The hard carbon shows a slightly higher capacity in Cs-containing electrolyte than in the control electrolyte.

**4. Effect of Cs-additive on cathode cycling stability.** The long-term cycling stability of several electrolytes both with and without $CsPF_6$ additive in Li half cells containing three cathodes $LiFePO_4$ (LFP) $LiNi_{0.80}Co_{0.15}Al_{0.05}O_2$ (NCA) from ANL and $LiNi_{1/3}Mn_{1/3}Co_{1/3}O_2$ (NMC) from an industry partner have been investigated. The NCA and NMC cells show fast capacity fading with cycling, even in conventional Li-ion battery electrolytes, indicating the poor quality of these two electrodes (figures not shown here). However, both of them show slightly better cycling performance for the electrolytes with $CsPF_6$ additive. As for the LFP electrode that was homemade, no significant difference was observed for about 1600 cycles (Figure VI - 260), and it seems no short circuit occurs even for the control electrolytes that did not contain $CsPF_6$. The main reason is probably the excellent stability of LFP at low LFP loading condition (1.7 mg/cm$^2$ or 0.29 mAh/cm$^2$). High loading LFP electrodes and high quality NCA and NMC electrodes are under development and will be used to test Cs-containing electrolytes.

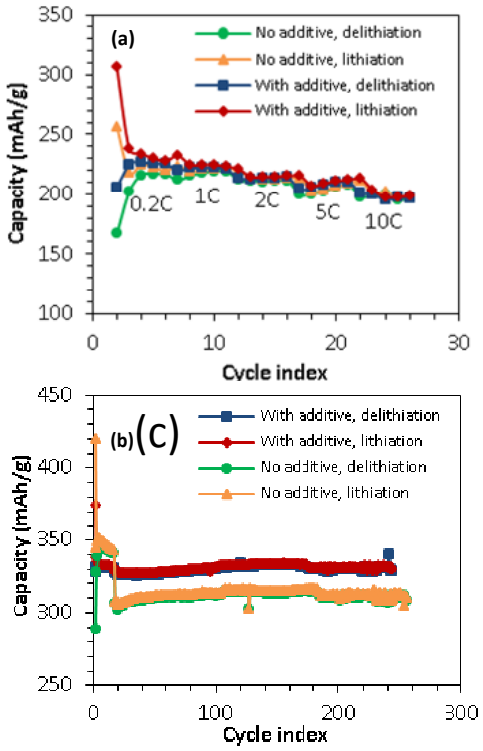


**Figure VI - 259: Rate capability (a) and long-term cycling stability (b) of electrolyte (1.0-M $LiPF_6$ in EC/PC/EMC) with and without 0.05-M $CsPF_6$ on hard carbon electrodes**

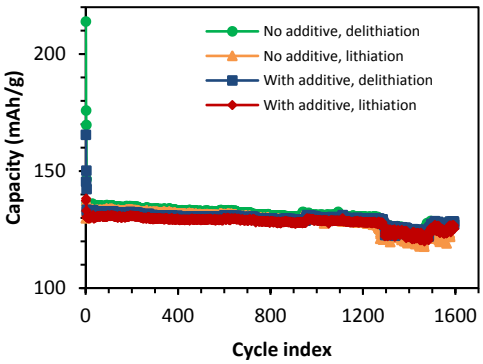


**Figure VI - 260: Long-term cycling stability of Li|LFP cells with electrolytes of 1.0-M $LiPF_6$ in PC both with and without 0.05-M $CsPF_6$**

## Conclusions and Future Directions

Dendrite-free Li films with high Coulombic efficiency of Li deposition/stripping have been demonstrated. Coulombic efficiency can be significantly improved by using appropriate EC-based electrolytes and by adding SEI film formation additives. The deposited Li

morphologies on Li and carbon anodes can be dendrite-free by adding small amount of a Cs additive. Such an additive also can prevent Li plating or dendrite formation on hard carbon anode during overcharging process. The addition of a Cs additive does not affect the rate capability and long-term cycling stability of a Li-metal anode, a hard carbon anode, and cathode materials. We will further investigate new electrolyte formulations to prevent Li dendrite formation on Li-metal and carbon anodes during overcharging and/or low temperature conditions as well as to improve the battery performance.

## FY 2013 Publications/Presentations


1. F. Ding, W. Xu*, G. L. Graff, J. Zhang, M. Sushko, X. Chen, Y. Shao, M. H. Engelhard, Z. Nie, J. Xiao, X. Liu, P. V. Sushko, J. Liu, J.-G. Zhang*, "Dendrite-Free Lithium Deposition via Self-Healing Electrostatic Shield Mechanism", *J. Am. Chem. Soc.*, 2013, **135**, 4450-4456.
2. F. Ding, W. Xu*, X. Chen, J. Zhang, M. H. Engelhard, Y. Zhang, B. R. Johnson, J. V. Crum, T. A. Blake, X. Liu, J.-G. Zhang*, "Effects of Carbonate Solvents and Lithium Salts on Morphology and Coulombic Efficiency of Lithium Electrode", *J. Electrochem. Soc*., 2013, 160, A1894-A1901.
3. W. Xu, F Ding, J. Zhang, X. Chen,M. H. Engelhard, M. Sushku, E. Nasybulin, J. Xiao, G. L. Graff, and J.-G. Zhang. "Enhanced Morphology and Cycling Efficiency of Li Metal Anode by Electrolyte Additives for Rechargeable Li Batteries," Presented in 222nd ECS Meeting, Oct. 7, 2012, Honolulu, Hawaii.
4. J.-G. Zhang, W. Xu, F. Ding, G. L. Graff, X. Chen, Y. Zhang, M. Sushku, "Self-Healing of Dendrite Growth in Li-Metal Batteries," Invitaed talk at 2013 International Battery Association Meeting, March 13, 2013, Barcelona, Spain.
5. J.-G. Zhang, W. Xu, F. Ding, X. Chen, Y. Zhang, E. Nasybulin, G. L. Graff, "Revival of Rechargeable Li Metal Batteries," Invited talk at Beyond Lithium-Ion VI, June 4-6, 2013, Boulder, Colorado.
6. W. Xu, M. H. Engelhard, E. Nasybulin, Y. Zhang, X. Chen, J.-G. Zhang, "XPS—A powerful technique for battery electrode surface analysis", Invited talk at 2013 Symposium of the Pacific Northwest Chapter of the AVS, September 19-20, 2013, Troutdale, Oregon.

# VI.G.8 Development of High Energy Lithium Sulfur Batteries (PNNL)

**Jie Xiao**
Pacific Northwest National Laboratory

Energy and Environment Directorate
902 Battelle Boulevard
Richland, WA 99352
Phone: (509) 375-4598; Fax: (509) 375-2186
E-mail: jie.xiao@pnnl.gov

**Jun Liu (Co-PI)**
Pacific Northwest National Laboratory
Energy and Environment Directorate
902 Battelle Boulevard
Richland, WA 99352
Phone: (509)375-4443;Fax: (509)371-6242
E-mail: jun.liu@pnnl.gov

Start Date: October 1, 2011
Projected End Date: September 30, 2015

## Objectives

- Develop high energy lithium-sulfur (Li-S) batteries
  - Investigate the fundamental chemistry and failure mechanism in the Li-S system
  - Apply fundamental research to help address the challenges in practical applications.

## Technical Barriers

- High cost of materials and synthesis routes
- Limited energy density and cycling ability.

## Technical Targets

- Systematic investigation of the sulfur/carbon (S/C) composite cathode in terms of carbon properties and electrochemical redistribution process of polysulfides
- Understand the interfacial reactions between the electrode and the electrolyte
- Explore novel strategies to mitigate the parasitic reactions that irreversibly consume polysulfides throughout cycling.

## Accomplishments

- Constructed a baseline S/C cathode with 80% S in the composite
- Identified key factors for obtaining reproducible results for Li-S batteries.
- Modified Li metal surface by using co-solvent to alleviate polysulfide contamination
- Developed a novel approach for fabricating a pinhole-free thick sulfur electrode with a sulfur loading of 2 to 8 mg/cm$^2$ over a large area.

✧ ✧ ✧ ✧ ✧

## Introduction

Li-S batteries have attracted increasing attention because of their high theoretical capacity, natural abundance of materials, low cost, and environmental friendliness. Assuming $Li_2S$ as the end-product, the maximum specific capacity and energy of Li-S batteries are 1675 Ah/kg and 2650 Wh/kg, respectively, which are significantly higher than those of state-of-the-art Li-ion batteries. However, the low electrical conductivity ($5 \times 10^{-30}$ S/cm) of sulfur and the "shuttle reaction" caused by the soluble polysulfides are detrimental to Li-S battery performances, leading to low utilization of sulfur, poor Coulombic efficiency, fast capacity fading and self-discharge.

## Approach

Although there are many approaches reported in literature for addressing the challenges in Li-S systems, the sulfur content in the S/C composite, the electrode thickness, and testing conditions vary largely in different groups, making direct comparison or evaluation of various methods difficult. The approaches we took included:

- Side-by-side comparison of different carbons by controlling 80% sulfur content in the composite
- Electrochemical understanding by using the baseline S/C cathode
- Evaluation of novel strategies in Li-S batteries by using baseline cathodes
- Application of the knowledge gained from the baseline cathode to a thick sulfur electrode for practical application.

## Results

**1. Baseline S/C composite cathode.** Four different carbons (e.g., Ketjenblack [KB], graphene, acetylene black [AB], and hollow carbon nanoSphere [HCNS]), were chosen to construct C/S composites. To eliminate other factors (e.g., sulfur content in the electrode) that may influence the accurate evaluation of carbon effects, sulfur in all C/S composites was controlled at ca. 80 wt%, and the sulfur loading on each electrode was approximately 1 mg/cm$^2$.

Figure VI - 261 compares the morphologies of different S (80%)/C composites. KB (1400 m$^2$/g) and graphene (840 m$^2$/g) both had high surface areas. KB manifested a highly porous structure (Figure VI - 261a3), while graphene only formed two-dimensional sheets (Figure VI - 261b3). On the other hand, AB and HCNS both had low surface areas of 124 m$^2$/g and 76 m$^2$/g, respectively, while the latter was hollow (Figure VI - 261d3) for the individual carbon particle. Incorporation of high sulfur content led to the complete coverage of sulfur on the outside surfaces of all different carbons (Figure VI - 261a2-Figure VI - 261d2) and the pore filling in most KB and HCNS (Figure VI - 261a3 and Figure VI - 261d3).

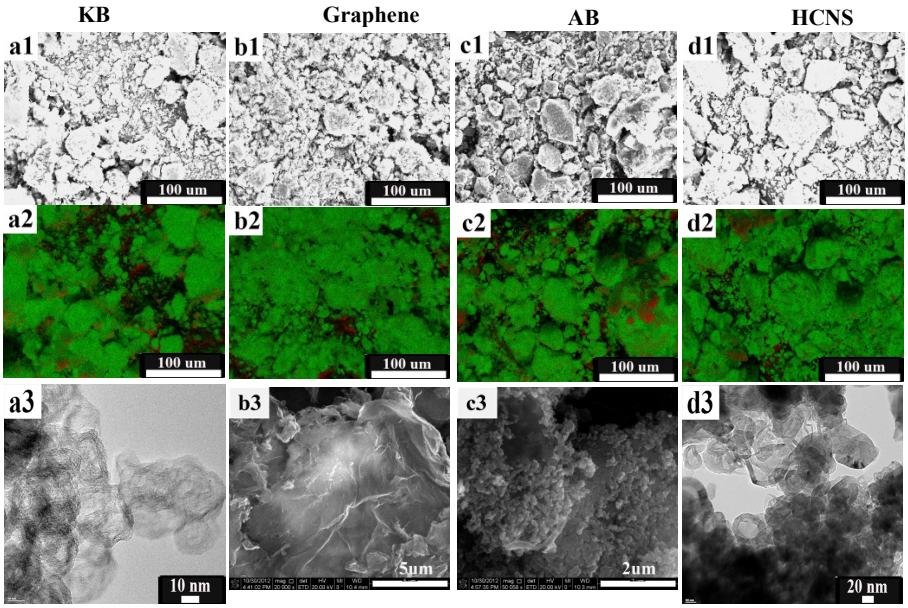


**Figure VI - 261: Morphology comparison of original S /C composites. a1-d1: Scanning electron microscope; a2-d2: Elemental mapping for sulfur in different carbon hosts; a3-d3: Transmission electron microscope (TEM) of these S/C composites**

Figure VI - 262a further reveals that, as the carbon surface area increases, the discharge capacity also increases. This can be explained by the increased utilization rate of sulfur in KB and graphene scaffolds. For carbons that contained similar surface areas, the capacity degradation rates followed exactly the same trend (Figure VI - 262a). At a relatively high rate of 0.5 C (Figure VI - 262a), the cycling data for KB and graphene overlap significantly, although KB has a porous structure while graphene does not. Similar phenomena were observed for AB and HCNS with the close low surface areas shown in Figure VI - 262a. The additional benefits from the pore volumes of KB and HCNS were seen only when the rate decreased to 0.2C (Figure VI - 262b). The lower rate (0.2C) provided sufficient time for soluble polysulfides to move from the cathode side during each cycle. The existence of porous structures on carbon slightly slowed down this “leaking” process for polysulfides by increasing the diffusion length within the carbon through the pores. Based on these results, KB with its high surface area and large pore volume was therefore chosen for the construction of the baseline sulfur electrode.

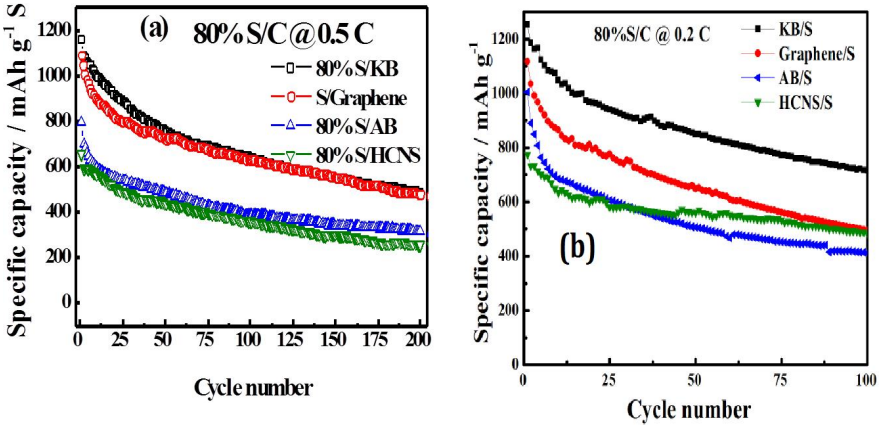


**Figure VI - 262: Comparison of the cycling stability of different S/C composites at (a) 0.5 C and (b) 0.2 C rates**

**2. Key parameters to obtain reproducible Li-S battery results.** For Li-ion batteries tested in the laboratory, excessive amount of electrolyte was always used to maximize the performance of active materials. Although it is not the case for practical applications, electrolyte-rich cells almost have become the default approach in the laboratory studies reported in the literature. However, for Li-S cells, the intermediate product is soluble, which allows the electrolyte content to directly influence the concentration of dissolved polysulfides and their subsequent nucleation and re-deposition. It was found that the relative S/electrolyte ratio significantly affected the cycling stability of Li-S cells and needed to be carefully controlled in each cell to generate reproducible/reliable results. Figure VI - 263a compares the cycling stability of Li-S cells in different amounts of electrolyte. The greater the amount of electrolyte (i.e., a lower S/L ratio), the higher the initial discharge capacity because of the increased utilization rate of sulfur caused by wetting. However, capacity decayed much faster in the presence of an excessive amount of electrolyte (i.e., S/L = 14 shown in Figure VI - 263a). The highest capacity retention rate is optimized at S/L = 50. It was found that the fast capacity degradation in the initial few cycles (circled area in Figure VI - 263a), which is commonly reported in the literature, was largely alleviated by reducing the relative amount of electrolyte in the cell.

Figure VI - 263b further compares electrode morphologies harvested from different cells. When the relative content of solid sulfur was low (S/L = 14 or 20 in Figure VI - 263b), more cracks and aggregates were found. The loss of cathode structure integration was probably related to the easy dissolution of polysulfide in the flooded cell. When the S/L ratio was increased to 75, the cathode exhibited a much smoother surface due to the much higher rate of polysulfide nucleation than growth in the concentrated electrolyte (S/L = 75), thus improving the Coulombic efficiency (data not shown here). Different morphology evolutions also were identified on the Li anode side. When electrolyte is excessively high (i.e., a low S/L ratio), more sulfur-containing electrolyte contacted with the Li anode and penetrated into the bulk lithium during cycling, which resulted in a rapid increase in cell impedance. When the electrolyte content was controlled (S/L >20) in the cell, Li corrosion was largely alleviated, which is consistent with the cycling stability results shown in Figure VI - 263a.

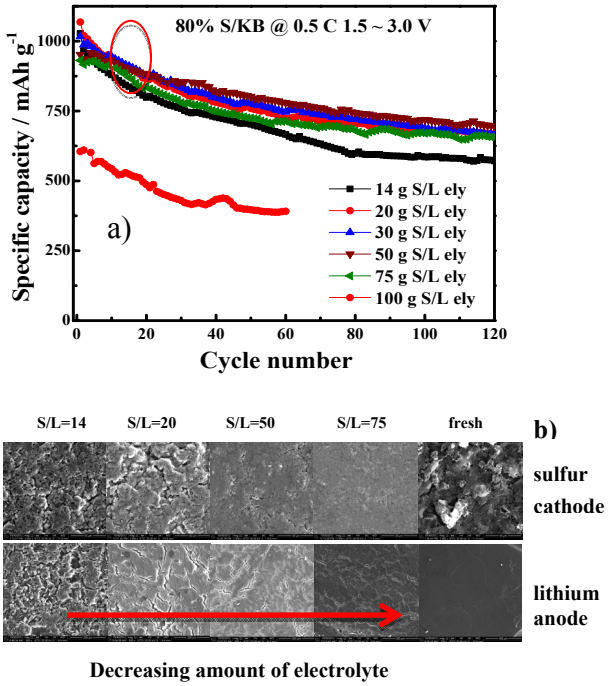


**Figure VI - 263: a) Cycling stability of baseline S/KB cathodes in different amounts of electrolyte. Numbers in the figure represent the solid-to-liquid ratio calculated from sulfur weight (in grams)/electrolyte volume (in liters). The higher ratio in a) corresponds to a smaller amount of electrolyte added in the cell. b) SEM images of cycled sulfur cathodes and Li anodes harvested from different cells in a)**

**3. Enhanced solid state electrolyte interface.** Parallel efforts also were pursued for the Li side focusing on the improvement of solid electrolyte interface (SEI) stability in the presence of corrosive polysulfides. Ionic liquid (IL) N-methyl-Nbutylpyrrolidinium bis(trifluoromethylsulfonyl)imide (Py14TFSI) was employed to modify the SEI layer shown in Figure VI - 264. When the 75% IL containing electrolyte was used in the Li–S battery, the electrochemical performance improved significantly, exhibiting high Coulombic efficiency and very stable cycling with high capacity retention of 94.3% for 120 cycles (Figure VI - 264). Integrated studies from SEM (insets of Figure VI - 264), EIS, and XPS (data not shown here) revealed that the ionic liquid facilitated formation of a more stable SEI layer and improved the quality of the Li metal surface (insets of Figure VI - 264). These improvements effectively prevent continuous penetration of soluble polysulfides into the bulk Li and slow down the otherwise rapid corrosion of Li and the rapid increase of the cell impedance.

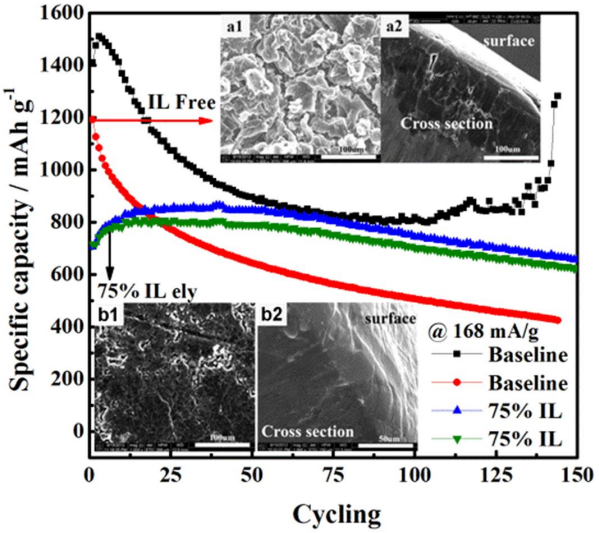


**Figure VI - 264. Comparison of cycling stability with and without ionic liquid (IL) as the co-solvent. The insets compare the surface and cross sectional images of Li metal cycled in (a1, a2) the baseline electrolyte and (b1, b2) in the presence of IL-co-solvent**

**4. Fabrication of thick sulfur electrode (S: 2 to 8 mg/cm$^2$).** Uniform coating of nanoparticles including S/C composite into thick electrode is always challenging but urgently needed for real applications of Li-S batteries. A novel and cost-effective method (for which a patent application has been submitted) has been developed at PNNL to prepare a practically usable sulfur cathode. Figure VI - 265a compares the coated sulfur electrode before and after modification. By using a newly developed method, the pinhole-free thick sulfur electrode displayed a large area of pinhole-free film, adaptable for mass production. The sulfur loading on the as-prepared electrode is also adjustable from 2 to 8 mg/cm$^2$ depending on the specific requirement.

Figure VI - 265b shows the cycling performance of as-prepared sulfur electrode with sulfur loading of 3.8 mg/cm$^2$. The areal specific capacity achieved was 4.5 mAh/cm$^2$ at 0.1 C, which is compatible with that of state-of-art electrodes for Li-ion batteries. Further increasing the rate to 0.2 C, a high area capacity of 3 mAh/cm$^2$ was still obtained. Of note, 1 C used in Figure VI - 265b was 1000 mA/g, translating to a current density of 3.8 mA/cm$^2$, which is much higher than that in traditional Li-ion batteries. By using the knowledge gained from our baseline S/C cathode, good cycling ability was observed in this thick electrode without complicated treatment on the electrodes (still under testing). This confirms the importance of the baseline cathode in assuring that the understanding is transferrable to electrodes with increased thickness and sulfur loadings. More work is underway to identify the balance between sulfur loading and electrochemical performance.

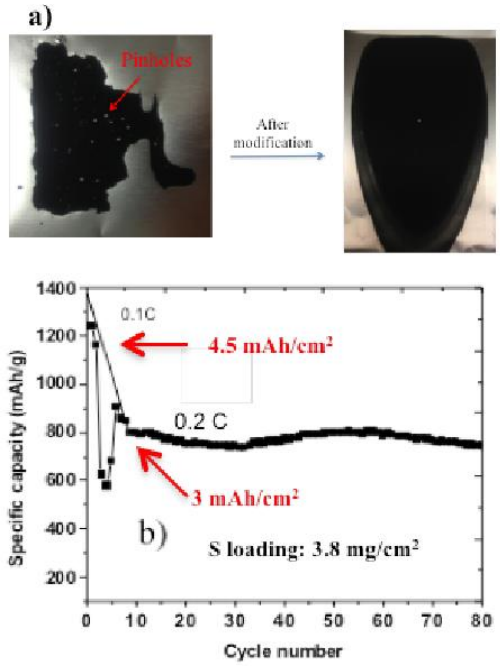


**Figure VI - 265: a) Comparison of as-coated thick sulfur electrodes before and after modification. b) Cycling performance of thick sulfur cathode. 0.1 C was used for the first two cycles, followed by 0.2 C in subsequent cycling (1 C = 1000 mA/g)**

## Conclusions and Future Directions

Beginning with construction of the sulfur baseline cathode, the Li-S battery system has been systematically

investigated during FY13. After correlating the carbon properties to electrochemical behavior of the S/C composite, high-surface-area KB with a porous structure was selected as the carbon host with a sulfur content of 80% in the composite. Based on the baseline electrode, the ratio between solid sulfur and liquid electrolyte was identified to significantly influence the reproducibility of Li-S battery results and optimized to be around 50 g/L for S/KB-type electrode. Ionic liquid was introduced as a co-solvent in the ether-based electrolyte to improve the quality of SEI film on the Li-metal anode side, which effectively improved the cycling stability of Li-S batteries. In addition, a cost-effective approach was invented to homogeneously coat S/C nanoparticles onto large-area pinhole-free cathode films. The sulfur loading is adjustable from 2 to 8 mg/cm$^2$ and the process is readily adaptable for mass production. Knowledge obtained from the baseline S/C cathode was successfully applied in the thick sulfur cathode, which led to considerably improved cycling stability with high areal specific capacity of 3 to 4 mAh/cm$^2$.

Future work will continue to investigate the electrochemical and chemical processes in Li-S batteries, with a focus on thick sulfur cathodes. Appropriate modifications of the anode side will be explored to further improve system performance. Advanced characterization techniques will be coupled with electrochemical measurements to develop fundamental understanding towards the practical application of lithium sulfur batteries for vehicle electrification.

## FY 2013 Publications/Presentations


1. J.Zheng, D. Lu, M.Gu, C.Wang, J.-G. Zhang, J. Liu and J. Xiao, "How to Obtain Reproducible Results for Lithium Sulfur Batteries?" *J. Electrochem. Soc*., **2013**, 160, A2288-2292.
2. J. Zheng, M.Gu, H. Chen, P. Meduri, M.H. Engelhard, J.-G. Zhang, J. Liu and J. Xiao, "Ionic liquid-enhanced solid state electrolyte interface (SEI) for lithium-sulfur batteries", *J. Mater. Chem. A*, **2013**, 1, 8464-8470.
3. J. Zheng, Me. Gu, C. Wang, P.Zuo, P.K. Koech, J.-G. Zhang, J. Liu and J. Xiao, "Controlled Nucleation and Growth Process of $Li_2S_2$/$Li_2S$ in Lithium-Sulfur Batteries", *J. Electrochem. Soc*., **2013**,160, A1992-A1996.
4. J. Zheng, M. Gu, M. J. Wagner, K. A. Hays, X. Li, P. Zuo, C. Wang, J.-G. Zhang, J. Liu, and J. Xiao, "Revisit Carbon/Sulfur Composite for Li-S Batteries", *J. Electrochem. Soc*., **2013**, 160, A1624-A1628.
5. J.Zheng, J. Xiao, H. Chen, M. Gu, P. Meduri, M.H. Engelhard, J.-G. Zhang, "Ionic Liquid Enhanced Solid Electrolyte Interface (SEI) for Lithium Sulfur Batteries", Materials Research Society (MRS) Spring Meeting, San Francisco, April, 2013.
6. J. Liu, "Recent Progress of Li-S and Na Batteries at Pacific Northwest National Laboratories", 7th U.S.-China Electric Vehicle and Battery Technology Workshop, Lawrence Berkeley National Laboratory, Berkeley, California, April, 2013.

# VI.G.9 Rechargeable Lithium-Air Batteries (PNNL)

**Ji-Guang Zhang**
Pacific Northwest National Laboratory

Energy & Environment Directorate
902 Battelle Boulevard, Mail Stop K2-44
Richland, WA 99352
Phone: (509) 372-6515; Fax: (509) 375-2186
E-mail: Jiguang.Zhang@pnnl.gov

**Wu Xu (Co-PI)**
Pacific Northwest National Laboratory
Energy & Environment Directorate
902 Battelle Boulevard
Richland, WA 99352
Phone: (509) 375-6934; Fax: (509) 375-2186
E-mail : wu.xu@pnnl.gov

Start Date: October 1, 2012
Projected End Date: September 30, 2015

## Objectives

- Identify stable components that can enable long-term, rechargeable operation of Li-air batteries for potential application in long-range EV.

## Technical Barriers

Reduced oxygen species ($O_2^{-\bullet}$, $LiO_2$, $O_2^{2-}$, $LiO_2^-$, and $Li_2O_2$) generated on the air electrode surface during the discharge of a Li-$O_2$ battery are strongly reactive. These reduced oxygen species attack all components in a Li-$O_2$ battery that are in contact with the liquid electrolyte and significantly limit the reversibility of rechargeable Li-$O_2$ batteries. In addition, the overvoltage that occurs during the charging process of a Li-$O_2$ battery also is high (i.e., normally over 1 V) and can lead to low Coulombic efficiency of the batteries.

## Technical Targets

- Identify appropriate substrates that will be stable with the reduced species of oxygen (i.e., superoxide radical anion, and $Li_2O_2$) and at high voltages in an oxygen atmosphere.
- Identify appropriate catalysts for the oxygen evolution reaction to lower the charging overvoltage of Li-air batteries.

## Accomplishments

- Identified polyethylene (PE) as the most stable polymer that can be used against superoxide radical and peroxide anions. PE can be used as the polymer binder for air-electrode construction.
- Developed poly(3,4-ethylenedioxythiophene) (PEDOT) as an organic catalyst to reduce overvoltage during charging process of Li-$O_2$ batteries.
- Developed a carbon nanotube/ruthenium (CNT/Ru) nanocomposite as an electrocatalytic substrate for improving cycling performance of Li-$O_2$ batteries.

✧ ✧ ✧ ✧ ✧

## Introduction

Li-air or Li-$O_2$ batteries have an ultra-high theoretical specific energy (~5200 Wh/kg when the weights of Li and $O_2$ are included), and are expected to have a practical specific energy of around 800 Wh/kg that is about four times of those of the state-of-the-art Li-ion batteries (ca. 200 Wh/kg). However, the development of rechargeable Li-$O_2$ batteries faces significant challenges including the decomposition of electrolyte, the large over-voltage that occurs during charge process, design of cathode materials with high capacity and stability, and protection of the Li anode. More importantly, highly reactive oxygen species ($O_2^{-\bullet}$, $LiO_2$, $O_2^{2-}$, $LiO_2^-$, and $Li_2O_2$) are generated on the air electrode surface during the discharge of a Li-$O_2$ battery, and these species attack every component in Li-$O_2$ batteries that are in contact with the liquid electrode and significantly limit the reversibility of the rechargeable Li-$O_2$ batteries. Therefore, the chemical and electrochemical stability of all Li-$O_2$ battery components, including the electrolyte solvent, electrolyte salt, cathode material (typically carbon-based), and binder, needs to be reevaluated in an $O_2$-rich environment. Also, good catalysts need to be developed to reduce the overvoltage during oxygen reduction and evolution reactions so the cycling stability of Li-$O_2$ batteries can be improved.

## Approach

The PNNL approach is to develop new non-carbon based air electrodes and oxygen evolution reaction

(OER) catalysts to avoid carbon oxidation, reduce the charging overvoltage, and improve the cycling stability of rechargeable Li-air batteries. The air electrode study also includes the investigation of the stability of polymer binders against superoxide radical anion and peroxide anion. Catalysts and non-carbon electronic-conductive substrates will be prepared, characterized, and investigated. Relatively stable electrolytes, $CF_3SO_3Li$ (i.e., LiTf) and tetraglyme (i.e., 4G) will be used in these investigations based on our previous investigations. The optimized components and compositions will improve the Coulombic efficiencies and cycle lives of rechargeable Li-$O_2$ batteries.

## Results

**1. Stability of polymer binders.** The effects of 11 polymers on the discharge performance of Li-$O_2$ batteries were evaluated using Ketjenblack-based air electrodes. The nature of the binder significantly affects discharge capacity. In general, a strong binder decreases the capacity by forming a strong bond among the carbon particles, thus reducing the active surface area and pore size/pore volume of the prepared air electrode.

The stability of the polymer binders with $KO_2$ was investigated using x-ray diffraction (XRD) patterns of ball milled powders (Figure VI - 266). The curves in the figure show that PVDF decomposes and forms $KHF_2$; PS decomposes and forms $Li_2CO_3$; PEO decomposes and forms amorphous products; PAN decomposes and forms KCN; PVC decomposes and forms KCl; PVP, PMMA and CMC decompose and form $K_2CO_3$, LiH, and presumably alkylcarbonates; PTFE, PE and PP are relatively stable against $KO_2$.

The stability of PE, PP, and PTFE along with PVDF was further investigated by x-ray photoelectron spectroscopy (XPS) to analyze corresponding powders after ball milling with $KO_2$ and $Li_2O_2$. The XPS results shown in Figure VI - 267 indicates signs of PTFE and PP decomposition when they are in contact with $Li_2O_2$ and $KO_2$. PE was found to be the only stable polymer under the applied experimental conditions. PE is completely stable even in the aggressive ball milling environment and, therefore, will certainly be beneficial to long-term operation of Li-$O_2$ batteries when stable electrolytes are developed.

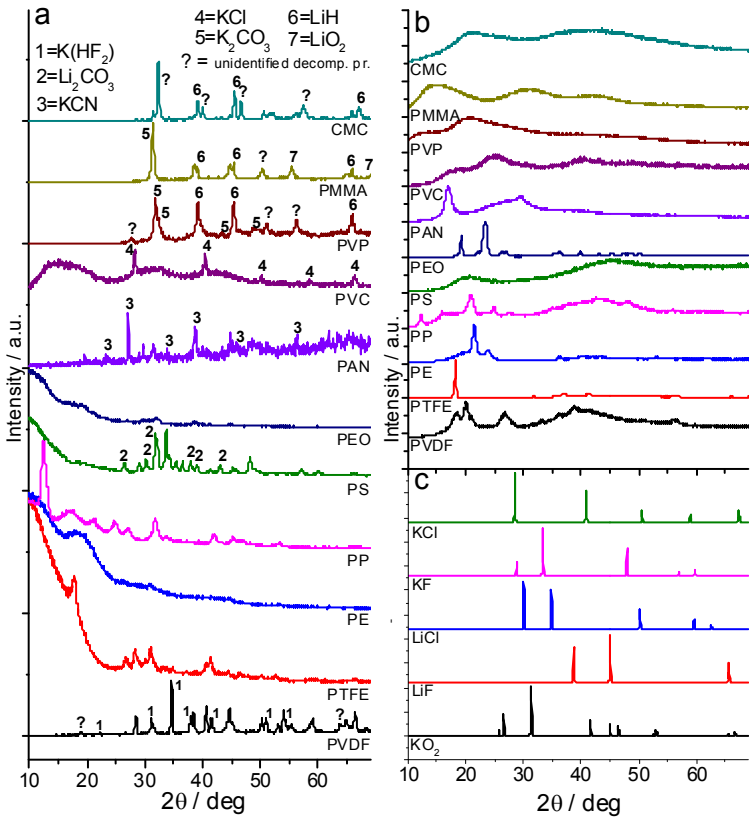


Figure VI - 266. XRD of reaction products of polymer with $KO_2$

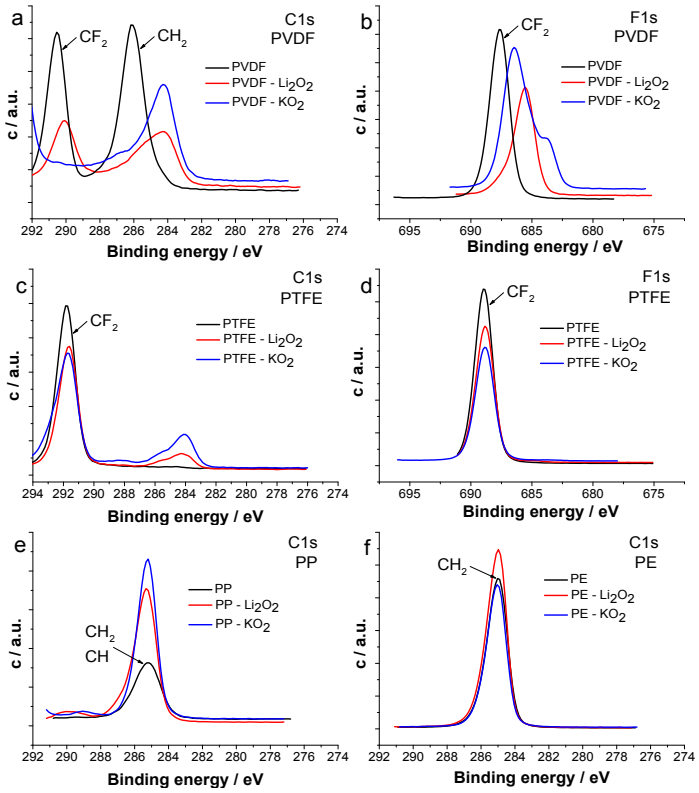


**Figure VI - 267: XPS spectra of the reaction products and pure polymers after ball milling with $KO_2$ and $Li_2O_2$**

## 2. Electrocatalytic effect of PEDOT

PEDOT was successfully polymerized inside Super P carbon (SP) using the chemical oxidative method. The composite of PEDOT-SP was confirmed by Fourier transform infrared spectroscopy (FTIR) and scanning electron microscopy (SEM) with energy dispersive x-ray spectroscopy mapping. The Li-$O_2$ batteries with the SP and PEDOT-SP air electrodes were compared. As shown in Figure VI - 268a, use of PEDOT significantly decreases the charging voltage (potential for oxygen evolution reaction [OER]) by 0.7 to 0.8 V and slightly increases discharge voltage (potential for oxygen reduction reaction) for the first cycle although the cycling performance is not significantly improved due to electrolyte decomposition and relatively high carbon loading. The electrocatalytic activity of PEDOT can be explained by its electrochemical activity in the applied potential range (Figure VI - 268b). PEDOT acts as a mediator in electron transfer between the discharge products and the carbon electrode, decreasing overpotential of the reactions. The electrocatalytic effect of PEDOT is reduced with cycling because of the irreversible decomposition of electrolyte and passivation of PEDOT by side reaction products.

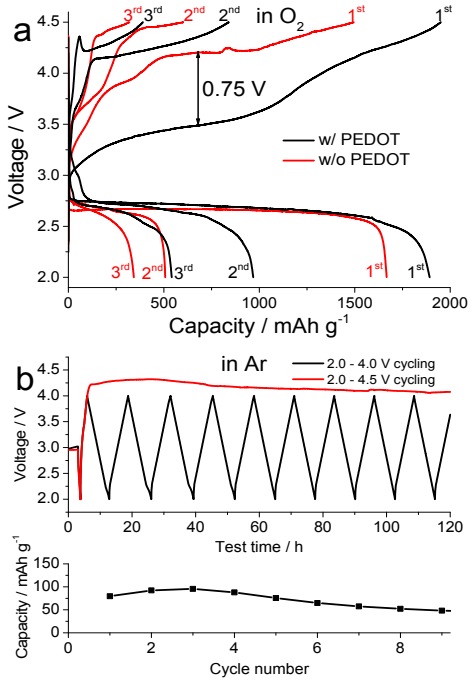


**Figure VI - 268: Voltage profiles for the PEDOT-containing battery and the control battery without PEDOT**

Formation/decomposition of discharge products as well as stability of PEDOT was analyzed by XPS (Figure VI - 269). $Li_2O_2$ was identified as a major discharge product with a contribution from a carbonate-based side product generated during electrode/electrolyte decomposition. After charging, $Li_2O_2$ disappeared while carbonate-based side products stay on the surface, greatly limiting cycling performance. Based on the XPS data, PEDOT with incorporated TFSI counter ions seems to be stable.

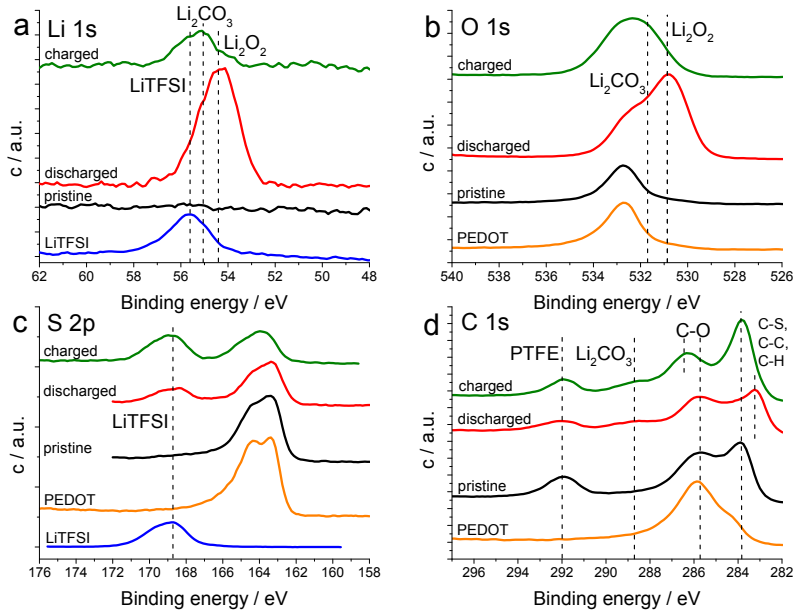


**Figure VI - 269: XPS results for the pristine, discharged, and charged PEDOT/SP/PTFE electrodes in $O_2$**

**3. Ru nanoparticle catalyst.** Ru-decorated CNTs were prepared by thermal reduction of $RuCl_3$ solution in water/glycerol mixture. SEM anlaysis showed an even distribution of Ru particles in the CNT matrix (Figure VI - 270a), while EDS elemental analysis demonstrated 46 wt% Ru in the composite (Figure VI - 270b). TEM analysis revealed that the Ru nanoparticles observed in SEM images represent aggregates of <2 to 4-nm Ru nanoparticles (Figure VI - 270c,d). The high-resolution TEM image (Figure VI - 270d, insert) shows single Ru nanoparticles with a characteristic 0.27-nm lattice space. XRD results (Figure VI - 271a) confirmed the characteristic Ru peaks at 44°, 38.2°, and 69° and a shoulder at 59° in the CNT/Ru nanocomposite. The cycling performance of CNTs/Ru nanocomposite was tested in Li-$O_2$ batteries with the LiTf-tetraglyme electrolyte at 0.1 mA/cm$^2$ current density.

Charge/discharge voltage profiles taken during the selected cycles of the batteries are shown in Figure VI - 271. Long cycle life was observed with a discharge capacity above 1000 mAh/g for nearly 50 cycles. The first cycle of the battery had a discharge capacity of 2500 mAh/g with a discharge plateau at 2.6 V. It is seen that Ru possesses electrocatalytic properties towards OER and decreases charge voltage by 0.3 to 0.5 V depending on loading. Ru also improves the cycle life of the Li-$O_2$ battery, although formation of side products (carbonates) takes over after 5 to 10 discharge cycles, similar to that occurring in non-catalyzed batteries.

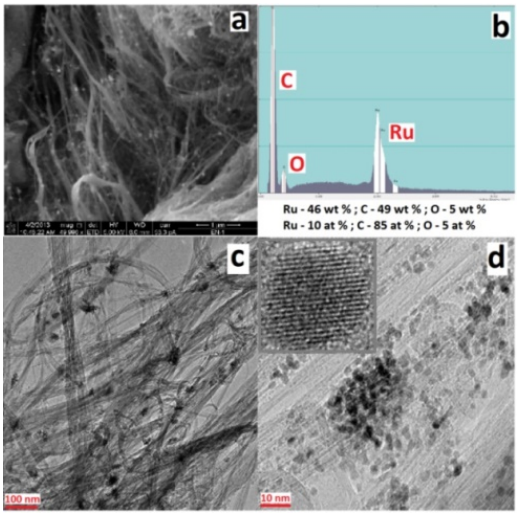


**Figure VI - 270: a) SEM image and b) EDS analysis of the prepared CNTs/Ru composite; c) and d) TEM images of the prepared CNTs/Ru composite**

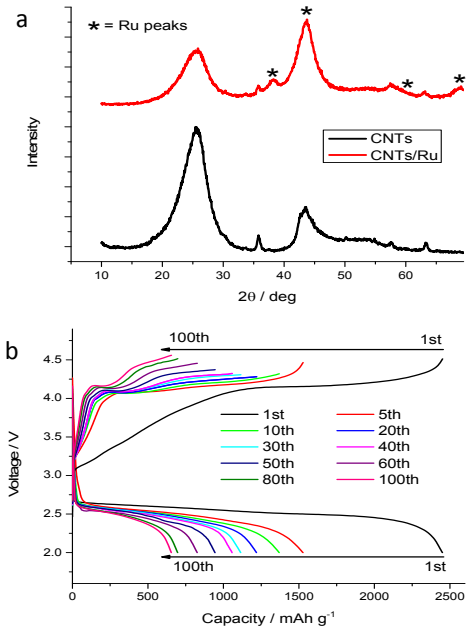


**Figure VI - 271: a) XRD spectra of CNTs and CNTs/Ru composite; b) cycling performance of CNTs/Ru electrode in Li-$O_2$ battery**

## Conclusions and Future Directions

Polyethylene has been identified as the most stable polymer binder for air electrodes. PEDOT proved to be a good organic catalyst for reducing overvoltage during the charging process of Li-$O_2$ batteries, and the CNT/Ru nanocomposite demonstrated good electrocatalytic effect on improving the cycling performance of Li-$O_2$ batteries.

Future work will focus on the investigation of the new electrolytes that are stable against the reactive reduced-oxygen species. Polymer encapsulated air electrodes will be prepared to improve the stability of carbon-based electrodes. The OER catalysts will be further studied to reduce charging overvoltage and improve the cycling stability of the Li-$O_2$ batteries.

## FY 2013 Publications/Presentations

1. Nasybulin, W. Xu,* M. H. Engelhard, Z. Nie, S. D. Burton, L. Cosimbescu, M. E. Gross, J.-G. Zhang,* "Effects of electrolyte salts on the performance of Li-$O_2$ batteries", *J. Phys. Chem. C*, 2013, **117**, 2635-2645.
2. Nasybulin, W. Xu,* M. H. Engelhard, S. X. Li, M. Gu, D. Hu, J.-G. Zhang,* "Electrocatalytic properties of poly(3,4-ethylenedioxythiophene) (PEDOT) in Li-$O_2$ battery", *Electrochem. Commun.*, 2013, **29**, 63-66.
3. Nasybulin, W. Xu,* M. H. Engelhard, Z. Nie, X. S. Li, J.-G. Zhang,* "Stability of polymer binders in Li-$O_2$ batteries", *J. Power Sources*, 2013, **243**, 899-907.
4. J.-G. Zhang, W. Xu, J. Xiao, E. Nasybulin Y. Shao, D. Mei, and J. Zhang, "Critical Components of Rechargeable Li-Air Batteries", Presented at the 222nd ECS Meeting, Oct. 7-11, 2012, Honolulu, HI.
5. E. Nasybulin, W. Xu, J.-G. Zhang, "The effects of electrolyte salts on the performance of Li-air batteries", Presented at the 222nd ECS Meeting, Oct. 7-11, 2012, Honolulu, HI.
6. W. Xu, E. Nasybulin, J.-G. Zhang, "Stability of Electrolyte Solvents, Salts and Electrode Binders in in Li-$O_2$ batteries", Invited talk at Beyond Lithium Ion VI, June 4-6, 2013, Boulder, CO.
7. W. Xu, M. H. Engelhard, E. Nasybulin, Y. Zhang, X. Chen, J.-G. Zhang, "XPS—A powerful technique for battery electrode surface analysis", Invited talk at 2013 Symposium of the Pacific Northwest Chapter of the AVS, September 19-20, 2013, Troutdale, OR.

# VI.G.10 Simulations and X-ray Spectroscopy of Li-S Chemistry (UCB)

**Nitash Balsara**
University of California, Berkeley

Dept. of Chemical and Biomolecular Engineering
201 C Gilman Hall
Berkeley, CA 94720
Phone: (510) 642-8973; Fax: (510) 642-5033
E-mail: nbalsara@berkeley.edu

**David Prendergast**
Lawrence Berkeley National Laboratory
1 Cyclotron Road
Berkeley, CA 94720
Phone: (510) 486-4948; Fax: (510) 486-7424
E-mail: dgprendergast@lbl.gov

Start Date: October 2013
Projected End Date: September 2016

## Objectives

- Develop a unique diagnostic tool to study Li-S battery reaction intermediates that employs X-ray spectroscopy and molecular modeling.
- Elucidate Li-S battery charge/discharge reaction mechanisms.
- Examine physical and chemical nature of Li-S battery reaction intermediates in electrolyte environment.

## Technical Barriers

As lithium-sulfur batteries are charged and discharged, $Li_2S_x$ reaction intermediates formed can leave the cathode, causing capacity fade and battery failure. Redox reaction mechanisms that form $Li_2S_x$ intermediates are still unclear. Elucidation of reaction pathways requires an experimental tool that can differentiate $Li_2S_x$ intermediates in their native environment. Little is known about the physical and chemical nature of $Li_2S_x$ intermediates dissolved in electrolytes.

## Technical Targets

- Obtain X-ray absorption spectroscopy (XAS) signatures for $Li_2S_x$ intermediates dissolved in electrolytes of poly(ethylene oxide) (PEO) and a diblock copolymer of polystyrene-poly(ethylene oxide) (SEO) by experiment and by simulations.
- Develop Li-S cell that facilitates use of soft and hard X-ray spectroscopy during charge-discharge cycles
- Perform detailed (first-principles or empirical force-field) molecular dynamics (MD) simulations to interpret associated X-ray spectra and reveal molecular nature of $Li_2S_x$ intermediates in electrolyte.

## Accomplishments

- Experimental XAS were obtained for $Li_2S_x$ (x = 2, 4, 6, 8) intermediates dissolved in PEO and a diblock copolymer of SEO.
- MD simulations of $Li_2S_x$ molecules dissolved in tetraglyme were performed. eXcited Core Hole (XCH) simulations were used to obtain theoretical $Li_2S_x$ X-ray signatures for representative *ab initio* molecular dynamic motifs.
- Li-S cells appropriate for *in situ* soft X-ray measurements were developed.

✧ ✧ ✧ ✧ ✧

## Introduction

The objectives of this work are to: (a) elucidate mechanisms by which redox reactions in the sulfur cathode proceed, and (b) study the physical and chemical nature of $Li_2S_x$ intermediates. Past studies of Li-S battery reaction mechanisms have been inconclusive due to the difficulty of $Li_2S_x$ molecule speciation. $Li_2S_x$ species cannot be isolated, and tend to undergo reversible disproportionation reactions in solution. The equilibrium constants and reaction kinetics governing disproportionation are system-dependent. A combination of XAS and simulations provides us with an unprecedented ability to detect $Li_2S_x$ molecules in solution and study their local chemical environments. Experimental XAS signatures were obtained for $Li_2S_x$ molecules dissolved in PEO and SEO. MD simulation of $Li_2S_x$ solvation revealed that lithium polysulfide molecules elect to form nano-agglomerates in solution. Theoretical XAS signatures for $Li_2S_x$/tetraglyme configurations were obtained and used to interpret signatures of experimental $Li_2S_x$/polymer electrolyte systems.

## Approach

- Obtain simulation results of $S_8$, $Li_2S_x$, and $Li_2S$ in tetraglyme (an oligomer analog of PEO).
- Obtain theoretical XAS signatures of $Li_2S_x$ molecules in tetraglyme using XCH methods at the sulfur K-edge.
- Obtain experimental sulfur K-edge XAS signatures for $Li_2S_x$ dissolved in thin films of solid-state PEO and SEO.
- Design a Li-S cell appropriate for measurement of X-ray spectra as a function of state of charge in cathode.

## Results

**MD simulations of $Li_2S_x$ molecules.** MD simulations of $Li_2S_x$ molecules dissolved in tetraglyme have shown that lithium polysulfide molecules elect to form nano-agglomerates in solution, and are not poly-dispersed as is commonly assumed. These nano-agglomerates are exemplified in Figure VI - 272a for $Li_2S_8$. The thermodynamics of agglomeration have been investigated by calculating the free energy of agglomeration for two $Li_2S_8$ molecules in tetraglyme (inset of Figure VI - 272b) using *ab initio* MD simulations. These studies show that the agglomerates are the thermodynamically stable state. A 0.4 kcal/mol (0.5 eV) barrier was calculated, which is accessible at room temperature. These simulations are the most extensive ever performed on this system and provide the first molecular level insights into the mechanism of lithium sulfide dissolution into the electrolyte and concurrently, the failure mechanism in Li/S batteries.

Spectroscopic signatures obtained using XCH methods for both single polysulfide molecules in tetraglyme and polysulfide molecules that have formed nano-crystals in simulation have been obtained. Due to computational limitations, the nano-agglomerates were modeled as solid phase structures. Then, the sulfur K-edge X-ray absorption spectra was calculated. As shown in Figure VI - 273, the nano-agglomerate of $Li_2S_8$ is in closer agreement with experiment than the isolated $Li_2S_8$ molecule. In particular, the separation between the pre-edge and main-edge peaks (labeled 'a' and 'b') is significant in the isolated molecule but absent in the $Li_2S_8$ solid and experiment. This result connects the experimental and computational spectra. Ongoing work involves understanding the physical basis of the observed differences in the isolated molecule and nano-agglomerates and quantifying this effect in other $Li_2S_x$ species.

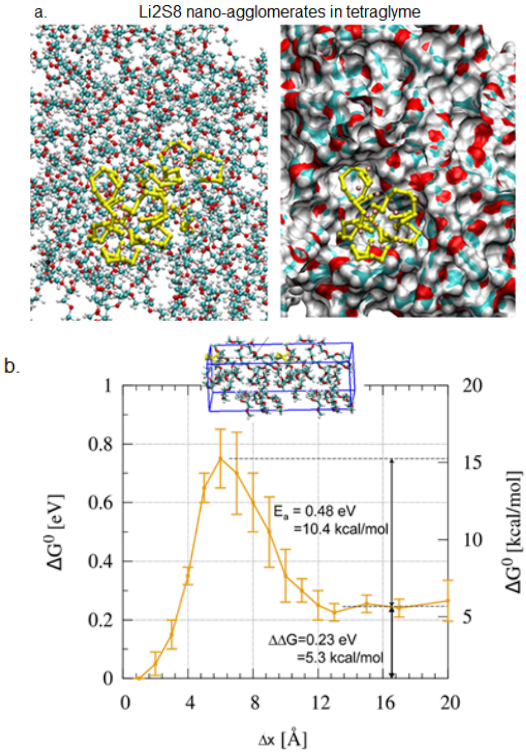


**Figure VI - 272: (a) Example of equilibrium structure of $Li_2S_8$ dissolved in tetraglyme from classical molecular dynamics simulations showing nano-aggregation. (b) Free energy *ab initio* molecular dynamics simulations of the association of 2 $Li_2S_8$ molecules in tetraglyme. This study reveals a 10.4 kcal/mol barrier for nano-agglomeration of $Li_2S_8$**

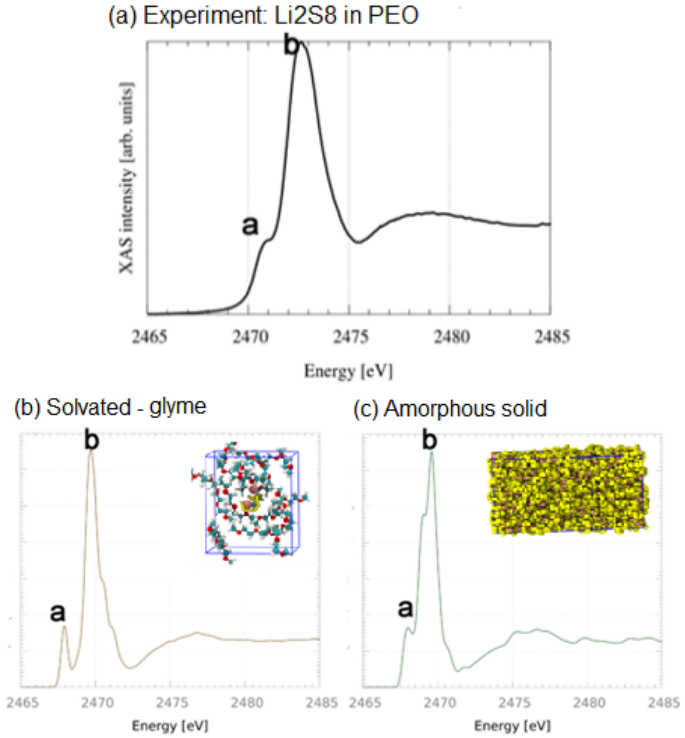


**Figure VI - 273: $Li_2S_8$ XAS Sulfur K-edge spectra from (a) experimental measurements (b) theoretical calculations of the isolated molecule in tetraglyme (c) theoretical calculations of the amorphous solid as a model of the nano-agglomerates. The pre-edge 'a' and main edge 'b' peak are labeled**

**XAS spectroscopy of $Li_2S_x$ intermediates.**
Experimental X-ray signatures were obtained for $Li_2S_x$ (x = 2, 4, 6, 8) dissolved in PEO and SEO. Samples were spin-cast solid-state thin films having a sulfur concentration of 30 wt%. XAS measurements were taken at the sulfur K-edge. Resulting spectra are shown in Figure VI - 274.

The set of $Li_2S_x$ spectra displayed three spectral features: a pre-edge peak at 2471.0 eV (attributable to anionic sulfur chain ends), a main-edge peak at 2472.7 eV (as typically found in S—S covalent bonds), and a broad peak from 2475-2485 eV (related to S—S bond length). The main-edge peak grows in intensity as polysulfide chain length increases, while the pre-edge peak decreases. This agrees with what would be expected, qualitatively, given the increasing ratio of S—S covalent bonds to anionic sulfur chain ends as polysulfide chain length increases. This trend was also seen in theoretical $Li_2S_x$ X-ray spectra, as shown in Figure VI - 275.

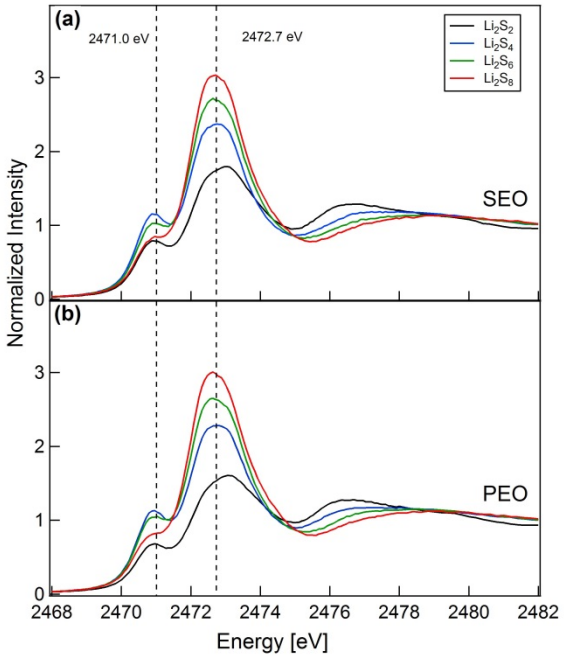


**Figure VI - 274: XAS sulfur K-edge spectra of $Li_2S_x$ dissolved in: (a) SEO, and (b) PEO**

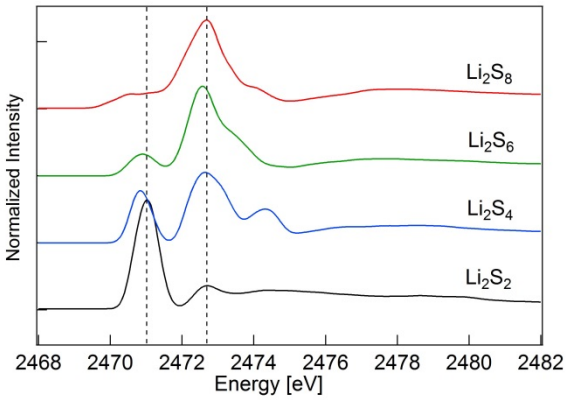


**Figure VI - 275: Theoretical $Li_2S_x$ spectra of $Li_2S_x$ amorphous solids.**

$Li_2S_x$ speciation is complicated by the fact that $Li_2S_x$ molecules may disproportionate in solution. While above, spectra were labeled with a given $Li_2S_x$ 'x' value, 'x' is an average value, and a distribution of $Li_2S_x$ species may be present in each system. For this reason, a principal component analysis (PCA) was performed on the system of $Li_2S_x$ spectra in attempt to deconvolute the spectra into spectra of individual mixture components. The PCA analysis revealed that the system of spectra could be represented by three unique components.

An iterative target factor analysis (ITFA) was then performed to convert abstract components generated by the PCA into spectra. Through linear combination, these components were then used to recreate experimental X-ray spectra. Component weightings needed to recreate each experimental spectrum were determined and are plotted in the ternary diagram in Figure VI - 276.

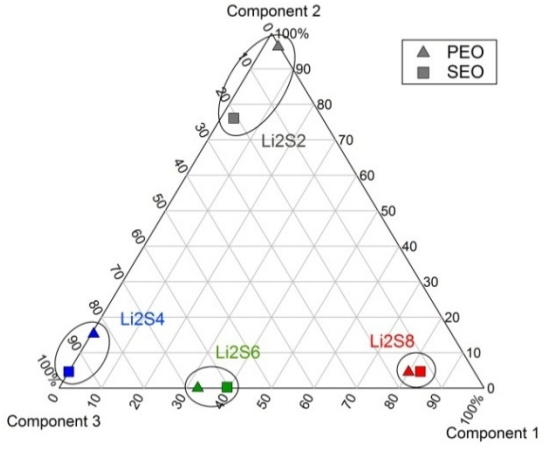


**Figure VI - 276: Ternary diagram of individual PCA/ITFA generated spectra weightings needed to recreate experimental $Li_2S_x$ spectra**

An important note regarding PCA/ITFA is that it cannot identify spectra/components as being unique if they truly are, in reality, a linear combination of other spectra/components.

**Li-S battery development for *in situ* XAS experiments.** Li-S cells for *in situ* X-ray experiments have been designed. As a first step, Li-S cells with a more traditional design have been assembled to study both the cathode and electrolyte composition effect on performance, the polysulfide shuttle process, and interfaces. The addition of $LiNO_3$ to the electrolyte has led to improved performance; discharge capacity of 600 mAh/g sulfur has been observed after 15 cycles with an initial discharge at C/50 and subsequent charging/discharging at C/20, as shown in Figure VI - 277.

## Conclusions and Future Directions

MD simulations of $Li_2S_x$ molecules have been used in conjunction with experimental XAS of $Li_2S_x$ species for: (a) elucidating Li-S battery chemistry, and (b) examining the fundamental nature of $Li_2S_x$/electrolyte systems. Simulations of $Li_2S_x$ molecules in tetraglyme revealed that $Li_2S_x$ molecules elect to form nano-agglomerates. Theoretical XAS spectra were obtained using XCH methods. When compared to experimental $Li_2S_x$ spectra, theoretical spectra suggest that $Li_2S_x$ molecules form nano-agglomerates in experimental $Li_2S_x$/PEO systems as well. Experimental XAS sulfur K-edge spectra were obtained for $Li_2S_x$ (x = 2, 4, 6, 8) in PEO an SEO. PCA/ITFA was used to determine that the $Li_2S_x$ systems may be comprised of three unique components. Weightings of each component needed to recreate experimental $Li_2S_x$/polymer system were determined. Cells for *in situ* XAS studies of Li-S battery cathodes during charging/discharging were assembled. Preliminary analysis has revealed that $LiNO_3$ increases specific capacity and efficiency of Li-S cells.

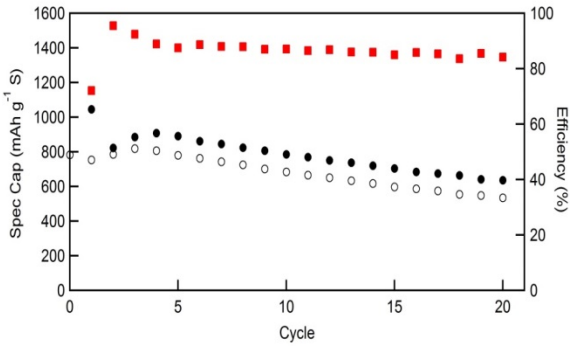


**Figure VI - 277: Li-S battery specific charge (full symbol) and discharge (open symbol) capacities at 90°C as a function of the cycle number. The efficiency for each cycle is indicated on the right Y-axis. The electrolyte and the cathode are made of SEO/LiTFSI(r=0.05)/$LiNO_3$(r=0.025) and $Li_2S_8$/SEO-LITFSI/Carbone (70/25/15$_{wt}$%), respectively**

Simulation work is now focused on: accessing the free energy of association barriers for all other $Li_2S_x$ species, accessing the role of solid lithium sulfide interfaces on the agglomeration barrier, and the development of a semi-classical forcefield to investigate $Li_2S_x$ inter-conversion and speciation. Experimental spectroscopy will focus on elucidating the Li-S battery reaction mechanisms by performing *in situ* XAS experiments during charge/discharge. Already obtained $Li_2S_x$ spectra will be used to interpret *in situ* spectra.

## FY 2013 Publications/Presentations

1. N.P. Balsara, "Polymer Electrolytes for Advanced Lithium Batteries," *2013 DOE Annual Merit Review*, May 2013, Washington, DC.

# VI.G.11 Lithium Batteries of Higher Capacity and Voltage (UT Austin)

**John B. Goodenough**
The University of Texas at Austin

Department of Mechanical Engineering
204 East Dean Keeton
C2201, ETC 9.184
Austin, TX 78712
Phone: (512) 471-1646; Fax: (512) 471-7681
E-mail: jgoodenough@mail.utexas.edu

Start Date: January 2013
Projected End Date: December 2016

## Objectives

- To increase cell voltage by:
  - enabling use of a lithium anode and,
  - allowing use of a liquid catholyte compatible with higher-voltage cathodes.
- To increase capacity by:
  - the elimination of the irreversible loss of Li from the cathode on first charge and,
  - the introduction of cathode strategies other than insertion-compound hosts.

## Technical Barriers

Technical problems in developing a hybrid redox flow battery with an aqueous catholyte and a thin garnet membrane as a separator turned out to be high interfacial $Li^+$-transfer impedance and chemical stability of the garnet pellet in water. Moreover, the ceramic membrane is brittle and not scalable to be used in a large-scale energy storage system. Therefore, a new type of $Li^+$-ion conducting membrane is required to overcome the problems of the ceramic electrolyte membrane. A polymer/ceramic composite membrane has been developed in UT Austin. New sets of problems have been identified in the new approach, and novel solutions were required to use the membrane for an electrochemical cell.

## Technical Targets

- Identify solid $Li^+$ electrolytes stable on contact with Lithium and having $\sigma_{Li} > 10^{-4}$ S $cm^{-1}$,
- Test their stability in various liquids: aqueous of different pH, organic, oxidative,
- Fabricate as a thin, durable membrane or coating, and,
- Test performance of single cells.

## Accomplishments

- Obtained $\sigma_{Li} > 5 \times 10^{-4}$ S/cm with an oxide garnet framework stable versus $Li^0$, but with a high $Li^+$-transfer impedance across its interface.
- Prepared robust $Al_2O_3$/PEO composite membrane with $\sigma_{Li} \approx 10^{-3}$ S/cm.
- Shown little crossover of $Al_2O_3$/PEO by 6-bromohexyl ferrocene redox molecule.
- Stabilized osmosis of liquid electrolyte across $Al_2O_3$/PEO membrane.
- Reduced absorption of anolyte into membrane by introducing gel PVdF-HFP (hexa fluoropropene) polymer electrolyte between $Li^0$ and membrane.

✧ ✧ ✧ ✧ ✧

## Introduction

UT Austin proposed to develop a solid $Li^+$-electrolyte separator that could block dendrites from a metallic lithium or sodium anode and allow the development of alternative cathode strategies. Two strategies were pursued: (a) development of the garnet $Li_{7-x}Zr_{2-x}Ta_xLa_3O_{12}$ as a solid that would allow a dual-electrolyte cell and (b) development of a flexible, mechanically robust $Al_2O_3$/PEO-polymer composite membrane that would block dendrites from an anode and allow a flow-through liquid cathode of high voltage for a high capacity battery. Although a Li-ion conductivity $\sigma_{Li} \geq 5 \times 10^{-4}$ S/cm was obtained for a bulk garnet, the oxide ions of the garnet structure proved to be too weakly bound by the garnet cations; the surface oxygen were attacked by Na from the furnace and Li was leached out on exposure to air to form $Li_2CO_3$ and $Li_2O$, on the surface, thus blocking Li transport across the garnet/liquid-electrolyte interface. Therefore, effort was concentrated on the porous $Al_2O_3$/PEO-polymer electrolyte which restricts the battery to a single liquid electrolyte. With this membrane, three of the four objectives of the proposal were realized.

## Approach

UT Austin has experience developing solid state $Li^+$-ion conducting materials, especially the garnet-

structured ceramics. The thin garnet pellets have been tested to be used in various electrochemical cells.

In parallel, a polymer composite membrane has been studied to make a thin, flexible, and mechanically robust $Li^+$-ion conducting separator. A PEO/$Al_2O_3$ composite membrane has been developed to block metal (lithium and sodium) dendrite penetration through the membrane. A PEDOT:PSS (polystyrene sulfonate)-coated polypropylene (PP) separator has been developed to block the redox molecule crossover.

## Results

**Garnet-type solid electrolytes for electrochemical cells.** A garnet-structured solid electrolyte, $Li_{7-x}La_3Zr_{2-x}Ta_xO_{12}$ (x=0.6) was synthesized via a solid-state reaction method. It showed a $Li^+$-ion conductivity of ~ 5 × $10^{-4}$ S/cm. A garnet pellet with a thickness of ~ 300 μm was used as a solid electrolyte and combined with a lithium metal electrode to check its electrochemical properties. The Li/garnet interface showed a very high electrochemical impedance (> 10,000 Ω), which hindered $Li^+$-ion transport through the interface. Since the origin of the high impedance is not clear, the surface chemistry of the garnet electrolyte and interface barriers should be responsible for that problem and will be further investigated.

**PEO/$Al_2O_3$ composite membrane.** A flexible PEO/$Al_2O_3$ (2/1 in weight) composite membrane has been developed as a solid electrolyte layer for a dual-electrolyte cell (see Figure VI - 278). The $Al_2O_3$ particles in the membrane are used to enhance the mechanical stability and to block lithium dendrite.

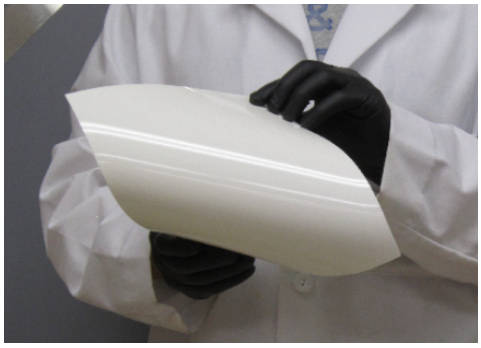

Figure VI - 278: A 68-72 membrane

The membrane was soaked with 1M LiTFSI in EC/DEC (1/1) electrolyte prior to electrochemical tests. Charging a Li|PEO/$Al_2O_3$(2/1)|Li symmetric cell has demonstrated that the lithium dendrite cannot penetrate the membrane. Cycling performance of Li|PEO/$Al_2O_3$(2/1)|Catholyte dual-electrolyte cell depends on the catholyte crossover and the osmotic pressure across the membrane. A redox molecule, 6-Bromohexyl ferrocene was used in the catholyte. After cycling, the crossover of the redox molecule has been identified by color change of the membrane. Controlling polymer structure was not successful enough to block the crossover, which initiated an extra activity to develop an electronic/ionic mixed conducting membrane. Another issue after cycling is the presence of the osmotic pressure across the membrane because it is semi-permeable to the $Li^+$-ion electrolyte, not to the big redox molecule. Higher concentration of the catholyte induced electrolyte transfer from the anode side, so the anode side was dried up at the end of cycles. It also affected the cell performance: a continuous increase in the cell polarization and drop in capacity were observed (see Figure VI - 279).

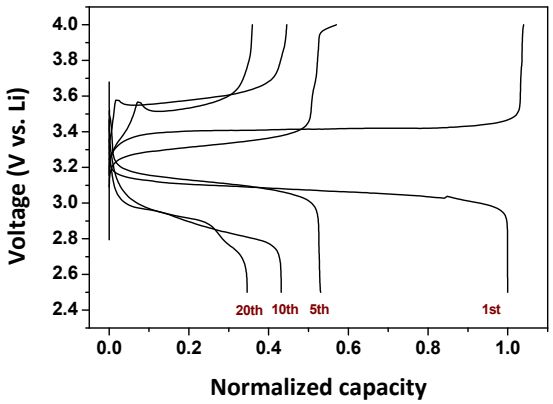


Figure VI - 279: Charge/discharge voltage curves of Li|PEO/$Al_2O_3$| 6-Bromohexyl ferrocene catholyte cell. Base electrolyte is 1M LiTFSI in EC/DEC (1/1)

The first approach to solve the issue was to balance the concentrations of anolyte and catholyte. A high molecular weight ionic liquid or soluble polymer could stabilize the cyclability and the polarization notably by inducing a dynamic equilibrium between catholyte and anolyte.

**PEDOT:PSS-coated PP separator.** An electronic/ionic mixed conducting membrane was tested as an additional layer to the PEO/$Al_2O_3$ membrane to block crossover while ensuring $Li^+$-ion transfer between cathode and anode.

First, amorphous vanadium oxide ($VO_x$) was coated on a commercial battery separator (Celgard 2500) by a drop casting method. However, a thin $VO_x$ film was immediately detached from the separator after wetting with catholyte. When the film got thicker, cell impedance greatly increased. It was suggested that to form a thin $Li^+$-ion-conductive film with good adhesion to the separator was necessary.

Second, a conducting polymer, PEDOT:PSS, was spin-coated on the PP separator. Concentration of the polymer solution and spinning speed were controlled to form a thin and uniform film without any macro-/micro-holes. A defect-free film was introduced between

electrodes to block the crossover of 6-bromohexyl ferrocene molecule from the catholyte. With this approach, stable charge/discharge cycle performance was achieved without a capacity fade over 50 cycles (see Figure VI - 280).

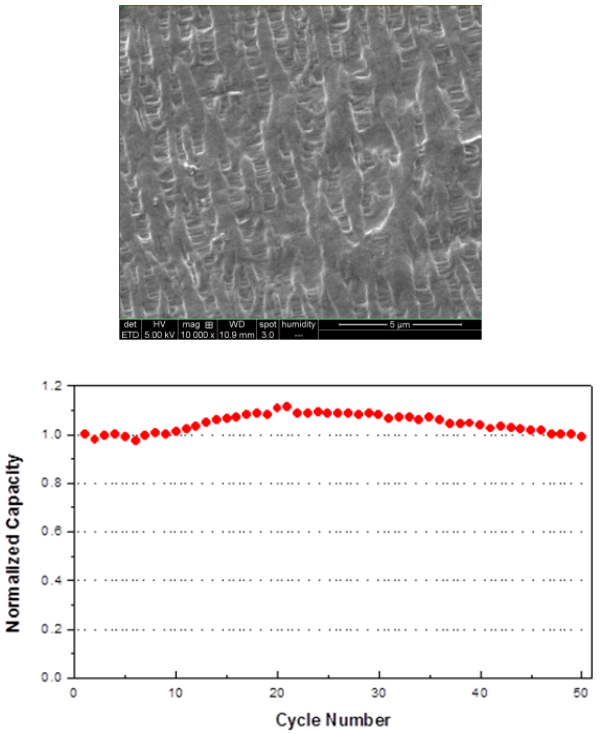


**Figure VI - 280: SEM image of a PEDOT:PSS-coated polypropylene separator and its electrochemical cycle performance of a Li/PVDF-HFP|PEO/$Al_2O_3$(2/1)|PEDOT:PSS/PP|6-bromohexyl ferrocene cell. Base electrolyte is 1M LiTFSI in EC/DEC (1/1) and the spectator molecule in anolyte is PEGDME (M.W. 500)**

## Conclusions and Future Directions

The development of a flexible, thin $Al_2O_3$/PEO-polymer membrane that allows penetration of a liquid electrolyte has been shown to block dendrites from a metallic lithium and also a sodium anode. This development allows safe use of a metallic anode and assembly of a charged cell rather than a discharged cell. As a result, a greater cell voltage and a greater capacity can be achieved for a given insertion-compound cathode since it eliminates loss of anode voltage and the loss of cathode capacity by formation of a Li-permeable SEI layer on the anode on the initial charge.

In order to develop the possibility of a redox flow-through liquid cathode, two problems were overcome: first, the problem of osmosis driving the liquid electrolyte from the anode to the cathode side of the membrane and, second, the development of a surface layer on the cathode side of the membrane that blocks crossover of the cathode redox molecule to the anode. Both of these problems were successfully solved.

Future work involves optimizing the composition, pore size, and thickness of an oxide/polymer composite membrane and development of alternative solid coatings on the surface of the $Al_2O_3$/polymer membrane that will allow realization of a dual liquid-electrolyte cell. In particular, the development of a solid that will block the small $Li_2S_2$ soluble molecules from the sulfur cathode of a Li-S cell and will also enable an aqueous catholyte for realization of a Li-air cell. Meanwhile, tests will continue for the membrane in a Na/cyano-perovskite cell that has a voltage of about 3.4 V to give a commercially viable Na-S cell.

## FY 2013 Publications/Presentations

1. Park, K.-S., Cho, J.H., Kadhiravan, S., Ellison, C.J., and Goodenough, J.B., "Chemical and ElectroChemical Properties of a Dual Electrolyte Cell Employing a Solid Electrolyte Membrane for Large Scale Energy Storage," *2013 ECS Fall Meeting* Presentation.
2. Lu, Y., Wang, L., Song, J., Zhang, D.W., Xu, M., and Goodenough, J.B., "Aluminium-Stabilized NASICON-Structured $Li_3V_2(PO_4)_3$," *J. Mater. Chem.*, **1,** 68-72 (2013).